ETH zürich

ETH Library

Carpy-Galy phases AnBnO3n+2 = ABOx : Overview, properties, special and hypothetical systems, and melt-grown synthesis of A- and O-deficient n = 5 types such as Sr19Nb19WO66 and Sr17Ca2Nb19WO64 and n = 6 type Ln6Ti4Fe2O20 and Ca6Nb5FeO20

Report

Author(s):
Lichtenberg, Frank

Publication date:
2020-07-06

Permanent link:
https://doi.org/10.3929/ethz-b-000424221

This page was generated automatically upon download from the ETH Zurich Research Collection.
For more information, please consult the Terms of use.

Rights / license:
In Copyright - Non-Commercial Use Permitted

This page was generated automatically upon download from the ETH Zurich Research Collection.
For more information, please consult the Terms of use.

Published in 2020 by the library of the ETH Zurich via doi 10.3929/ethz-b-000424221

Carpy-Galy phases $A_nB_nO_{3n+2} = ABO_x$: Overview, properties, special and hypothetical systems, and melt-grown synthesis of *A*- and O-deficient *n* = 5 types such as $Sr_{19}Nb_{19}WO_{66}$ and $Sr_{17}Ca_2Nb_{19}WO_{64}$ and *n* = 6 type $Ln_6Ti_4Fe_2O_{20}$ and $Ca_6Nb_5FeO_{20}$

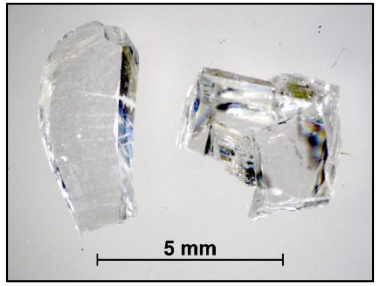

$Sr_4Nb_4O_{14}$
n = 4
ferroelectric

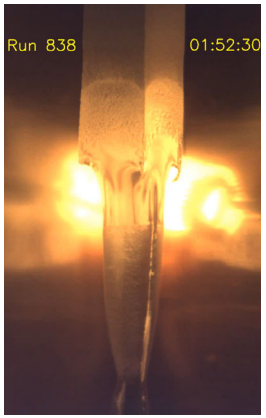

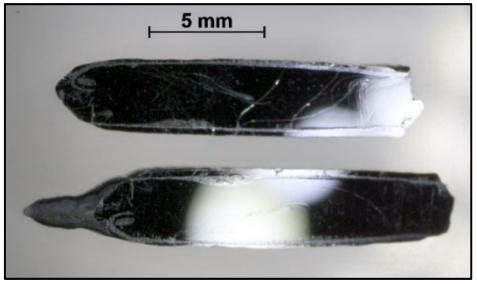

$Sr_{17}Ca_2Nb_{19}WO_{64}$
A- and O- deficient *n* = 5
quasi-1D metal ?

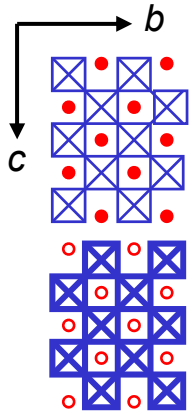

n = 5

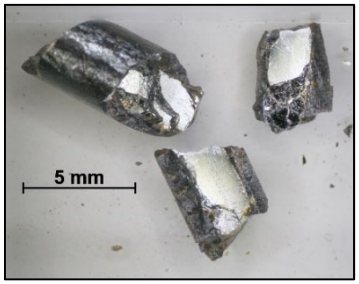

$Ca_6Nb_5FeO_{20}$
n = 6
ferroelectric ?

Frank Lichtenberg

ETH Zurich • Department of Materials • Division of Prof. Nicola Spaldin

8093 Zurich • Switzerland • https://theory.mat.ethz.ch/lab

Version 1 from 4 July 2020

ETH
Eidgenössische Technische Hochschule Zürich
Swiss Federal Institute of Technology Zurich

Copyright © 2020 Frank Lichtenberg • ETH Zurich

This paper in form of a presentation comprises 477 pages, about 400 figures or pictures, 33 tables, 17 videos, and a content overview. It is published by the library of the ETH Zurich / ETH Research Collection via doi 10.3929/ethz-b-000424221:

https://dx.doi.org/10.3929/ethz-b-000424221

It allows the download of

- this paper as pdf document
- this paper as ppsx type PowerPoint show with 17 embedded videos from the synthesis of melt-grown materials in a mirror furnace
- two Excel files with powder x-ray diffraction data of melt-grown $Ca_6Nb_5FeO_{20}$ and $Sr_{17}Ca_2Nb_{19}WO_{64}$

Part	**Content overview 1 / 8**	Page(s)
	Acknowledgement	11 – 12
1	Introduction	13 – 19
2	The crystal structure of $A_nB_nO_{3n+2} = ABO_x$ and other perovskite-related layered oxides	20 – 44
3	How the name Carpy-Galy phases for oxides of the type $A_nB_nO_{3n+2} = ABO_x$ comes about	45 – 46
4	Melt-grown synthesis of oxides and study of their properties by powder-x-ray diffraction, thermogravimetry, and a SQUID magnetometer	47 – 74
5	Insulating, ferroelectric and potential multiferroic Carpy-Galy phases $A_nB_nO_{3n+2} = ABO_x$	75 – 145
5.1	Insulators and ferroelectrics	76 – 83

Part	**Content overview 2 / 8**	Page(s)
5.2	Multiferroicity and magnetoelectricity: Abstracts of two papers and properties of various modifications of Fe_2O_3	84 – 87
5.3	Materials in the context of potential multiferroic Carpy-Galy phases $A_nB_nO_{3n+2} = ABO_x$	88 – 145
5.3.1	Compounds in the system La – Ti^{4+} – Fe^{3+} (Mn^{3+}) – O like the n = 6 type $La_6Ti_4Fe_2O_{20}$	89 – 100
5.3.2	Melt-grown n = 6 types $Ln_6Ti_4Fe_2O_{20}$ (Ln = Ce, Pr, Nd, Sm, $Sm_{0.9}Eu_{0.1}$, Eu) and $Ca_6Nb_5FeO_{20}$ prepared at the ETH Zurich	101 – 134
5.3.3	Other known, hypothetical, and suggested compounds / systems	135 – 145
6	Conducting and metallic Carpy-Galy phases $A_nB_nO_{3n+2} = ABO_x$	146 – 436
6.1	$LaTiO_x$ and the n = 5 type quasi-1D metal $La_5Ti_5O_{17} = LaTiO_{3.4}$	147 – 157

Part	**Content overview 3 / 8**	Page(s)
6.2	*n* = 4, *n* = 4.5, and *n* = 5 type quasi-1D metals (Sr,La)NbO_x	158 – 178
6.2.1	Photoinduced properties of the quasi-1D metals $SrNbO_{3.45}$ (*n* = 4.5) and $Sr_{0.95}NbO_{3.37}$ (Sr- and O-deficient *n* = 5)	179 – 180
6.3	Why Carpy-Galy phases $A_nB_nO_{3n+2}$ = ABO_x might have a potential to create superconductors	181 – 188
6.4	Potential polar or ferroelectric metals such as the *n* = 4 type $Sr_{0.8}La_{0.2}NbO_{3.5}$ and the hypothetical *n* = 5 type $Bi_5Ti_5O_{17}$	189 – 192
6.5	The history how the quasi-1D metallic behavior was revealed and results of resistivity measurements with various types of electrical contacts and methods	193 – 207
6.6	The size of the *a*-axis and crystallographic unit cell of the *n* = 5 type quasi-1D metal $SrNbO_{3.4}$ = $Sr_5Nb_5O_{17}$ = $Sr_{20}Nb_{20}O_{68}$ and other *n* = 5 type Sr-based niobates	208 – 210

Part	**Content overview 4 / 8**	Page(s)
6.7	The Schückel-Müller-Buschbaum phase $SrNbO_{3.2} = Sr_5Nb_5O_{16} = Sr_{20}Nb_{20}O_{64}$ and the $n = 5$ type quasi-1D metal $SrNbO_{3.4} = Sr_5Nb_5O_{17} = Sr_{20}Nb_{20}O_{68}$	211 – 227
6.8	Prepared and studied at the University of Augsburg and structurally and compositionally related to the Schückel-Müller-Buschbaum phase: Melt-grown *A*- and O-deficient $n = 5$ type titanates $A_{0.95}TiO_{3.2} = A_{4.75}Ti_5O_{16} = A_{19}Ti_{20}O_{64}$ without pronounced crystalline appearance	228 – 236
6.9	Prepared and studied at the ETH Zurich and structurally, compositionally, and electronically related to the Schückel-Müller-Buschbaum phase: Melt-grown Sr- and O-deficient $n = 5$ type materials $(Sr,Ca,Ba)_{19}Nb_{19}WO_x$ ($64 \leq x \leq 66$) with pronounced crystalline appearance	237 – 397

Part	**Content overview 5 / 8**	Page(s)
6.9.1	Overview of the melt-grown compounds $(Sr,Ca,Ba)_{19}Nb_{19}WO_x$ ($64 \leq x \leq 66$) and general experimental details	238 – 246
6.9.2	Towards a Schückel-Müller-Buschbaum type phase: Synthesis and properties of $Sr_{19}Nb_{19}WO_{66}$	247 – 264
6.9.3	Towards a Schückel-Müller-Buschbaum type phase: Synthesis and properties of $Sr_{17}CaBaNb_{19}WO_{65.5}$	265 – 284
6.9.4	Towards a Schückel-Müller-Buschbaum type phase: Synthesis and properties of $Sr_{17}CaBaNb_{19}WO_{65.3}$	285 – 305
6.9.5	A Schückel-Müller-Buschbaum type phase: Synthesis and properties of $Sr_{17}CaBaNb_{19}WO_{64}$	306 – 329
6.9.6	A Schückel-Müller-Buschbaum type phase: Synthesis and properties of $Sr_{17}Ca_2Nb_{19}WO_{64}$	330 – 354

Part	**Content overview 6 / 8**	Page(s)
6.9.7	Magnetic susceptibility χ(T) of the five compounds of the type $(Sr,Ca,Ba)_{19}Nb_{19}WO_x$ ($64 \leq x \leq 66$) in one graphics	355 – 357
6.9.8	The Sr-deficient Schückel-Müller-Buschbaum type phases $Sr_{17}Ca_2Nb_{19}WO_{64}$ and $Sr_{17}CaBaNb_{19}WO_{64}$: Comments and open questions	358 – 373
6.9.9	A nonlinear behavior of the magnetic moment M(H) of the crossover region from a polycrystalline to a crystalline material suggests the existence of ferromagnetism in the system Sr - Ca - Ba - Nb - W - O or in one of its subsystem	374 – 397
6.10	Examples of synthesis experiments and processed compositions which did not result in a single phase melt-grown n = 5 type material: $Sr_{19}Nb_{18}W_2O_{70-y}$, $Sr_{18}CaBaNb_{19}WO_{70.5-y}$, $Ca_{19}BaNb_{19}WO_{68}$, $Sr_{20}Nb_{19}O_{67.5-y}$, $Ca_{20}Nb_{19}O_{65}$, and $Eu_{20}Ti_{20}O_{67}$	398 – 431

Part	**Content overview 7 / 8**	Page(s)
6.11	Magnetic properties of lanthanide ions Ln^{3+} in titanates of the type $Ln_nTi_nO_{3n+2}$ = $LnTiO_x$	432 – 436
7	Stability ranges of Carpy-Galy phases $A_nB_nO_{3n+2}$ = ABO_x and polymorphism in the systems $LnTiO_{3.5}$, $(Pr,Ca)(Ti,Nb)O_{3.5}$, $SmTiO_x$, $Ln_6Ti_4Fe_2O_{20}$, and $NaWO_{3.5}$	437 – 447
8	Carpy-Galy phases $A_nB_nO_{3n+2}$ = ABO_x allow a special kind of micro or nano patterning by an electron beam	448 – 458
8.1	A basic observation which was published in 1993	449 – 450
8.2	Conducting $n = \infty$ type $SrNbO_3$ micropillars or nanopillars in an n = 4 type ferroelectric $SrNbO_{3.5}$ matrix or in an n = 5 type $SrNbO_{3.4}$ matrix	451 – 454

Part	**Content overview 8 / 8**	Page(s)
8.3	A potential novel magnetoelectric or multiferroic system: Weak ferromagnetic $LaTiO_3$ micropillars in a ferroelectric matrix $LaTiO_{3.5}$	455 – 456
8.4	Another suggested system: $NaWO_x$ ($3 \leq x < 3.5$) micropillars in a $NaWO_{3.5}$ matrix	457 – 458
9	Indications for high-T_c superconductivity in the system Na – W – O and a hypothetical involvement of Carpy-Galy phases $A_nB_nO_{3n+2} = ABO_x$	459 – 463
10	Pictures and properties of some melt-grown perovskite-related layered oxides which are not Carpy-Galy phases such as Sr_2RuO_4 , $SrLaFeO_4$, $BaCa_{0.6}La_{0.4}Nb_2O_7$, $Sr_5Nb_4O_{15}$, and $Sr_6Nb_5O_{18}$	464 – 477

Acknowledgement ☺ Frank Lichtenberg thanks

S. C. Abrahams
Ulrich Aschauer
Teguh Citra Asmara
Bertram Batlogg
Johannes Georg Bednorz
Florian Biebl
Nicholas Bingham
Susanne Blatter
Vid Bobnar
Klaus Peter Bohnen
Peter Bornhauser
Martin Brändle
Norbert Büttgen
Chunlin Chen
Peter Daniels
Philipp Dorscht
Martin Dressel
Vincenzo Fiorentini
Matthias Frontzek
Boris Gorshunov
Lin Gu
Jonathan Guevarra
German Hammerl
Joachim Hemberger
Alexander Herrnberger
Yuichi Ikuhara
Stanislav Kamba
Lassi Karvonen
Thilo Kopp
Jan Kroupa
Hans-Albrecht Krug von Nidda
Christine A. Kuntscher
Ingo Loa
Dmitry Logvinovich
D. H. Lu
Peter Lunkenheimer
Yoshiteru Maeno
Jochen Mannhart
Dirk van der Marel
Marisa Medarde
Mickael Morin
Maribel Nunez
Marc Petitmermet
Anna Radi
Armin Reller
Michael A. Rübhausen
Andrivo Rusydi
Mitsuhiro Saito
Sebastien Saitzek
Eleonore Saladie
Maxim Savinov
Barbara Scherrer
Darrell G. Schlom
Helmut Schmalle
Michael Schmidt
Stefan Schuppler
Sander van Smaalen
Nicola Spaldin
Walter Steurer
Karl Syassen
Masaru Tsukada
Susumu Tsukimoto
Franz Waldner
Zhongchang Wang
Jens-Erik Weber
Thomas Weber
Daniel Widmer
Klaus Wiedenmann
Tim Williams
Hermann Winter
Alexander Wölfel
and many others

for various kinds of special contributions and / or support

Acknowledgement ☺

Nicola Spaldin and Frank Lichtenberg
thank the Körber Foundation
for financial support

1 Introduction ...

Introduction 1 / 6

The homologous series $A_nB_nO_{3n+2} = ABO_x$ stands for a special class of perovskite-related layered oxides. The layers comprise an arrangement of BO_6 octahedra which are $[110]_{perovskite}$ oriented along the *c*-axis. The index or structure type *n* describes the thickness of the layers which are *n* BO_6 octahedra thick along the *c*-axis. For $n = \infty$ the non-layered perovskite structure ABO_3 is obtained.

Why are oxides of the type $A_nB_nO_{3n+2} = ABO_x$ interesting ?

- They comprise the highest-T_c ferroelectrics such as the $n = 4$ type $La_4Ti_4O_{14} = La_2Ti_2O_7 = LaTiO_{3.5}$ with $T_c = 1770$ K
- They comprise quasi-1D metals where the delocalized electrons are embedded in a ferroelectric-like environment with high dielectric permittivity. An example is the $n = 5$ type $Sr_5Nb_5O_{17} = SrNbO_{3.4}$
- The quasi-1D metals display particular photoinduced properties: Teguh Citra Asmara et al., to be published in Communications Physics (2020)
- They might have a potential to create multiferroics and / or superconductors

Introduction 2 / 6

Why are oxides of the type $A_nB_nO_{3n+2}$ = ABO_x interesting ? continued

- They allow the fabrication of novel micro or nano patterned systems by an electron beam such as conducting $n = \infty$ pervoskite type $SrNbO_3$ micro/nano pillars in a ferroelectric $n = 4$ type $SrNbO_{3.5}$ matrix
- There are non-integral series members such as the $n = 4.5$ type quasi-1D metal $SrNbO_{3.45}$ which comprise an ordered stacking sequence of layers with different thickness
- Many compounds can be synthesized in a single phase and crystalline form via a solidification from the melt by floating zone melting
- There are many possible chemical compositions including non-stoichiometric compounds
- Presence of a partial or full occupational order
    - at the *A* or *B* site when there are cations *A*' and *A*'' or *B*' and *B*'' with a different valence such as *B* = (Ti^{4+}, Fe^{3+})
    - at the O site in case of oxygen vacancies

Introduction 3 / 6

This work presents concepts, results, and materials from own research and from other scientists and publications. Several materials synthesis experiments are described in detail with many pictures and several fast mode and real time videos from the floating zone melting process in a Cyberstar mirror furnace.

Examples from the content of this work:

As an extension of the already reported n = 6 type $La_6Ti_4Fe_2O_{20}$ related melt-grown n = 6 type materials $Ln_6Ti_4Fe_2O_{20}$ (Ln = Ce, Pr, Nd, Sm, $Sm_{0.9}Eu_{0.1}$, Eu) and $Ca_6Nb_5FeO_{20}$ are presented.

A focus topic in this paper is $Sr_5Nb_5O_{16}$ and related compounds. $Sr_5Nb_5O_{16}$ is reported by K. Schückel and Hk. Müller-Buschbaum in Zeitschrift für Anorganische und Allgemeine Chemie 528 (1985) 91. Small crystals were obtained by a very special technique, the non-centrosymmetric crystal structure was determined by single crystal x-ray diffraction, and physical properties are not reported.

Introduction 4 / 6

As already communicated in
Progress in Solid State Chemistry 36 (2008) 253

- the crystal structure of the non-centrosymmetric $Sr_5Nb_5O_{16}$ can be considered as an oxygen-deficient variant of the *n* = 5 type and centrosymmetric quasi-1D metal $SrNbO_{3.4} = Sr_5Nb_5O_{17} = Sr_{20}Nb_{20}O_{68}$ with fully ordered oxygen vacancies
- attempts to prepare the Schückel-Müller-Buschbaum phase $SrNbO_{3.2} = Sr_5Nb_5O_{16} = Sr_{20}Nb_{20}O_{64}$ via the melt were unsuccessful

In contrast to the quasi-1D metal $Sr_5Nb_5O_{17}$ a layer or slab of $Sr_5Nb_5O_{16}$ comprises along the *c*-axis an asymmetric distribution of the

- Nb^{4+} ($4d^1$) and Nb^{5+} ($4d^0$) ions
- Nb – O polyhedra distortions

Maybe these particular details of this structure type and its reported non-centrosymmetricity can bring forth special physical properties.

Introduction 5 / 6

To enable the verification of the crystal structure reported by K. Schückel and Hk. Müller-Buschbaum and the study of the physical properties it was tried to prepare related melt-grown compounds.

This work presents five melt-grown Sr- and O-deficient *n* = 5 type materials which are related to $Sr_5Nb_5O_{16} = Sr_{20}Nb_{20}O_{64}$ and appear single phase within the detection limit of powder x-ray diffraction:

$Sr_{19}Nb_{19}WO_{66}$
$Sr_{17}CaBaNb_{19}WO_{65.5}$
$Sr_{17}CaBaNb_{19}WO_{65.3}$
$Sr_{17}Ca_2Nb_{19}WO_{64}$
$Sr_{17}CaBaNb_{19}WO_{64}$

The temperature dependence of the magnetic moment or susceptibility of these five compounds suggests that they are potentially quasi-1D metals. The two latter are Sr-deficient Schückel-Müller-Buschbaum type phases because their oxygen content is 64.

Introduction 6 / 6

Examples of crystalline pieces from the melt-grown materials:

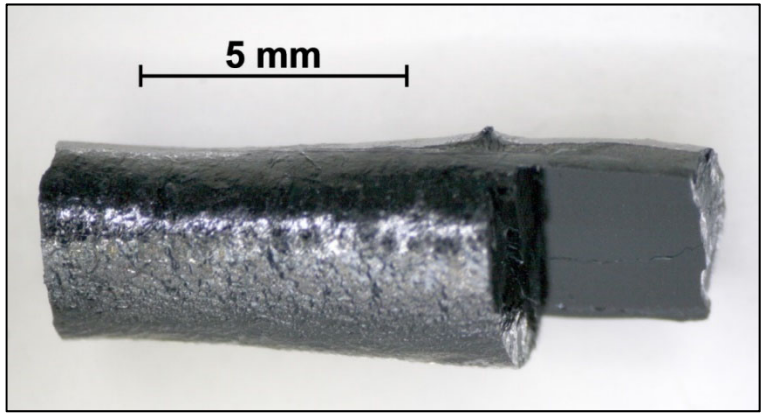

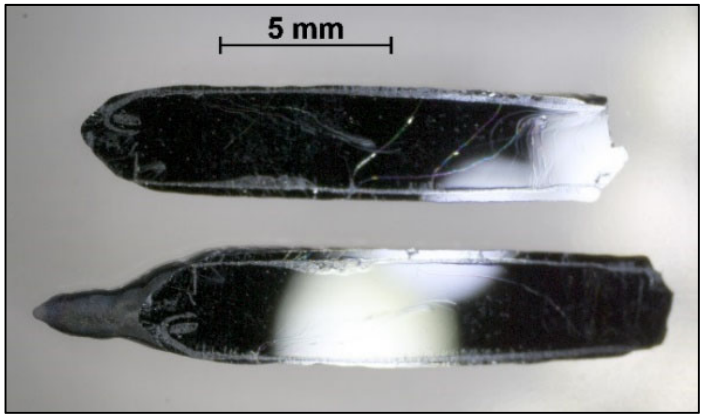

$Sr_{19}Nb_{19}WO_{66}$ 6.9 $Sr_{17}Ca_2Nb_{19}WO_{64}$ 11.1

Number of d-electrons from Nb^{4+} / $4d^1$ and W^{4+} / $5d^2$ per formula

For comparison: 4 in $Sr_{20}Nb_{20}O_{68}$ and 12 in $Sr_{20}Nb_{20}O_{64}$

These materials give rise to several questions such as: Have the compounds with oxygen content 64 the same non-centrosymmetric but Sr-deficient crystal structure as that of $Sr_5Nb_5O_{16}$ = $Sr_{20}Nb_{20}O_{64}$ reported by K. Schückel and Hk. Müller-Buschbaum ? Do the W ions occupy specific *B* or Nb sites ? Are there also related insulating materials which are potentially ferroelectric, magnetoelectric, or multiferroic ?

2 The crystal structure of $A_nB_nO_{3n+2} = ABO_x$ and other perovskite-related layered oxides...

The perovskite structure of compounds of the type ABX_3 or ABO_3

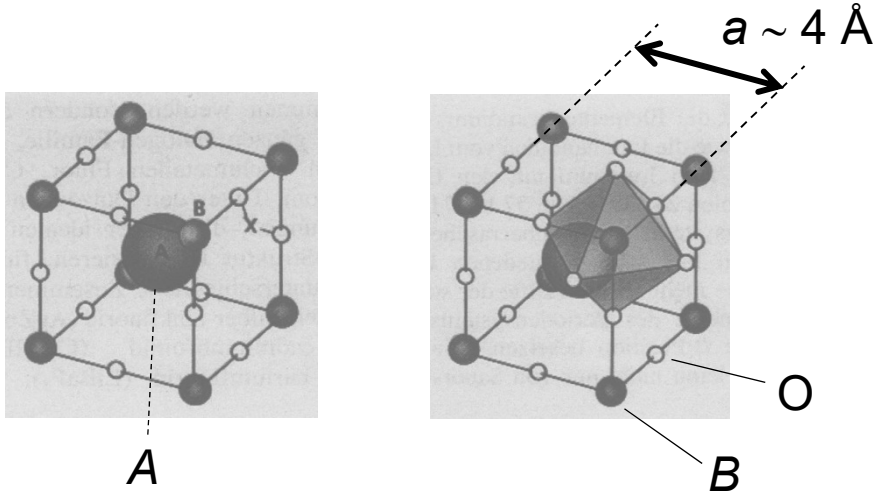

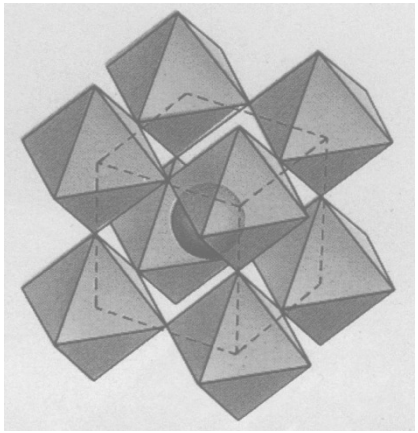

a = 3.9 Å for cubic $SrTiO_3$

Most ABO_3 compounds are distorted and adopt e.g. an orthorhombic structure

ABO_3

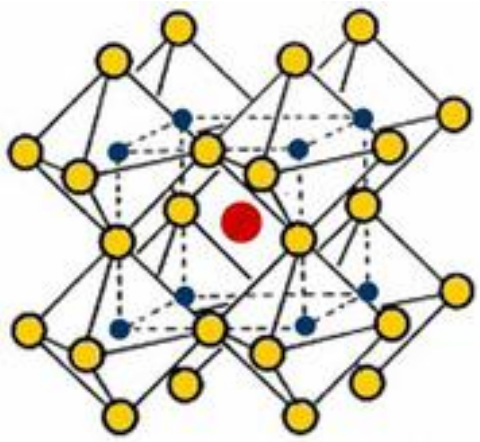

Image source:
www.iam.kit.edu/wpt/184.php

Progress in Solid State Chemistry 36 (2008) 253

Viewing the 3D perovskite structure ABO_3 from different directions and their 2D projections

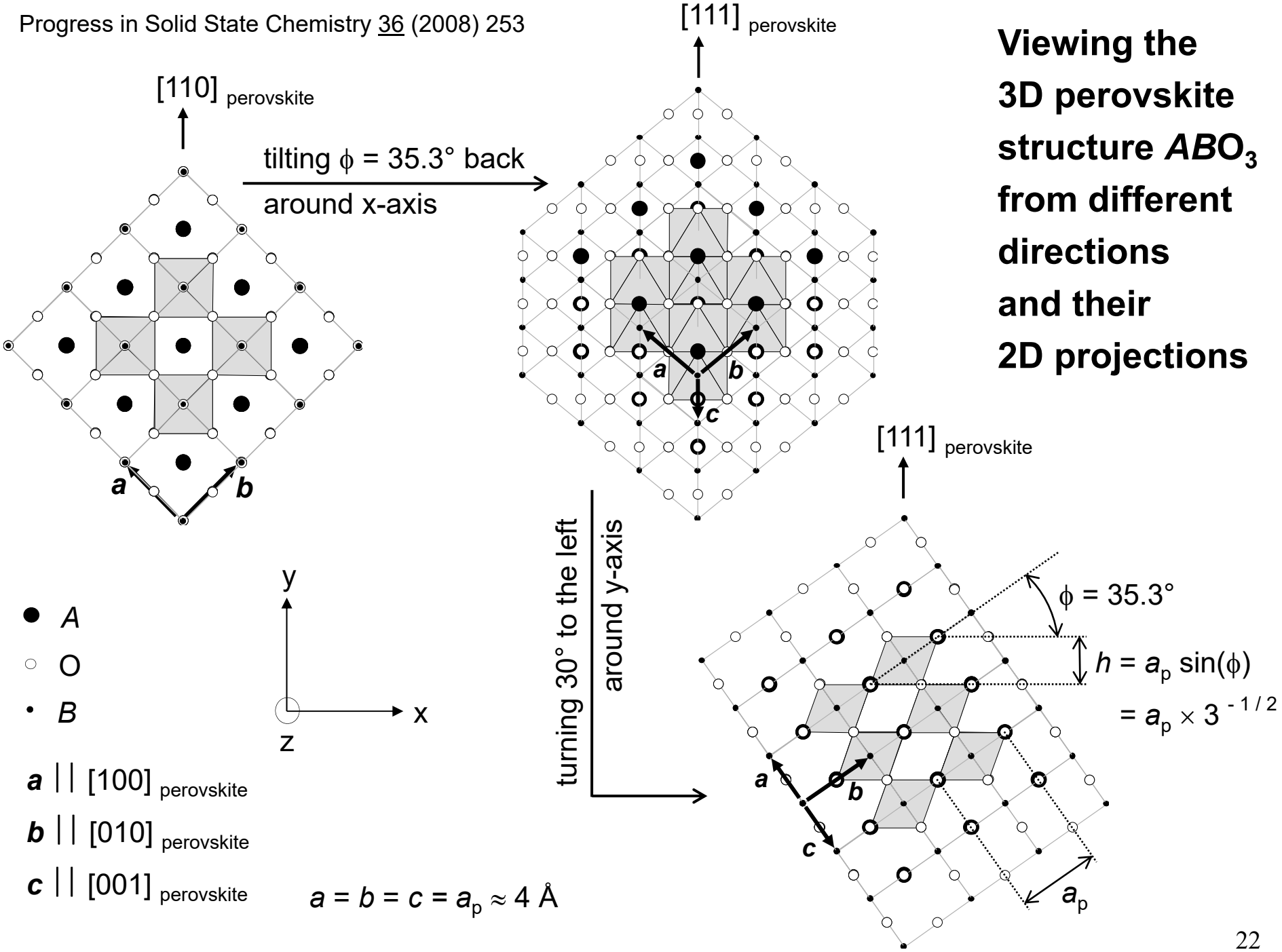

Viewing the 3D perovskite structure ABO_3 from different directions and their 2D projections

= BO_6 octahedra (O located at corners, *B* hidden in center)

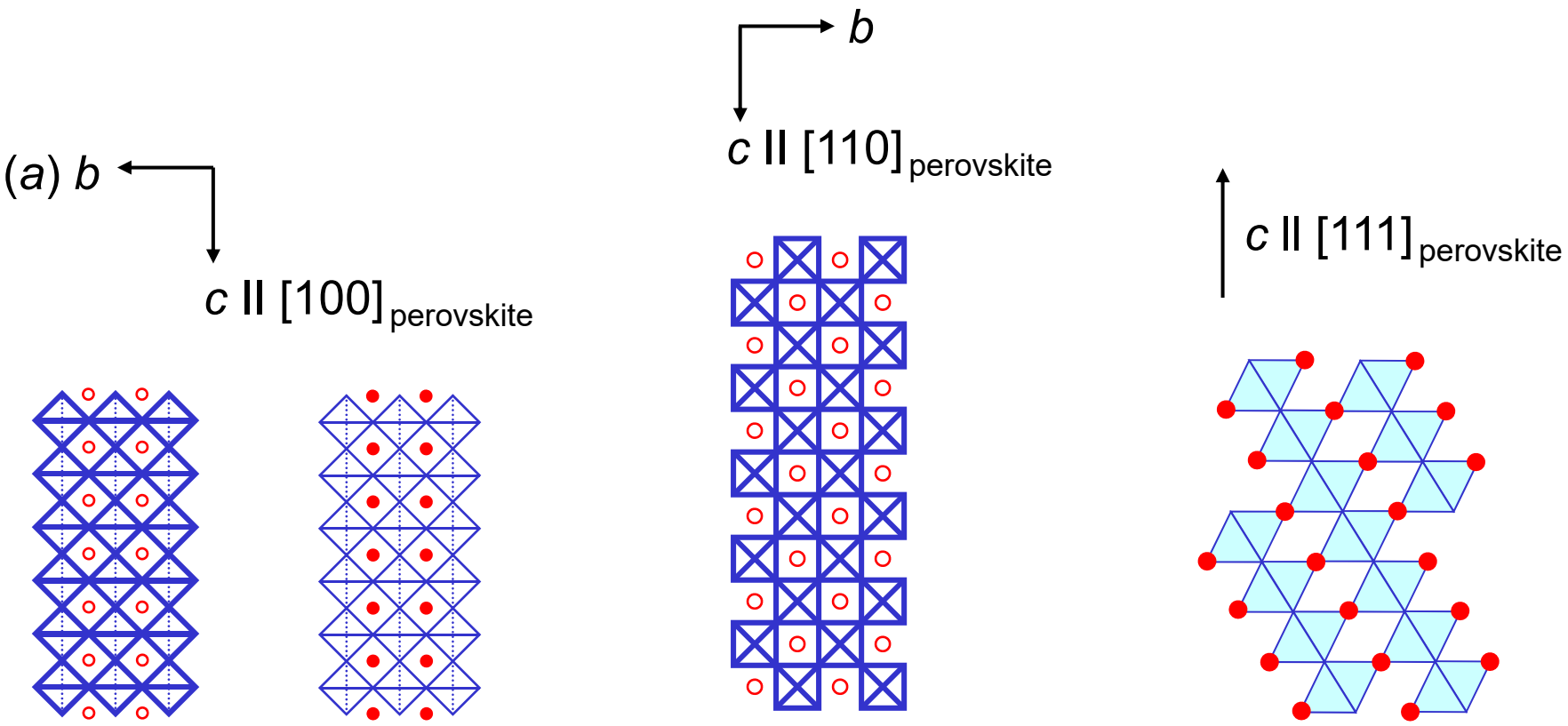

Cutting the perovskite structure ABO_3 along specific planes and inserting additional O (and *A*) leads to perovskite-related layered structures ABO_{3+y} ($A_{1+w}BO_{3+y}$) …

Example of a perovskite-related layered structure

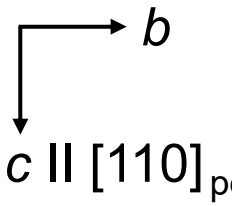

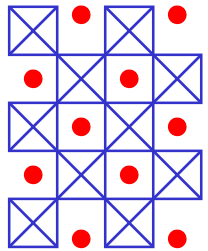

= BO_6 octahedra
(O located at corners,
B hidden in center)

Cut and insert additional oxygen until all octahedra are complete again and shift adjacent slabs perpendicular to the drawing plane

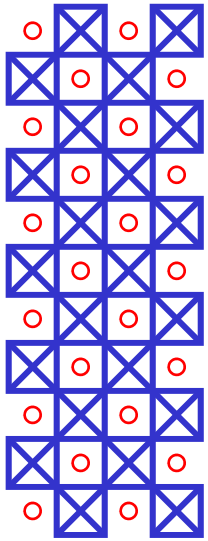

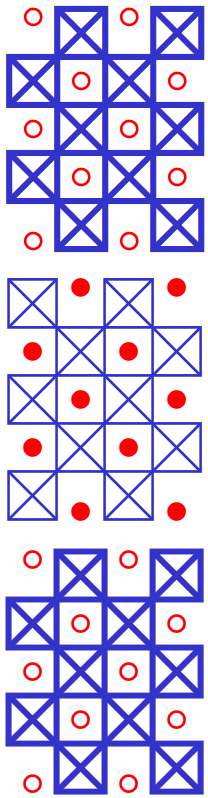

Light and bold BO_6 octahedra and filled and open circles indicate a height difference perpendicular to the drawing plane of about 2 Å, the *B* – O bond length:

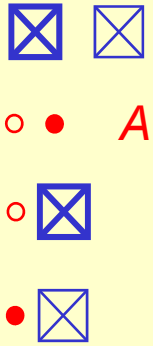

ABO_3 perovskite

$n = \infty$ of $A_nB_nO_{3n+2} = ABO_x$

$ABO_{3.40} = A_5B_5O_{17}$

$n = 5$ of $A_nB_nO_{3n+2} = ABO_x$

2D sketch of perovskite-related layered oxides of the type

$A_{j+1}B_jO_{3j+1}$, $A'A_{k-1}B_kO_{3k+1}$, $A_nB_nO_{3n+2}$, and hexagonal $A_mB_{m-1}O_{3m}$

B = Al, Ti, V, Cr, Mn, Fe, Cu, Ru ... Comprises j = 1 type $(La,Ba)_2CuO_4$ in which J. G. Bednorz and K. A. Müller discovered in 1986 superconductivity up to 30 K

B = Ti, Nb, Ta

- Layers are constituted by corner-shared BO_6 octahedra and extend along *ab*-plane
- Layer thickness along *c*-axis: $j = k = n = m - 1$ BO_6 octahedra
- $j = k = n = m = \infty \rightarrow$ Perovskite structure ABO_3

Progress in Solid State Chemistry 36 (2008) 253

= BO_6 octahedra (O located at corners, *B* hidden in center)

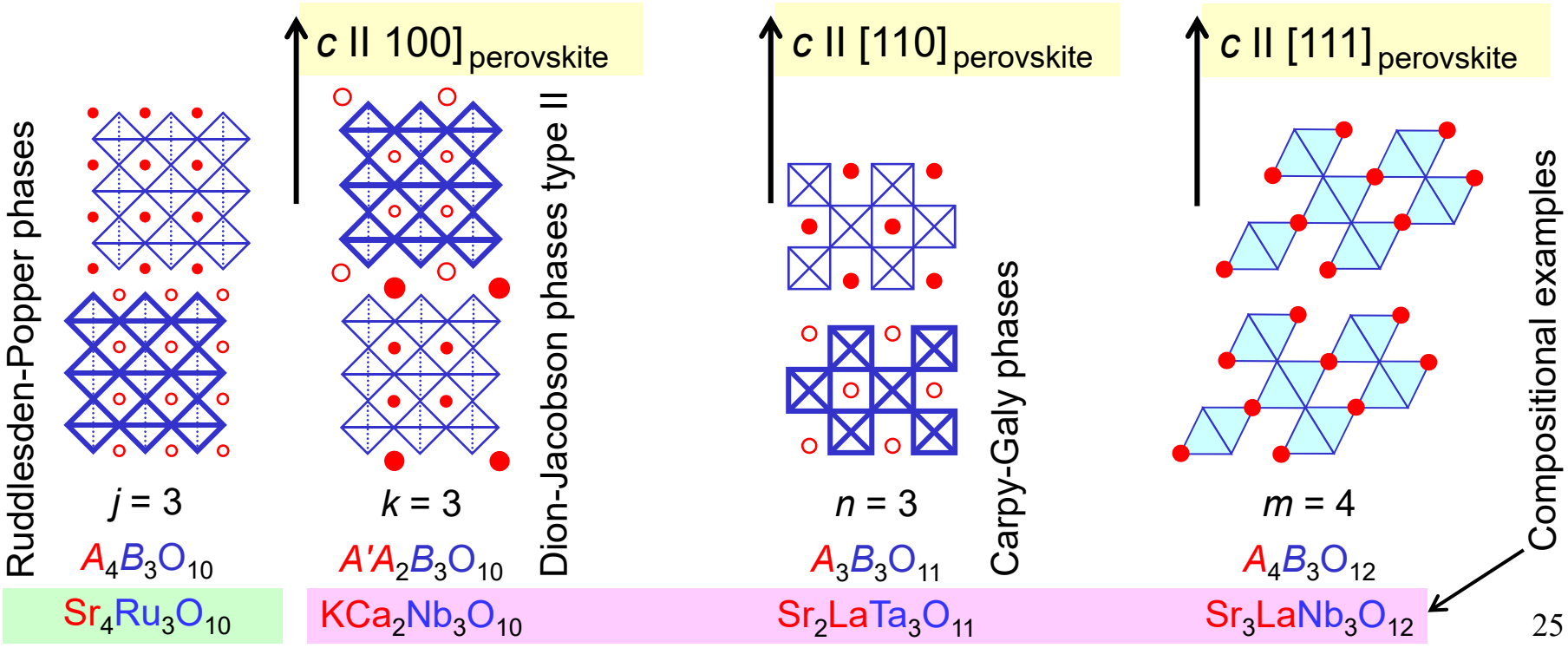

2D sketch of perovskite-related layered oxides of the type

$A_{j+1}B_jO_{3j+1}$, $A'A_{k-1}B_kO_{3k+1}$, $A_nB_nO_{3n+2}$, and hexagonal $A_mB_{m-1}O_{3m}$

Examples of melt-grown materials and their properties of these three homologous series are presented in part 10

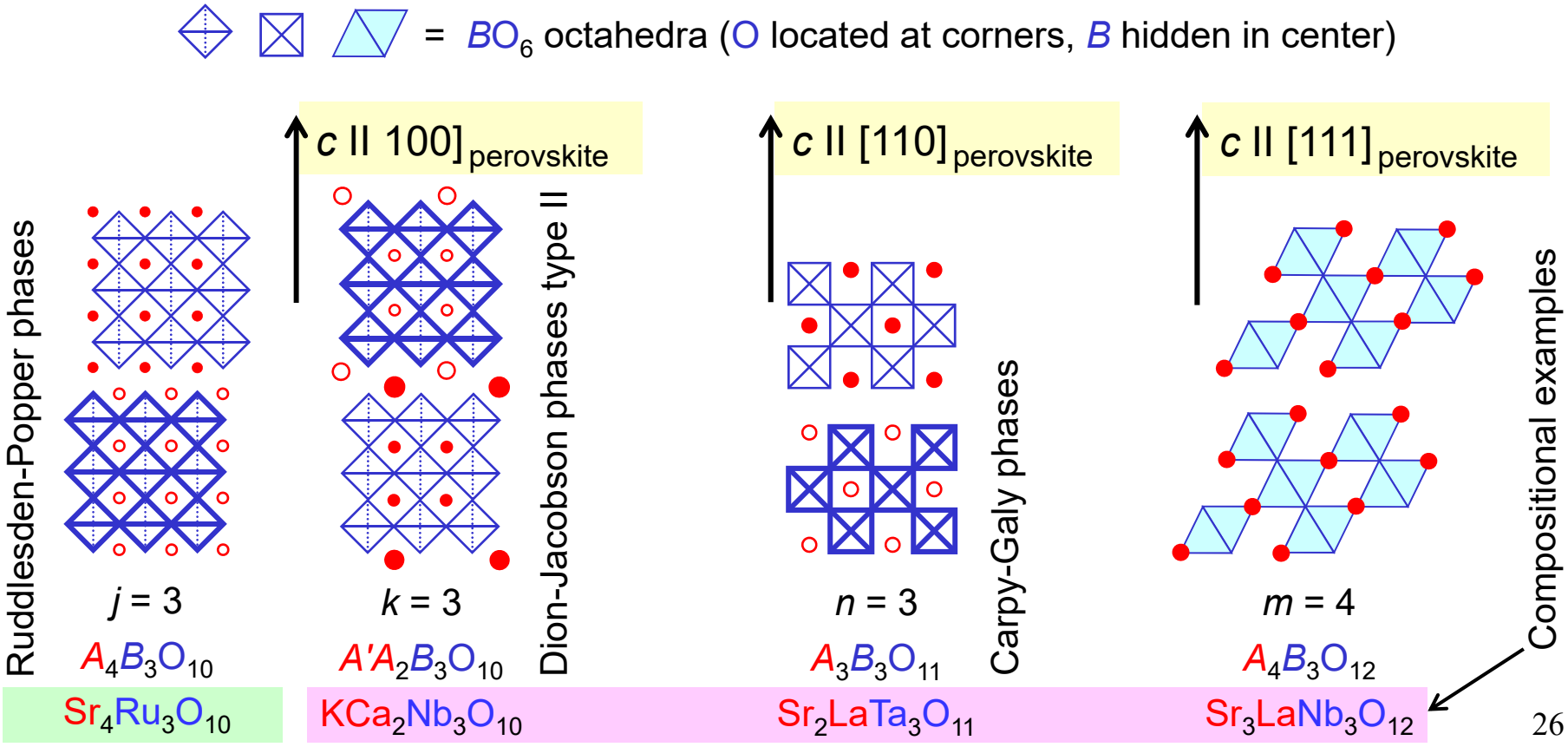

2D sketch of perovskite-related layered oxides of the type

$A_{j+1}B_jO_{3j+1}$, $A'A_{k-1}B_kO_{3k+1}$, $A_nB_nO_{3n+2}$, and hexagonal $A_mB_{m-1}O_{3m}$

Special features of $A_nB_nO_{3n+2} = ABO_x$ when compared to the other homologous series:

- Marked structural in-plane anisotropy, see also page 34
- The structure type *n* can be altered by changing only the oxygen content *x*. This allows a special kind of micro or nano patterning by an electron beam which is presented in part 8

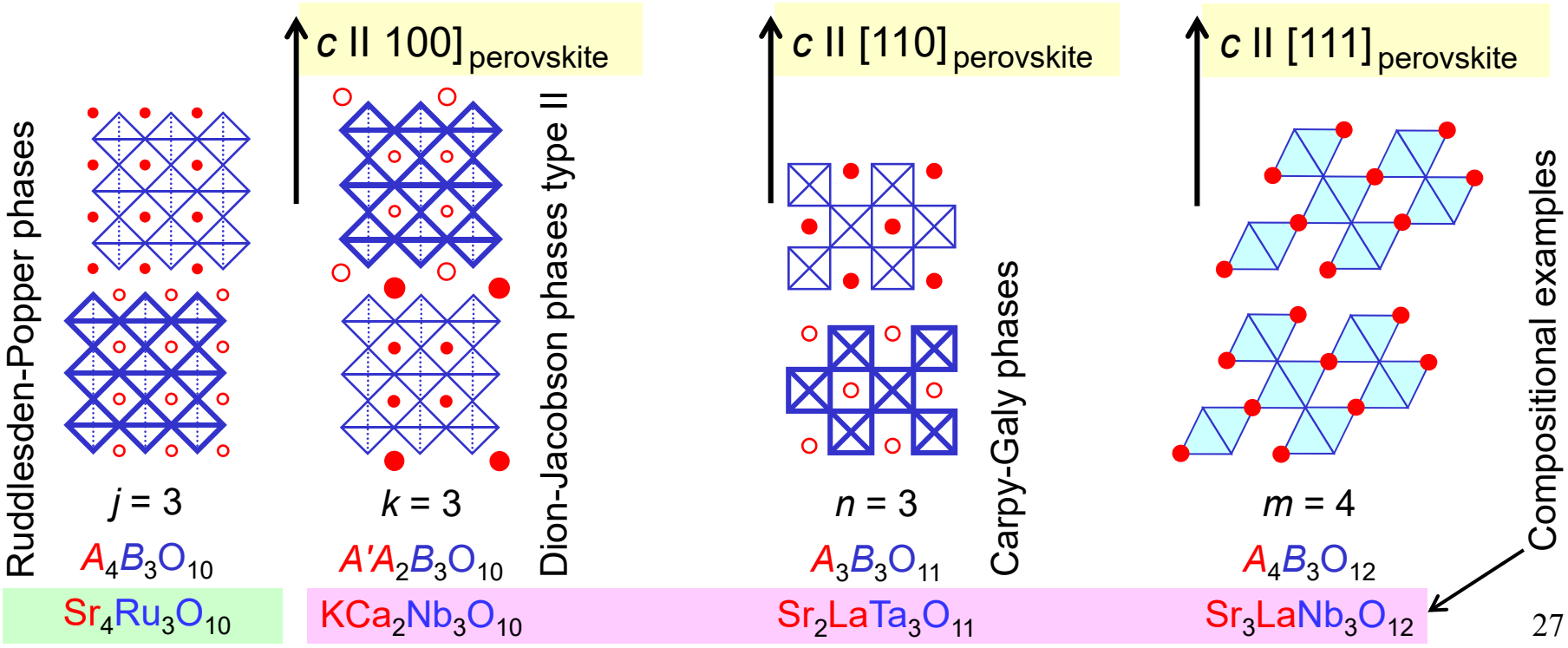

Sketch of the perovskite-related structure of

$A_nB_nO_{3n+2} = ABO_x$

B = Ti, Nb, Ta

⊠ = BO_6 octahedra (O located at corners, B hidden in center)

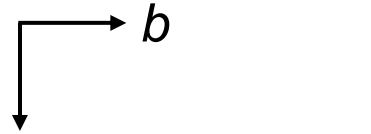

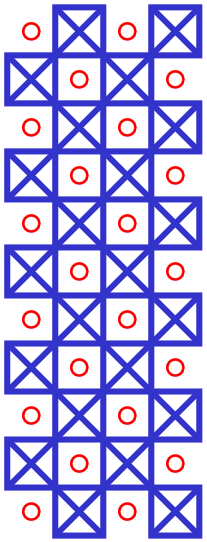

$n = \infty$

ABO_3 perovskite

Progress in Solid State Chemistry 29 (2001) 1 and 36 (2008) 253

Sketch of the perovskite-related structure of

$A_nB_nO_{3n+2} = ABO_x$

B = Ti, Nb, Ta

n = layer thickness
= number of BO_6 octahedra along c-axis per layer

☒ = BO_6 octahedra (O located at corners, B hidden in center)

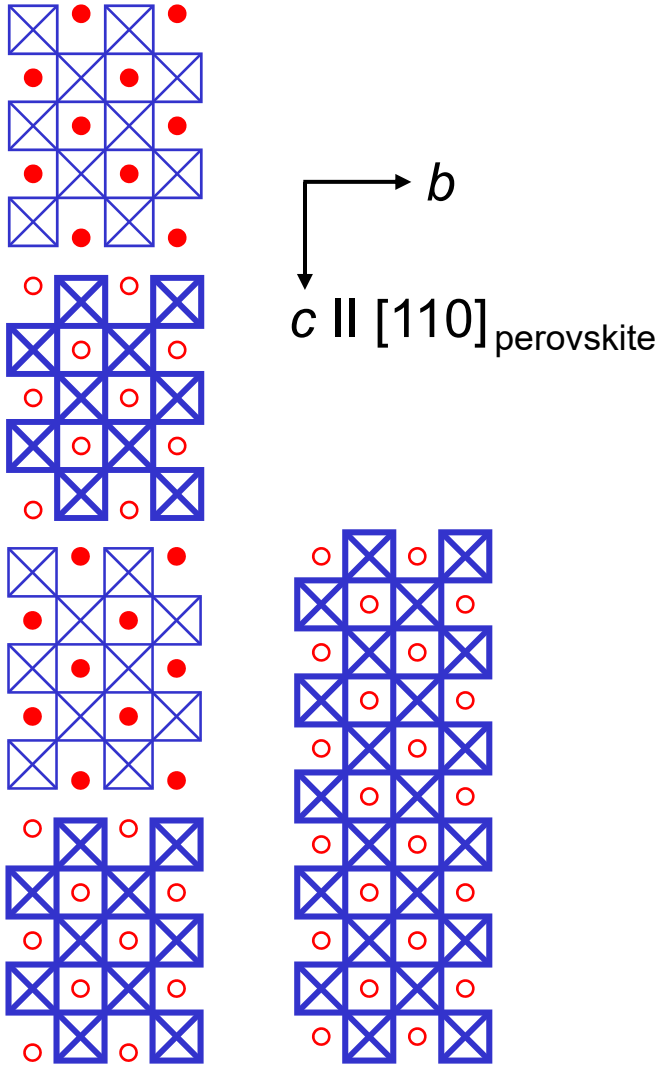

Progress in Solid State Chemistry 29 (2001) 1 and 36 (2008) 253

Sketch of the perovskite-related structure of

$A_nB_nO_{3n+2} = ABO_x$

B = Ti, Nb, Ta

n = layer thickness
= number of BO_6 octahedra along *c*-axis per layer

☒ = BO_6 octahedra (O located at corners, *B* hidden in center)

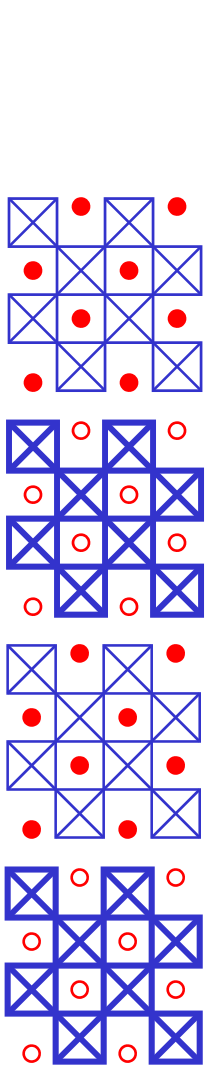

n = 4

$ABO_{3.50}$

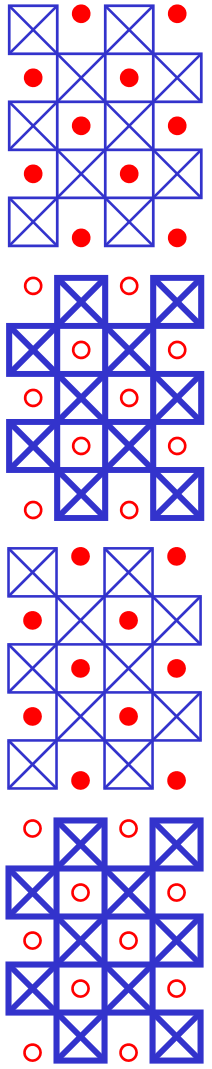

n = 5

$ABO_{3.40}$

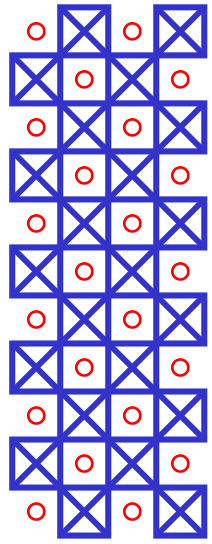

n = ∞

ABO_3 perovskite

Sketch of the perovskite-related structure of

$A_nB_nO_{3n+2} = ABO_x$

B = Ti, Nb, Ta

n = layer thickness
= number of BO_6 octahedra along *c*-axis per layer

Existence of non-integral series members such as *n* = 4.5 with an ordered stacking sequence of layers with different thickness

⊠ = BO_6 octahedra (O located at corners, *B* hidden in center)

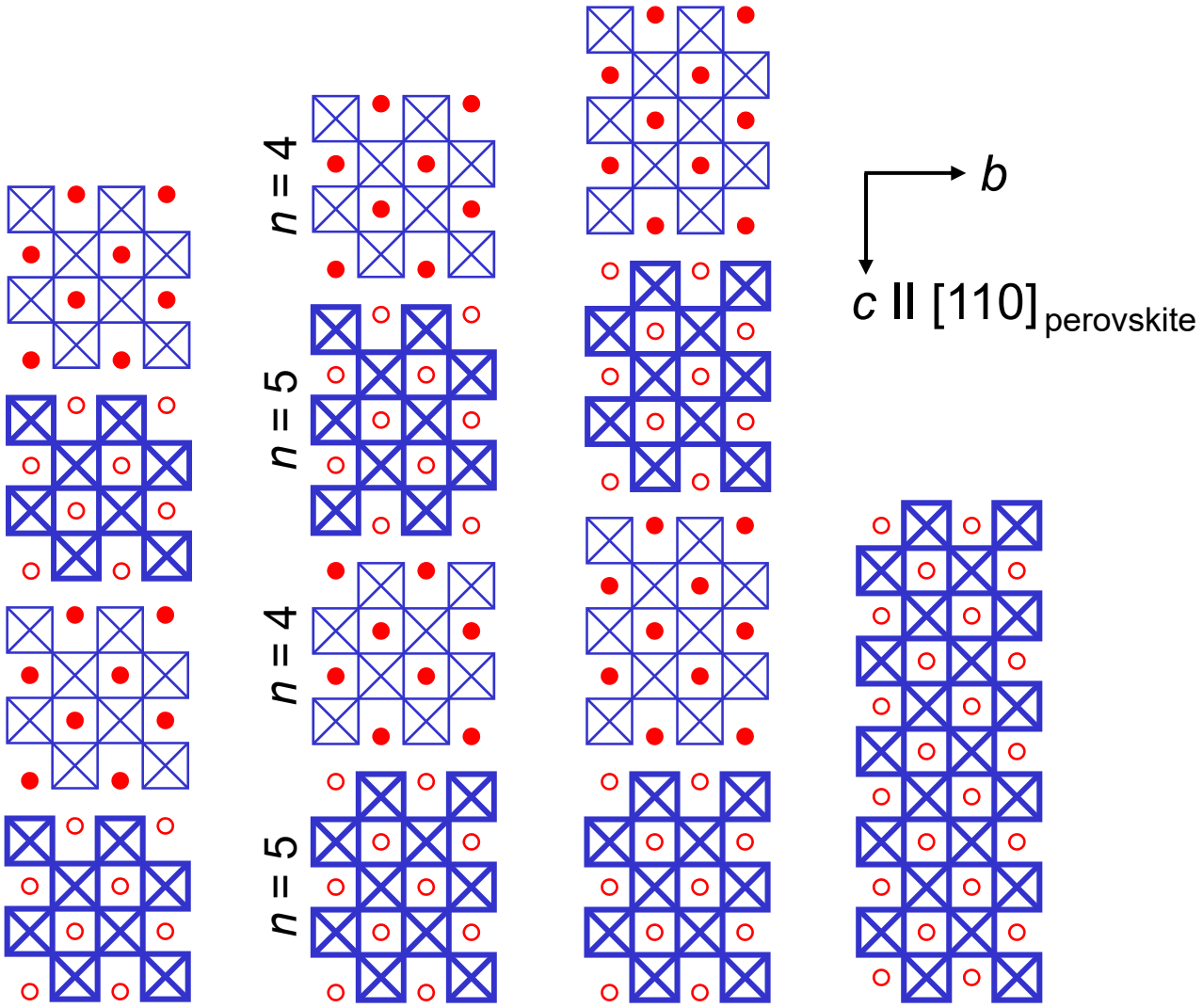

Progress in Solid State Chemistry 29 (2001) 1 and 36 (2008) 253

Sketch of the perovskite-related structure of

$A_nB_nO_{3n+2} = ABO_x$

B = Ti, Nb, Ta

n = layer thickness
= number of BO_6 octahedra along c-axis per layer

Existence of non-integral series members such as $n = 4.5$ with an ordered stacking sequence of layers with different thickness

⊠ = BO_6 octahedra (O located at corners, B hidden in center)

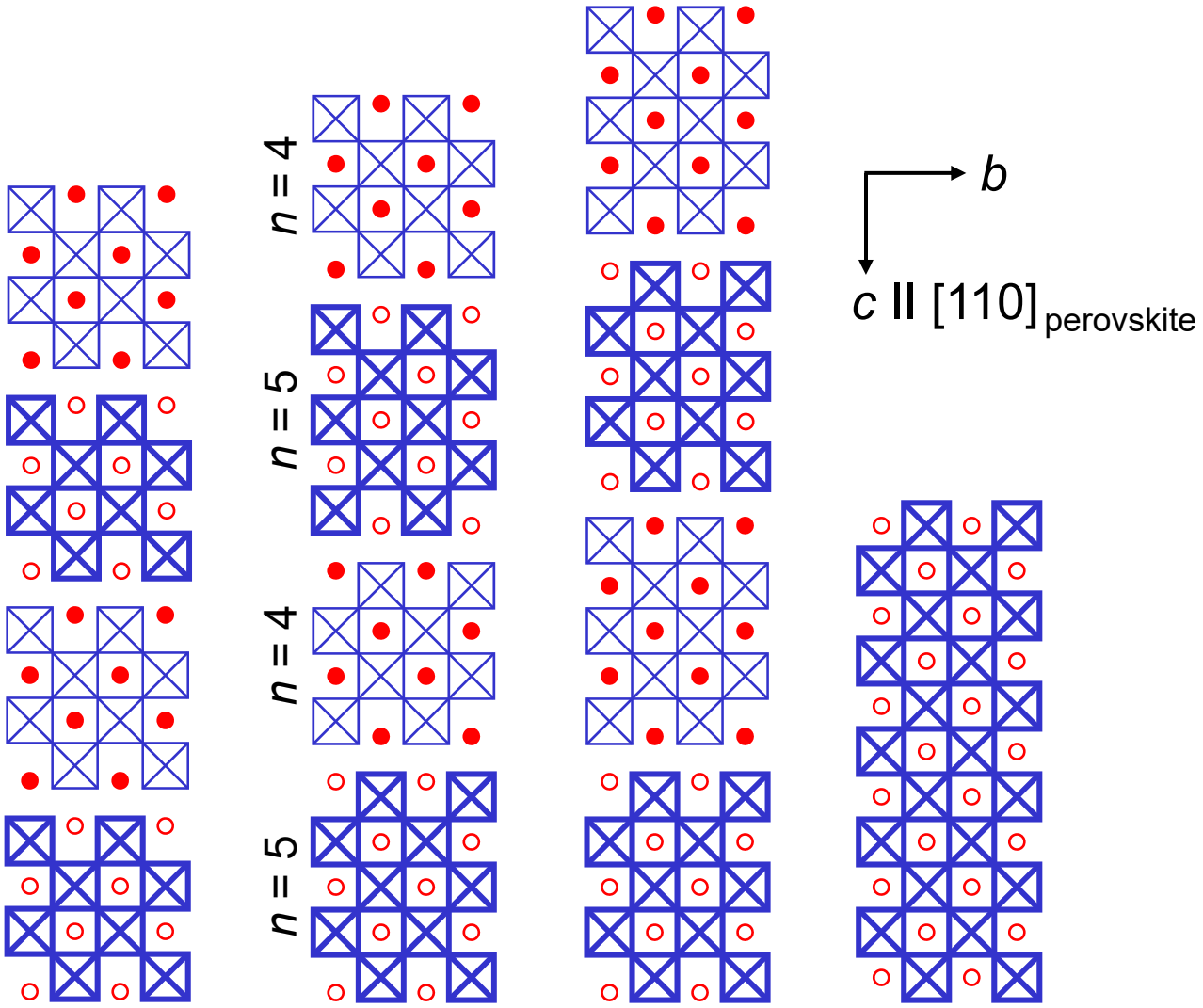

	$n = 4$	$n = 4.5$	$n = 5$	$n = \infty$
	$ABO_{3.50}$	$ABO_{3.44}$	$ABO_{3.40}$	ABO_3 perovskite
Compositional examples →	$SrNbO_{3.50}$	$SrNbO_{3.44}$	$SrNbO_{3.40}$	$SrNbO_3$
Physical properties →	ferroelectric	quasi-1D metals		metal

High-resolution transmission electron microscopy image from the n = 4.5 type quasi-1D metal $SrNbO_{3.45}$ ($c \approx 59$ Å)

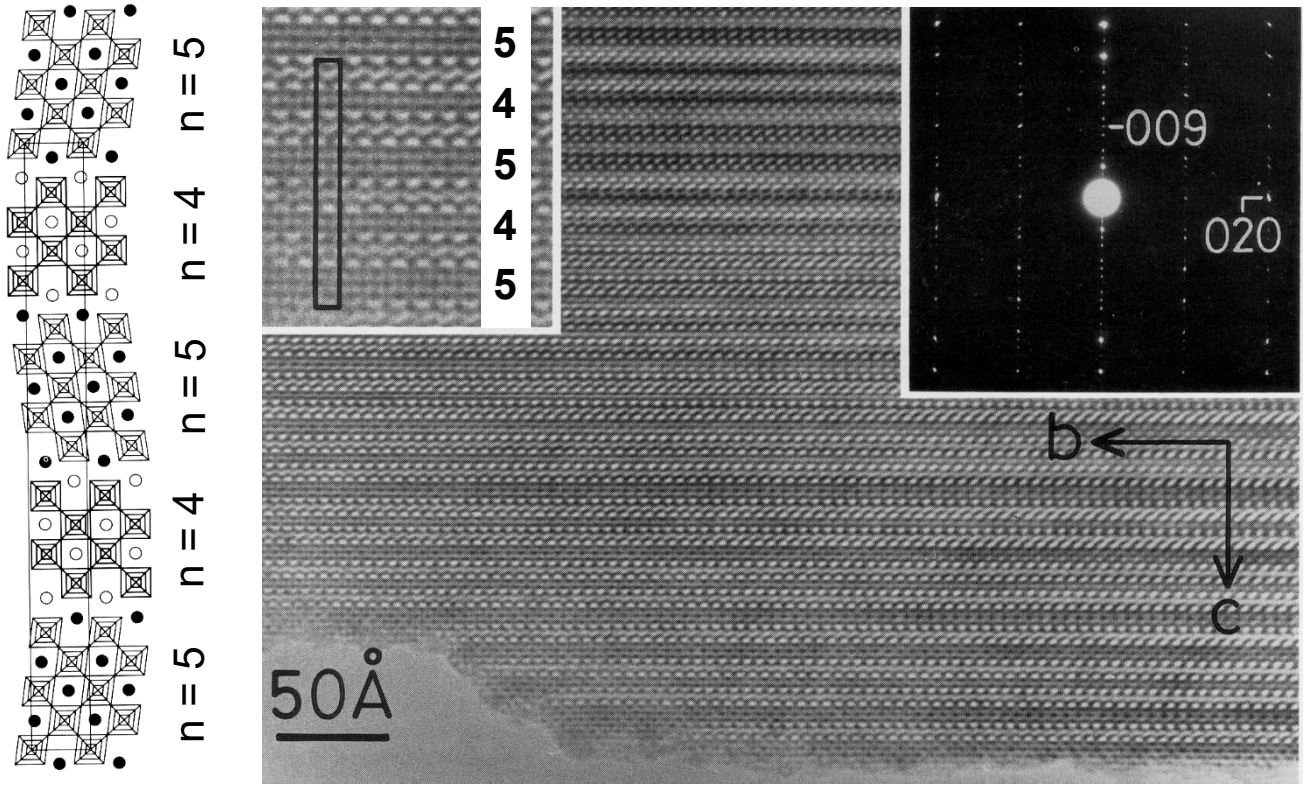

TEM image made by Tim Williams

T. Williams et al., Journal of Solid State Chemistry 103 (1993) 375 • F. Lichtenberg et al., Zeitschrift für Physik B Condensed Matter 84 (1991) 369 and Progress in Solid State Chemistry 29 (2001) 1 • D. H. Lu et al., Physica C 282 - 287 (1997) 995 • C. A. Kuntscher et al., Physical Review B 70 (2004) 245123 and B 61 (2000) 1876

BO_6 octahedra (O located at corners, *B* hidden in center) =

Sketch of the pronounced structural anisotropy of $A_nB_nO_{3n+2}$ = ABO_x by using *n* = 5 as example

Distortion of BO_6 octahedra in percent

Typical values for *n* = 5

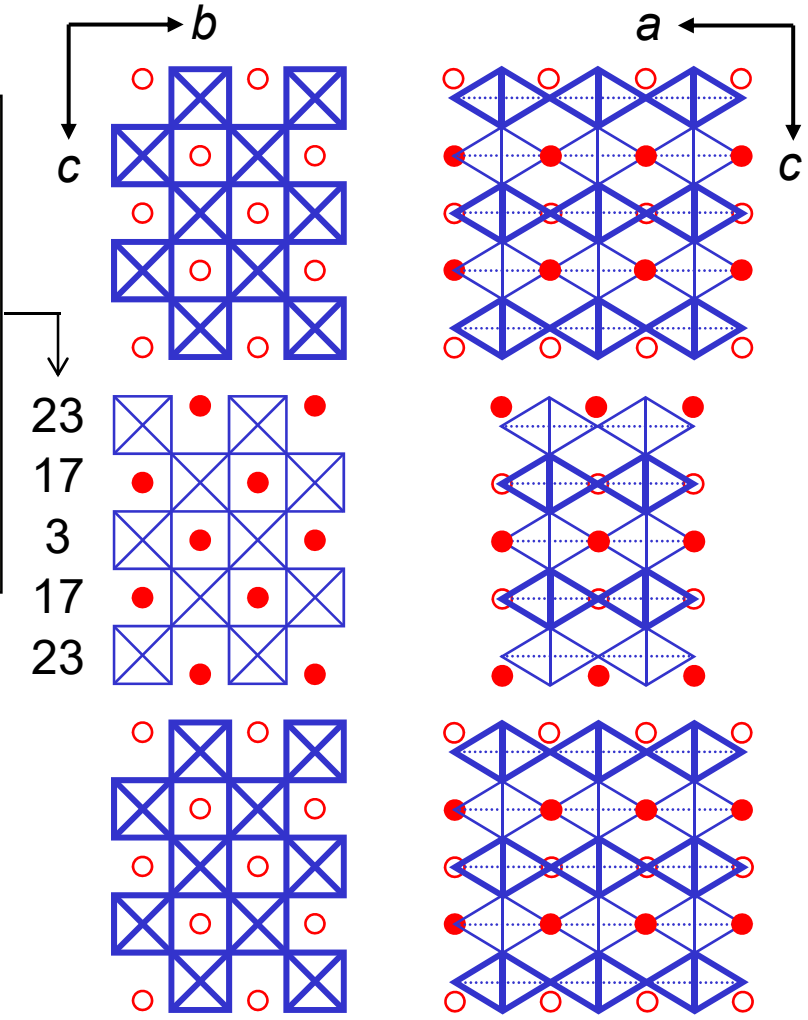

n = 5 type $A_5B_5O_{17}$ = $ABO_{3.4}$

B – O linkage:

- zig-zag along *b*-axis
- chains along *a*-axis
- interruptions along *c*-axis
  → layered crystal structure

Progress in Solid State Chemistry
29 (2001) 1 and 36 (2008) 253

☺ Another sketch of the n = 5 type structure of $A_nB_nO_{3n+2}$ ☺

Cake made by Silvana from miyuko.ch in December 2012

Vegan and 95 % organic

Thanks also to D. Grenzler from https://www.miyuko.ch

Atomic structure of a $SrNbO_{3.4}$ (n = 5) / $SrNbO_3$ (n = ∞) interface

Small amounts of $SrNbO_3$ in a melt-grown n = 5 type $SrNbO_x$ crystal which was studied by transmission electron microscopy (TEM)

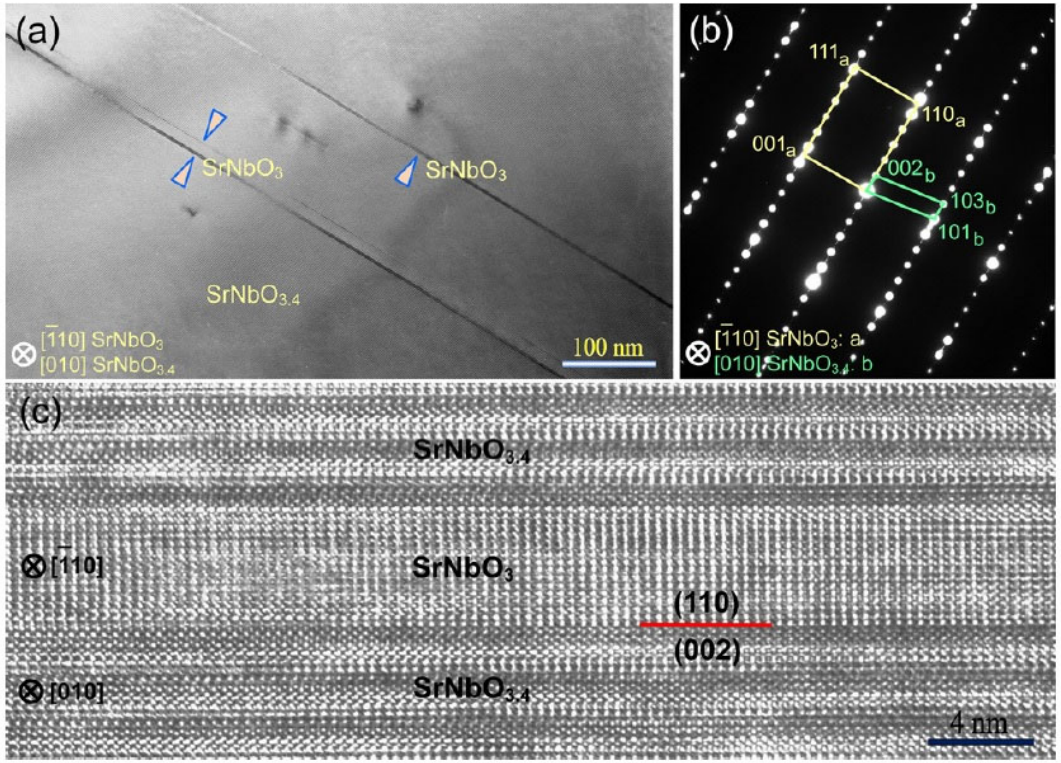

(a) Bright-field TEM image, (b) Selected area diffraction pattern, and (c) HRTEM image. The $SrNbO_{3.4}$ / $SrNbO_3$ interface is very flat without any misfit dislocations

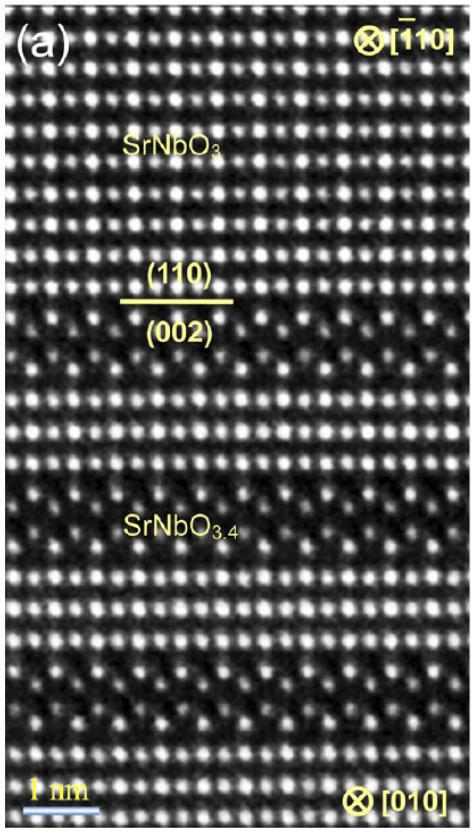

High angle annular dark field (HAADF) image of the interface region. The interface is coherent and atomically abrupt

Chunlin Chen, Shuhui Lv, Zhongchang Wang, Kazuto Akagi, Frank Lichtenberg, Yuichi Ikuhara, and Johannes Georg Bednorz
Applied Physics Letters 105 (2014) 221602 (1 - 5)

Sketch of the perovskite-related structure of

$A_nB_nO_{3n+2} = ABO_x$

= BO_6 octahedra (O located at corners, *B* hidden in center)

= BO_4 (O located at corners, *B* in the center)

b

c II [110]$_{perovskite}$

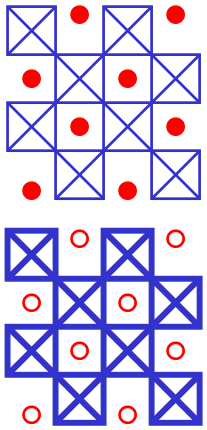

n = 4

$ABO_{3.5}$

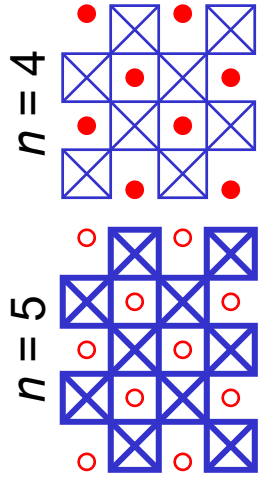

n = 4.5

$ABO_{3.44}$

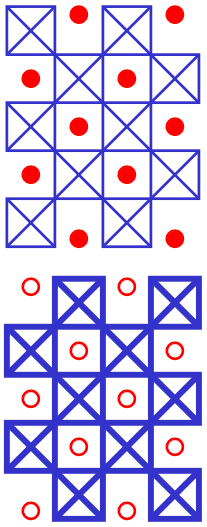

n = 5 (I)

$ABO_{3.4}$

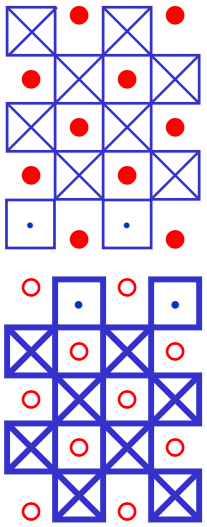

n = 5 (II)

$ABO_{3.2}$

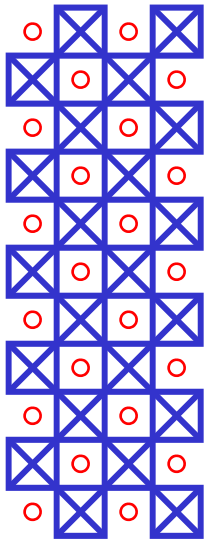

n = ∞

ABO_3

Progress in Solid State Chemistry 36 (2008) 253 and references therein, Zeitschrift für Anorganische und Allgemeine Chemie 528 (1985) 91 , and part 5.1 , 6.2 and 6.7 in this work

Sketch of the perovskite-related structure of

$A_nB_nO_{3n+2} = ABO_x$

⊠ = BO_6 octahedra (O located at corners, *B* hidden in center)

⊡ = BO_4 (O located at corners, *B* in the center)

Examples from the system $SrNbO_x$ with Nb^{5+} ($4d^0$) and / or Nb^{4+} ($4d^1$)

b

c II [110]$_{perovskite}$

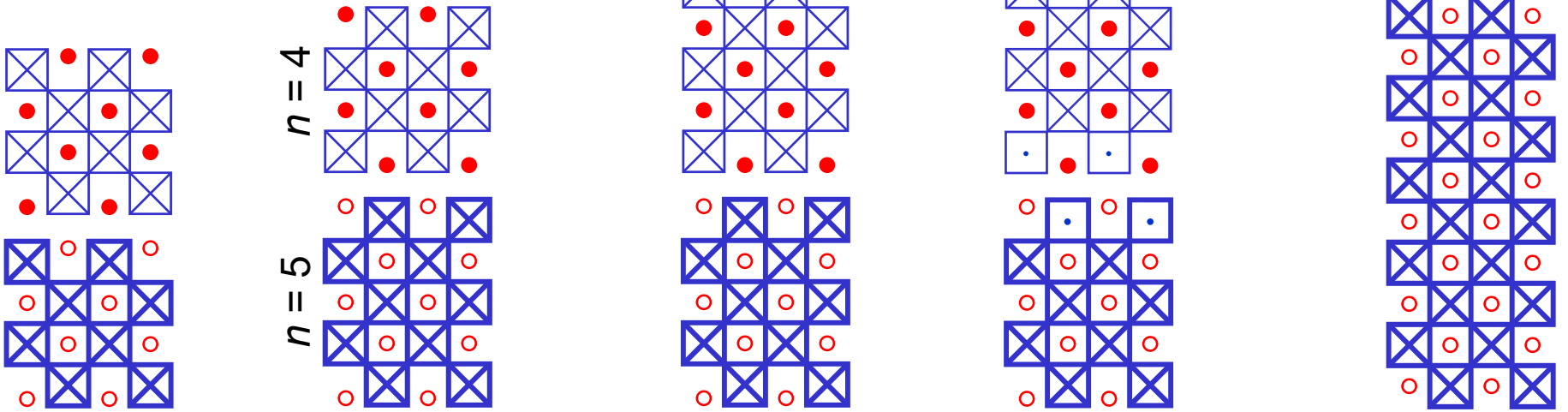

n = 4	*n* = 4.5	*n* = 5 (I)	*n* = 5 (II)	*n* = ∞
$ABO_{3.5}$	$ABO_{3.44}$	$ABO_{3.4}$	$ABO_{3.2}$	ABO_3
$SrNbO_{3.5}$	$SrNbO_{3.44}$	$SrNbO_{3.4}$	$SrNbO_{3.2}$	$SrNbO_3$
non-centrosym. ferroelectric	centrosymmetric quasi-1D metals		non-centrosym. quasi-1D metal ?	centrosym. metal

Progress in Solid State Chemistry 36 (2008) 253 and references therein, Zeitschrift für Anorganische und Allgemeine Chemie 528 (1985) 91 , and part 5.1 , 6.2 and 6.7 in this work

Sketch of the perovskite-related structure of

$A_nB_nO_{3n+2} = ABO_x$

☒ = BO_6 octahedra (O located at corners, *B* hidden in center)

b

c II [110]$_{perovskite}$

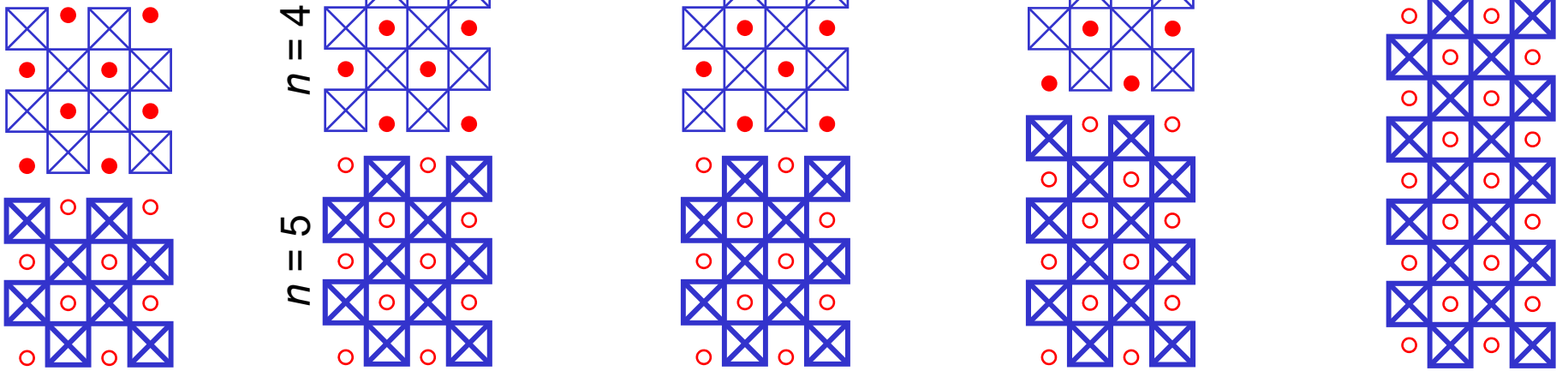

n = 4 $ABO_{3.5}$

n = 4.5 $ABO_{3.44}$

n = 5 $ABO_{3.4}$

n = 6 $ABO_{3.33}$

n = ∞ ABO_3

Progress in Solid State Chemistry 36 (2008) 253 and references therein

Sketch of the perovskite-related structure of
$A_nB_nO_{3n+2}$ = ABO_x

⊠ = BO_6 octahedra (O located at corners, *B* hidden in center)

Examples from the system $Sr(Nb,Ti)O_x$ with Nb^{5+} ($4d^0$) and Ti^{4+} ($3d^0$)

b

c II [110]$_{perovskite}$

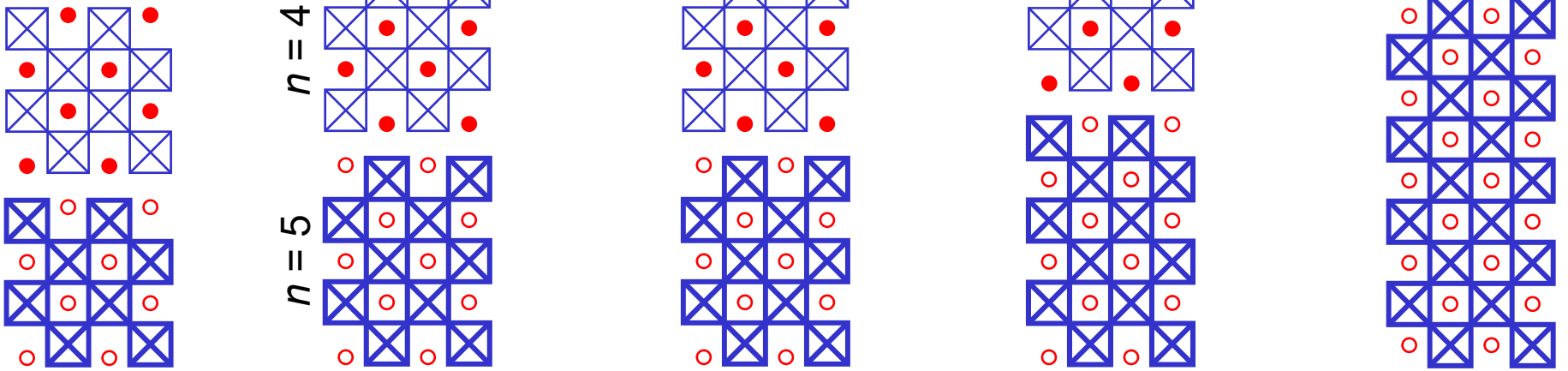

n = 4	*n* = 4.5	*n* = 5	*n* = 6	*n* = ∞
$ABO_{3.5}$	$ABO_{3.44}$	$ABO_{3.4}$	$ABO_{3.33}$	ABO_3
$SrNbO_{3.5}$	$SrNb_{0.89}Ti_{0.11}O_{3.44}$	$SrNb_{0.8}Ti_{0.2}O_{3.4}$	$SrNb_{0.67}Ti_{0.33}O_{3.33}$	$SrTiO_3$
non-centrosym. ferroelectric	centrosymmetric insulator	centrosymmetric antiferroelectric	non-centrosym. ferroelectric	centrosym. insulator

Progress in Solid State Chemistry 36 (2008) 253 and references therein

Sketch of the perovskite-related structure of

$A_nB_nO_{3n+2}$ = ABO_x

⊠ = BO_6 octahedra (O located at corners, *B* hidden in center)

b

c II [110]$_{perovskite}$

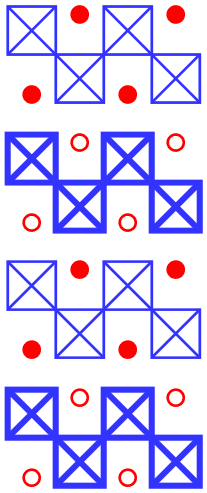

n = 2

ABO_4

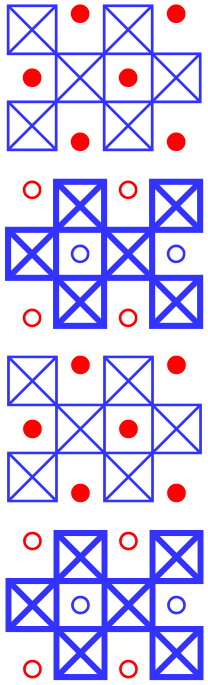

n = 3 (I)

$ABO_{3.67}$

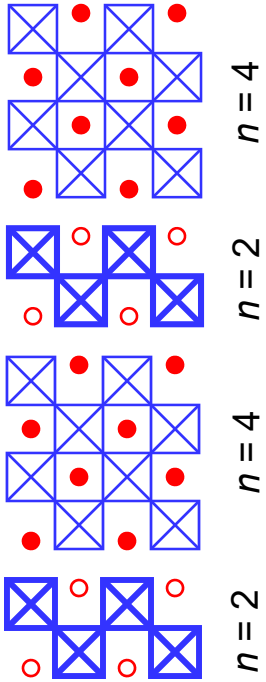

n = 3 (II)

$ABO_{3.67}$

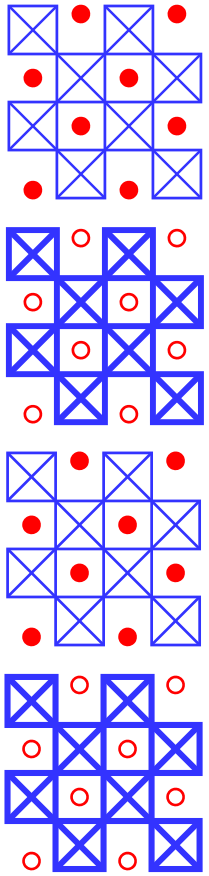

n = 4

$ABO_{3.5}$

Progress in Solid State Chemistry 36 (2008) 253 and references therein

Sketch of the perovskite-related structure of $A_nB_nO_{3n+2} = ABO_x$

⊠ = BO_6 octahedra (O located at corners, *B* hidden in center)

Examples from the system (La,Sr)(Ta,Ti)O_x with Ta^{5+} ($5d^0$) and Ti^{4+} ($3d^0$)

b

c II [110]$_{perovskite}$

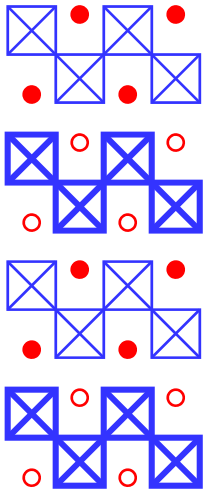

n = 2

ABO_4

$LaTaO_4$

non-centrosymmetric

potentially ferroelectric

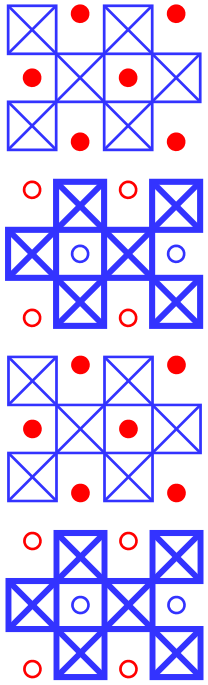

n = 3 (I)

$ABO_{3.67}$

$Sr_{0.67}La_{0.33}TaO_{3.67}$

centrosymmetric

insulator

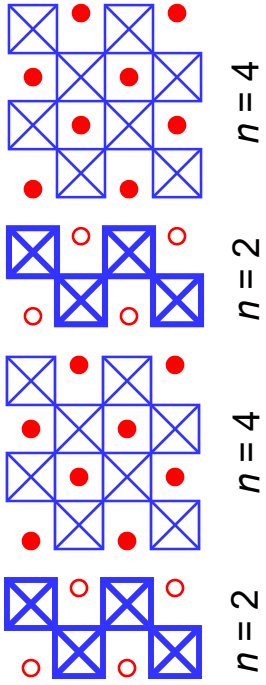

n = 3 (II)

$ABO_{3.67}$

$LaTi_{0.67}Ta_{0.33}O_{3.67}$

non-centrosym.

potentially ferroelectric

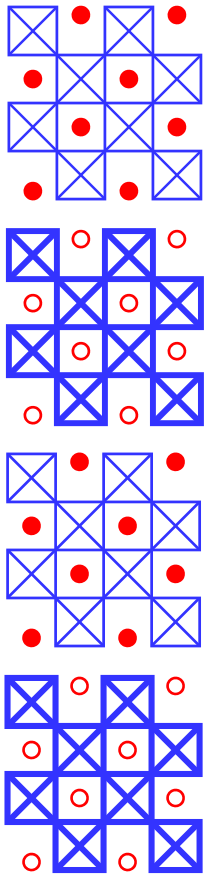

n = 4

$ABO_{3.5}$

$LaTiO_{3.5}$

non-centrosym.

ferroelectric

Progress in Solid State Chemistry 36 (2008) 253 and references therein

Approximate lattice parameters of oxides of the type $A_nB_nO_{3n+2} = ABO_x$

Lattice parameters		Structure type *n*
a (Å)	~ 3.9 or ~ 2 × 3.9 = 7.8	all *n*
b (Å)	~ 5.5	all *n*
c (Å)	~ 44	*n* = 7
	~ 19 or ~ 2 × 19 = 38	*n* = 6
	~ 31	*n* = 5
	~ 58	*n* = 4.5
	~ 83	*n* = 4.33
	~ 13 or ~ 2 × 13 = 26	*n* = 4
	~ 20	*n* = 3
	~ 7.5 or ~ 2 × 7.5 = 15	*n* = 2
β (°)	90 (orthorhombic) or ~ 96 (monoclinic)	all *n*

Progress in Solid State Chemistry 29 (2001) 1 and 36 (2008) 253 and references therein

Powder x-ray diffraction pattern at low angles of some melt-grown materials of the type $A_nB_nO_{3n+2} = ABO_x$

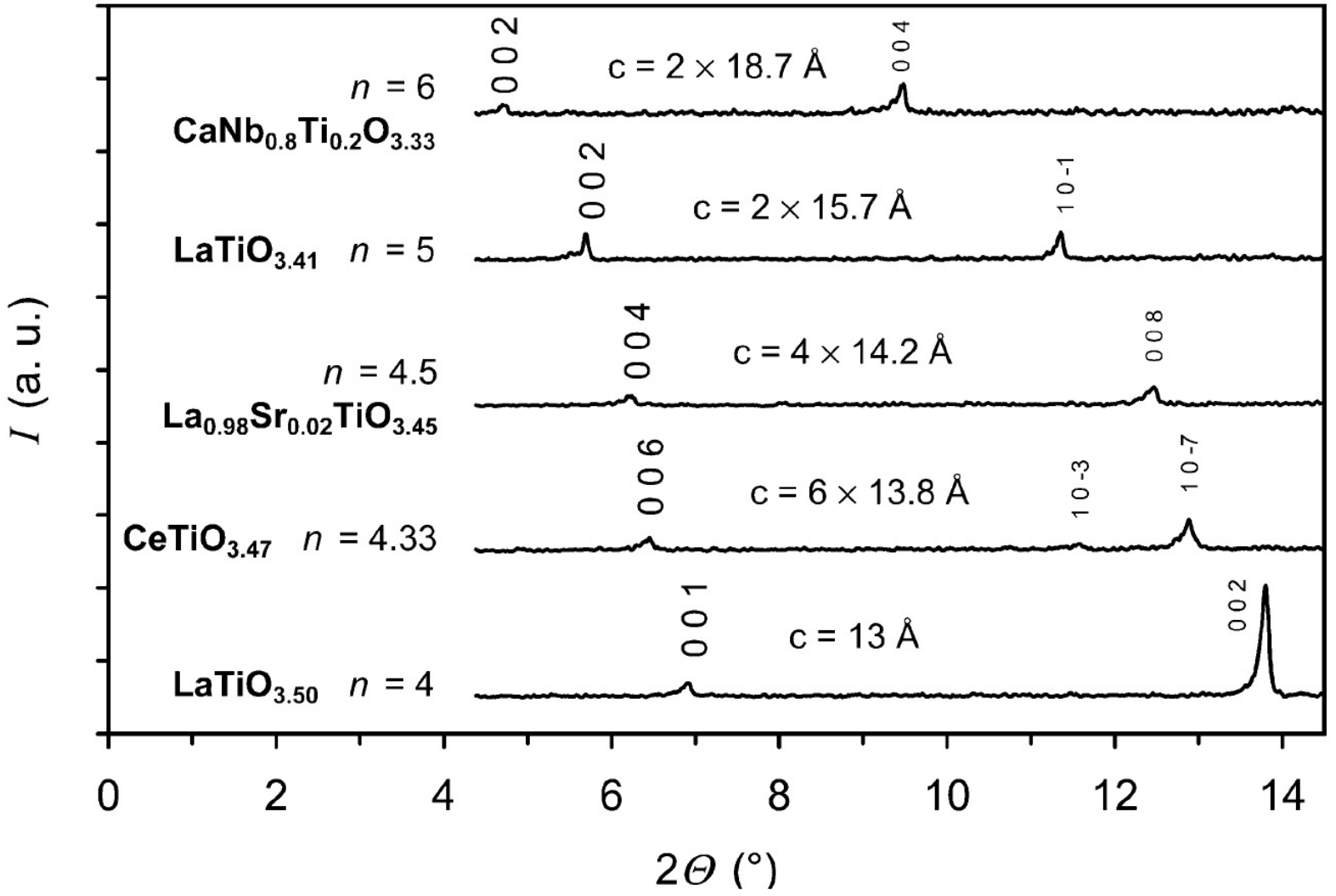

The low angle peak indicates the structure type *n*

Progress in Solid State Chemistry 29 (2001) 1

3 How the name Carpy-Galy phases for oxides of the type $A_nB_nO_{3n+2} = ABO_x$ comes about ...

A name for the oxides of the type $A_nB_nO_{3n+2}$ = ABO_x: Carpy-Galy phases

To the best of our knowledge the first publications about oxides of the type $A_nB_nO_{3n+2}$ were published by Alain Carpy et al. in 1972 and 1973 for $Ca_2Nb_2O_7$ and compounds in the system $Ca_2Nb_2O_7$ - $NaNbO_3$:

Alain Carpy, Pierre Amestoy, and Jean Galy

Contribution a l'etude du pyroniobate de calcium $Ca_2Nb_2O_7$ Paper in French

Comptes Rendus des Seances de L'Academie des Sciences, Paris, Serie C, 275 (14) (1972) 833 - 835

Alain Carpy, Pierre Amestoy, and Jean Galy

Systeme $Ca_2Nb_2O_7$ - $NaNbO_3$: synthèse et etude radiocristallographique de membres de la serie $A_nB_nX_{3n+2}$ (n =4, 5, 6) Paper in French

Comptes Rendus des Seances de L'Academie des Sciences, Paris, Serie C, 277 (1) (1973) 501 - 506

Many compounds and publications are presented and cited in
V. A. Isupov , Ferroelectrics 220 (1999) 79 - 103 https://doi.org/10.1080/00150199908007997
F. Lichtenberg et al. , Progress in Solid State Chemistry 29 (2001) 1 - 70 and 36 (2008) 253 - 387
https://dx.doi.org/10.1016/S0079-6786%2801%2900002-4 & https://dx.doi.org/10.1016/j.progsolidstchem.2008.10.001

In 2019 Maribel Nunez Valdez and Nicola A. Spaldin introduced in their following paper for the oxides of the type $A_nB_nO_{3n+2}$ the name Carpy-Galy phases:

Origin and evolution of ferroelectricity in the layered rare-earth titanate, $R_2Ti_2O_7$, Carpy-Galy phases

Polyhedron 171 (2019) 181 - 192 , https://doi.org/10.1016/j.poly.2019.07.018

4 Melt-grown synthesis of oxides and study of their properties by powder x-ray diffraction, thermogravimetry, and a SQUID magnetometer ...

Experimental details are presented in the following publications:

Progress in Solid State Chemistry 29 (2001) 1 - 70
https://dx.doi.org/10.1016/S0079-6786%2801%2900002-4

Progress in Solid State Chemistry 36 (2008) 253 - 387
https://dx.doi.org/10.1016/j.progsolidstchem.2008.10.001

Presentation of a lab for the synthesis and study of melt-grown oxides, published by the library of the ETH Zurich / ETH Research Collection in 2017 (438 pages):
https://dx.doi.org/10.3929/ethz-a-010817148

Experimental details and used equipment at the ETH Zurich like

- an analytical balance Mettler Toledo MS 204 for weighing powders
- special mortars and pestles for the mingling of powders
- custom-made pressing dies made of magnesia-stabilized zirconia or quartz glass for the preparation of polycrystalline sintered rods for floating zone melting in a mirror furnace
- a laboratory chamber furnace Linn High Therm VMK 1600
- a GERO tube furnace
- Cyberstar mirror furnace
- custom-made sample holders made of yttria-stabilized zirconia and custom-made screws made of Pt-Rh for the fixation and centering of polycrystalline sintered rods at the lower and upper shaft of the mirror furnace
- an oxygen analyzer ZIROX SGM7 to measure the oxygen content of argon at the gas outlet of the GERO tube furnace and the Cyberstar mirror furnace
- a thermogravimetric analyzer NETZSCH TG 209 F1 Libra and how to determine the oxygen content of oxides by thermogravimetry
- the mechanical fixation of a sample within a straw by pieces of another straw for magnetic measurements in a SQUID magnetometer
- the measurement of the magnetic moment M(T) or M(H) of a sample by a Quantum Design SQUID magnetometer MPMS3

are presented in https://dx.doi.org/10.3929/ethz-a-010817148

Examples of furnaces

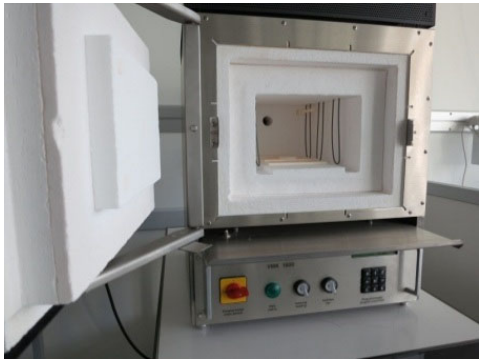

Non-gas-tight laboratory chamber furnace

For removing moisture of starting materials, pre-reactions, calcination, sintering or synthesis of polycrystalline materials in air

Gas-tight tube furnace

For preparation or sintering of polycrystalline materials under various non-air atmospheres such as oxygen, argon, argon plus hydrogen, or vacuum

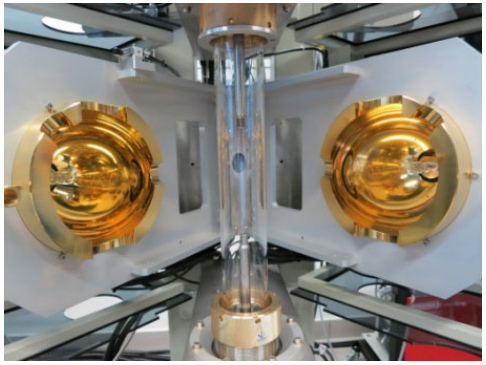

Gas-tight mirror furnace / floating zone melting furnace

For synthesis of crystalline oxides via a solidification from the melt under various atmospheres like oxygen, air, argon, argon plus hydrogen or vacuum

https://dx.doi.org/10.3929/ethz-a-010817148

Sketch of the sample preparation

1) ☺ It starts always with an idea about a known, new or apriori hypothetical oxide material, i.e. devise a chemical composition such as $La_6Ti_4Fe_2O_{20}$ or $Sr_5Nb_5O_{17}$

2) Select appropriate starting materials from commercially available powders such as oxides La_2O_3 , TiO_2 , Fe_2O_3 or Nb_2O_5 , carbonates like $CaCO_3$, and / or metals such as Nb

3) Calculate the amounts (mass, weight) of the selected starting materials according to the devised or desired chemical composition

4) Weighing the calculated amounts of the starting materials by a spatula, weighing paper, and an analytical balance

5) Mingle the weighed starting materials by a mortar and pestle. If steps 6 - 8 are omitted, then a part of the as-mingled startimg materials is pressed into two rods and it is continued with step 9

6) Pre-reaction in air: Heat the mingled starting materials in a laboratory chamber furnace to elevated temperatures

Sketch of the sample preparation

7) Grind the pre-reacted starting materials into powder and mingle it by a mortar and pestle – in some cases another starting material is added to the pre-reacted starting materials

8) Press a part of the powder obtained in step 7 into two rods

9) Sinter the as-pressed rods at elevated temperatures under an appropriate atmosphere such as under air in a laboratory chamber furnace or under argon in a tube furnace or molybdenum furnace

10) Try to synthesize the devised or desired oxide material in a crystalline form via a solidification from the melt by processing the sintered rods by floating zone melting in a mirror furnace under an appropriate atmosphere such as air or argon. In some cases reduced mixed-valence titanates or niobates can be prepared by processing sintered rods with a fully oxidized composition by floating zone melting under argon plus hydrogen

Examples of commercially available starting materials

Fe_2O_3 powder

WO_3 powder

$SrCO_3$ powder

Nd_2O_3 powder

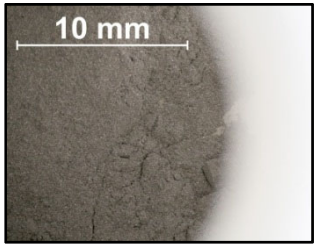

Nb powder

Storage of starting materials in an alumina crucible in a desiccator

Mn_2O_3 powder in this example

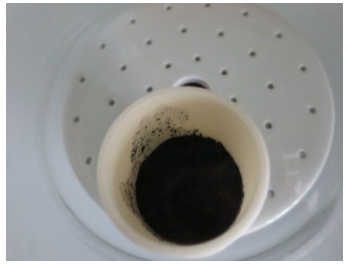

https://dx.doi.org/10.3929/ethz-a-010817148

Preparation and handling of powder mixtures

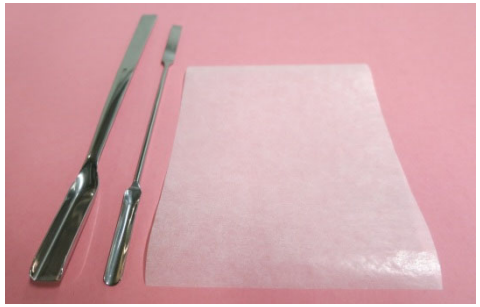

Spatula and weighing paper

Analytical balance

Mingle the starting materials by a pestle in a mortar

Alumina crucible filled with powder

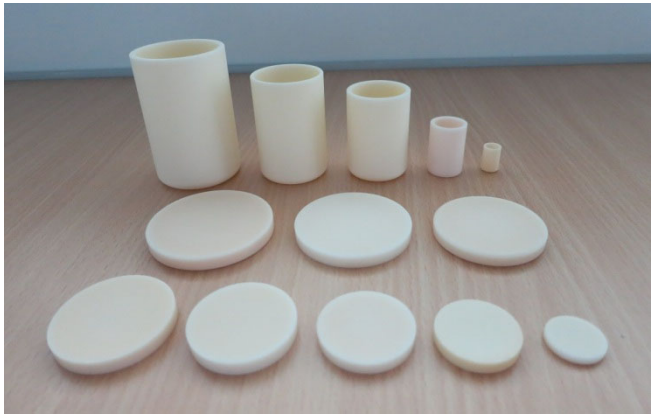

High temperature ceramics: Various types of crucibles and discs / lids made of alumina

High temperature ceramics: Various types of boats and boxes made of alumina

https://dx.doi.org/10.3929/ethz-a-010817148

Pressing dies for the preparation of rods for the mirror furnace

Custom-made pressing dies made of technical ceramics

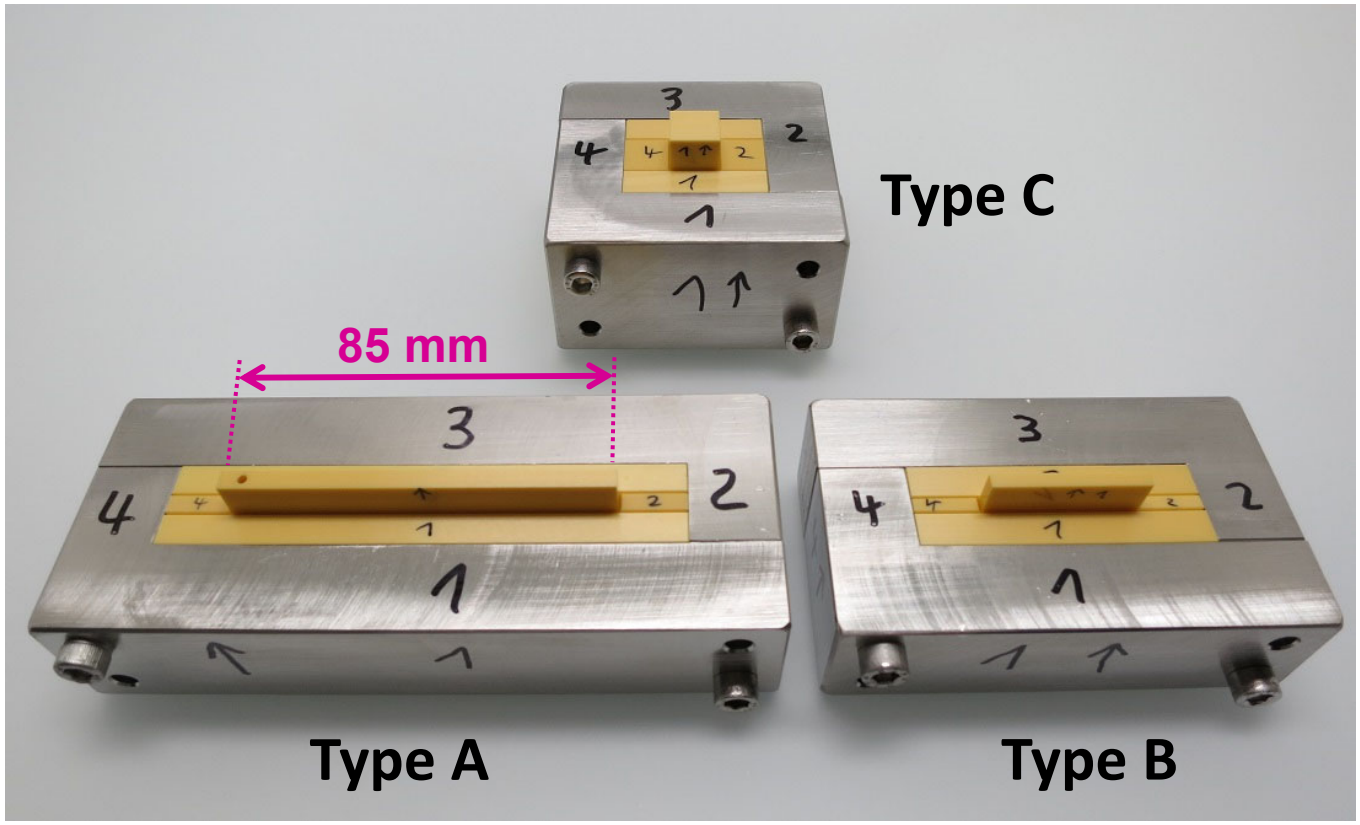

Type C with square punch for other samples

Type B with rectangular punch for seed rods with length 35 mm and width 3,5 mm

Type A with rectangular punch for feed rods with length 85 mm and width 4,5 mm

Yellow parts made of magnesia stabilized zirconia (FRIATEC FRIALIT FZM) by FRIATEC AG (Germany), purchased and delivered from stone-ware gmbh (Switzerland)

https://dx.doi.org/10.3929/ethz-a-010817148

Metal frames made in the metal workshop of the Department of Materials of the ETH Zurich by C. Roth and M. Elsener

Several types of lower punches on which the powder is pressed

Lower punches for the pressing die type A (feed rod), type B (seed rod) and type C

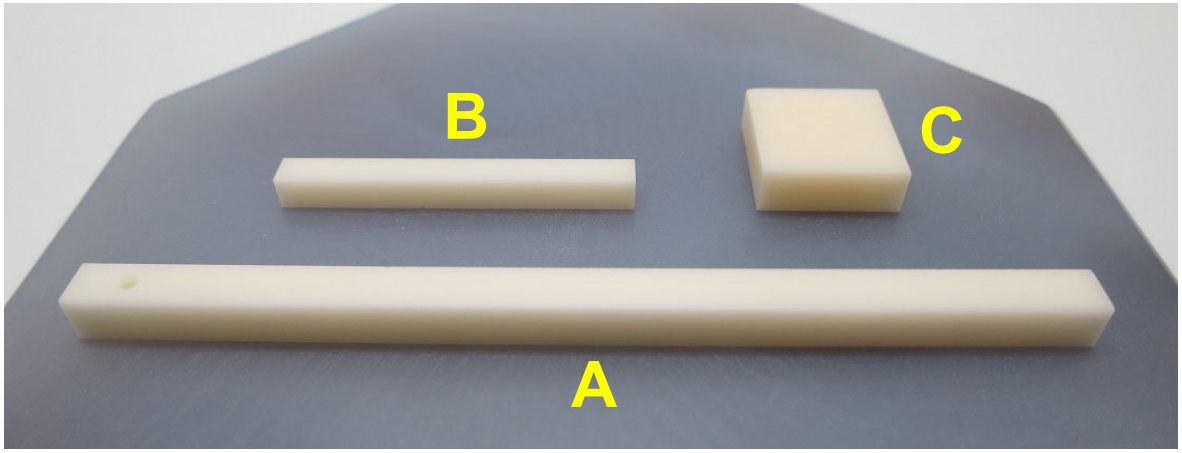

Lower punches
made of alumina
(FRIATEC FRIALIT F 99,7)
- usable up to 1950 °C

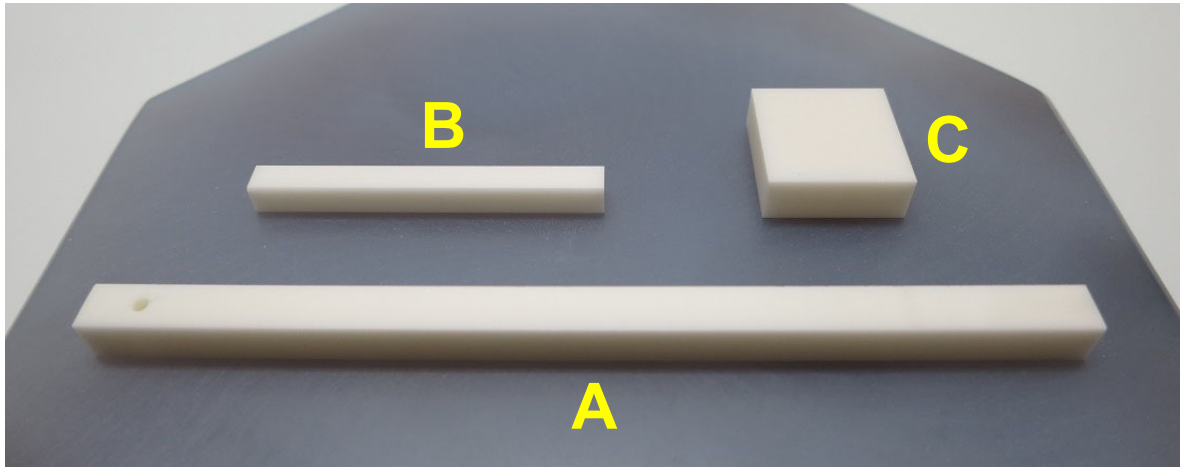

Lower punches made of
yttria stabilized zirconia
(FRIATEC DEGUSSIT FZY)
- usable up to 1500 °C

Made by FRIATEC AG (Germany), purchased and
delivered from stone-ware gmbh (Switzerland)

https://dx.doi.org/10.3929/ethz-a-010817148

Example of an as-pressed feed rod for the mirror furnace

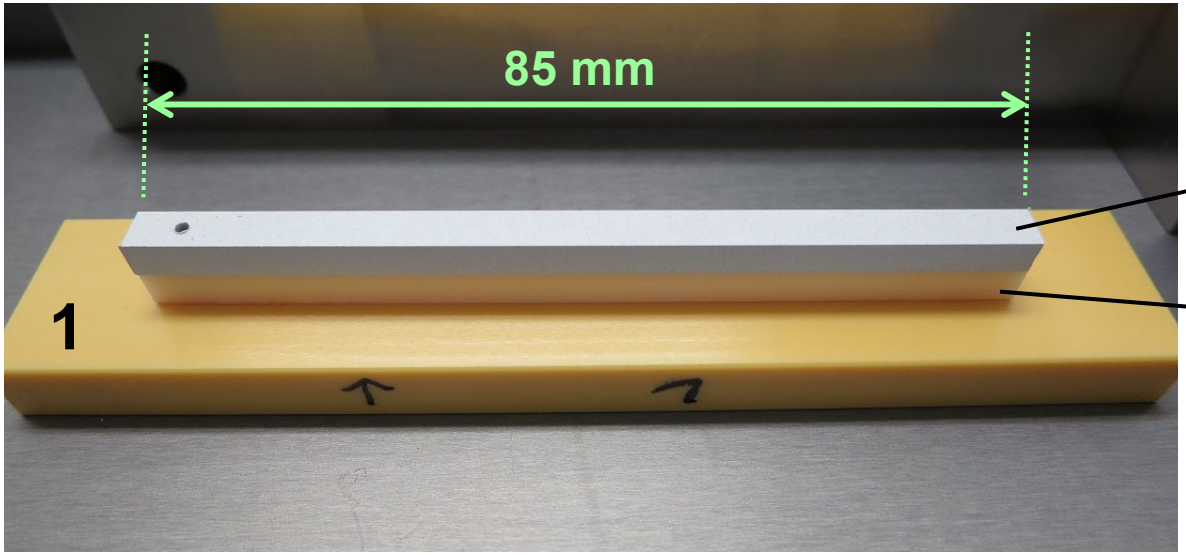

3 Rectangular rod with a continuous hole - made of pressed powder
Chemical composition of the pressed powder in this example: 0,6 Nb + 0,2 Nb_2O_5

2 Lower punch - made of alumina (FRIATEC FRIALIT F 99,7)

1 Base plate - made of magnesia stabilized zirconia (FRIATEC FRIALIT FZM)

The powder was pressed with a pressing force of 1 kN. The as-pressed rod is mechanically not stable. If it is touched in a not very careful way, then it becomes damaged or destroyed. However, the rod is needed in a mechanically stable form. Therefore the lower punch and the pressed rod will be placed into an alumina box and heated to an appropriate high temperature under a suitable atmosphere which results in sintering and chemical solid state reactions

https://dx.doi.org/10.3929/ethz-a-010817148

Feed rod and seed rod for the mirror furnace before and after sintering

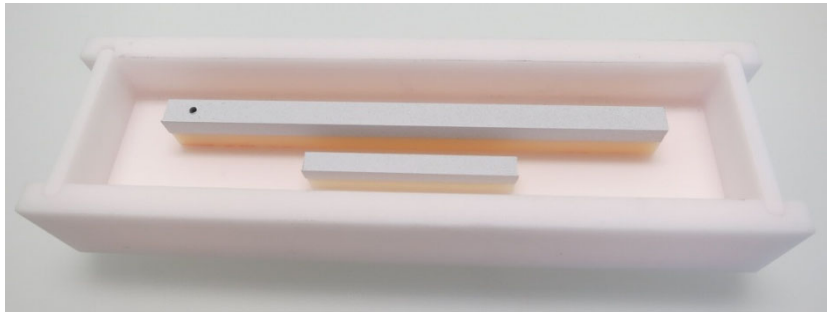

Pressed rods on their lower alumina punch in an alumina box before sintering

Chemical composition of the powder in this example: 0,6 Nb + 0,2 Nb_2O_5

Pressed rods on their lower alumina punch in an alumina box after sintering them for 1 h at 1150 °C under argon

The color change of the rods from white-grey to black is due to chemical solid state reactions like 0,6 Nb + 0,2 Nb_2O_5 → NbO

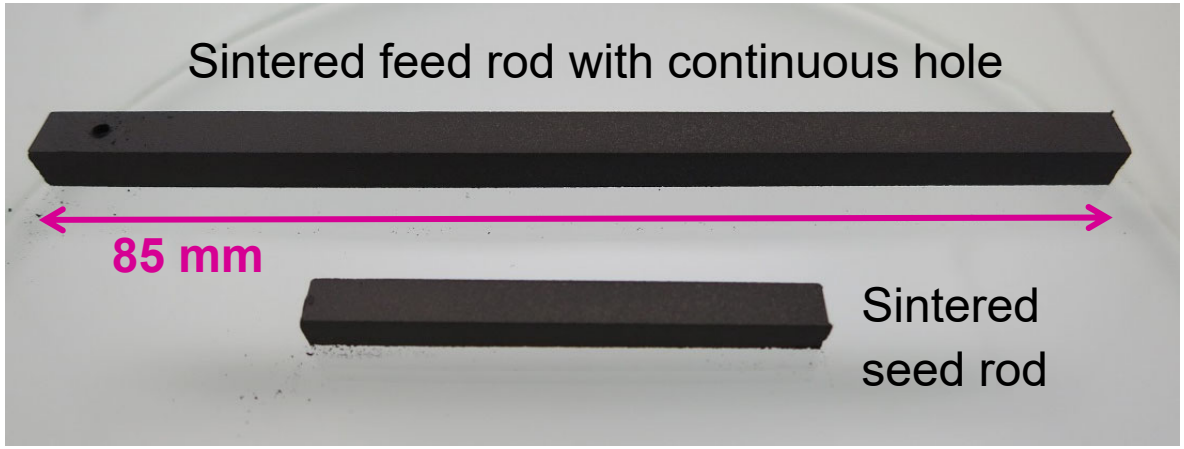

https://dx.doi.org/10.3929/ethz-a-010817148

Another pressing dies for the preparation of rods for the mirror furnace

Custom-made pressing dies made of glass

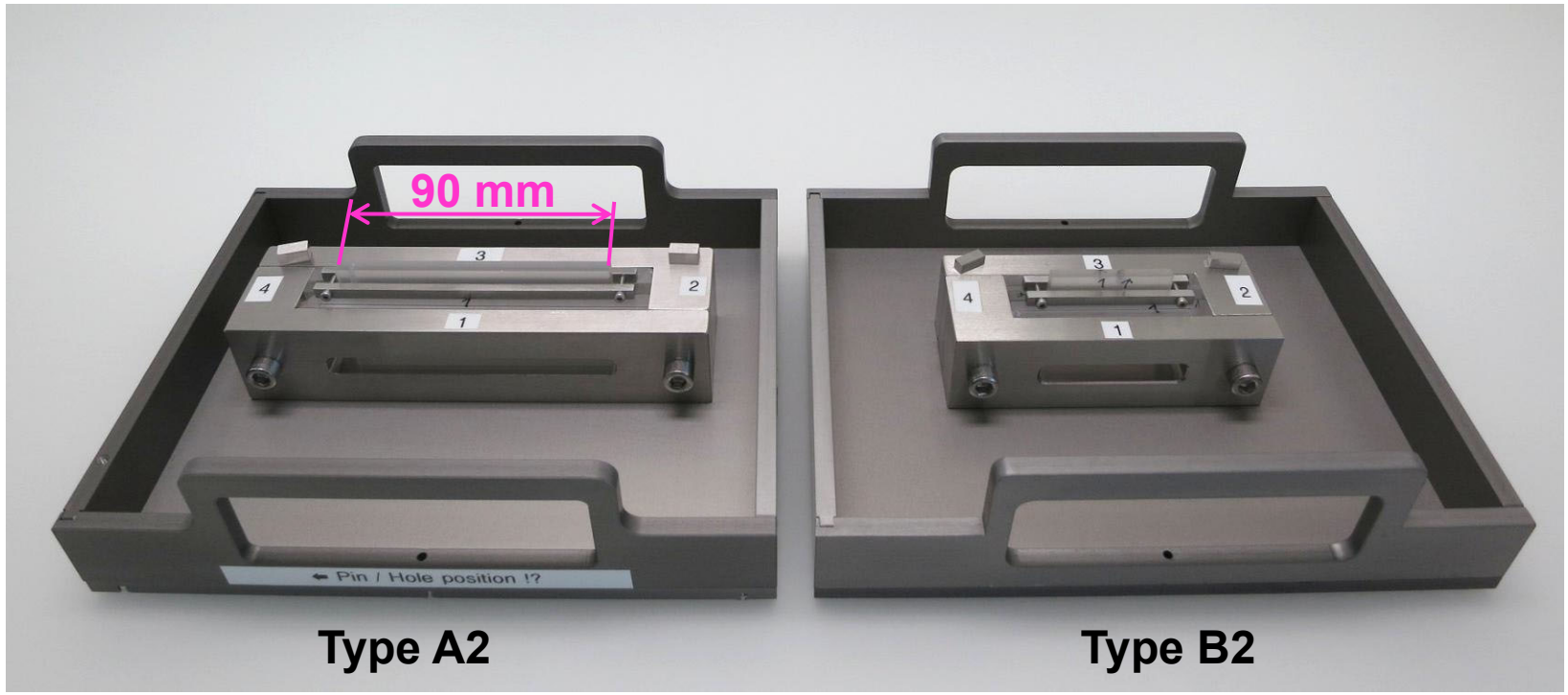

Type A2 with rectangular punch for feed rods with length 90 mm and width 5 mm

Type B2 with rectangular punch for seed rods with length 40 mm and width 4 mm

Glass parts purchased and delivered from EMATAG AG (Switzerland)

Metal frames, trays and other metal parts made in the metal workshop of the Department of Materials of the ETH Zurich by C. Roth and M. Elsener

https://dx.doi.org/10.3929/ethz-a-010817148

Example of an as-pressed feed rod for the mirror furnace

An as-pressed rod inside the pressing die when the metal frame is removed. The applied pressing force was 1 kN

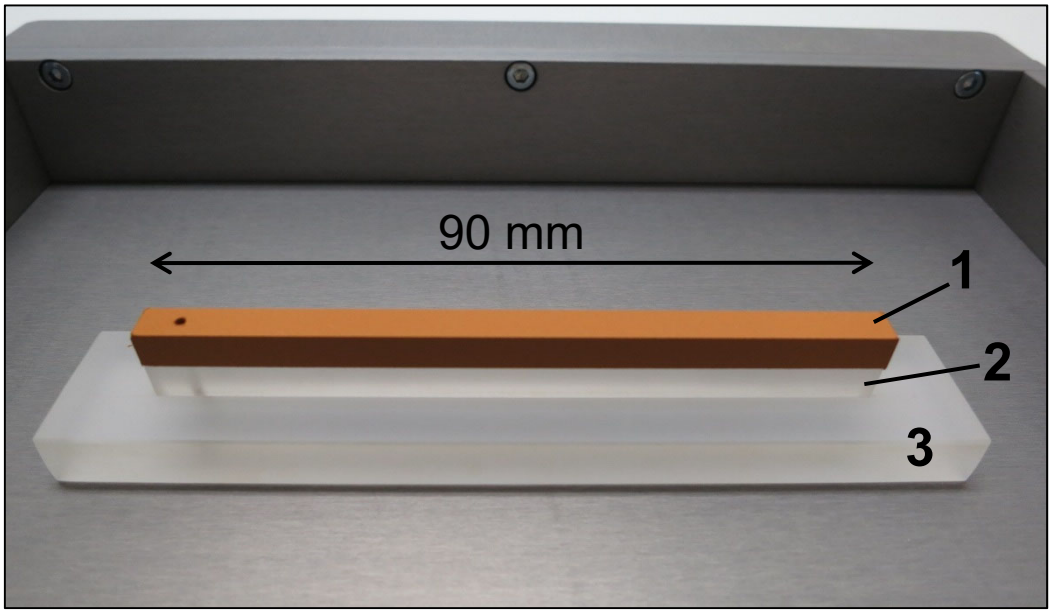

View when the side panels are removed:

As-pressed rod (1) on a lower punch (2) which is made of sapphire. The lower punch (2) is located on the base plate (3) which is made of quartz glass

https://dx.doi.org/10.3929/ethz-a-010817148

Cyberstar mirror furnace

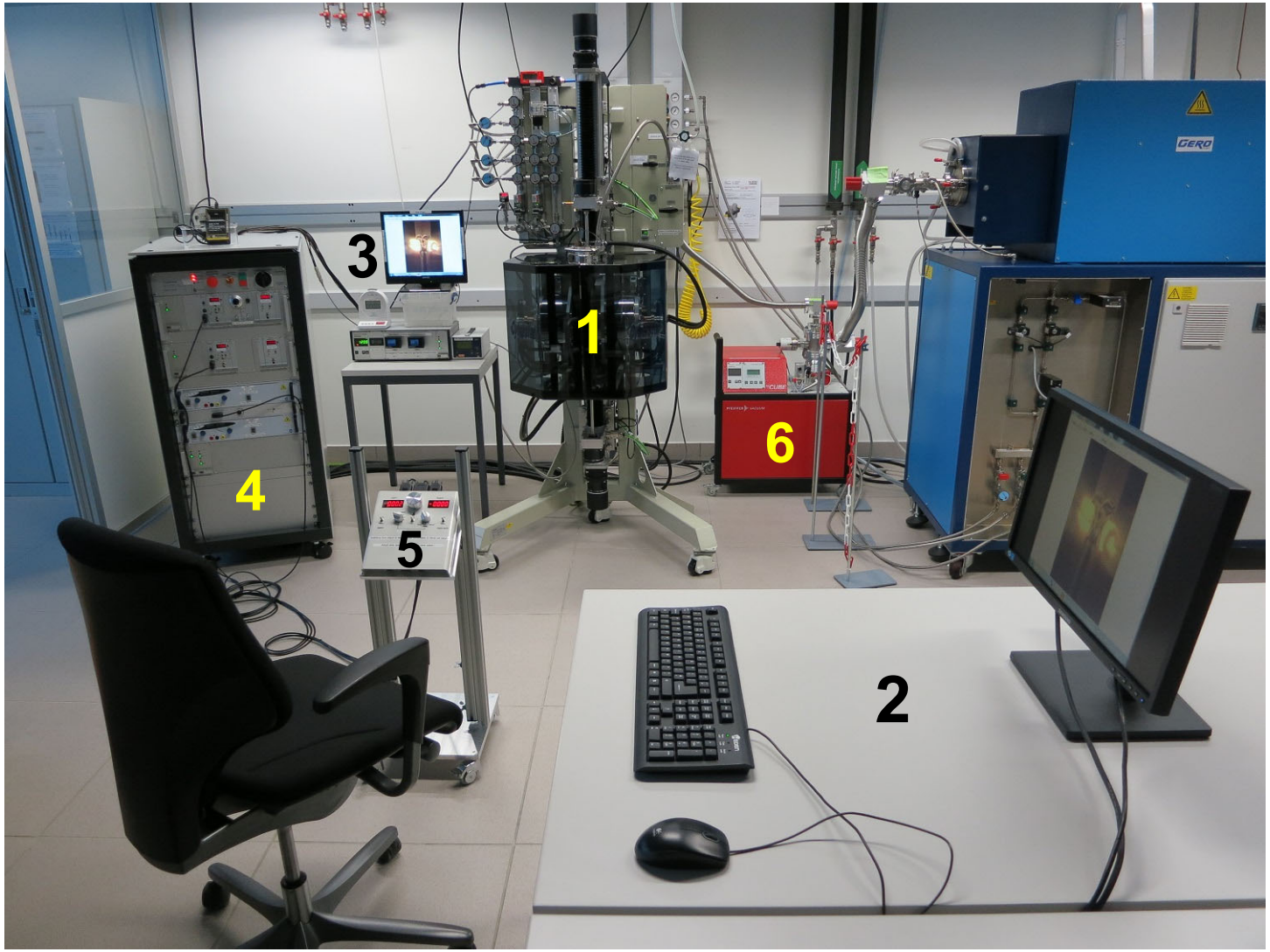

1 Mirror furnace

2 Monitor and keyboard of the video recording and processing system which is equipped with the software HIRIS from R&D Vision

3 Second monitor

4 Control cabinet

5 Movable control unit for lamp power and fast motion of seed and feed rod

6 Turbo pumping station

https://dx.doi.org/10.3929/ethz-a-010817148

Cyberstar mirror furnace – Casing open and mirrors M1 and M2 locked

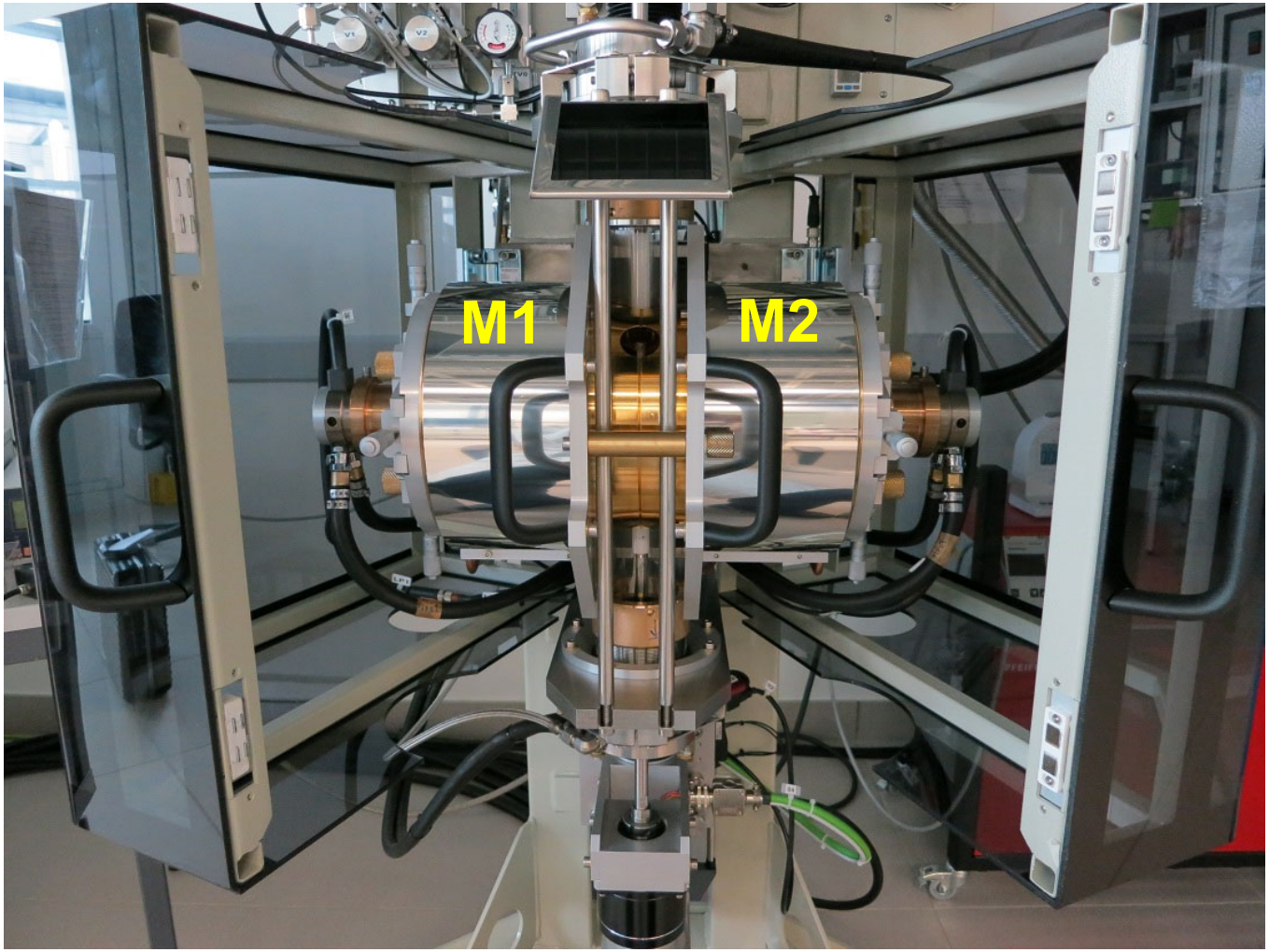

https://dx.doi.org/10.3929/ethz-a-010817148

Cyberstar mirror furnace – Mirrors unlocked

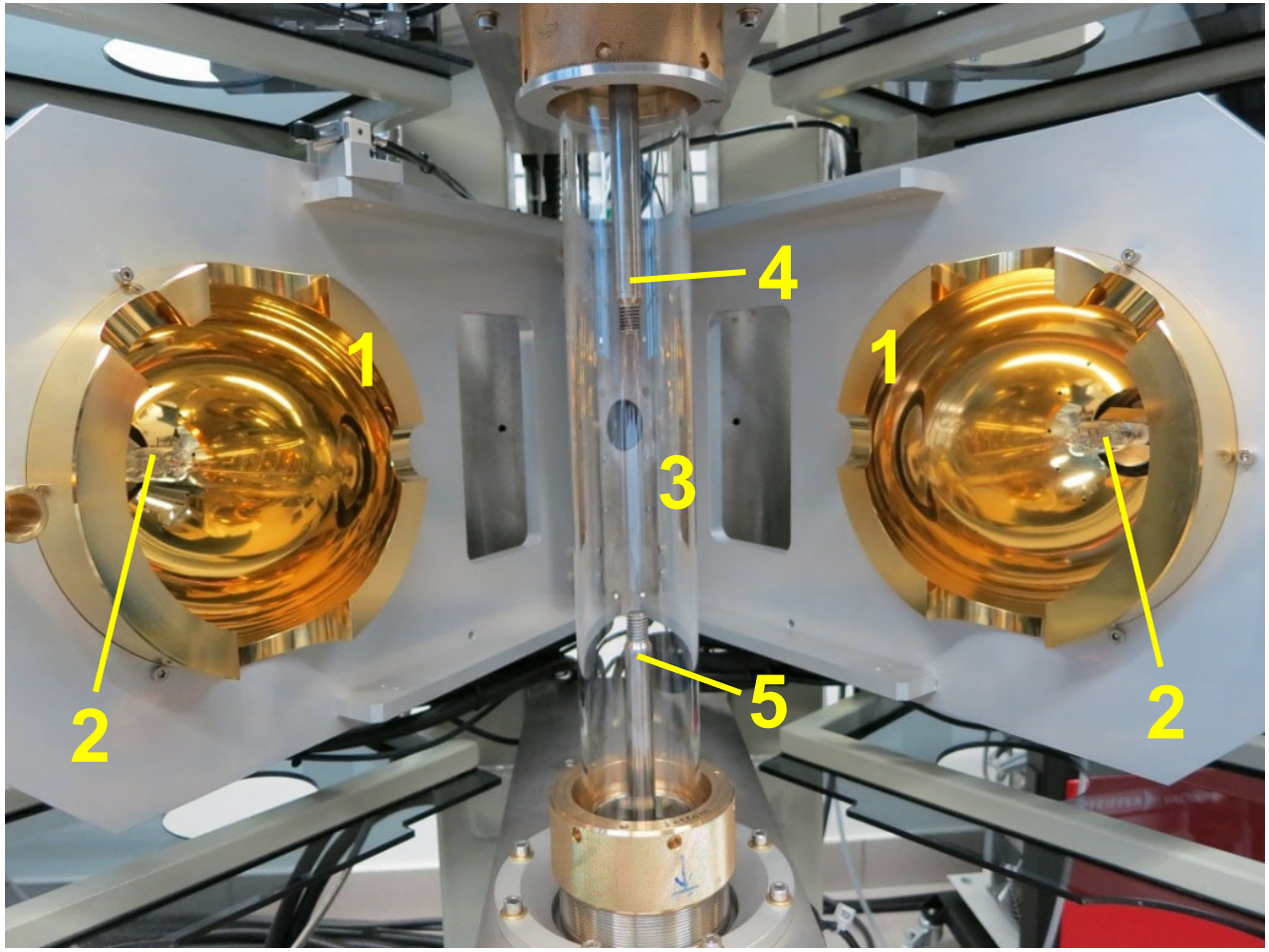

1 Elliptical and gold-coated mirror

2 Lamp
P_{max} = 1000 W

3 Quartz glass tube

4 Upper shaft

5 Lower shaft

Mirrors and lamps are cooled by cooling water and a flow of compressed air

- Mirrors focus radiation from lamps into a small volume. If a material is located at that volume, then it can be molten if the lamp power is high enough
- Heating-up and melting of a material takes mainly place by its infrared absorption
- Mirrors are gold-coated because that enhances their infrared reflectivity

https://dx.doi.org/10.3929/ethz-a-010817148

Synthesis of crystalline materials by a mirror furnace requires desired chemical composition in form of two rods

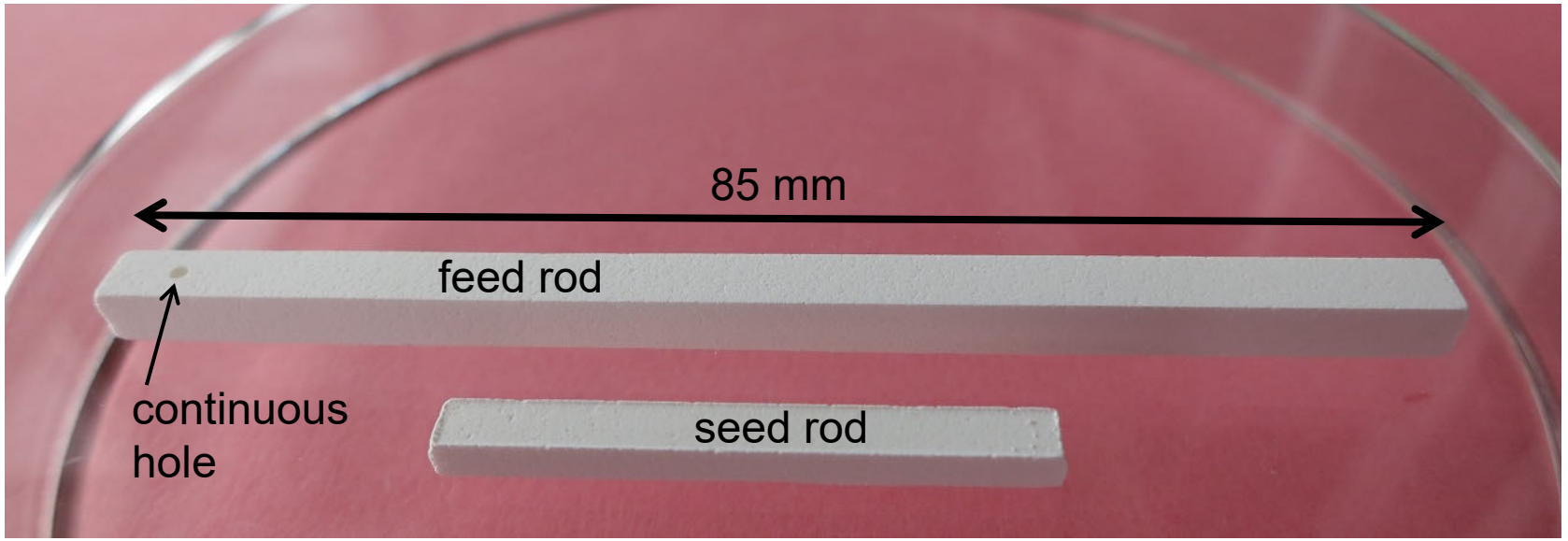

Example of two polycrystalline sintered rods with same chemical composition such as $La_2Ti_2O_7$

Fixation of the rods at the lower and upper shaft by special sample holders ...

https://dx.doi.org/10.3929/ethz-a-010817148

Cyberstar mirror furnace equipped with rods and quartz glass tube

Feed rod (4) fixed by a sample holder (5) which is screwed on the upper shaft (6)

Seed rod (3) fixed by a sample holder (2) which is screwed on the lower shaft (1)

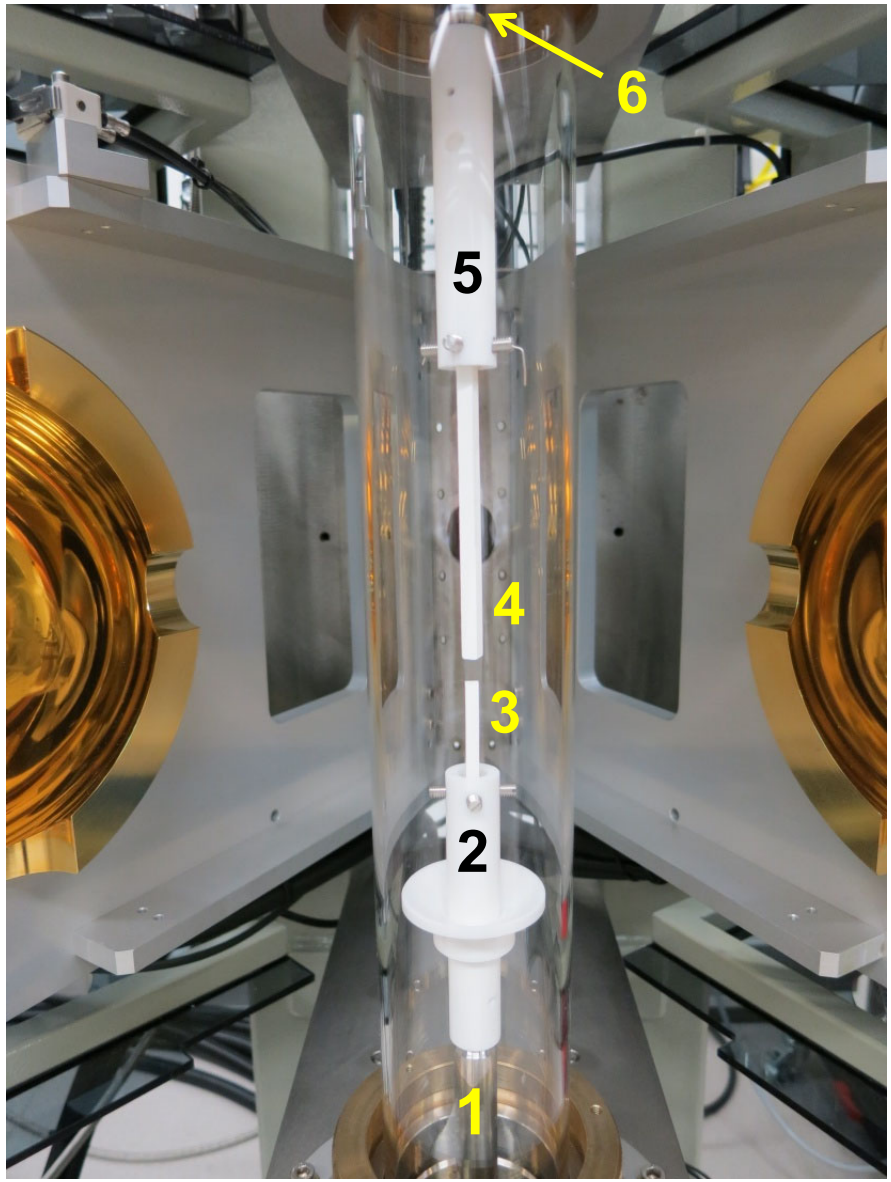

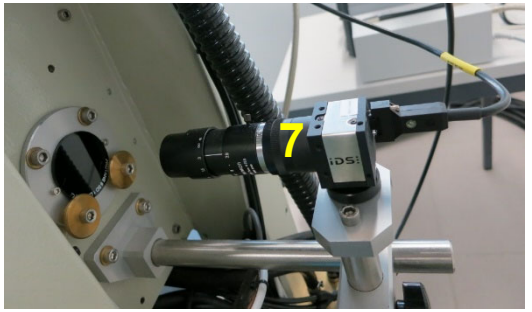

Digital video camera (7) at the rear side

https://dx.doi.org/10.3929/ethz-a-010817148

Synthesis of melt-grown oxides by the Cyberstar mirror furnace

Example of a snap shot of a floating zone melting process

The polycrystalline feed rod is converted via the melt into a crystalline material which is created by a solidification from the melt

2 Slow downwards motion of the feed rod, e.g. 10 mm / h

1 Slow downward motion of the seed rod, e.g. 8 mm / h

The crystalline material grows onto the upper part of the seed rod which is not visible in this image. The seed rod is located below the bottom boundary of this picture

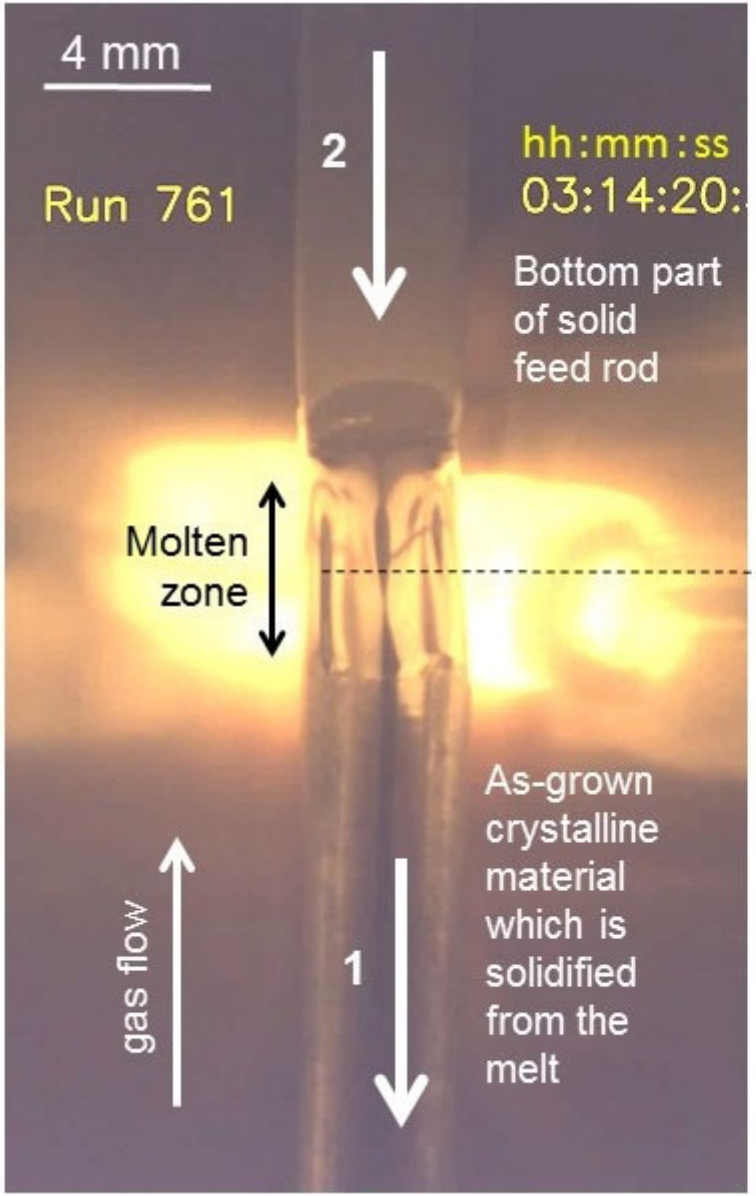

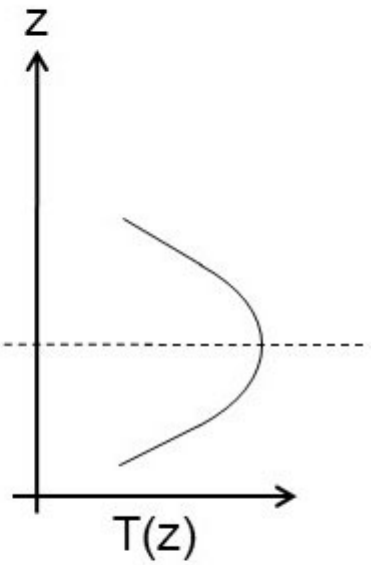

Sketch of the temperature profile T(z) along the z - direction

https://dx.doi.org/10.3929/ethz-a-010817148

Nice-looking ☺ example of a melt-grown oxide prepared by a mirror furnace

$Ca_4EuNb_5O_{17}$ – Eu^{2+} / $4f^7$ and $Nb^{4.8+}$ / $4d^{0.2}$

Grown with 15 mm / h in argon • Blue-black electrical conductor • Sample No. 510

Structure type n = 5 of the layered perovskite-related Carpy-Galy phases $A_nB_nO_{3n+2}$

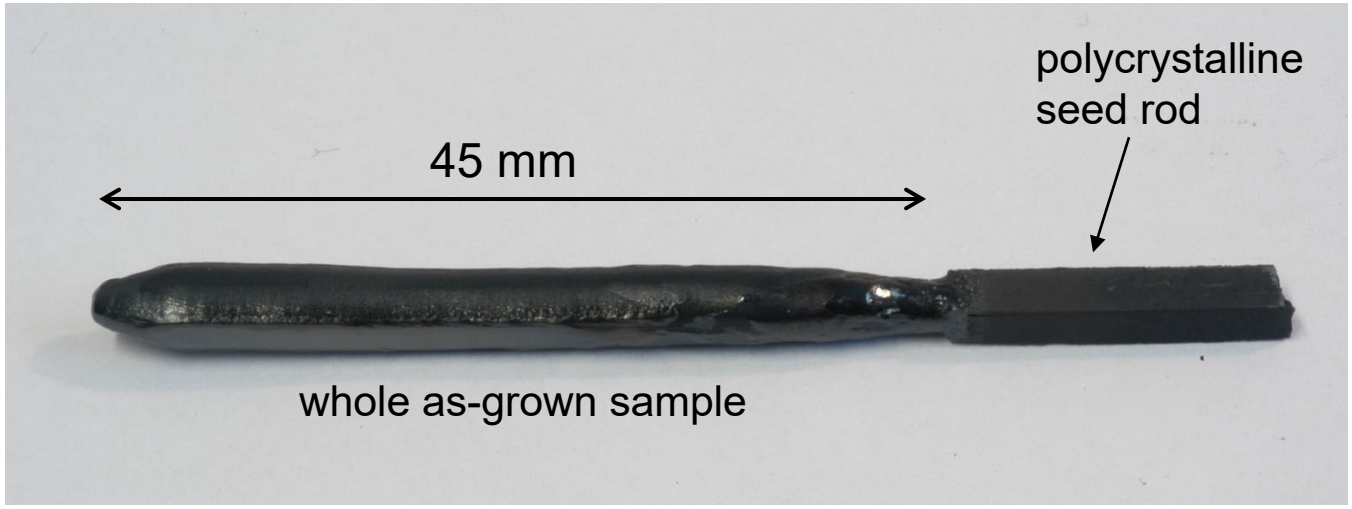

Part of the as-grown sample

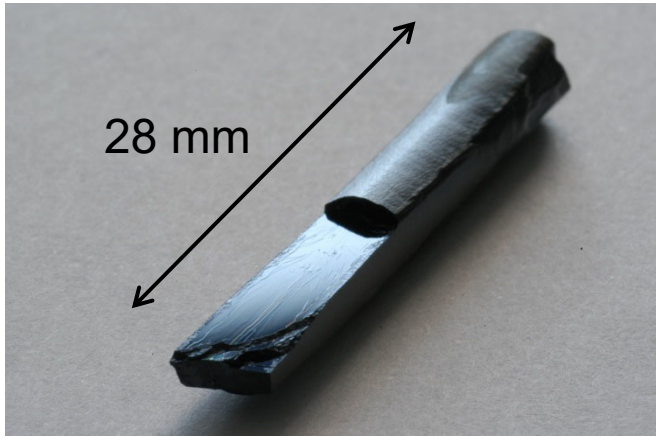

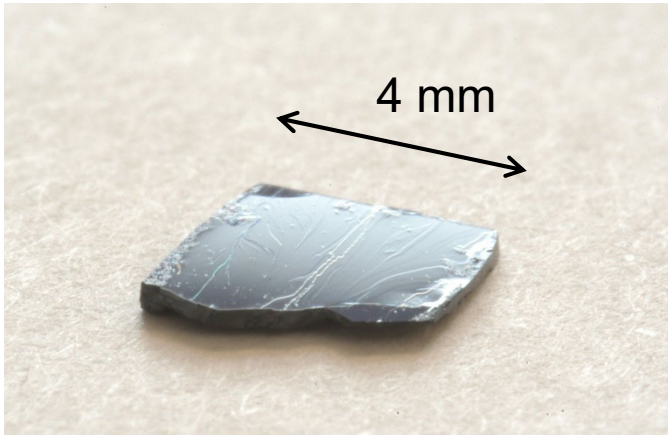

Plate-like crystal obtained by crushing / cleaving the as-grown sample

Prepared at the University of Augsburg by a GERO mirror furnace

Progress in Solid State Chemistry 36 (2008) 253

Nice-looking ☺ examples of melt-grown oxides prepared by a mirror furnace

Layered perovskite-related Carpy-Galy phases $A_nB_nO_{3n+2} = ABO_x$

Pieces and plate-like crystals from as-grown samples

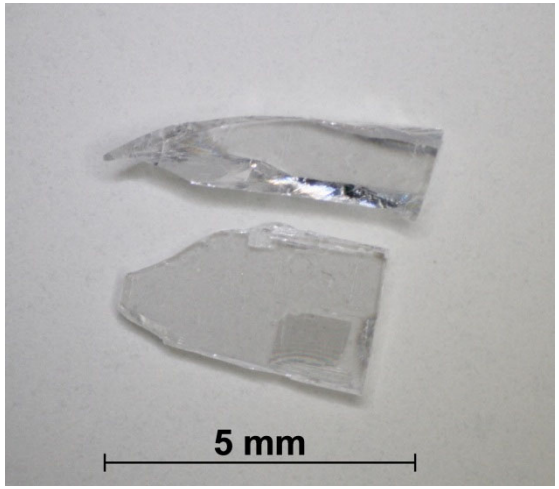

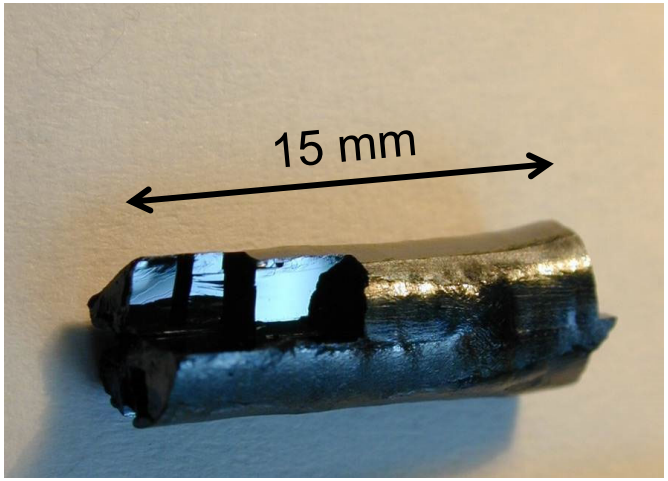

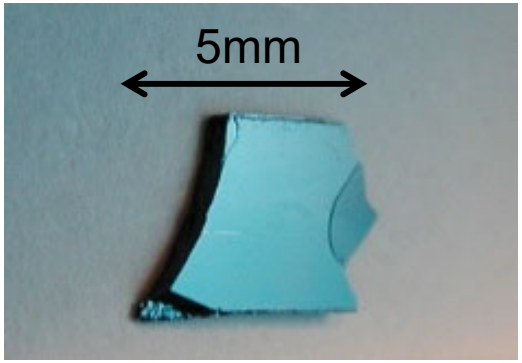

$Sr_4Nb_4O_{14} = SrNbO_{3.50}$

Nb^{5+} / $4d^0$ Sample No. 169

Grown in air

White transparent
high-T_c ferroelectric insulator
T_c = 1615 K

Structure type *n* = 4

$Sr_5Nb_5O_{17.05} = SrNbO_{3.41}$

$Nb^{4.82+}$ / $4d^{0.18}$ Sample No. 71

Grown in argon

Black-blue quasi-1D metal

Structure type *n* = 5

Progress in Solid State Chemistry 29 (2001) 1 and 36 (2008) 253
Physical Review B 70 (2004) 245123 • Physical Review Letters 89 (2002) 236403
Samples prepared at the University of Augsburg by a GERO mirror furnace
Photo of $Sr_4Nb_4O_{14} = SrNbO_{3.5}$ taken at the ETH Zurich

Powder x-ray diffraction

Used diffractometer at the

X-Ray Service Platform / Laboratory of Crystallography
https://xray.mat.ethz.ch / www.crystal.mat.ethz.ch

of the Department of Materials of the ETH Zurich:

PANALYTICAL X`Pert PRO MPD diffractometer equipped with a Ge monochromator (Cu $K\alpha_1$ radiation)

Some of the used measurement conditions:

- Measured diffraction angle range $3° \leq 2\Theta \leq 73°$
- Step size 0.0084° and time per step 99.695 s
- Irradiated and observed length 10 mm
- Rotating sample with a revolution time of 2 seconds

Data evaluation and lattice parameter refinement with PANALYTICAL software HighScore Plus. Available crystallographic database: ICDD PDF 4+ with annual renewal. ICDD = International Center for Diffraction Data

Acknowledgement

Frank Lichtenberg thanks Thomas Weber from the X-Ray Service Platform and the former Laboratory of Crystallography as well as Walter Steurer from the former Laboratory of Crystallography for their support

Powder x-ray diffraction

Preparation of powder for the measurement

A sample holder from PANALYTICAL for powder x-ray diffraction. The inner part (gray) is made of single crystalline silicon with an orientation which displays no diffraction peaks in the measurement range of the diffractometer. The diameter of the inner deepening (D) is 15 mm

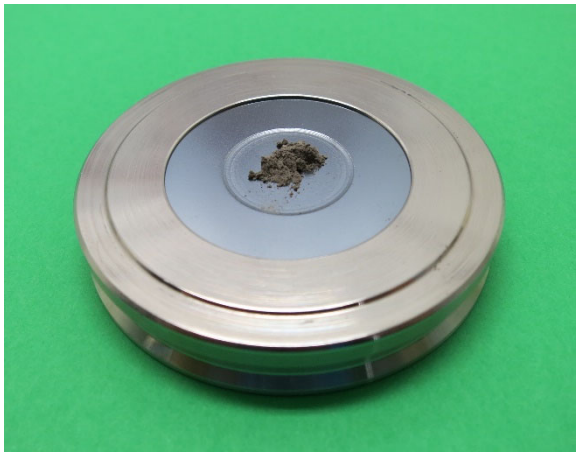

The inner deepening of the sample holder is loaded with a small powder heap. The powder can be dispersed by adding a few droplets of ethanol and a subsequent manual horizontal oscillating motion

The powder is dispersed in a flat manner within the inner deepening. It is important that the powder is on the same height as the gray silicon (S). Now it is ready for a powder XRD measurement

Powder x-ray diffraction

To verify the accuracy of the measured peak positions each measurement or series of measurements was followed by a separate measurement with a polycrystalline silicon sample from PANALYTICAL

Solid disk from PANALYTICAL made of polycrystalline silicon. Its diameter is 3 cm

Silicon disk in a sample holder from PANALYTICAL

Powder x-ray diffraction

PANALYTICAL
X`Pert PRO MPD
diffractometer

Picture taken
in July 2019

Powder x-ray diffraction

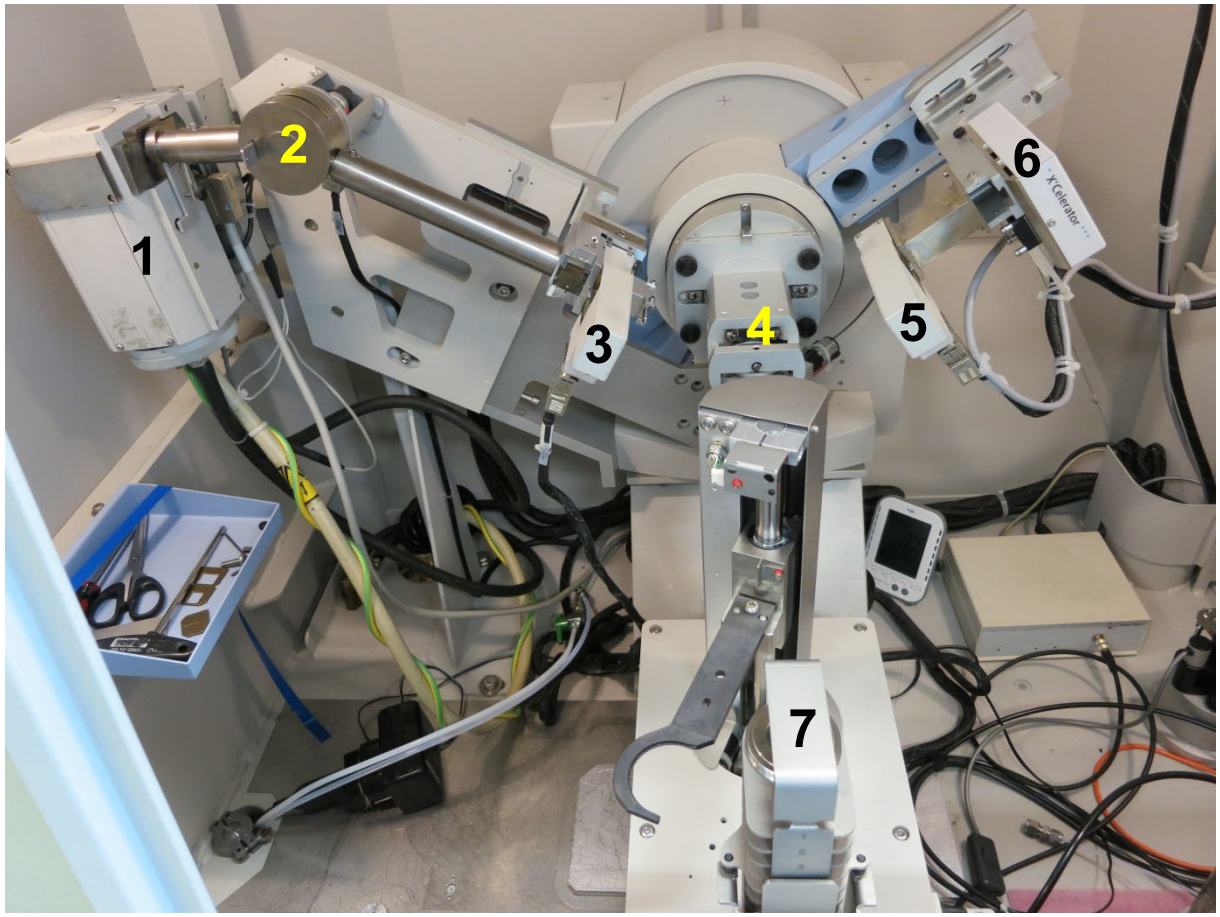

At this diffractometer the diffraction angle Θ or 2Θ is changed by changing the angular position of the sample and the detector. The position of the x-ray tube / source remains unchanged.

View into the PANALYTICAL X`Pert PRO MPD diffractometer

Picture taken in July 2019

1) Water-cooled x-ray tube / source
2) Ge monochromator
3) Programmable slit for the incident beam
4) Sample position
5) Programmable slit for the diffracted beam
6) Detector
7) Stage for several samples

Powder x-ray diffraction

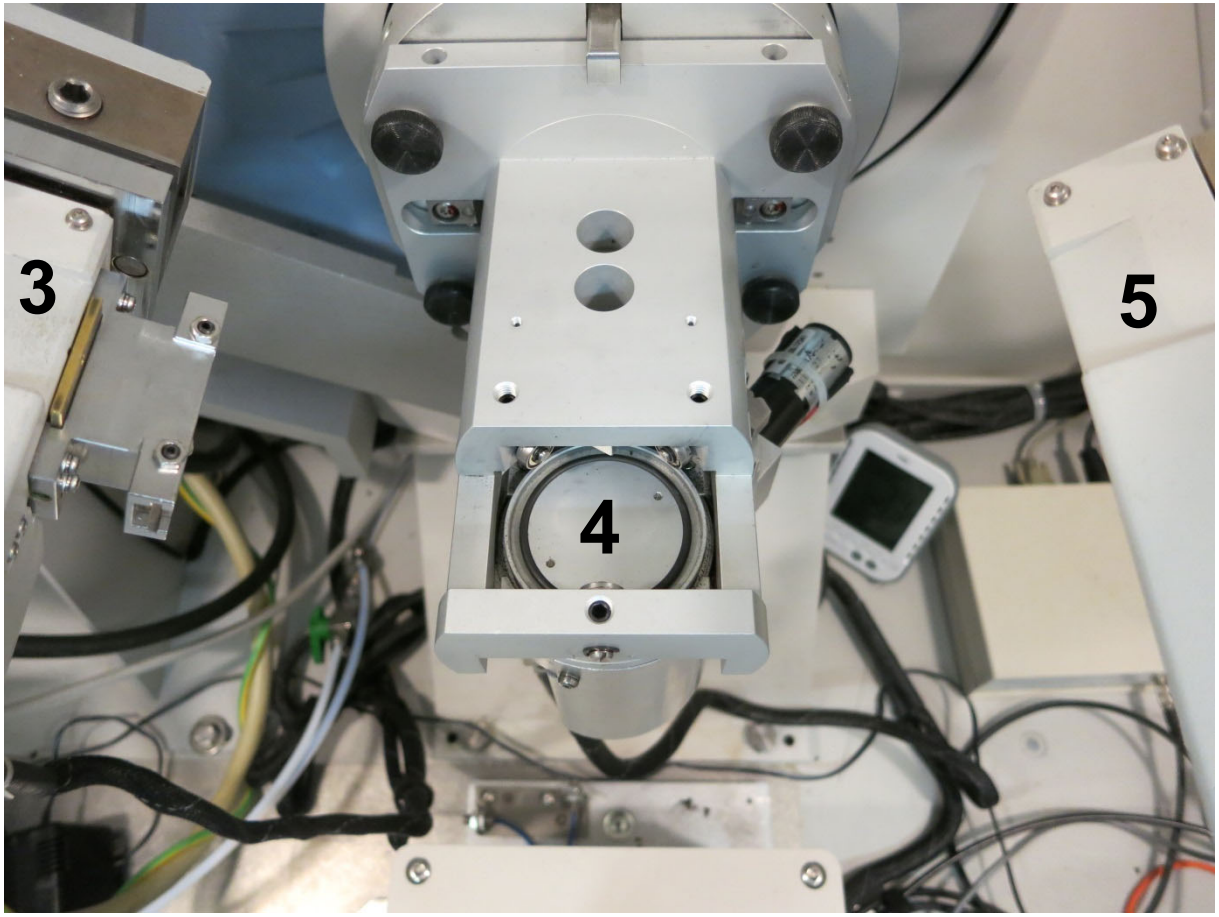

View into the
PANALYTICAL
X`Pert PRO MPD
diffractometer

Picture taken in July 2019

3) Programmable slit for the incident beam

4) Sample position

5) Programmable slit for the diffracted beam

Powder x-ray diffraction

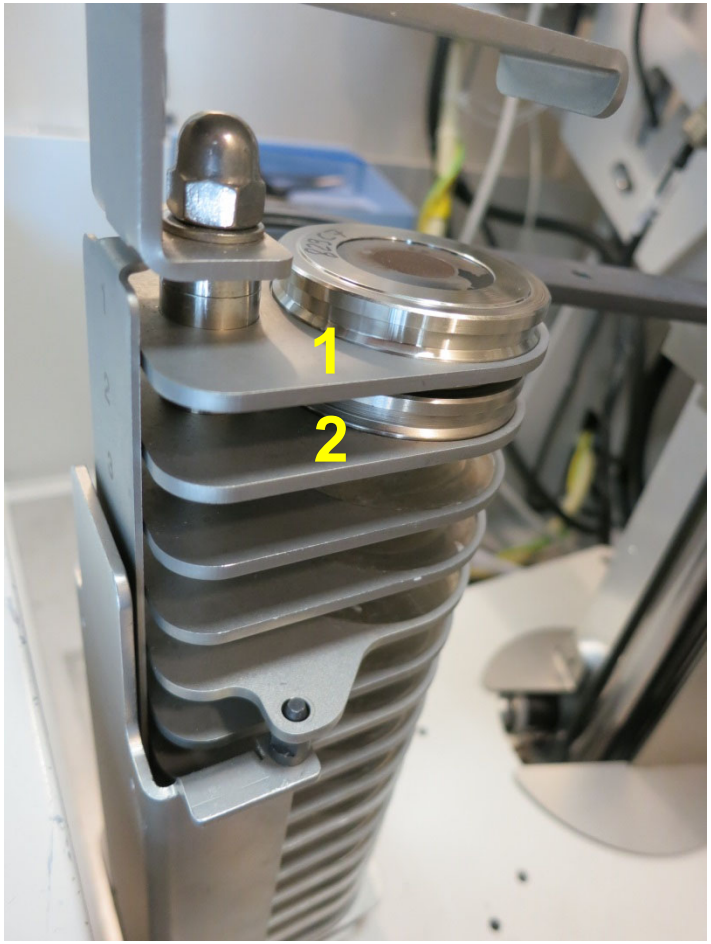

Sample stage in the PANALYTICAL X`Pert PRO MPD diffractometer

In this example the stage is loaded with two samples (1) and (2). Each sample is carried by a sample holder from PANALYTICAL

Picture taken in July 2019

5 Insulating, ferroelectric, and potential multiferroic Carpy-Galy phases $A_nB_nO_{3n+2} = ABO_x$ ...

5.1 Insulators and ferroelectrics ...

$A_nB_nO_{3n+2} = ABO_x$ type insulators and ferroelectrics (B = Ti^{4+}, Nb^{5+}, Ta^{5+})

- The highest-T_c ferroelectrics are n = 4 type oxides, e.g. $LaTiO_{3.50}$ with T_c = 1770 K and $CaNbO_{3.50}$ which is ferroelectric up to its melting point of 1850 K !

  S. Nanamatsu et al., Ferroelectrics 8 (1974) 511 ● S. Nanamatsu and M. Kimura, J. Phys. Soc. Jpn. 36 (1974) 1495

  Definition of highest-T_c ferroelectrics: Compounds with $T_c > T_c(LiNbO_3)$ = 1480 K

- Ferroelectrics $\rightarrow$ n is an even number like n = 2, 4, 6 (non-centrosymmetric)
  Antiferroelectrics $\rightarrow$ n is an odd number like n = 3, 5, 7 (centrosymmetric)

- Compounds with non-integral n
  e.g. $CaNb_{0.89}Ti_{0.11}O_{3.44}$ (n = 4.5) M. Nanot et al. , Journal of Solid State Chemistry 28 (1979) 137

- Single phase bulk materials known for n = 2 , 3 , 4 , 4.33 , 4.5 , 5 , 6 , 7

- Complex structural details like incommensurate modulations
  e.g. in $SrNbO_{3.50}$ (n = 4) P. Daniels et al. , Acta Crystallographica Section B 58 (2002) 970

- Another ions B' = Al^{3+}, Fe^{3+} … can occupy the B site:
  $B = (Ti, Nb, Ta)_{1-y}B'_y$ whereby so far $y \leq 0.33$

Examples of melt-grown $A_nB_nO_{3n+2}$ = ABO_x type insulators with B = Nb^{5+}

Crystalline pieces from the as-grown materials which were grown under synth. air

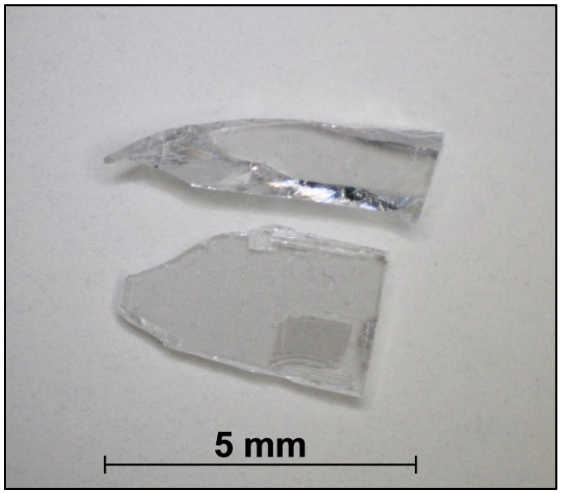

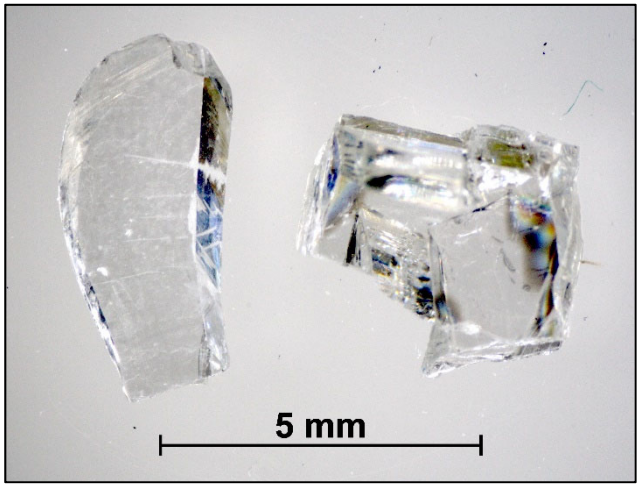

$Sr_4Nb_4O_{14}$ = $Sr_2Nb_2O_7$ = $SrNbO_{3.5}$

Sample No. 169

White transparent ferroelectric insulator with T_c = 1615 K

J. Phys. Soc. Jpn. 38 (1975) 817

Structure type n = 4

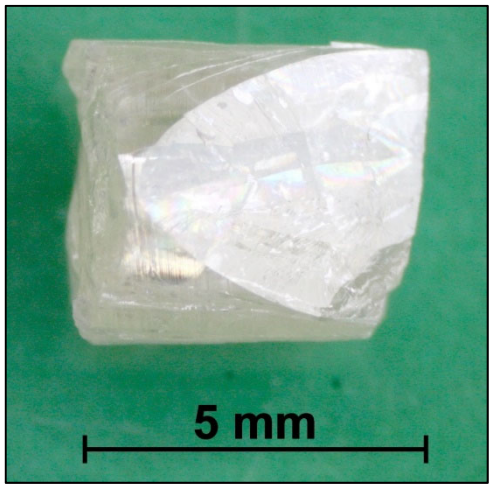

$Ca_4Nb_4O_{14}$ = $Ca_2Nb_2O_7$ = $CaNbO_{3.5}$

Sample No. 84

White transparent insulator which is ferroelectric up to the melting point of 1850 K

J. Phys. Soc. Jpn. 36 (1974) 1495

Structure type n = 4

Prog. Solid State Chem. 29 (2001) 1 • As-grown materials prepared at the University of Augsburg with a GERO mirror furnace • Photos taken at the ETH Zurich

Ferroelectric *n* = 4 type

$Sr_4Nb_4O_{14} = Sr_2Nb_2O_7 = SrNbO_{3.5}$

T_c = 1340 °C

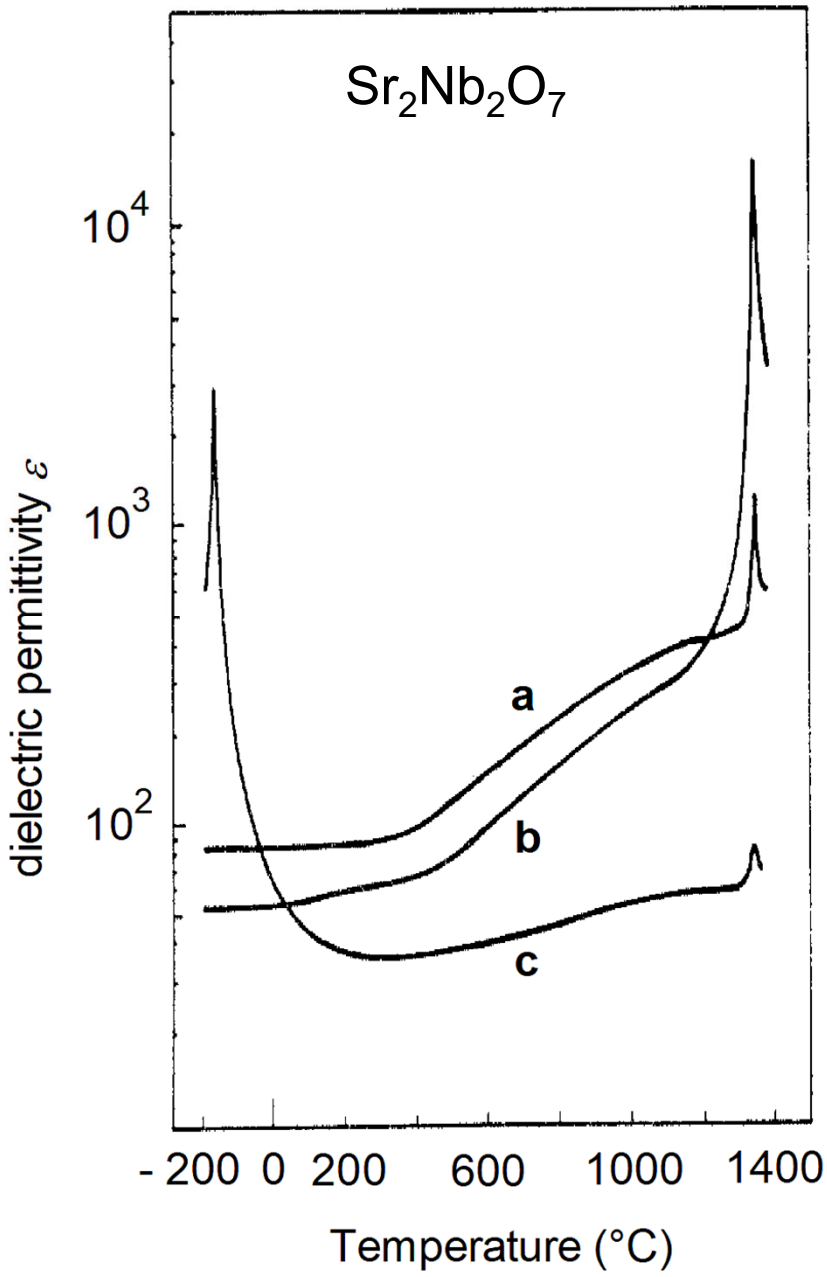

Crystallographic and Dielectric Properties of Ferroelectric $A_2B_2O_7$ (A=Sr, B=Ta, Nb) Crystals and Their Solid Solutions

Satoshi Nanamatsu, Masakazu Kimura, and Tsutomu Kawamura

Journal of the Physical Society of Japan 38 (1975) 817 - 824

https://doi.org/10.1143/JPSJ.38.817

Example of a melt-grown $A_nB_nO_{3n+2} = ABO_x$ type insulator with $B = Ti^{4+}$

Crystalline piece from the as-grown material which was grown under synth. air

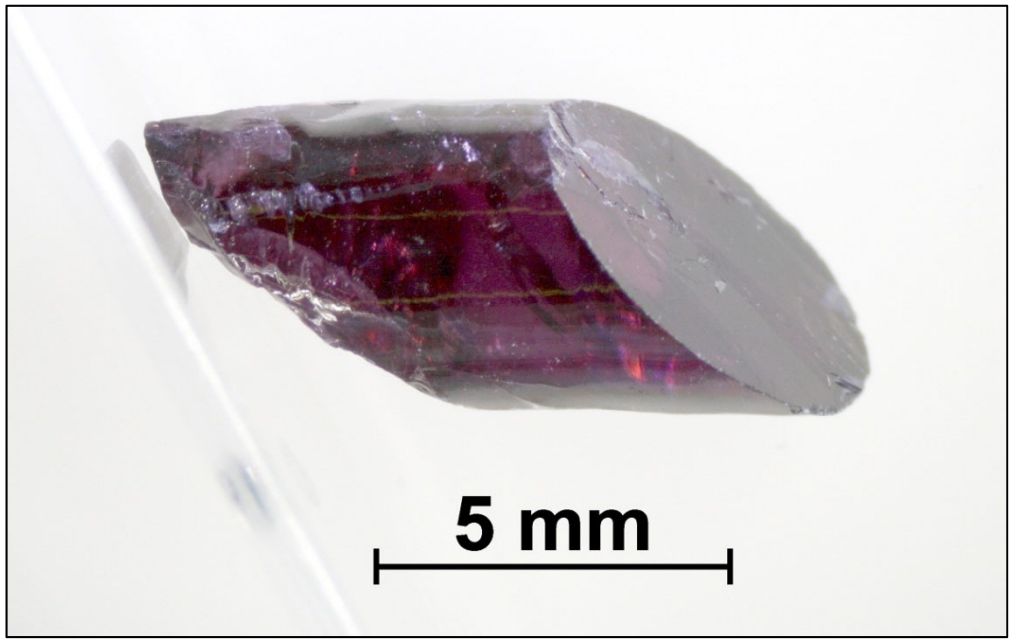

Sample No. Z 267

As-grown material prepared at the IBM Zurich Research Laboratory with an IBM mirror furnace

Photo taken at the ETH Zurich

$Nd_4Ti_4O_{14} = Nd_2Ti_2O_7 = NdTiO_{3.5}$ with Nd^{3+}

Violet transparent ferroelectric insulator with $T_c > 1770$ K

Japanese Journal of Applied Physics 13 (1974) 1473

Structure type $n = 4$

Example of a melt-grown $A_nB_nO_{3n+2}$ = ABO_x type insulator with B = Ti^{4+}

Crystalline pieces from the as-grown material which was grown under synth. air

Sample No. 385

As-grown material prepared at the University of Augsburg with a GERO mirror furnace

Photo taken at the ETH Zurich

Progress in Solid State Chemistry 36 (2008) 253

$La_{0.4}Sm_{3.6}Ti_4O_{14}$ = $La_{0.2}Sm_{1.8}Ti_2O_7$ = $La_{0.1}Sm_{0.9}TiO_{3.5}$ with La^{3+} and Sm^{3+}

Yellow transparent (ferroelectric) insulator

Structure type n = 4

Composition is nearby the stability limit of the n = 4 type structure because $Sm_2Ti_2O_7$ = $SmTiO_{3.5}$ crystallizes in the cubic pyrochlore structure

Example of a melt-grown $A_nB_nO_{3n+2}$ = ABO_x type insulator with B = Ti^{4+}

Crystalline pieces from the as-grown material which was grown under synth. air

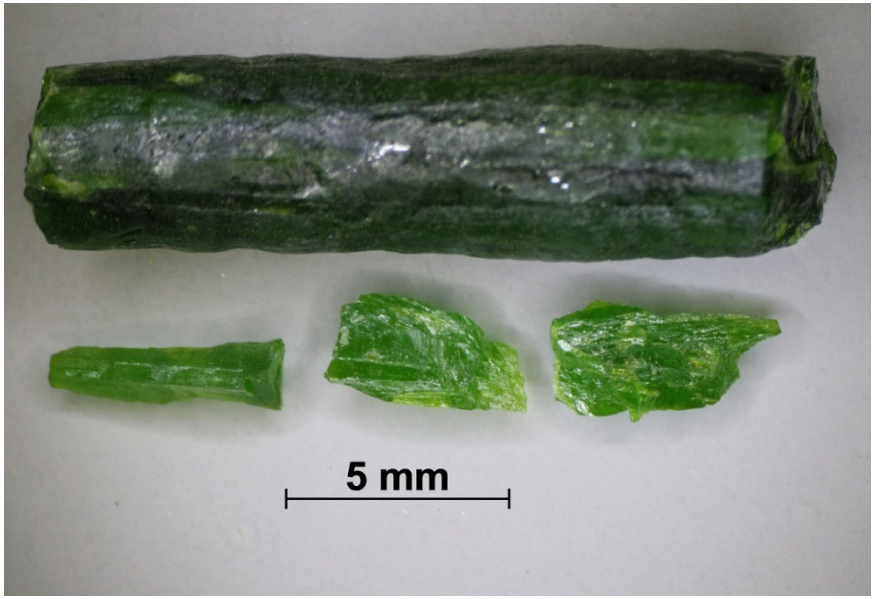

Sample No. 461

As-grown material prepared at the University of Augsburg with a GERO mirror furnace

Photo taken at the ETH Zurich

Progress in Solid State Chemistry 36 (2008) 253

$Pr_5Ti_4AlO_{17}$ = $PrTi_{0.8}Al_{0.2}O_{3.4}$ with Pr^{3+}

Green transparant insulator

Structure type n = 5

Example of a melt-grown $A_nB_nO_{3n+2}$ = ABO_x type insulator with B = Ta^{5+}

Crystalline pieces from the as-grown material which was grown under synth. air

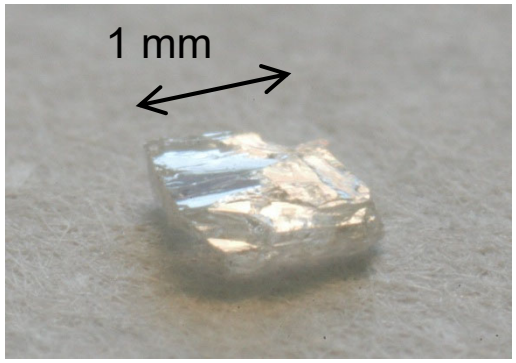

Sample No. 276

As-grown material prepared at the University of Augsburg with a GERO mirror furnace

Progress in Solid State Chemistry 36 (2008) 253

$Sr_2LaTa_3O_{11}$ = $Sr_{0.67}La_{0.33}TaO_{3.67}$

Light colored transparent insulator

Structure type n = 3

Further insulators, namely such with B = (Ti,Fe) , (Ti,Mn) , and (Nb,Fe) , are presented in part 5.3.1 and 5.3.2

5.2 Multiferroicity and magnetoelectricity: Abstracts of two papers and properties of various modifications of Fe_2O_3 ...

Why are there so few magnetic ferroelectrics ?

Why are there so few magnetic ferroelectrics ?
Nicola A. Hill
The Journal of Physical Chemistry B 104 (2000) 6694 - 6709
https://doi.org/10.1021/jp000114x

Abstract

Multiferroic magnetoelectrics are materials that are both ferromagnetic and ferroelectric in the same phase. As a result, they have a spontaneous magnetization that can be switched by an applied magnetic field, a spontaneous polarization that can be switched by an applied electric field, and often some coupling between the two. Very few exist in nature or have been synthesized in the laboratory. In this paper, we explore the fundamental physics behind the scarcity of ferromagnetic ferroelectric coexistence. In addition, we examine the properties of some known magnetically ordered ferroelectric materials. We find that, in general, the transition metal d electrons, which are essential for magnetism, reduce the tendency for off-center ferroelectric distortion. Consequently, an additional electronic or structural driving force must be present for ferromagnetism and ferroelectricity to occur simultaneously.

Epitaxial $BiFeO_3$ (Fe^{3+} / $3d^5$) Multiferroic Thin Film Heterostructures

Epitaxial $BiFeO_3$ Multiferroic Thin Film Heterostructures

J. Wang, J. B. Neaton, H. Zheng, V. Nagarajan, S. B. Ogale, B. Liu, D. Viehland, V. Vaithyanathan, D. G. Schlom, U. V. Waghmare, N. A. Spaldin, K. M. Rabe, M. Wuttig, and R. Ramesh

Science 299 (2003) 1719 - 1722

https://doi.org/10.1126/science.1080615

Abstract

Enhancement of polarization and related properties in heteroepitaxially constrained thin films of the ferroelectromagnet, $BiFeO_3$, is reported. Structure analysis indicates that the crystal structure of film is monoclinic in contrast to bulk, which is rhombohedral. The films display a room-temperature spontaneous polarization (50 to 60 microcoulombs per square centimeter) almost an order of magnitude higher than that of the bulk (6.1 microcoulombs per square centimeter). The observed enhancement is corroborated by first-principles calculations and found to originate from a high sensitivity of the polarization to small changes in lattice parameters. The films also exhibit enhanced thickness-dependent magnetism compared with the bulk. These enhanced and combined functional responses in thin film form present an opportunity to create and implement thin film devices that actively couple the magnetic and ferroelectric order parameters.

Some structural and physical properties of Fe_2O_3 (Fe^{3+} / $3d^5$)

α - Fe_2O_3 (Hematite)

- Corundum type structure
- Neel temperature $T_N \approx 685$ °C
- Low temperature magnetic transition $T_c \approx 260$ K
- Weak ferromagnetic between T_c and T_N

γ - Fe_2O_3 (Maghemite)

- Cation-deficient spinel structure
- Ferrimagnetic with $T_c \approx 950$ K
- Magnetic moment about 2.5 Bohr magnetons per formula unit
- Used as magnetic pigment in electronic recording media

Polar (!) ε - Fe_2O_3

- So far prepared only as nanoparticles and thin films
- Difficult to prepare in a single phase form
- At room temperature non-centrosymmetric $GaFeO_3$ structure
- Ferrimagnetic with $T_c \approx 510$ K
- Coupling between magnetic and dielectric properties

R. Dronskowski, Advanced Functional Materials 11 (2001) 27 • M. Gich et al. , Applied Physics Letters 96 (2010) 112508 and references therein • M. Gich et al. , Nanotechnology 17 (2006) 687

5.3 Materials in the context of potential multiferroic Carpy-Galy phases $A_nB_nO_{3n+2} = ABO_x$ ...

5.3 Materials in the context of potential multiferroic Carpy-Galy phases $A_nB_nO_{3n+2} = ABO_x$

5.3.1 Compounds in the system La – Ti^{4+} – Fe^{3+} (Mn^{3+}) – O like the n = 6 type $La_6Ti_4Fe_2O_{20}$ ...

Ti^{4+} ($3d^0$) and Fe^{3+} ($3d^5$) insulators of the type $La_n(Ti,Fe)_nO_{3n+2}$ = $La(Ti,Fe)O_x$

⊠ = TiO_6 octahedra (O located at the corners, Ti^{4+} hidden in the center)

⊠ = FeO_6 octahedra (O located at the corners, Fe^{3+} hidden in the center)

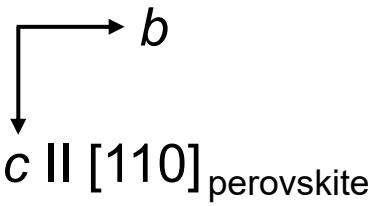

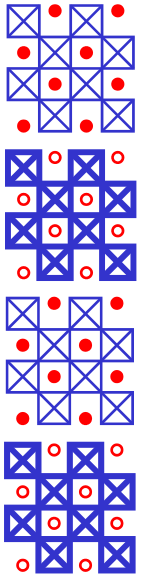

n = 4

$LaTiO_{3.50}$

ferroelectric

T_c = 1770 K

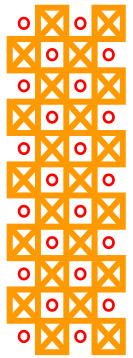

n = ∞

$LaFeO_3$ perovskite

canted AFM / weak FM

T_N = 740 K

Ti^{4+} ($3d^0$) and Fe^{3+} ($3d^5$) insulators of the type $La_n(Ti,Fe)_nO_{3n+2}$ = $La(Ti,Fe)O_x$

⊠ = TiO_6 octahedra (O located at the corners, Ti^{4+} hidden in the center)

⊠ = FeO_6 octahedra (O located at the corners, Fe^{3+} hidden in the center)

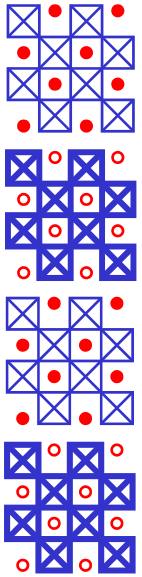

n = 4

$LaTiO_{3.50}$

ferroelectric

T_c = 1770 K

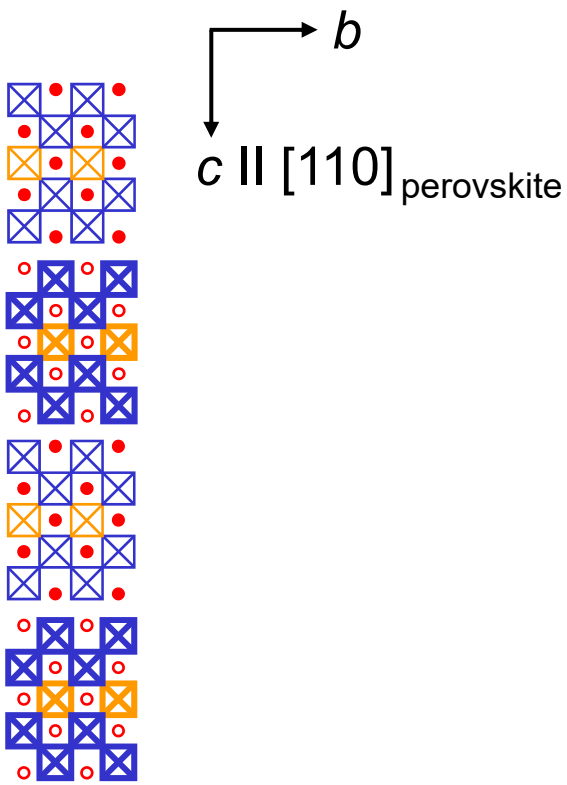

n = 5

$LaTi_{0.8}Fe_{0.2}O_{3.40}$

Full occupational order of Fe reported by Y. Titov et al

Centrosymmetric

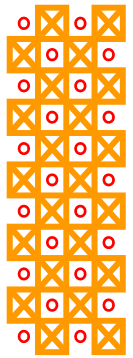

n = ∞

$LaFeO_3$ perovskite

canted AFM / weak FM

T_N = 740 K

Ti^{4+} ($3d^0$) and Fe^{3+} ($3d^5$) insulators of the type $La_n(Ti,Fe)_nO_{3n+2}$ = $La(Ti,Fe)O_x$

⊠ = TiO_6 octahedra (O located at the corners, Ti^{4+} hidden in the center)

⊠ = FeO_6 octahedra (O located at the corners, Fe^{3+} hidden in the center)

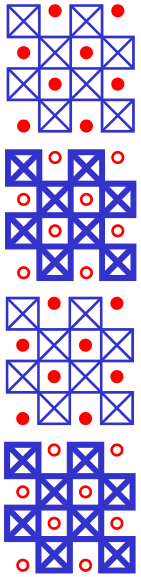

n = 4

$LaTiO_{3.50}$

ferroelectric

T_c = 1770 K

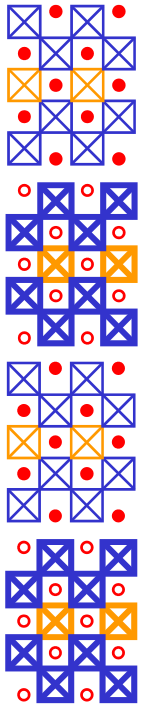

n = 5

$LaTi_{0.8}Fe_{0.2}O_{3.40}$

Full occupational order of Fe reported by Y. Titov et al

Centrosymmetric

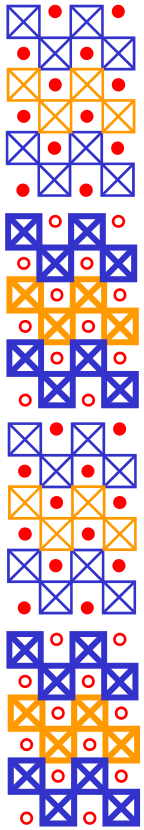

n = 6

$LaTi_{0.67}Fe_{0.33}O_{3.33}$

Hypothetical compound

Non-centrosymmetric

Example of a ferroelectric *n* = 6 type material:

$Sr_6Nb_4Ti_2O_{20}$ (T_c = 630 °C)

V. A. Isupov et al , Soviet Physics Solid State 18 (1976) 835 and 19 (1977) 544

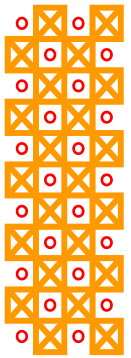

n = ∞

$LaFeO_3$ perovskite

canted AFM / weak FM

T_N = 740 K

Ti^{4+} ($3d^0$) and Fe^{3+} ($3d^5$) insulators of the type $La_n(Ti,Fe)_nO_{3n+2}$ = $La(Ti,Fe)O_x$

Coexistence of (anti)ferroelectric and magnetic order

in $La_n(Ti,Fe)_nO_{3n+2}$ = $La(Ti,Fe)O_x$?

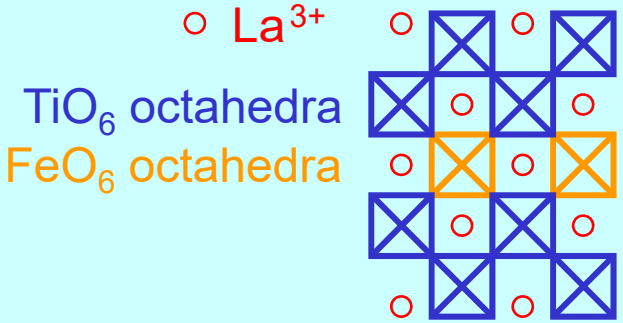

Ti^{4+} and Fe^{3+} ions are fully ordered

Y. A. Titov et al. , Rep. Natl. Sci. Ukraine 12 (2005) 149

Fe – O linkage linear along *a*-axis → 1 D

n = 5 type $La_5Ti_4FeO_{17}$

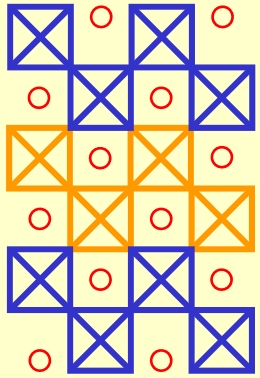

?

Fe – O linkage linear along *a*-axis, zig-zag along *b*-direction → 2 D

n = 6 type $La_6Ti_4Fe_2O_{20}$

⇨ Probably different magnetic behavior of Fe^{3+} ($3d^5$) in *n* = 5 and *n* = 6

Structure reported by Y. A. Titov et al. bases on powder x-ray diffraction. Desirable is a verification by a structural study based on single crystal x-ray diffraction

Melt-grown $La_5Ti_4FeO_{17}$ (n = 5) and $La_6Ti_4Fe_2O_{20}$ (n = 6)

Ti^{4+} / $3d^0$ and Fe^{3+} / $3d^5$

Pieces of as-grown samples which were grown in air with 15 mm / h

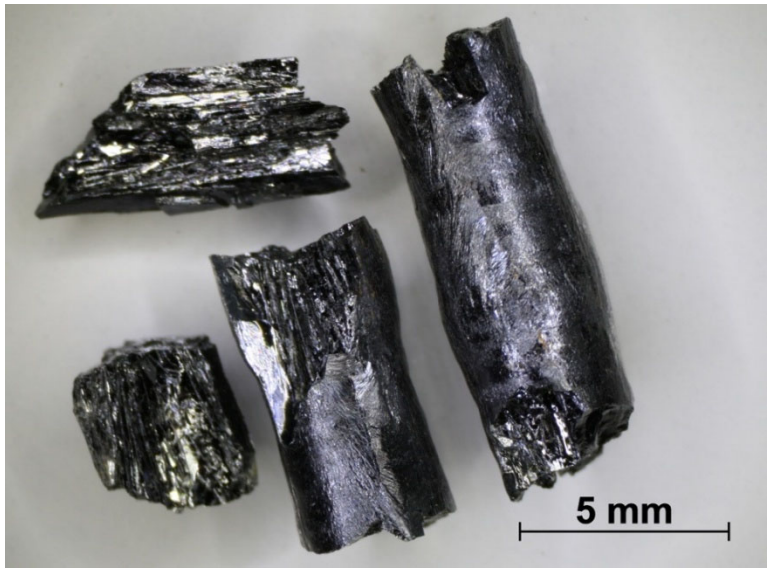

$La_5Ti_4FeO_{17}$ (n = 5) Sample No. 522

$La_6Ti_4Fe_2O_{20}$ (n = 6) Sample No. 523

- No large plate-like crystals
- Powder x-ray diffraction → single phase n = 5 and n = 6 materials
- Single crystal x-ray diffraction peaks and structural refinement:
  FWHM (n = 6) > FWHM (n = 5) and $R_{F\,\mathrm{obs}}$ (n = 6) > $R_{F\,\mathrm{obs}}$ (n = 5)
  → crystal quality of n = 5 better than that of n = 6

F. Lichtenberg et al., Progress in Solid State Chemistry 36 (2008) 253 • A. Wölfel et al., Journal of Physics: Condensed Matter 25 (2013) 076003 • Samples prepared at the University of Augsburg - Photos taken at the ETH Zurich

Melt-grown monoclinic $La_5Ti_4FeO_{17}$ (n = 5) and $La_6Ti_4Fe_2O_{20}$ (n = 6)

Crystal structure and B = (Ti^{4+}, Fe^{3+}) site occupancies from single crystal x-ray diffraction

Fe^{3+} occupancy in % at 295 K
Distortion of (Ti^{4+}, Fe^{3+})O_6 octahedra in %

} averaged over two non-equivalent sites along a-axis

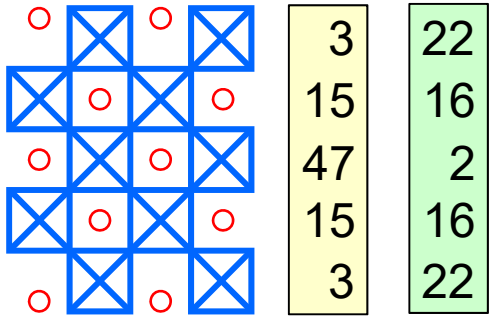

3	22
15	16
47	2
15	16
3	22

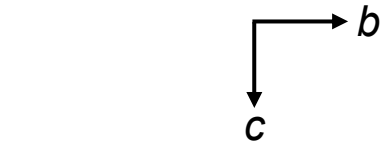

= BO_6 octahedra
(O located at corners,
B hidden in center)

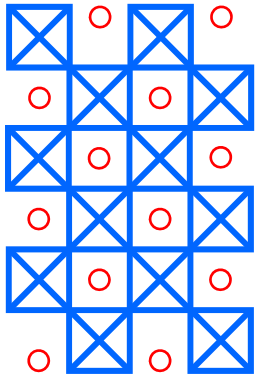

5	23
24	17
68	4
68	4
24	17
5	23

n = 5 type $La_5Ti_4FeO_{17}$
Centrosymmetric

n = 6 type $La_6Ti_4Fe_2O_{20}$
Non-centrosymmetric

- Partial occupational order of Fe^{3+} and Ti^{4+} at B site
- Fe^{3+} (Ti^{4+}) concentrated at the center (border) of the layers or slabs
- For $La_6Ti_4Fe_2O_{20}$ (n = 6) the Fe^{3+} occupancy at the two central sheets is larger than 59 % which is the percolation limit of a 2D square lattice
- Not confirmed: Full occupational order in $La_5Ti_4FeO_{17}$ (n = 5) reported by Titov et al.

A. Wölfel , F. Lichtenberg , S. van Smaalen , Journal of Physics: Condensed Matter 25 (2013) 076003
A. Wölfel , P. Dorscht , F. Lichtenberg , S. van Smaalen , Acta Crystallographica Section B 69 (2013) 137

Melt-grown $La_5Ti_4FeO_{17}$ (n = 5) and $La_6Ti_4Fe_2O_{20}$ (n = 6)

Inverse magnetic susceptibility $\chi(T)$
H = 500 G parallel to the layers

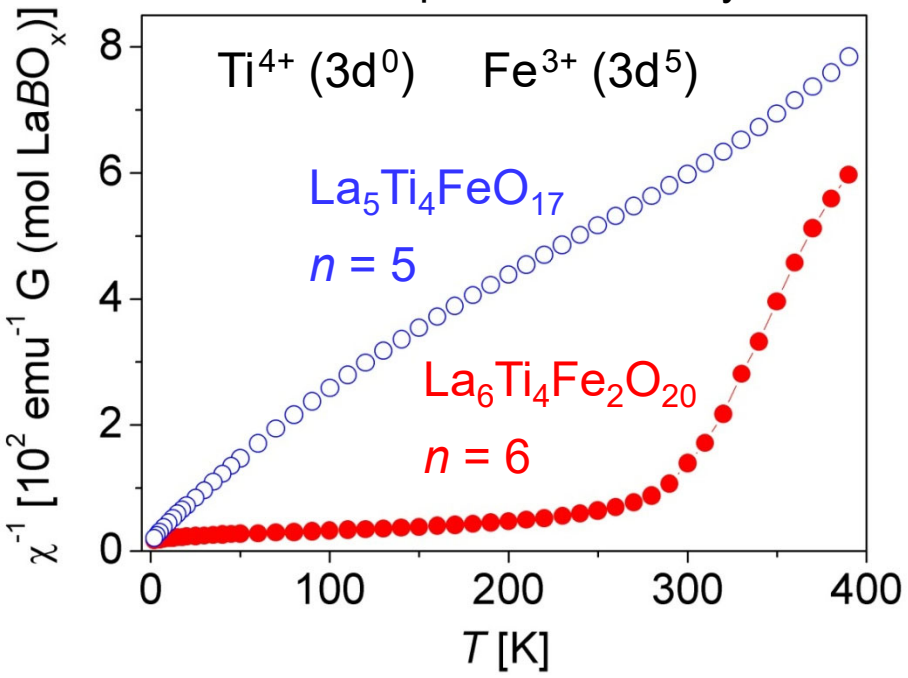

***n* = 5** Curie-Weiss behavior $\chi = C/(T - \Theta)$ for $T > 130$ K and change of slope at $T \approx 300$ K:
$\Theta = -69$ K for $T \leq 290$ K → AFM interaction
$\Theta = +35$ K for $T \geq 330$ K → FM interaction

Fit to Curie-Weiss formula: ***n* = 6**
$\Theta = -196$ K for 50 K $\leq T \leq$ 150 K
$\Theta = +281$ K for 310 K $\leq T \leq$ 380 K

At high temperatures ferromagnetic interaction between Fe^{3+} ions !

→ Ferromagnetic ordering if Fe^{3+} occupancy at central *B* sites can be further increased ?!

Model consideration of magnetic behavior

***n* = 6:** Fe^{3+} occupancy at central *B* sites = 0.71 > 0.59 = percolation limit of 2D square lattice
Above about 300 K: Ferromagnetic interaction between Fe^{3+} ions
Below about 300 K: Formation of ferromagnetic Fe^{3+} clusters with a size of about 52 Fe^{3+} ions and antiferromagnetic interaction between clusters

***n* = 5:** Absence of crossover behavior because Fe^{3+} occupancy at central *B* sites is < 0.59

F. Lichtenberg , A. Herrnberger , K. Wiedenmann , Progress in Solid State Chemistry 36 (2008) 253
A. Wölfel , F. Lichtenberg , S. van Smaalen , Journal of Physics: Condensed Matter 25 (2013) 076003

Reported properties of melt-grown $La_6Ti_4Fe_2O_{20}$ (n = 6) by X. Cheng et al.

Multiferroic properties of the layered perovskite-related oxide $La_6(Ti_{0.67}Fe_{0.33})_6O_{20}$

Xiangyi Cheng et al. , Journal of Materials Chemistry C 3 (2015) 4482 - 4489

https://doi.org/10.1039/C5TC00188A

Abstract: The magnetic and electrical properties of the layered perovskite-related oxide $La_6(Ti_{0.67}Fe_{0.33})_6O_{20}$ are investigated. The material possesses the structure of six ABO_3 layers with iron ions concentrated towards the center of the slabs. The valence state of La, Ti and Fe ions was determined using X-ray photoelectron spectroscopy. The "glassy" magnetic behavior of $La_6(Ti_{0.67}Fe_{0.33})_6O_{20}$ can be understood by the coexistence and competition between two different types of interaction, which originate from both the antiferromagnetic interactions between Fe^{3+} – O – Fe^{3+} in the central layers of the slabs and ferromagnetic coupling that is induced by the oxygen vacancies from the titanium ion enrichment zone at the borders, owing to the nonrandom distribution of magnetic Fe^{3+} ions. The observed ferromagnetism can be ascribed to the ferromagnetic coupling and spin canting of the antiferromagnetic coupling via the Dzyaloshinskii–Moriya interaction. The frequency-dependent behavior of the dielectric loss peak in $La_6(Ti_{0.67}Fe_{0.33})_6O_{20}$ manifests itself as a thermally activated relaxation process. The P – E hysteresis loops and local piezoresponse loops confirm the ferroelectric behavior of $La_6(Ti_{0.67}Fe_{0.33})_6O_{20}$

Reported properties of melt-grown $La_6Ti_4Fe_2O_{20}$ (n = 6) by X. Cheng et al.

Multiferroic properties of the layered perovskite-related oxide $La_6(Ti_{0.67}Fe_{0.33})_6O_{20}$

Xiangyi Cheng et al. , Journal of Materials Chemistry C 3 (2015) 4482 - 4489

https://doi.org/10.1039/C5TC00188A

P(E) curve at 100 Hz and room temperature from dielectric measurements

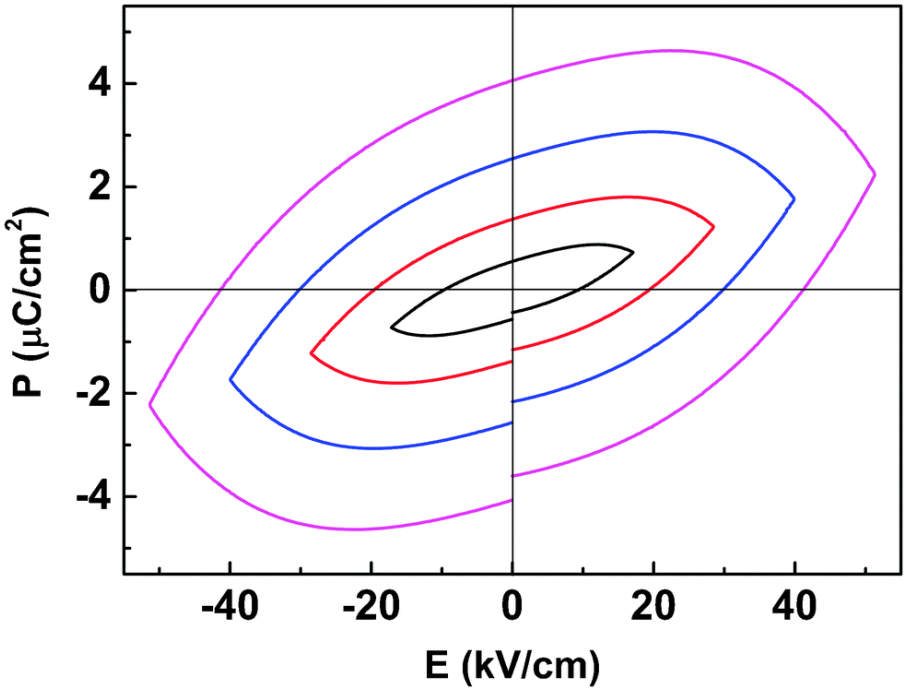

Citation from the paper:

The sample exhibits FE hysteresis loops at room temperature even though the loops are not really saturated, which represents a partial reversal of the polarization. It can be seen that remnant polarization increases gradually with an increase in the electric field, indicating that the electric field provides higher level of driving power, which is responsible for the reversal of ferroelectric domains. In addition, leaky behavior is deduced from the curvature of the polarization maxima at higher fields. The lossy character of the sample may result from the existence of oxygen vacancies

Melt-grown $La_5Ti_4XO_{17}$ and $La_6Ti_4X_2O_{20}$ with X = Fe^{3+} or Mn^{3+}

Ti^{4+} / $3d^0$ Fe^{3+} / $3d^5$ Mn^{3+} / $3d^4$

Pieces of as-grown materials which were grown in synth. air with 15 or 17 mm / h

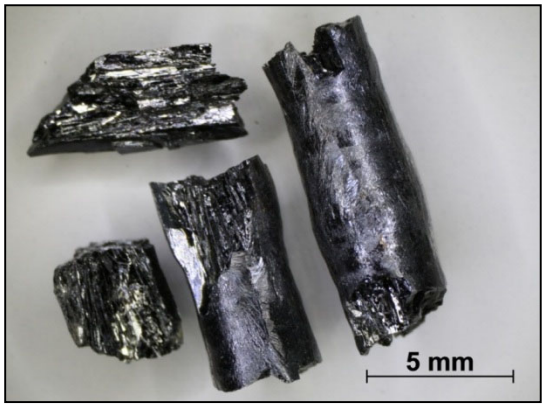

$La_5Ti_4FeO_{17}$

Sample No. 522

Structure type *n* = 5

$La_6Ti_4Fe_2O_{20}$

Sample No. 523

Structure type *n* = 6

$La_5Ti_4MnO_{17}$

Sample No. 541

Structure type *n* = 5

$La_6Ti_4Mn_2O_{20}$ = $LaTi_{0.67}Mn_{0.33}O_{3.33}$

Sample No. 543

Structure type not *n* = 6 but O-deficient *n* = 5

Progress in Solid State Chemistry 36 (2008) 253

Samples prepared at the University of Augsburg - Photos taken at the ETH Zurich

Melt-grown $La_6Ti_4X_2O_{20}$ with X = Mn^{3+} and / or Fe^{3+}

Ti^{4+} / $3d^0$ Fe^{3+} / $3d^5$ Mn^{3+} / $3d^4$

Pieces of as-grown materials which were grown in synth. air with 14, 15 or 17 mm / h

$La_6Ti_4Mn_2O_{20}$ = $LaTi_{0.67}Mn_{0.33}O_{3.33}$

Sample No. 543

Structure type not *n* = 6 but O-deficient *n* = 5

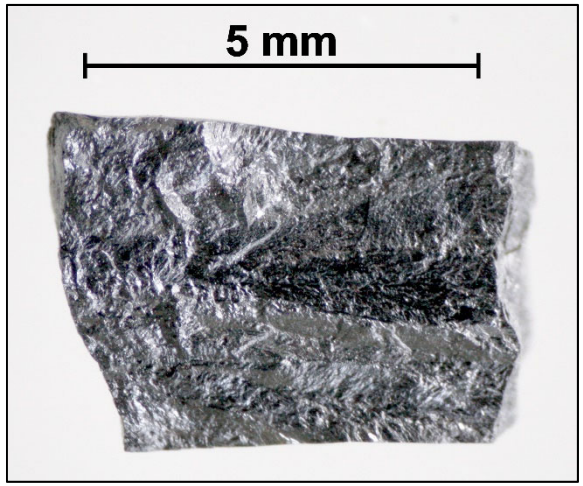

$La_6Ti_4MnFeO_{20}$ = $LaTi_{0.67}Mn_{0.165}Fe_{0.165}O_{3.33}$

Sample No. 730 • Prepared at the ETH Zurich in 2014

Structure type not *n* = 6 but O-deficient *n* = 5

$La_6Ti_4Fe_2O_{20}$ = $LaTi_{0.67}Fe_{0.33}O_{3.33}$

Sample No. 523

Structure type *n* = 6

Progress in Solid State Chemistry 36 (2008) 253
Samples prepared at the University of Augsburg
Photos taken at the ETH Zurich

5.3 Materials in the context of potential multiferroic Carpy-Galy phases $A_nB_nO_{3n+2} = ABO_x$

5.3.2 Melt-grown $n = 6$ type $Ln_6Ti_4Fe_2O_{20}$ (Ln = Ce, Pr, Nd, Sm, $Sm_{0.9}Eu_{0.1}$, Eu) and $Ca_6Nb_5FeO_{20}$ prepared at the ETH Zurich ...

Melt-grown $n = 6$ type compositions $Ln_6Ti_4Fe_2O_{20}$

The lanthanides *Ln* from La to Eu:

La	Ce	Pr	Nd	Pm	Sm	Eu
57	58	59	60	61	62	63

In 2014 - 2016 and 2018 polycrystalline sintered rods with composition

- $Ce_6Ti_4Fe_2O_{20}$
- $Pr_6Ti_4Fe_2O_{20 + y}$
- $Nd_6Ti_4Fe_2O_{20}$
- $Sm_6Ti_4Fe_2O_{20}$
- $Sm_{5.4}Eu_{0.6}Ti_4Fe_2O_{20}$
- $Eu_6Ti_4Fe_2O_{20}$
- $Ca_6Nb_5FeO_{20}$

Nb^{5+} / $4d^0$	Eu^{3+} / $4f^6$
Fe^{3+} / $3d^5$	Sm^{3+} / $4f^5$
Ti^{4+} / $3d^0$	Nd^{3+} / $4f^3$
	Pr^{3+} / $4f^2$

were processed at the ETH Zurich by floating zone melting in a Cyberstar mirror furnace. Starting materials (powder) were CeO_2 , $Pr_6O_{11} = PrO_{1.83}$ or PrO_x with thermogravimetriically determined oxygen content x , Nd_2O_3 , Sm_2O_3 , Eu_2O_3 , TiO , TiO_2 , Fe_2O_3 , $CaCO_3$, and Nb_2O_5 with a purity $\geq$ 99.9 %. The oxygen content of Fe_2O_3 was verified by a thermogravimetric reduction to Fe as described on page 62 (Fig. 41) in https://dx.doi.org/10.3929/ethz-b-000220998 . To remove moisture from the starting materials – apart from PrO_x and TiO – they were heated at appropriate temperatures under air and subsequently stored in a desiccator.

One of several unsuccessful attempts to prepare $n = 6$ type $Ce_6Ti_4Fe_2O_{20}$

Most lanthanide oxides are commercially available as Ln_2O_3 (Ln^{3+}) and therefore one can try to prepare $Ln_6Ti_4Fe_2O_{20}$ in the following way under air:

$$3\ Ln_2O_3 + 4\ TiO_2 + Fe_2O_3 \rightarrow Ln_6Ti_4Fe_2O_{20}$$

However, cerium oxide is offered only as CeO_2 (Ce^{4+}) and it is relatively stable, even at high temperatures in the presence of other elements. One of several potential approaches to synthesize $n = 6$ type $Ce_6Ti_4Fe_2O_{20}$ is the folllowing:

$$6\ CeO_2 + 3\ TiO + TiO_2 + Fe_2O_3 \xrightarrow[\text{rods under argon and perform floating zone melting under argon}]{\text{Sinter as-pressed}} Ce_6Ti_4Fe_2O_{20}$$

The oxygen content of TiO and that of the prepared powder mixture
$6\ CeO_2 + 3\ TiO + TiO_2 + Fe_2O_3 = Ce_6Ti_4Fe_2O_{20}$
was verified thermogravimetrically.

One of several unsuccessful attempts to prepare *n* = 6 type $Ce_6Ti_4Fe_2O_{20}$

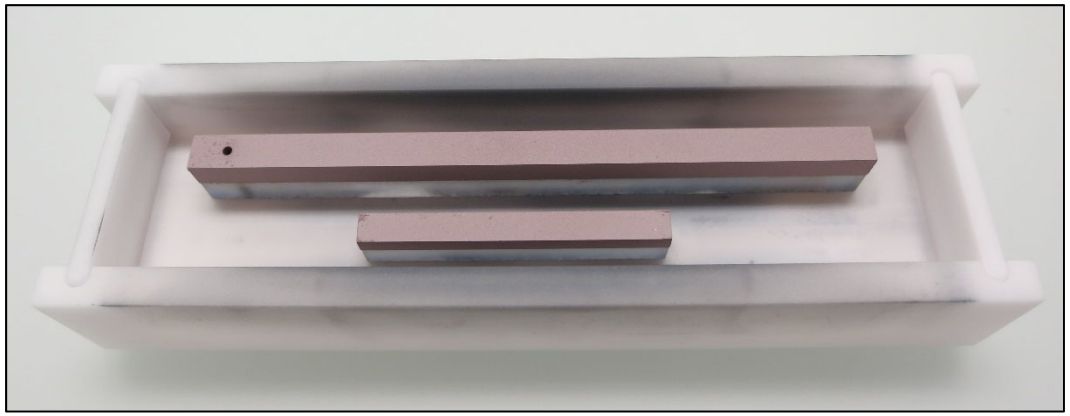

As-pressed rods
with composition
6 CeO_2 + 3 TiO + TiO_2 + Fe_2O_3
on their lower punch made of sapphire in an alumina box. The length of the long rod is 9 cm

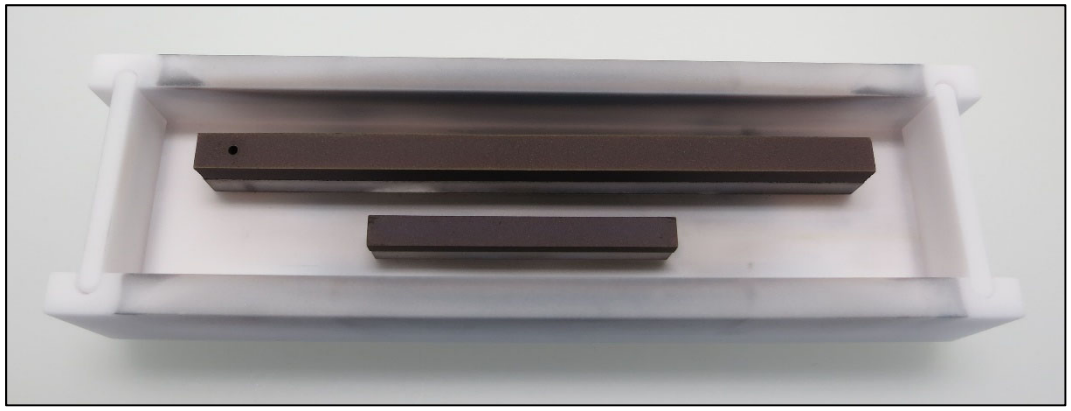

Rods after sintering for 2 h at 1200 °C under argon in the GERO tube furnace

Run / Sample No. 831

One of several unsuccessful attempts to prepare *n* = 6 type $Ce_6Ti_4Fe_2O_{20}$

Log-linear plot of recorded data of a tube furnace run on 31 October and 1 November 2018 with rods No. 831 on lower punches in an alumina box covered with a Nb sheet. Before starting the run: 2 × evacuated (3.5×10^{-3} / 2.0×10^{-3} mbar at the gas outlet after 6 / 6 min) and flushed with Ar. Gas (Ar) flow rate 400 sccm (24 L / h). Heating and cooling rate 250 °C / h (set values). Dwell time 2 h at 1200 °C . The O_2 content of Ar at the gas outlet becomes zero at elevated temperatures because the Nb sheet getters oxygen. Ar purity 6.0

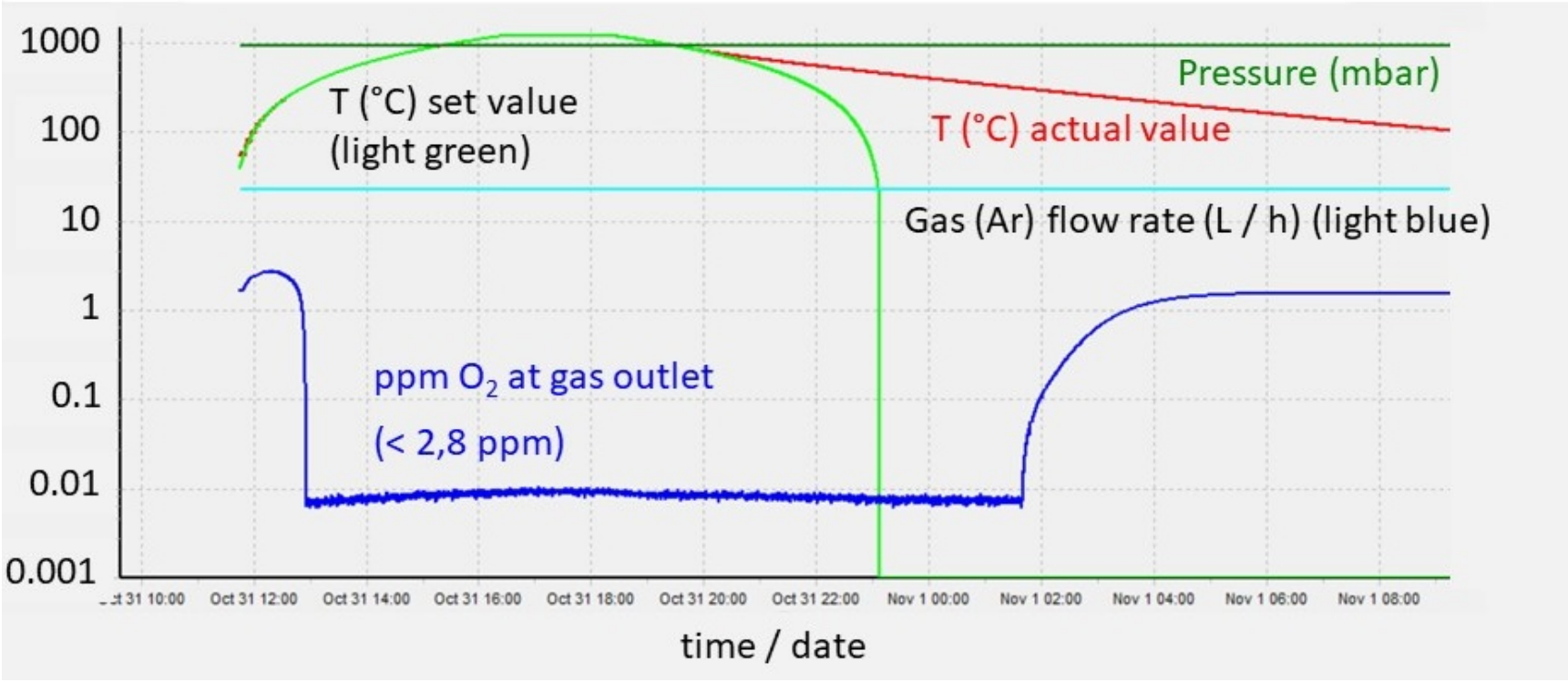

One of several unsuccessful attempts to prepare *n* = 6 type $Ce_6Ti_4Fe_2O_{20}$

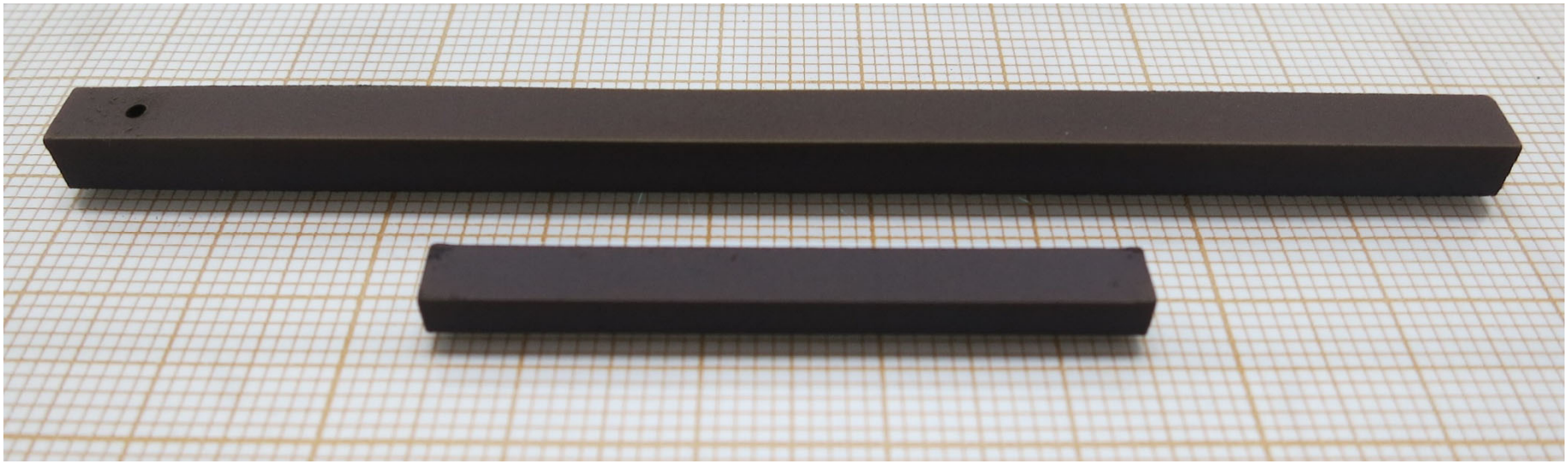

Sintered rods with composition 6 CeO_2 + 3 TiO + TiO_2 + Fe_2O_3 = $Ce_6Ti_4Fe_2O_{20}$

Run / Sample No. 831

Prepared at the ETH Zurich in 2018

One of several unsuccessful attempts to prepare *n* = 6 type $Ce_6Ti_4Fe_2O_{20}$

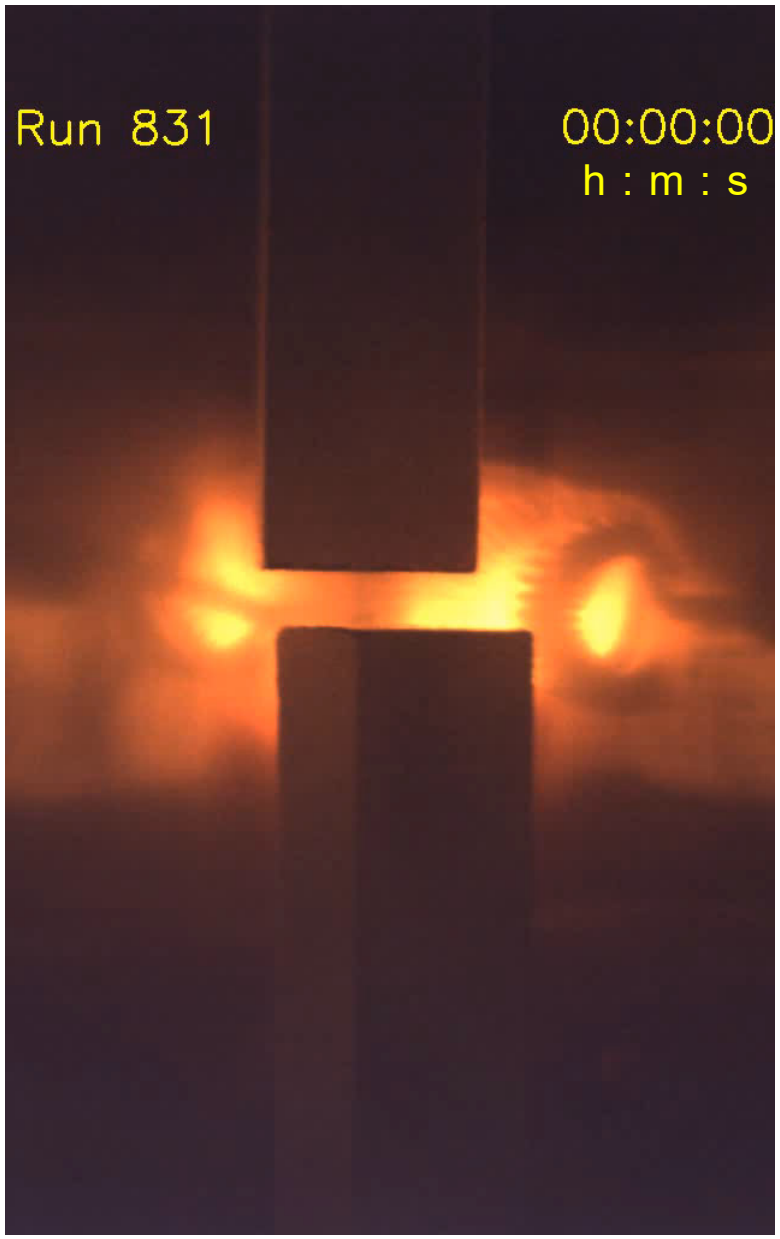

Run / Sample No. 831

Fast mode video (~ 2 min) of the overall run (~ 4 h) in the Cyberstar mirror furnace. The video is only running in the ppsx type version of this publication, see page 2

The composition of the polycrystalline sintered rods is $Ce_6Ti_4Fe_2O_{20}$ and the floating zone melting is performed under flowing Ar

Lamp power to maintain the molten zone: 2 × (404 - 325) W

Speed of the lower shaft and seed rod (crystal growth speed): 14 mm / h

The gas outlet is equipped with a oxygen analyzer ZIROX SGM7 and at the beginning of the run the oxygen content of argon was about 1 ppm. Subsequently it increased stepwise to 25 ppm, i.e. the solid and / or molten material did release somewhat oxygen

One of several unsuccessful attempts to prepare *n* = 6 type $Ce_6Ti_4Fe_2O_{20}$

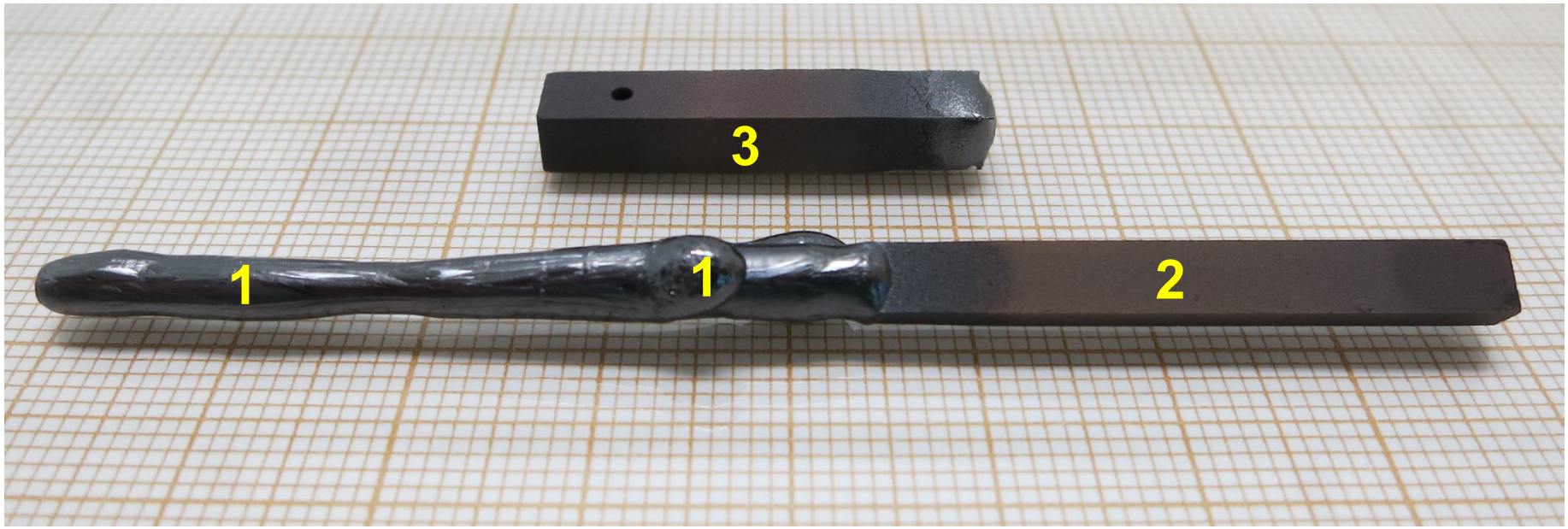

45 mm long as-grown crystalline material (1), polycrystalline see rod (2), and remaining part of the polycrystalline feed rod (3)

Run / Sample No. 831

Prepared at the ETH Zurich in 2018

One of several unsuccessful attempts to prepare *n* = 6 type $Ce_6Ti_4Fe_2O_{20}$

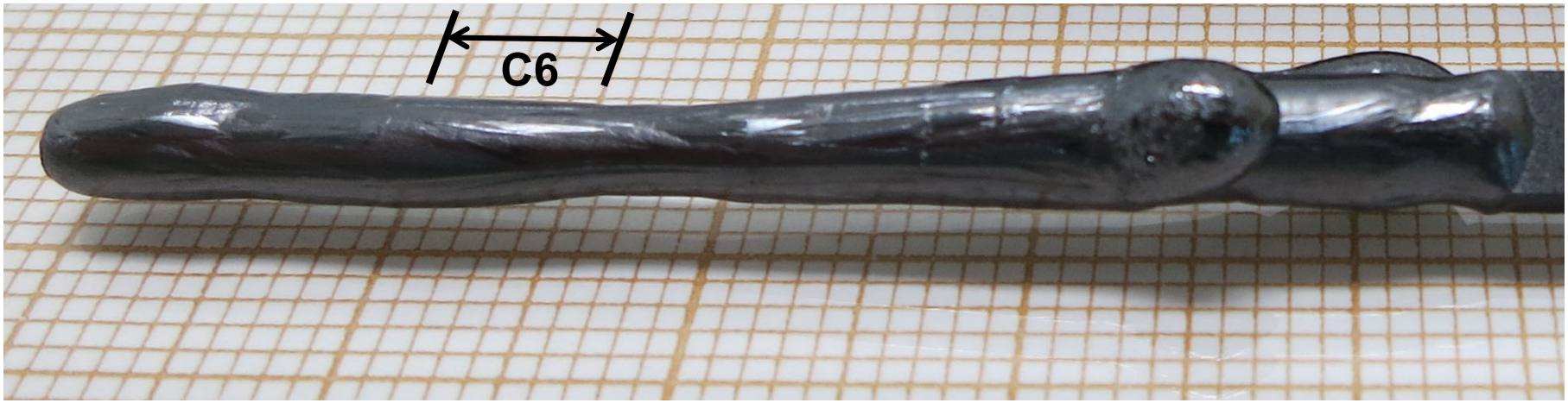

45 mm long as-grown crystalline material Sample No. 831

A crystalline piece from section C6.

Powder x-ray diffraction of pulverized crystalline pieces from section C6 indicates the presence of a $Ce(Ti,Fe)O_3$ perovskite type phase, a *n* = 5 type phase $Ce_5Ti_5O_{17}$ which is reported in Progress in Solid State Chemistry 36 (2008) 253, and another unidentified phases. The presence of several phases in this material is also suggested by the non-constant lamp power $2 \times (404 - 325)$ W to maintain the molten zone during the mirror furnace run. This indicates an incongruent melting and solidification and therefore a multiphase material.

Synthesis of melt-grown $n = 6$ type $Pr_6Ti_4Fe_2O_{20}$ and $Nd_6Ti_4Fe_2O_{20}$

Most lanthanide oxides such as Nd_2O_3 are commercially available as Ln_2O_3 (Ln^{3+}) and therefore one can try to prepare $Ln_6Ti_4Fe_2O_{20}$ in the following way under air:

$$3\ Ln_2O_3 + 4\ TiO_2 + Fe_2O_3 \rightarrow Ln_6Ti_4Fe_2O_{20}$$

However, praseodymium oxide is offered only as $Pr_6O_{11} = PrO_{1.83}$ and it is advisable to study its actual composition or oxygen content by thermogravimetry. At elevated temperatures and in the presence of other elements Pr_6O_{11} releases oxygen and all Pr ions adopt the valence state Pr^{3+}

Thermogravimeteric study of Pr_6O_{11} = $PrO_{1.83}$ or PrO_x

Pr_6O_{11} = $PrO_{1.83}$ from various suppliers was analyzed thermogravimetrically, i.e. they were reduced under flowing argon plus hydrogen towards Pr_2O_3 = $PrO_{1.50}$. These studies did reveal a significant deviation from their assumed composition. If the difference between the assumed and actual composition is expressed in terms of an assumed formula PrO_x , then the investigated powder correspond to x = 2 and x = 2.07. Their actual composition is, however, most probably something like $PrO_xH_yC_z$. Nevertheless, the results from thermogravimetric analysis enable a correct stoichiometric calculation by taking into account the weight difference between the assumed and actual composition.

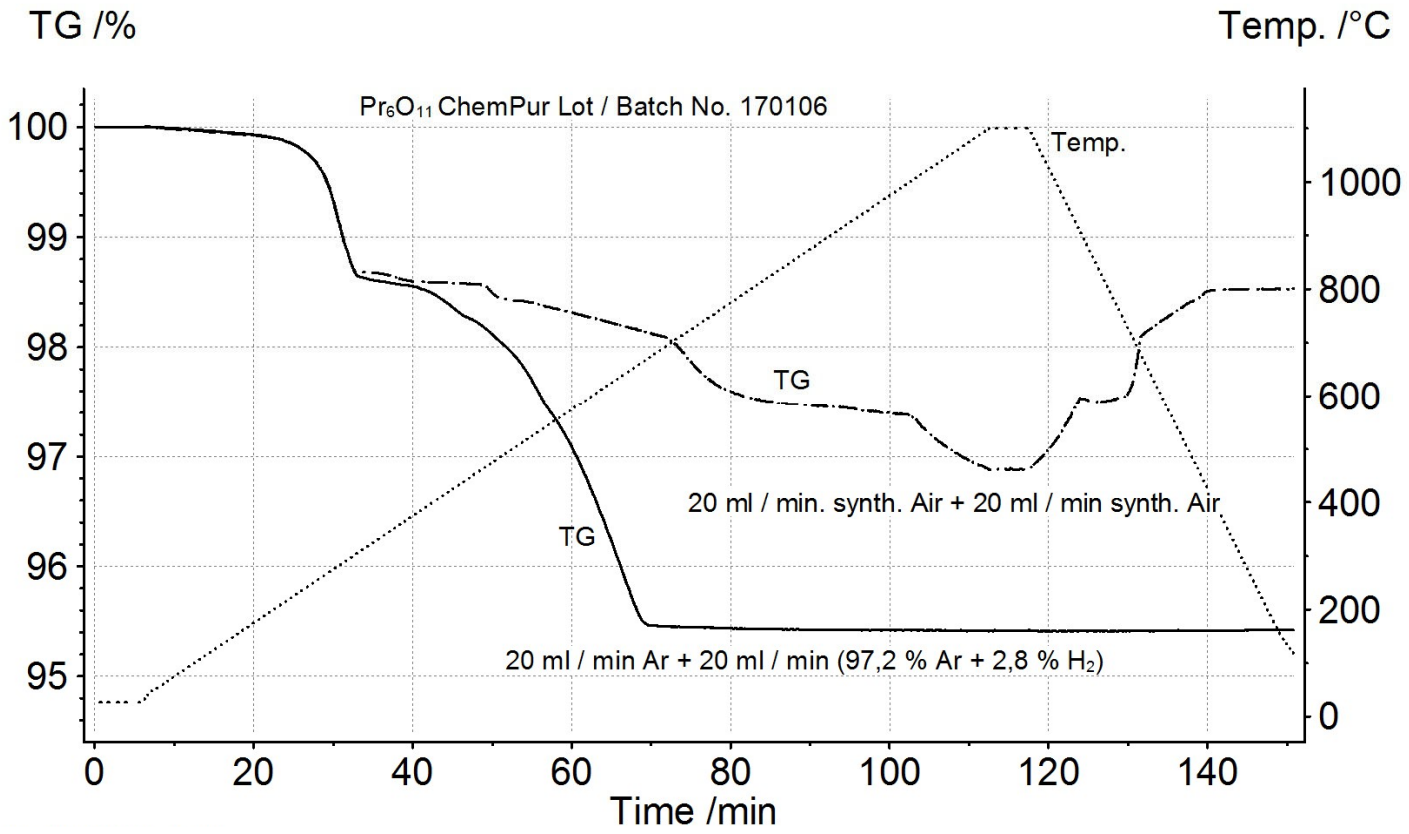

Melt-grown $n = 6$ type materials $Pr_6Ti_4Fe_2O_{20}$ and $Nd_6Ti_4Fe_2O_{20}$

Nd^{3+} / $4f^3$

Pr^{3+} / $4f^2$

Fe^{3+} / $3d^5$

Ti^{4+} / $3d^0$

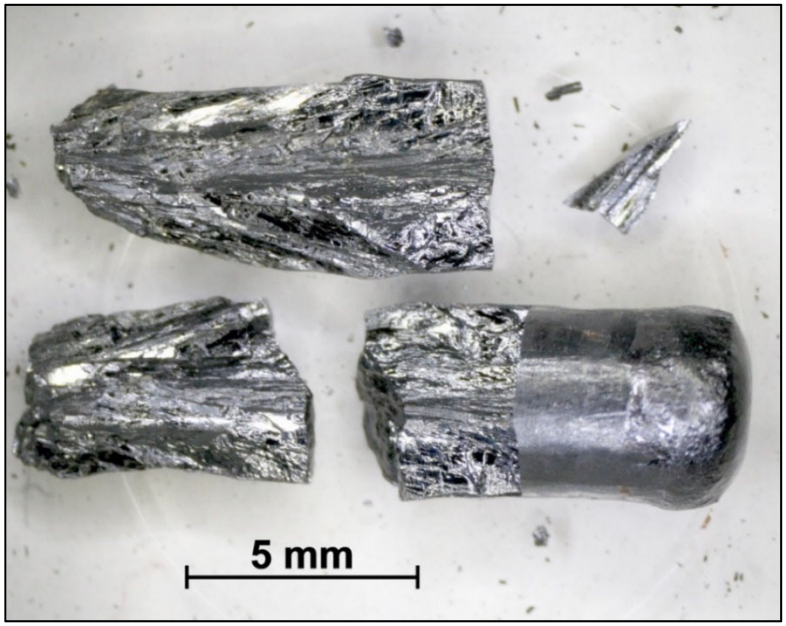

$Pr_6Ti_4Fe_2O_{20}$ Sample No. 727

$Nd_6Ti_4Fe_2O_{20}$ Sample No. 731

Prepared at the ETH Zurich in 2014 • Grown with 10 - 14 mm / h under flowing 90 % Ar + 10 % O_2 • Powder x-ray diffraction indicates in both cases a single phase $n = 6$ type material

Both mirror furnace runs were overall relatively difficult because the molten zone did often break down. Therefore after the normal run a **reverse run** was performed, i.e. the crystalline material was molten again and converted via a molten zone into a new crystalline material which grew onto the bottom end of the remaining part of the feed rod

Melt-grown *n* = 6 type materials $Sm_6Ti_4Fe_2O_{20}$ and $Sm_{5.4}Eu_{0.6}Ti_4Fe_2O_{20}$

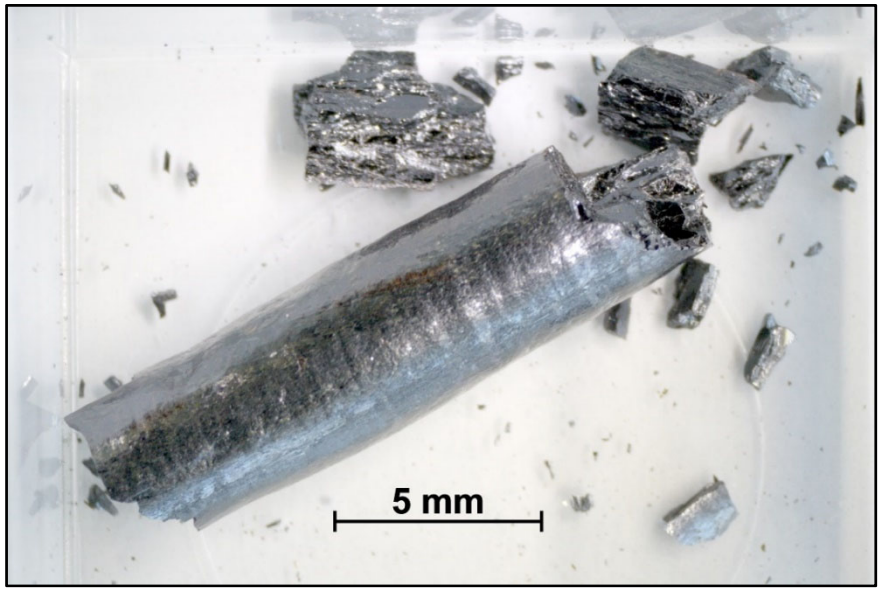

Eu^{3+} / $4f^6$

Sm^{3+} / $4f^5$

Fe^{3+} / $3d^5$

Ti^{4+} / $3d^0$

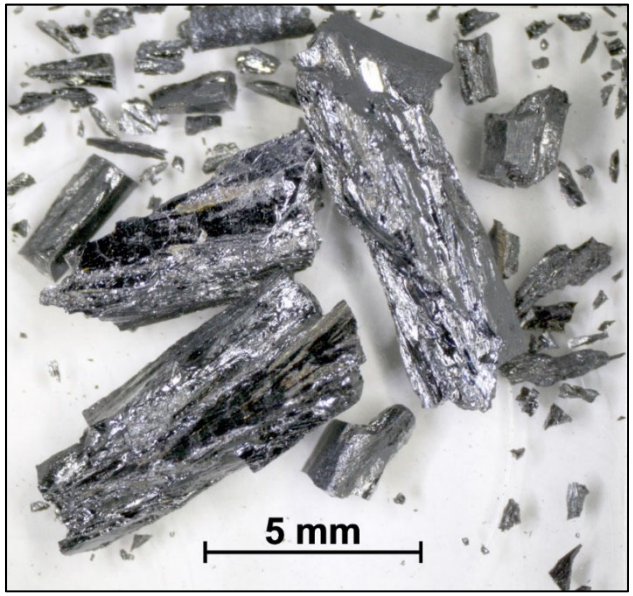

$Sm_6Ti_4Fe_2O_{20}$
Sample No. 718
Prepared at the ETH Zurich in 2014
Grown with 14 mm / h under
flowing synthetic air

$Sm_{5.4}Eu_{0.6}Ti_4Fe_2O_{20}$
Sample No. 752
Prepared at the ETH Zurich in 2015
Grown with 10 mm / h under
flowing 90 % Ar + 10 % O_2

Powder x-ray diffraction indicates in both cases an *n* = 6 type material.
In both cases there is 1 unindexed peak at $2\Theta = 32.75°$ with 2 % relative intensity. This suggests the presence of small amounts of $(Sm,Eu)FeO_3$ because its highest intensity peak is located at $2\Theta \approx 32.7°$

n = 6 type $Sm_{5.4}Eu_{0.6}Ti_4Fe_2O_{20}$ • Melt-grown under normal and high pressure

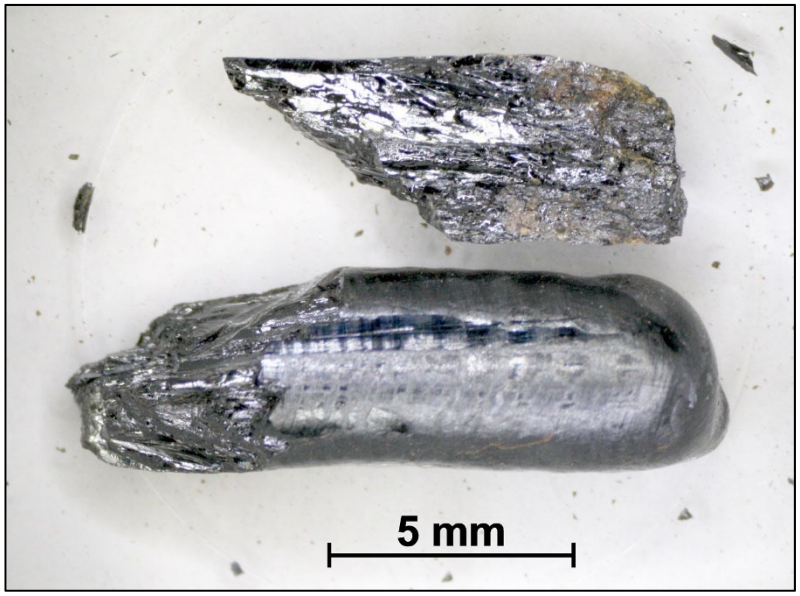

$Sm_{5.4}Eu_{0.6}Ti_4Fe_2O_{20}$
Sample No. 753
Prepared at the ETH Zurich in 2015
Grown with 10 mm / h under flowing
90 % Ar + 10 % O_2 with high pressure 9 - 10 bar

Eu^{3+} / $4f^6$

Sm^{3+} / $4f^5$

Fe^{3+} / $3d^5$

Ti^{4+} / $3d^0$

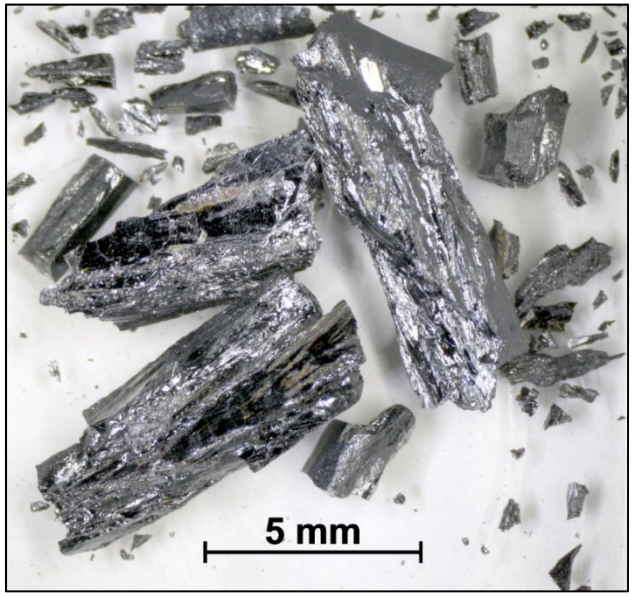

$Sm_{5.4}Eu_{0.6}Ti_4Fe_2O_{20}$
Sample No. 752
Prepared at the ETH Zurich in 2015
Grown with 10 mm / h under
flowing 90 % Ar + 10 % O_2

Powder x-ray diffraction indicates in both cases an n = 6 type material

All observed peaks fit to an n = 6 type structure. This indicates that the synthesis under high pressure has suppressed the formation of a small amount of $(Sm,Eu)FeO_3$

1 unindexed peak at $2\Theta = 32.75°$ with 2 % relative intensity. This suggests the presence of a small amount of $(Sm,Eu)FeO_3$ because its highest intensity peak is located at $2\Theta \approx 32.7°$

Melt-grown materials with n = 6 type composition $Eu_6Ti_4Fe_2O_{20}$

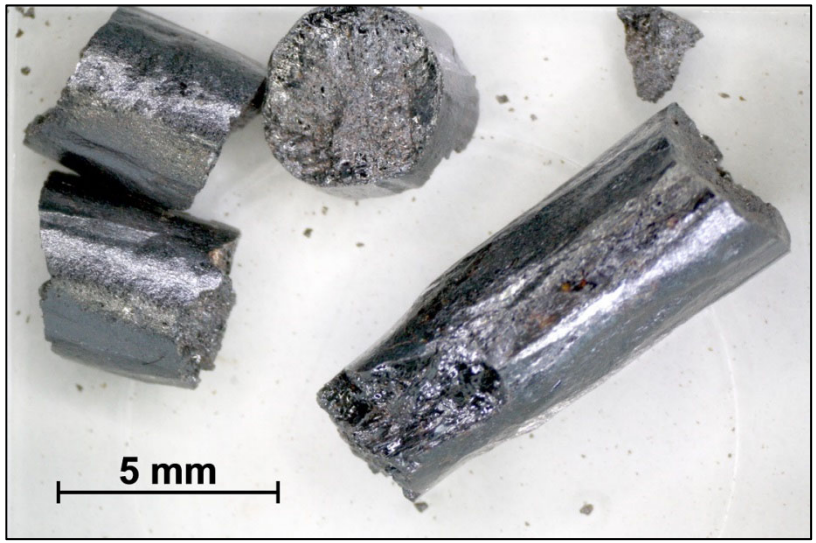

Pieces from sample No. 720 grown with 8 mm / h under flowing synthetic air and normal pressure. Powder x-ray diffraction indicates a multiphase material which consists mainly of a cubic pyrochlore $Eu_2Ti_2O_7$ and an orthorhombic perovskite $EuFeO_3$

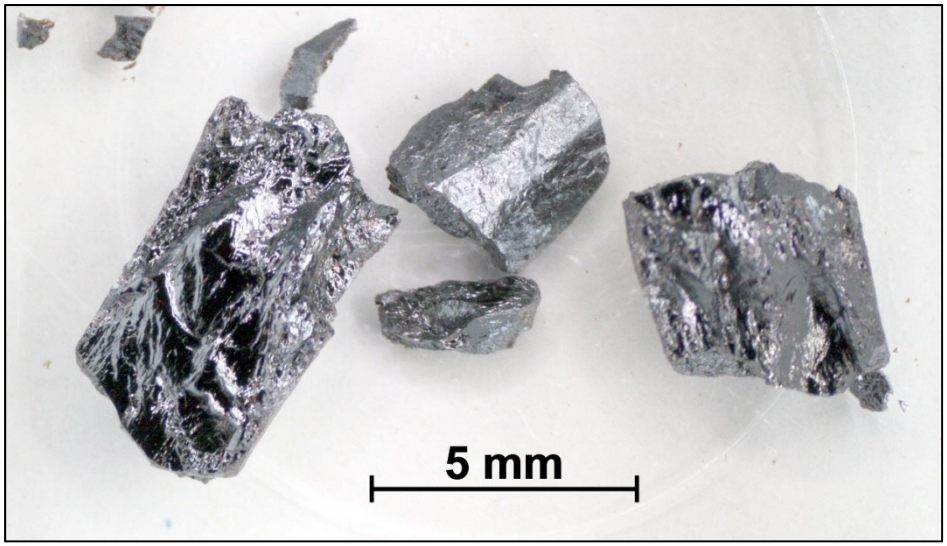

Pieces from sample No. 721 grown with 8 mm / h under flowing synthetic air under a high pressure of 9.2 - 9.7 bar. Powder x-ray diffraction indicates a multiphase material but most phases could not be identified. The amount of pyrochlore $Eu_2Ti_2O_7$ seems to be smaller than that in sample No. 720

In both cases no indications for a phase of the type n = 6 of $A_nB_nO_{3n+2}$

Prepared at the ETH Zurich in 2014

Stability limit of melt-grown $n = 6$ type $Sm_{6-y}Eu_yTi_4Fe_2O_{20}$

The lanthanides *Ln* from La to Eu:

La	Ce	Pr	Nd	Pm	Sm	Eu
57	58	59	60	61	62	63

The results which are shown on the two previous pages indicate that the $n = 6$ stability limit $y = y_{max}$ is located in the range $0.6 \leq y_{max} < 6$

For comparison: The stability range of the $n = 4$ type ferroelectric insulators $Ln_4Ti_4O_{14} = Ln_2Ti_2O_7 = LnTiO_{3.5}$ ranges from *Ln* = La to *Ln* = Nd. $SmTiO_{3.5}$ and $EuTiO_{3.5}$ crystallize in a cubic pyrochlore structure. However, the conducting material $SmTiO_{3.37}$ adopts a $n = 5$ type structure

Progress in Solid State Chemistry 36 (2008) 253 and references therein

Melt-grown $n = 6$ type $Ca_6Nb_5FeO_{20}$ Nb^{5+} / $4d^0$ Fe^{3+} / $3d^5$

Run / Sample No.		766	777	779
Growth speed (mm / h)		14	12	6
Grown under flowing		90 % Ar + 10 % O_2		
Powder x-ray diffraction and results from lattice parameter refinement of a monoclinic P type cell FOM = Figure of merit of refinement	*a* (Å)	7.68	7.68	7.68
	b (Å)	5.49	5.48	5.47
	c (Å)	37.68	37.97	37.96
	β (°)	95.7	96.0	96.0
	V (Å^3)	1579	1589	1586
	FOM	3.2	3.8	3.2
	Remarks	67 indexed peaks $\lvert 2\Theta_{calc} - 2\Theta_{obs} \rvert \leq 0.098°$ 4 unindexed peaks with rel. intensity < 2 %	74 indexed peaks $\lvert 2\Theta_{calc} - 2\Theta_{obs} \rvert \leq 0.084°$ 2 unindexed peaks with rel. intensity 1 %	72 indexed peaks $\lvert 2\Theta_{calc} - 2\Theta_{obs} \rvert \leq 0.091°$ 2 unindexed peaks with rel. intensity < 2 %

Prepared at the ETH Zurich in 2016

Melt-grown $n = 6$ type $Ca_6Nb_5FeO_{20}$ Nb^{5+} / $4d^0$ Fe^{3+} / $3d^5$

Run / Sample No.		766	777	779
Growth speed (mm / h)		14	12	6
Grown under flowing		90 % Ar + 10 % O_2		
Powder x-ray diffraction and results from lattice parameter refinement of a monoclinic P type cell FOM = Figure of merit of refinement	*a* (Å)	7.68	7.68	7.68
	b (Å)	5.49	5.48	5.47
	c (Å)	37.68	37.97	37.96
	β (°)	95.7	96.0	96.0
	V (Å^3)	1579	1589	1586
	FOM	3.2	3.8	3.2
	Remarks	67 indexed peaks $\lvert 2\Theta_{calc} - 2\Theta_{obs} \rvert \leq 0.098°$ 4 unindexed peaks with rel. intensity < 2 %	74 indexed peaks $\lvert 2\Theta_{calc} - 2\Theta_{obs} \rvert \leq 0.084°$ 2 unindexed peaks with rel. intensity 1 %	Available is an Excel file with the powder-x-ray diffraction data. It is provided via the link which is specified on page 2

Prepared at the ETH Zurich in 2016

Melt-grown $n = 6$ type $Ca_6Nb_5FeO_{20}$ $Nb^{5+} / 4d^0$ $Fe^{3+} / 3d^5$

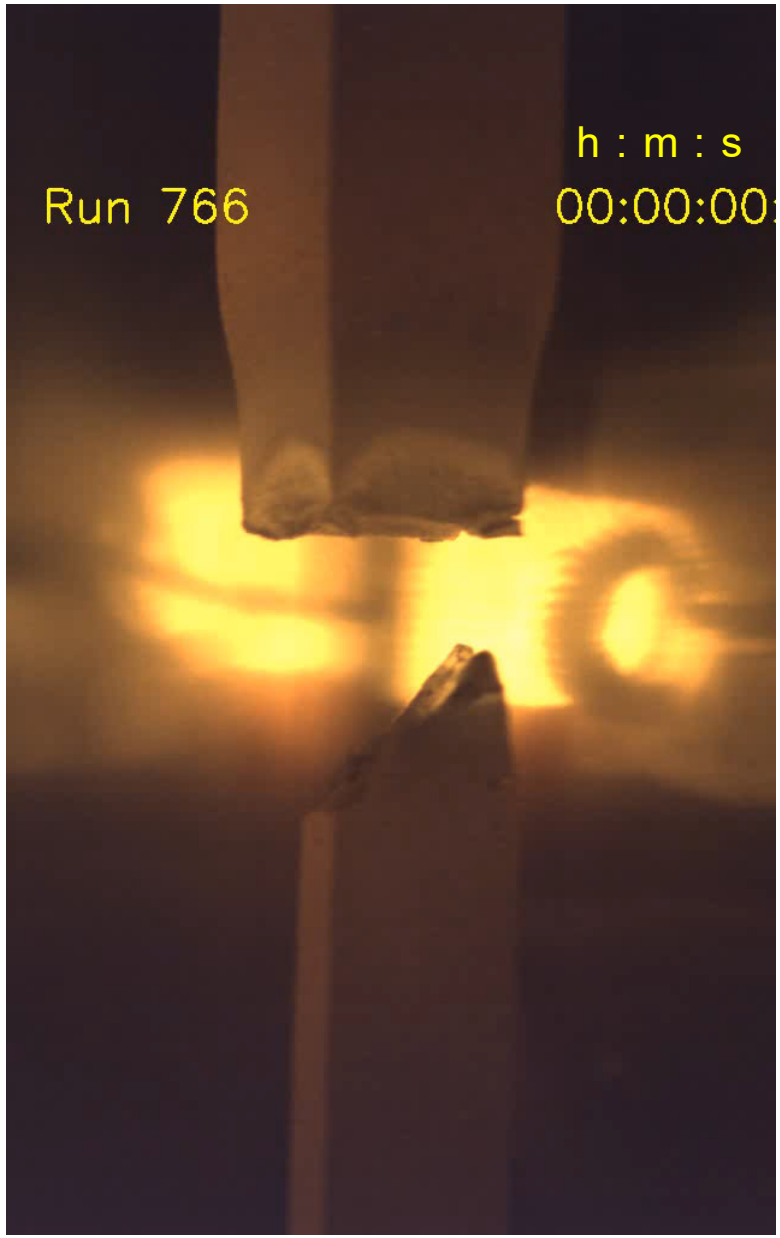

Run / Sample No. 766

Fast mode video (~ 4 min) of the overall run (~ 4 h) in the Cyberstar mirror furnace. The video is only running in the ppsx type version of this publication, see page 2

The composition of the polycrystalline sintered rods is $Ca_6Nb_5FeO_{20}$ and the floating zone melting is performed under flowing 90 % Ar + 10 % O_2

Lamp power to maintain the molten zone: 2 × 327 W

Speed of the lower shaft and seed rod (crystal growth speed): 14 mm / h

At the video time ~ 03 : 00 : 00 an exceptionally large gas-liquid region arises in the molten zone and persists for an unusually long time

Melt-grown *n* = 6 type $Ca_6Nb_5FeO_{20}$ Nb^{5+} / $4d^0$ Fe^{3+} / $3d^5$

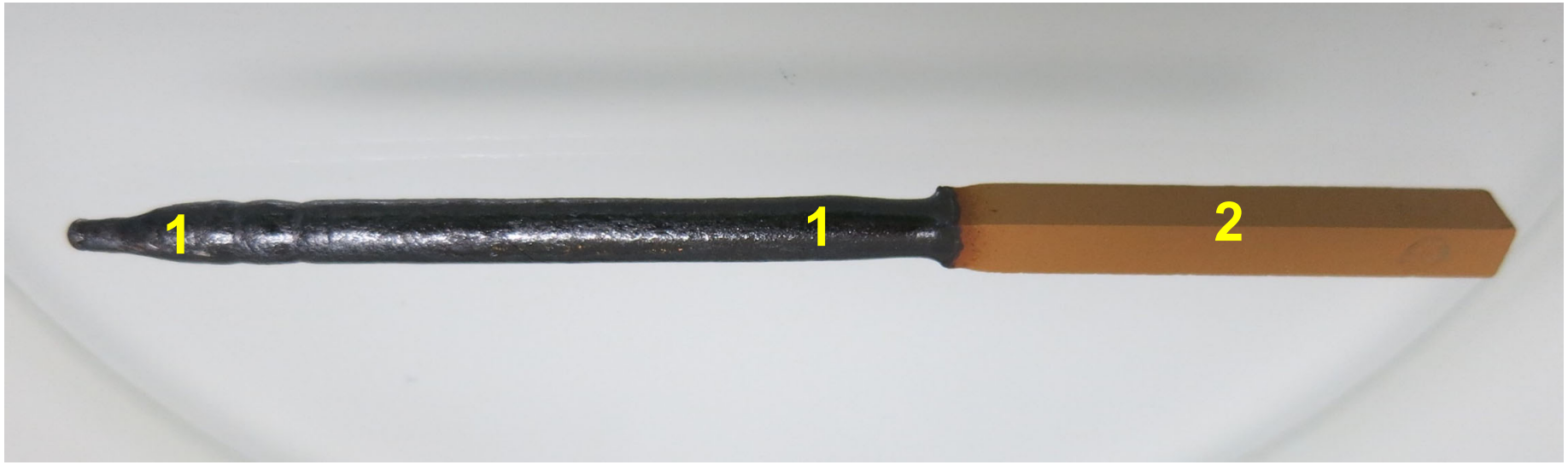

5 cm long as-grown crystalline material (1) plus polycrystalline seed rod (2)

Run or sample No. 766

Grown with 14 mm / h under 90 % Ar + 10 % O_2

Prepared at the ETH Zurich in 2016

Melt-grown $n = 6$ type $Ca_6Nb_5FeO_{20}$ $Nb^{5+} / 4d^0$ $Fe^{3+} / 3d^5$

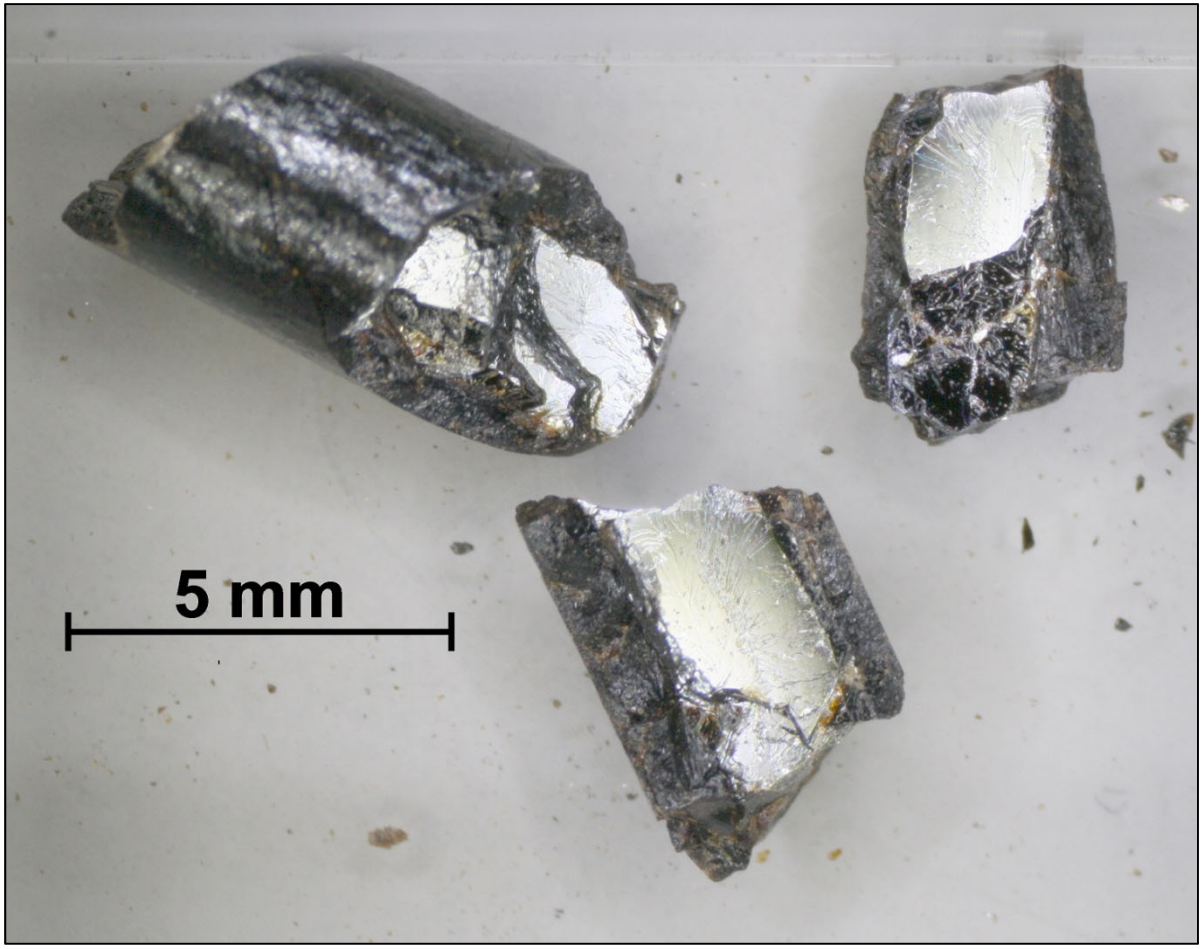

Crystalline pieces from the as-grown sample No. 766

Grown with 14 mm / h under 90 % Ar + 10 % O_2

Powder XRD:

Some peaks display an unusual shape

4 unindexed peaks with relative intensity < 2 %

Melt-grown *n* = 6 type $Ca_6Nb_5FeO_{20}$ Nb^{5+} / $4d^0$ Fe^{3+} / $3d^5$

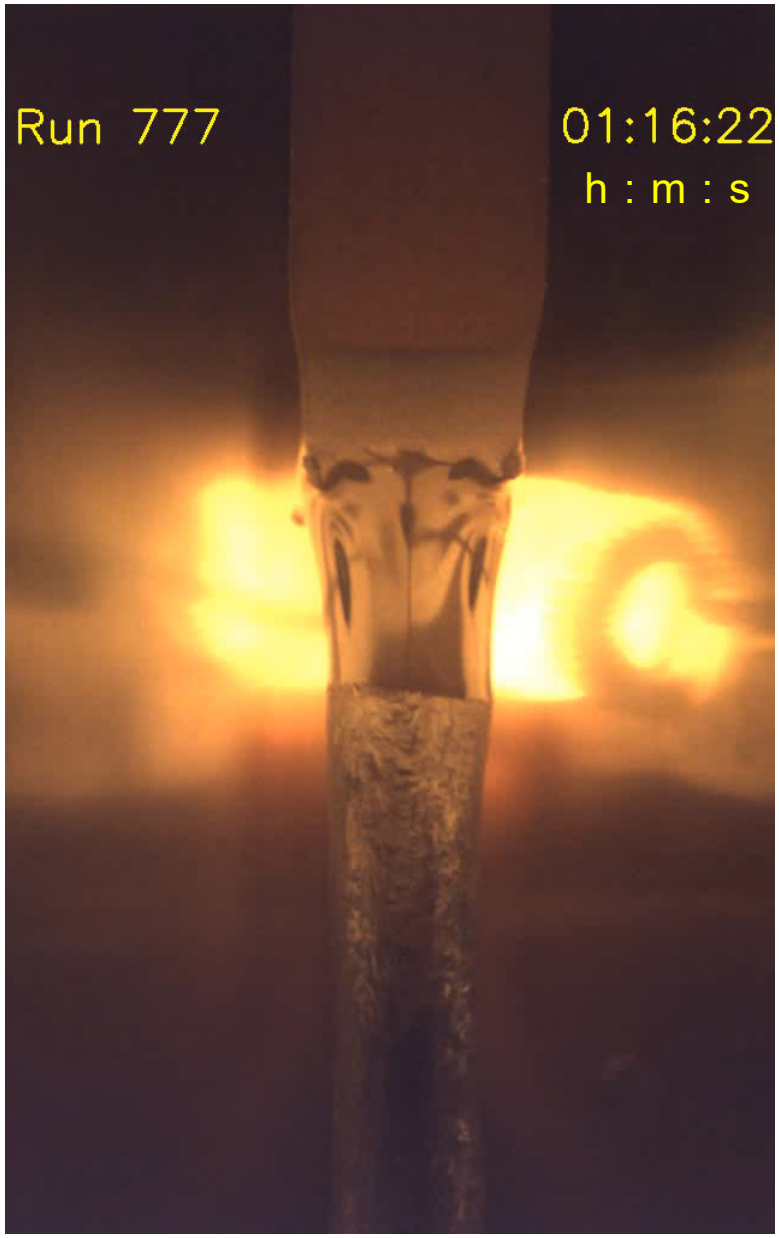

Run / Sample No. 777

Real time video (~ 1 min) of a short section of the overall run in the Cyberstar mirror furnace. The video is only running in the ppsx type version of this publication, see page 2

The composition of the polycrystalline sintered rods is $Ca_6Nb_5FeO_{20}$ and the floating zone melting is performed under flowing 90 % Ar + 10 % O_2

Lamp power to maintain the molten zone: about 2 × 310 W

Speed of the lower shaft and seed rod (crystal growth speed): 12 mm / h

During this run the upper feed rod was not rotated

Melt-grown *n* = 6 type $Ca_6Nb_5FeO_{20}$ Nb^{5+} / $4d^0$ Fe^{3+} / $3d^5$

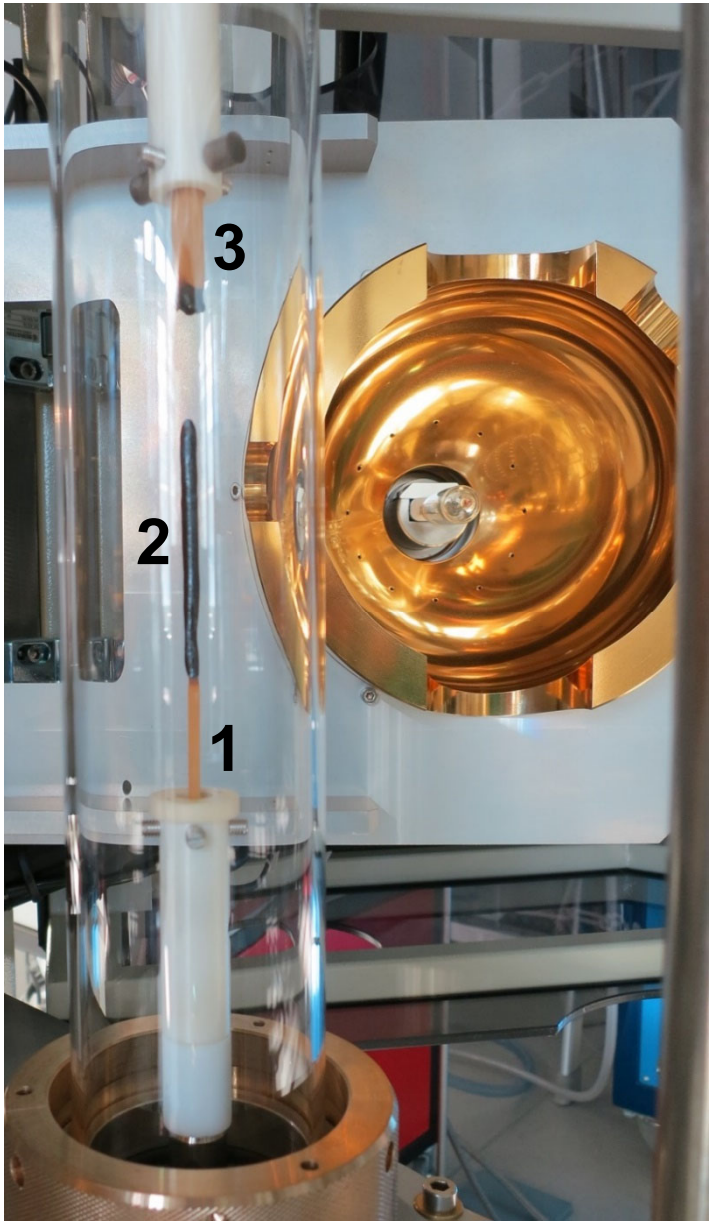

Run / Sample 777

Visible within the quartz glass tube of the Cyberstar mirror furnace after the run:

3 Remaining part of the polycrystalline feed rod

2 As-grown crystalline material

1 Polycrystalline seed rod

Melt-grown *n* = 6 type $Ca_6Nb_5FeO_{20}$ Nb^{5+} / $4d^0$ Fe^{3+} / $3d^5$

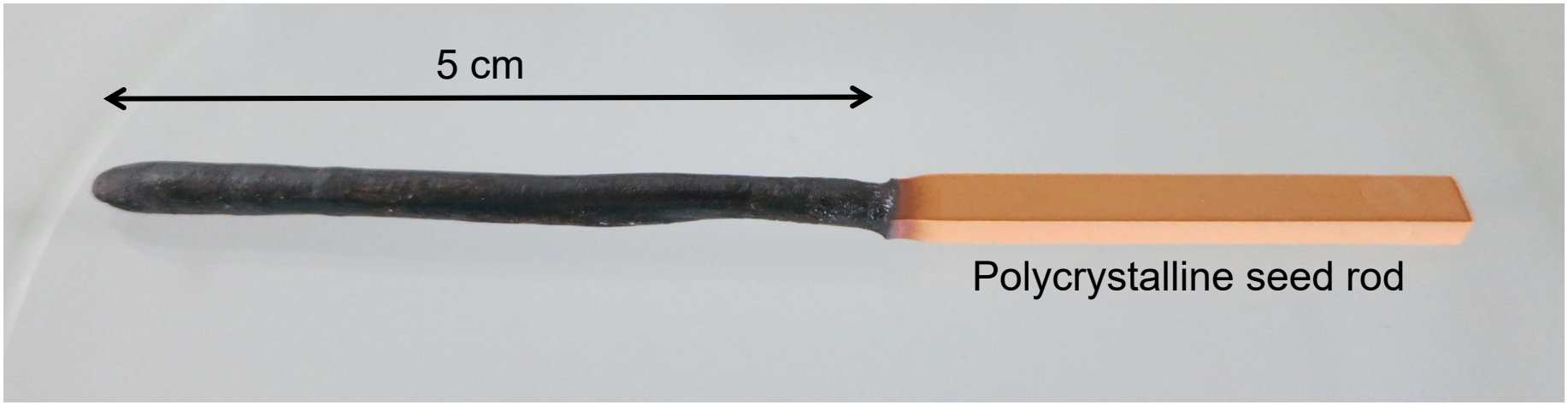

5 cm long as-grown crystalline material plus polycrystalline seed rod

Sample No. 777

Grown with 12 mm / h under 90 % Ar + 10 % O_2

Prepared at the ETH Zurich in 2016

Melt-grown *n* = 6 type $Ca_6Nb_5FeO_{20}$ Nb^{5+} / $4d^0$ Fe^{3+} / $3d^5$

Run / Sample No. 779

Fast mode video (~ 2 min) of the overall run (~ 5 h) in the Cyberstar mirror furnace. The video is only running in the ppsx type version of this publication, see page 2

The composition of the polycrystalline sintered rods is $Ca_6Nb_5FeO_{20}$ and the floating zone melting is performed under flowing 90 % Ar + 10 % O_2

Lamp power to maintain the molten zone: 2 × 318 W

Speed of the lower shaft and seed rod (crystal growth speed): 6 mm / h

Melt-grown *n* = 6 type $Ca_6Nb_5FeO_{20}$ Nb^{5+} / $4d^0$ Fe^{3+} / $3d^5$

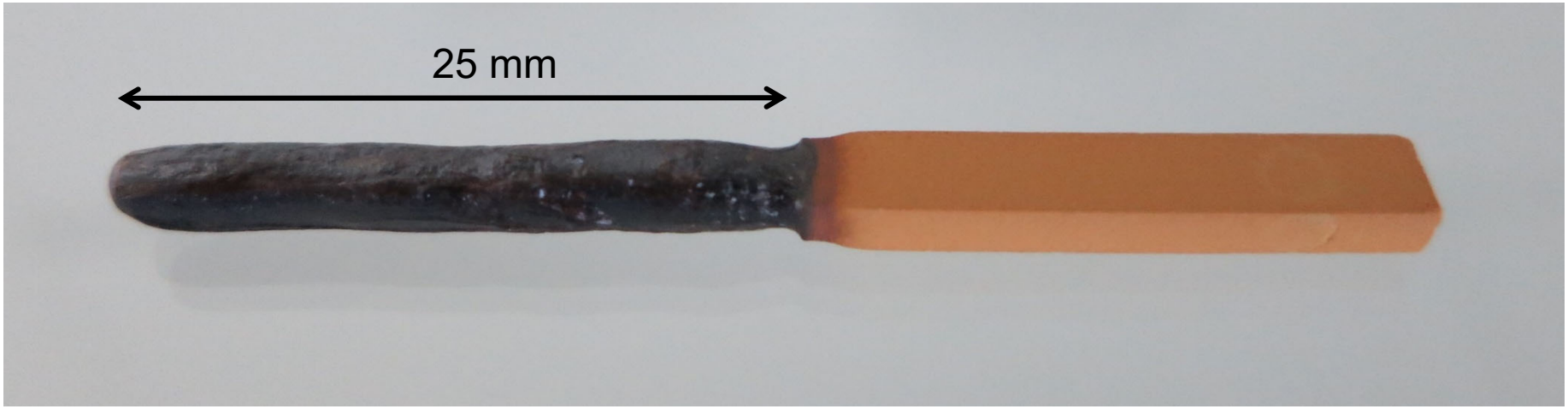

25 mm long as-grown crystalline material plus polycrystalline seed rod

Run or sample No. 779

Grown with 6 mm / h under 90 % Ar + 10 % O_2

Prepared at the ETH Zurich in 2016

Melt-grown $n = 6$ type $Ca_6Nb_5FeO_{20}$ $Nb^{5+} / 4d^0$ $Fe^{3+} / 3d^5$

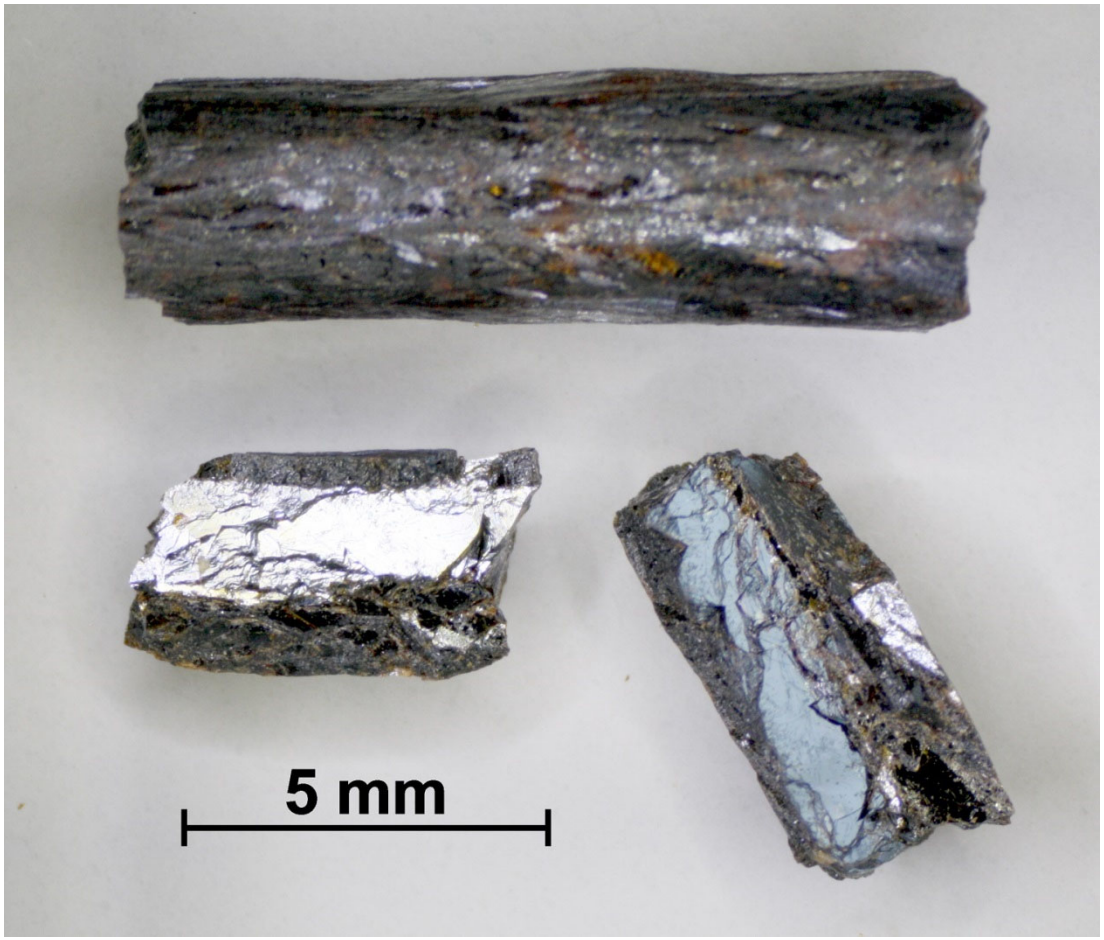

Crystalline pieces from the as-grown sample No. 779

Grown with 6 mm / h under 90 % Ar + 10 % O_2

Melt-grown $n = 6$ type $Ca_6Nb_5FeO_{20}$ $Nb^{5+} / 4d^0$ $Fe^{3+} / 3d^5$

Powder x-ray diffraction pattern of a pulverized crystalline piece of sample No. 779
Background subtracted

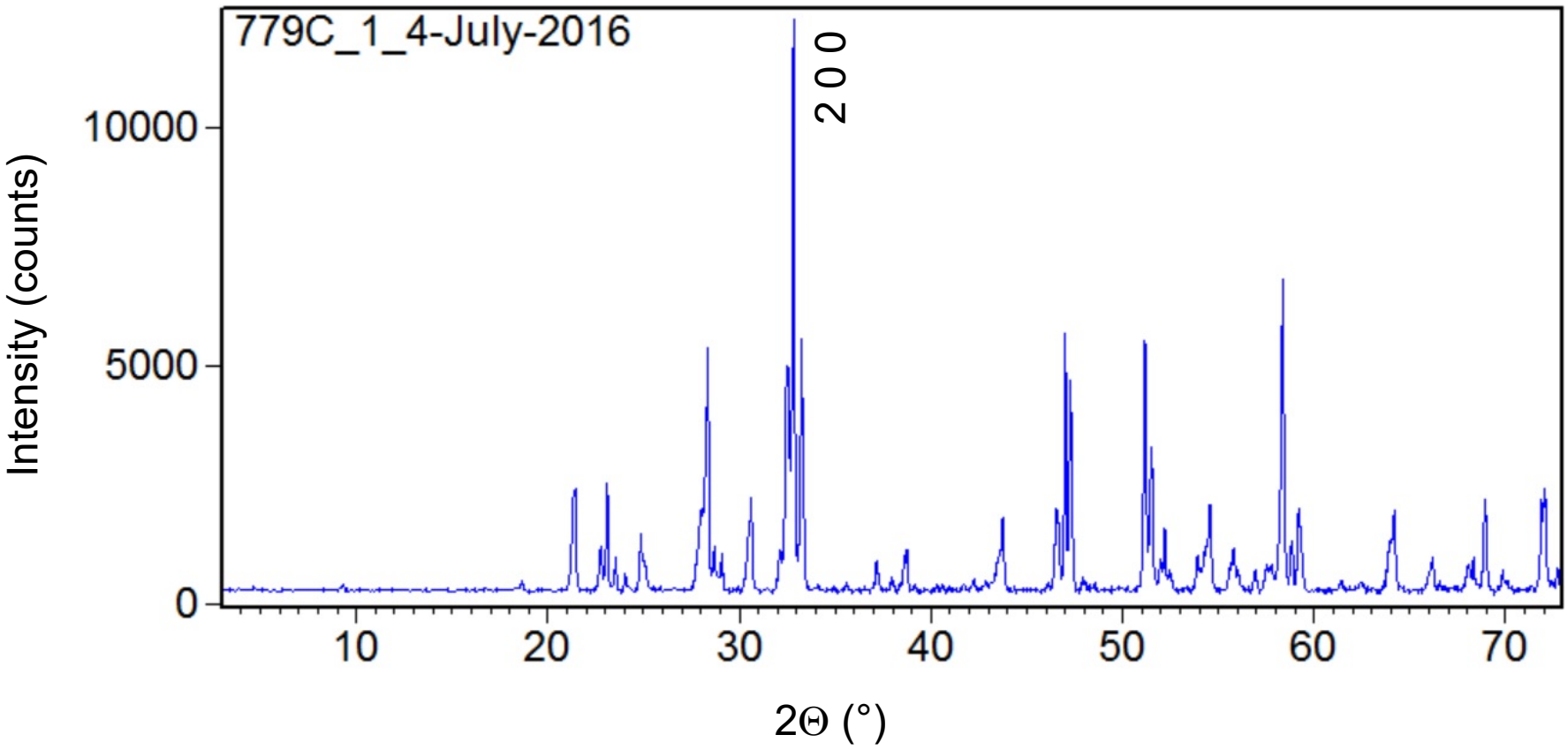

Available is an Excel file with the powder-x-ray diffraction data.
It is provided via the link which is specified on page 2

Melt-grown $n = 6$ type $Ca_6Nb_5FeO_{20}$ $Nb^{5+} / 4d^0$ $Fe^{3+} / 3d^5$

Powder x-ray diffraction pattern of a pulverized crystalline piece of sample No. 779
Background subtracted

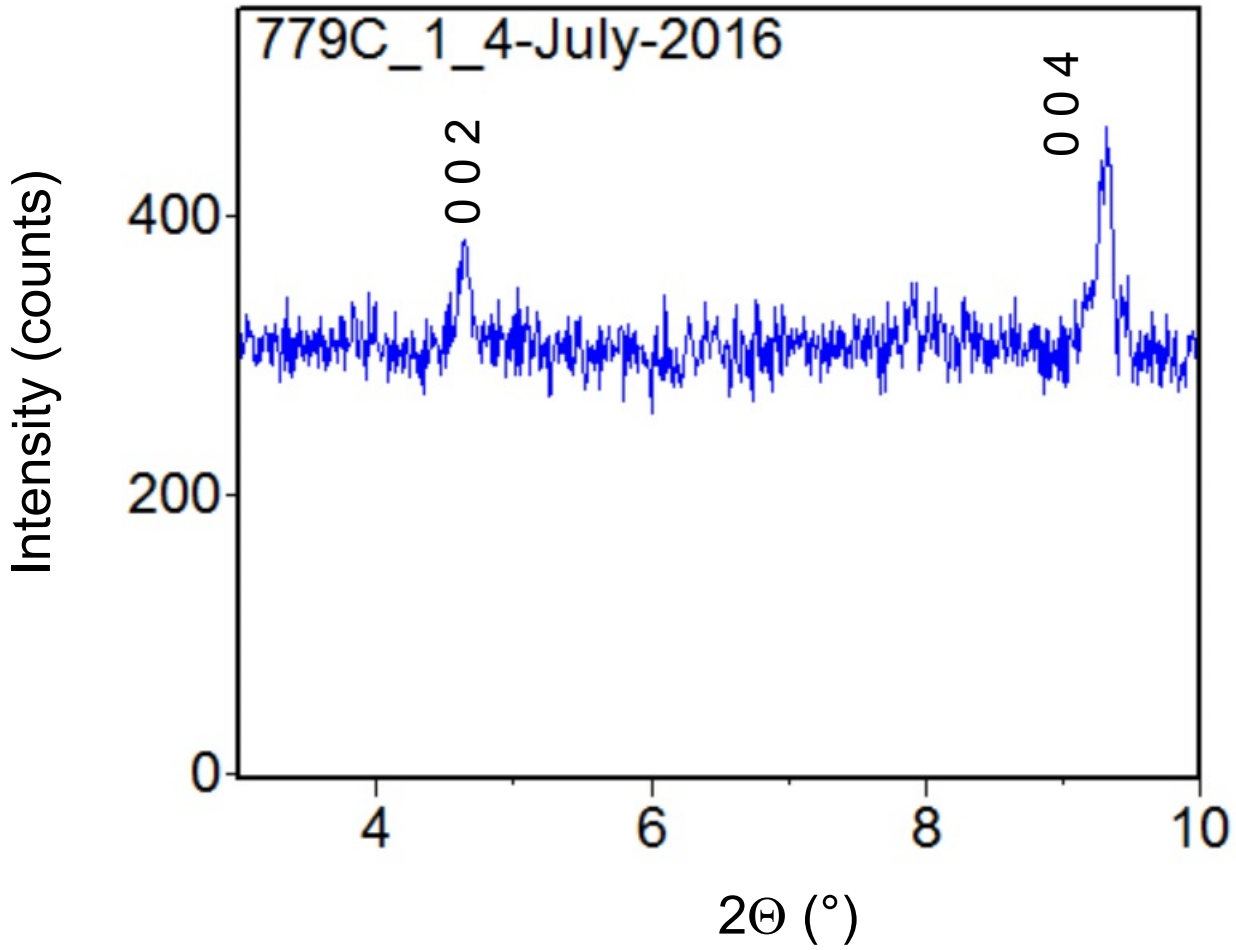

Available is an Excel file with the powder-x-ray diffraction data. It is provided via the link which is specified on page 2

Melt-grown $n = 6$ type $Ca_6Nb_5FeO_{20}$ Nb^{5+} / $4d^0$ Fe^{3+} / $3d^5$

The magnetic moment M(T) of a crystalline piece of sample No. 779 was measured by a SQUID magnetometer MPMS3. The magnetic field H was approximately oriented parallel to the layers. Shown is the plot of the inverse magnetic susceptibility $\chi(T)$

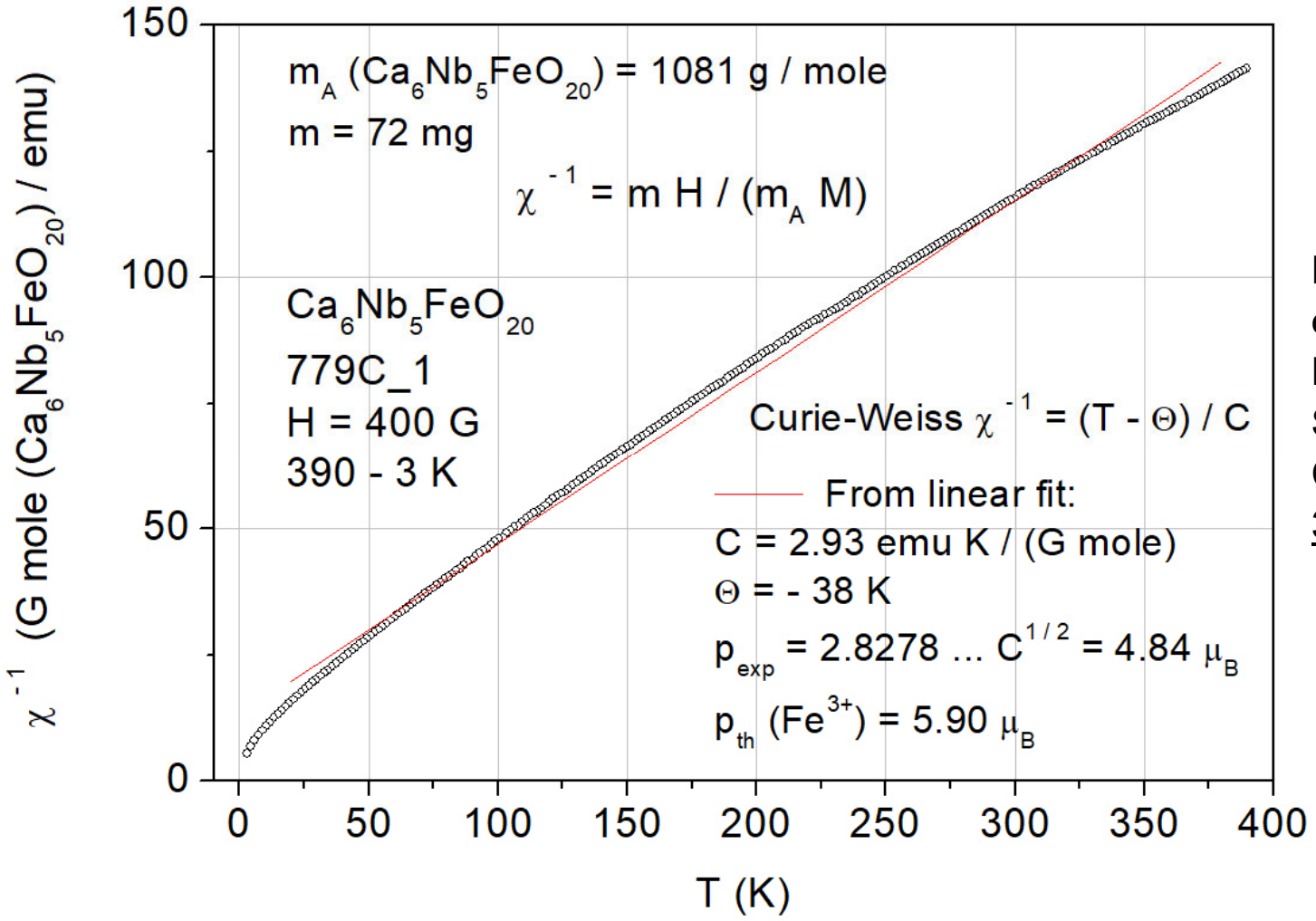

Ref. for data evaluation: Progress in Solid State Chemistry 36 (2008) 253

Inverse χ(T) of melt-grown n = 6 type $La_6Ti_4Fe_2O_{20}$ and $Ca_6Nb_5FeO_{20}$

Ti^{4+} / $3d^0$ Fe^{3+} / $3d^5$ Nb^{5+} / $4d^0$

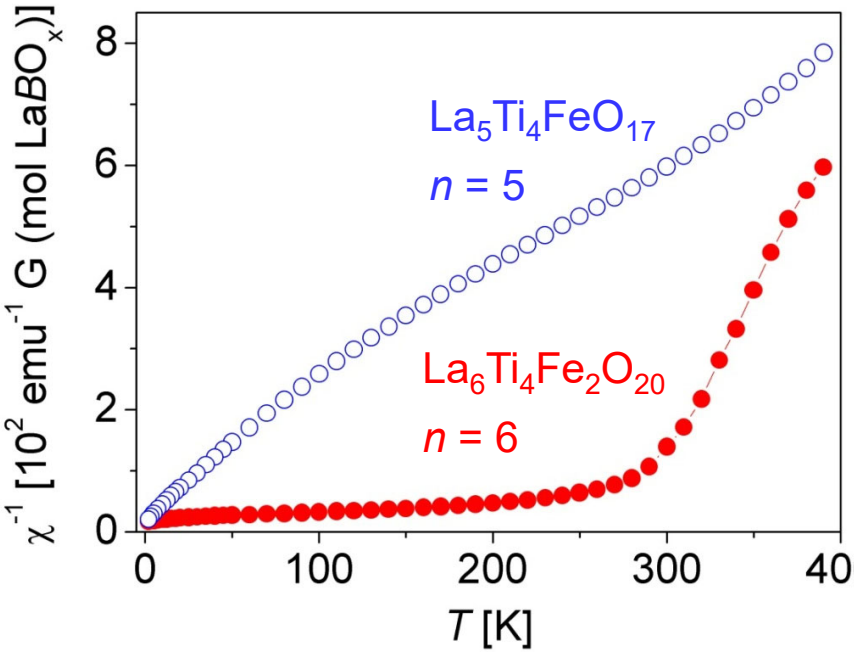

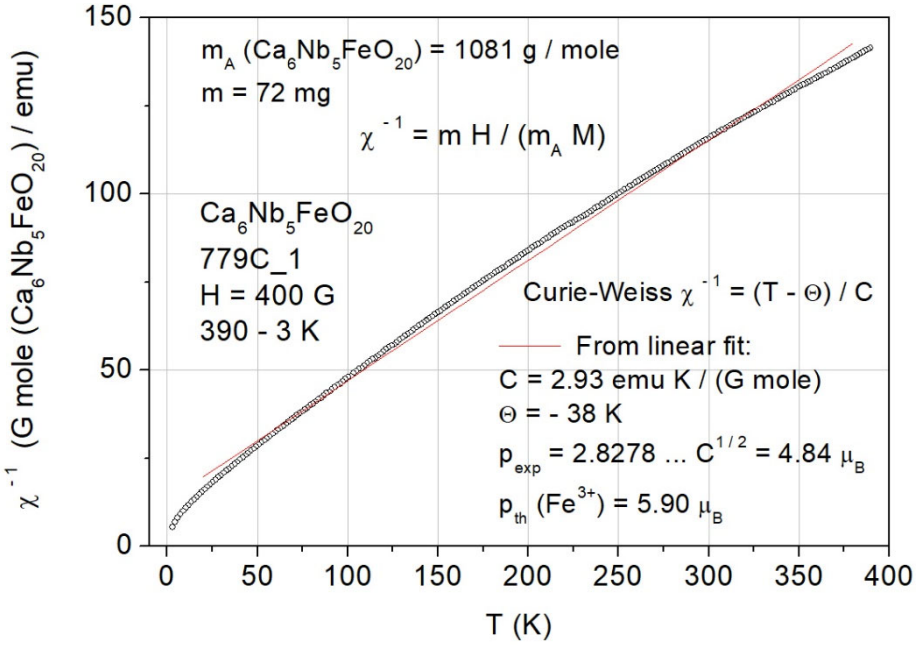

No indication for long-range magnetic ordering in $Ca_6Nb_5FeO_{20}$ because the Fe content is probably too small for that. See also the two following pages ...

$La_6Ti_4Fe_2O_{20}$: Progress in Solid State Chemistry 36 (2008) 253 and Journal of Physics: Condensed Matter 25 (2013) 076003 • $Ca_6Nb_5FeO_{20}$: This work

Melt-grown n = 6 type $Ln_6Ti_4Fe_2O_{20}$ and $Ca_6Nb_5FeO_{20}$

Fe^{3+} occupancy in % at 295 K

Distortion of $(Ti^{4+}, Fe^{3+})O_6$ octahedra in %

} averaged over two non-equivalent sites along *a*-axis

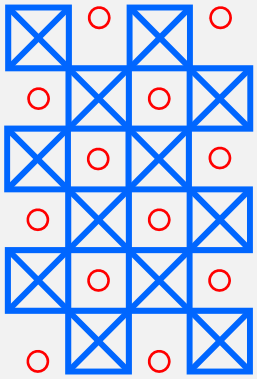

5	23
24	17
68	4
68	4
24	17
5	23

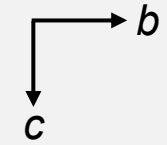

= BO_6 octahedra
(O located at corners,
B hidden in center)

n = 6 type $La_6Ti_4Fe_2O_{20}$
Non-centrosymmetric

A. Wölfel et al.: Journal of Physics: Condensed Matter 25 (2013) 076003 , Acta Crystallographica Section B 69 (2013) 137

Some open questions

- Is it possible to synthesize a material with *B* = (Ti,Fe) and a Fe^{3+} occupancy > 68 % at the central BO_6 octahedra ?
- Compared to Ti^{4+} and Fe^{3+} the both ions Nb^{5+} and Fe^{3+} have a larger difference of their valence. Does this imply for $Ca_6Nb_5FeO_{20}$ a sharper concentration gradient of Fe^{3+} and a larger Fe^{3+} occupancy at the central BO_6 octahedra ?

Melt-grown n = 6 type $Ln_6Ti_4Fe_2O_{20}$ and $Ca_6Nb_5FeO_{20}$

Fe^{3+} occupancy in % at 295 K

Distortion of $(Ti^{4+}, Fe^{3+})O_6$ octahedra in %

} averaged over two non-equivalent sites along *a*-axis

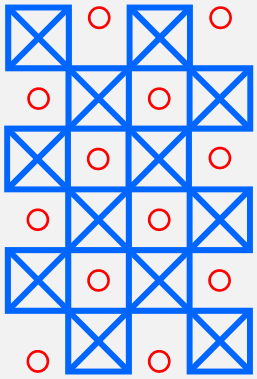

5	23
24	17
68	4
68	4
24	17
5	23

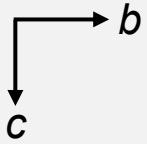

= BO_6 octahedra
(O located at corners,
B hidden in center)

n = 6 type $La_6Ti_4Fe_2O_{20}$
Non-centrosymmetric

A. Wölfel et al.: Journal of Physics: Condensed Matter 25 (2013) 076003 , Acta Crystallographica Section B 69 (2013) 137

Some open questions

- Is $Ca_6Nb_5FeO_{20}$ non-centrosymmetric and polar or ferroelectric ?
- Is it possible to prepare a material of the type $A_6Nb_4Fe_2O_{20}$ with Nb^{5+} and Fe^{3+} ?
  It was already attempted to prepare melt-grown n = 6 type $Ca_4La_2Nb_4Fe_2O_{20}$ (run / sample No. 775). However, the melting and solidification behavior was difficult and the obtained melt-grown material is multiphase.

An unsuccessful attempt to prepare melt-grown $Sr_6Nb_5FeO_{20}$

Polycrystalline sintered rods with the composition $Sr_6Nb_5FeO_{20}$ (run / sample No. 772) were used for an attempt to prepare melt-grown *n* = 6 type $Sr_6Nb_5FeO_{20}$ which is potentially isostructural to the *n* = 6 type $Ca_6Nb_5FeO_{20}$. However, when processing the rods with the composition $Sr_6Nb_5FeO_{20}$ in the Cyberstar mirror furnace a very difficult melt and solidification behavior was observed. It indicated a strong deviation from congruent melting and solidification. The mirror furnace run was soon terminated because it was not possible to achieve a steady state of melting and solidification.

5.3 Materials in the context of potential multiferroic Carpy-Galy phases $A_nB_nO_{3n+2} = ABO_x$

5.3.3 Other known, hypothetical, and suggested compounds / systems ...

Already known: Multiferroic non-oxides $A_nB_nF_{3n+2}$ of the type $n = 2$

☒ = BF_6 octahedra (F located at the corners, B hidden in the center)

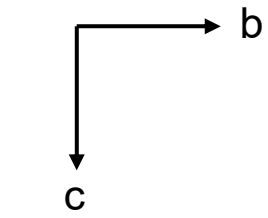

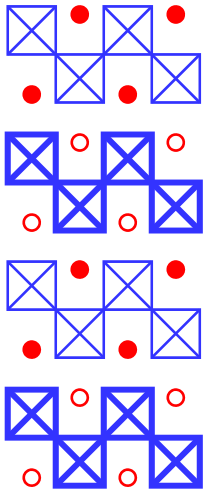

$n = 2$

$A_2B_2F_8$

ABF_4

- $n = 2$ type flourine compounds $A_2B_2F_8 = ABF_4$ are known for A = Ba and B = Mg, Mn, Fe, Co, Ni or Zn
- B^{2+}: Mn^{2+} / $3d^5$ Fe^{2+} / $3d^6$ Co^{2+} / $3d^7$ Ni^{2+} / $3d^8$ Zn^{2+} / $3d^0$
- B = Mn, Fe, Co or Ni: Antiferromagnetic (T_N about 20 - 70 K) and ferroelectric up to melting point (720 - 970 °C)

C. Ederer and N. Spaldin, Physical Review B 74 (2006) 024102
C. Ederer and N. Spaldin, Physical Review B 74 (2006) 020401 (R)
E. T. Keve et al., The Journal of Chemical Physics 51 (1969) 4928
Table 2 in Progress in Solid State Chemistry 29 (2001) 1

Hypothetical *n* = 4 type compounds

☒ = BO_6 octahedra (O located at the corners, *B* hidden in the center)

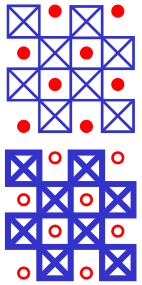

n = 4

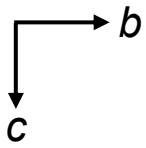

- Theoretical / computational study about ferroelectric *n* = 4 type $La_4Ti_4O_{14} = La_2Ti_2O_7$: Ab initio study of proper topological ferroelectricity in layered perovskite $La_2Ti_2O_7$, J. Lopez-Perez and J. Iniguez , Physical Review B 84 (2011) 075121
  - Significant polar character in structural distortions that are typically nonpolar
  - Observed proper ferroelectricity driven by O_6 rotations provides ideal conditions to obtain strong magnetoelectric effects
  - Strong magnetoelectric effects if the *B* site is occupied by magnetic ions such as Mn^{4+} / $3d^3$ and hypothetical *n* = 4 type material $La_4Mn_4O_{14} = La_2Mn_2O_7$
- Potential *n* = 4 type thin films $Ln_2Ti_{2-w}Mn_wO_7$ (w > 0) on (110)-oriented $SrTiO_3$ with $Ti^{4+}$and Mn^{4+} are suggested: Zhenmian Shao, Sebastien Saitzek, Pascal Roussel, and Rachel Desfeux, Journal of Materials Chemistry 22 (2012) 24894

Hypothetical $n = 4$ type compounds

☒ = BO_6 octahedra (O located at the corners, *B* hidden in the center)

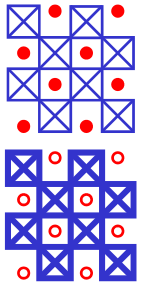

$n = 4$

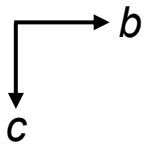

- Theoretical / computational study suggests multiferroicity in $n = 4$ type V-doped $La_2Ti_2O_7$, i.e. in $La_2Ti_{2-w}V_wO_7$ ($w > 0$): Marco Scarrozzaa, Alessio Filippetti, and Vincenzo Fiorentini, The European Physical Journal B 86 (2013) 128

Estimation about the level of difficulty to synthesize the suggested materials

$La_2Mn_2O_7$ → Very difficult

$Ln_2Ti_{2-y}Mn_yO_7$ ($y > 0$) → Increases with increasing y

$La_2Ti_{2-w}V_wO_7$ ($w > 0$) → Relatively easy if w is not too large. An open question is the valence distribution among the Ti and V ions. Ti^{4+} and V^{4+} seems to be the most likely scenario

Suggested epitaxial (110)-oriented thin film hetreostructures 1 / 3

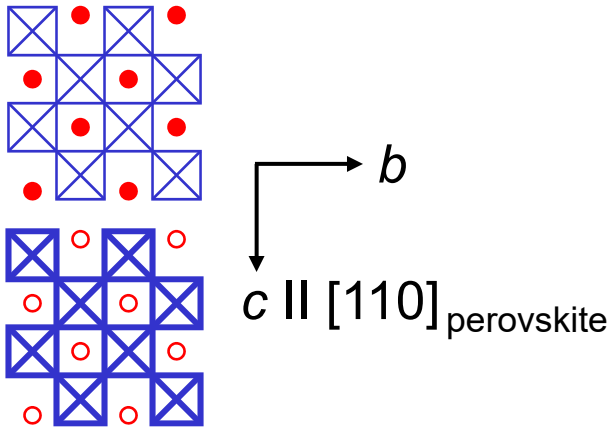

n = 4 type $ABO_{3.5}$

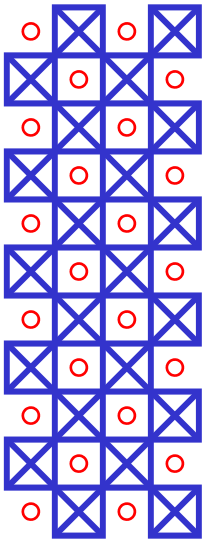

n = ∞ type ABO_3 perovskite

The following suggested heterostructures are examples of a potential artificial extension of the (110)-oriented stacking of slabs or layers in the Carpy-Galy phases $A_nB_nO_{3n+2}$ = ABO_x ...

Suggested epitaxial (110)-oriented thin film hetreostructures 2 / 3

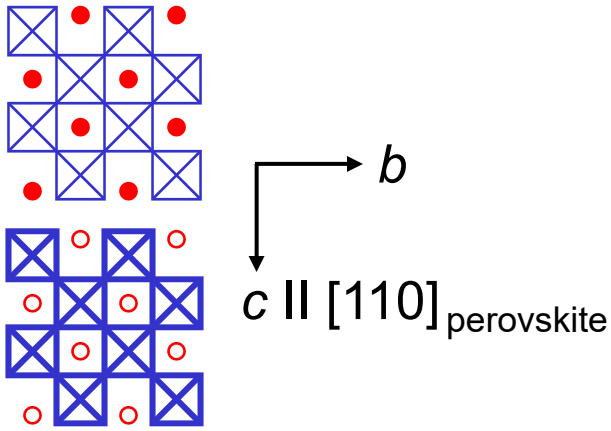

n = 4 type $ABO_{3.5}$

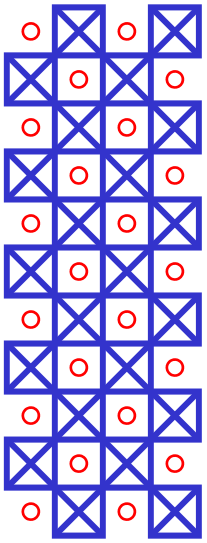

n = ∞ type ABO_3 perovskite

Suggested $LaTiO_3$ / $LaTiO_{3.5}$ heterostructures

The n = 4 type $LaTiO_{3.5}$ is known as a high-T_c ferroelectric with T_c = 1770 K. The n = ∞ type perovskite $LaTiO_3$ is known as a weak ferromagnet / canted antiferromagnet with $T_N \approx$ 150 K.

If it is possible to create epitaxial and (110)-oriented heterostructures which consist of thin films of ferroelectric n = 4 type $LaTiO_{3.5}$ and weak ferromagnetic n = ∞ type $LaTiO_3$, then the electric and magnetic properties / quantities are potentially coupled. If yes, then this represents potentially a novel magnetoelectric or multiferroic system.

(110)-oriented n = 4 type $LaTiO_{3.5}$
(110)-oriented n = ∞ type $LaTiO_3$
(110)-oriented n = 4 type $LaTiO_{3.5}$
(110)-oriented n = ∞ type $LaTiO_3$
substrate such as (110)-oriented $SrTiO_3$

Suggested epitaxial (110)-oriented thin film hetreostructures 3 / 3

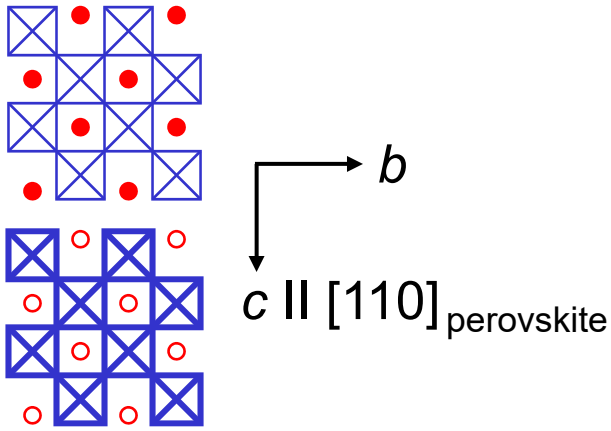

n = 4 type $ABO_{3.50}$

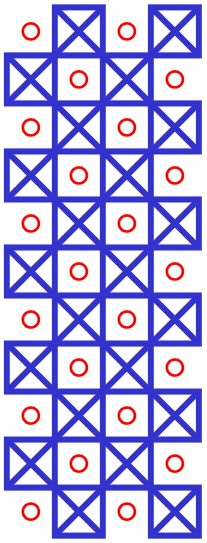

n = ∞ type ABO_3 perovskite

Suggested $LaFeO_3$ / $LaTiO_{3.5}$ heterostructures

The n = 4 type $LaTiO_{3.5}$ is known as a high-T_c ferroelectric with T_c = 1770 K. The n = ∞ type perovskite $LaFeO_3$ is known as a weak ferromagnet / canted antiferromagnet with $T_N \approx$ 740 K.

If it is possible to create epitaxial and (110)-oriented heterostructures which consist of thin films of ferroelectric n = 4 type $LaTiO_{3.5}$ and weak ferromagnetic n = ∞ type $LaFeO_3$, then the electric and magnetic properties / quantities are potentially coupled. If yes, then this represents potentially a novel magnetoelectric or multiferroic system.

(110)-oriented n = 4 type $LaTiO_{3.5}$
(110)-oriented n = ∞ type $LaFeO_3$
(110)-oriented n = 4 type $LaTiO_{3.5}$
(110)-oriented n = ∞ type $LaFeO_3$
substrate such as (110)-oriented $SrTiO_3$

Another suggested system:
$n = \infty$ type $LaTiO_3$ micropillars in a ferroelectric $n = 4$ type $LaTiO_{3.5}$ matrix

Presented in part 8:
$n = \infty$ type $SrNbO_3$ micro/nanopillars were created by an electron beam in a $n = 4$ type ferroelectric $SrNbO_{3.5}$ matrix

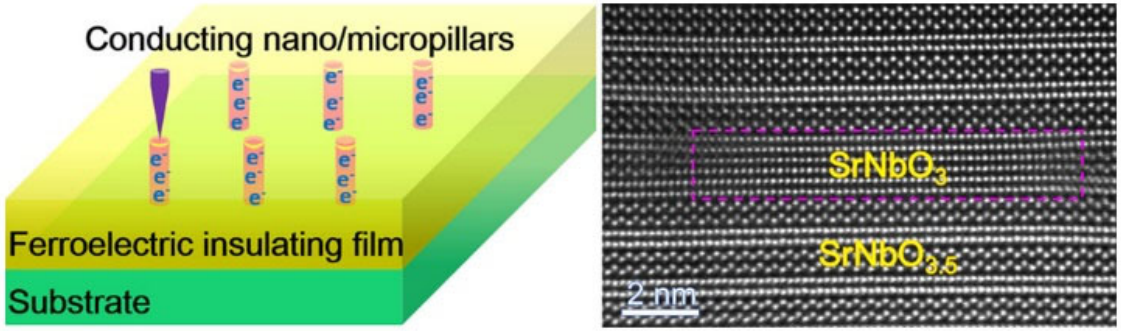

Image source: Tingting Yao et al., Nano Letters 20 (2020) 1047 - 1053
https://doi.org/10.1021/acs.nanolett.9b04210

The $n = \infty$ perovskite type $LaTiO_3$ is known as a weak ferromagnet / canted anti-ferromagnet with $T_N \approx 150$ K. The $n = 4$ type $LaTiO_{3.5}$ is known as a high-T_c ferroelectric with $T_c = 1770$ K. If it is possible to create weak ferromagnetic $LaTiO_3$ micropillars in a ferroelectric $LaTiO_{3.5}$ matrix, then the electric and magnetic properties / quantities are potentially coupled. If yes, then this represents a novel magnetoelectric system and potentially also a novel multiferroic system.

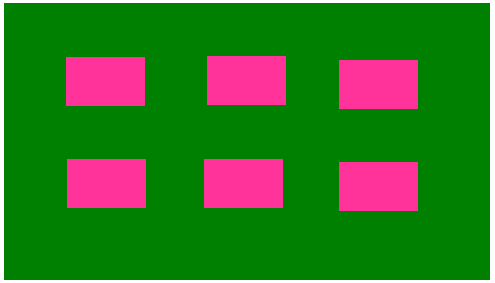

Sketch of a hypothetical system:
Weak ferromagnetic $LaTiO_3$ micropillars
in a ferroelectric $LaTiO_{3.5}$ matrix

Hypothetical materials related to the Schückel-Müller-Buschbaum phase

= NbO_6 octahedra (O located at the corners, Nb hidden in the center)

= NbO_4 (O located at the corners, Nb in the center)

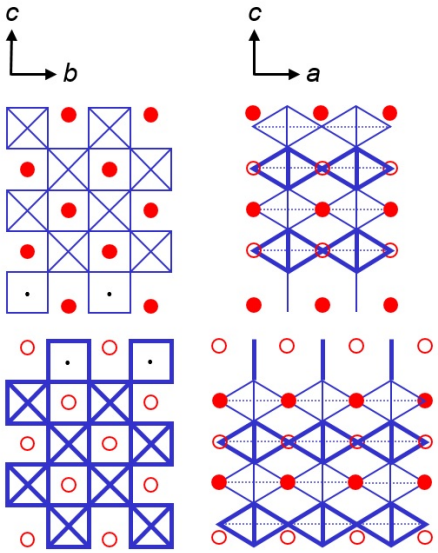

Sketch of the crystal structure of the Schückel-Müller-Buschbaum phase $SrNbO_{3.2} = Sr_5Nb_5O_{16} = Sr_{20}Nb_{20}O_{64}$ which is related to the $n = 5$ type quasi-1D metal $SrNbO_{3.4} = Sr_5Nb_5O_{17} = Sr_{20}Nb_{20}O_{68}$

Presented in part 6.7 – 6.9 are

- the non-centrosymmetric and O-deficient $n = 5$ type Schückel-Müller-Buschbaum phase $SrNbO_{3.2} = Sr_5Nb_5O_{16} = Sr_{20}Nb_{20}O_{64}$ in which the oxygen vacancies are fully ordered K. Schückel and Hk. Müller-Buschbaum, Zeitschrift für Anorganische und Allgemeine Chemie 528 (1985) 91
  F. Lichtenberg et al., Progress in Solid State Chemistry 36 (2008) 253
  S. C. Abrahams et al., Acta Crystallographica Section B 54 (1998) 399

- related Sr- and O-deficient $n = 5$ type electrical conductors such as $Sr_{17}Ca_2Nb_{19}WO_{64}$

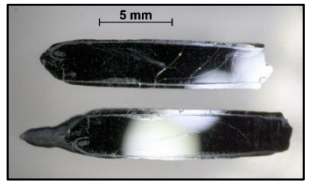

Open question: Are there also related non-centrosymmetric insulators which are potentially ferroelectric, magnetoelectric, and / or multiferroic ? It should be noted that compositions like $SrNbO_{3.2} = Sr_{20}Nb_{20}O_{64}$ and $A_{0.95}BO_{3.2} = A_{19}B_{20}O_{64}$ are close to that of the perovskite $ABO_3 = A_{20}B_{20}O_{60}$

The crystal structure of La_2RuO_5 in comparison to $n = 2$ of $A_nB_nO_{3n+2}$

As sketched on the following page La_2RuO_5 (Ru^{4+} / $4d^4$) crystallizes in a particular crystal structure which is related to $n = 2$ of $A_nB_nO_{3n+2}$

La_2RuO_5 is a $m = 2$ member of a hypothetical homologous series $A_{m+2}B_mO_{3m+4}$ and it is an open question if other and also non-centrosymmetric compounds belonging to this series exist / can be prepared. If yes, then there are potentially novel magnetoelectric or multiferroic materials among them.

The crystal structure of La_2RuO_5 in comparison to $n = 2$ of $A_nB_nO_{3n+2}$

= BO_6 octahedra (O located at the corners, *B* hidden in the center)

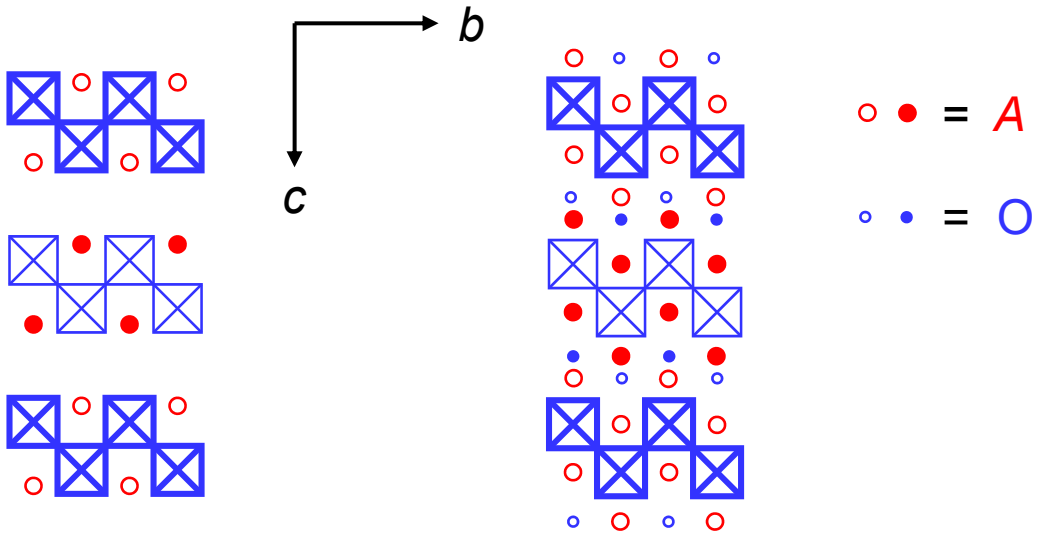

La_2RuO_5 : Seminconductor-to-semiconductor transition and (antiferro ?) magnetic ordering at $T \approx 160$ K, centrosymmetric

$LaTaO_4$: Non-centrosymmetric as well as centrosymmetric modifications are reported

$n = 2$ of $A_nB_nO_{3n+2}$

$A_2B_2O_8 = ABO_4$

$La_2Ta_2O_8 = LaTaO_4$

$Ta^{5+} / 5d^0$

$m = 2$ of hypothetical series $A_{m+2}B_mO_{3m+4}$

$A_4B_2O_{10} = A_2BO_5$

$La_4Ru_2O_{10} = La_2RuO_5$

$Ru^{4+} / 4d^4$

Open question: Are there other and also non-centrosymmetric compounds of the type $A_{m+2}B_mO_{3m+4}$?

La_2RuO_5 : P. Boullay et al., J. Solid State Chem. 170 (2003) 294 • S. Ebbinghaus, Acta Cryst. C i96 (2005) 61
P. Khalifah et al., Science 297 (2002) 2237 • S. K. Malik et al., Solid State Comm. 135 (2005) 16
F. Lichtenberg et al., Prog. Solid State Chem. 36 (2008) 253

$LaTaO_4$: For references see Table 15 in Prog. Solid State Chem. 36 (2008) 253

6 Conducting and metallic Carpy-Galy phases $A_nB_nO_{3n+2} = ABO_x$ ...

6 Conducting and metallic Carpy-Galy phases $A_nB_nO_{3n+2} = ABO_x$

6.1 $LaTiO_x$ and the n = 5 type quasi-1D metal $La_5Ti_5O_{17} = LaTiO_{3.4}$ ...

$A_nB_nO_{3n+2}$ = ABO_x type electrical conductors

No publications before 1991 apart from the following structural study on conducting $CaNbO_x$ ($3.4 \leq x < 3.5$) in which no physical properties are not reported:

M. Hervieu et al. , Journal of Solid State Chemistry 22 (1977) 273

Systematic study of $A_nB_nO_{3n+2} = ABO_x$ electronic conductors started with a study of melt-grown $La_nTi_nO_{3n+2} = LaTiO_x$

Synthesis and study of $LaTiO_x$ between the end members $LaTiO_3$ and $LaTiO_{3.5}$ which were already known

F. Lichtenberg, Dissertation, University of Zurich (1991)

F. Lichtenberg et al., Zeitschrift für Physik B Condensed Matter 82 (1991) 211

T. Williams et al., Journal of Solid State Chemistry 93 (1991) 534 and 103 (1993) 375

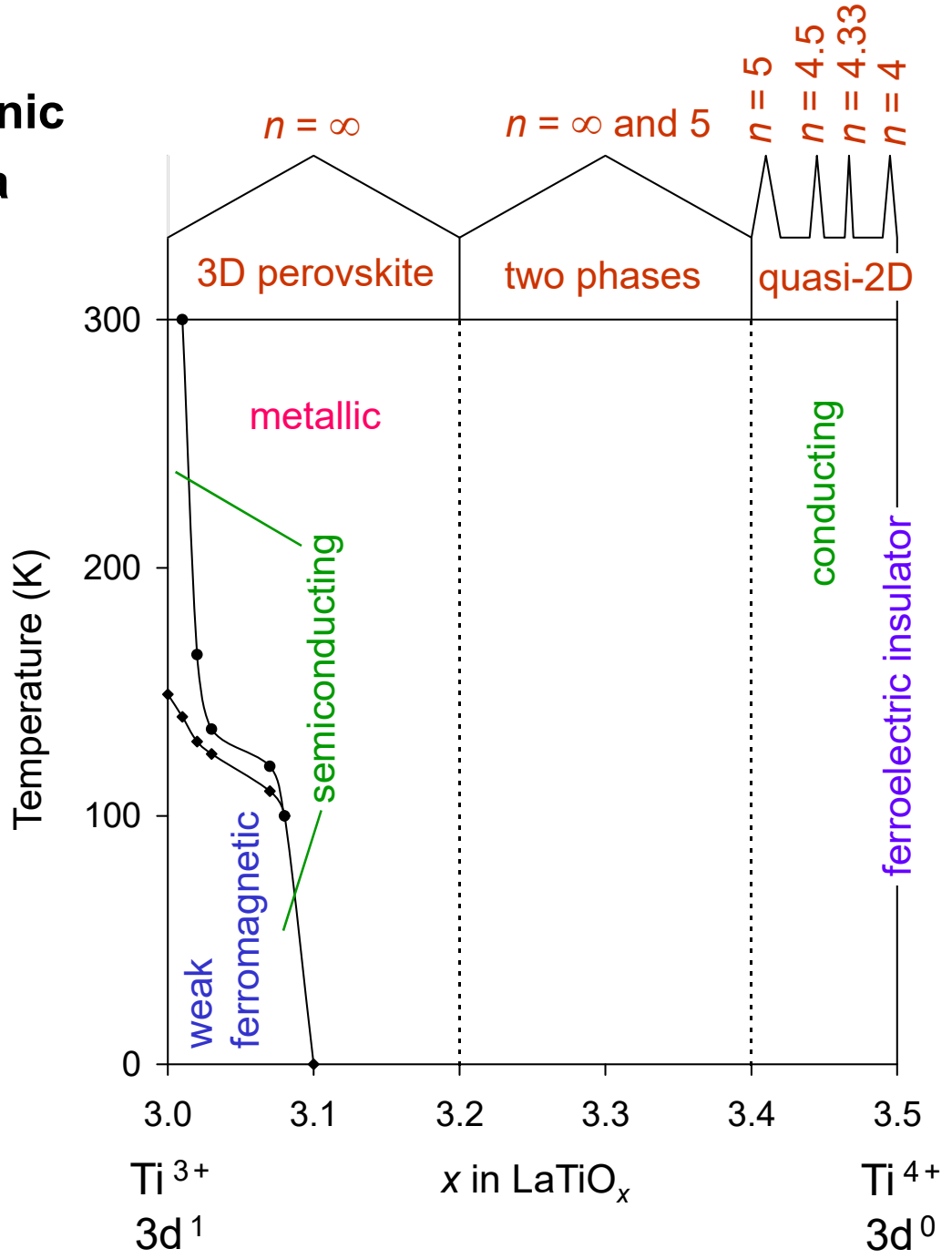

Systematic study of $A_nB_nO_{3n+2} = ABO_x$ electronic conductors started with a study of melt-grown $La_nTi_nO_{3n+2} = LaTiO_x$

Synthesis and study of $LaTiO_x$ between the end members $LaTiO_3$ and $LaTiO_{3.5}$ which were already known

F. Lichtenberg, Dissertation, University of Zurich (1991)

F. Lichtenberg et al., Zeitschrift für Physik B Condensed Matter 82 (1991) 211

T. Williams et al., Journal of Solid State Chemistry 93 (1991) 534 and 103 (1993) 375

F. Lichtenberg et al., Progress in Solid State Chemistry 29 (2001) 1

C. A. Kuntscher et al., Physical Review B 67 (2003) 035105

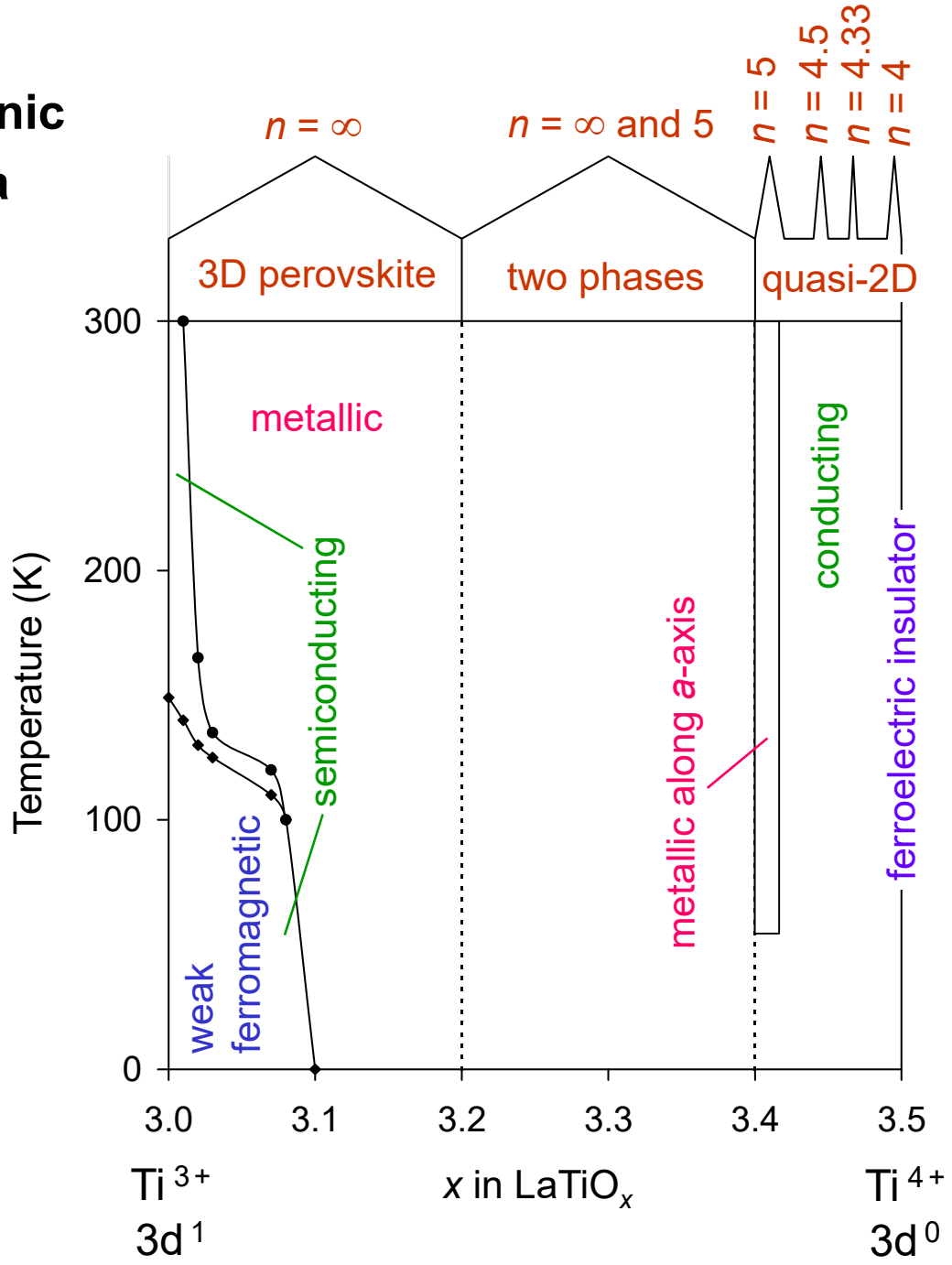

Pictures from melt-grown $LaTiO_x$

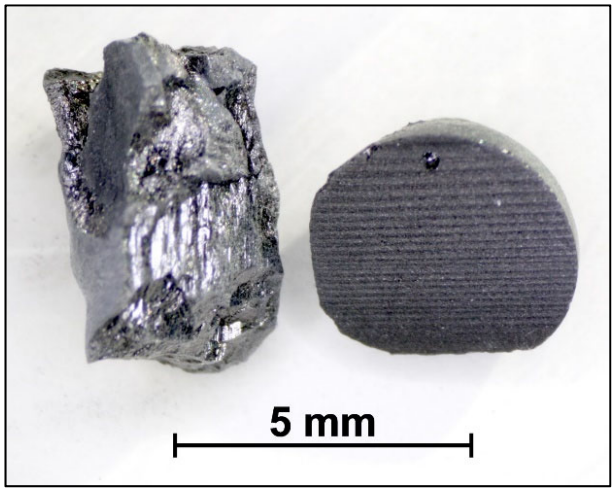

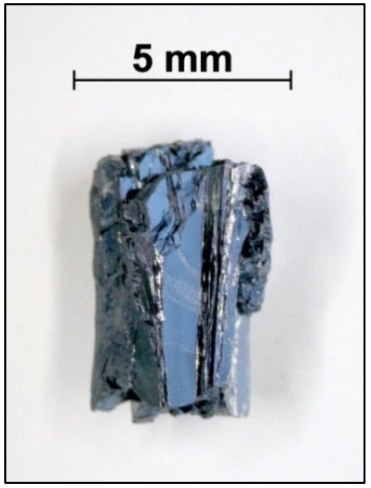

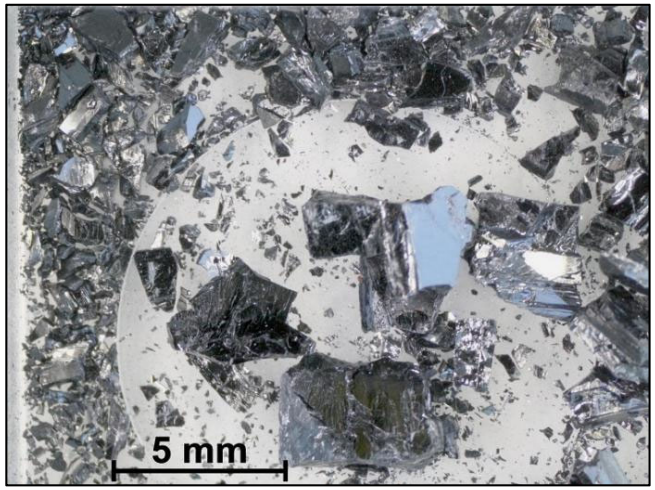

$n = \infty$ type $LaTiO_3$ Sample No. 442

Pieces from the as-grown material which was prepared by processing rods with the composition $LaTiO_3$ under Ar in a GERO mirror furnace at the University of Augsburg

Photo taken at the ETH Zurich

Physical Review B 68 (2003) 245108

$n = 5$ type $LaTiO_{3.4}$ Sample No. Z 187

Pieces from the as-grown material which was prepared by processing rods with the composition $LaTiO_{3.4}$ under Ar in an IBM mirror furnace at the IBM Zurich Research Laboratory

Photos taken at the ETH Zurich

Zeitschrift für Physik B Condensed Matter 82 (1991) 211

Pictures from melt-grown $LaTiO_x$

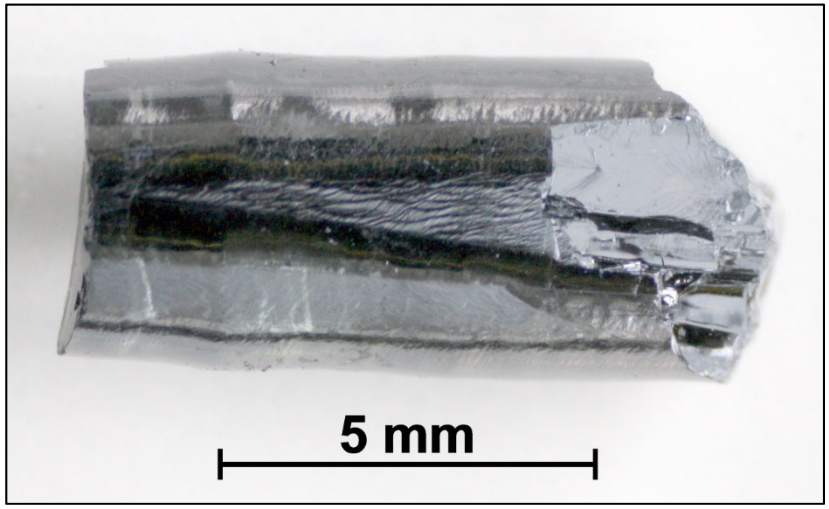

n = 5 type $LaTiO_{3.41}$ Sample No. 353

A piece from the as-grown material which was prepared by processing rods with the fully oxidized composition $LaTiO_{3.5}$ under 98 % Ar plus 2 % H_2 in a GERO mirror furnace at the University of Augsburg

Photo taken at the ETH Zurich

Progress in Solid State Chemistry 29 (2001) 1

Table 35 in Progress in Solid State Chemistry 36 (2008) 253 and references therein

n = 4 type $LaTiO_{3.5}$ Sample No. 168

Pieces from the as-grown material which was prepared by processing rods with the composition $LaTiO_{3.5}$ under air in a GERO mirror furnace at the University of Augsburg

Photo taken at the ETH Zurich

Progress in Solid State Chemistry 29 (2001) 1

The large homogeneity range of the $n = \infty$ perovskite type $LaTiO_x$

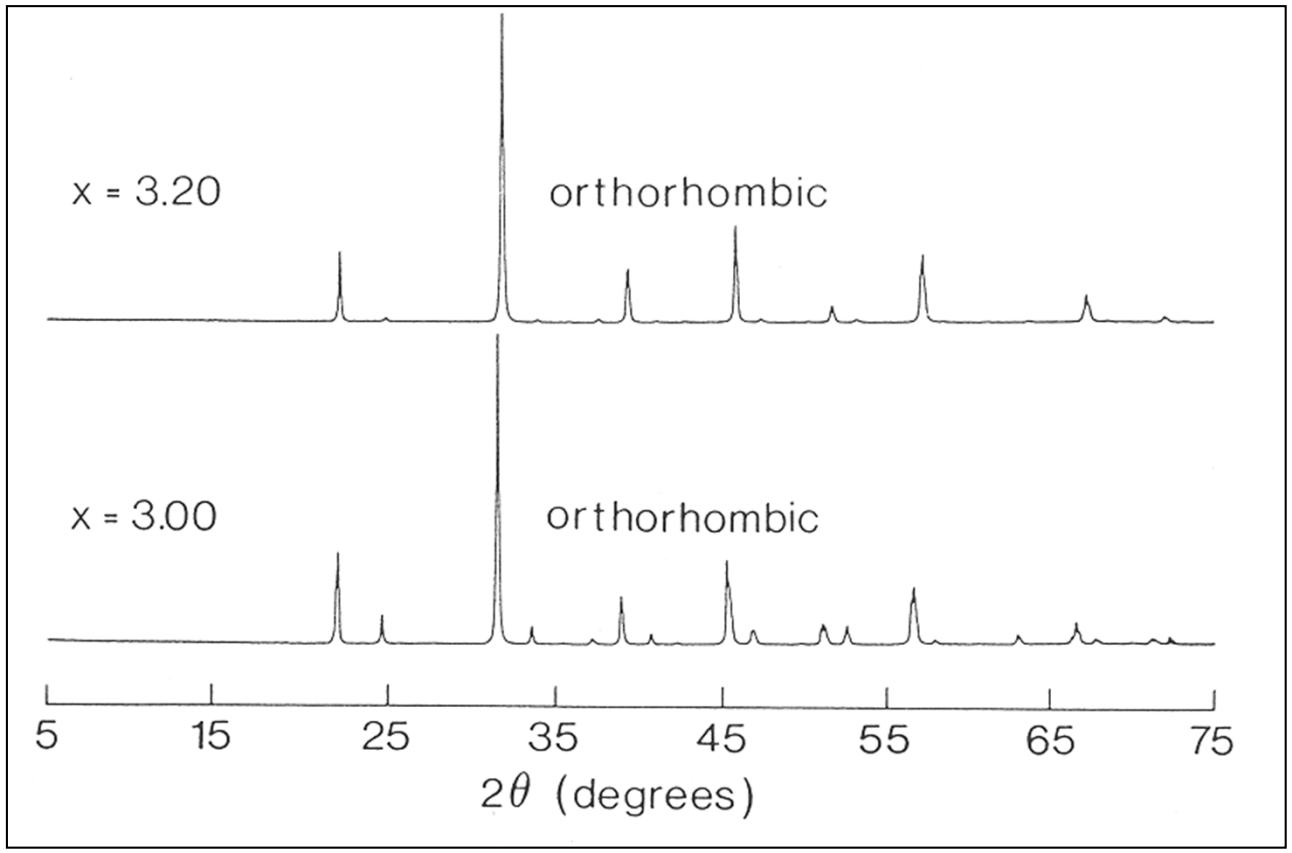

Powder x-ray diffraction pattern of melt-grown $LaTiO_{3.2}$ and $LaTiO_3$

$n = \infty$ perovskite type $LaTiO_x$

$x = 3.20$: Unit cell volume $V = 243$ Å^3

$x = 3.00$: Unit cell volume $V = 250$ Å^3

$\rightarrow$ Lattice contraction with increasing x

$\rightarrow$ Cation deficiency $La_yTi_yO_3$ with $0.94 \leq y \leq 1$?!

F. Lichtenberg, Dissertation, University of Zurich (1991)

Zeitschrift für Physik B Ccndensed Matter 82 (1991) 211

Progress in Solid State Chemistry 29 (2001) 1

The monoclinic $n = 5$ titanate $La_5Ti_5O_{17} = LaTiO_{3.4}$ ($Ti^{3.8+}$, $3d^{0.2}$)

Magnetic susceptibility $\chi(T)$

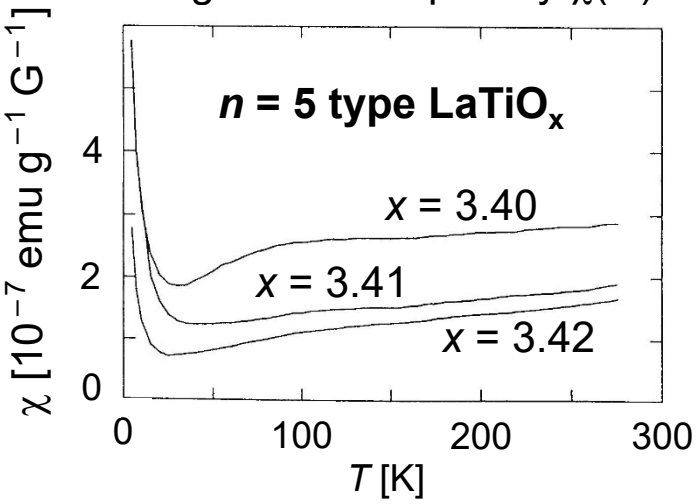

Resistivity ρ(T) along *a*- and *b*-axis and ⊥ *ab*-plane

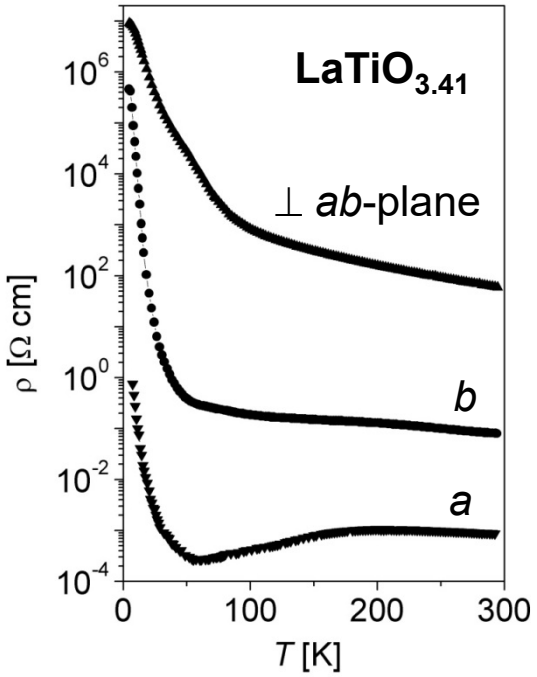

Optical reflectivity vs. frequency along *a*- and *b*-axis

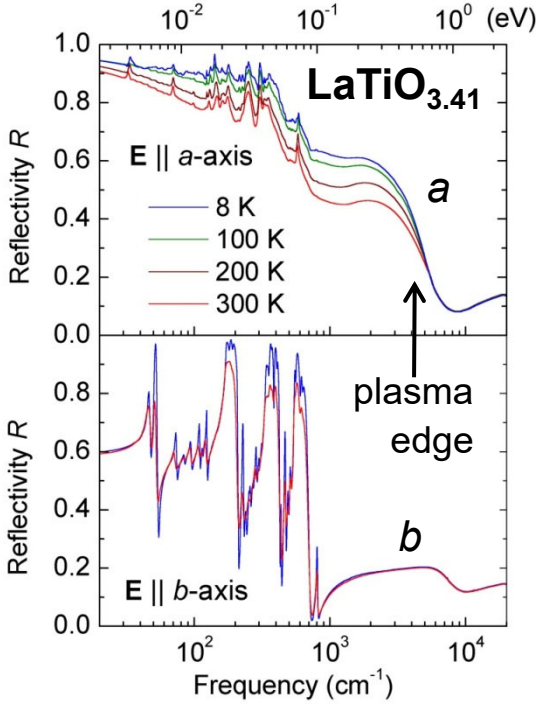

Highly anisotropic conductor and quasi-1D metal • At $T \approx 100$ K metal-to-semiconductor transition / indications for a phase transition • Below $T \approx 100$ K very small energy gap of ≈ 6 meV along *a*-axis • Indications for strong electron-phonon coupling • Crystal structure detemined by single crystal x-ray diffraction • Studies under high pressure indicate a stable structure up to 18 GPa, a sluggish structural phase transition from 18 to 24 GPa, and near 15 GPa an onset of a dimensional crossover from a quasi-1D to a quasi-2D metal

F. Lichtenberg et al: Progress in Solid State Chemistry 36 (2008) 253 and 29 (2001) 1 and Zeitschrift für Physik B Condensed Matter 84 (1991) 369 • C. A. Kuntscher et al: Physical Review B 74 (2006) 054105 and 67 (2003) 035105 • I. Loa et al., Physical Review B 69 (2004) 224105 • P. Daniels et al., Acta Crystallographica Section C 59 (2003) i15

The *n* = 5 quasi-1D metal $La_5Ti_5O_{17}$ ($Ti^{3.8+}$, $3d^{0.2}$)

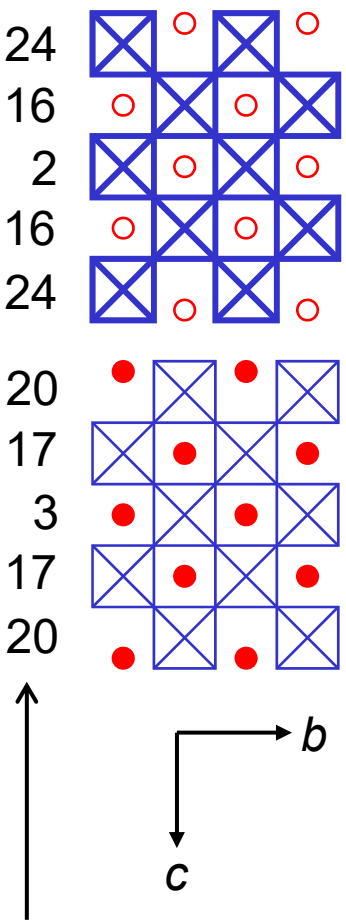

distortion of TiO_6 octahedra in percent

⊠ = TiO_6 octahedra (O located at corners, Ti hidden in center)

Experimental and theoretical / computational study on melt-grown *n* = 5 type $La_5Ti_5O_{17.05}$ = $LaTiO_{3.41}$ by Z. Wang et al:

"Spontaneous Structural Distortion and Quasi-One-Dimensional Quantum Confinement in a Single-Phase Compound"

- Structural investigation by state-of-the-art high-angle annular dark-field (HAADF) and annular bright-field (ABF) transmission electron microscopy (TEM)
- Valence state study by electron energy-loss spectroscopy (EELS)
- Density functional theory (DFT) calculations
  by using atomic coordinates and structural data obtained from single crystal x-ray diffraction by P. Daniels et al., Acta Cryst. C 59 (2003) i15
- investigation of non-linear quantum transport by calculatiing the (electrical) transmission function of three devised Pt / $La_5Ti_5O_{17}$ / Pt systems along the *a*- , *b*- and *c*-axis

Z. Wang, L. Gu, M. Saito, S. Tsukimoto, M. Tsukada, F. Lichtenberg, Y. Ikuhara, and J. G. Bednorz, Advanced Materials 25 (2013) 218 • Octahedra distortions from Fig. 15 in Progress in Solid State Chemistry 36 (2008) 253

The n = 5 quasi-1D metal $La_5Ti_5O_{17}$ ($Ti^{3.8+}$, $3d^{0.2}$)

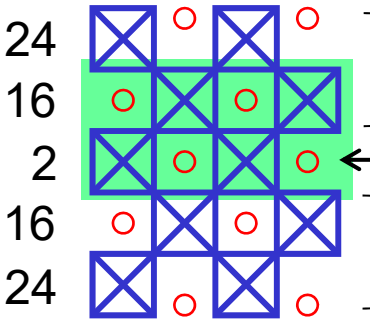

almost only Ti^{4+} / $3d^0$

almost only Ti^{3+} / $3d^1$

almost only Ti^{4+} / $3d^0$

⊠ = TiO_6 octahedra (O located at corners, Ti hidden in center)

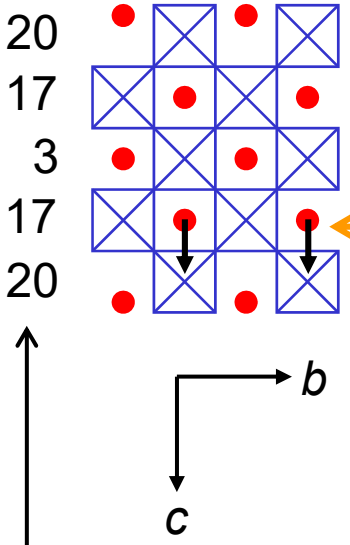

distortion of TiO_6 octahedra in percent

- Confinement of charge (delocalized 3d electrons) to the central octahedra / center of the layers or slabs
- Within unit cell metal-insulator-like interfaces which are similar to those in thin film heterostructures !
- DFT calculations indicate ferromagnetic ordering / spin-polarized quasi-1D electron gas. Experimentally not observed but the real material might be close to a state of itinerant ferromagnetism. Or computational artefact ?
- Assuming that one La sheet surrounding the central Ti is displaced down by 0.2 Å as indicated by the black arrows → DFT calculations result in a quasi-2D dispersion of valence bands around Fermi energy → Quasi-1D metallic behavior is related to the overall structure and not only due to the presence of Ti – O chains along the a-axis !

Z. Wang, L. Gu, M. Saito, S. Tsukimoto, M. Tsukada, F. Lichtenberg, Y. Ikuhara, and J. G. Bednorz, Advanced Materials 25 (2013) 218 • Octahedra distortions from Fig. 15 in Progress in Solid State Chemistry 36 (2008) 253

An example of a melt-grown non-stoichiometric lanthanum titanate

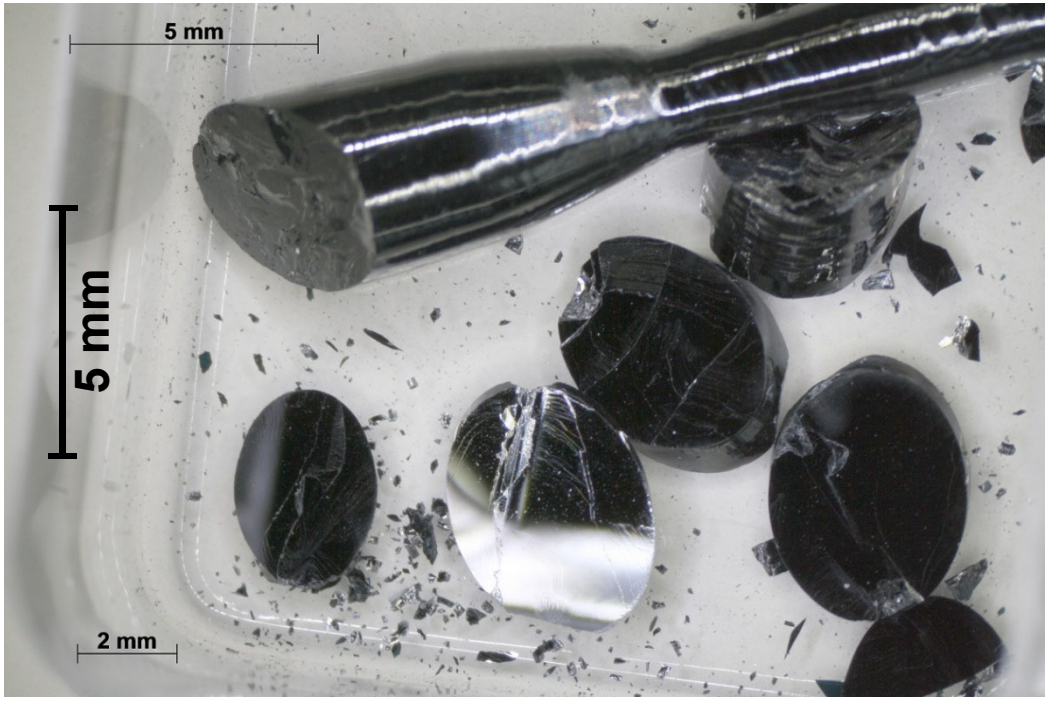

La- and O-deficient n = 4.5 type $La_{0.95}TiO_{3.38}$ ($Ti^{3.9+}$ / $3d^{0.1}$) Sample No. 205

Pieces from the as-grown material which was prepared by processing rods with composition $La_{0.95}TiO_{3.38}$ under Ar in a GERO mirror furnace at the University of Augsburg. This material is potentially a quasi-1D metal.
The ideal n = 4.5 type composition is $LaTiO_{3.44}$ ($Ti^{3.9+}$ / $3d^{0.1}$)

Photo taken at the ETH Zurich

Progress in Solid State Chemistry 36 (2008) 253

6 Conducting and metallic Carpy-Galy phases $A_nB_nO_{3n+2} = ABO_x$

6.2 $n = 4$, $n = 4.5$, and $n = 5$ type quasi-1D metals $(Sr,La)NbO_x$ ...

Melt-grown n = 4 type $SrNbO_{3.5}$ and $Sr_{0.8}La_{0.2}NbO_{3.5}$

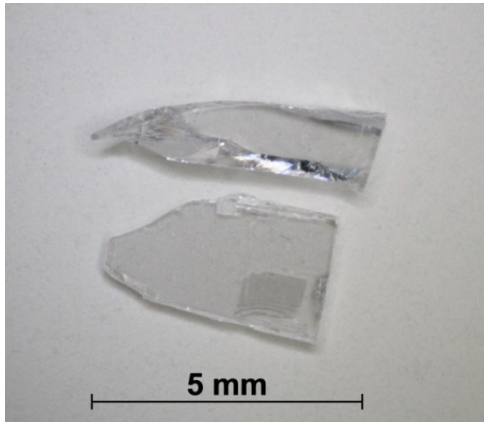

Examples of n = 4 type crystalline pieces from the as-grown materials

Grown under synth. air (left) or argon (right) at the University of Augsburg. Photos taken at the ETH Zurich

$Sr_4Nb_4O_{14} = SrNbO_{3.50}$

Nb^{5+} / $4d^0$ Sample No. 169

White transparent high-T_c ferroelectric insulator with T_c = 1615 K

→ Replacing Sr^{2+} partly by La^{3+}

$Sr_{3.2}La_{0.8}Nb_4O_{14} = Sr_{0.8}La_{0.2}NbO_{3.50}$

$Nb^{4.8+}$ / $4d^{0.2}$ Sample No. 72

Black-blue electrical conductor

- Optical spectroscopy, angle-resolved photoelectron spectroscopy and resistivity measurements → Weakly pronounced quasi-1D metal
- Optical spectroscopy indicates presence of ferroelectric soft mode → Is this a polar or ferroelectric metal ?

C. A. Kuntscher et al., Physical Review B 70 (2004) 245123

V. Bobnar et al., Physical Review B 65 (2002) 155115

F. Lichtenberg et al., Progress in Solid State Chemistry 29 (2001) 1 and 36 (2008) 253

Satoshi Nanamatsu et al., Journal of the Physical Society of Japan 38 (1975) 817

Melt-grown n = 4 type $SrNbO_{3.5}$ and n = 5 type $SrNbO_{3.4}$

Examples of crystalline pieces from the as-grown materials

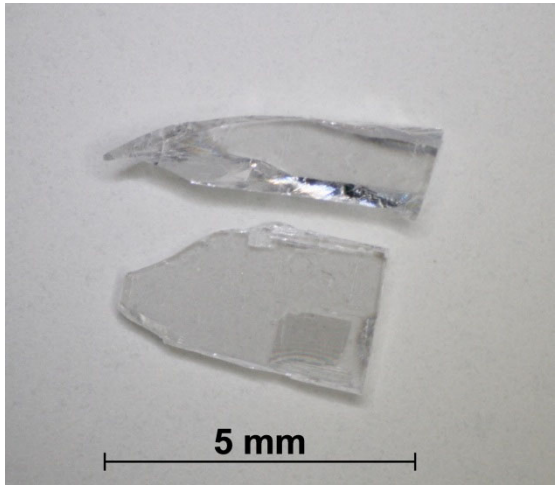

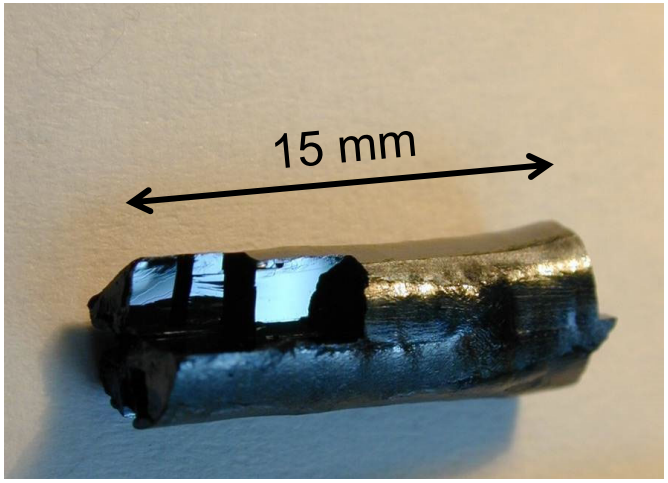

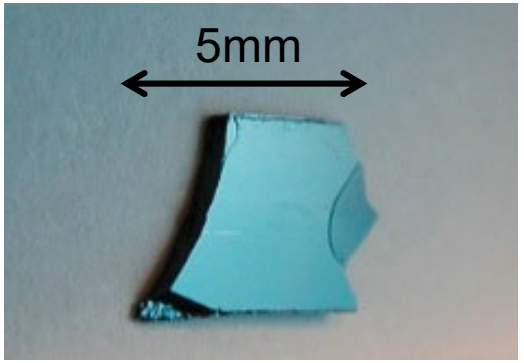

$Sr_4Nb_4O_{14} = SrNbO_{3.50}$

$Nb^{5+} / 4d^0$ Sample No. 169

Grown under synthetic air

White transparent high-T_c ferroelectric insulator with T_c = 1615 K

Structure type n = 4

$Sr_5Nb_5O_{17.05} = SrNbO_{3.41}$

$Nb^{4.82+} / 4d^{0.18}$ Sample No. 71

Grown under argon

Black-blue quasi-1D metal

Structure type n = 5

Progress in Solid State Chemistry 29 (2001) 1 and 36 (2008) 253
Physical Review B 65 (2002) 155115 and B 70 (2004) 245123
Physical Review Letters 89 (2002) 236403
Journal of the Physical Society of Japan 38 (1975) 817

Samples prepared at the University of Augsburg
Photo of $Sr_4Nb_4O_{14} = SrNbO_{3.5}$ taken at the ETH Zurich

Melt-grown n = 4.5 type $(Sr,Ba)NbO_{3.45}$

Examples of crystalline pieces from the as-grown materials

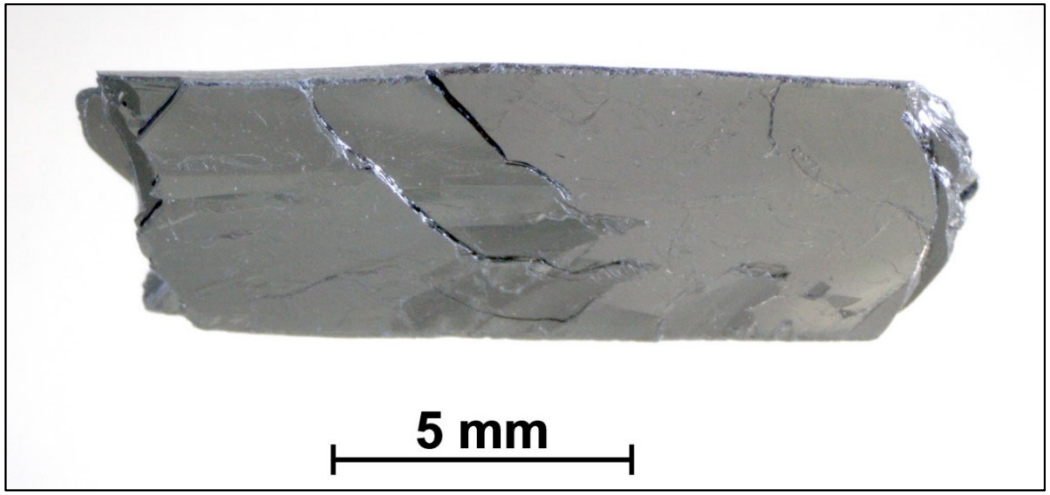

$SrNbO_{3.45}$

$Nb^{4.9+}$ / $4d^{0.1}$

Sample No. 126

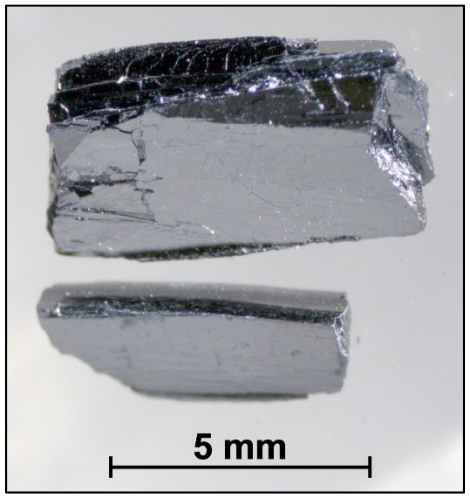

$Sr_{0.96}Ba_{0.04}NbO_{3.45}$

$Nb^{4.9+}$ / $4d^{0.1}$

Sample No. 127

Grown under 98 % Ar + 2 % H_2

Structure type n = 4.5

Quasi-1D metals

Physica C 282 - 287 (1997) 995 • Progress in Solid State Chemistry 29 (2001) 1 and 36 (2008) 253
Physical Review B 61 (2000) 1876 and B 65 (2002) 155115 and B 70 (2004) 245123
Samples prepared at the University of Augsburg - Photos taken at the ETH Zurich

Melt-grown $n = 5$ type $Sr_{0.95}NbO_{3.37}$ and $Sr_{0.9}La_{0.1}NbO_{3.4}$

Examples of crystalline pieces from the as-grown materials

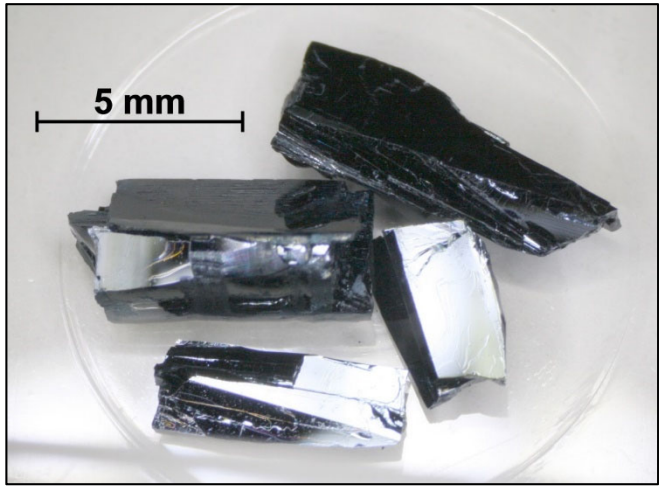

$Sr_{0.95}NbO_{3.37}$ Sample No. 181

$Nb^{4.84+}$ / $4d^{0.16}$

Grown under 98 % Ar + 2 % H_2

Structure type Sr- and O-deficient $n = 5$

Quasi-1D metal

F. Lichtenberg et al.,
Progress in Solid State Chemistry 29 (2001) 1

Teguh Citra Asmara et al.,
to be published in Communications Physics (2020)
See also part 6.2.1

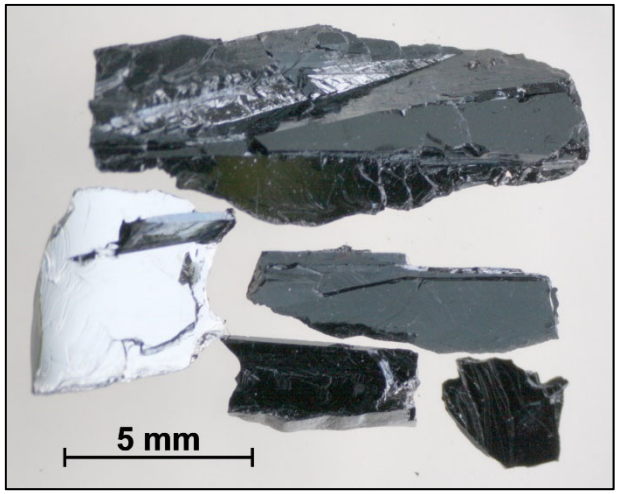

$Sr_{0.9}La_{0.1}NbO_{3.4}$ Sample No. 167

$Nb^{4.7+}$ / $4d^{0.3}$

Grown under argon

Structure type $n = 5$

Quasi-1D metal

F. Lichtenberg et al.,
Progress in Solid State Chemistry 29 (2001) 1

C. A. Kuntscher et al.,
Physical Review B 61 (2000) 1876

Samples prepared at the University of Augsburg - Photos taken at the ETH Zurich

Resistivity $\rho(T)$ of some $A_nNb_nO_{3n+2}$ = $ANbO_x$ along the *a*- , *b*- and *c*-axis

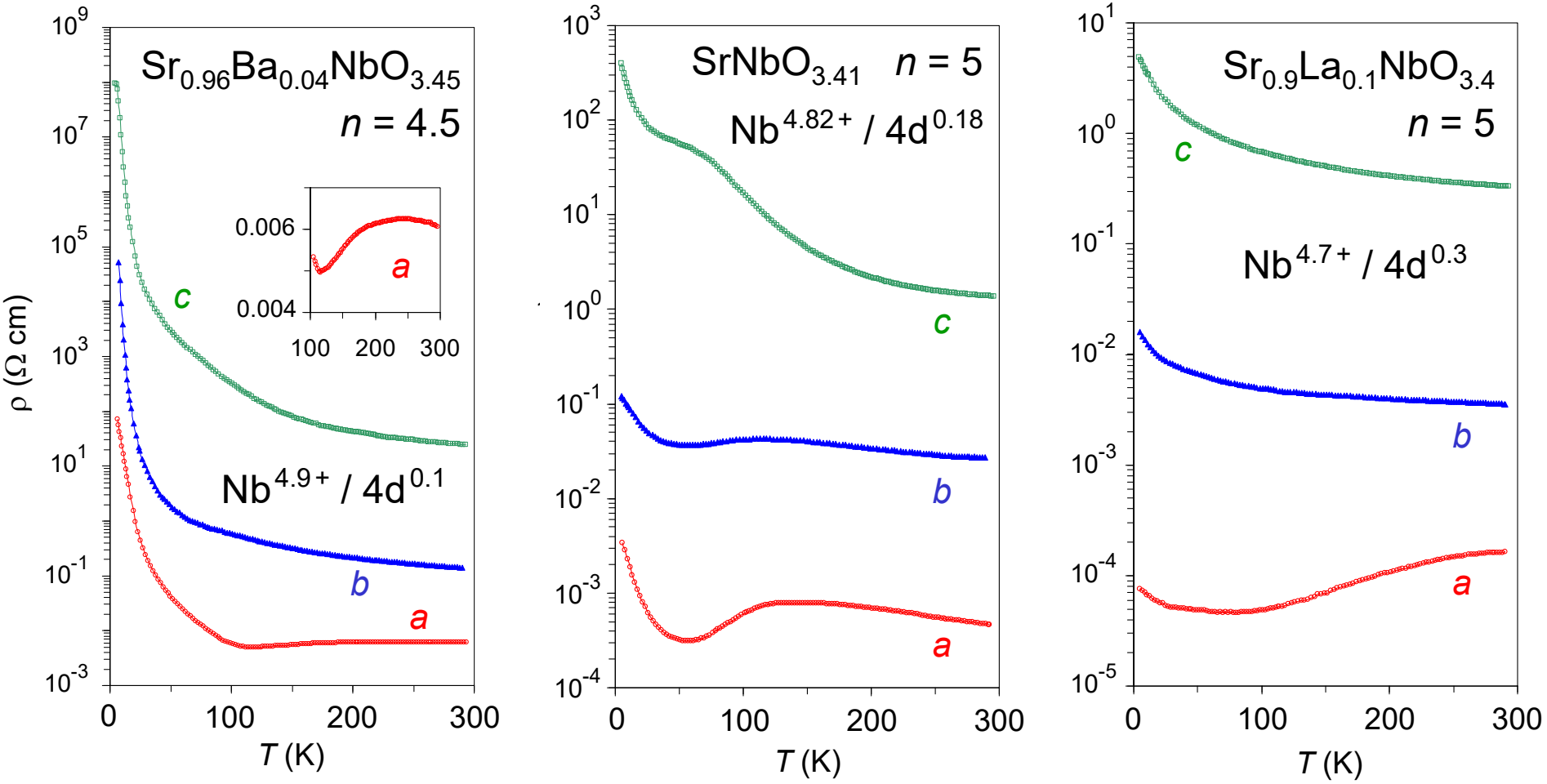

Progress in Solid State Chemistry 29 (2001) 1

- Highly anisotropic conductors
- Quasi-1D metals along *a*-axis. The quasi-1D metallic behavior is confirmed or revealed by angle-resolved photoemission (ARPES) and optical spectroscopy. For references see the previous pages and the pages after the next two pages
- Metal-to-semiconductor transition at low *T*

Resistivity $\rho(T)$ of the $n = 5$ type $SrNbO_{3.41}$

and the Sr- and O-deficient $n = 5$ type $Sr_{0.95}NbO_{3.37}$

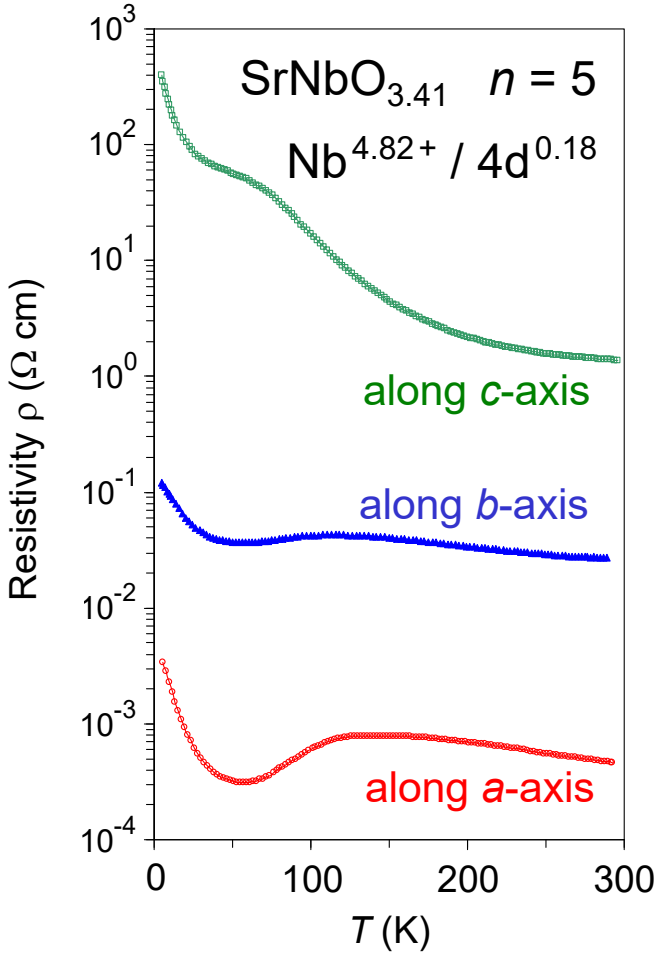

F. Lichtenberg et al., Progress in Solid State Chemistry 29 (2001) 1

Resistivity $\rho(T)$ of the $n = 5$ type $SrNbO_{3.41}$

and the Sr- and O-deficient $n = 5$ type $Sr_{0.95}NbO_{3.37}$

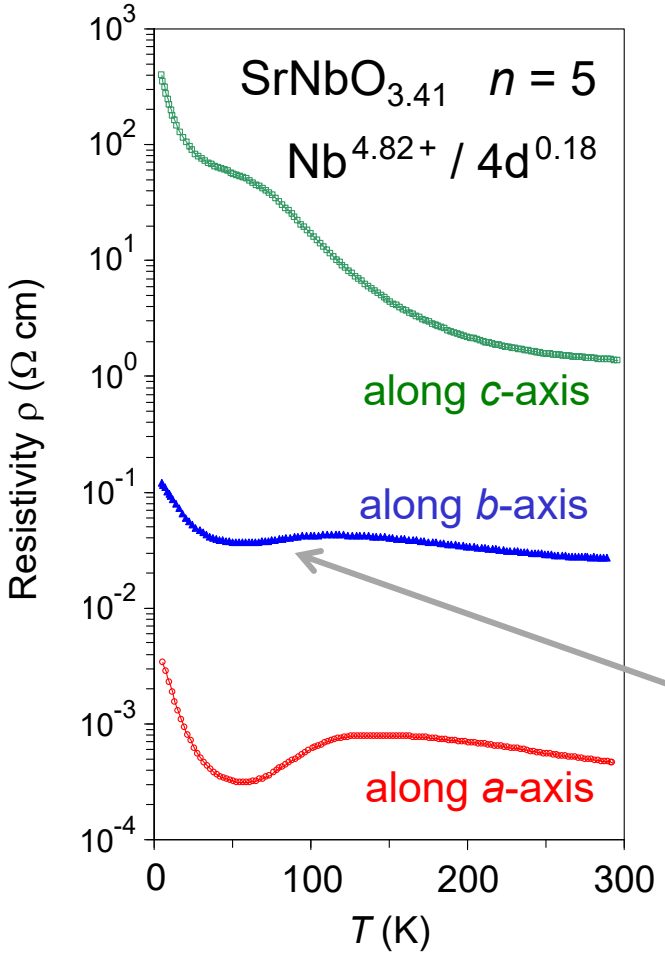

This section with a metallic temperature dependence along the *b*-axis could be due to an intermixture of a contribution from the *a*-axis

F. Lichtenberg et al., Progress in Solid State Chemistry 29 (2001) 1

Resistivity $\rho(T)$ of the $n = 5$ type $SrNbO_{3.41}$ and the Sr- and O-deficient $n = 5$ type $Sr_{0.95}NbO_{3.37}$

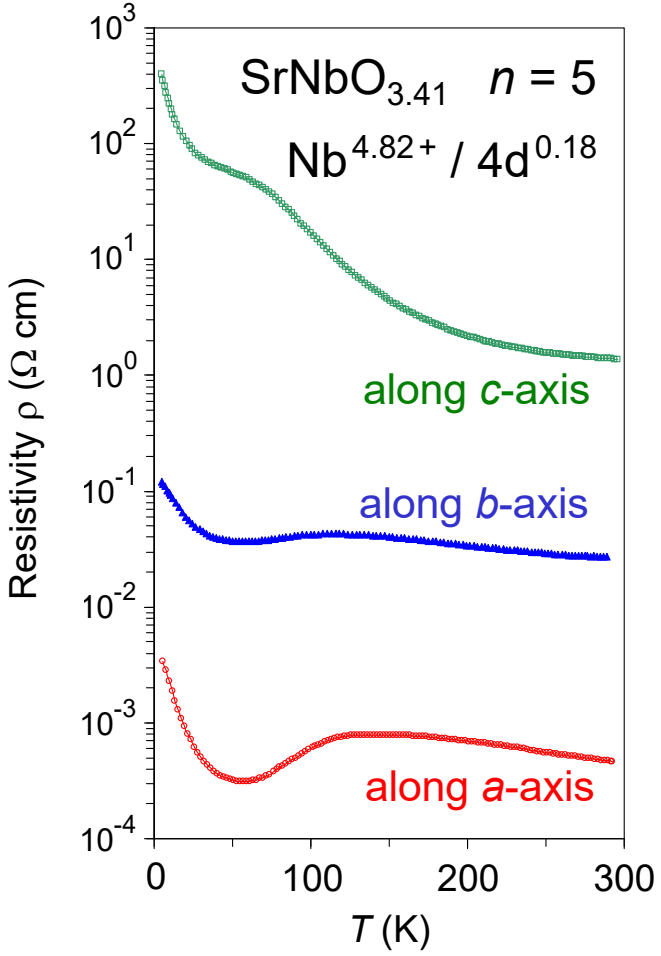

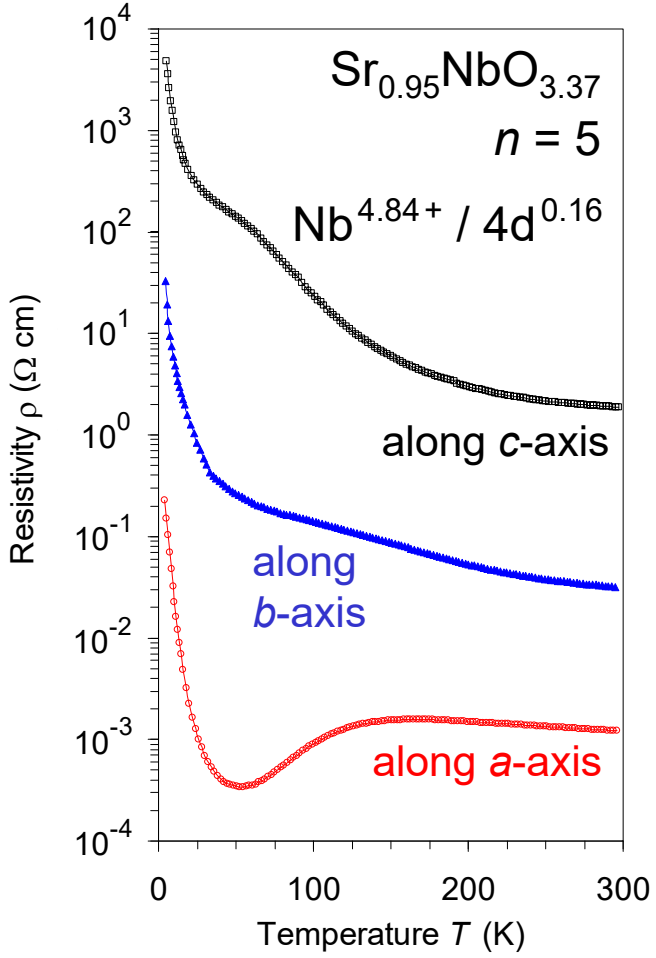

Optical spectroscopy confirmed or revealed that both materials are quasi-1D metals

$SrNbO_{3.41}$:
C. A. Kuntscher et al., Physical Review Letters 89 (2002) 236403 and Physical Review B 70 (2004) 245123

$Sr_{0.95}NbO_{3.37}$:
Teguh Citra Asmara et al., to be published in Communications Physics (2020).
See also part 6.2.1

F. Lichtenberg et al., Progress in Solid State Chemistry 29 (2001) 1

Comprehensive studies on $A_nNb_nO_{3n+2}$ = $ANbO_x$ by angle-resolved photo-emission (ARPES) and optical spectroscopy: Example n = 5 type $SrNbO_{3.41}$

ARPES probes occupied electronic states and their dispersion $E(k)$, $k = k(\theta)$

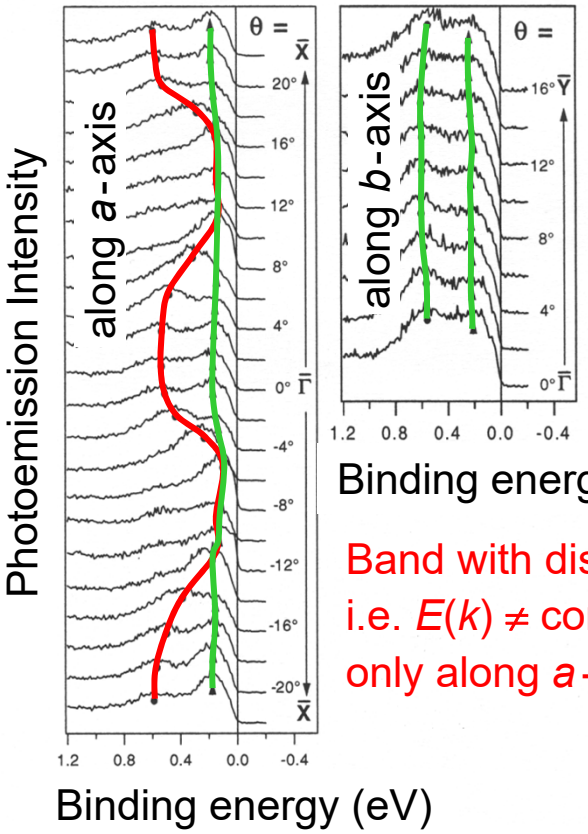

T = 75 K

Band with dispersion, i.e. $E(k) \neq$ constant, only along a-axis

→

Quasi-1D metal along a-axis

←

Inset: Reflectivity $R(\nu)$

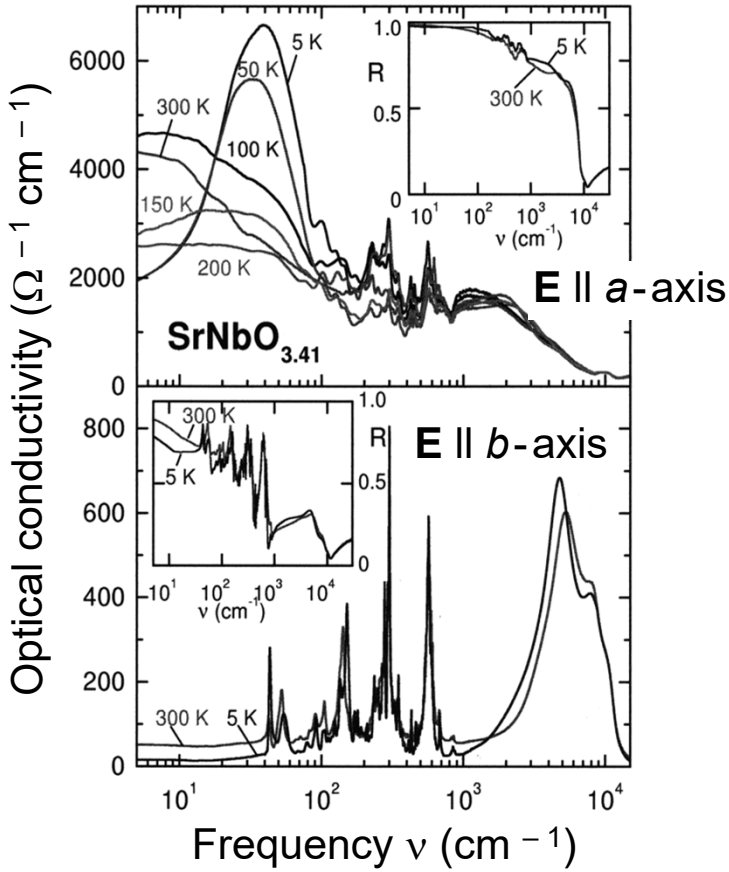

- Metal-to-semiconductor transition at T < 100 K
- High-resolution ARPES at 25 K, resistivity $\rho(T)$ & optical conductivity → Semiconducting state with extremely small energy gap $\Delta \approx 5$ meV, the smallest Δ of all known quasi-1D metals
- Experimental findings appear inconsistent with Peierls or 1D Mott-Hubbard picture

C. A. Kuntscher et al.: Phys. Rev. B 61 (2000) 1876 & 70 (2004) 245123 and Phys. Rev. Lett. 89 (2002) 236403

Comprehensive studies on $A_nNb_nO_{3n+2}$ = $ANbO_x$ by ARPES, optical spectroscopy, resistivity measurements, and electronic band structure calculations

n = 4	$Sr_{0.8}La_{0.2}NbO_{3.50}$	$4d^{0.20}$	→ Weakly pronounced quasi-1D metal No energy gap at low T along a-axis
n = 4.5	$SrNbO_{3.45}$	$4d^{0.10}$	} Quasi-1D metals Small energy gap at low T along a-axis
n = 5	$SrNbO_{3.41}$	$4d^{0.18}$	
n = 5	$Sr_{0.9}La_{0.1}NbO_{3.4}$	$4d^{0.3}$	

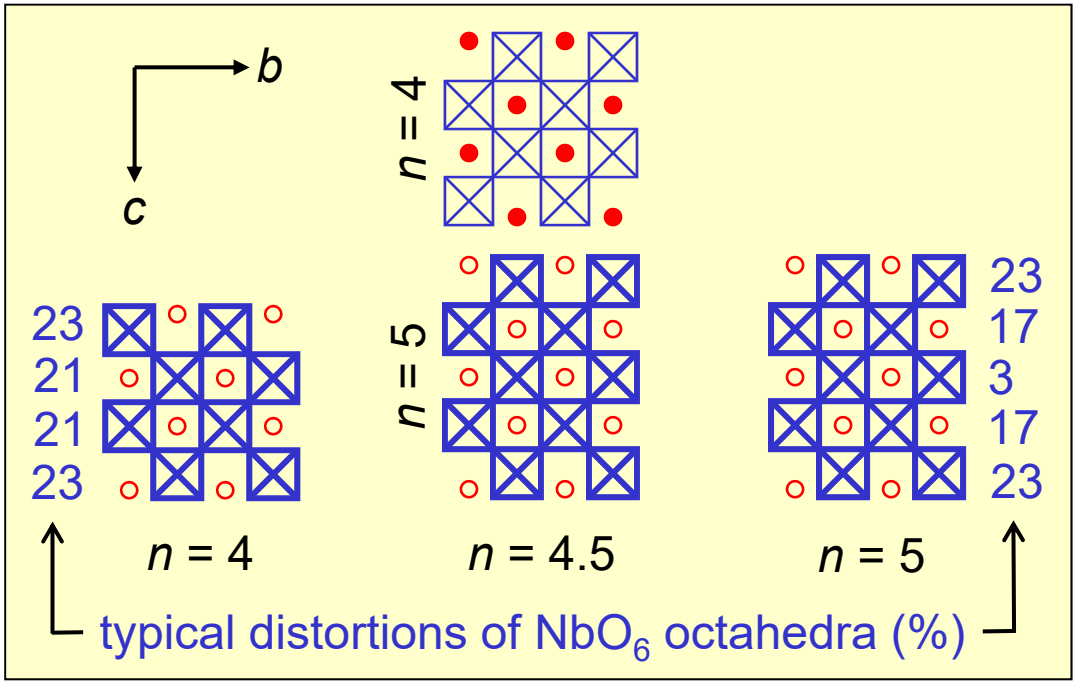

Special role of layers which are 5 NbO_6 octahedra thick:

Electrons from the Nb ions located in the central and nearly undistorted octahedra contribute most to the metallic character

C. A. Kuntscher et al.: Physical Review B 61 (2000) 1876 and 70 (2004) 245123 as well as Physical Review Letters 89 (2002) 236403 • F. Lichtenberg et al.: Progress in Solid State Chemistry 29 (2001) 1 and 36 (2008) 253

LDA calculations of the electronic band structure of the n = 5 quasi-1D metal $SrNbO_{3.41}$

Good agreement with results from angle-resolved photoelectron spectroscopy (ARPES) with respect to lowest band

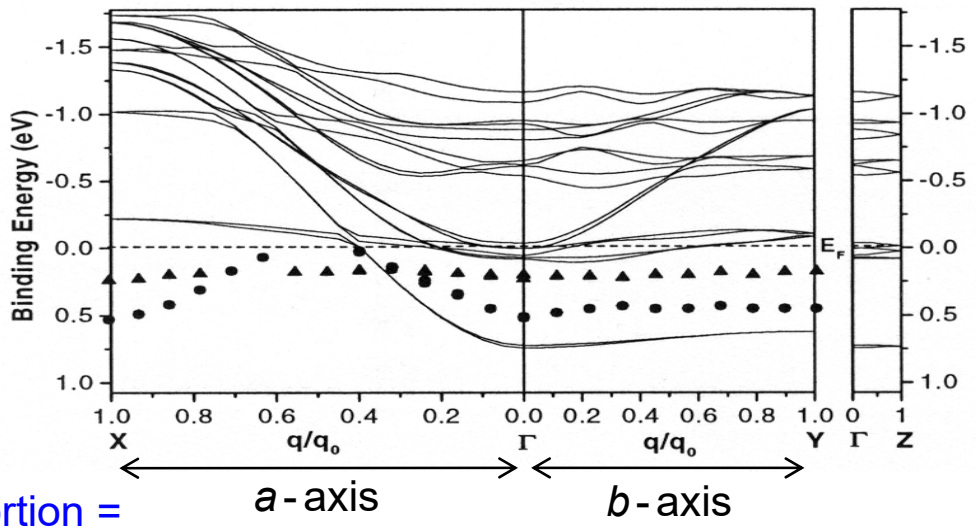

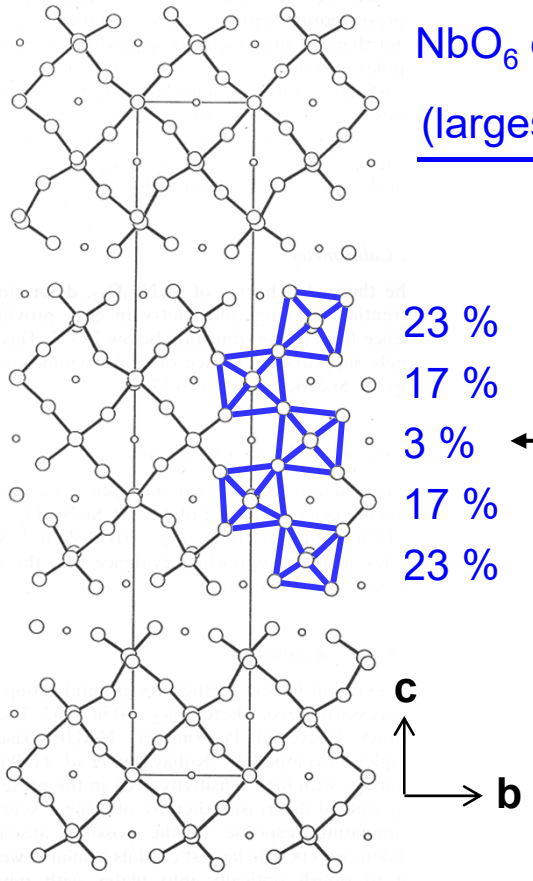

NbO_6 octadedron distortion =

$$\frac{\text{(largest Nb – O distance) – (smallest Nb – O distance)}}{\text{average Nb – O distance}}$$

Nb atoms of least distorted octahedra contribute most to the electronic density of states (DOS) at the Fermi energy E_F

Quasi-1D features along a-axis related to octahedra distortions

LDA predicts further bands around E_F which disperse along a- and b-axis, but they are not observed by ARPES: Subtle structural details ? Electronic correlations ? ARPES resolution ?

C. A. Kuntscher et al.
Phys. Rev. B
61 (2000) 1876

H. Winter et al.
J. Phys. Cond. Matter
12 (2000) 1735

S. C. Abrahams et al.
Acta Cryst. B
54 (1998) 399

F. Lichtenberg et al.
Prog. Solid State Chem.
29 (2001) 1

A special feature of the $A_nB_nO_{3n+2}$ = ABO_x type quasi-1D metals

Structural, compositional and electronical proximity to (anti)ferroelectric insulators !

This distinguishes them from all other known quasi-1D metals such as $K_{0.3}MoO_3$, $Li_{0.9}Mo_6O_{17}$, $NbSe_3$, $(SN)_y$ and organic conductors like TTF-TCNQ

Examples:

n = 4: Ferroelectric $SrNbO_{3.5}$ ($4d^0$) $\rightarrow$ Poor quasi-1D metal $Sr_{0.8}La_{0.2}NbO_{3.5}$ ($4d^{0.2}$)

n = 5: Antiferroelectric $SrNb_{0.8}Ti_{0.2}O_{3.4}$ ($4d^0$) $\rightarrow$ Quasi-1D metal $SrNbO_{3.4}$ ($4d^{0.2}$)

↓

Intrinsic coexistence of metallic conductivity and large dielectric polarizability in $A_nB_nO_{3n+2}$ type systems !?

Usually these both features exclude each other

Intrinsic coexistence of these both features might be useful for the creation of superconductors

↓

The following experimental observations support the presence of such an intrinsic coexistence …

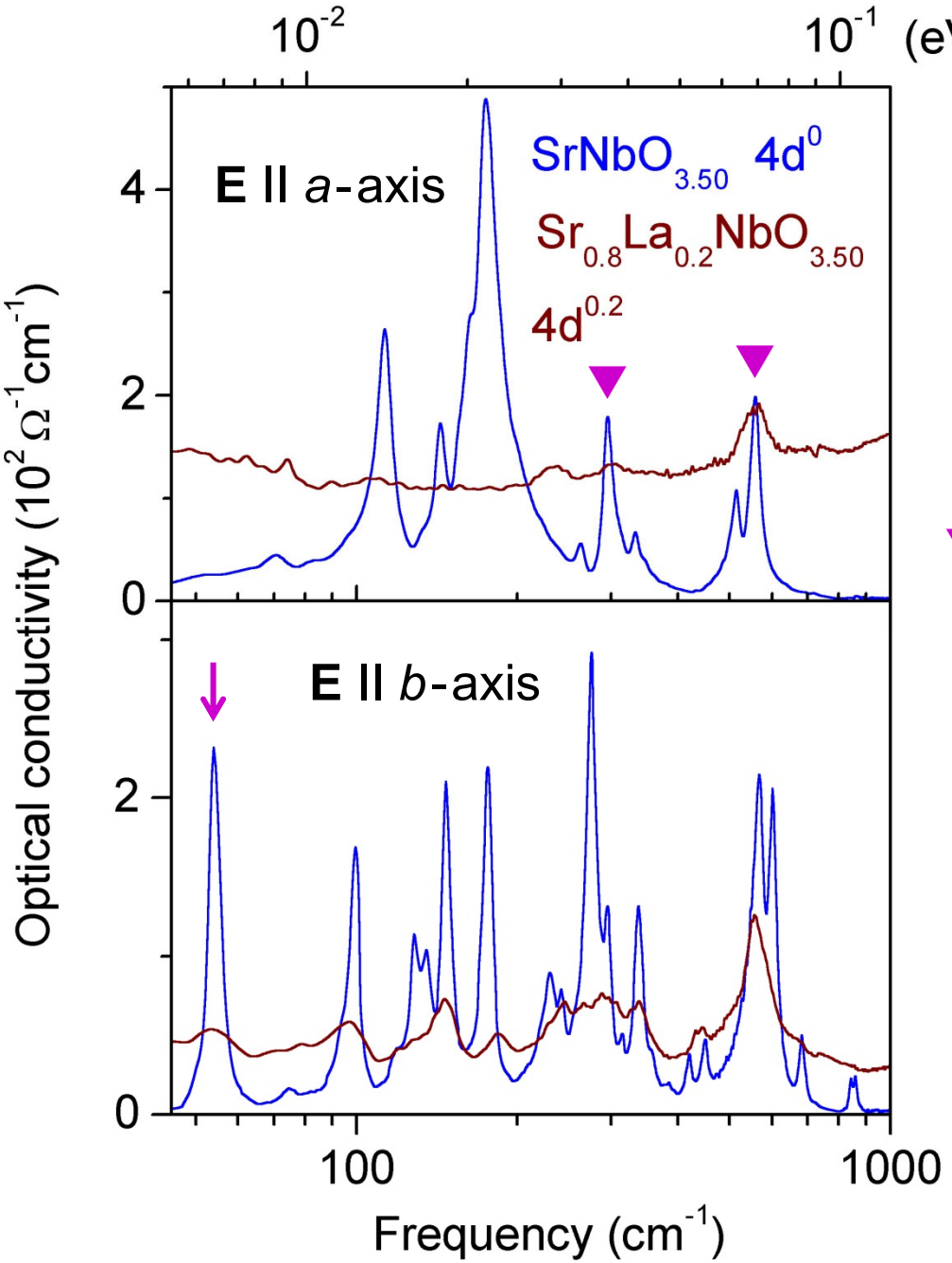

Optical conductivity at T = 300 K along *a*- and *b*-axis of n = 4 ferroelectric insulator $SrNbO_{3.50}$ and weakly pronounced n = 4 quasi-1D metal $Sr_{0.8}La_{0.2}NbO_{3.50}$

▼ = Phonon peaks which survive in the conducting oxide

↓ = Ferroelectric soft mode (phonon peak associated with ferroelectric phase transition)

Ferroelectric soft mode peak occurs also in the weakly pronounced quasi-1D metal !

C. A. Kuntscher et al.
Physical Review B 70 (2004) 245123

Is the n = 4 type $Sr_{0.8}La_{0.2}NbO_{3.50}$ a polar or ferroelectric metal ?

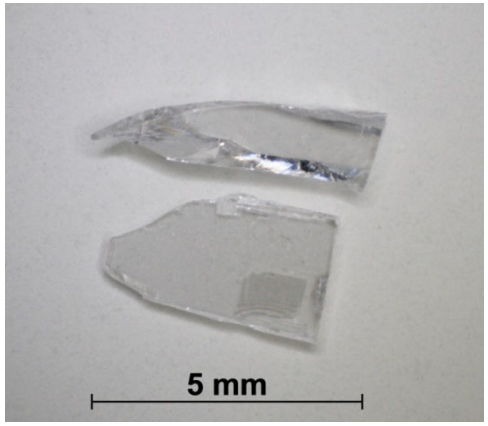

Examples of n = 4 type crystalline pieces from the as-grown materials

Grown under synth. air (left) or argon (right) at the University of Augsburg. Photos taken at the ETH Zurich

$Sr_4Nb_4O_{14} = SrNbO_{3.50}$

Nb^{5+} / $4d^0$ Sample No. 169

White transparent high-T_c ferroelectric insulator with T_c = 1615 K

→ Replacing Sr^{2+} partly by La^{3+}

$Sr_{3.2}La_{0.8}Nb_4O_{14} = Sr_{0.8}La_{0.2}NbO_{3.50}$

$Nb^{4.8+}$ / $4d^{0.2}$ Sample No. 72

Black-blue electrical conductor

- Optical spectroscopy, angle-resolved photoelectron spectroscopy and resistivity measurements → Weakly pronounced quasi-1D metal
- Optical spectroscopy indicates presence of ferroelectric soft mode → Is this a polar or ferroelectric metal ?

C. A. Kuntscher et al., Physical Review B 70 (2004) 245123

V. Bobnar et al., Physical Review B 65 (2002) 155115

F. Lichtenberg et al., Progress in Solid State Chemistry 29 (2001) 1 and and 36 (2008) 253

Satoshi Nanamatsu et al., Journal of the Physical Society of Japan 38 (1975) 817

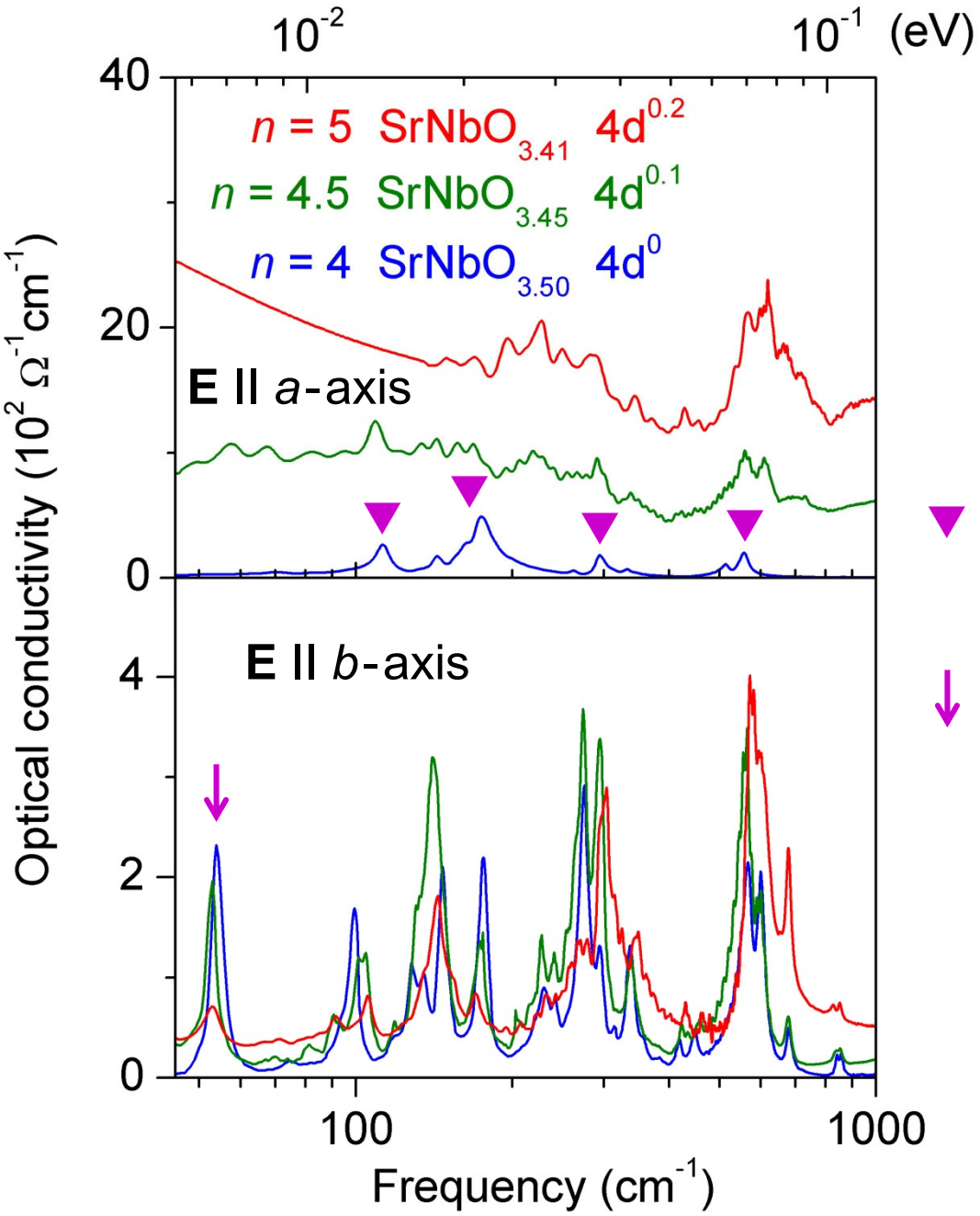

Optical conductivity at T = 300 K along a- and b-axis of n = 4 ferroelectric insulator $SrNbO_{3.50}$, n = 4.5 quasi-1D metal $SrNbO_{3.45}$ and n = 5 quasi-1D metal $SrNbO_{3.41}$

▼ = Phonon peaks which survive in the conducting oxides

↓ = Ferroelectric soft mode (phonon peak associated with ferroelectric phase transition)

Ferroelectric soft mode peak occurs also in the quasi-1D metals !

C. A. Kuntscher et al.
Physical Review B 70 (2004) 245123

Ferroelectric insulator $SrNbO_{3.5}$ (n = 4) and quasi-1D metal $SrNbO_{3.4}$ (n = 5)

Examples of crystalline pieces from the as-grown materials

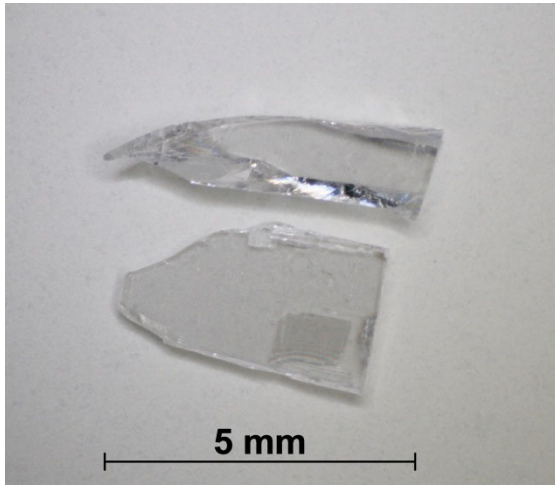

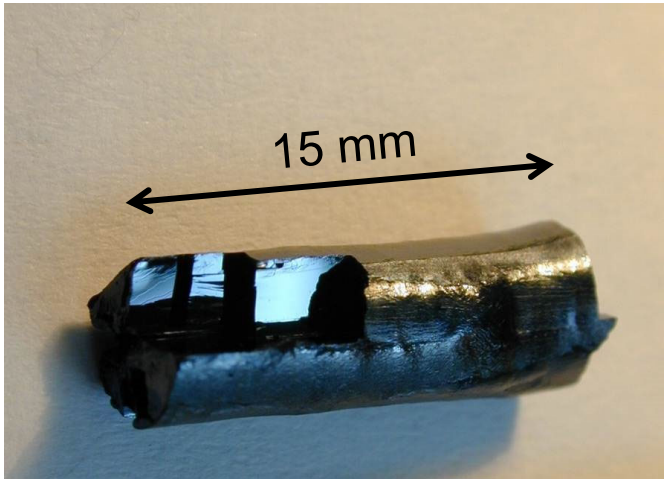

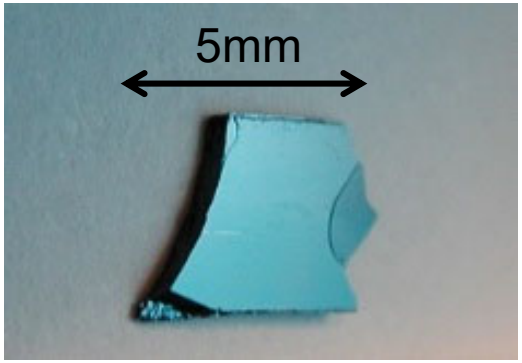

$Sr_4Nb_4O_{14} = SrNbO_{3.50}$

$Nb^{5+} / 4d^0$ Sample No. 169

Grown under synthetic air

White transparent high-T_c ferroelectric insulator with T_c = 1615 K

Structure type n = 4

$Sr_5Nb_5O_{17.05} = SrNbO_{3.41}$

$Nb^{4.82+} / 4d^{0.18}$ Sample No. 71

Grown under argon

Black-blue quasi-1D metal

Structure type n = 5

Progress in Solid State Chemistry 29 (2001) 1 and 36 (2008) 253
Physical Review B 65 (2002) 155115 and B 70 (2004) 245123
Physical Review Letters 89 (2002) 236403
Journal of the Physical Society of Japan 38 (1975) 817

Samples prepared at the University of Augsburg

Photo of $Sr_4Nb_4O_{14} = SrNbO_{3.5}$ taken at the ETH Zurich

Intrinsic high-frequency dielectric permittivity of the *n* = 5 quasi-1D metal $SrNbO_{3.41}$ along the *c*-axis

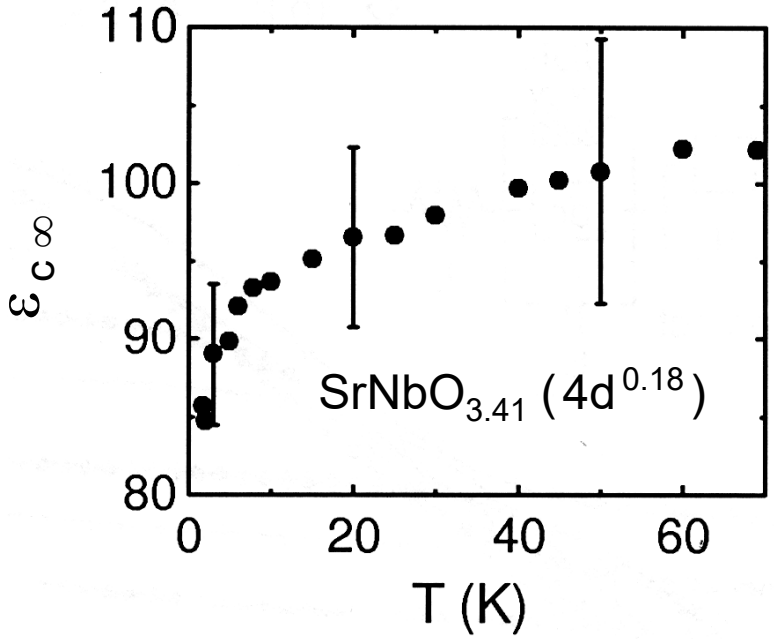

Large permittivity: $\varepsilon_{c\infty} \approx 100$

$T > 70$ K: Measurement prevented by too high conductivity

V. Bobnar et al.
Physical Review B 65 (2002) 155115

$T \approx 70$ K: Metallic along *a*-axis according to ARPES and resistivity $\rho(T)$

C. A. Kuntscher et al., Physical Review B 70 (2004) 245123

F. Lichtenberg et al., Progress in Solid State Chemistry 29 (2001) 1

→ Coexistence of large intrinsic high-frequency dielectric permittivity $\varepsilon_{c\infty}$ along *c*-axis and metallic behavior along *a*-axis

Note: Largest possible intrinsic dielectric permittivity in non-ferroelectrics of the order of $\varepsilon_{\infty} \approx 100$!?

P. Lunkenheimer et al., Physical Review B 66 (2002) 052105

Magnetic susceptibility $\chi(T)$ of the ferroelectric insulator $SrNbO_{3.5}$ and quasi-1D metals of the type $(Sr,La,)NbO_x$

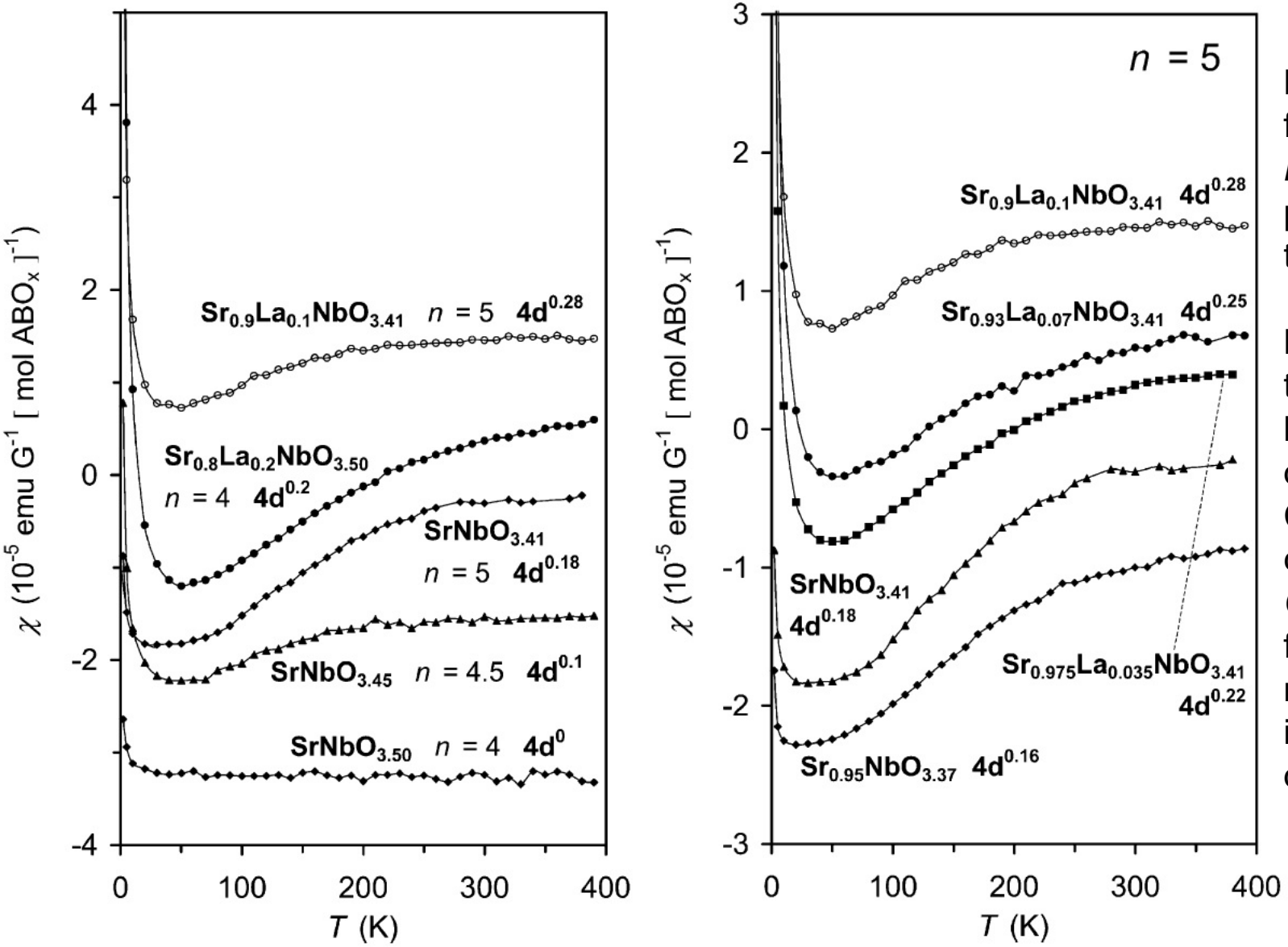

Magnetic field $H \leq 1000$ G parallel to the layers

Low temperature behavior is due to a Curie contribution C / T from para-magnetic impurities or defect states

Progress in Solid State Chemistry 29 (2001) 1

Model considerations of $\chi(T)$ of the n = 5 type quasi-1D metal $SrNbO_{3.41}$

Bulk susceptibility $\chi(T)$ can be interpreted as arising from almost localized spins in a 1D Heisenberg chain with an exchange constant of J = 530 K

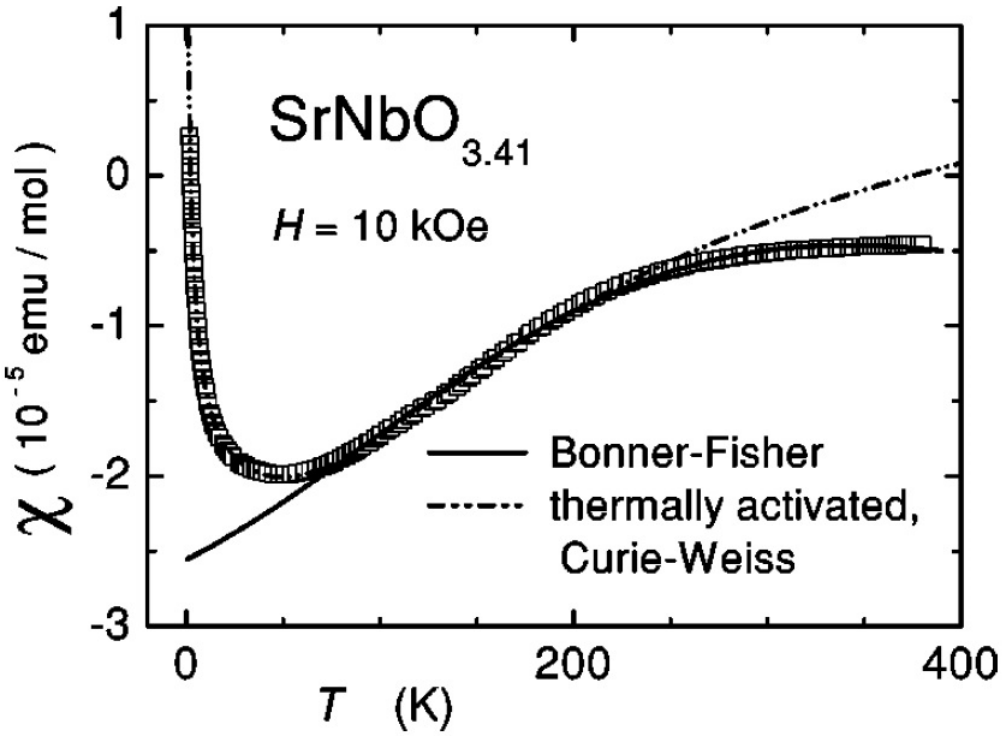

J.-E. Weber, C. Kegler, N. Büttgen, H.-A. Krug von Nidda, A. Loidl, and F. Lichtenberg, Physical Review B 64 (2001) 235414

Approach 1: Diamagnetic contribution from closed electron shells plus Curie-Weiss tail at low T from defect states plus Pauli paramagnetism from thermally activated charge carriers:

$$\chi(T) = \chi_{\mathrm{dia}} + \frac{C}{T-\theta} + \chi_{\mathrm{Pauli}} \exp\left(-\frac{E_g}{k_B T}\right)$$

Approach 2: Bonner-Fisher model of an 1D antiferromagnetic S = 1/2 Heisenberg spin chain for $T \geq 0.3\ J$:

$$\chi_{1\mathrm{D}}(T) = \chi_{\mathrm{dia}} + \frac{V\Gamma}{T} \times \frac{0.25 + 0.0774975 J/T + 0.075235 (J/T)^2}{1 + 0.9931 J/T + 0.172135 (J/T)^2 + 0.757825 (J/T)^3}$$

50 K $\leq T \leq$ 400 K and J = 530 K

Examples of conducting materials which show another behavior of $\chi(T)$

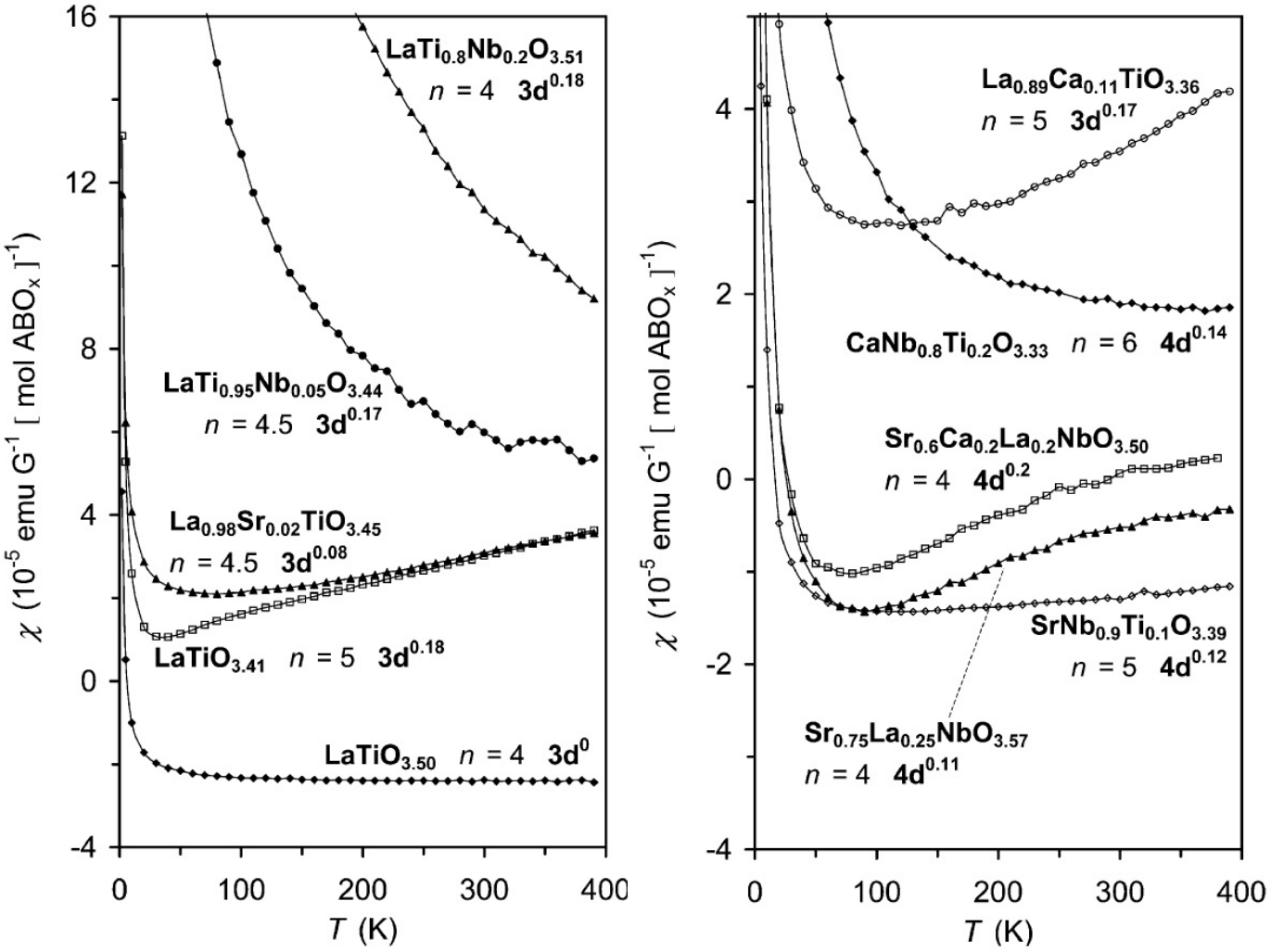

Progress in Solid State Chemistry 29 (2001) 1

For the $n = 4$ type $LaTi_{0.8}Nb_{0.2}O_{3.51}$, the $n = 4.5$ type $LaTi_{0.95}Nb_{0.05}O_{3.44}$, and the $n = 6$ type $CaNb_{0.8}Ti_{0.2}O_{3.33}$ the magnetic susceptibility $\chi(T)$ increases with decreasing temperature. These compounds are conducting but probably not metallic

6 Conducting and metallic Carpy-Galy phases $A_nB_nO_{3n+2} = ABO_x$

6.2.1 Photoinduced properties of the quasi-1D metals $SrNbO_{3.45}$ (n = 4.5) and $Sr_{0.95}NbO_{3.37}$ (Sr- and O-deficient n = 5) ...

Photoinduced properties of the quasi-1D metals $SrNbO_{3.45}$ (n = 4.5) and $Sr_{0.95}NbO_{3.37}$ (Sr- and O-deficient n = 5)

Photoinduced metastable exciton-driven metal-insulator transitions in quasi-one-dimensional transition metal oxides

Teguh Citra Asmara, Frank Lichtenberg, Florian Biebl, Tao Zhu, Pranab Kumar Das, Muhammad Avicenna Naradipa, Ping Yang, Philipp Lenzen, Sören Buchenau, Benjamin Grimm-Lebsanft, Dongyang Wan, Paolo E. Trevisanutto, Mark B. H. Breese, T. Venkatesan, Michael Rübhausen, and Andrivo Rusydi

to be published in Communications Physics (2020)

Abstract: Photoinduced phase transitions in matter have gained tremendous attention over the past few years. However, their ultrashort lifetime makes their study and possible control very challenging. Here, we report on new photoinduced metal-insulator transitions (MITs) in quasi-one-dimensional metals $Sr_{1-y}NbO_x$ using Mueller-Matrix spectroscopic ellipsometry, transient ultraviolet Raman spectroscopy, transient mid-infrared reflectivity and angular-resolved photoemission spectroscopy supported with density functional theory. The MITs are driven by photo-pumping of *d*-*d* excitons, causing the metallic *a*-axis to become insulating while the insulating *b*- and *c*-axis concomitantly become a correlated metal. We assign these effects to the melting of charge and lattice orderings along the different anisotropic optical axes. The long lifetime in the order of several seconds of the metastable MITs gives a greater flexibility to study and manipulate the transient excitonic state. Fundamental questions associated with coherent excitonic states such as Bose-Einstein condensates and potential applications in exciton-based optoelectronic devices could now be addressed.

6 Conducting and metallic Carpy-Galy phases $A_nB_nO_{3n+2} = ABO_x$

6.3 Why Carpy-Galy phases $A_nB_nO_{3n+2} = ABO_x$ might have a potential to create superconductors ...

Potential for high-T_c superconductivity in $A_nB_nO_{3n+2}$ = ABO_x quasi-1D metals from the perspective of so-called excitonic superconductivity

A hypothetical possibility to realize superconductivity at room temperature is given by the so-called excitonic mechanism of superconductivity (electron-electron mediated):

- Original proposal by W. A. Little for hypothetical **quasi-1D** organic conductors:

  Conducting chains surrounded by electronically polarizable side branches

  - In: Novel Superconductivity, Plenum Press (1987) 341
  - Journal de Physique Colloque C3 Supplement No 6 (1983) 819
  - Int. Journal of Quantum Chemistry (Quantum Chemistry Symposium) 15 (1981) 545
  - Scientific American 212 (1965) 21
  - Physical Review 134 (1964) A1416

- Original proposal by V. L. Ginzburg for **quasi-2D** systems:

  Thin metallic sheet surrounded by two dielectric layers

  - Soviet Physics Uspekhi 72 (1970) 335

The results of the studies on $La_5Ti_5O_{17}$ = $LaTiO_{3.4}$ and (Sr,La)NbO_x , see part 6.1 and part 6.2 , suggest the following scenario ...

Potential for high-T_c superconductivity in $A_nB_nO_{3n+2}$ = ABO_x quasi-1D metals from the perspective of so-called excitonic superconductivity

For example, the types n = 4.5 and n = 5 seem to be interesting from Little's and from Ginzburg's point of view: • Quasi-2D crystal structure • Electronically quasi-1D by B – O chains and delocalized electrons along a-axis • Electronically polarizable units by electronic band structure, fluctuating valence states of rare earth ions at A site … ?

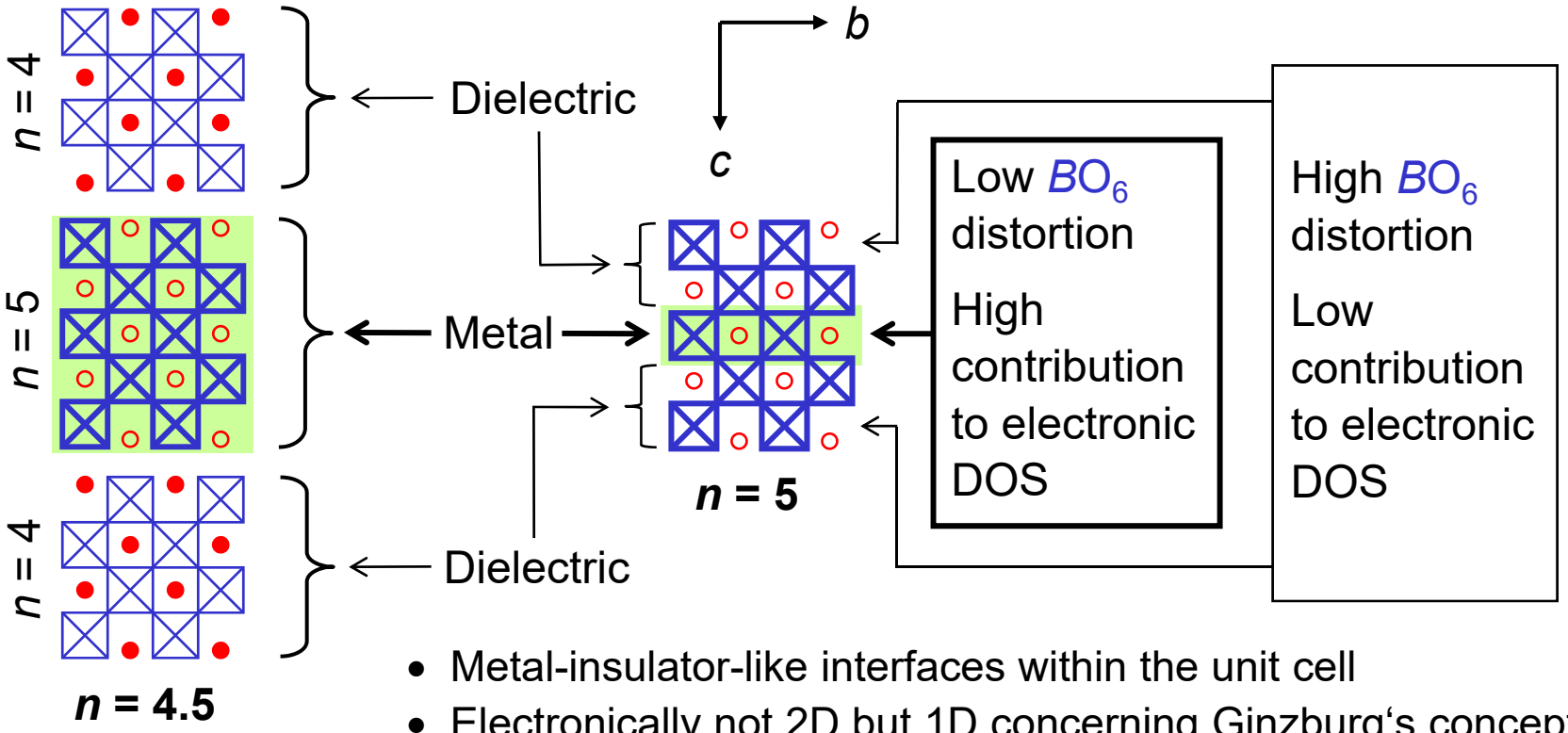

- Metal-insulator-like interfaces within the unit cell
- Electronically not 2D but 1D concerning Ginzburg's concept
- Also quasi-2D metals among $A_nB_nO_{3n+2}$ type oxides ?

Progress in Solid State Chemistry 36 (2008) 253 and Advanced Materials 25 (2013) 218

Searching for high-T_c and ambient temperature superconductors

- Excitonic superconductivity only in a very small region of the compositional parameter space (W. A. Little, V. L. Ginzburg)

- “Therefore, synthesizing a room temperature superconductor, one must pay attention to its structure: the ”distance” between failure and success can be as small as 0.01 Å in the lattice constant”.

  Cited from Andrei Mourachkine‘s book “Room-Temperature Superconductivity“, 2004 (ISBN 1 – 904602 – 27 – 4), pages 292 and 293

Indications for high-T_c superconductivity in the system Na – W – O

WO_3 (W^{6+} / $5d^0$)

- Antiferroelectric insulator with $T_c \approx 1000$ K
- Distorted ReO_3 type crystal structure which can be considered as distorted perovskite ABO_3 with absent A

Sodium tungsten bronze Na_xWO_3 (W^{6+} / $5d^0$ and W^{5+} / $5d^1$) with $0 < x < 1$

- Na-deficient perovskite structure and metallic conductor
- Superconducting with $T_c < 2$ K for $0.16 \leq x \leq 0.4$, T_c increases with decreasing x

B. W. Brown and E. Banks, Journal of the American Chemical Society 76 (1954) 963 • Ch. J. Raub et al., Physical Review Letters 13 (1964) 746 • N. N. Garif'yanov et al., Czechoslovak Journal of Physics 46 Supplement S2 (1996) 855 • A. Garcia-Ruiz and Bokhimi, Physica C 204 (1992) 79

Superconducting islands with $T_c \approx 90$ K on the surface of Na-doped WO_3

S. Reich et al., The European Physical Journal B 9 (1999) 1 • A. Shengelaya et al., The European Physical Journal B 12 (1999) 13 • S. Reich et al., Journal of Superconductivity 13 (2000) 855

- Strong experimental evidence for high-T_c superconductivity without Cu
- In spite of many efforts the superconducting phase could not be identified

Speculation: High-T_c superconducting phase Na_xWO_y could be of the type $A_nB_nO_{3n+2}$

Progress in Solid State Chemistry 36 (2008) 253

$NaWO_x$ ($3.5 \geq x \geq 3$) and $A_nB_nO_{3n+2} = ABO_x$

x in $NaWO_x$	$x = 3.5$ W^{6+} ($5d^0$) insulator	$3.5 > x > 3$ Conducting	$x = 3$ W^{5+} ($5d^1$) metal
Structure type after normal pressure synthesis	Orthorhombic Centrosymmetric WO_6 octahedra and WO_4 tetrahedra $[W_2O_7]^{2-}$ chains along *a*-axis K. Okada, H. Morikawa, F. Marumo, and S. Iwai, Acta Cryst. B 31 (1975) 1200	W^{6+} ($5d^0$) / W^{5+} ($5d^1$) ? Hypothetical $4 \leq n \leq 6$ Supercon-ducting ? Progress in Solid State Chemistry 36 (2008) 253	
Structure type after high pressure synthesis	Orthorhombic $n = 4$ Non-centrosymmetric Potentially ferroelectric Single crystals were grown by cooling normal pressure synthesized $Na_2W_2O_7$ slowly from 1200 °C under 20 – 30 kbar K.-J. Range and H. Haase, Acta Cryst. C 46 (1990) 317		Cubic perovskite Yuya Ikeuchi et al., Inorganic Chemistry 58 (2019) 6790

No indications for superconductivity in a polycrystalline sintered *n* = 5 type composition $NaWO_{3.4}$

Synthesis approach:

$0.5\ Na_2CO_3 + 0.8921\ WO_3 + 0.1079\ WO_{1.98} \rightarrow NaWO_{3.39} + 0.5\ CO2 \uparrow$

$WO_{1.98}$ = Tungsten dioxide with thermogravimetrically determined oxygen content 1.98

Pre-reacted for 6 h at 600 °C under air. After mingling the pre-reacted material with $WO_{1.98}$ the obtained powder was pressed into a reactangular shape and heated and sintered for 6 h at 700 °C under argon in the GERO tube furnace.

A polycrystalline sintered *n* = 5 type composition $NaWO_{3.4}$

Sample No. 704 • Prepared at the ETH Zurich in 2012

Material is probably multiphase

Powder x-ray diffraction was not performed

The magnetic moment M(T) and susceptibility $\chi(T)$ of a piece from this material was measured by a SQUID magnetometer in the temperature range $2\ K \leq T \leq 330\ K$. $\chi(T)$ is weakly diamagnetic and nearly temperature-independent and no indication for superconductivity was detected.

Acknowledgement: F. L. thanks Bertram Batlogg (ETH Zurich) who performed the magnetic measurement with his Qantum Design SQUID Magnetometer MPMS XL

No indications for superconductivity in a polycrystalline sintered *n* = 6 type composition $NaWO_{3.33}$

Synthesis approach analogous to what is described on the previous page but with another appropriate ratio WO_3 / $WO_{1.98}$

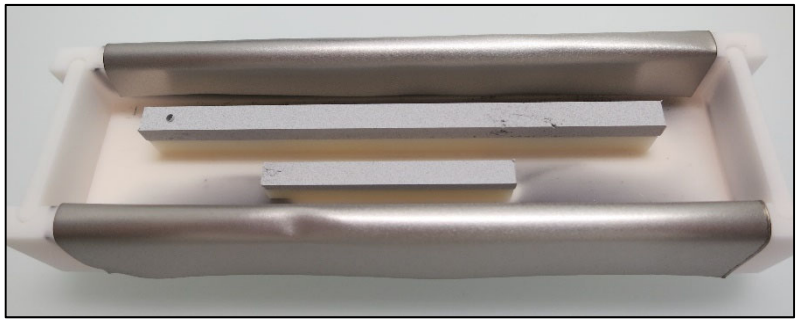

Two as-pressed rods with composition $NaWO_{3.33}$

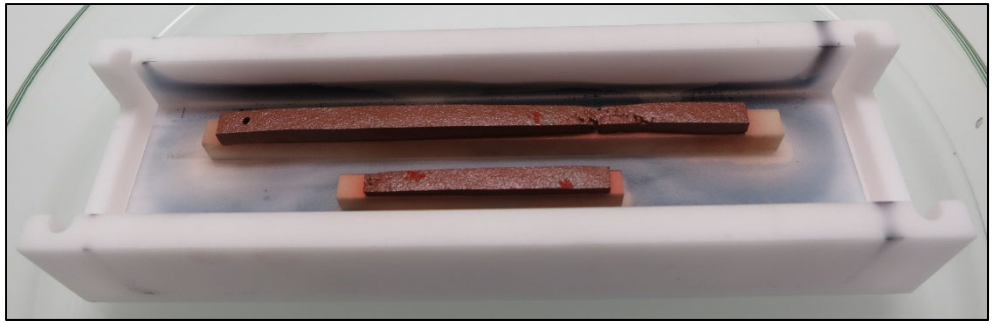

Rods with composition $NaWO_{3.33}$ after they were heated and sintered under argon

Run / Sample No. 711 • Prepared at the ETH Zurich in 2013

Material is probably multiphase • Powder x-ray diffraction was not performed

Processing the sintered rods by floating zone melting did not work because of a difficult melting behavior and strong bending of the seed rod in the mirror furnace

The magnetic moment M(T) of a piece from the sintered rods was measured by a SQUID magnetometer in the temperature range 2 K ≤ T ≤ 300 K and no indication for superconductivity was detected. **Acknowledgement:** F. L. thanks Marisa Medarde (PSI) and Mickael Morin (PSI) for performing a magnetic measurement with a Quantum Design SQUID magnetometer MPMS XL and Nicholas Bingham (PSI) for performing a magnetic measurement with a Quantum Design SQUID magnetometer MPMS3

6 Conducting and metallic Carpy-Galy phases $A_nB_nO_{3n+2} = ABO_x$

6.4 Potential polar or ferroelectric metals such as the $n = 4$ type $Sr_{0.8}La_{0.2}NbO_{3.5}$ and the hypothetical $n = 5$ type $Bi_5Ti_5O_{17}$ ...

Is the n = 4 type $Sr_{0.8}La_{0.2}NbO_{3.5}$ a polar or ferroelectric metal ?

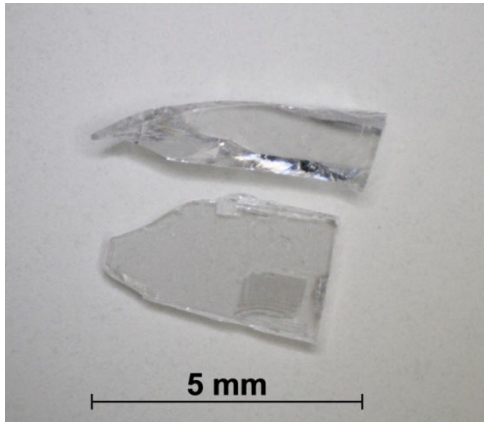

Examples of n = 4 type crystalline pieces from the as-grown materials

Grown under synth. air (left) or argon (right) at the University of Augsburg. Photos taken at the ETH Zurich

$Sr_4Nb_4O_{14} = SrNbO_{3.50}$

Nb^{5+} / $4d^0$ Sample No. 169

White transparent high-T_c ferroelectric insulator with T_c = 1615 K

→ Replacing Sr^{2+} partly by La^{3+}

$Sr_{3.2}La_{0.8}Nb_4O_{14} = Sr_{0.8}La_{0.2}NbO_{3.50}$

$Nb^{4.8+}$ / $4d^{0.2}$ Sample No. 72

Black-blue electrical conductor

- Optical spectroscopy, angle-resolved photoelectron spectroscopy and resistivity measurements → Weakly pronounced quasi-1D metal
- Optical spectroscopy indicates presence of ferroelectric soft mode → Is this a polar or ferroelectric metal ?

C. A. Kuntscher et al., Physical Review B 70 (2004) 245123

V. Bobnar et al., Physical Review B 65 (2002) 155115

F. Lichtenberg et al., Progress in Solid State Chemistry 29 (2001) 1 and 36 (2008) 253

Satoshi Nanamatsu et al., Journal of the Physical Society of Japan 38 (1975) 817

See also part 6.2

A hypothetical *n* = 5 type material which is potentially a ferroelectric metal: $Bi_5Ti_5O_{17}$

Prediction of a native ferroelectric metal

Alessio Filippetti, Vincenzo Fiorentini, Francesco Ricci, Pietro Delugas & Jorge Iniguez
Nature Communications 7 (2016) 11211 (1 - 7)
https://doi.org/10.1038/ncomms11211

To the best of our knowledge there is so far no publication about the synthesis of $Bi_5Ti_5O_{17}$. It is probably very difficult to prepare, if at all possible

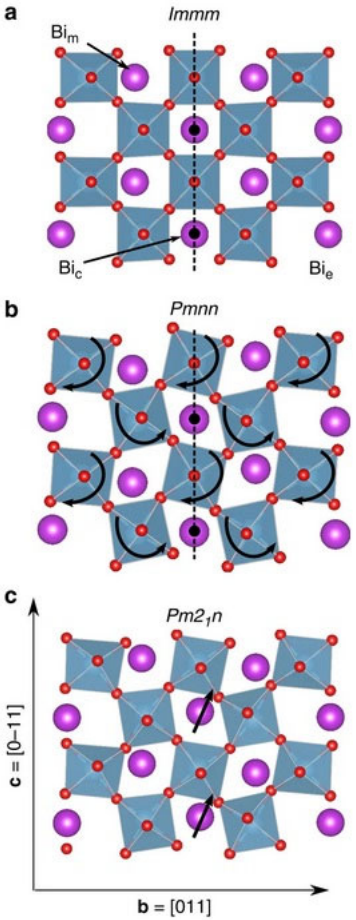

Abstract

Over 50 years ago, Anderson and Blount discussed symmetry-allowed polar distortions in metals, spawning the idea that a material might be simultaneously metallic and ferroelectric. While many studies have ever since considered such or similar situations, actual ferroelectricity - that is, the existence of a switchable intrinsic electric polarization - has not yet been attained in a metal, and is in fact generally deemed incompatible with the screening by mobile conduction charges. Here we refute this common wisdom and show, by means of first-principles simulations, that native metallicity and ferroelectricity coexist in the layered perovskite $Bi_5Ti_5O_{17}$. We show that, despite being a metal, $Bi_5Ti_5O_{17}$ can sustain a sizable potential drop along the polar direction, as needed to reverse its polarization by an external bias. We also reveal striking behaviours, as the self-screening mechanism at work in thin $Bi_5Ti_5O_{17}$ layers, emerging from the interplay between polar distortions and carriers in this compound.

Another potential polar or ferroelectric metals

$SrNbO_{3.4} = Sr_5Nb_5O_{17} = Sr_{20}Nb_{20}O_{68}$ is a centrosymmetric *n* = 5 type quasi-1D metal which is described in part 6.2 and 6.5 – 6.7

There is a related O-deficient *n* = 5 type niobate, namely the non-centrosymmetric Schückel-Müller-Buschbaum phase
$SrNbO_{3.2} = Sr_5Nb_5O_{16} = Sr_{20}Nb_{20}O_{64}$
which is presented in part 6.7 . Its physical properties are not yet known. If the non-centrosymmetric $Sr_5Nb_5O_{16} = Sr_{20}Nb_{20}O_{64}$ is a quasi-1D metal, then it is potentially a polar or ferroelectric metal.

Melt-grown Schückel-Müller-Buschbaum type phases, namely the Sr- and O-deficient *n* = 5 type $Sr_{17}Ca_2Nb_{19}WO_{64}$ and $Sr_{17}CaBaNb_{19}WO_{64}$, are presented in part 6.9.1 and 6.9.5 – 6.9.8 . If they are likewise non-centrosymmetric and if they are quasi-1D metals, then they are potentially polar or ferroelectric metals.

6 Conducting and metallic Carpy-Galy phases $A_nB_nO_{3n+2} = ABO_x$

6.5 The history how the quasi-1D metallic behavior was revealed and results of resistivity measurements with various types of electrical contacts and methods ...

Results of resistivity measurements on crystals of melt-grown $LaTiO_{3.41}$ published in 1991 – Electrical contacts made with silver paint

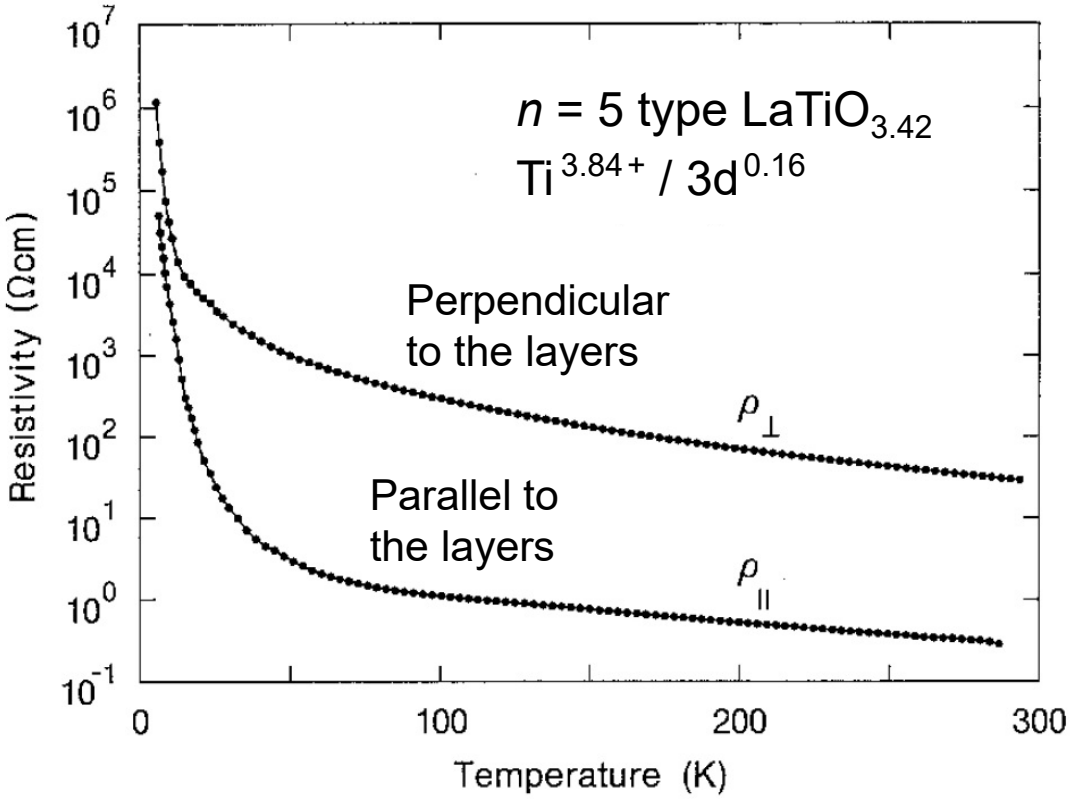

Resistivity measurements between room temperature and 4.2 K were performed on platelets obtained by cleaving the melt-grown samples. Typical dimensions of these crystals were (2 mm) × (1 mm) × (0.1 mm) but larger ones were also used. Electrical contacts in a four-point configuration were made with thin indium or thin gold-beryllium wires and silver paint

- Also the electrical voltage contacts were prepared by silver paint and thin wires
- The in-plane direction of the electrical current with respect to the *a*- and *b*- axis was / is not known
- A metallic temperature dependence of the resistivity was not detected

F. Lichtenberg, T. Williams, A. Reller, J. G. Bednorz, and D. Widmer, Zeitschrift für Physik B Condensed Matter 84 (1991) 369 • F. Lichtenberg, Dissertation, University of Zurich (1991)

Results of resistivity measurements on crystals of melt-grown $CaNbO_{3.35}$ published in 1991 – Electrical contacts made with silver paint

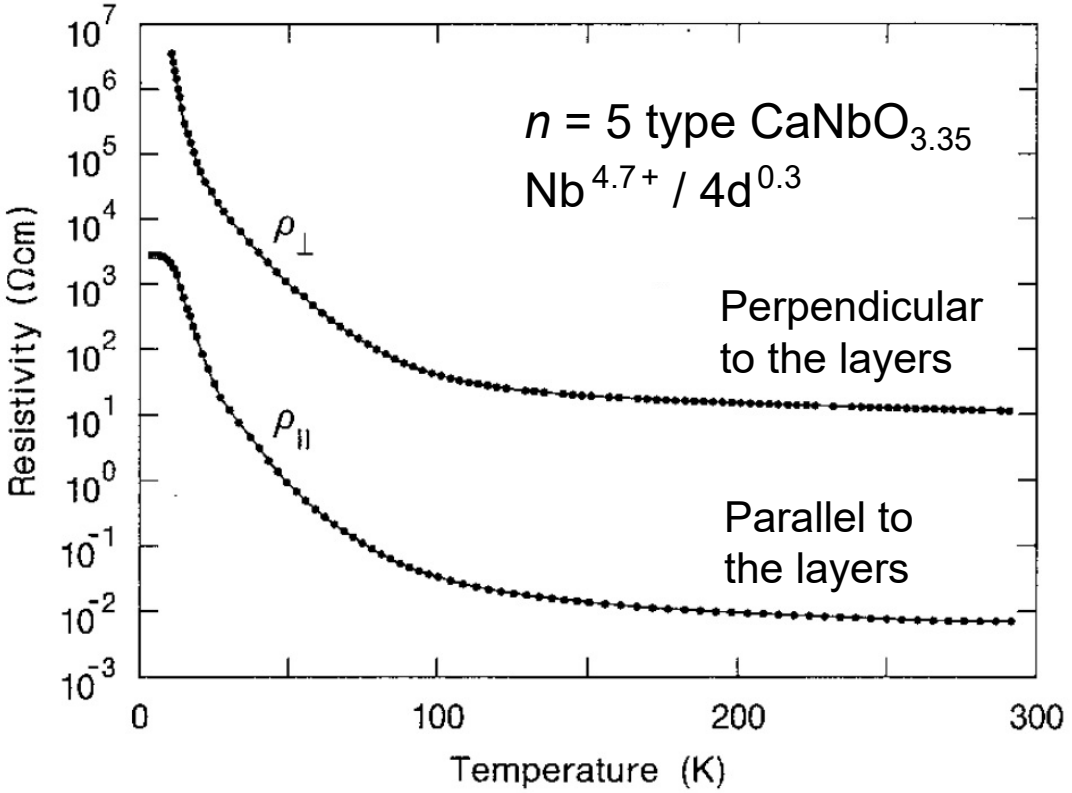

Resistivity measurements between room temperature and 4.2 K were performed on platelets obtained by cleaving the melt-grown samples. Typical dimensions of these crystals were (2 mm) × (1 mm) × (0.1 mm) but larger ones were also used. Electrical contacts in a four-point configuration were made with thin indium or thin gold-beryllium wires and silver paint

- Also the electrical voltage contacts were prepared by silver paint and thin wires
- The in-plane direction of the electrical current with respect to the *a*- and *b*- axis was / is not known
- A metallic temperature dependence of the resistivity was not detected

F. Lichtenberg, T. Williams, A. Reller, J. G. Bednorz, and D. Widmer, Zeitschrift für Physik B Condensed Matter 84 (1991) 369 • F. Lichtenberg, Dissertation, University of Zurich (1991)

Results of resistivity measurements on crystals of melt-grown $SrNbO_{3.45}$ published in 1991 – Electrical contacts made with silver paint

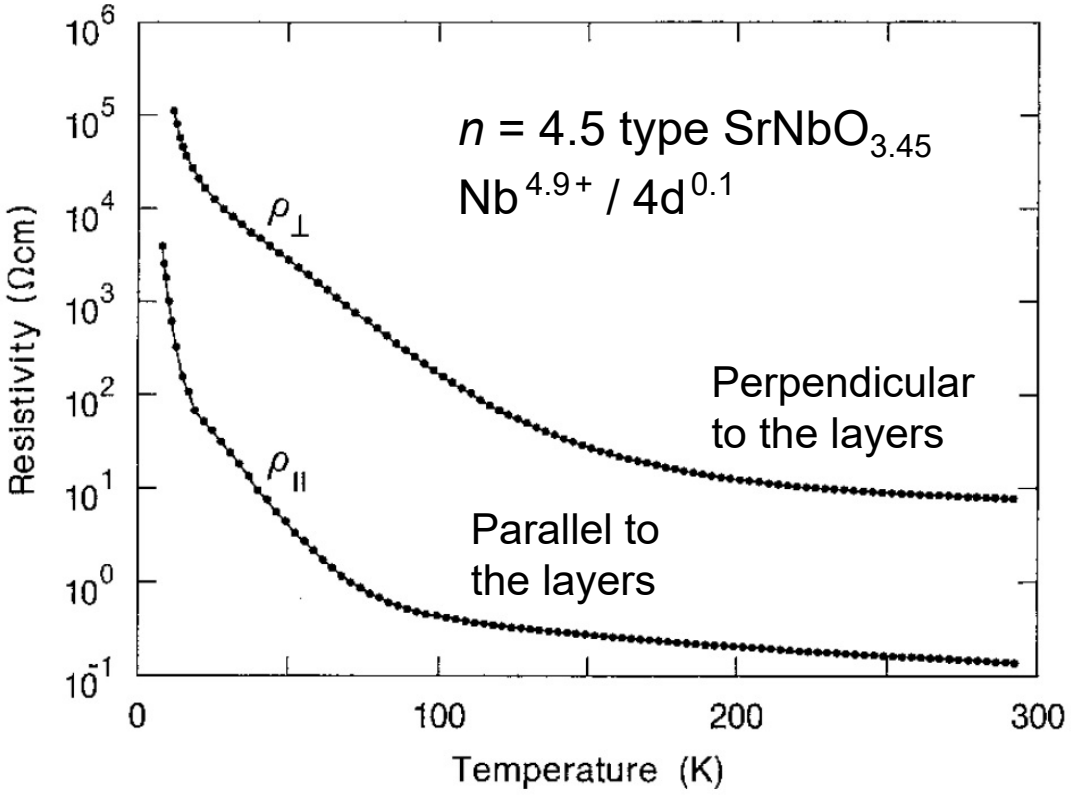

Resistivity measurements between room temperature and 4.2 K were performed on platelets obtained by cleaving the melt-grown samples. Typical dimensions of these crystals were (2 mm) × (1 mm) × (0.1 mm) but larger ones were also used. Electrical contacts in a four-point configuration were made with thin indium or thin gold-beryllium wires and silver paint

- Also the electrical voltage contacts were prepared by silver paint and thin wires
- The in-plane direction of the electrical current with respect to the *a*- and *b*- axis was / is not known
- A metallic temperature dependence of the resistivity was not detected

F. Lichtenberg, T. Williams, A. Reller, J. G. Bednorz, and D. Widmer, Zeitschrift für Physik B Condensed Matter 84 (1991) 369 • F. Lichtenberg, Dissertation, University of Zurich (1991)

Results of angle-resolved photoemission spectroscopy (ARPES) on crystals of melt-grown n = 4.5 type $SrNbO_{3.45}$ published in 1997

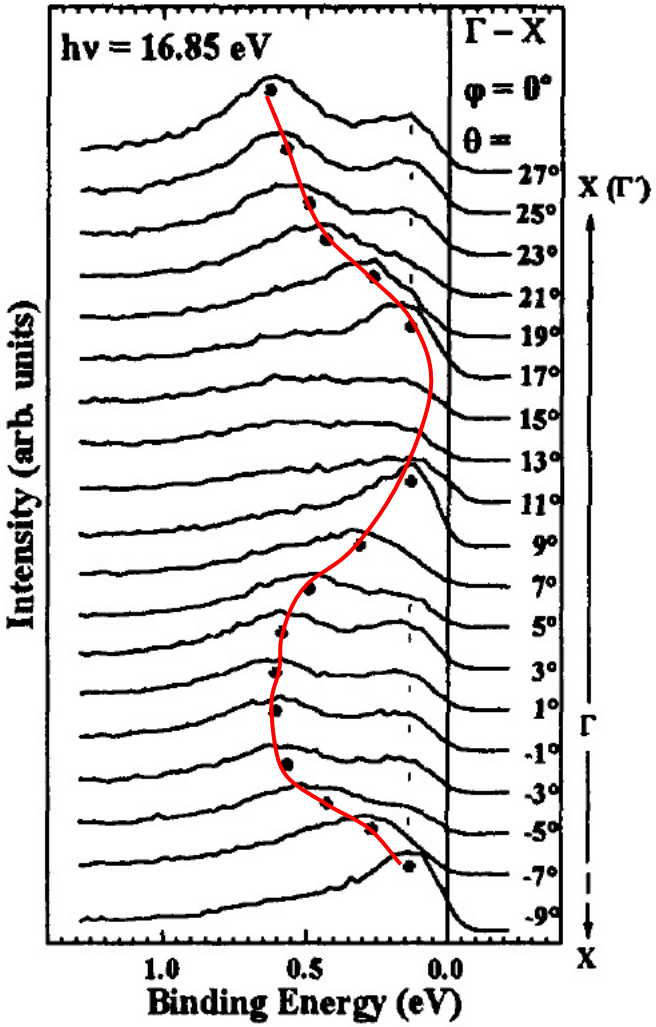

ARPES probes the occupied electronic states and their dispersion $E(k)$, $k = k(\theta)$

A band with dispersion, i.e. $E(k) \neq$ constant, was detected only along the *a*-axis

This result which was published by D. H. Lu et al. in 1997 was the first indication that the n = 4.5 type $SrNbO_{3.45}$ could be a quasi-1D metal

D. H. Lu, C. S. Gopinath, M. Schmidt, T. R. Cummins, N. Nücker, S. Schuppler, and F. Lichtenberg, Physica C 282 - 287 (1997) 995

Subsequently this and other $A_nB_nO_{3n+2} = ABO_x$ type niobates and titanates were comprehensively studied by optical spectroscopy and ARPES by C. A. Kuntscher et al. and by resistivity measurements with special electrical voltage contacts by F. Lichtenberg et al. As presented in part 6.1 and 6.2 the corresponding results clearly show that many of the studied materials are quasi-1D metals.

The result by D. H. Lu et al. triggered some attempts to detect the quasi-1D metallic behavior also in resistivity measurements by using improved or special electrical voltage contacts ...

Electrical contacts for resistivity measurements on crystals

After the ARPES results from D. H. Lu et al. on n = 4.5 type $SrNbO_{3.45}$ it was attempted to detect the quasi-1D metallic behavior also in temperature-dependent resistivity measurements. When compared to the former approach whose results were published in 1991 two modifications were implemented :

- Laue diffraction was used to determine the orientation of the crystals and in-plane current and voltage contacts along the *a*- and *b*-axis were attached
- Some attempts of using different types of in-plane voltage contacts resulted in the conclusion that only ultrasonically bonded wires lead to the detection of a metallic resistivity behavior along the *a*-axis

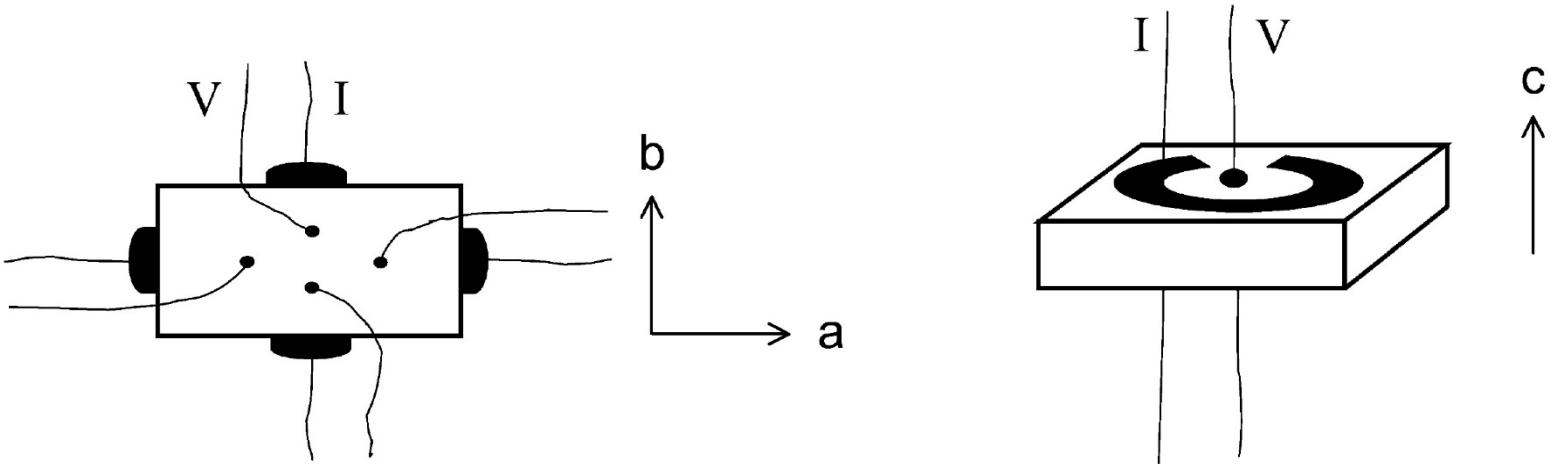

Sketch of the arrangement of electrical contacts for resistivity measurements in a four-point configuration on a rectangular plate-like crystal along the *a*-, *b*- and *c*-axis. V and I denote the voltage and current contacts, respectively

F. Lichtenberg, A. Herrnberger, K. Wiedenmann, and J. Mannhart, Progress in Solid State Chemistry 29 (2001) 1

Electrical contacts for resistivity measurements on crystals

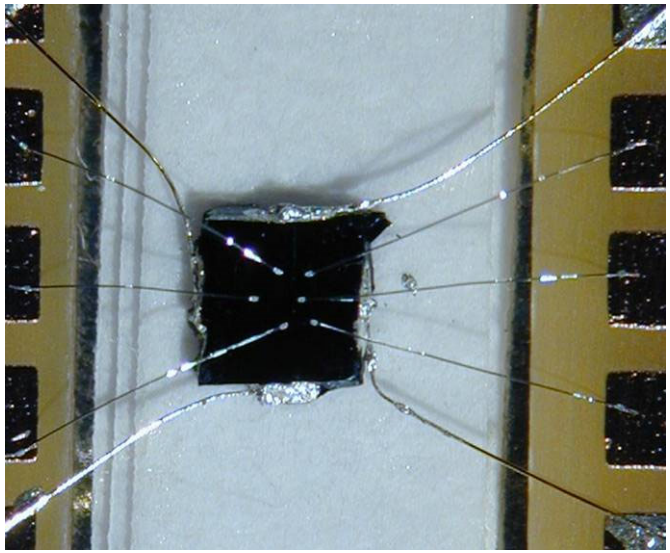

A crystal prepared for four-point resistivity measurements along two different directions within the *ab*-plane, usually along the *a*- and *b*-axis. The size of this crystal is (1.7 mm) × (1.7 mm) × (0.3 mm). At the four sides the current leads, 50 µm diameter Au wires, are attached with silver paint. On the top there are six voltage contacts, 25 µm diameter Al wires, which were mechanically fixed by ultrasonic bonding. Although one current direction requires only two voltage contacts, the presence of more contacts can be very useful, e.g. if one of them fails.

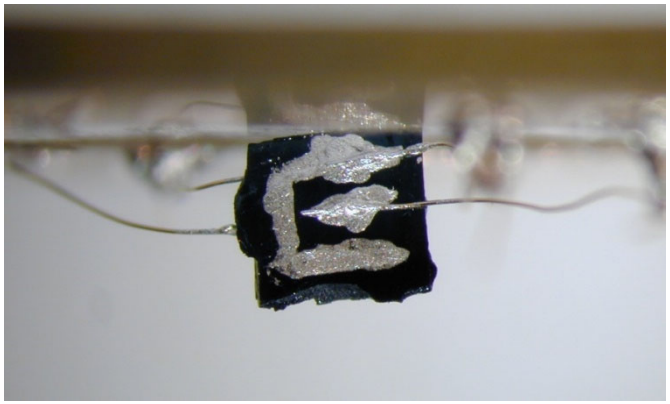

The same crystal as shown above but now with contacts for a four-point resistivity measurement perpendicular to the layers. Shown is one of the both sides with two contacts which were prepared by silver paint and 50 µm diameter Au wires. The U-like shape is used as current contact and the other in the middle as voltage contact. There are two corresponding contacts on the other side of the crystal.

F. Lichtenberg, A. Herrnberger, and K. Wiedenmann, Progress in Solid State Chemistry 36 (2008) 253

Examples of results of resistivity measurements on plate-like crystals with ultrasonically bonded in-plane voltage contacts published in 2001

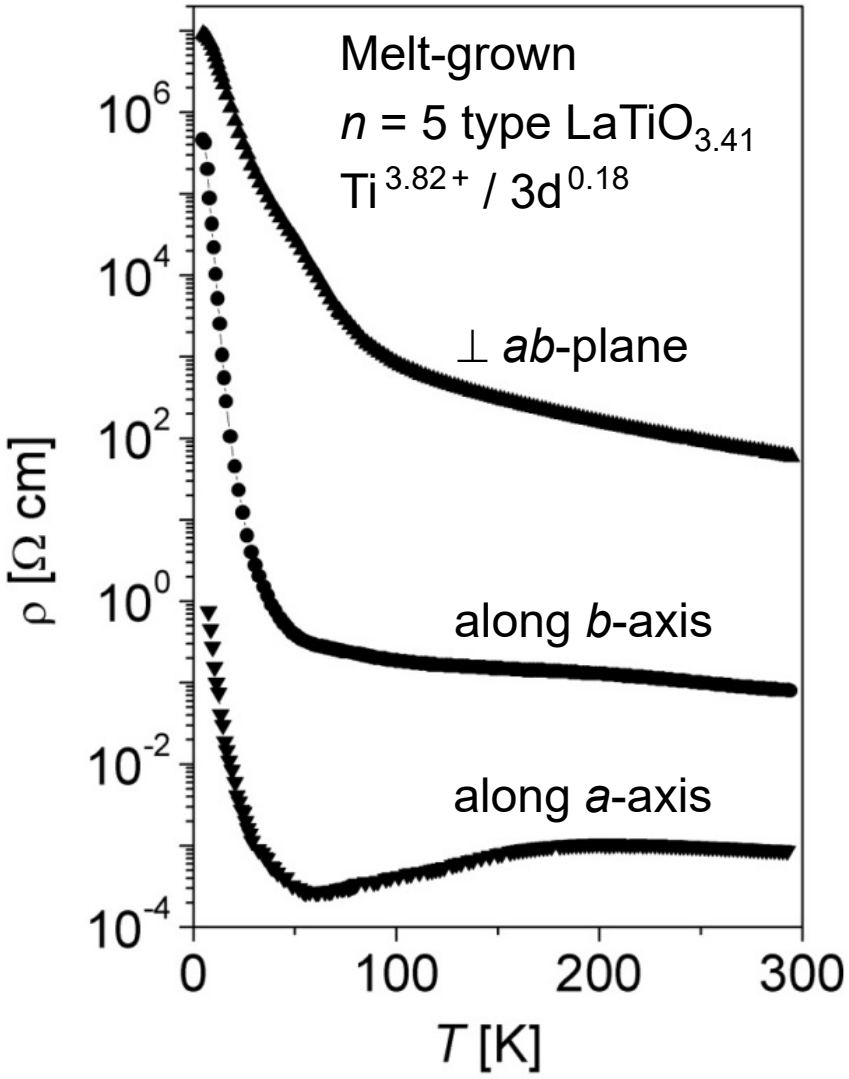

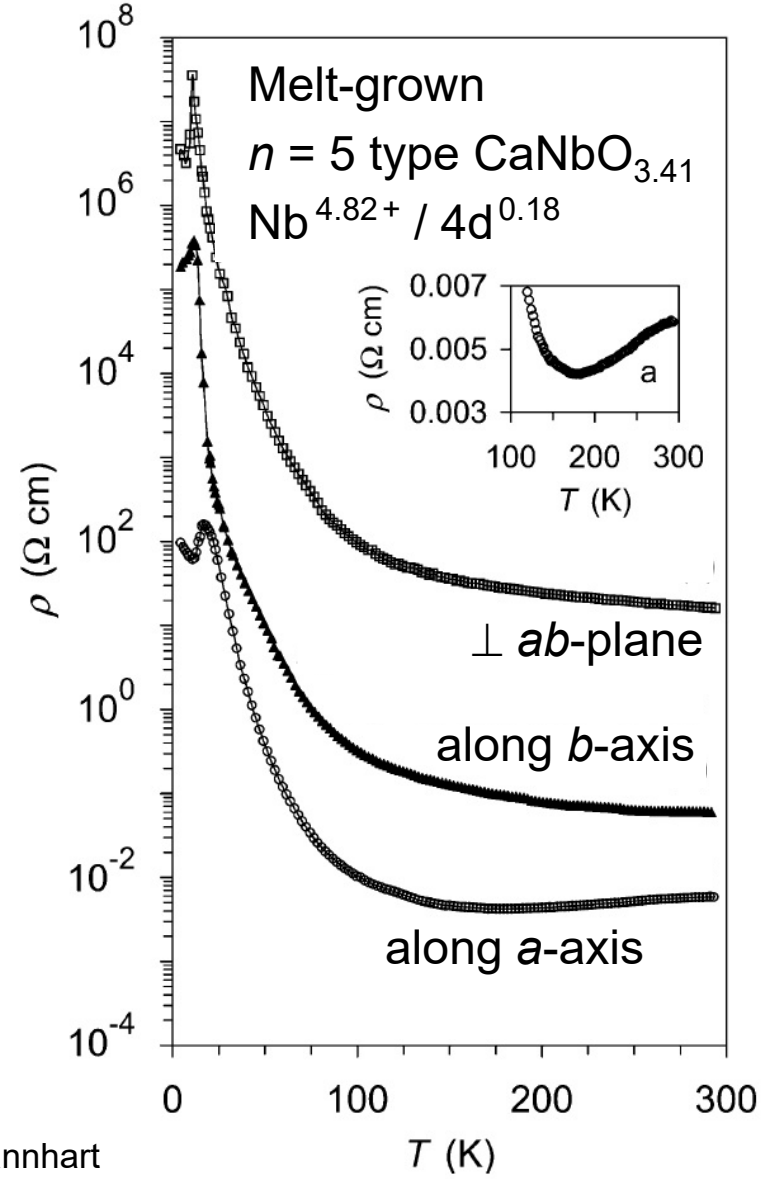

F. Lichtenberg, A. Herrnberger, K. Wiedenmann, and J. Mannhart
Progress in Solid State Chemistry 29 (2001) 1

Types of electrical in-plane voltage contacts for resistivity measurements on crystals

It is an open question why in-plane voltage contacts made of thin wires and silver paint are not able to detect the metallic resistivity behavior along the *a*-axis

- In contrast to silver paint voltage contacts, which are just attached on the surface of the crystal, ultrasonically bonded voltage contacts penetrate somewhat into the surface of the crystal

- A. Moini et al. reports that initial measurements on crystals of structurally and electronically low-dimensional $La_2Mo_2O_7$ with silver paste contacts lead to erratic results, but the problem was solved by ultrasonically soldered indium contacts

  A. Moini, A. Subramanian, A. Clearfield, F. J. DiSalvo, and W. H. McCarroll
  Journal of Solid State Chemistry 66 (1987) 136

  Note: The crystal structure of $La_2Mo_2O_7$ is not of the type $A_nB_nO_{3n+2}$

Results of resistivity measurements on crystals of melt-grown $n = 5$ type $SrNb_{0.964}O_{3.41-y}$ published by A. de Campos et al. in 2010

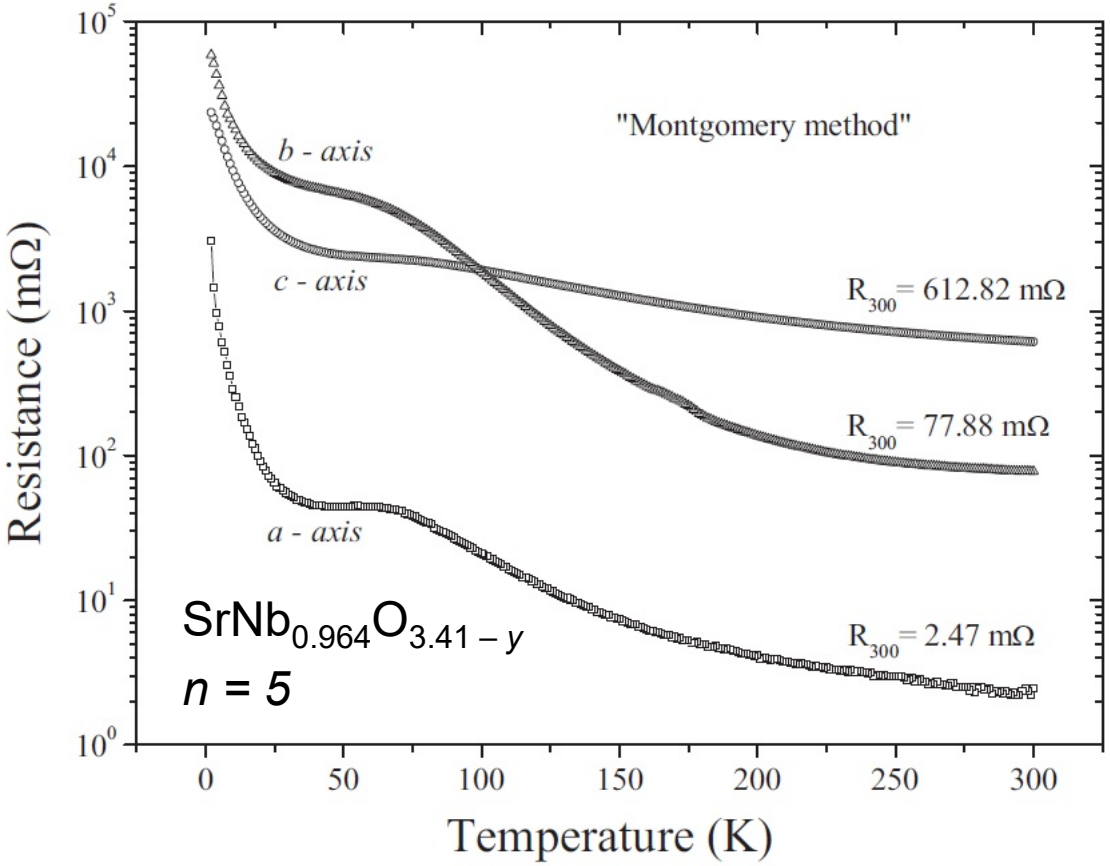

Reference and image source: Physical properties of quasi-one-dimensional $SrNbO_{3.41}$ and Luttinger liquid analysis of electrical transport • A. de Campos, M. S. da Luz, C. A. M. dos Santos, A. T. Rice, A. M. Deml, B. D. White, J. J. Neumeier, and J. L. Cohn • Physical Review B 82 (2010) 125117 http://dx.doi.org/10.1103/PhysRevB.82.125117

Melt-grown Nb- and O-deficient $n = 5$ type $SrNb_{0.964}O_{3.41-y}$ was prepared by sintering polycrystalline rods with fully oxidized Nb^{5+} composition $SrNb_{0.964}O_{3.41}$ under 97 % Ar + 3 % H_2 followed by processing the sintered rods by floating zone melting under 97 % Ar + 3 % H_2 with a gas flow rate of 72 L / h. The growth speed was 5 mm / h. The oxygen content $x = 3.41 - y$ is not specified but a single phase $n = 5$ type material was confirmed by x-ray-diffraction. The electrical resistance and resistivity was determined by the Montgomery method with low-resistance vapor-deposited gold contacts as well as by the four-point method.

Results of resistivity measurements on crystals of melt-grown $n = 5$ type $SrNb_{0.964}O_{3.41-y}$ published by A. de Campos et al. in 2010

The Montgomery method may provide a better assessment of the resistivity behavior than the four-point method because the latter may comprise an intermixture of resistivity contributions from different directions or crystallographic axes.

The diagonal components of the electrical resistivity tensor of $SrNb_{0.964}O_{3.41-y}$ were determined by the Montgomery method. The results confirm a quasi-1D behavior with a smaller anisotropy than previously reported by F. Lichtenberg et al. in 2001 on crystals of melt-grown $n = 5$ type $SrNbO_{3.41}$

Reference: Physical properties of quasi-one-dimensional $SrNbO_{3.41}$ and Luttinger liquid analysis of electrical transport • A. de Campos, M. S. da Luz, C. A. M. dos Santos, A. T. Rice, A. M. Deml, B. D. White, J. J. Neumeier, and J. L. Cohn
• Physical Review B 82 (2010) 125117 • http://dx.doi.org/10.1103/PhysRevB.82.125117

Note: The composition of the melt-grown $n = 5$ type $SrNb_{0.964}O_{3.41-y}$ (y not specified) and the melt-grown $n = 5$ type $SrNbO_{3.41}$ ($Nb^{4.82+}$ / $4d^{0.18}$) is not the same. That could be also a reason why the resistivity behavior and anisotropy of these both materials are (somewhat) different.

Examples of results of resistivity measurements on crystals of melt-grown *n* = 5 type Sr-based niobates published in 2001

Four-point method
with ultrasonically
bonded
in-plane
voltage contacts

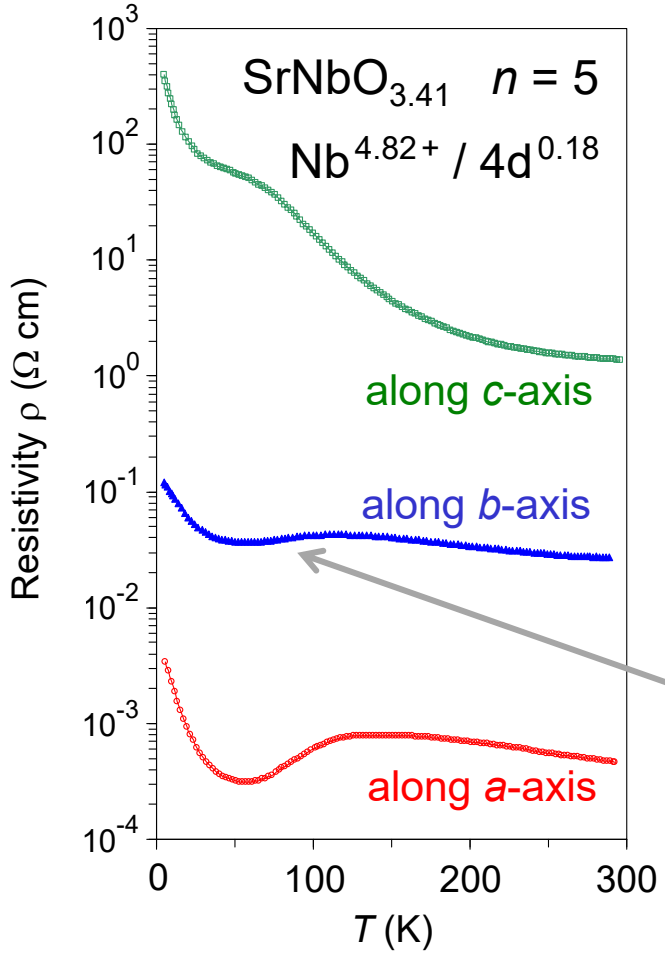

This section with a metallic temperature dependence along the *b*-axis could be due to an intermixture of a contribution from the *a*-axis

F. Lichtenberg et al., Progress in Solid State Chemistry 29 (2001) 1

Examples of results of resistivity measurements on crystals of melt-grown *n* = 5 type Sr-based niobates published in 2001

Four-point method with ultrasonically bonded in-plane voltage contacts

Optical spectroscopy confirmed / revealed that both materials are quasi-1D metals

$SrNbO_{3.41}$:
See part 6.2

$Sr_{0.95}NbO_{3.37}$:
Teguh Citra Asmara et al., to be published in Communications Physics (2020).
See also part 6.2.1

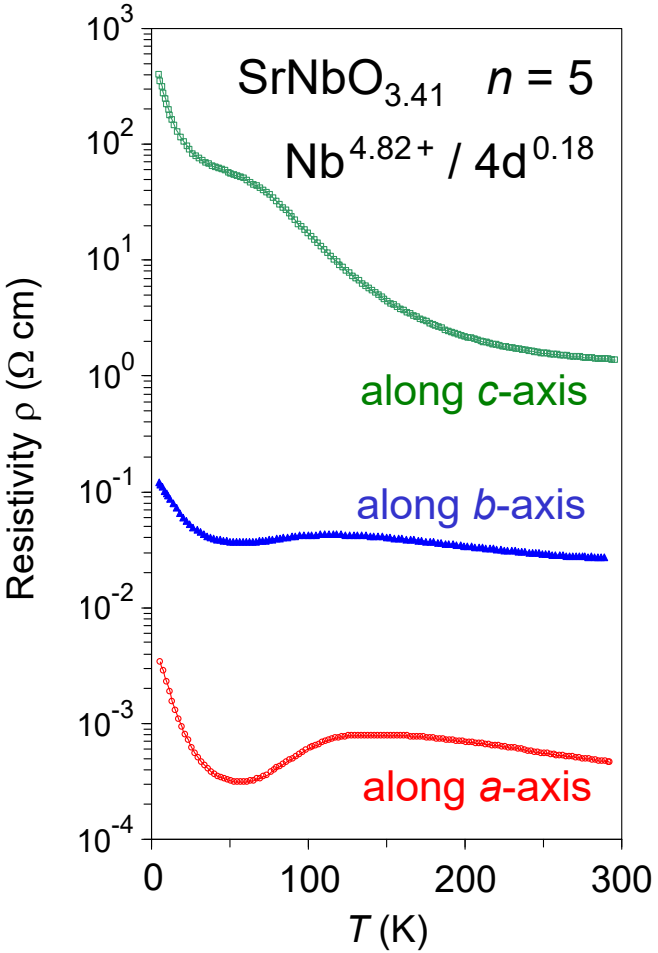

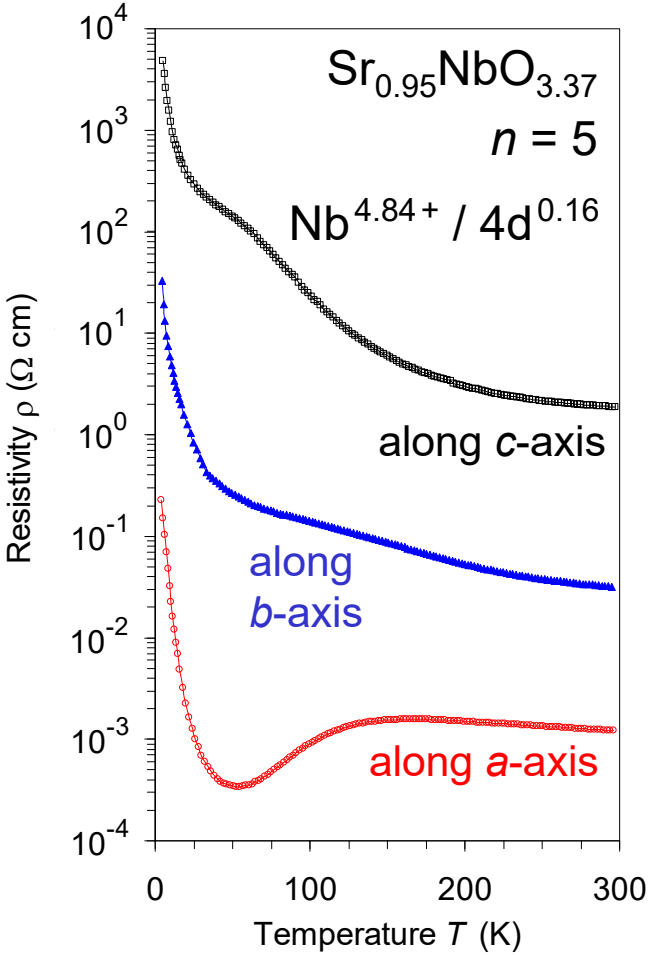

F. Lichtenberg et al., Progress in Solid State Chemistry 29 (2001) 1

Results of resistivity measurements on crystals of melt-grown n = 5 type $SrNbO_{3.43}$ published by W. Kobayashi et al. in 2011 – Electrical contacts made with silver paint

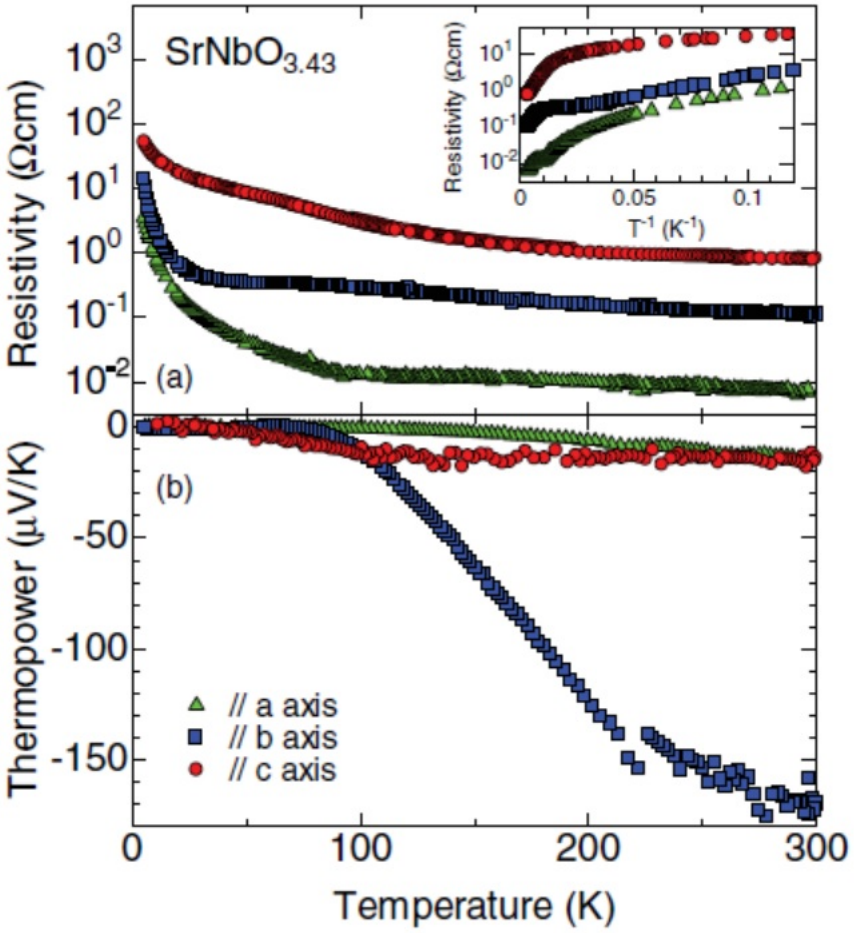

Melt-grown n = 5 type $SrNbO_{3.43}$ was prepared by processing polycrystalline sintered rods with fully oxidized Nb^{5+} composition $SrNbO_{3.5}$ by floating zone melting under 97 % Ar + 3 % H_2 with a gas flow rate of 12 L / h. The growth speed was 10 mm / h. The oxygen content $x = 3.5 - y = 3.43$ was determined thermogravimetrically. A single phase n = 5 type material was confirmed by synchrotron powder x-ray-diffraction measurements. The specified orthorhombic lattice parameteres are a = 3.988 Å, b = 5.676 Å, and c = 32.467 Å. The electrical resistivity was measured by the four-point method and gold wires which were attached on the crystal by silver paint.

Reference and image source: Anisotropic thermoelectric properties associated with dimensional crossover in quasi-one-dimensional $SrNbO_{3.4+d}$ ($d \sim 0.03$) • W. Kobayashi, Y. Hayashi, M. Matsushita, Y. Yamamoto, I. Terasaki, A. Nakao, H. Nakao, Y. Murakami, Y. Moritomo, H. Yamauchi, and M. Karppinen • Physical Review B 84 (2011) 085118 • http://dx.doi.org/10.1103/PhysRevB.84.085118

Results of resistivity measurements on crystals of melt-grown $n = 5$ type $SrNbO_{3.43}$ published by W. Kobayashi et al. in 2011 – Electrical contacts made with silver paint

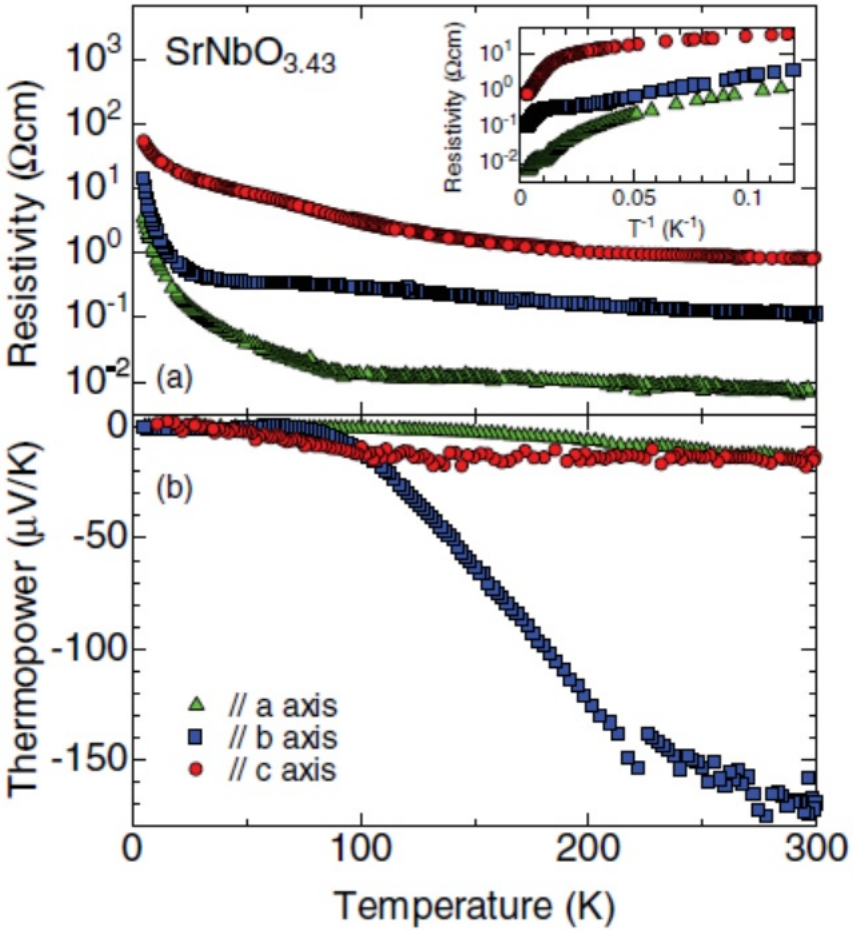

Note: $x = 3.43$ is the largest possible upper end of the homogeneity or stability range of $n = 5$ type $SrNbO_x$ because for $x = 3.44$ an $n = 4.5$ type structure is formed

A reported value for the upper end of the homogeneity or stability range of $n = 5$ type $SrNbO_x$ is $x = 3.42$

Zeitschrift für Physik B Condensed Matter 84 (1991) 369 • Progress in Solid State Chemistry 29 (2001) 1

Image source: Anisotropic thermoelectric properties associated with dimensional crossover in quasi-one-dimensional $SrNbO_{3.4+d}$ ($d \sim 0.03$) • W. Kobayashi, Y. Hayashi, M. Matsushita, Y. Yamamoto, I. Terasaki, A. Nakao, H. Nakao, Y. Murakami, Y. Moritomo, H. Yamauchi, and M. Karppinen • Physical Review B 84 (2011) 085118
• http://dx.doi.org/10.1103/PhysRevB.84.085118

6 Conducting and metallic Carpy-Galy phases $A_nB_nO_{3n+2} = ABO_x$

6.6 The size of the *a*-axis and crystallographic unit cell of the *n* = 5 type quasi-1D metal $SrNbO_{3.4} = Sr_5Nb_5O_{17} = Sr_{20}Nb_{20}O_{68}$ and other *n* = 5 type Sr-based niobates ...

Results of single crystal x-ray diffraction studies of ternary *n* = 5 types

Composition	$LaTiO_{3.4}$ = $La_5Ti_5O_{17}$ = $La_{20}Ti_{20}O_{68}$	$CaNbO_{3.4}$ = $Ca_5Nb_5O_{17}$ = $Ca_{20}Nb_{20}O_{68}$	$SrNbO_{3.4}$ = $Sr_5Nb_5O_{17}$ = $Sr_{20}Nb_{20}O_{68}$	
Crystal system	Monoclinic	Monoclinic	Orthorhombic	
Space group	$P2_1/c$ (No. 14)	$P2_1/c$ (No. 14)	Pnnm (No. 58)	
Number Z of formula units per unit cell and corresponding composition formula	4 $La_{20}Ti_{20}O_{68}$	4 $Ca_{20}Nb_{20}O_{68}$	2 $Sr_{10}Nb_{10}O_{34}$	4 $Sr_{20}Nb_{20}O_{68}$
a (Å)	7.86	7.75	8.00 / 2 = 4.00	2 × 4 = 8
b (Å)	5.53	5.49	5.67	
c (Å)	31.45	32.24	32.46	
β (°)	97.2	96.8	90	
V (Å^3)	1356	1363	1472 / 2 = 736	
References	P. Daniels, F. Lichtenberg, S. van Smaalen, Acta Cryst.C 59 (2003) i15	J. Guevarra, S. van Smaalen, N. Rotiroti, C. Paulmann, F. Lichtenberg, J. Solid State Chem. 178 (2005) 2934	S. C. Abrahams, H. W. Schmalle, T. Williams, A. Reller, F. Lichtenberg, D. Widmer, J. G. Bednorz, R. Spreiter, Ch. Bosshard, P. Gunter, Acta Cryst. B 54 (1998) 399	S. van Smaalen, private communi-cation (2008)

Results of single crystal x-ray diffraction studies of *n* = 5 type $Sr_5Nb_5O_{17}$

	Orthorhombic $SrNbO_{3.4}$ = $Sr_5Nb_5O_{17}$ = $Sr_{20}Nb_{20}O_{68}$	
Space group	Pnnm (No. 58)	
Number Z of formula units per unit cell and corresponding composition formula	2 $Sr_{10}Nb_{10}O_{34}$	4 $Sr_{20}Nb_{20}O_{68}$
a (Å)	4.00	2 × 4 = 8
b (Å) , *c* (Å)	5.67 , 32.46	
References and comments	Centrosymmetric or noncentrosymmetric? Case study, Generalization, and Structural Redetermination of $Sr_5Nb_5O_{17}$ S. C. Abrahams et al., Acta Cryst. B 54 (1998) 399. This work is based on a dataset whose evaluation results were published in 1995: H. Schmalle et al., Acta Cryst. C 51 (1995) 1243	A dataset from about 2008 clearly reveals a doubled *a*-axis. The detection of the corresponding superstructure peaks is probably related to an advanced detector technology when compared to that around 1995. S. van Smaalen, private communication (2008). Therefore it is assumed that all Sr-based *n* = 5 type niobates have a doubled *a*-axis which implies an unit cell with 20 + 20 + 68 lattice sites which is in case of a stoichiometric composition described by the formula $Sr_{20}Nb_{20}O_{68}$

6 Conducting and metallic Carpy-Galy phases $A_nB_nO_{3n+2} = ABO_x$

6.7 The Schückel-Müller-Buschbaum phase $SrNbO_{3.2} = Sr_5Nb_5O_{16} = Sr_{20}Nb_{20}O_{64}$ and the $n = 5$ type quasi-1D metal $SrNbO_{3.4} = Sr_5Nb_5O_{17} = Sr_{20}Nb_{20}O_{68}$ ...

Introduction of the name Schückel-Müller-Buschbaum phase

In 1985 K. Schückel and Hk. Müller-Buschbaum have published the following paper about the synthesis of $SrNbO_{3.2} = Sr_5Nb_5O_{16} = Sr_{20}Nb_{20}O_{64}$ and its structure determination by single crystal x-ray diffraction:

Ein weiteres gemischtvalentes Oxoniobat: $Sr_5Nb_3^{4+}Nb_2^{5+}O_{16}$
K. Schückel and Hk. Müller-Buschbaum
Zeitschrift für anorganische und allgemeine Chemie 528 (1985) 91 - 97
https://doi.org/10.1002/zaac.19855280909
Paper in German but title and abstract also in English

Title: About a Mixed Valence Oxoniobate: $Sr_5Nb_3^{4+}Nb_2^{5+}O_{16}$

Abstract: The hitherto unknown compound $Sr_5Nb_5O_{16}$ was prepared and examined by X-ray single crystal work. It crystallizes with orthorhombic symmetry (space group D_{2h}^7 – $Pmn2_1$, *a* = 3.992(1) , *b* = 5.677(2) , *c* = 32.476(10) , *Z* = 2). $Sr_5Nb_5O_{16}$ consists of stacked perovskite-like blocks cut by a plane perpendicular to the cube face diagonal of the perovskite structure. The coordination relations of the intersections between those blocks and the distribution of Nb^{5+} and Nb^{4+} are discussed. Compared to the original text *b* and *c* are swapped so that they correspond to the assignment used in this work

In this work we suggest and introduce for $SrNbO_{3.2} = Sr_5Nb_5O_{16} = Sr_{20}Nb_{20}O_{64}$ and its reported crystal structure the name Schückel-Müller-Buschbaum phase.

The Schückel-Müller-Buschbaum phase $Sr_5Nb_5O_{16}$

In 1985 K. Schückel and Hk. Müller-Buschbaum have published the following paper about the synthesis of $SrNbO_{3.2} = Sr_5Nb_5O_{16} = Sr_{20}Nb_{20}O_{64}$ and its structure determination by single crystal x-ray diffraction:

Ein weiteres gemischtvalentes Oxoniobat: $Sr_5Nb_3^{4+}Nb_2^{5+}O_{16}$
K. Schückel and Hk. Müller-Buschbaum
Zeitschrift für anorganische und allgemeine Chemie 528 (1985) 91 - 97
https://doi.org/10.1002/zaac.19855280909
Paper in German but title and abstract also in English

Synthesis and analysis (translated from German into English): Mingled 2 SrO + Nb_2O_5 was pressed into a disk. On it a layer of Nb metal powder was pressed. The disk which consisted of an oxide layer and a metal layer was heated in a H_2 / H plasma at about 2000 °C (surface temperature) for 30 minutes. The H_2 / H plasma was generated by a low pressure and high frequency plasma torch. The metal powder layer couples to the high frequency field and intensifies at the oxide / metal interface the effect of the plasma torch. The reaction takes place at the 2 SrO + Nb_2O_5 / Nb interface where small blue-gray crystals did arise. The Sr and Nb content of the crystals was determined by energy dispersive x-ray spectroscopy (EDX). The oxygen content could only be determined with a complete structure analysis by single crystal x-ray diffraction.

The Schückel-Müller-Buschbaum phase $Sr_5Nb_5O_{16}$

In 1985 K. Schückel and Hk. Müller-Buschbaum have published the following paper about the synthesis of $SrNbO_{3.2}$ = $Sr_5Nb_5O_{16}$ = $Sr_{20}Nb_{20}O_{64}$ and its structure determination by single crystal x-ray diffraction:

Ein weiteres gemischtvalentes Oxoniobat: $Sr_5Nb_3^{4+}Nb_2^{5+}O_{16}$
K. Schückel and Hk. Müller-Buschbaum
Zeitschrift für anorganische und allgemeine Chemie 528 (1985) 91 - 97
https://doi.org/10.1002/zaac.19855280909
Paper in German but title and abstract also in English

Notes

- Physical properties are not reported / were not studied
- Oxides of the type $A_nB_nO_{3n+2}$ and a relationship to the structure type n = 5 are not mentioned

The mixed valence and conducting niobates $Sr_5Nb_5O_{16}$ and $Sr_5Nb_5O_{17}$

Composition		$SrNbO_{3.2}$ = $Sr_5Nb_5O_{16}$ = $Sr_{20}Nb_{20}O_{64}$	$SrNbO_{3.4}$ = $Sr_5Nb_5O_{17}$ = $Sr_{20}Nb_{20}O_{68}$
Synthesis approach		2 SrO + Nb_2O_5 with Nb on surface was heated in a H_2 / H plasma → Small crystals. Synthesis via melt did not work (incongruent melting)	Floating zone melting of the composition $Sr_5Nb_5O_{17}$ under Ar
Structure type		Schückel-Müller-Buschbaum phase Oxygen-deficient *n* = 5 type with fully ordered oxygen vacancies	*n* = 5 type Carpy-Galy phase ABO_x = $A_nB_nO_{3n+2}$
Space group		$Pmn2_1$ / Non-centrosymmetric	Pnnm / Centrosymmetric
Published / actual or assumed orthorhombic lattice parameters	*a* (Å)	3.99 / 2 × 3.99	4.00 / 2 × 4
	b (Å)	5.68	5.67
	c (Å)	32.48	32.46
Number of 4d electrons from Nb^{4+} / $4d^1$ per unit cell		12	4
Physical properties		?	Quasi-1D metal
References		Z. Anorg. Allg. Chem. 528 (1985) 91 Prog. Solid State Chem. 36 (2008) 253 Part 6.6 in this work	See part 6.2 and 6.6 in this work Part 6.6 in this work

The crystal structure of $Sr_5Nb_5O_{16}$ and the *n* = 5 type $Sr_5Nb_5O_{17}$

= NbO_6 octahedra (O located at the corners, Nb hidden in the center)

= NbO_4 (O located at the corners, Nb in the center) = Sr

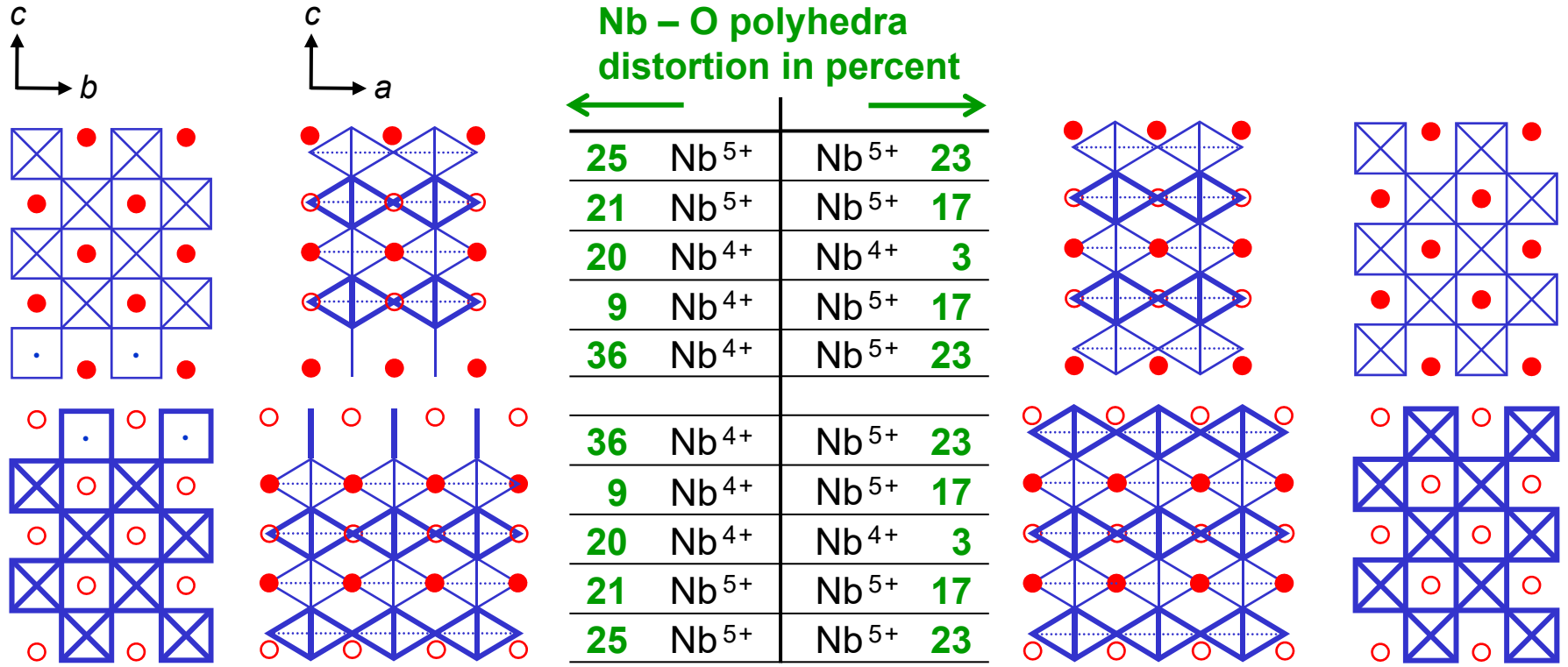

Nb – O polyhedra distortion in percent

25	Nb^{5+}	Nb^{5+}	23
21	Nb^{5+}	Nb^{5+}	17
20	Nb^{4+}	Nb^{4+}	3
9	Nb^{4+}	Nb^{5+}	17
36	Nb^{4+}	Nb^{5+}	23
36	Nb^{4+}	Nb^{5+}	23
9	Nb^{4+}	Nb^{5+}	17
20	Nb^{4+}	Nb^{4+}	3
21	Nb^{5+}	Nb^{5+}	17
25	Nb^{5+}	Nb^{5+}	23

$SrNbO_{3.2} = Sr_5Nb_5O_{16} = Sr_{20}Nb_{20}O_{64}$

Non-centrosymmetric !

Physical properties = ?

K. Schückel and Hk. Müller-Buschbaum
Z. Anorg. Allg. Chem. 528 (1985) 91

Nb^{5+} / $4d^0$

Nb^{4+} / $4d^1$

F. Lichtenberg et al., Prog. Solid State Chem. 36 (2008) 253

$SrNbO_{3.4} = Sr_5Nb_5O_{17} = Sr_{20}Nb_{20}O_{68}$

Centrosymmetric

Quasi-1D metal

S. C. Abrahams et al.
Acta Cryst. B 54 (1998) 399

The crystal structure of $Sr_5Nb_5O_{16}$ and the *n* = 5 type $Sr_5Nb_5O_{17}$

= NbO_6 octahedra (O located at the corners, Nb hidden in the center)

= NbO_4 (O located at the corners, Nb in the center)

(Fully ordered) oxygen vacancies are located at opposite boundaries of the layers or slabs

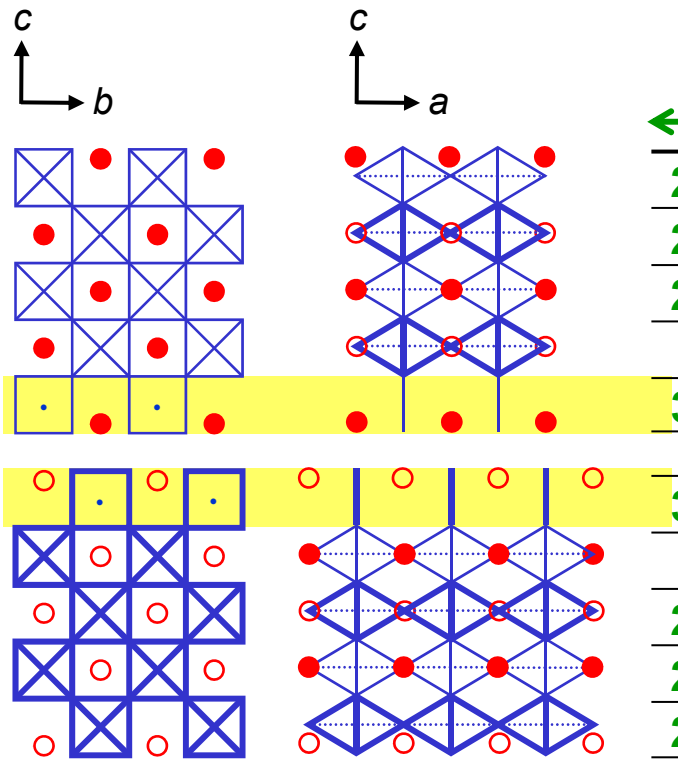

Nb – O polyhedra distortion in percent

25	Nb^{5+}	Nb^{5+}	23
21	Nb^{5+}	Nb^{5+}	17
20	Nb^{4+}	Nb^{4+}	3
9	Nb^{4+}	Nb^{5+}	17
36	Nb^{4+}	Nb^{5+}	23
36	Nb^{4+}	Nb^{5+}	23
9	Nb^{4+}	Nb^{5+}	17
20	Nb^{4+}	Nb^{4+}	3
21	Nb^{5+}	Nb^{5+}	17
25	Nb^{5+}	Nb^{5+}	23

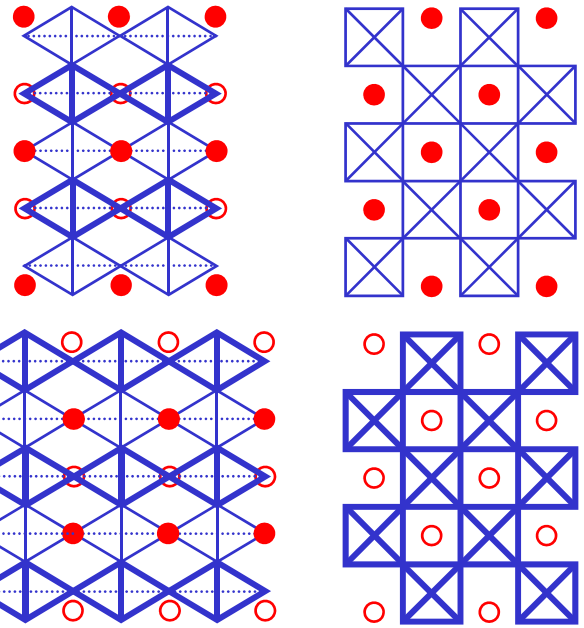

$SrNbO_{3.2} = Sr_5Nb_5O_{16} = Sr_{20}Nb_{20}O_{64}$

Non-centrosymmetric !

Physical properties = ?

K. Schückel and Hk. Müller-Buschbaum
Z. Anorg. Allg. Chem. 528 (1985) 91

Nb^{5+} / $4d^0$

Nb^{4+} / $4d^1$

F. Lichtenberg et al., Prog. Solid State Chem. 36 (2008) 253

$SrNbO_{3.4} = Sr_5Nb_5O_{17} = Sr_{20}Nb_{20}O_{68}$

Centrosymmetric

Quasi-1D metal

S. C. Abrahams et al.
Acta Cryst. B 54 (1998) 399

The crystal structure of $Sr_5Nb_5O_{16}$ and the *n* = 5 type $Sr_5Nb_5O_{17}$

= NbO_6 octahedra (O located at the corners, Nb hidden in the center)

= NbO_4 (O located at the corners, Nb in the center)

Along *c*-axis symmetric distribution of Nb^{5+} and Nb^{4+} and distortions

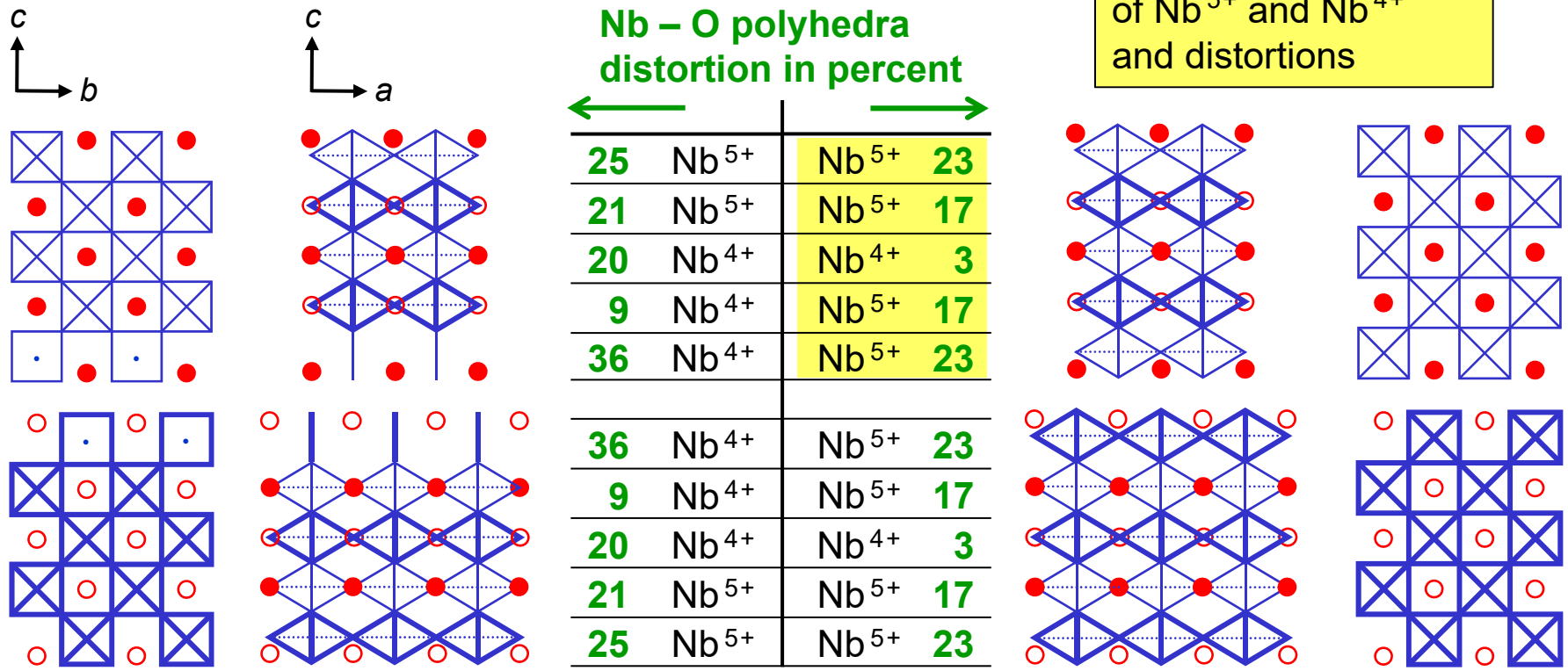

Nb – O polyhedra distortion in percent

25	Nb^{5+}	Nb^{5+}	23
21	Nb^{5+}	Nb^{5+}	17
20	Nb^{4+}	Nb^{4+}	3
9	Nb^{4+}	Nb^{5+}	17
36	Nb^{4+}	Nb^{5+}	23
36	Nb^{4+}	Nb^{5+}	23
9	Nb^{4+}	Nb^{5+}	17
20	Nb^{4+}	Nb^{4+}	3
21	Nb^{5+}	Nb^{5+}	17
25	Nb^{5+}	Nb^{5+}	23

$SrNbO_{3.2} = Sr_5Nb_5O_{16} = Sr_{20}Nb_{20}O_{64}$

Non-centrosymmetric !

Physical properties = ?

Nb^{5+} / $4d^0$

Nb^{4+} / $4d^1$

$SrNbO_{3.4} = Sr_5Nb_5O_{17} = Sr_{20}Nb_{20}O_{68}$

Centrosymmetric

Quasi-1D metal

K. Schückel and Hk. Müller-Buschbaum
Z. Anorg. Allg. Chem. 528 (1985) 91

F. Lichtenberg et al., Prog. Solid State Chem. 36 (2008) 253

S. C. Abrahams et al.
Acta Cryst. B 54 (1998) 399

The crystal structure of $Sr_5Nb_5O_{16}$ and the *n* = 5 type $Sr_5Nb_5O_{17}$

= NbO_6 octahedra (O located at the corners, Nb hidden in the center)

= NbO_4 (O located at the corners, Nb in the center)

Along *c*-axis asymmetric distribution of Nb^{5+} and Nb^{4+} and distortions

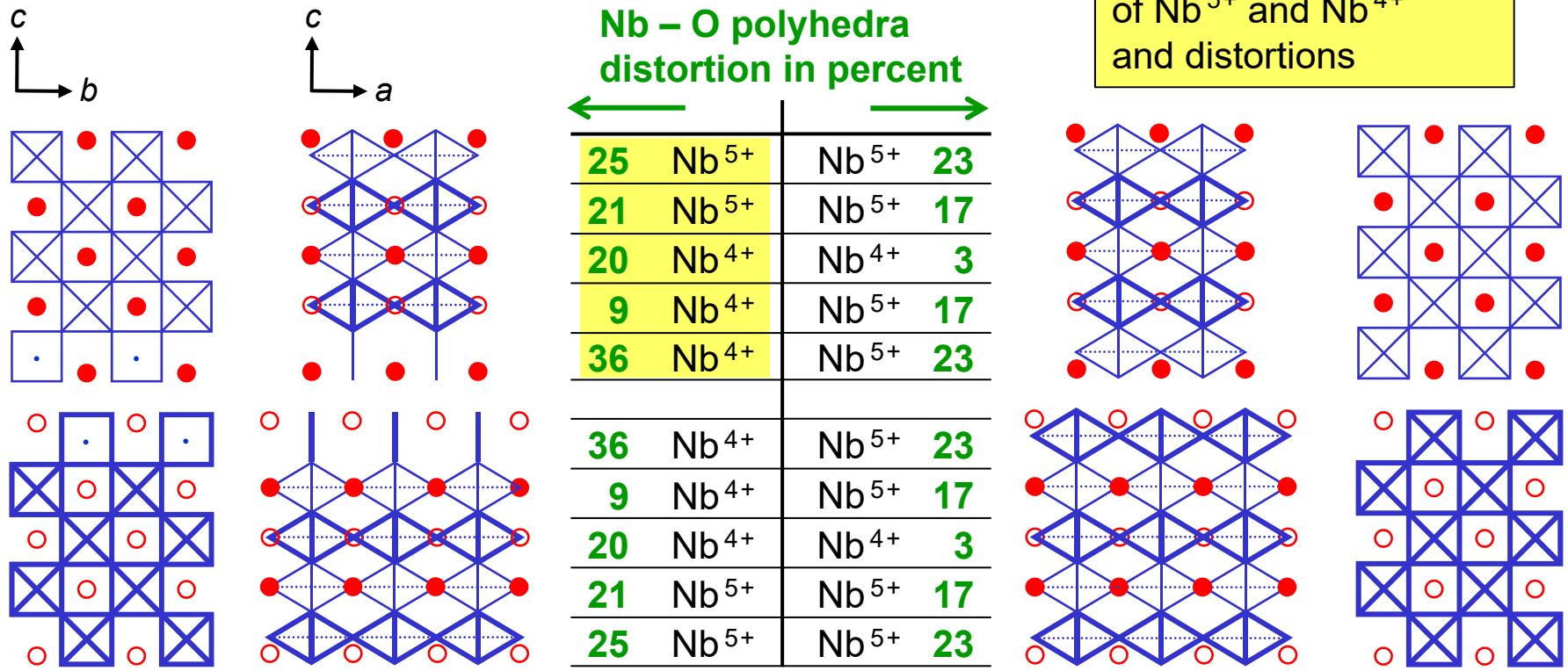

Nb – O polyhedra distortion in percent

25	Nb^{5+}	Nb^{5+}	23
21	Nb^{5+}	Nb^{5+}	17
20	Nb^{4+}	Nb^{4+}	3
9	Nb^{4+}	Nb^{5+}	17
36	Nb^{4+}	Nb^{5+}	23
36	Nb^{4+}	Nb^{5+}	23
9	Nb^{4+}	Nb^{5+}	17
20	Nb^{4+}	Nb^{4+}	3
21	Nb^{5+}	Nb^{5+}	17
25	Nb^{5+}	Nb^{5+}	23

$SrNbO_{3.2} = Sr_5Nb_5O_{16} = Sr_{20}Nb_{20}O_{64}$

Non-centrosymmetric !

Physical properties = ?

Nb^{5+} / $4d^0$

Nb^{4+} / $4d^1$

$SrNbO_{3.4} = Sr_5Nb_5O_{17} = Sr_{20}Nb_{20}O_{68}$

Centrosymmetric

Quasi-1D metal

K. Schückel and Hk. Müller-Buschbaum
Z. Anorg. Allg. Chem. 528 (1985) 91

F. Lichtenberg et al., Prog. Solid State Chem. 36 (2008) 253

S. C. Abrahams et al.
Acta Cryst. B 54 (1998) 399

The crystal structure of $Sr_5Nb_5O_{16}$ and the *n* = 5 type $Sr_5Nb_5O_{17}$

= NbO_6 octahedra (O located at the corners, Nb hidden in the center)

= NbO_4 (O located at the corners, Nb in the center)

Largest contribution to electronic DOS / metallic behavior from these regions, see part 6.2

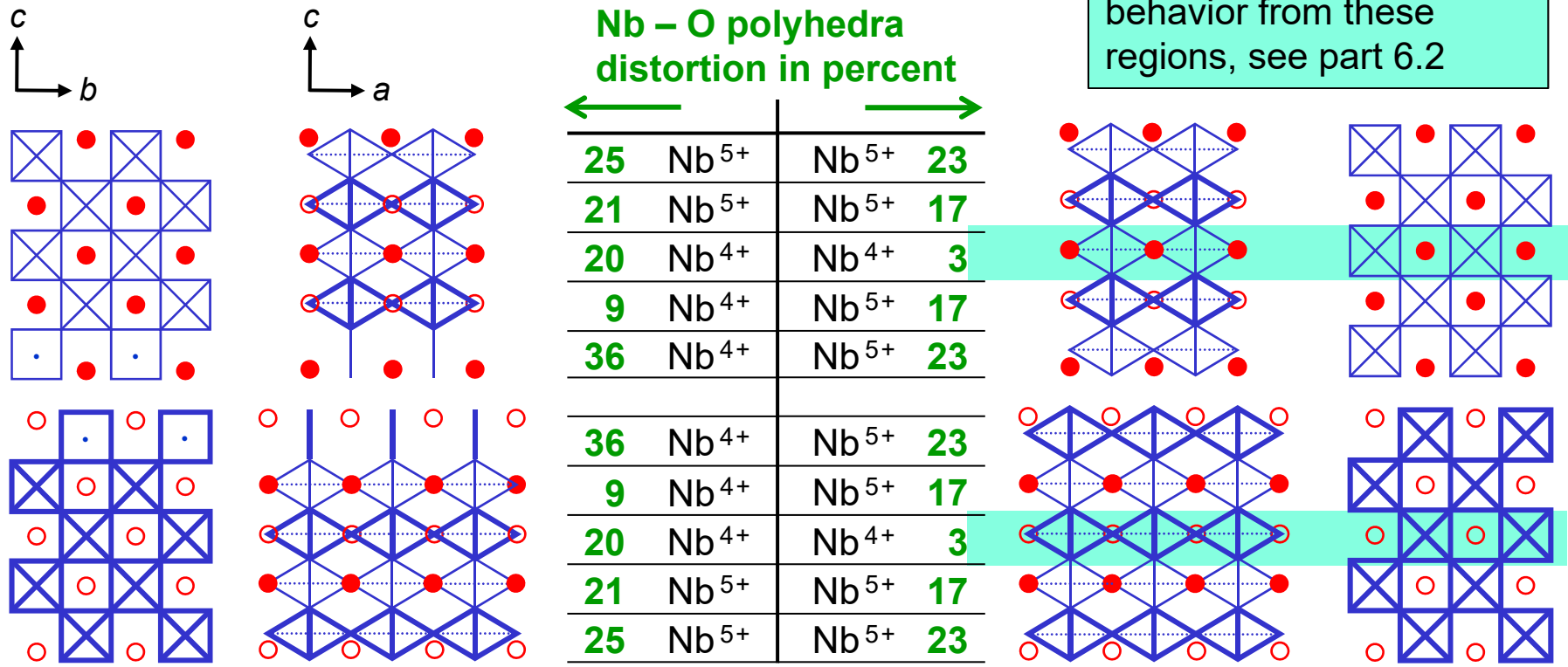

Nb – O polyhedra distortion in percent

25	Nb^{5+}	Nb^{5+}	23
21	Nb^{5+}	Nb^{5+}	17
20	Nb^{4+}	Nb^{4+}	3
9	Nb^{4+}	Nb^{5+}	17
36	Nb^{4+}	Nb^{5+}	23
36	Nb^{4+}	Nb^{5+}	23
9	Nb^{4+}	Nb^{5+}	17
20	Nb^{4+}	Nb^{4+}	3
21	Nb^{5+}	Nb^{5+}	17
25	Nb^{5+}	Nb^{5+}	23

$SrNbO_{3.2} = Sr_5Nb_5O_{16} = Sr_{20}Nb_{20}O_{64}$

Non-centrosymmetric !

Physical properties = ?

K. Schückel and Hk. Müller-Buschbaum
Z. Anorg. Allg. Chem. 528 (1985) 91

Nb^{5+} / $4d^0$

Nb^{4+} / $4d^1$

F. Lichtenberg et al., Prog. Solid State Chem. 36 (2008) 253

$SrNbO_{3.4} = Sr_5Nb_5O_{17} = Sr_{20}Nb_{20}O_{68}$

Centrosymmetric

Quasi-1D metal

S. C. Abrahams et al.
Acta Cryst. B 54 (1998) 399

The crystal structure of $Sr_5Nb_5O_{16}$ and the *n* = 5 type $Sr_5Nb_5O_{17}$

= NbO_6 octahedra (O located at the corners, Nb hidden in the center)

= NbO_4 (O located at the corners, Nb in the center)

Largest contribution to electronic DOS / potential metallic behavior from these regions ?

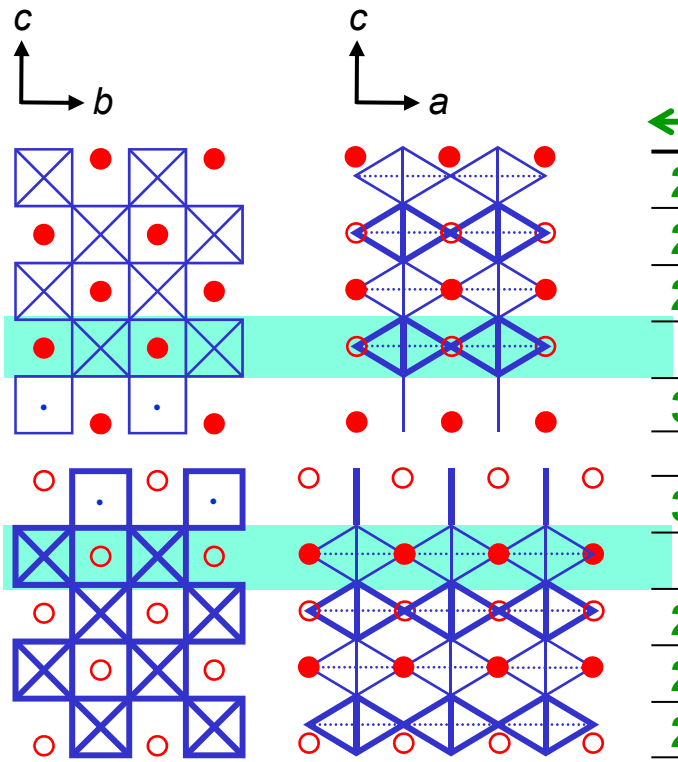

Nb – O polyhedra distortion in percent

25	Nb^{5+}	Nb^{5+}	23
21	Nb^{5+}	Nb^{5+}	17
20	Nb^{4+}	Nb^{4+}	3
9	Nb^{4+}	Nb^{5+}	17
36	Nb^{4+}	Nb^{5+}	23
36	Nb^{4+}	Nb^{5+}	23
9	Nb^{4+}	Nb^{5+}	17
20	Nb^{4+}	Nb^{4+}	3
21	Nb^{5+}	Nb^{5+}	17
25	Nb^{5+}	Nb^{5+}	23

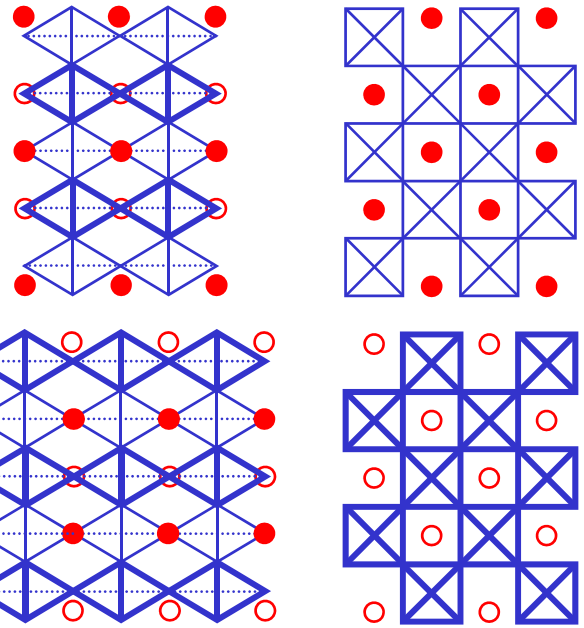

$SrNbO_{3.2} = Sr_5Nb_5O_{16} = Sr_{20}Nb_{20}O_{64}$

Non-centrosymmetric !

Physical properties = ?

K. Schückel and Hk. Müller-Buschbaum
Z. Anorg. Allg. Chem. 528 (1985) 91

$Nb^{5+} / 4d^0$

$Nb^{4+} / 4d^1$

F. Lichtenberg et al., Prog. Solid State Chem. 36 (2008) 253

$SrNbO_{3.4} = Sr_5Nb_5O_{17} = Sr_{20}Nb_{20}O_{68}$

Centrosymmetric

Quasi-1D metal

S. C. Abrahams et al.
Acta Cryst. B 54 (1998) 399

The crystal structure of $Sr_5Nb_5O_{16}$ and the *n* = 5 type $Sr_5Nb_5O_{17}$

= NbO_6 octahedra (O located at the corners, Nb hidden in the center)

= NbO_4 (O located at the corners, Nb in the center)

Region with a metal-insulator-like interface, see part 6.3

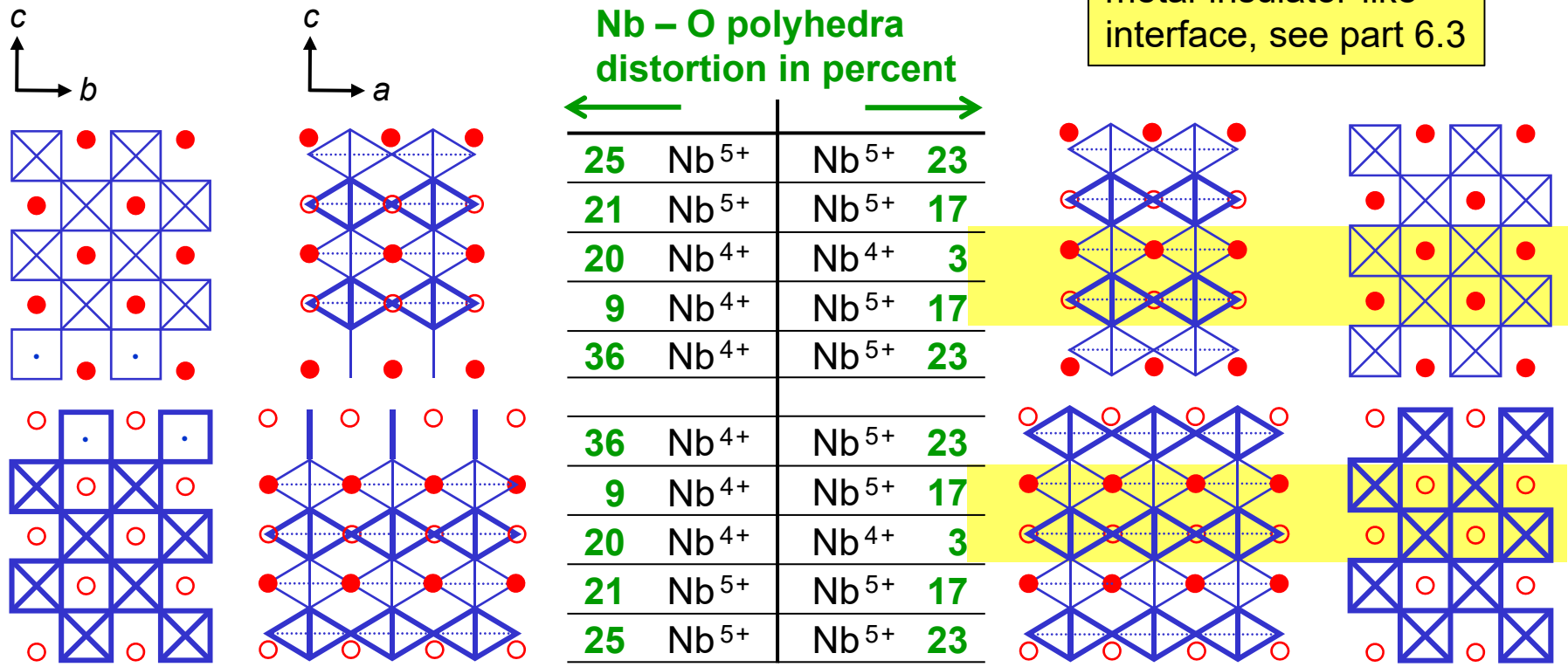

Nb – O polyhedra distortion in percent

25	Nb^{5+}	Nb^{5+}	23
21	Nb^{5+}	Nb^{5+}	17
20	Nb^{4+}	Nb^{4+}	3
9	Nb^{4+}	Nb^{5+}	17
36	Nb^{4+}	Nb^{5+}	23
36	Nb^{4+}	Nb^{5+}	23
9	Nb^{4+}	Nb^{5+}	17
20	Nb^{4+}	Nb^{4+}	3
21	Nb^{5+}	Nb^{5+}	17
25	Nb^{5+}	Nb^{5+}	23

$SrNbO_{3.2} = Sr_5Nb_5O_{16} = Sr_{20}Nb_{20}O_{64}$

Non-centrosymmetric !

Physical properties = ?

K. Schückel and Hk. Müller-Buschbaum
Z. Anorg. Allg. Chem. 528 (1985) 91

Nb^{5+} / $4d^0$

Nb^{4+} / $4d^1$

F. Lichtenberg et al., Prog. Solid State Chem. 36 (2008) 253

$SrNbO_{3.4} = Sr_5Nb_5O_{17} = Sr_{20}Nb_{20}O_{68}$

Centrosymmetric

Quasi-1D metal

S. C. Abrahams et al.
Acta Cryst. B 54 (1998) 399

The crystal structure of $Sr_5Nb_5O_{16}$ and the *n* = 5 type $Sr_5Nb_5O_{17}$

= NbO_6 octahedra (O located at the corners, Nb hidden in the center)

= NbO_4 (O located at the corners, Nb in the center)

Region with a metal-insulator-like interface ?

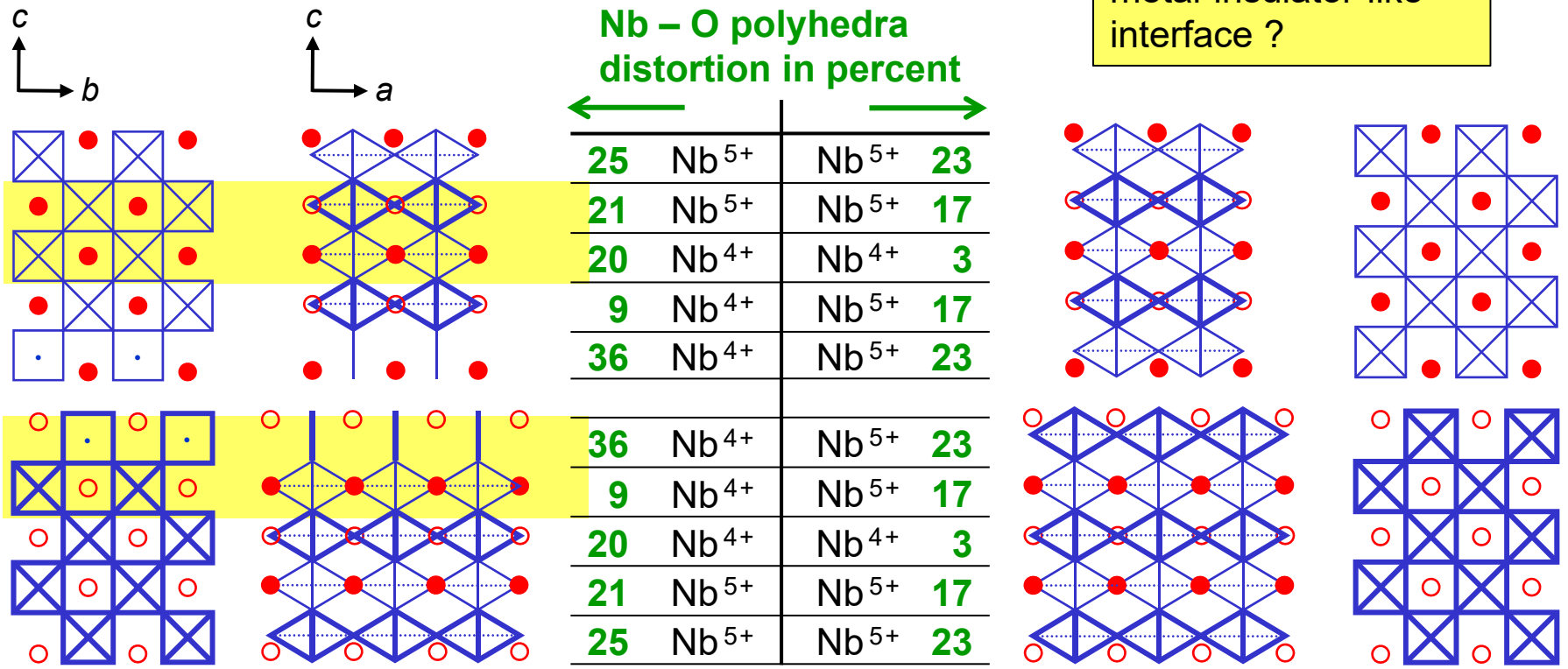

Nb – O polyhedra distortion in percent

25	Nb^{5+}	Nb^{5+}	23
21	Nb^{5+}	Nb^{5+}	17
20	Nb^{4+}	Nb^{4+}	3
9	Nb^{4+}	Nb^{5+}	17
36	Nb^{4+}	Nb^{5+}	23
36	Nb^{4+}	Nb^{5+}	23
9	Nb^{4+}	Nb^{5+}	17
20	Nb^{4+}	Nb^{4+}	3
21	Nb^{5+}	Nb^{5+}	17
25	Nb^{5+}	Nb^{5+}	23

$SrNbO_{3.2} = Sr_5Nb_5O_{16} = Sr_{20}Nb_{20}O_{64}$

Non-centrosymmetric !

Physical properties = ?

Nb^{5+} / $4d^0$

Nb^{4+} / $4d^1$

$SrNbO_{3.4} = Sr_5Nb_5O_{17} = Sr_{20}Nb_{20}O_{68}$

Centrosymmetric

Quasi-1D metal

K. Schückel and Hk. Müller-Buschbaum
Z. Anorg. Allg. Chem. 528 (1985) 91

F. Lichtenberg et al., Prog. Solid State Chem. 36 (2008) 253

S. C. Abrahams et al.
Acta Cryst. B 54 (1998) 399

The reported and a hypothetical structure of $Sr_5Nb_5O_{16}$

= NbO_6 octahedra (O located at the corners, Nb hidden in the center)

= NbO_4 (O located at the corners, Nb in the center) ● ○ = Sr

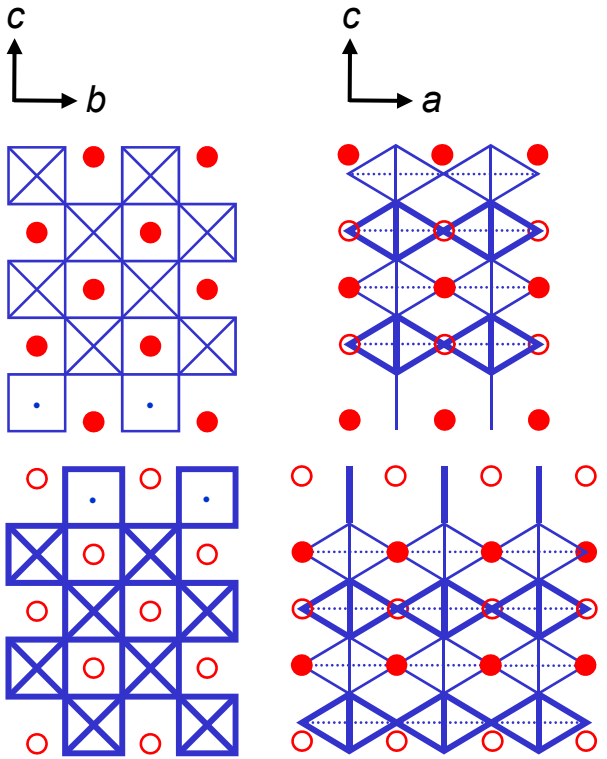

Nb – O polyhedra distortion in percent

25	Nb^{5+}	Nb^{5+}
21	Nb^{5+}	Nb^{4+}
20	Nb^{4+}	Nb^{4+}
9	Nb^{4+}	Nb^{4+}
36	Nb^{4+}	Nb^{5+}
36	Nb^{4+}	Nb^{5+}
9	Nb^{4+}	Nb^{4+}
20	Nb^{4+}	Nb^{4+}
21	Nb^{5+}	Nb^{4+}
25	Nb^{5+}	Nb^{5+}

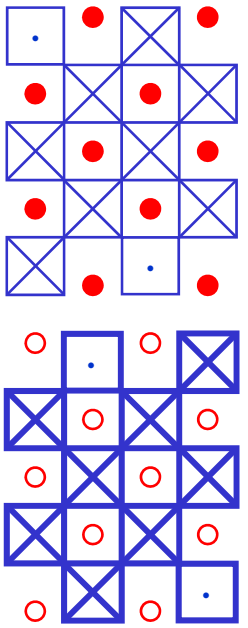

A hypothetical variant with a symmetric distribution of Nb^{4+} and Nb^{5+} in one slab or layer along the *c*-axis

Energetically unfavorable ?

NbO_4 polyhedra with Nb^{5+} ?

Reported by K. Schückel and Hk. Müller-Buschbaum

Nb^{5+} / $4d^0$

Nb^{4+} / $4d^1$

Z. Anorg. Allg. Chem. 528 (1985) 91 and
Prog. Solid State Chem. 36 (2008) 253

The Schückel-Müller-Buschbaum phase $SrNbO_{3.2} = Sr_5Nb_5O_{16}$

Comments and open questions

- In contrast to the quasi-1D metal $Sr_5Nb_5O_{17}$ a layer or slab of $Sr_5Nb_5O_{16}$ comprises along the *c*-axis an asymmetric distribution of the Nb^{4+} ($4d^1$) and Nb^{5+} ($4d^0$) ions and Nb – O polyhedra distortions. Maybe these particular details of the $Sr_5Nb_5O_{16}$ type structure can bring forth special physical properties

- What are its physical properties ?
  - Is it a quasi-1D metal like the related *n* = 5 type $SrNbO_{3.4} = Sr_5Nb_5O_{17}$? If yes, is $Sr_5Nb_5O_{16}$ because if its non-centrosymmetric structure a polar or ferroelectric metal ?

- Are there related materials which can be prepared via the melt ?
  - If yes, then larger amounts of crystalline material / larger crystals could be obtained. That would facilitate the study of the physical properties
  - Can the crystal structure reported by K. Schückel and Hk. Müller-Buschbaum be confirmed ?

The Schückel-Müller-Buschbaum phase $SrNbO_{3.2} = Sr_5Nb_5O_{16}$

Comments and open questions

- Its reported crystal structure can be considered as an oxygen-deficient $n = 5$ type structure with fully ordered oxygen vacancies. Therefore the Schückel-Müller-Buschbaum phase and potential related compounds with the same type of crystal structure, i.e. Schückel-Müller-Buschbaum type phases, represent a special subset of the Carpy-Galy phases $A_nB_nO_{3n+2} = ABO_x$

- The oxygen-deficient $n = 5$ type structure of $SrNbO_{3.2}$ is perovskite-related and layered and its composition is close to that of the non-layered $n = \infty$ type perovskite $SrNbO_3$

  For comparison: In the system $LaTiO_x$ the $n = \infty$ type perovskite structure has a large homogeneity range, namely $3.00 \leq x \leq 3.20$, i.e. it extends up to the composition $LaTiO_{3.2}$ (see part 6.1)

The Schückel-Müller-Buschbaum phase $SrNbO_{3.2} = Sr_5Nb_5O_{16}$

Comments and open questions

- The overall homogeneity range of $n = 5$ type $SrNbO_x$ seems to be $3.20 \leq x \leq 3.42$ whereby $x = 3.40$ corresponds to the stoichiometric composition

  - When having prepared a series of niobates $SrNbO_x$ with an oxygen content ranging from $x = 3.40$ to $x = 3.20$: Is there a specific oxygen content x_c or a two-phase oxygen content range which separates the two single phases
    - centrosymmetric / non-centrosymmetric
    - symmetric / asymmetric distribution of the Nb^{4+} and Nb^{5+} ions
    - symmetric / asymmetric distribution of the Nb – O polyhedra distortions ?

  - For $x \approx 3.33$ basically an $n = 6$ type phase could arise but for $SrNbO_x$ there are no indications for that. An example for an $n = 6$ type material is the ferrorelectric insulator $SrNb_{0.67}Ti_{0.33}O_{3.33}$ (Nb^{5+} / $4d^0$ and Ti^{4+} / $3d^0$)

6 Conducting and metallic Carpy-Galy phases $A_nB_nO_{3n+2} = ABO_x$

6.8 Prepared and studied at the University of Augsburg and structurally and compositionally related to the Schückel-Müller-Buschbaum phase: Melt-grown *A*- and O-deficient *n* = 5 type titanates $A_{0.95}TiO_{3.2} = A_{4.75}Ti_5O_{16} = A_{19}Ti_{20}O_{64}$ without pronounced crystalline appearance ...

Published in 2008: *A*-deficient and conducting $n = 5$ type titanates with the same oxygen content as that of the Schückel-Müller-Buschbaum phase $SrNbO_{3.2} = Sr_5Nb_5O_{17} = Sr_{20}Nb_{20}O_{64}$ ...

Melt-grown *A*- and O-deficient *n* = 5 type titanates

$A_{0.95}TiO_{3.2} = A_{4.75}Ti_5O_{16} = A_{19}Ti_{20}O_{64}$

Composition		$La_{0.75}Ca_{0.2}TiO_{3.21}$ = $La_{3.75}CaTi_5O_{16.05}$ = $La_{15}Ca_4Ti_{20}O_{64.2}$	$La_{0.75}Ba_{0.2}TiO_{3.21}$ = $La_{3.75}BaTi_5O_{16.05}$ = $La_{15}Ba_4Ti_{20}O_{64.2}$	
Synthesis approach		Processing the above-mentioned composition by floating zone melting under Ar		
Monoclinic lattice parameters	a (Å)	7.83	7.86	
	b (Å)	5.52	5.54	
	c (Å)	31.36	31.48	
	β (°)	97.0	96.7	
Number of 3d electrons from Ti^{3+} / $3d^1$ per unit cell		4.6 The Schückel-Müller-Buschbaum phase has 12 4d electrons per unit cell		
Physical properties		Potentially quasi-1D metals because above 150 K the magnetic moment increases with increasing temperature		

F. Lichtenberg, A. Herrnberger, and K. Wiedenmann, Progress in Solid State Chemistry 36 (2008) 253

Melt-grown *A*- and O-deficient *n* = 5 type titanates $A_{0.95}TiO_{3.2} = A_{4.75}Ti_5O_{16} = A_{19}Ti_{20}O_{64}$ and another related *n* = 5 titanate

Composition		$La_{0.75}Ca_{0.2}TiO_{3.21}$ = $La_{3.75}CaTi_5O_{16.05}$ = $La_{15}Ca_4Ti_{20}O_{64.2}$	$La_{0.75}Ba_{0.2}TiO_{3.21}$ = $La_{3.75}BaTi_5O_{16.05}$ = $La_{15}Ba_4Ti_{20}O_{64.2}$	$La_{0.85}Ca_{0.1}TiO_{3.26}$ = $La_{4.25}Ca_{0.5}Ti_5O_{16.3}$ = $La_{17}Ca_2Ti_{20}O_{65.2}$
Synthesis approach		Processing the above-mentioned composition by floating zone melting under Ar		
Monoclinic lattice parameters	a (Å)	7.83	7.86	7.84
	b (Å)	5.52	5.54	5.52
	c (Å)	31.36	31.48	31.41
	β (°)	97.0	96.7	97.0
Number of 3d electrons from Ti^{3+} / $3d^1$ per unit cell		4.6 The Schückel-Müller-Buschbaum phase has 12 4d electrons per unit cell		
Physical properties		Potentially quasi-1D metals because above 150 K or 50 K the magnetic moment increases with increasing temperature		

F. Lichtenberg, A. Herrnberger, and K. Wiedenmann, Progress in Solid State Chemistry 36 (2008) 253

Melt-grown $La_{0.75}Ba_{0.2}TiO_{3.21}$ = $La_{3.75}BaTi_5O_{16.05}$ = $La_{15}Ba_4Ti_{20}O_{64.2}$

A- and O-deficient *n* = 5 type of $ABO_x = A_nB_nO_{3n+2}$

Number of 3d electrons from Ti^{3+} / $3d^1$ per unit cell: 4.6

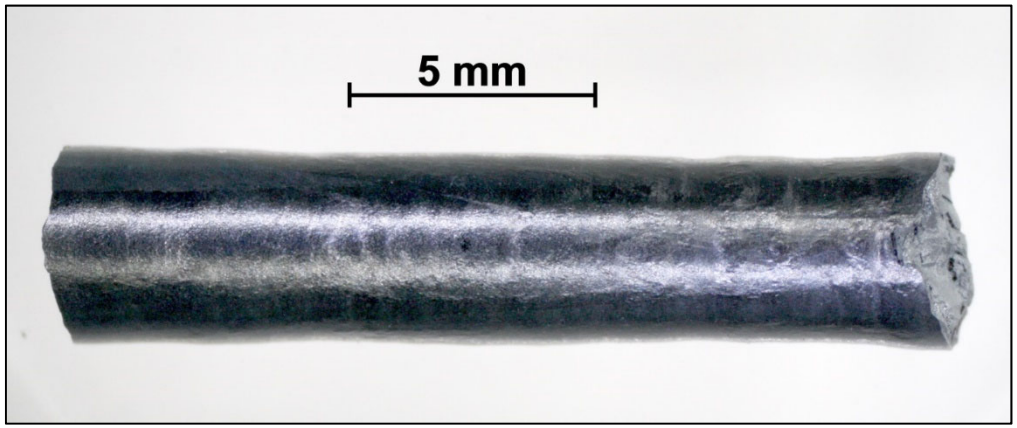

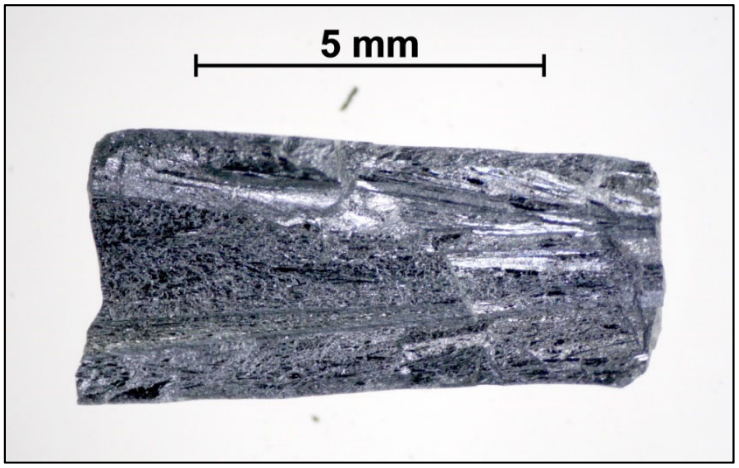

Pictures of crystalline pieces from the as-grown material

Sample No. 488

Progress in Solid State Chemistry 36 (2008) 253

Prepared at the University of Augsburg in 2005

Pictures taken at the ETH Zurich in 2019

Melt-grown $La_{0.75}Ca_{0.2}TiO_{3.21}$ = $La_{3.75}CaTi_5O_{16.05}$ = $La_{15}Ca_4Ti_{20}O_{64.2}$

A- and O-deficient *n* = 5 type of $ABO_x = A_nB_nO_{3n+2}$

Number of 3d electrons from Ti^{3+} / $3d^1$ per unit cell: 4.6

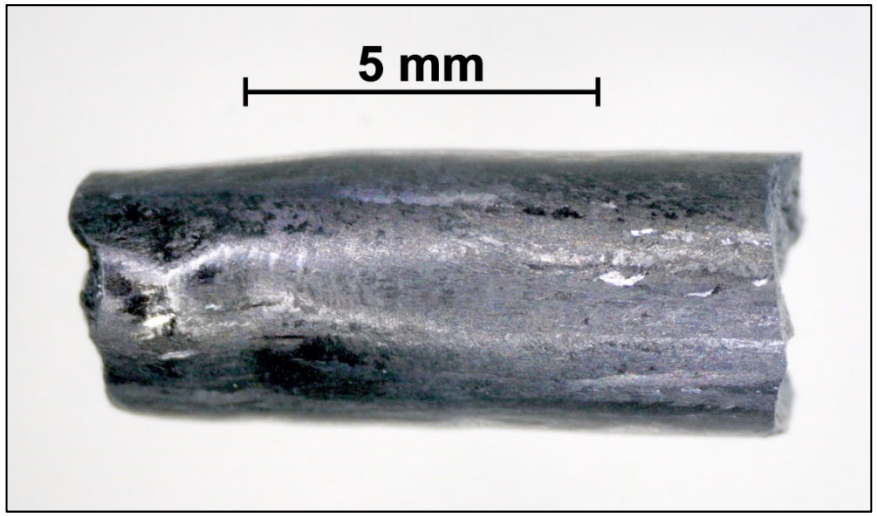

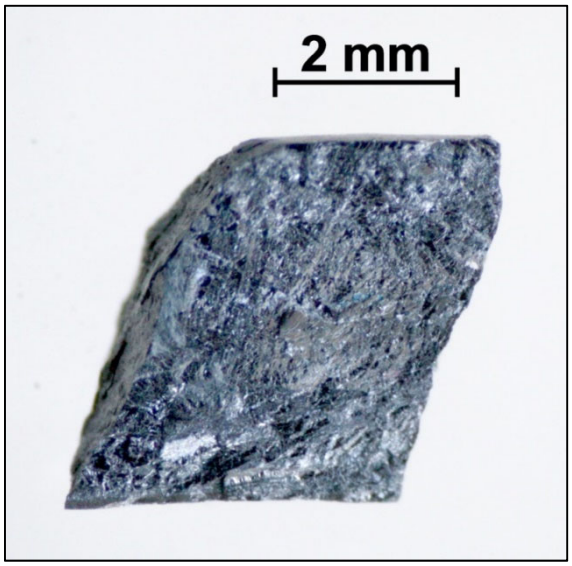

Pictures of crystalline pieces from the as-grown material

Sample No. 462

Progress in Solid State Chemistry 36 (2008) 253

Prepared at the University of Augsburg in 2005

Pictures taken at the ETH Zurich in 2019

Melt-grown $La_{0.85}Ca_{0.1}TiO_{3.26}$ = $La_{4.25}Ca_{0.5}Ti_5O_{16.3}$ = $La_{17}Ca_2Ti_{20}O_{65.2}$

A- and O-deficient *n* = 5 type of $ABO_x = A_nB_nO_{3n+2}$

Number of 3d electrons from Ti^{3+} / $3d^1$ per unit cell: 4.6

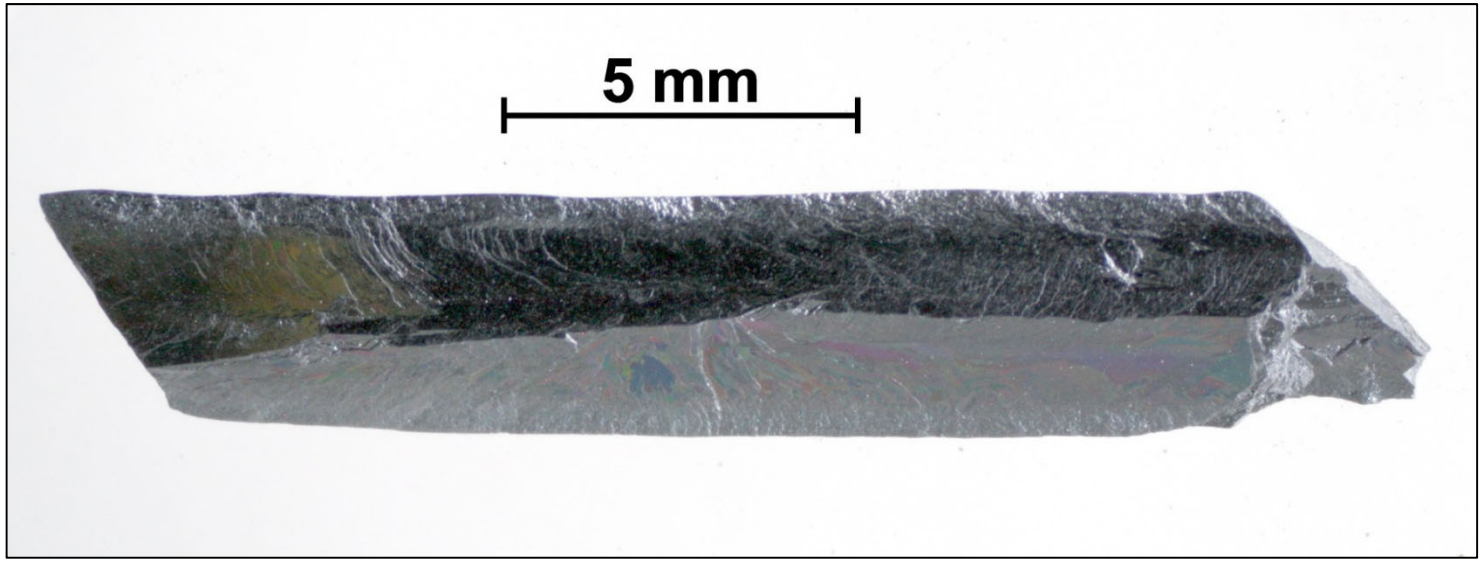

Picture of a crystalline piece from the as-grown material

Sample No. 458

Progress in Solid State Chemistry 36 (2008) 253

Prepared at the University of Augsburg in 2005

Pictures taken at the ETH Zurich in 2019

Molar magnetic susceptibility $\chi(T)$ in fields H ≤ 1000 G of $La_{0.75}Ca_{0.2}TiO_{3.21}$, $La_{0.75}Ba_{0.2}TiO_{3.21}$, $La_{0.85}Ca_{0.1}TiO_{3.26}$, and other melt-grown *n* = 5 type titanates

F. Lichtenberg, A. Herrnberger, and K. Wiedenmann, Progress in Solid State Chemistry 36 (2008) 253

$LaTiO_{3.41}$ and $La_{0.9}Ca_{0.1}TiO_{3.38}$ were also studied by optical and resistivity measurements which revealed a quasi-1D metallic behavior along the *a*-axis

K. Thirunavukkuarasu, F. Lichtenberg, and C. A. Kuntscher, Journal of Physics: Condensed Matter 18 (2006) 9173

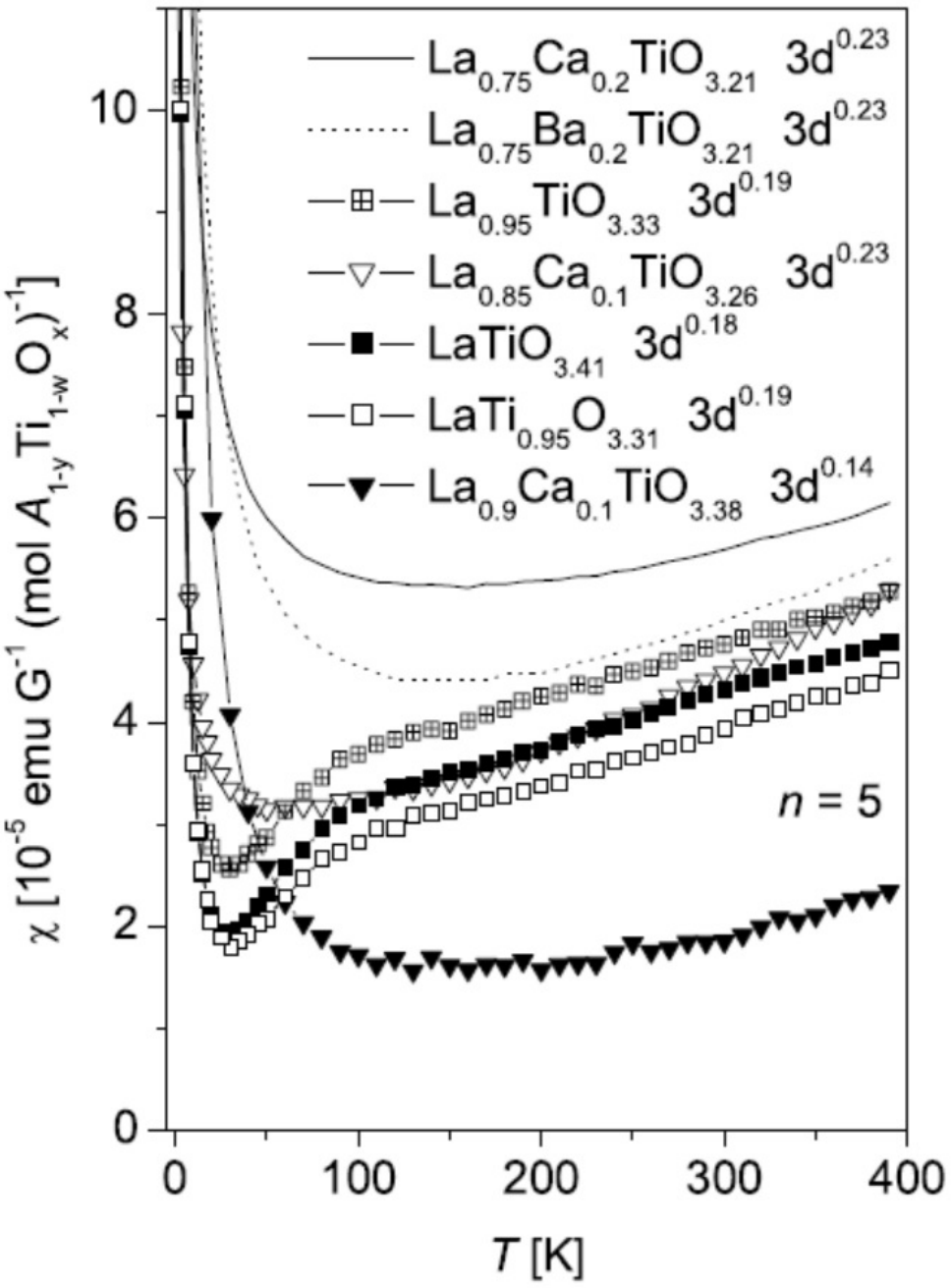

Melt-grown $n = 5$ type $La_{0.75}Ca_{0.2}TiO_{3.2}$, $La_{0.75}Ca_{0.2}TiO_{3.2}$, and $SrNbO_{3.4}$

No pronounced crystalline appearance

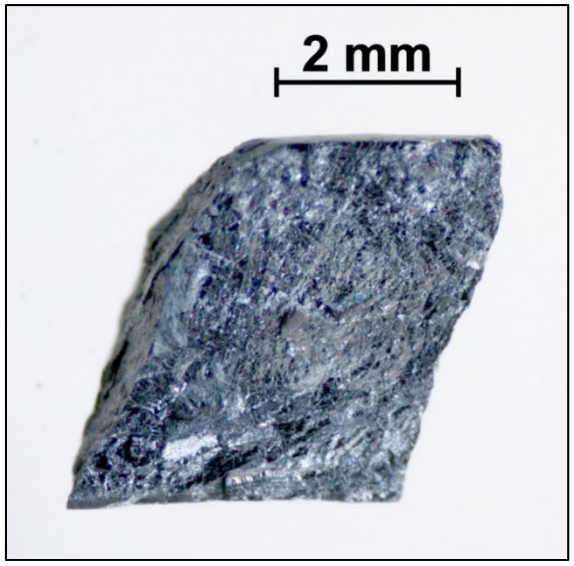

$La_{0.75}Ca_{0.2}TiO_{3.21}$

$Ti^{3.77+}$ / $3d^{0.23}$

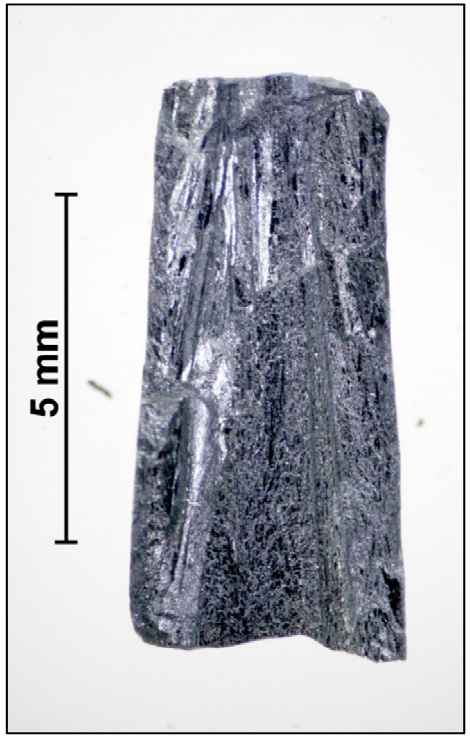

$La_{0.75}Ba_{0.2}TiO_{3.21}$

$Ti^{3.77+}$ / $3d^{0.23}$

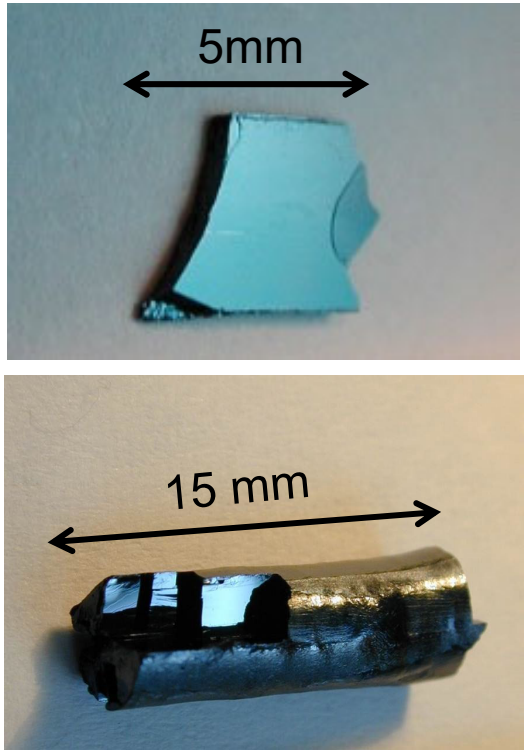

$SrNbO_{3.41}$

$Nb^{4.82+}$ / $4d^{0.18}$

Progress in Solid State Chemistry 29 (2001) 1 and 36 (2008) 253 • Samples prepared at the University of Augsburg • Pictures of $La_{0.75}Ca_{0.2}TiO_{3.21}$ and $La_{0.75}Ba_{0.2}TiO_{3.21}$ taken at the ETH Zurich

Schückel-Müller-Buschbaum phase $SrNbO_{3.2}$: $Nb^{4.4+}$ / $4d^{0.6}$. The following part 6.9 presents melt-grown $n = 5$ and $ABO_{3.2}$ type materials with an average number of 0.55 d-electrons per *B* site and a crystalline appearance like that of $SrNbO_{3.4}$ ...

6 Conducting and metallic Carpy-Galy phases $A_nB_nO_{3n+2} = ABO_x$

6.9 Prepared and studied at the ETH Zurich and structurally, compositionally, and electronically related to the Schückel-Müller-Buschbaum phase: Melt-grown Sr- and O-deficient $n = 5$ type materials $(Sr,Ca,Ba)_{19}Nb_{19}WO_x$ ($64 \leq x \leq 66$) with pronounced crystalline appearance ...

6 Conducting and metallic Carpy-Galy phases $A_nB_nO_{3n+2} = ABO_x$

6.9.1 Overview of the melt-grown compounds $(Sr,Ca,Ba)_{19}Nb_{19}WO_x$ ($64 \leq x \leq 66$) and general experimental details ...

Before presenting the Sr- and O-deficient n = 5 type materials $(Sr,Ca,Ba)_{19}Nb_{19}WO_x$ ($64 \leq x \leq 66$) , which were prepared by floating zone melting of the fully oxidized compositions $(Sr,Ca,Ba)_{19}Nb_{19}WO_{69.5}$ under argon plus hydrogen, let's first consider some melt-grown niobates $SrNbO_{3.5-y}$ and $Sr_{0.95}NbO_{3.45-y}$ which were likewise synthesized under argon plus hydrogen ...

Melt-grown $SrNbO_{3.5-y}$ and $Sr_{0.95}NbO_{3.45-y}$

Run / Sample No.	126	181	713	714
Composition	$SrNbO_{3.45}$	$Sr_{0.95}NbO_{3.37}$ = $Sr_{19}Nb_{20}O_{67.4}$	$Sr_{0.95}NbO_{3.38}$ = $Sr_{19}Nb_{20}O_{67.6}$	$Sr_{0.95}NbO_{3.35}$ = $Sr_{19}Nb_{20}O_{67}$
Synthesized by floating zone melting of the fully oxidized Nb^{5+} / $4d^0$ composition (y = 0) under flowing	98 % Ar + 2 % H_2	with a gas flow rate 250 sccm (15 L / h) , growth speed 10 mm / h and lamp power 2 × (515 - 505) W in a GERO mirror furnace	97.2 % Ar + 2.8 % H_2 with a gas flow rate 300 sccm (18 L / h) , growth speed 10 mm / h and the following lamp power to maintain the molten zone in the Cyberstar mirror furnace: 2 × (390 - 400) W	2 × 490 W
Degree y of reduction	0.05	0.08	0.07	0.10
Structure type	n = 4.5	Sr- and O-deficient n = 5		
Prepared at the ... in	University of Augsburg		ETH Zurich	
	1999	2001	2013	2013
Reference	Prog. Solid State Chem. 29 (2001) 1		This work	This work

Melt-grown synthesis under a high gas pressure of about 9 bar

Overview of the melt-grown compounds $(Sr,Ca,Ba)_{19}Nb_{19}WO_x$ ($64 \leq x \leq 66$) and general experimental details ...

Melt-grown Sr- and O-deficient $n = 5$ type $(Sr,Ca,Ba)_{19}Nb_{19}WO_x$ with $64 \leq x \leq 66$

Run / Sample No.		812	826
Prepared and studied at ETH Zurich in		2017 and 2018	2019
Composition		$Sr_{19}Nb_{19}WO_{66.03}$	$Sr_{17}Ca_2Nb_{19}WO_{63.97}$
Synthesized by floating zone melting of the fully oxidized Nb^{5+} / $4d^0$ and W^{6+} / $5d^0$ composition (x = 69.5) under		97.2 % Ar + 2.8 % H_2	95 % Ar + 5 % H_2
		with gas flow rate 24 L / h and growth speed 14 mm / h	
Powder XRD: Number of observed / indexed peaks		87 / 87	97 / 97
Orthorhombic lattice parameters FOM = Figure of merit of the refinement	a (Å)	7.98	7.96
	b (Å)	5.68	5.67
	c (Å)	32.51	32.46
	V ($Å^3$)	1474	1465
	FOM	8	17
Number of d electrons from Nb^{4+} / $4d^1$ and W^{4+} / $5d^2$ per unit cell		6.9	11.1
Physical properties		Potentially quasi-1D metals because above 100 K (No. 812) and 70 K (No. 826) the magnetic moment increases with increasing temperature	

Melt-grown Sr- and O-deficient $n = 5$ type $(Sr,Ca,Ba)_{19}Nb_{19}WO_x$ with $64 \leq x \leq 66$

Run / Sample No.		828	836	838
Prepared and studied at ETH Zurich in		2018	2019	2019
Composition		$Sr_{17}CaBaNb_{19}WO_x$		
x from thermogravimetric analysis		65.45	65.27	64.06
Synthesized by floating zone melting of the fully oxidized Nb^{5+} / $4d^0$ and W^{6+} / $5d^0$ composition (x = 69.5) under		97.2 % Ar + 2.8 % H_2		95 % Ar + 5 % H_2
		with gas flow rate 24 L / h and growth speed 14 mm / h		
Powder XRD: Number of observed / indexed peaks		95 / 95	98 / 98	103 / 103
Orthorhombic lattice parameters FOM = Figure of merit of the refinement	a (Å)	7.98	7.98	7.98
	b (Å)	5.68	5.68	5.68
	c (Å)	32.51	32.51	32.50
	V (Å^3)	1474	1474	1473
	FOM	17	18	14
Number of d electrons from Nb^{4+} / $4d^1$ and W^{4+} / $5d^2$ per unit cell		8.1	8.5	10.9
Physical properties		Potentially quasi-1D metals because above 105 K (# 828), 110 K (# 836), and 65 K (# 838) the magnetic moment increases with increasing temperature		

Melt-grown synthesis under a high gas pressure of about 9.5 bar

Synthesis approach

$19\,(s\,SrCO_3 + c\,CaCO_3 + b\,BaCO_3) + 9.5\,Nb_2O_5\,(Nb^{5+}) + WO_3\,(W^{6+})$

$s + c + b = 1$

↓

Pre-reaction at elevated temperatures under air

↓

Composition $(Sr,Ca,Ba)_{19}Nb_{19}WO_{69.5}$ + 19 CO_2 ↑

↓

Melt and solidify polycrystalline sintered rods
with fully oxidized composition $(Sr,Ca,Ba)_{19}Nb_{19}WO_{69.5}$
under an argon-hydrogen atmosphere

↓

Melt-grown crystalline material with reduced composition
$(Sr,Ca,Ba)_{19}Nb_{19}WO_{69.5-y}$ ($y > 0$)

Its oxygen content $x = 69.5 - y$ can be determined by thermogravimetric oxidation towards the fully oxidized $x = x_F = 69.5$. Fully oxidized composition means that all Nb and W ions are in their highest valence state 5+ and 6+, respectively

The valence or oxidation state of the W ions in melt-grown reduced $(Sr,Ca,Ba)_{19}Nb_{19}WO_{69.5-y}$

When comparing a W-free composition ... Nb_{20} ... with a corresponding W-containing composition ... $Nb_{19}W$ ... then the presence of W results in a significantly enhanced degree of reduction, i.e. $y\ (Nb_{19}W) > y\ (Nb_{20})$

To the best of our knowledge W^{4+} / $5d^2$ is the lowest valence or oxidation state of W in oxides and W^{6+} / $5d^0$ can be reduced easier than Nb^{5+} / $4d^0$

Therefore the most likely scenario seems to be W^{4+} / $5d^2$

Starting materials (powder) and preparation of sintered rods

Starting material	Supplier	Lot or Ch. No.	Purity (%) metals basis if not otherwise specified	Before using the powder it was heated under air at ... (°C) and subsequently stored in a desiccator	Calculated amount (g) for run / sample No. 838
$SrCO_3$	ChemPur	150916	99.994	250	4.1828
$CaCO_3$	ChemPur	120717	99.9	250	0.1668
$BaCO_3$	ChemPur	050514	99.999	250	0.3289
Nb_2O_5	Alfa Aesar	W10A029	99.9	400	4.2087
WO_3	Alfa Aesar	10183650	99.998 excluding Mo Mo 100 ppm	400	0.3864

The starting materials were mingled by an agate mortar and pestle and then pre-reacted for 4 h at a temperature around 1200 °C under air in an alumina crucible which was placed into a laboratory chamber furnace Linn High Therm VMK 1600. Afterwards the pre-reacted and somewhat sintered powder mixture was grinded into powder which was mingled by an agate mortar and pestle. Subsequently a part of the pre-reacted powder was pressed into the shape of two rectangular rods by using special pressing dies made of magnesia-stabilized zirconia. Then the as-pressed rods were sintered under air.

6 Conducting and metallic Carpy-Galy phases $A_nB_nO_{3n+2} = ABO_x$

6.9.2 Towards a Schückel-Müller-Buschbaum type phase: Synthesis and properties of $Sr_{19}Nb_{19}WO_{66}$ ...

Sintered rods with composition $Sr_{19}Nb_{19}WO_{69.5}$ Run No. 812

Polycrystalline sintered rods with fully oxidized composition $Sr_{19}Nb_{19}WO_{69.5}$, i.e. all Nb and W ions are in their highest valence or oxidation state Nb^{5+} and W^{6+}, respectively

The as-pressed rods were 4 h sintered at 1280 °C under air. The sintering did result in a shrinkage of their length, namely $\Delta L \approx$ - 6 mm for the long rod and $\Delta L \approx$ - 3 mm for the short rod

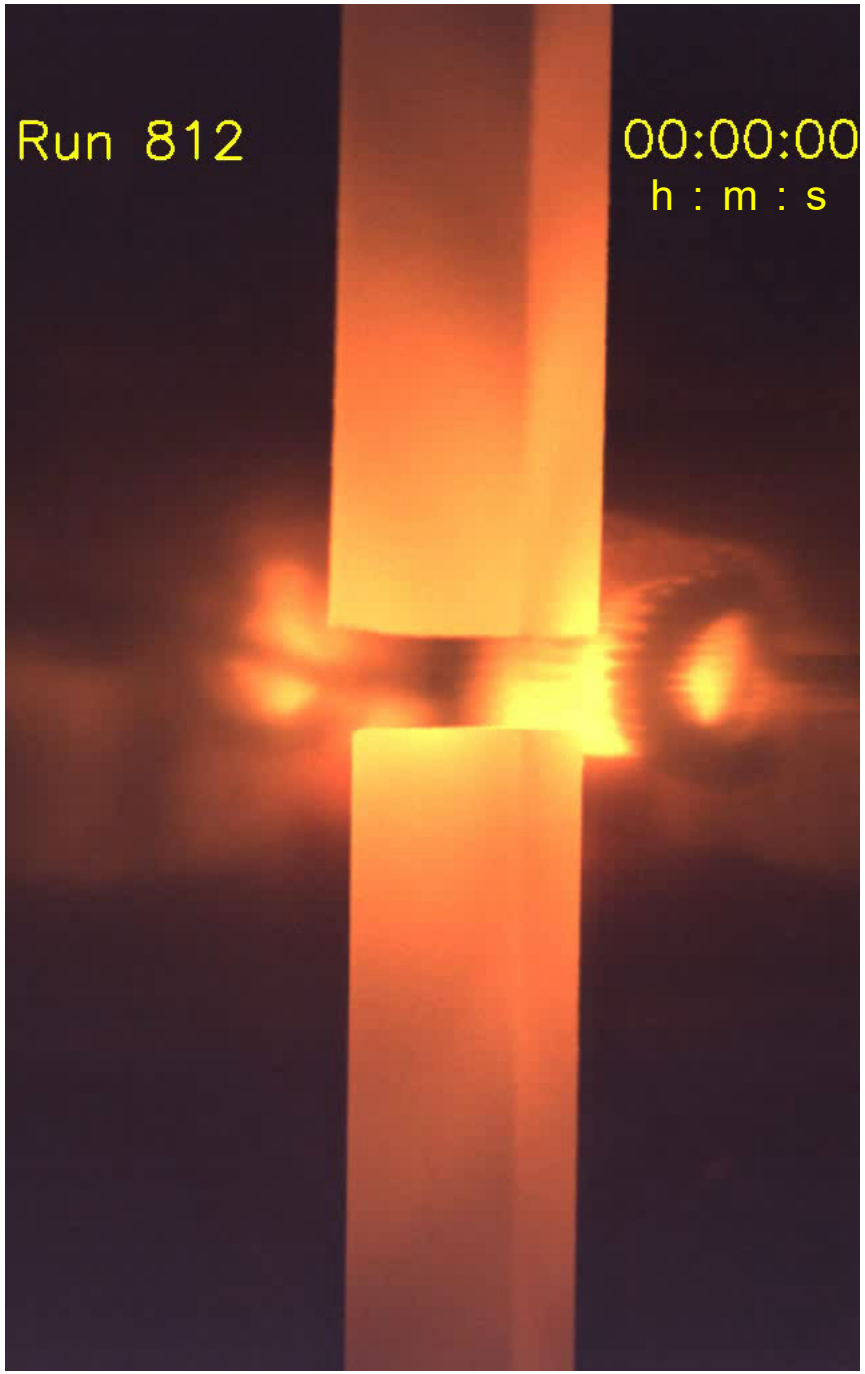

Melt-grown synthesis of $Sr_{19}Nb_{19}WO_{69.5 - y}$

Starting materials for the mirror furnace run: Polycrystalline sintered rods with fully oxidized composition $Sr_{19}Nb_{19}WO_{69.5}$

Fast mode video from the overall melt-grown synthesis of $Sr_{19}Nb_{19}WO_{69.5 - y}$ under 97.2 % Ar + 2.8 % H_2 in the Cyberstar mirror furnace. The video is only running in the ppsx type version of this publication, see page 2

Gas flow rate: 400 sccm (24 L / h)
Gas type setting at the mass flow controller: Ar

Lamp power to maintain the molten zone: 2 × 383 W

Speed of the lower shaft and seed rod (crystal growth speed): 14 mm / h

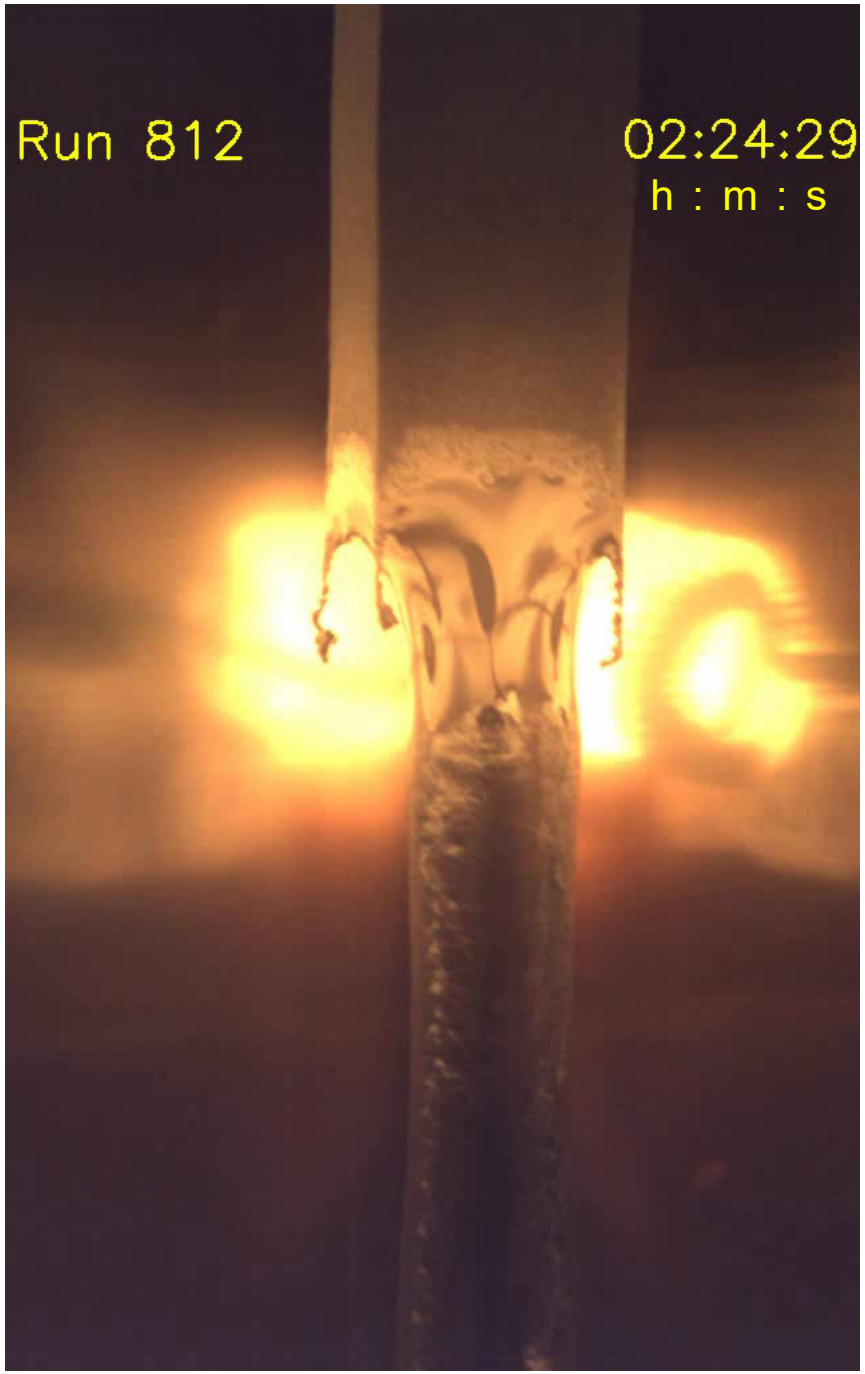

Melt-grown synthesis of $Sr_{19}Nb_{19}WO_{69.5 - y}$

Starting materials for the mirror furnace run: Polycrystalline sintered rods with fully oxidized composition $Sr_{19}Nb_{19}WO_{69.5}$

Real time video of a short section from the melt-grown synthesis of $Sr_{19}Nb_{19}WO_{69.5 - y}$ under 97.2 % Ar + 2.8 % H_2 in the Cyberstar mirror furnace. The video is only running in the ppsx type version of this publication, see page 2

Gas flow rate: 400 sccm (24 L / h)
Gas type setting at the mass flow controller: Ar

Lamp power to maintain the molten zone: 2 × 383 W

Speed of the lower shaft and seed rod (crystal growth speed): 14 mm / h

As-grown crystalline material $Sr_{19}Nb_{19}WO_{69.5-y}$ and polycrystalline rods

Run / Sample No. 812

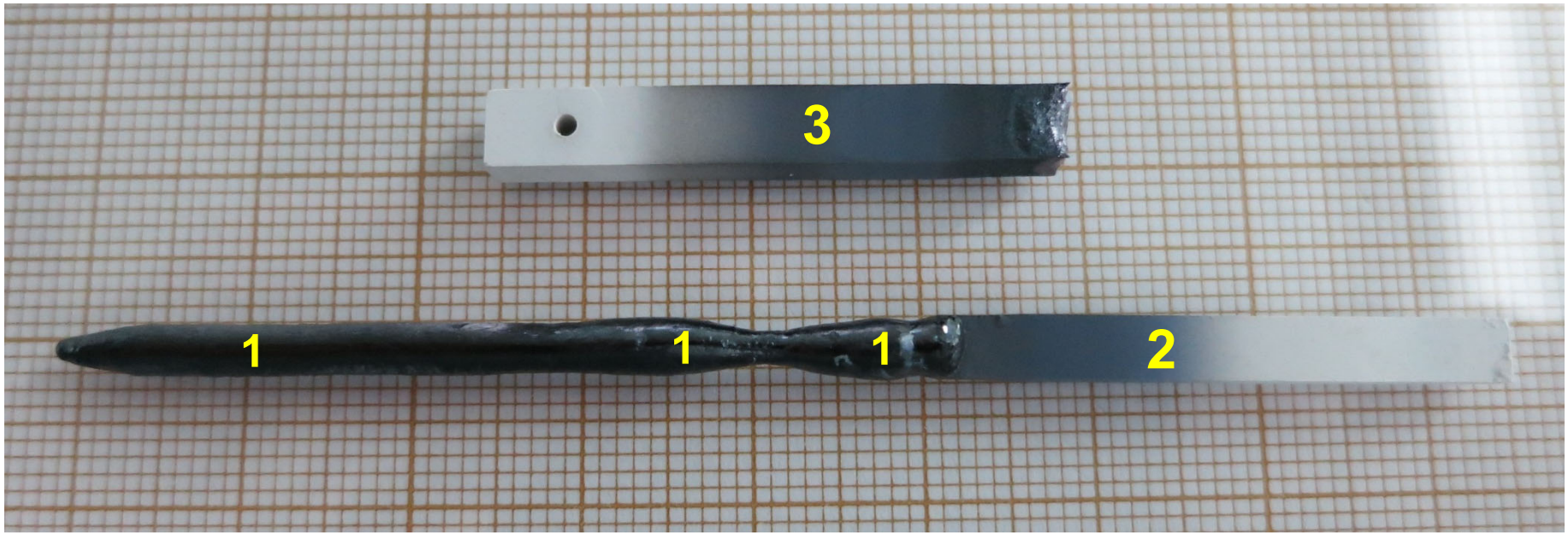

5 cm long as-grown crystalline material (1) plus polycrystalline seed rod (2) and remaining part of the polycrystalline feed rod (3)

Prepared at the ETH Zurich in 2017

As-grown crystalline material $Sr_{19}Nb_{19}WO_{69.5 - y}$

Sample No. 812

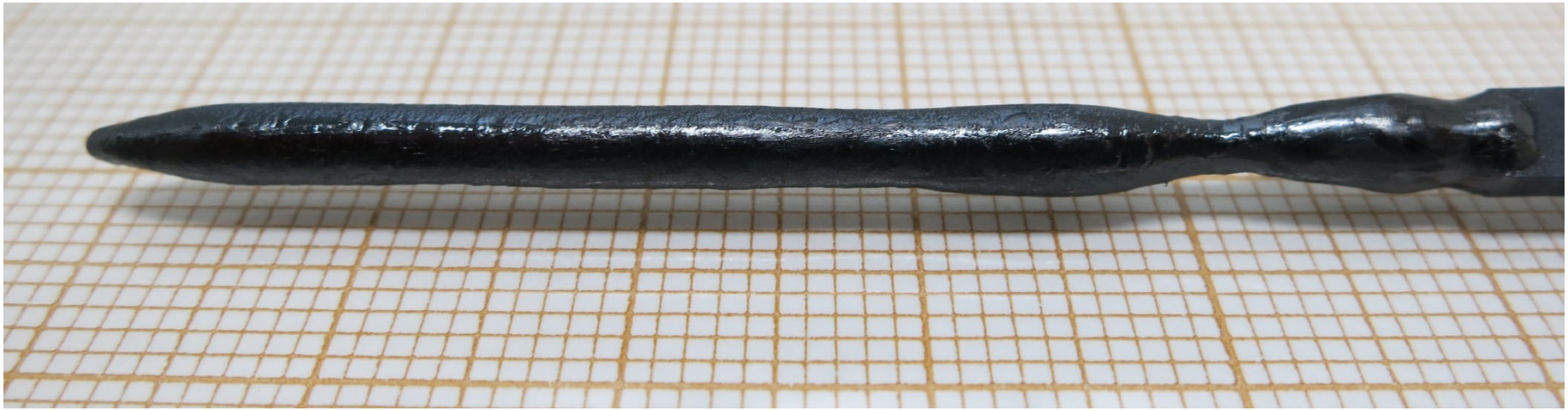

5 cm long as-grown crystalline material

As-grown crystalline material $Sr_{19}Nb_{19}WO_{69.5 - y}$

Sample No. 812

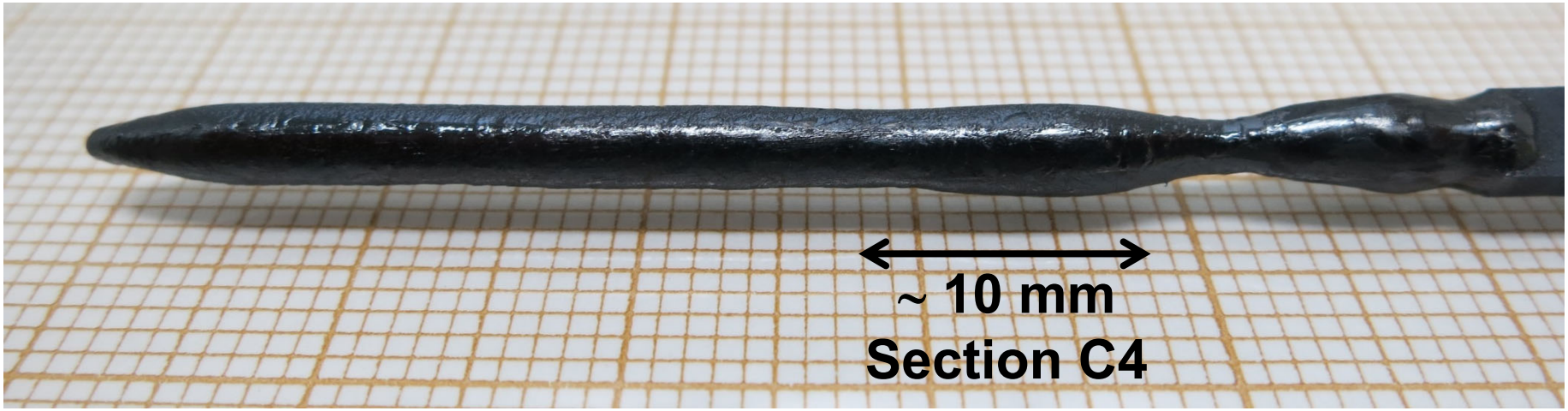

5 cm long as-grown crystalline material

As-grown crystalline material $Sr_{19}Nb_{19}WO_{69.5 - y}$

Sample No. 812

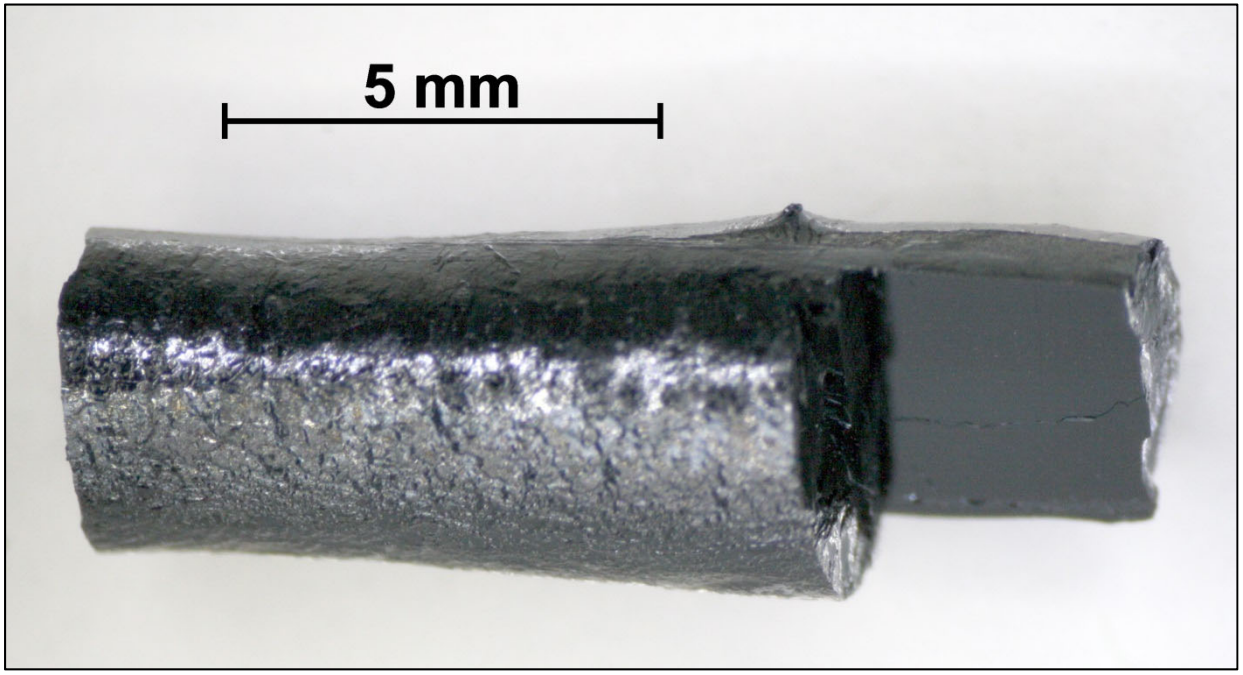

Crystalline piece from section C4 of the as-grown material

812 C4 $Sr_{19}Nb_{19}WO_x$ Thermogravimetry

Thermogravimetric oxidation in flowing synth. air up to the fully oxidized composition with $x = x_F = 69.5$ for the determination of the oxygen content $x = 69.5 - y$ by using a thermogravimetric analyzer NETZSCH TG 209 F1 Libra

Pulverized crystalline material from section C4 of the as-grown sample → $x = 66.03$

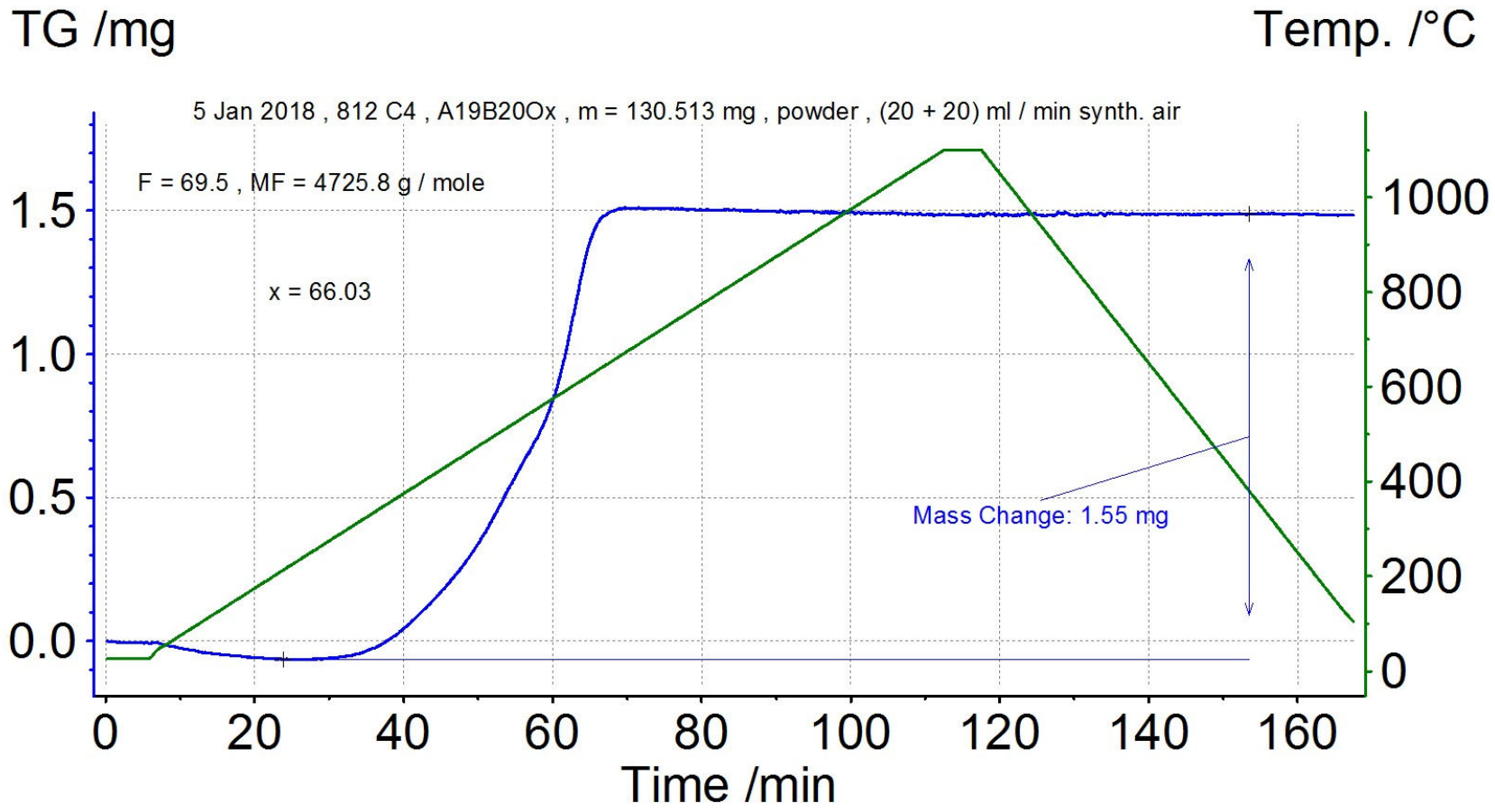

$Sr_{19}Nb_{19}WO_{66.03}$ Valences of the Nb and W ions

Valence or oxidation states of the
Nb and W ions in $Sr_{19}Nb_{19}WO_{66.03}$

The most likely scenario is W^{4+} / $5d^2$

↓

Charge neutrality and Sr^{2+} and O^{2-} → $Nb^{4.74+}$ / $4d^{0.26}$

↓

2 (5d) + 19 × 0.26 (4d) = 6.94 d-electrons
per formula and assumed size of the unit cell

812 C4 $Sr_{19}Nb_{19}WO_{66}$ Powder x-ray diffraction

Powder x-ray diffraction pattern of pulverized crystalline material from section C4

Square root - linear plot • Background subtracted

All observed peaks fit to an orthorhombic *n* = 5 type structure

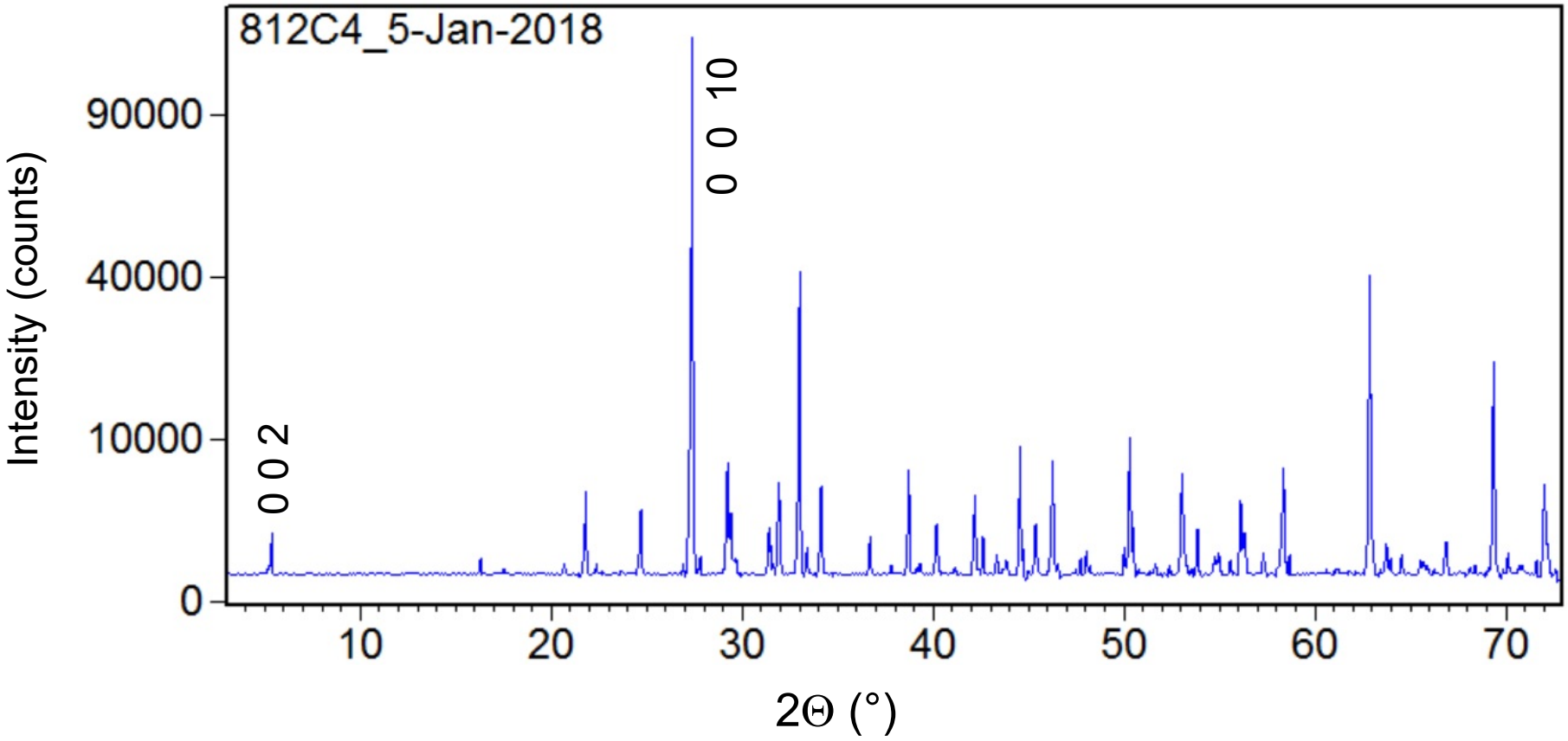

812 C4 $Sr_{19}Nb_{19}WO_{66}$ Powder x-ray diffraction

	Observed peak position (°2θ)	d-spacing (Å)	Relative intensity (%)	h k l from lattice parameter refinement
Lowest angle peak Its position indicates the structure type of $A_nB_nO_{3n+2}$, namely n = 5 in this case	5.38	16.42	1	0 0 2
Highest intensity peak	27.38	3.25	100	0 0 10

812 C4 $Sr_{19}Nb_{19}WO_{66}$ Powder x-ray diffraction

Results of lattice parameter refinement with $(h\ k\ l)_{max} = (10\ \ 10\ \ 20)$

Number of observed peaks	87
Number of indexed peaks	87
Number of unindexed peaks	0
Crystal structure type	$n = 5$ of $A_nB_nO_{3n+2}$
Crystal system	Orthorhombic
Bravais lattice	P
a (Å)	7.98
b (Å)	5.68
c (Å)	32.51
V (Å^3)	1474
$\lvert 2\theta_{obs} - 2\theta_{calc} \rvert$ of observed and calculated peaks	$\leq 0.067°$ for 86 peaks $= 0.094°$ for 1 peak with $I_{rel} = 0.2$ %
Figure of merit of the refinement or fit	8.2
Chi square of the refinement or fit	6.5×10^{-6}

812 C4 $Sr_{19}Nb_{19}WO_{66}$ Magnetic measurements

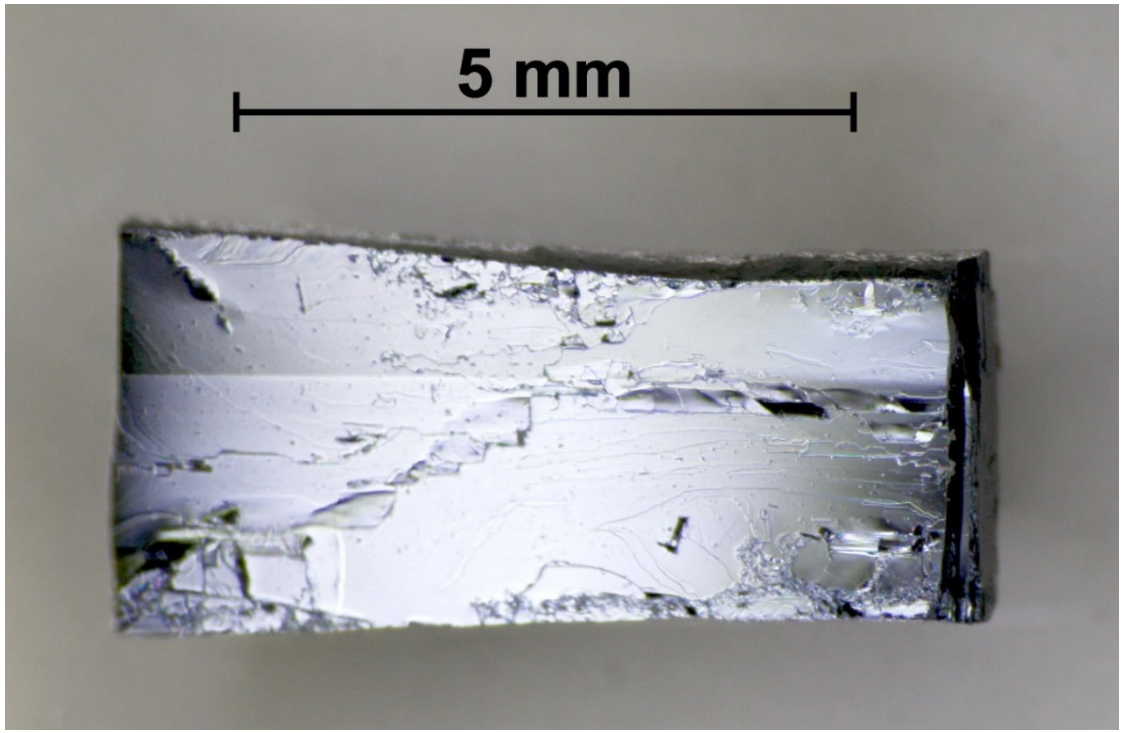

Crystalline piece C4-1 from section C4

This piece with a mass m = 187 mg
was used to study its magnetic
properties by a SQUID magnetometer

After magnetic
measurements
by a SQUID
magnetometer
the electrical
resistance R of a
part of this piece,
called 814 C4 R,
was measured
by a multimeter
$\rightarrow$ $R \geq 10\ \Omega$

812 C4 $Sr_{19}Nb_{19}WO_{66}$ Magnetic susceptibility $\chi(T)$

DC magnetic moment M(T) measured by a Quantum Design SQUID magnetometer MPMS3

6.9 d-electrons from Nb^{4+} / $4d^1$ and W^{4+} / $5d^2$

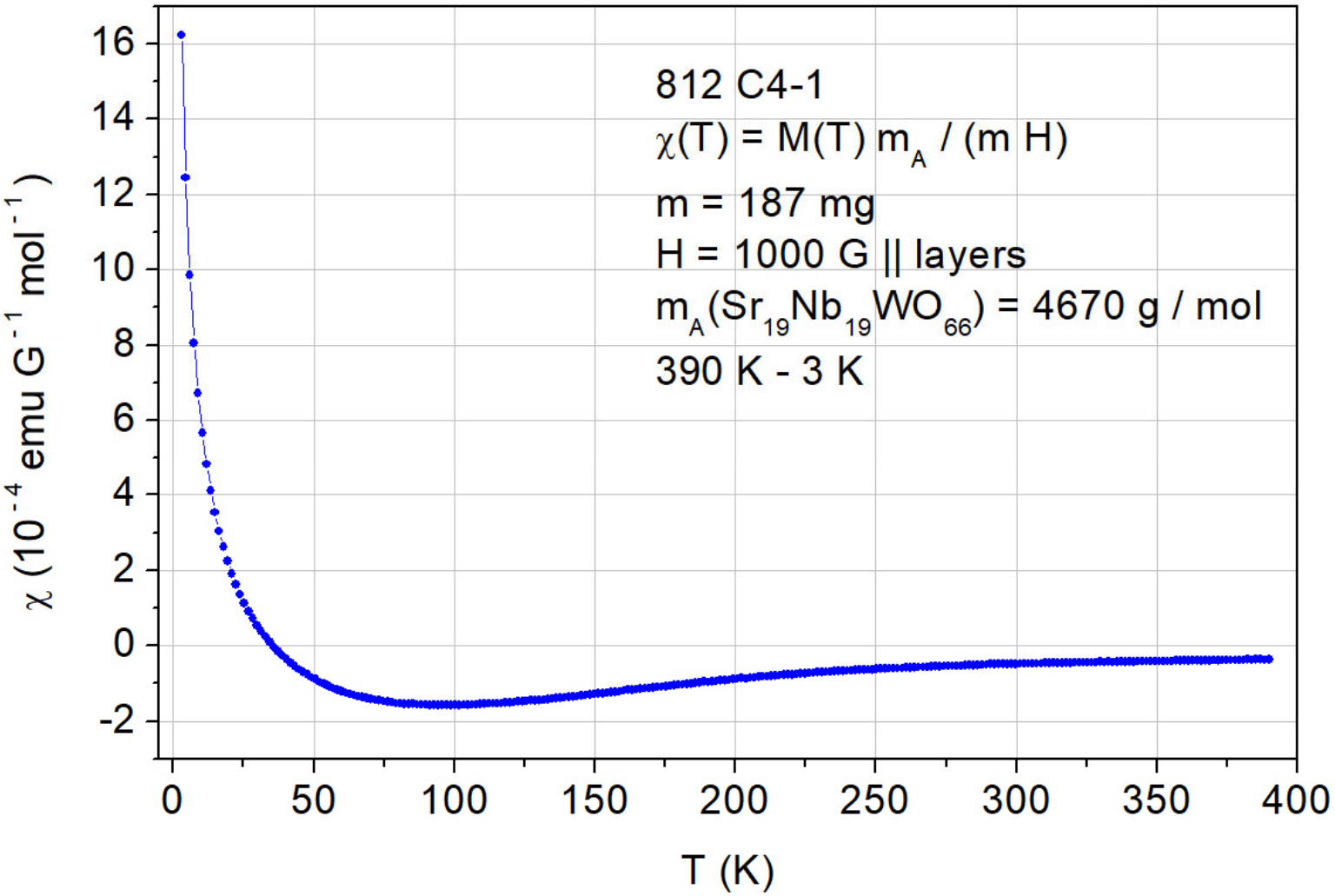

812 C4 $Sr_{19}Nb_{19}WO_{66}$ Magnetic susceptibility $\chi(T)$

DC magnetic moment M(T) measured by a Quantum Design SQUID magnetometer MPMS3

6.9 d-electrons from Nb^{4+} / $4d^1$ and W^{4+} / $5d^2$

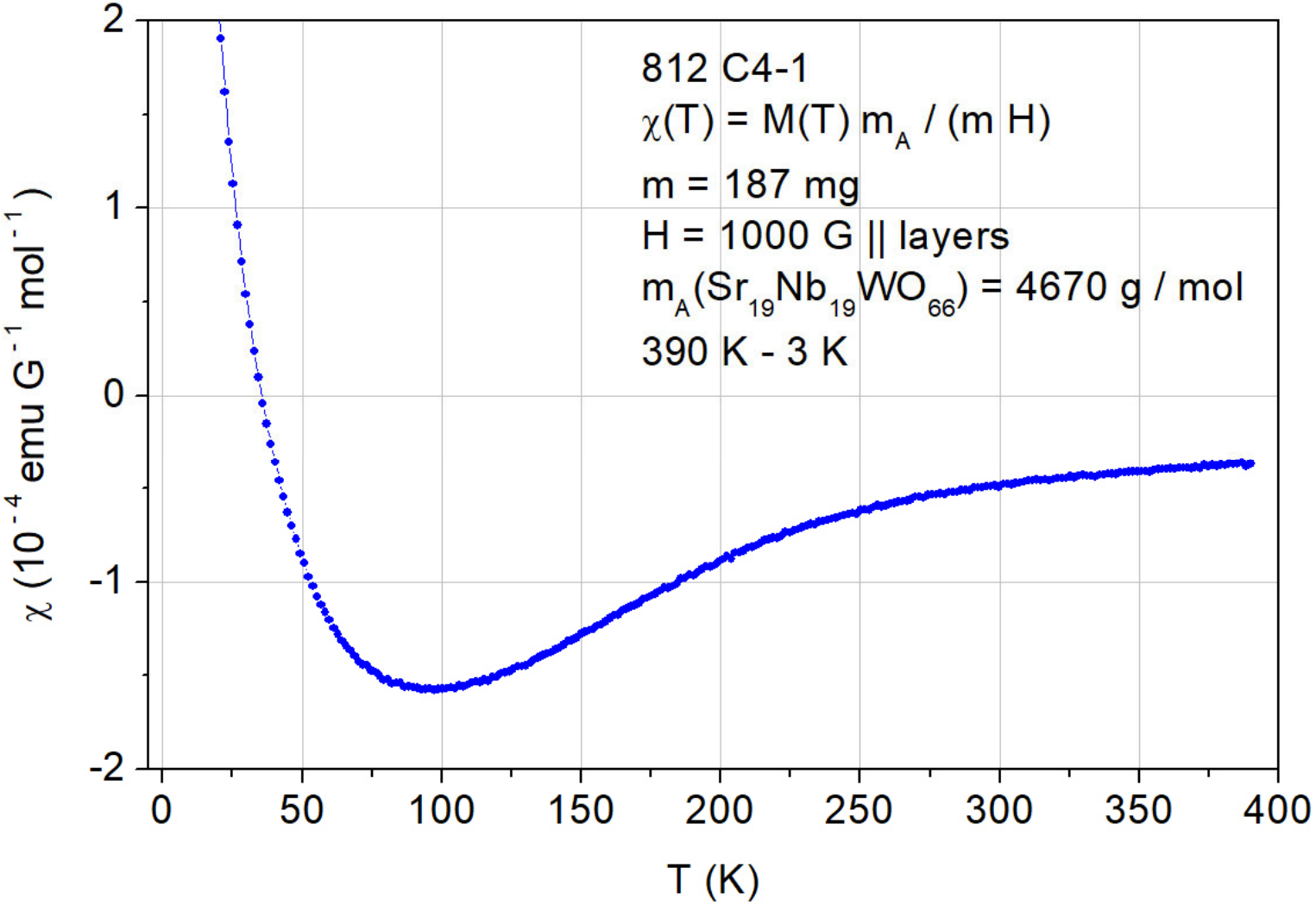

The behavior of $\chi(T)$ in the range from 390 K to 100 K is similar to that of $A_nB_nO_{3n+2}$ type quasi-1D metals. Thus this n = 5 type material is potentially also a quasi-1D metal

812 C4 $Sr_{19}Nb_{19}WO_{66}$ Magnetic susceptibility $\chi(T)$

DC magnetic moment M(T) measured by a Quantum Design SQUID magnetometer MPMS3

6.9 d-electrons from Nb^{4+} / $4d^1$ and W^{4+} / $5d^2$

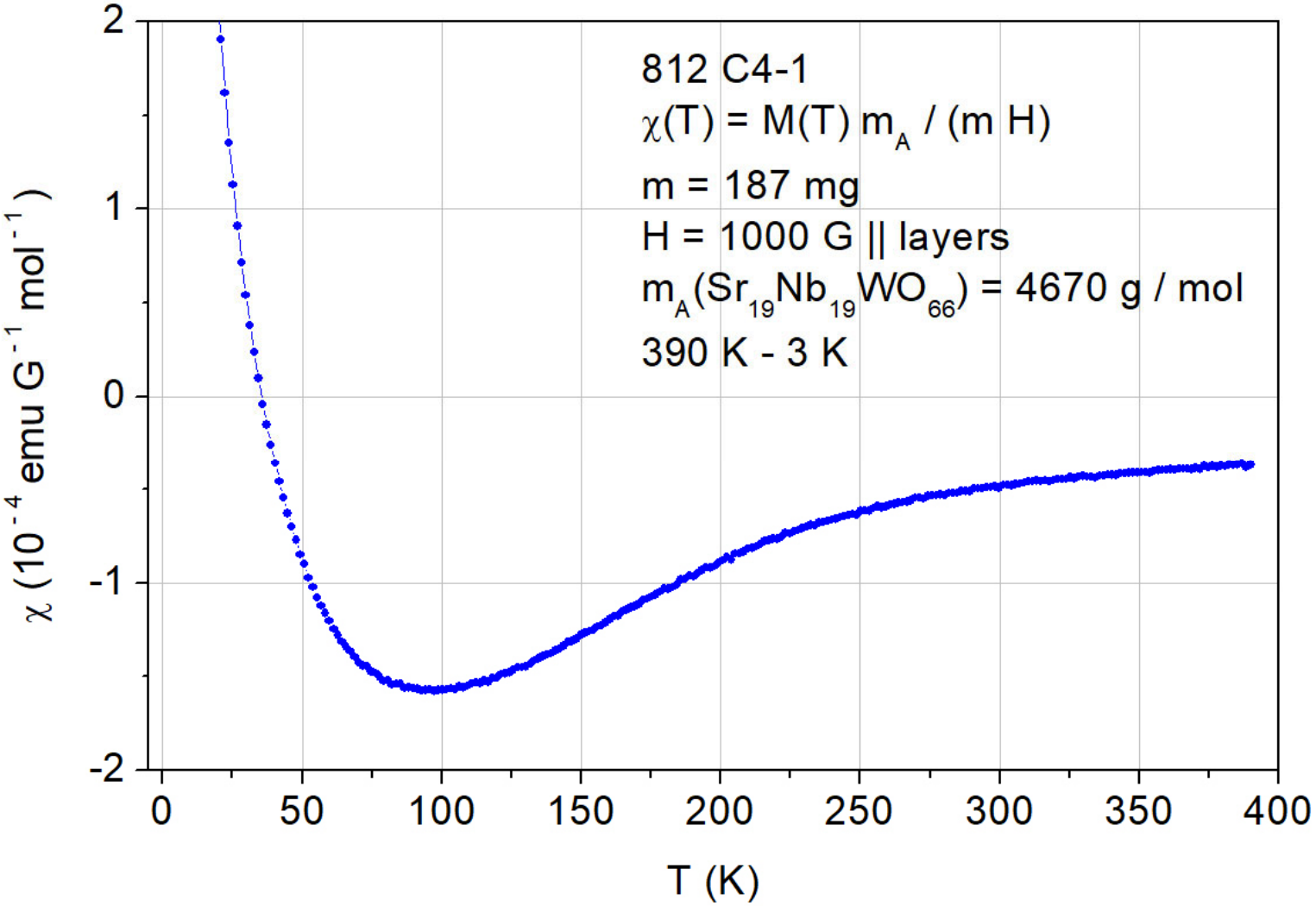

Increase of $\chi(T)$ below 90 K probably not due to paramagnetic impurities or defect states because they give usually a signal only at lower temperatures. Increase below 90 K due to 5d electrons which become localized ?

812 C4 $Sr_{19}Nb_{19}WO_{66}$ Magnetic susceptibility $\chi(T)$

DC magnetic moment M(T) measured by a Quantum Design SQUID magnetometer MPMS3

6.9 d-electrons from Nb^{4+} / $4d^1$ and W^{4+} / $5d^2$

D = diamagnetic contribution from closed electron shells of Sr^{2+}, Nb^{5+}, W^{6+}, and O^{2-}

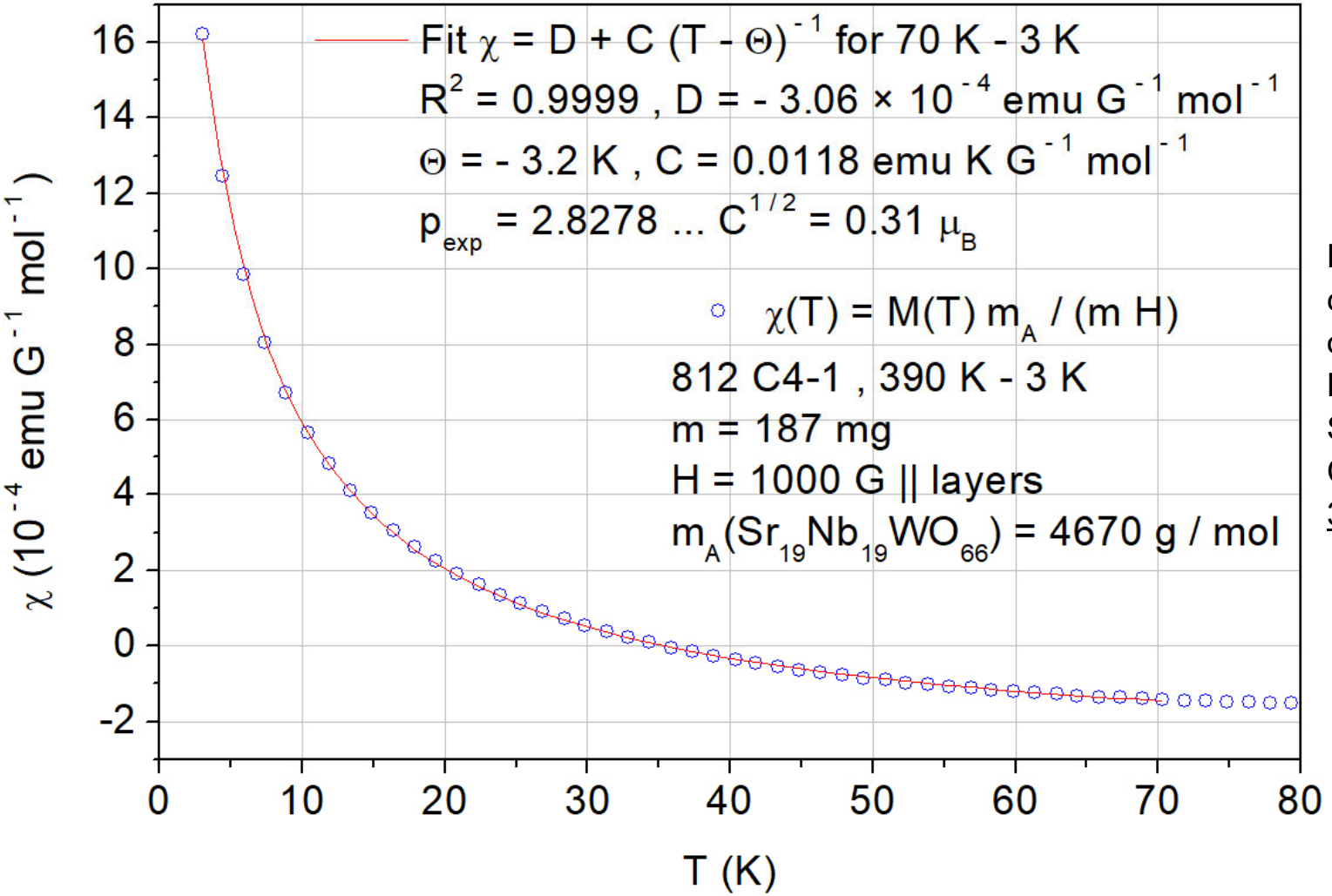

Ref. for the calculation of p_{exp}: Progress in Solid State Chemistry 36 (2008) 253

6 Conducting and metallic Carpy-Galy phases $A_nB_nO_{3n+2} = ABO_x$

6.9.3 Towards a Schückel-Müller-Buschbaum type phase: Synthesis and properties of $Sr_{17}CaBaNb_{19}WO_{65.5}$ ...

As-pressed rods with composition $Sr_{17}CaBaNb_{19}WO_{69.5}$ Run No. 828

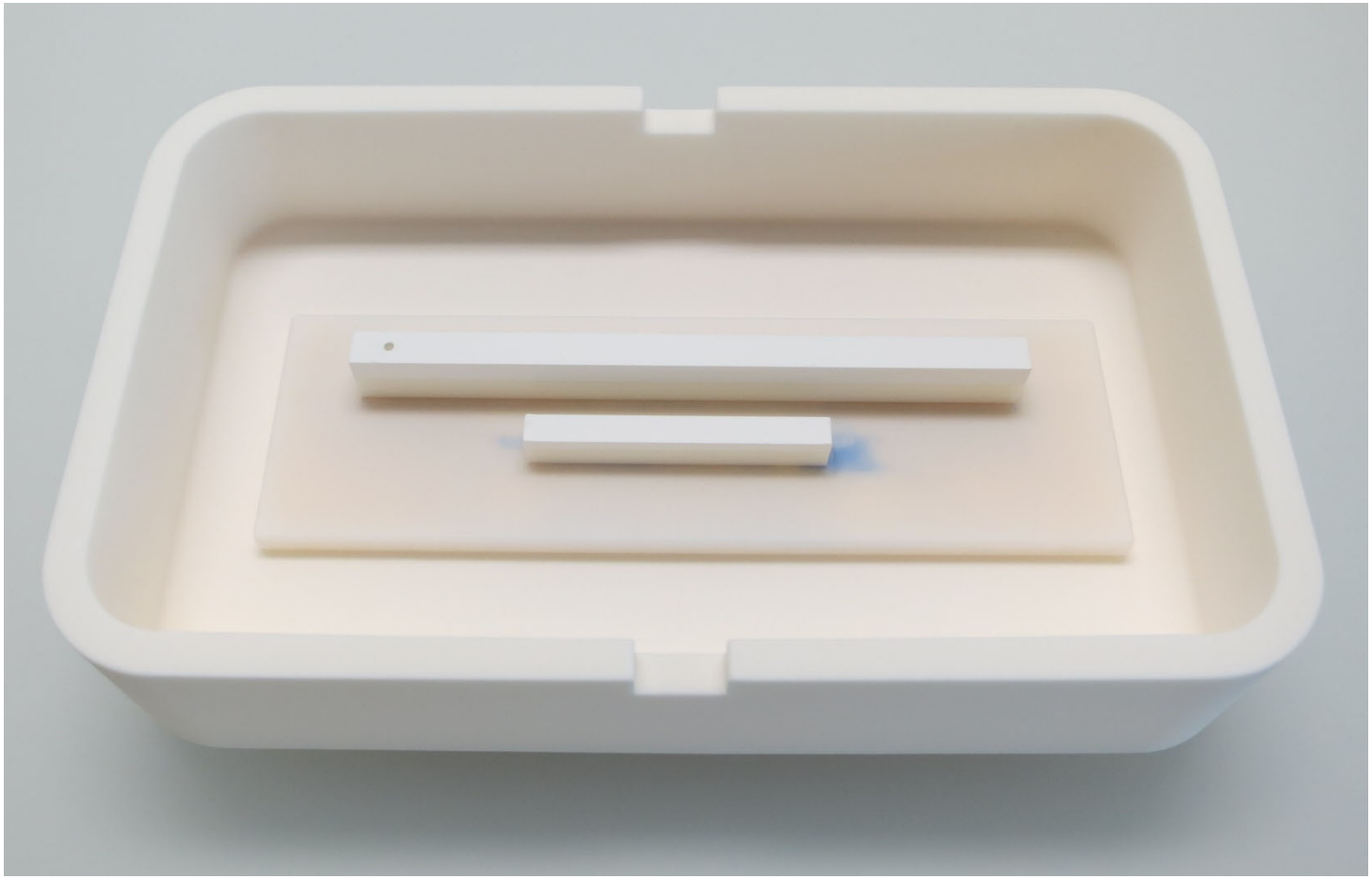

As-pressed rods in an alumina box. Ready for sintering under air. The as-pressed rods are located on a lower punch which is made of yttria-stabilized zirconia. The length of the long rod is 9 cm

Both as-pressed rods have the fully oxidized composition $Sr_{17}CaBaNb_{19}WO_{69.5}$, i.e. all Nb and W ions are in their highest valence or oxidation state Nb^{5+} and W^{6+}, respectively

Sintered rods with composition $Sr_{17}CaBaNb_{19}WO_{69.5}$ Run No. 828

The as-pressed rods were 4 h sintered at 1240 °C under air.
The sintering did result in a shrinkage of their length, namely
$\Delta L \approx$ - 5 mm for the long rod and $\Delta L \approx$ - 2.5 mm for the short rod

A somewhat lower sintering temperature would have been better because the sintered rods were attached on their lower punch. Fortunately it was possible to remove the rods from their lower punch without damaging the rods.
Later related experiments revealed that lower punches made of alumina are more suitable

Sintered rods with composition $Sr_{17}CaBaNb_{19}WO_{69.5}$ Run No. 828

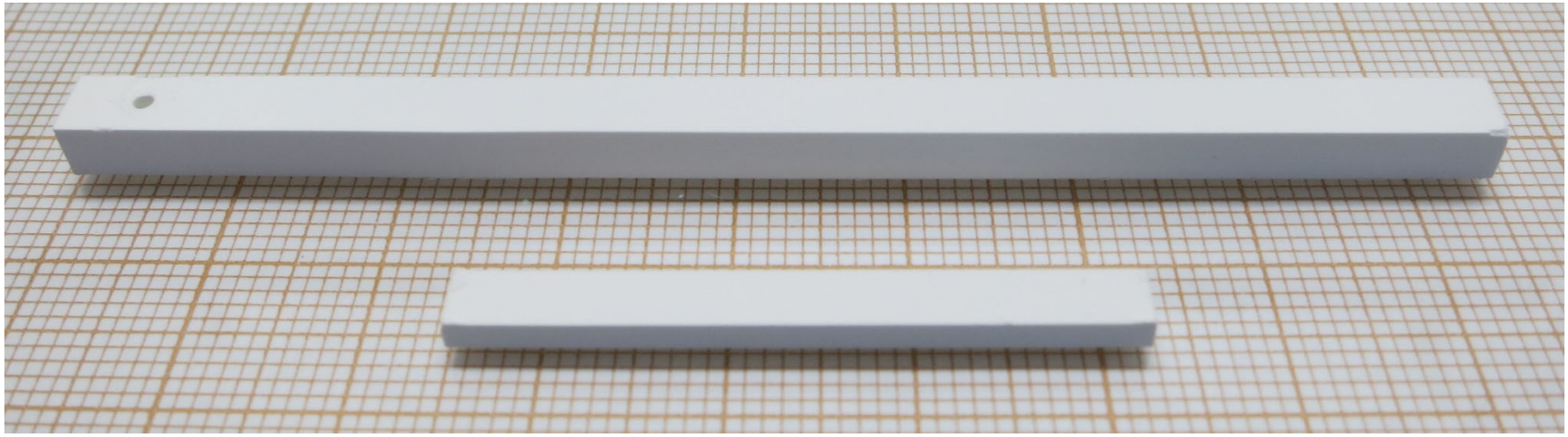

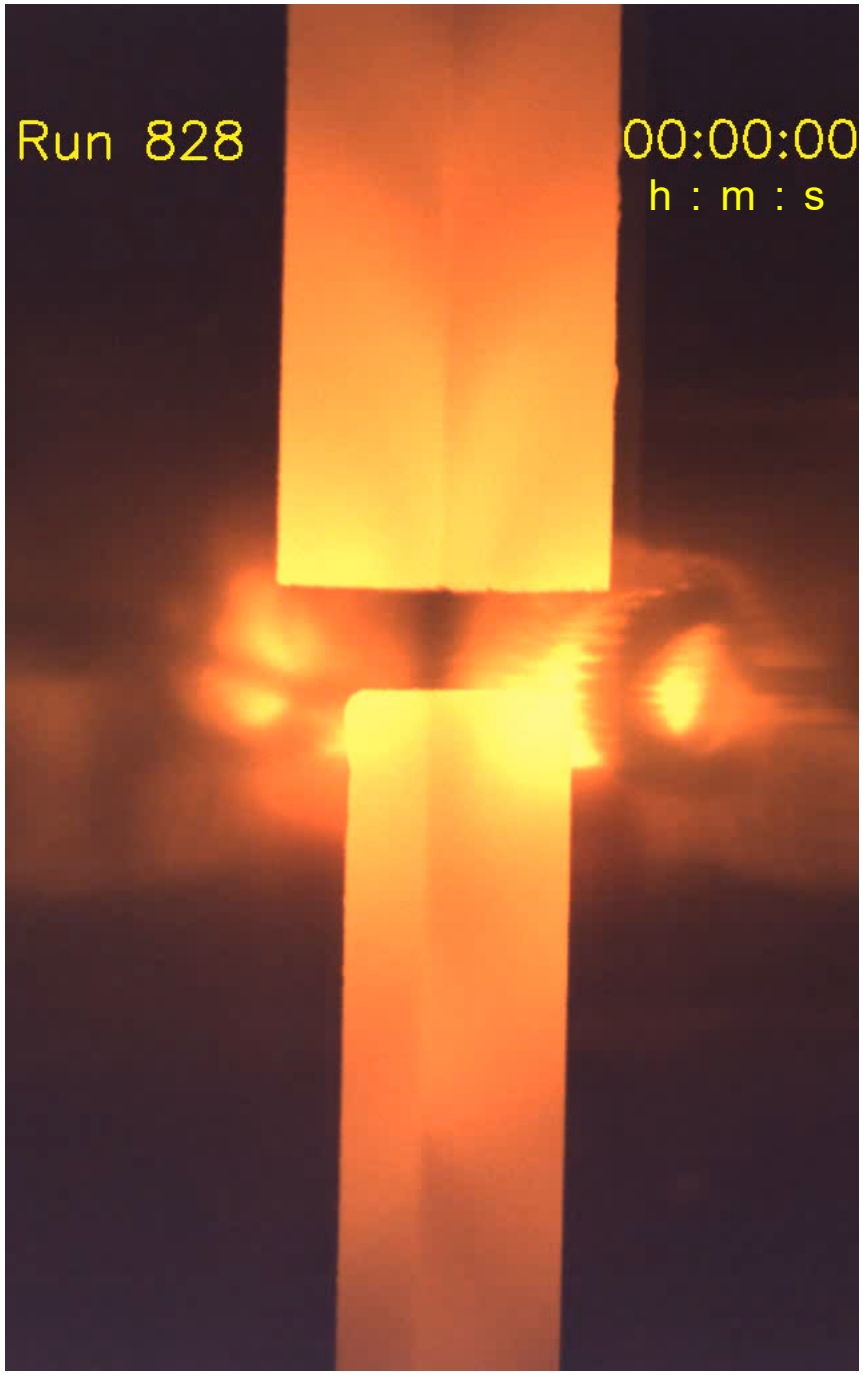

Melt-grown synthesis of $Sr_{17}CaBaNb_{19}WO_{69.5 - y}$

Starting materials for the mirror furnace run: Polycrystalline sintered rods with fully oxidized composition $Sr_{17}CaBaNb_{19}WO_{69.5}$

Fast mode video from the overall melt-grown synthesis of $Sr_{17}CaBaNb_{19}WO_{69.5 - y}$ under 97.2 % Ar + 2.8 % H_2 in the Cyberstar mirror furnace. The video is only running in the ppsx type version of this publication, see page 2

Gas flow rate: 400 sccm (24 L / h)
Gas type setting at the mass flow controller: Ar

Lamp power to maintain the molten zone: 2 × 368 W

Speed of the lower shaft and seed rod (crystal growth speed): 14 mm / h

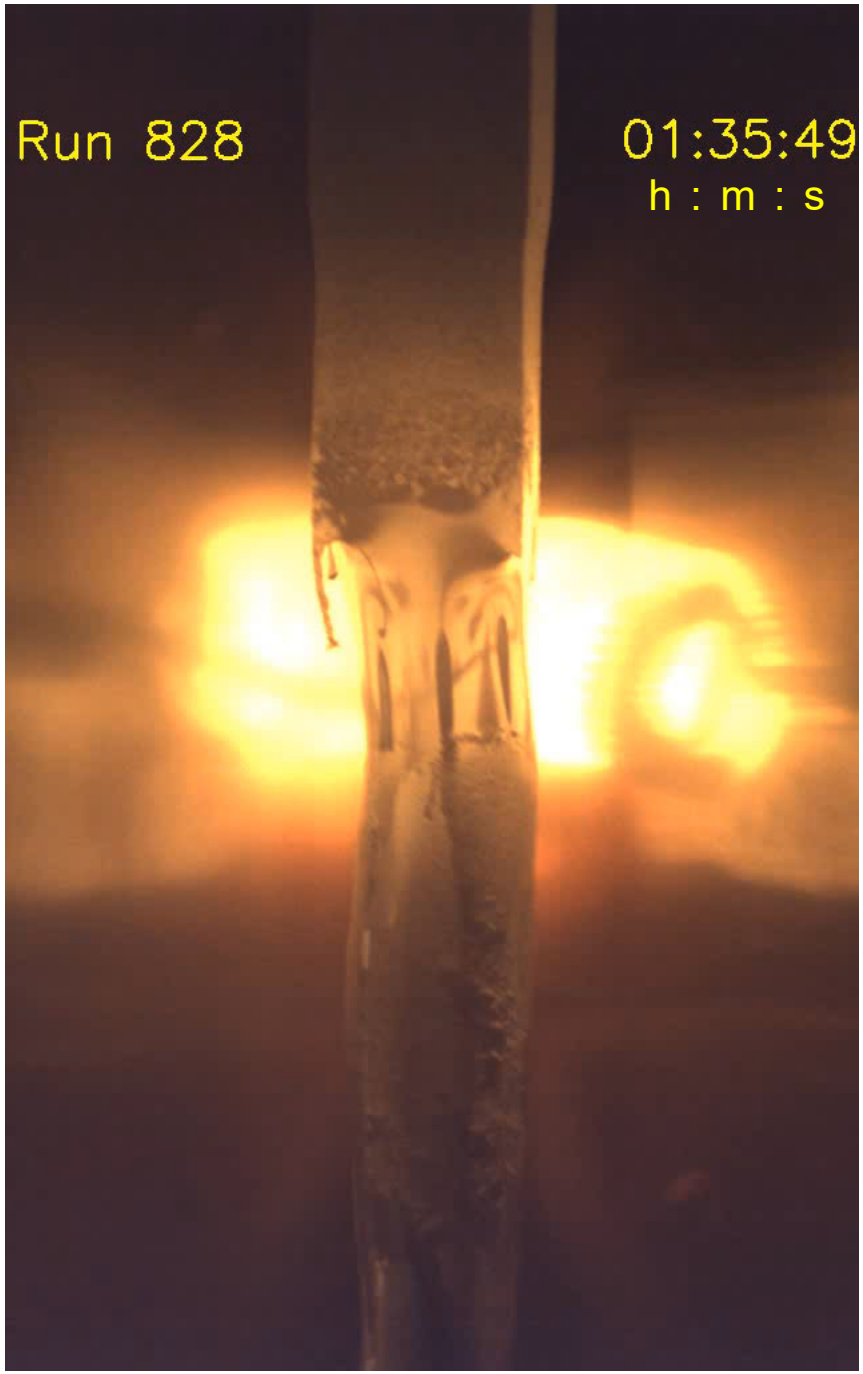

Melt-grown synthesis of $Sr_{17}CaBaNb_{19}WO_{69.5-y}$

Starting materials for the mirror furnace run: Polycrystalline sintered rods with fully oxidized composition $Sr_{17}CaBaNb_{19}WO_{69.5}$

Real time video of a short section from the melt-grown synthesis of $Sr_{17}CaBaNb_{19}WO_{69.5-y}$ under 97.2 % Ar + 2.8 % H_2 in the Cyberstar mirror furnace. The video is only running in the ppsx type version of this publication, see page 2

Gas flow rate: 400 sccm (24 L / h)
Gas type setting at the mass flow controller: Ar

Lamp power to maintain the molten zone: 2 × 368 W

Speed of the lower shaft and seed rod (crystal growth speed): 14 mm / h

As-grown crystalline $Sr_{17}CaBaNb_{19}WO_{69.5-y}$ and polycrystalline rods

Run / Sample No. 828

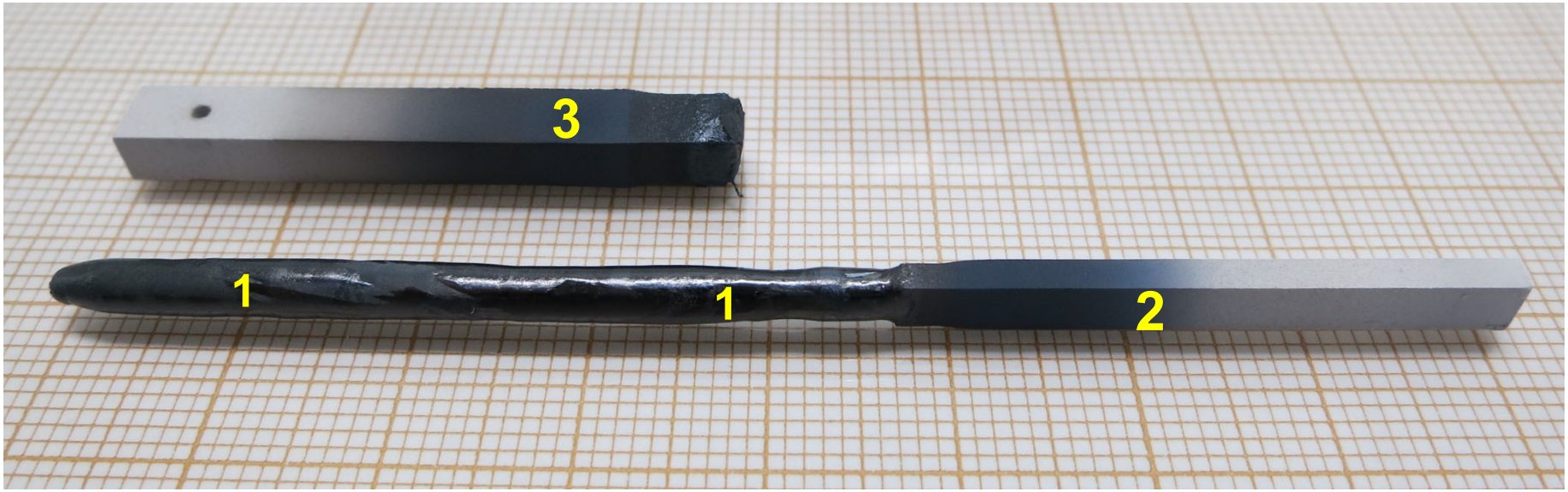

47 mm long as-grown crystalline material (1) plus polycrystalline seed rod (2) and remaining part of the polycrystalline feed rod (3)

Prepared at the ETH Zurich in 2018

As-grown crystalline material $Sr_{17}CaBaNb_{19}WO_{69.5 - y}$

Sample No. 828

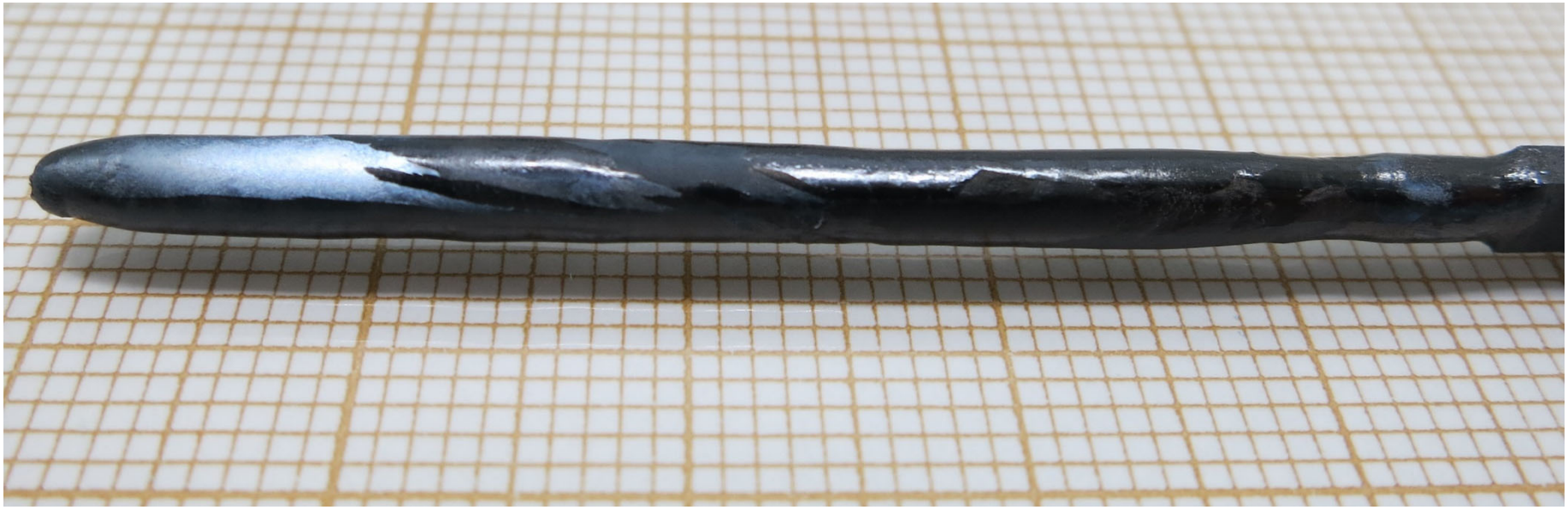

47 mm long as-grown crystalline material

As-grown crystalline material $Sr_{17}CaBaNb_{19}WO_{69.5 - y}$

Sample No. 828

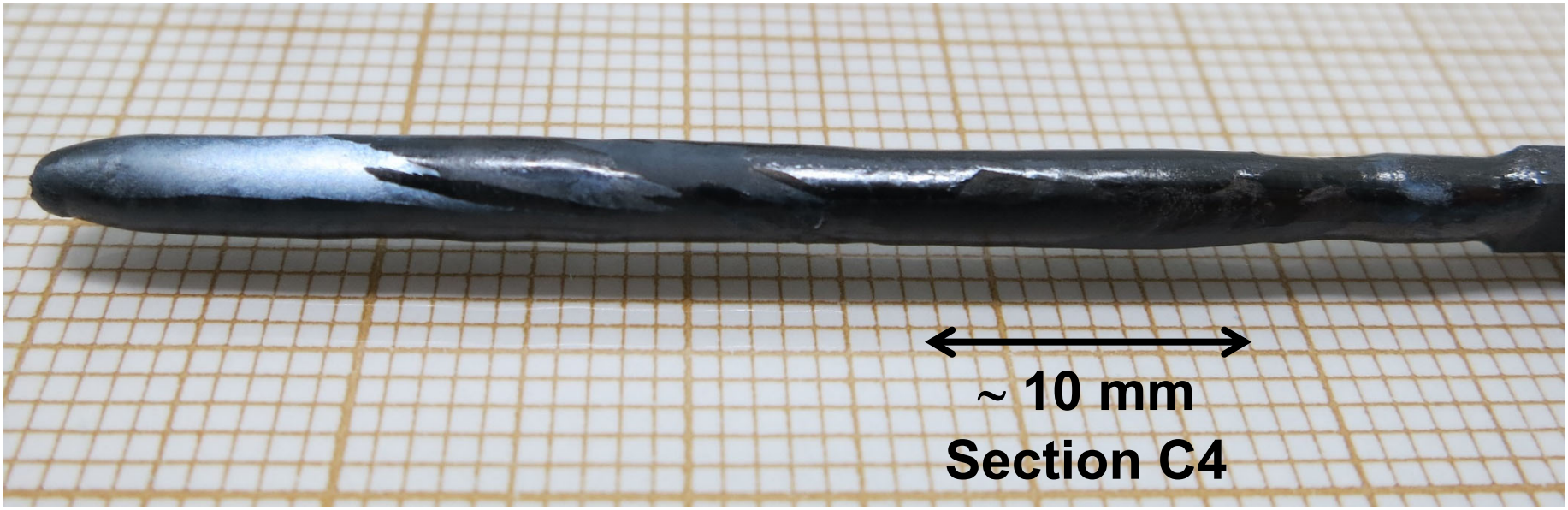

47 mm long as-grown crystalline material

As-grown crystalline material $Sr_{17}CaBaNb_{19}WO_{69.5 - y}$

Sample No. 828

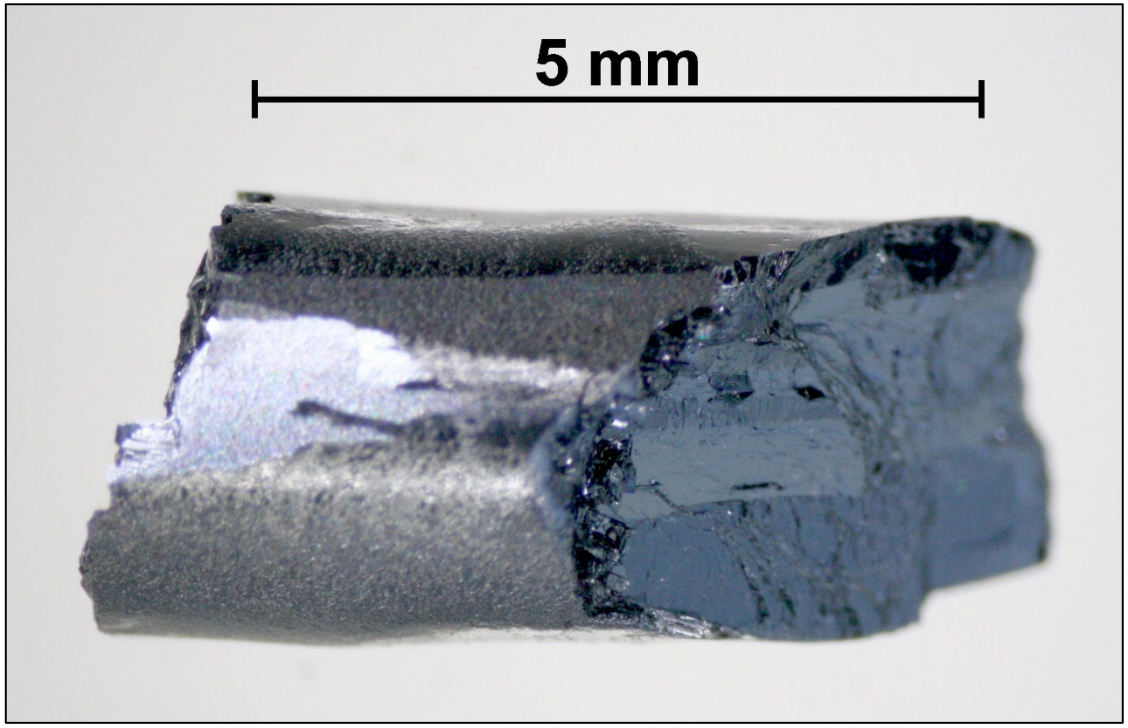

Crystalline piece from section C4 of the as-grown material

828 C4 $Sr_{17}CaBaNb_{19}WO_x$ Thermogravimetry

Thermogravimetric oxidation in flowing synth. air up to the fully oxidized composition with $x = x_F = 69.5$ for the determination of the oxygen content $x = 69.5 - y$ by using a thermogravimetric analyzer NETZSCH TG 209 F1 Libra

Pulverized crystalline material from section C4 of the as-grown sample $\rightarrow$ $x = 65.45$

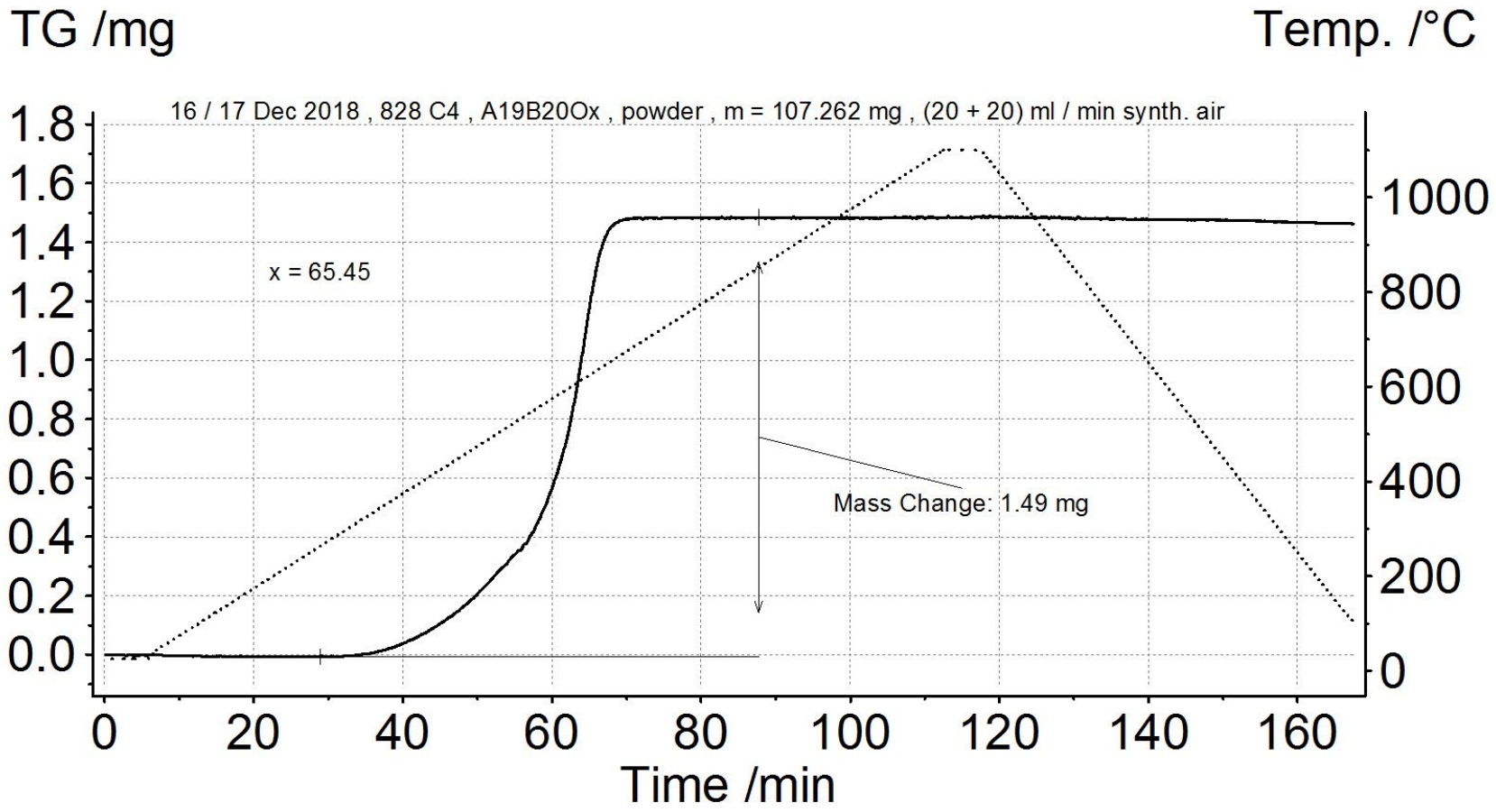

$Sr_{17}CaBaNb_{19}WO_{65.45}$ Valences of the Nb and W ions

Valence or oxidation states of the
Nb and W ions in $Sr_{17}CaBaNb_{19}WO_{65.45}$

The most likely scenario is W^{4+} / $5d^{2}$

↓

Charge neutrality and Sr^{2+}, Ca^{2+}, Ba^{2+}, and O^{2-} → $Nb^{4.679+}$ / $4d^{0.321}$

↓

2 (5d) + 19 × 0.321 (4d) = 8.1 d-electrons
per formula and assumed size of the unit cell

828 C4 $Sr_{17}CaBaNb_{19}WO_{65.5}$ Powder x-ray diffraction

Powder x-ray diffraction pattern of pulverized crystalline material from section C4

Square root - linear plot • Background subtracted

All observed peaks fit to an orthorhombic *n* = 5 type structure

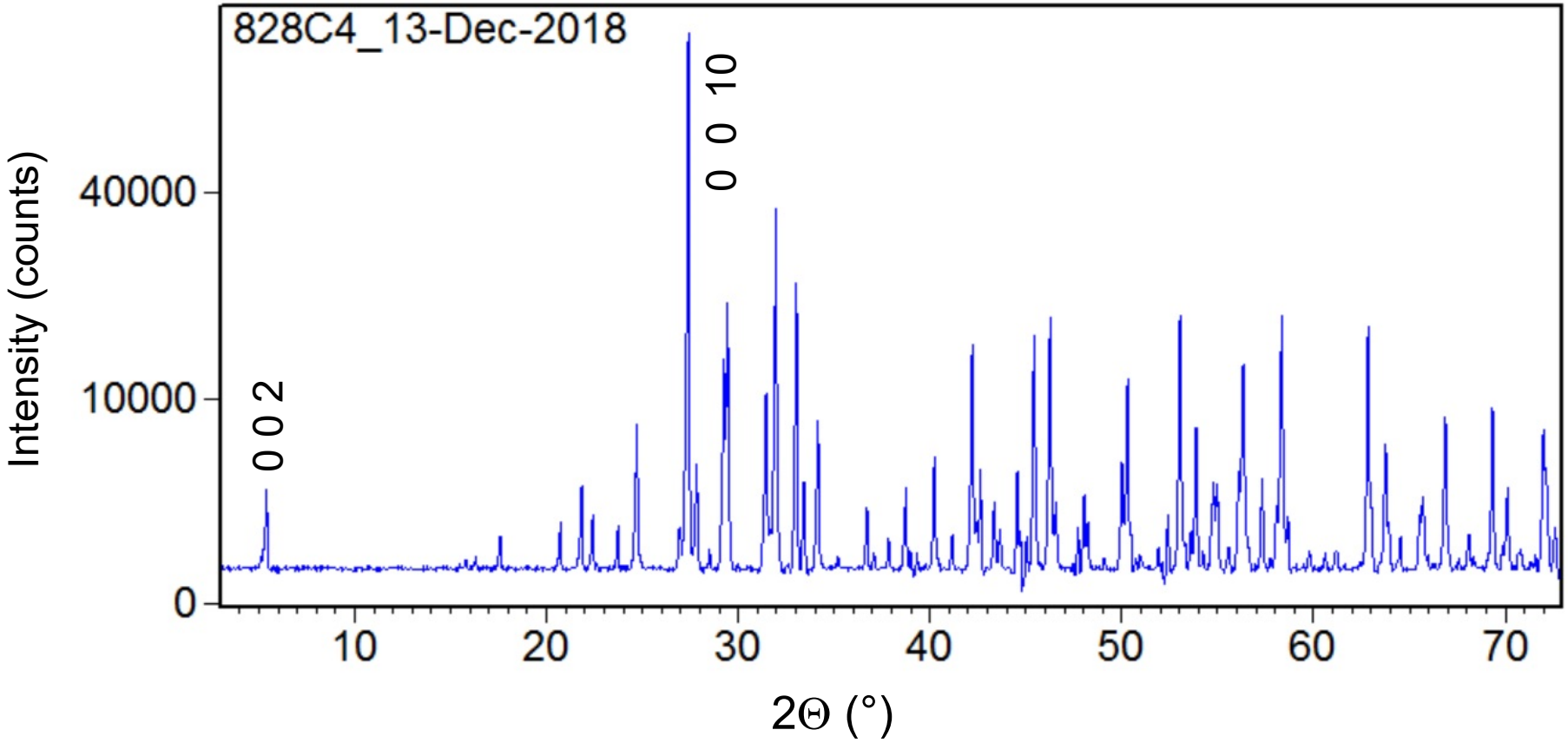

828 C4 $Sr_{17}CaBaNb_{19}WO_{65.5}$ Powder x-ray diffraction

	Observed peak position (°2θ)	d-spacing (Å)	Relative intensity (%)	h k l from lattice parameter refinement
Lowest angle peak Its position indicates the structure type of $A_nB_nO_{3n+2}$, namely n = 5 in this case	5.41	16.34	4	0 0 2
Highest intensity peak	27.39	3.25	100	0 0 10

828 C4 $Sr_{17}CaBaNb_{19}WO_{65.5}$ Powder x-ray diffraction

Results of lattice parameter refinement with $(h\ k\ l)_{max}$ = (10 10 20)

Number of observed peaks	95
Number of indexed peaks	95
Number of unindexed peaks	0
Crystal structure type	n = 5 of $A_nB_nO_{3n+2}$
Crystal system	Orthorhombic
Bravais lattice	P
a (Å)	7.98
b (Å)	5.68
c (Å)	32.51
V (Å^3)	1474
$\lvert 2\theta_{obs} - 2\theta_{calc} \rvert$ for all observed and calculated peaks	$\leq 0.033°$
Figure of merit of the refinement or fit	17.3
Chi square of the refinement or fit	1.8×10^{-6}

828 C4 $Sr_{17}CaBaNb_{19}WO_{65.5}$ Magnetic measurements

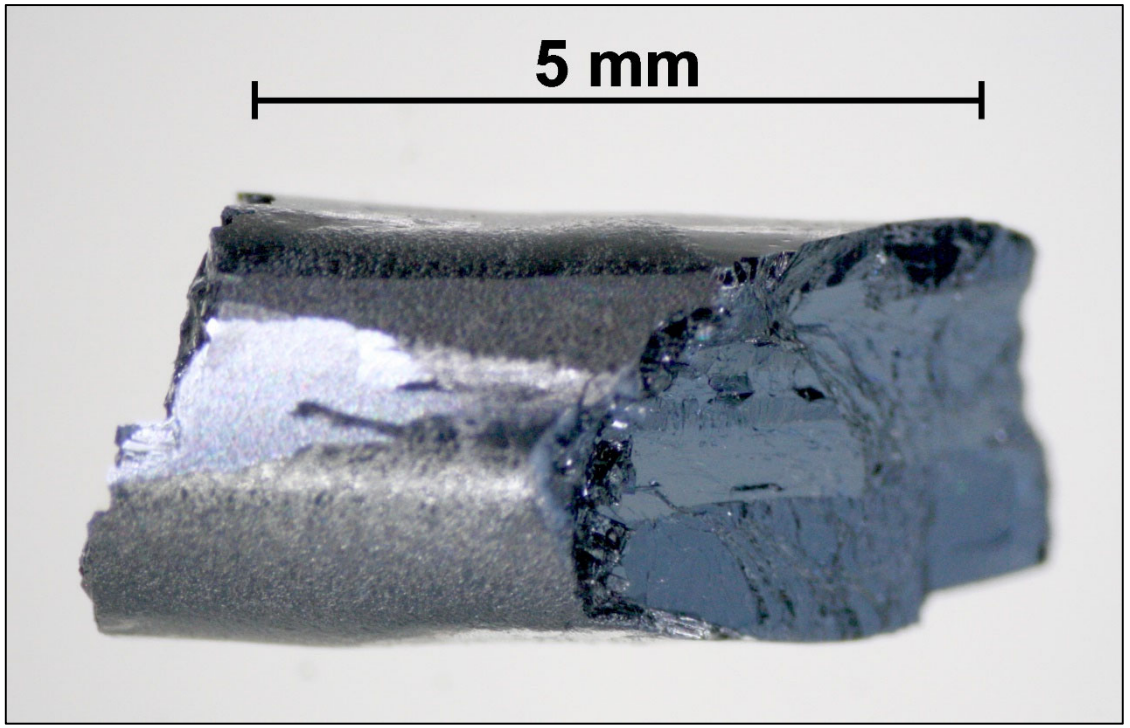

Crystalline piece C4-1 with m = 168 mg
from section C4 of the as-grown material

This piece was used to study its magnetic
properties by a SQUID magnetometer

828 C4 $Sr_{17}CaBaNb_{19}WO_{65.5}$ Magnetic susceptibility $\chi(T)$

DC magnetic moment M(T) measured by a Quantum Design SQUID magnetometer MPMS3

8.1 d-electrons from Nb^{4+} / $4d^1$ and W^{4+} / $5d^2$

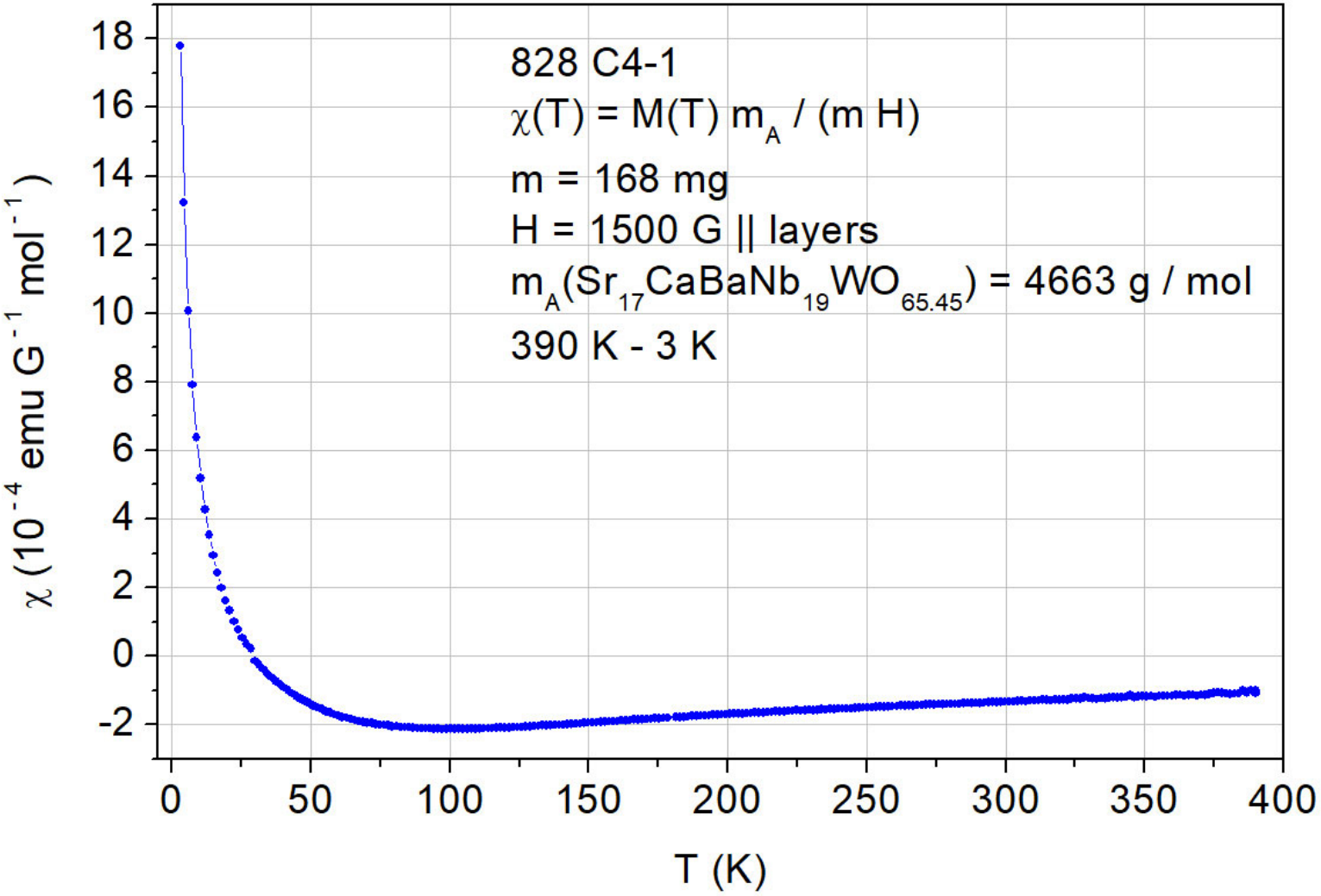

828 C4 $Sr_{17}CaBaNb_{19}WO_{65.5}$ Magnetic susceptibility $\chi(T)$

DC magnetic moment M(T) measured by a Quantum Design SQUID magnetometer MPMS3

8.1 d-electrons from Nb^{4+} / $4d^1$ and W^{4+} / $5d^2$

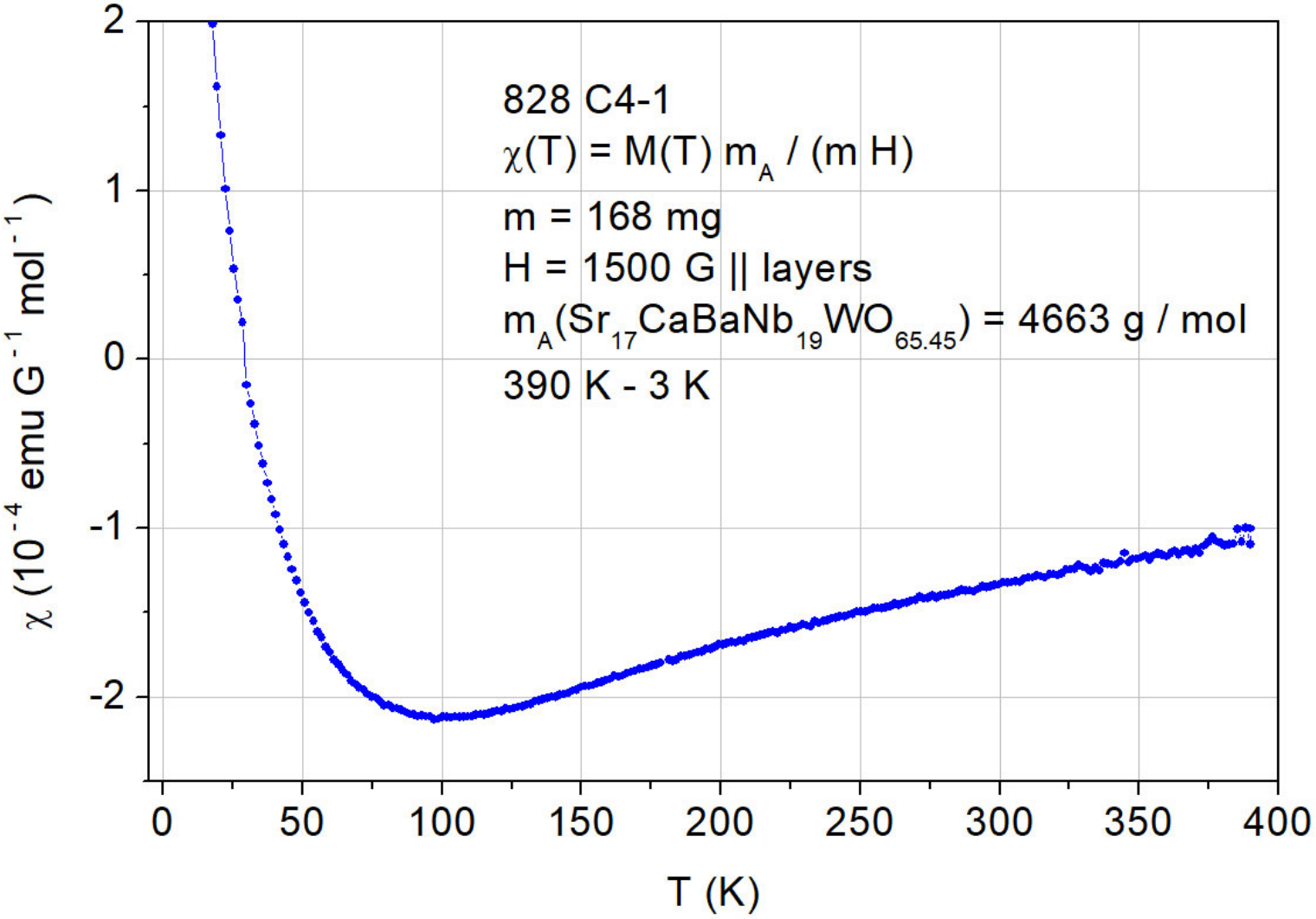

The behavior of $\chi(T)$ in the range from 390 K to 105 K is similar to that of $A_nB_nO_{3n+2}$ type quasi-1D metals. Thus this n = 5 type material is potentially also a quasi-1D metal

828 C4 $Sr_{17}CaBaNb_{19}WO_{65.5}$ Magnetic susceptibility $\chi(T)$

DC magnetic moment M(T) measured by a Quantum Design SQUID magnetometer MPMS3

8.1 d-electrons from Nb^{4+} / $4d^1$ and W^{4+} / $5d^2$

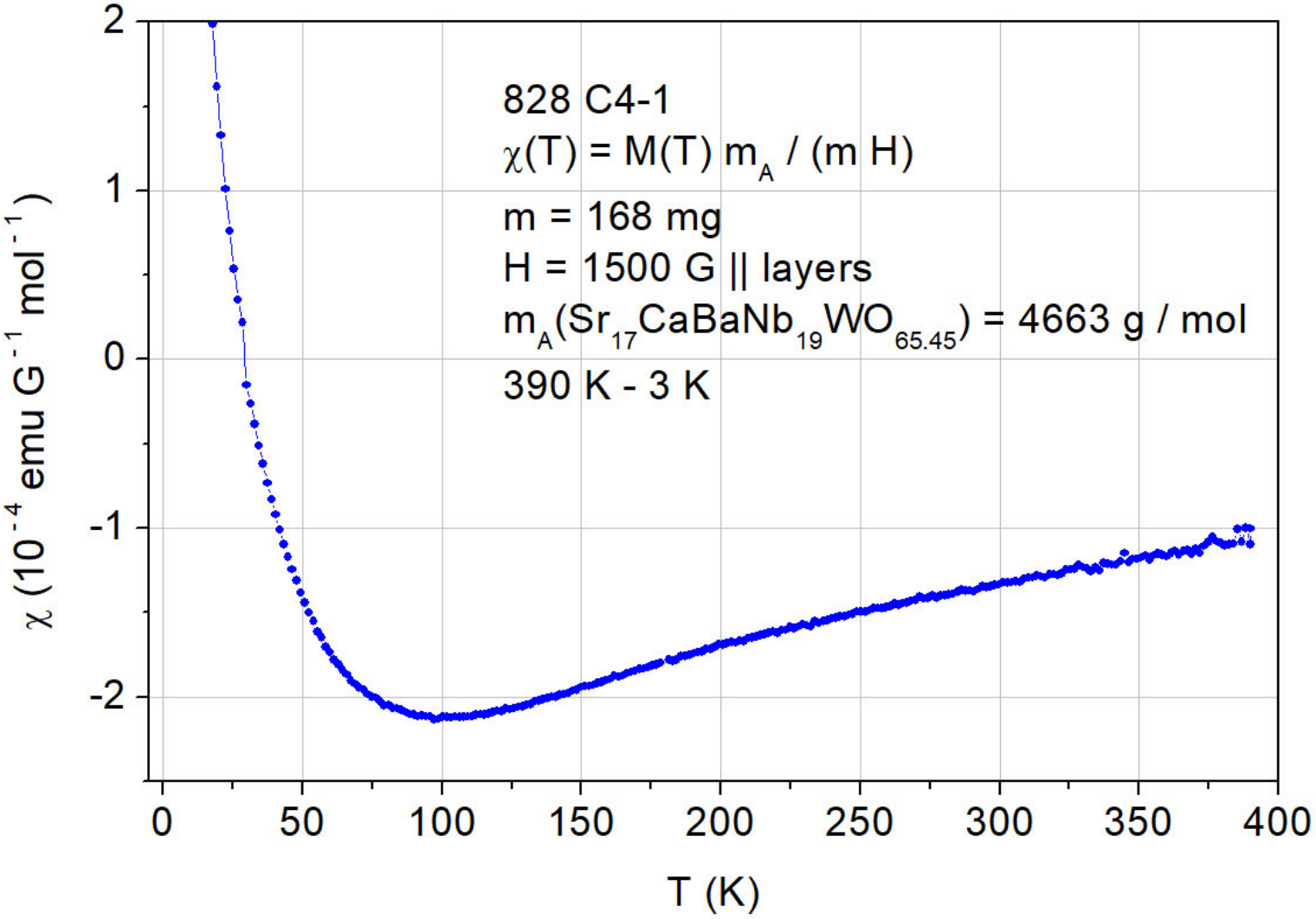

Increase of $\chi(T)$ below 95 K probably not due to paramagnetic impurities or defect states because they give usually a signal only at lower temperatures. Increase below 95 K due to 5d electrons which become localized ?

828 C4 $Sr_{17}CaBaNb_{19}WO_{65.5}$ Magnetic susceptibility $\chi(T)$

DC magnetic moment M(T) measured by a Quantum Design SQUID magnetometer MPMS3

8.1 d-electrons from Nb^{4+} / $4d^1$ and W^{4+} / $5d^2$

D = diamagnetic contribution from closed electron shells of Sr^{2+}, Ca^{2+}, Ba^{2+}, Nb^{5+}, W^{6+}, and O^{2-}

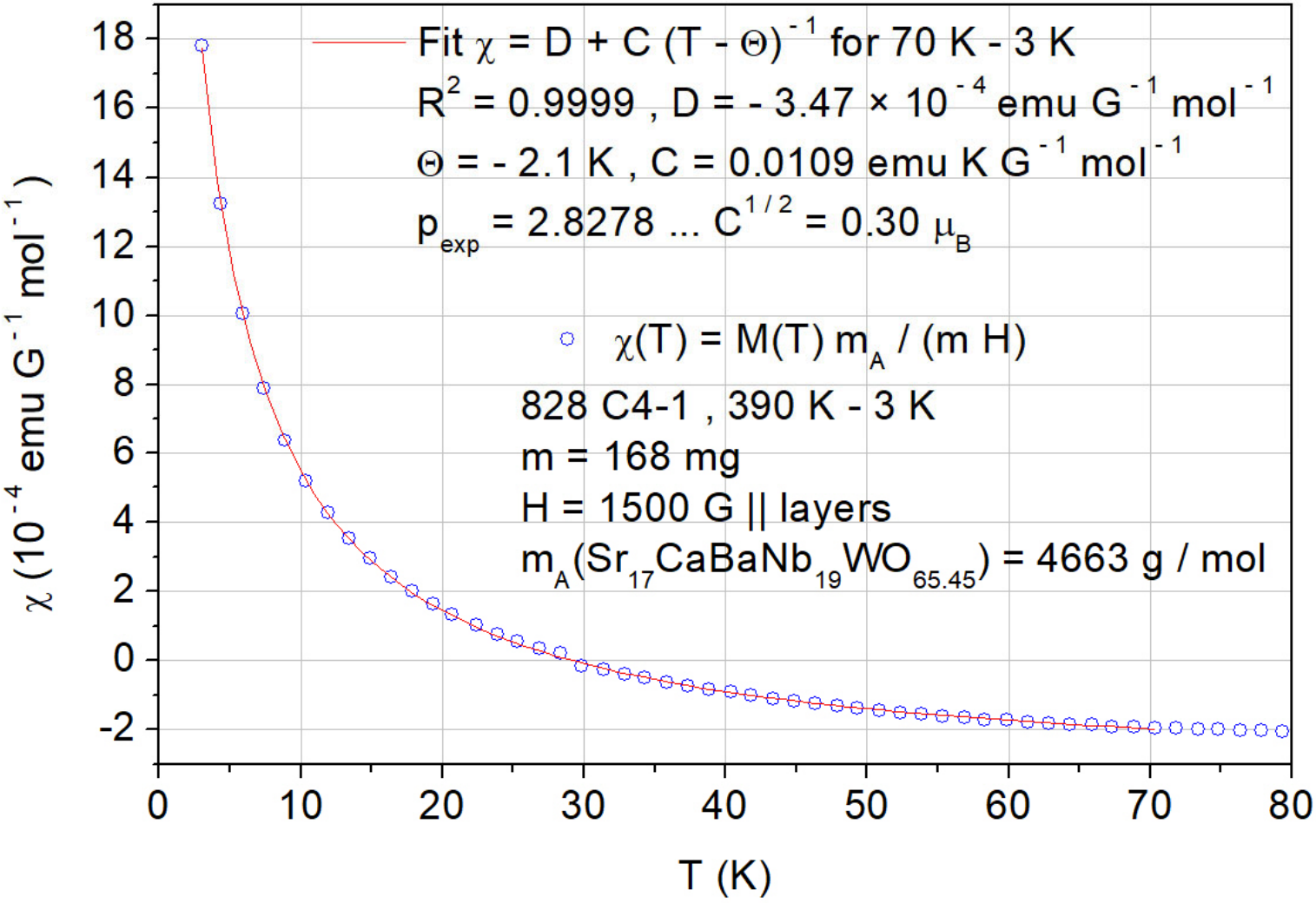

Ref. for the calculation of p_{exp}: Progress in Solid State Chemistry 36 (2008) 253

6 Conducting and metallic Carpy-Galy phases $A_nB_nO_{3n+2} = ABO_x$

6.9.4 Towards a Schückel-Müller-Buschbaum type phase: Synthesis and properties of $Sr_{17}CaBaNb_{19}WO_{65.3}$ ...

Melt-grown synthesis of $Sr_{17}CaBaNb_{19}WO_{69.5 - y}$ under a gas pressure of about 9.5 bar

Run No. 836

Intention of this run

In the previous part 6.9.3 the run / sample No. 828 is presented. It describes the melt-grown synthesis of $Sr_{17}CaBaNb_{19}WO_{65.45}$ which was prepared by reducing the fully oxidized composition $Sr_{17}CaBaNb_{19}WO_{69.5}$ under flowing 97.2 % Ar + 2.8 % H_2 with an ambient or normal gas pressure.

The intention of this run No. 836 was to repeat run No. 828 with only one difference, namely using instead of a normal gas pressure a high gas pressure of about 9.5 bar. The enhanced gas pressure results in a higher melting point which implies usually a higher degree of the reduction. This was indeed confirmed by the thermogravimetrically determined oxygen content $x = 69.5 - y$. However, the increased degree of reduction was smaller than anticipated so that a desired oxygen content of $x \approx 64$ could not be obtained in this way.

As-pressed rod with composition $Sr_{17}CaBaNb_{19}WO_{69.5}$ Run No. 836

As-pressed feed rod in an alumina box. Ready for sintering under air. The as-pressed rod is located on a lower punch which is made of yttria-stabilized zirconia. The length of the rod is 9 cm

As-pressed feed rod with fully oxidized composition $Sr_{17}CaBaNb_{19}WO_{69.5}$, i.e. all Nb and W ions are in their highest valence or oxidation state Nb^{5+} and W^{6+}, respectively. A second rod, the seed rod, was not prepared because the remaining seed rod from run No. 828 was used in this run

Sintered rod with composition $Sr_{17}CaBaNb_{19}WO_{69.5}$ Run No. 836

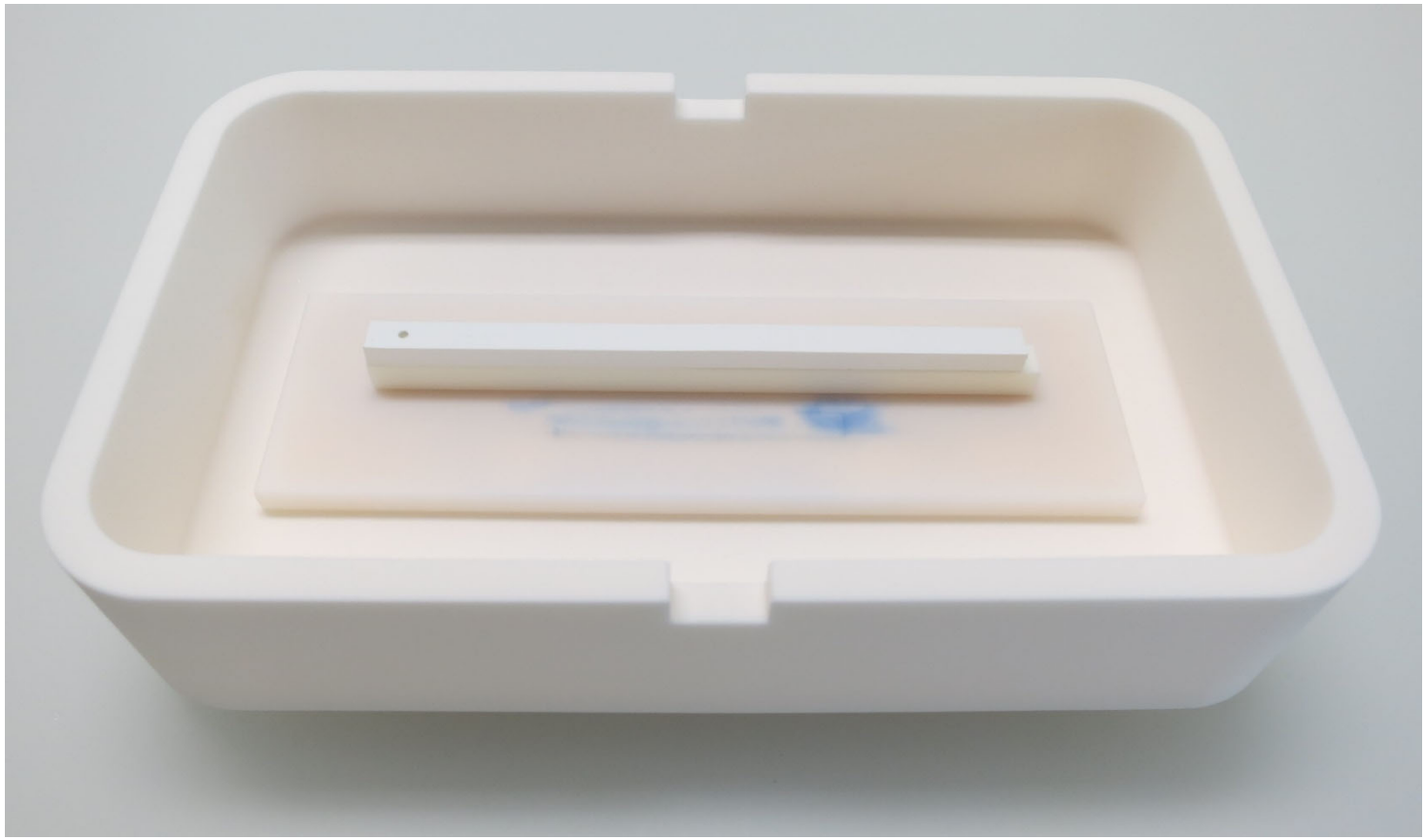

The as-pressed feed rod was 4 h sintered at 1230 °C under air. The sintering did result in a shrinkage of its length, namely $\Delta L \approx -3$ mm

A somewhat lower sintering temperature would have been better because the sintered rod was attached on its lower punch. Fortunately it was possible to remove the rod from its lower punch without damaging the rod. Later related experiments revealed that lower punches made of alumina are more suitable

Sintered rod with composition $Sr_{17}CaBaNb_{19}WO_{69.5}$ Run No. 836

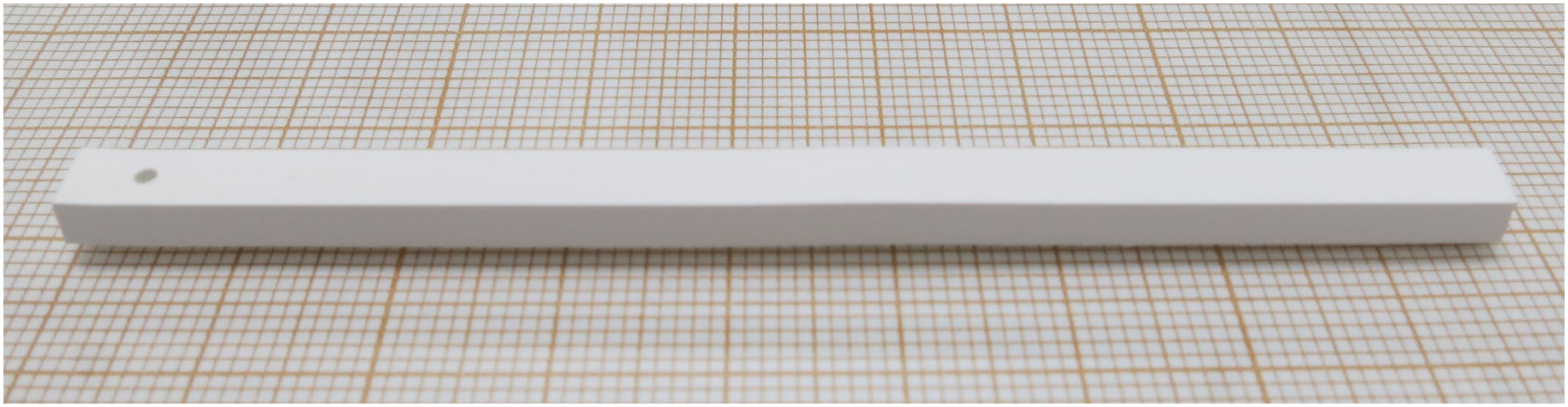

A second rod, the seed rod, was not prepared because the remaining seed rod from run No. 828 was used in this run

Melt-grown synthesis of $Sr_{17}CaBaNb_{19}WO_{69.5-y}$ under a gas pressure of about 9.5 bar

Starting materials for the mirror furnace run: Polycrystalline sintered rods with fully oxidized composition $Sr_{17}CaBaNb_{19}WO_{69.5}$

Fast mode video from the overall melt-grown synthesis of $Sr_{17}CaBaNb_{19}WO_{69.5-y}$ under ≈ 9.5 bar 97.2 % Ar + 2.8 % H_2 in the Cyberstar mirror furnace. The video is only running in the ppsx type version of this publication, see page 2

Gas flow rate: 400 sccm (24 L / h)
Gas type setting at the mass flow controller: Ar

Lamp power to maintain the molten zone: 2 × (480 - 460) W

Speed of the lower shaft and seed rod (crystal growth speed): 14 mm / h

Melt-grown synthesis of $Sr_{17}CaBaNb_{19}WO_{69.5-y}$ under a gas pressure of about 9.5 bar

Starting materials for the mirror furnace run: Polycrystalline sintered rods with fully oxidized composition $Sr_{17}CaBaNb_{19}WO_{69.5}$

Real time video of a short section from the melt-grown synthesis of $Sr_{17}CaBaNb_{19}WO_{69.5-y}$ under ≈ 9.5 bar 97.2 % Ar + 2.8 % H_2 in the Cyberstar mirror furnace. The video is only running in the ppsx type version of this publication, see page 2

Gas flow rate: 400 sccm (24 L / h)
Gas type setting at the mass flow controller: Ar

Lamp power to maintain the molten zone: 2 × (480 - 460) W

Speed of the lower shaft and seed rod (crystal growth speed): 14 mm / h

As-grown crystalline $Sr_{17}CaBaNb_{19}WO_{69.5-y}$ and polycrystalline rods

Run / Sample No. 836

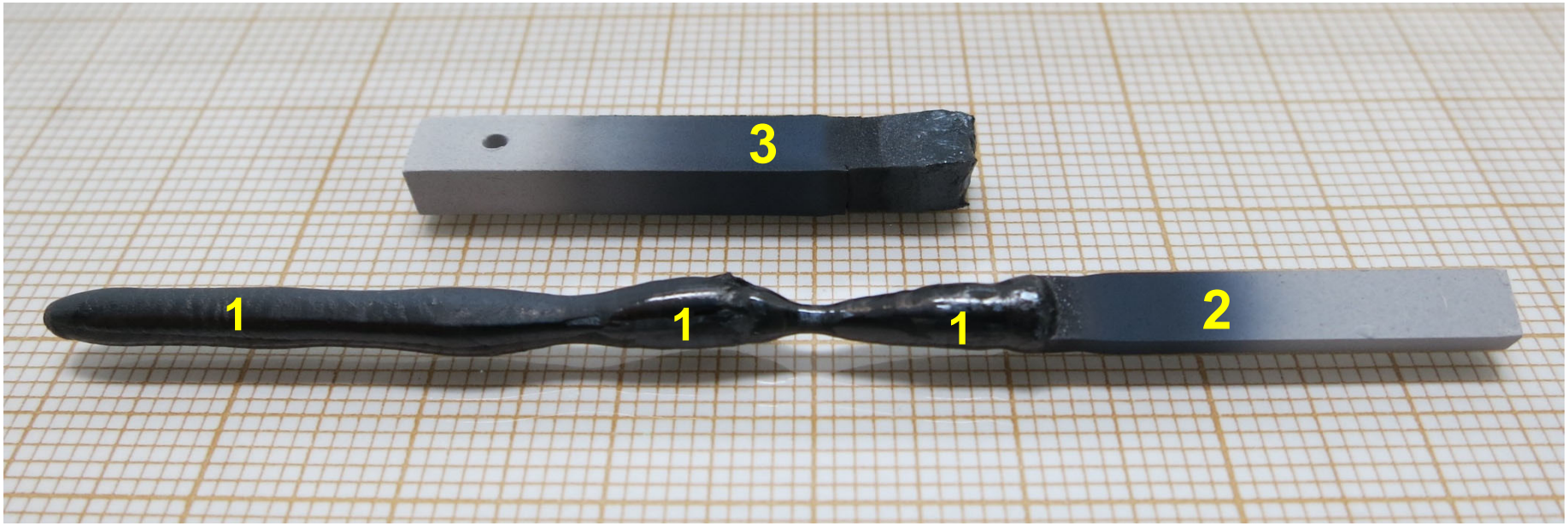

5 cm long as-grown crystalline material (1) plus polycrystalline seed rod (2) and remaining part of the polycrystalline feed rod (3)

Prepared at the ETH Zurich in 2019

As-grown crystalline material $Sr_{17}CaBaNb_{19}WO_{69.5 - y}$

Sample No. 836

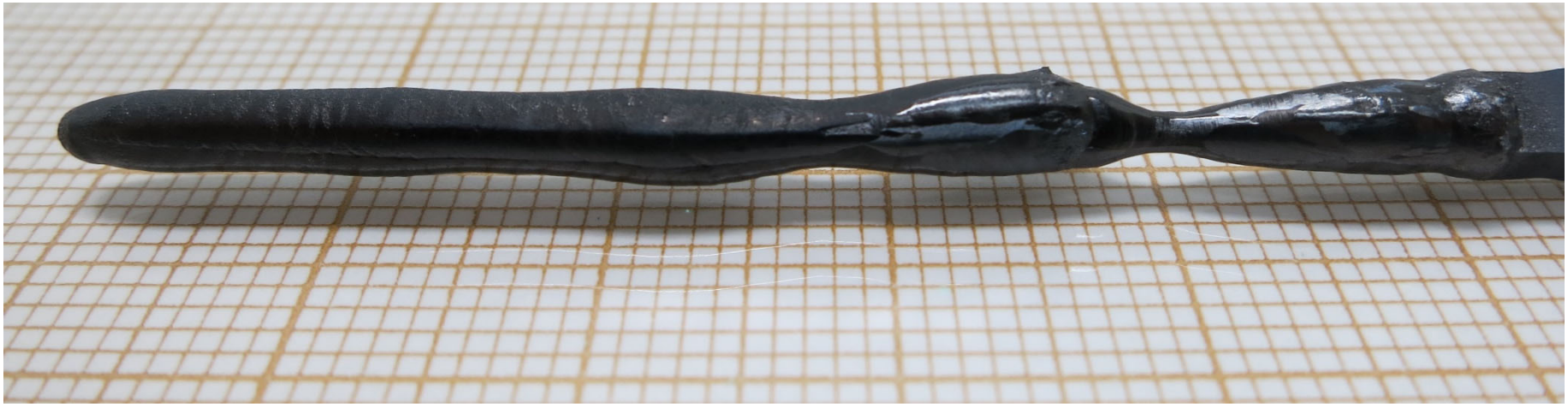

5 cm long as-grown crystalline material

As-grown crystalline material $Sr_{17}CaBaNb_{19}WO_{69.5 - y}$

Sample No. 836

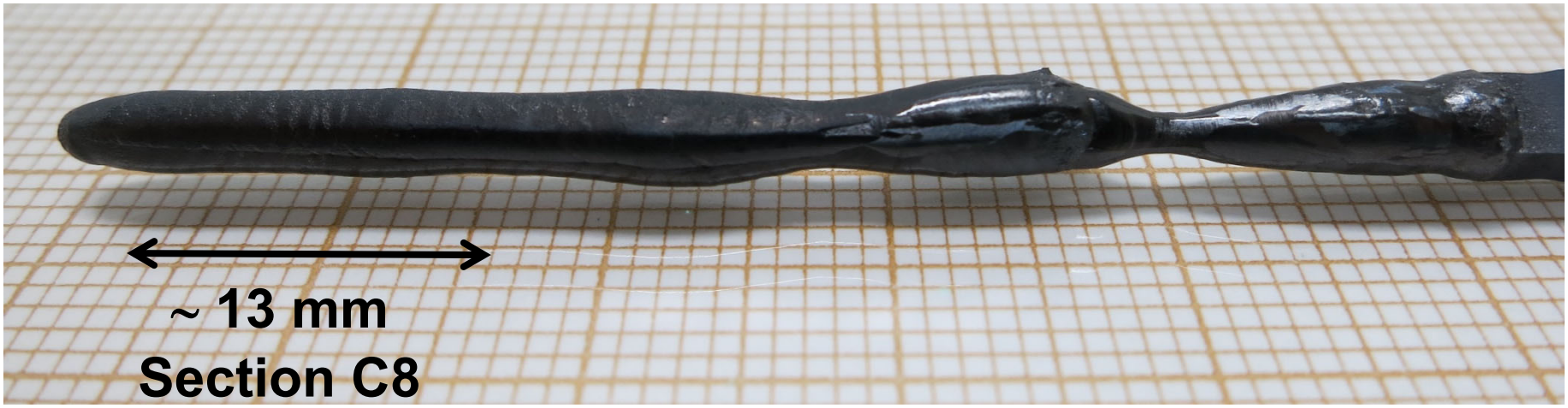

5 cm long as-grown crystalline material

As-grown crystalline material $Sr_{17}CaBaNb_{19}WO_{69.5 - y}$

Sample No. 836

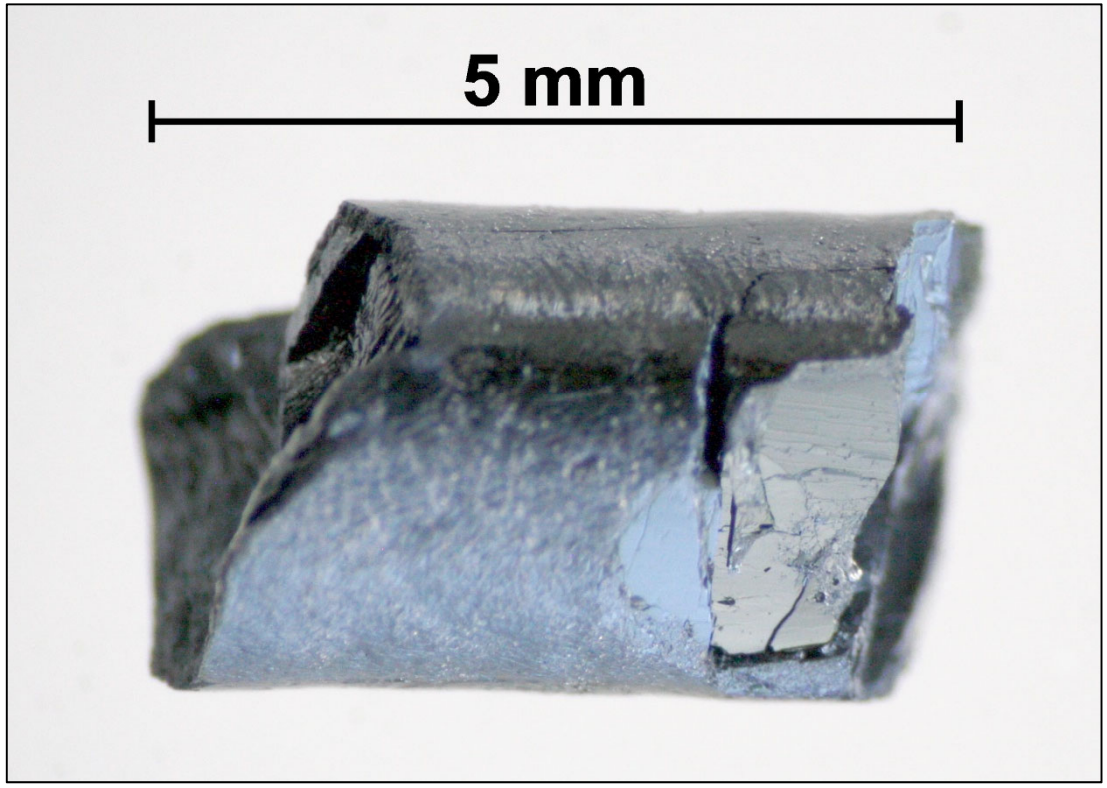

Crystalline piece from section C8 of the as-grown material

836 C8 $Sr_{17}CaBaNb_{19}WO_x$ Thermogravimetry

Thermogravimetric oxidation in flowing synth. air up to the fully oxidized composition with $x = x_F = 69.5$ for the determination of the oxygen content $x = 69.5 - y$ by using a thermogravimetric analyzer NETZSCH TG 209 F1 Libra

Pulverized crystalline material from section C8 of the as-grown sample $\rightarrow$ $x = 65.27$

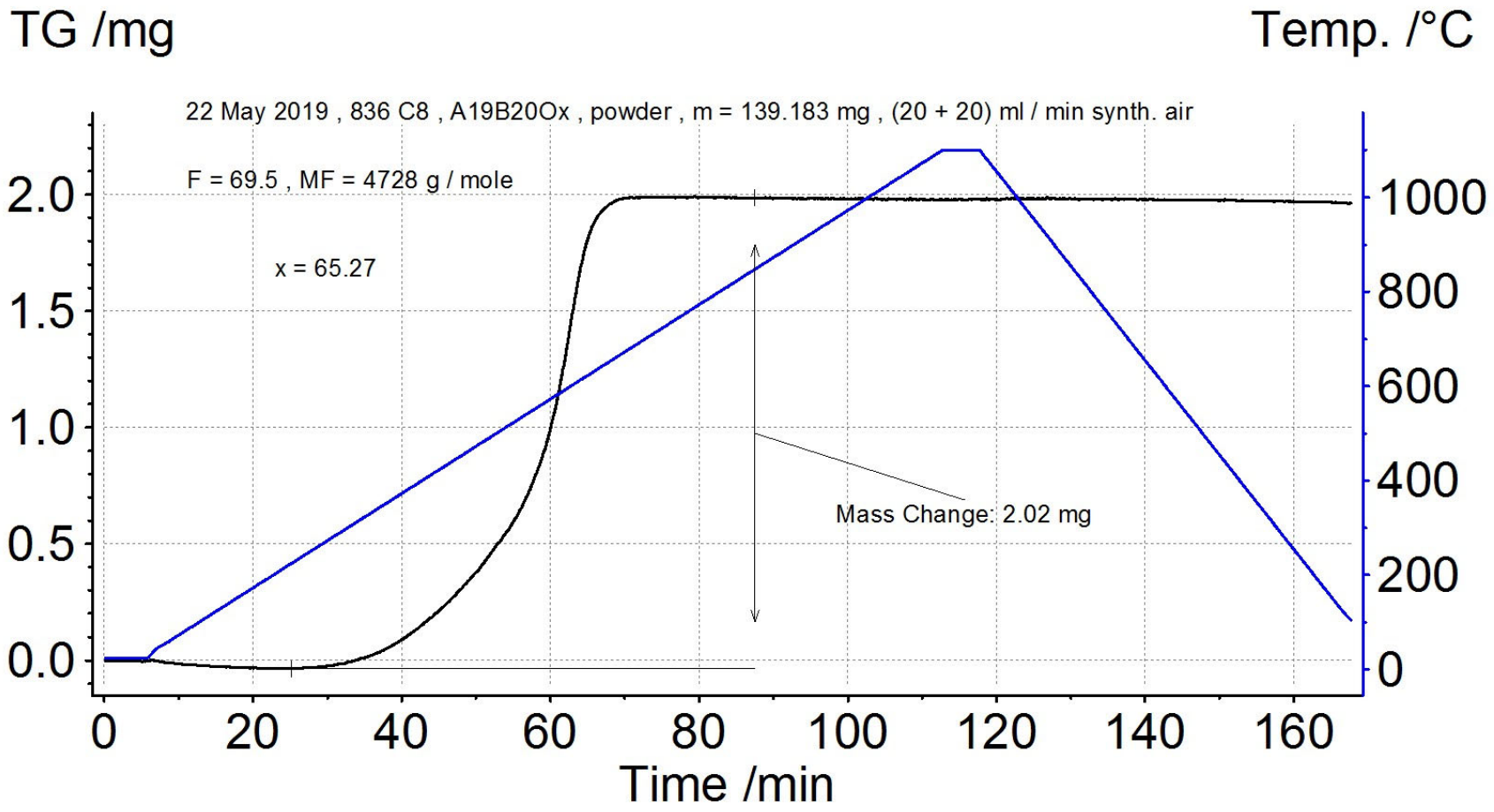

836 C8 $Sr_{17}CaBaNb_{19}WO_{65.27}$ Valences of the Nb and W ions

Valence or oxidation states of the
Nb and W ions in $Sr_{17}CaBaNb_{19}WO_{65.45}$

The most likely scenario is W^{4+} / $5d^2$

↓

Charge neutrality and Sr^{2+}, Ca^{2+}, Ba^{2+}, and O^{2-} → $Nb^{4.66+}$ / $4d^{0.34}$

↓

2 (5d) + 19 × 0.34 (4d) = 8.46 d-electrons
per formula and assumed size of the unit cell

836 C8 $Sr_{17}CaBaNb_{19}WO_{65.3}$ Powder x-ray diffraction

Powder x-ray diffraction pattern of pulverized crystalline material from section C8

Square root - linear plot • Background subtracted

All observed peaks fit to an orthorhombic *n* = 5 type structure

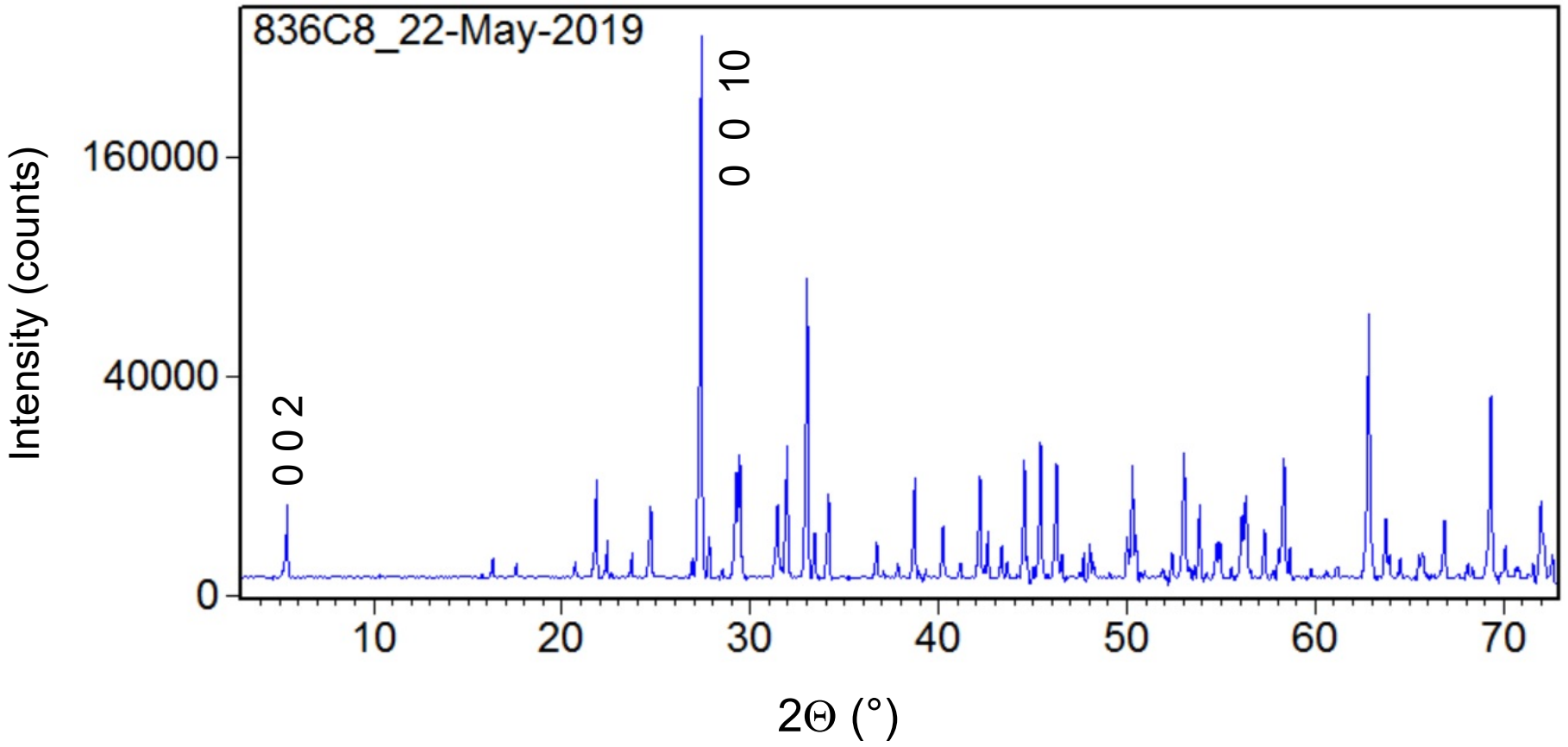

836 C8 $Sr_{17}CaBaNb_{19}WO_{65.3}$ Powder x-ray diffraction

	Observed peak position (°2θ)	d-spacing (Å)	Relative intensity (%)	h k l from lattice parameter refinement
Lowest angle peak Its position indicates the structure type of $A_nB_nO_{3n+2}$, namely n = 5 in this case	5.41	16.34	3	0 0 2
Highest intensity peak	27.39	3.25	100	0 0 10

836 C8 $Sr_{17}CaBaNb_{19}WO_{65.3}$ Powder x-ray diffraction

Results of lattice parameter refinement with $(h\ k\ l)_{max}$ = (10 10 20)

Number of observed peaks	98
Number of indexed peaks	98
Number of unindexed peaks	0
Crystal structure type	n = 5 of $A_nB_nO_{3n+2}$
Crystal system	Orthorhombic
Bravais lattice	P
a (Å)	7.98
b (Å)	5.68
c (Å)	32.51
V (Å^3)	1474
$\lvert 2\theta_{obs} - 2\theta_{calc} \rvert$ for all observed and calculated peaks	$\leq 0.043°$
Figure of merit of the refinement or fit	17.8
Chi square of the refinement or fit	2.2×10^{-6}

836 C8 $Sr_{17}CaBaNb_{19}WO_{65.3}$ Magnetic measurements

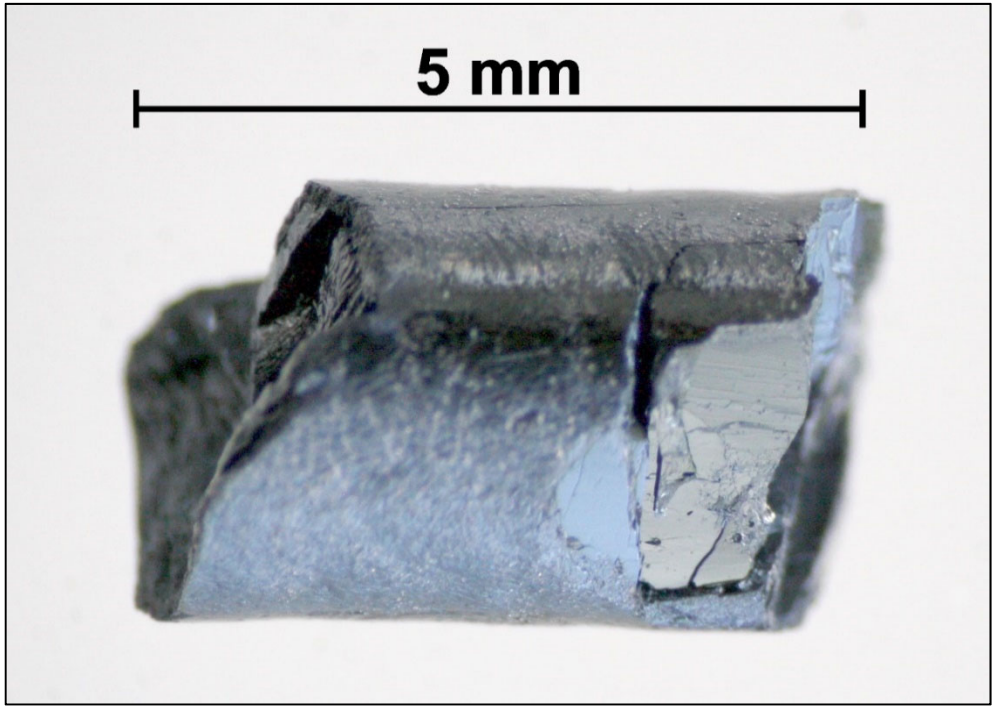

Crystalline piece C8-1 with m = 134 mg from section C8 of the as-grown material

This piece was used to study its magnetic properties by a SQUID magnetometer

836 C8 $Sr_{17}CaBaNb_{19}WO_{65.3}$ Magnetic susceptibility $\chi(T)$

DC magnetic moment M(T) measured by a Quantum Design SQUID magnetometer MPMS3

8.5 d-electrons from Nb^{4+} / $4d^1$ and W^{4+} / $5d^2$

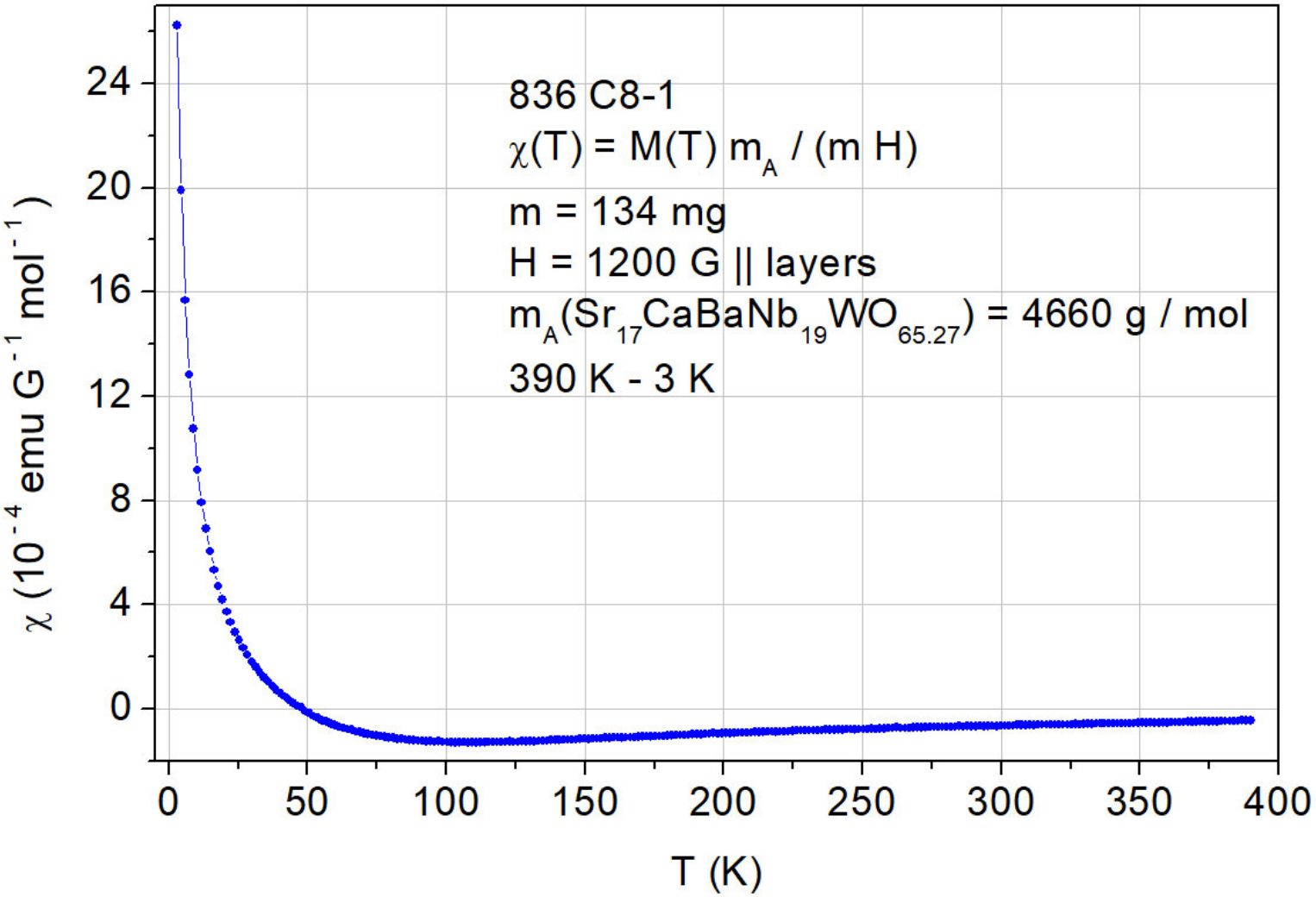

836 C8 $Sr_{17}CaBaNb_{19}WO_{65.3}$ Magnetic susceptibility $\chi(T)$

DC magnetic moment M(T) measured by a Quantum Design SQUID magnetometer MPMS3

8.5 d-electrons from Nb^{4+} / $4d^1$ and W^{4+} / $5d^2$

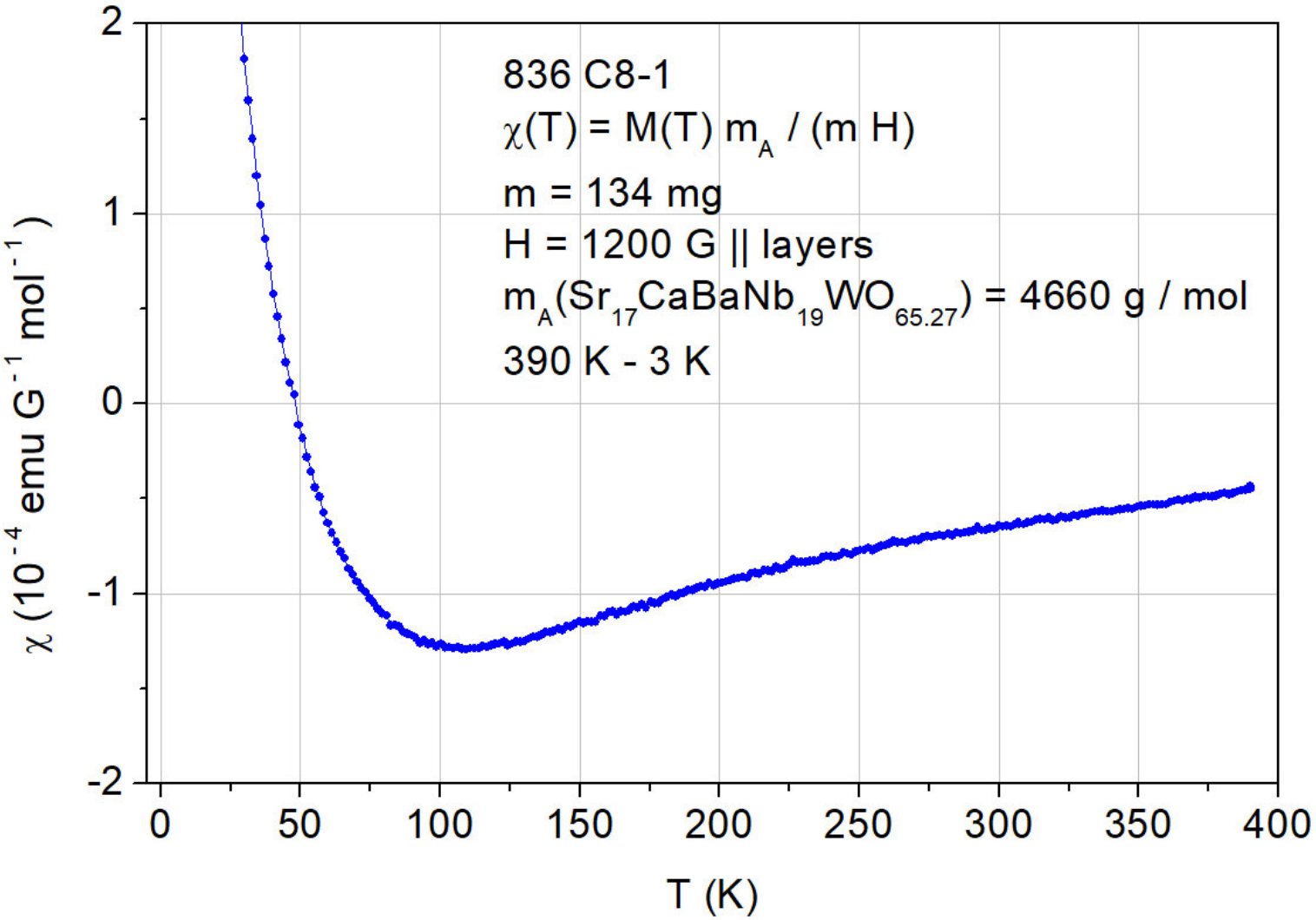

The behavior of $\chi(T)$ in the range from 390 K to about 110 K is similar to that of $A_nB_nO_{3n+2}$ type quasi-1D metals. Thus this n = 5 type material is potentially also a quasi-1D metal

836 C8 $Sr_{17}CaBaNb_{19}WO_{65.3}$ Magnetic susceptibility $\chi(T)$

DC magnetic moment M(T) measured by a Quantum Design SQUID magnetometer MPMS3

8.5 d-electrons from Nb^{4+} / $4d^1$ and W^{4+} / $5d^2$

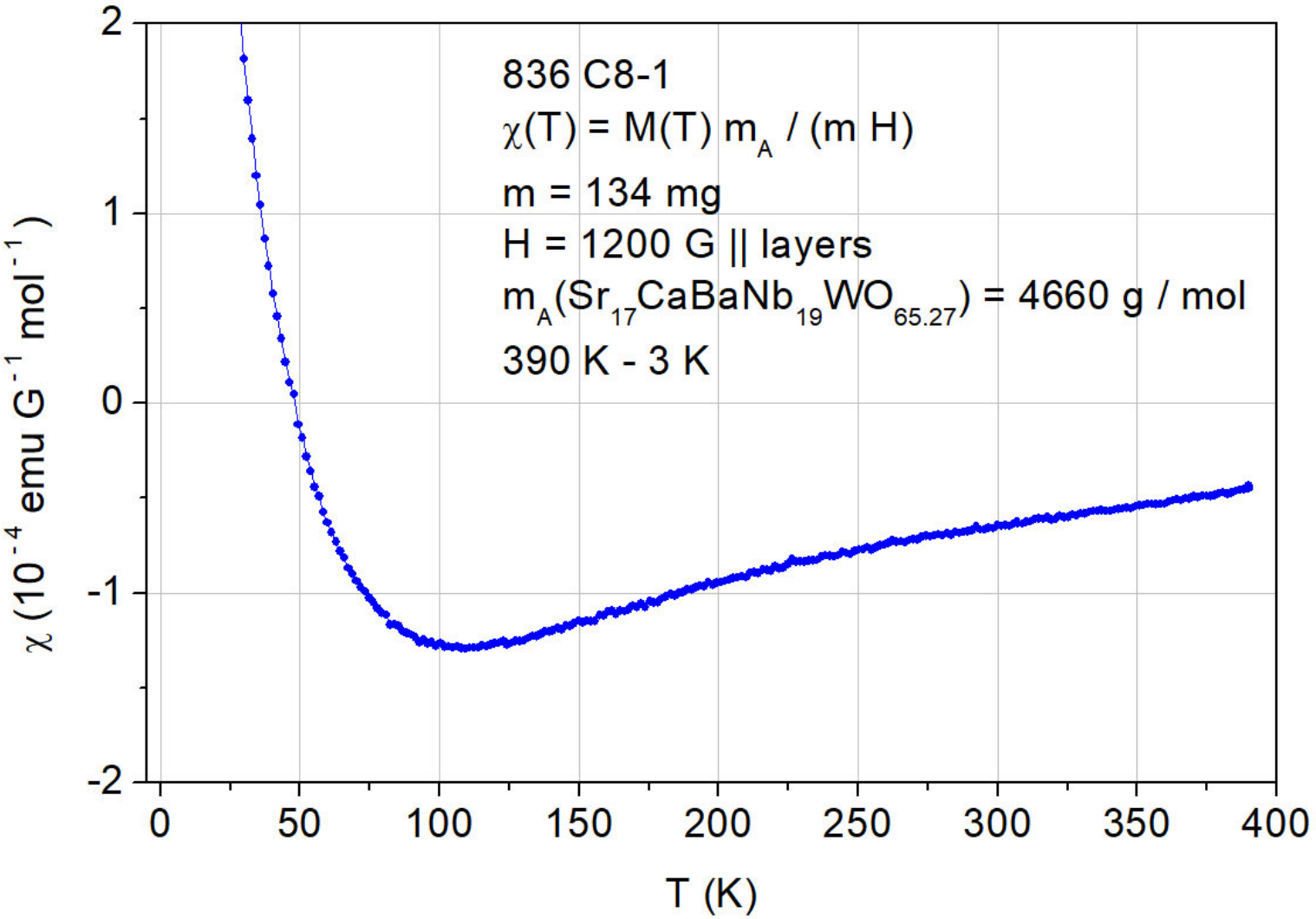

Increase of $\chi(T)$ below 110 K probably not due to paramagnetic impurities or defect states because they give usually a signal only at lower temperatures. Increase below 110 K due to 5d electrons which become localized ?

836 C9 $Sr_{17}CaBaNb_{19}WO_{65.3}$ Magnetic susceptibility $\chi(T)$

DC magnetic moment M(T) measured by a Quantum Design SQUID magnetometer MPMS3

8.5 d-electrons from Nb^{4+} / $4d^1$ and W^{4+} / $5d^2$

D = diamagnetic contribution from closed electron shells of Sr^{2+}, Ca^{2+}, Ba^{2+}, Nb^{5+}, W^{6+}, and O^{2-}

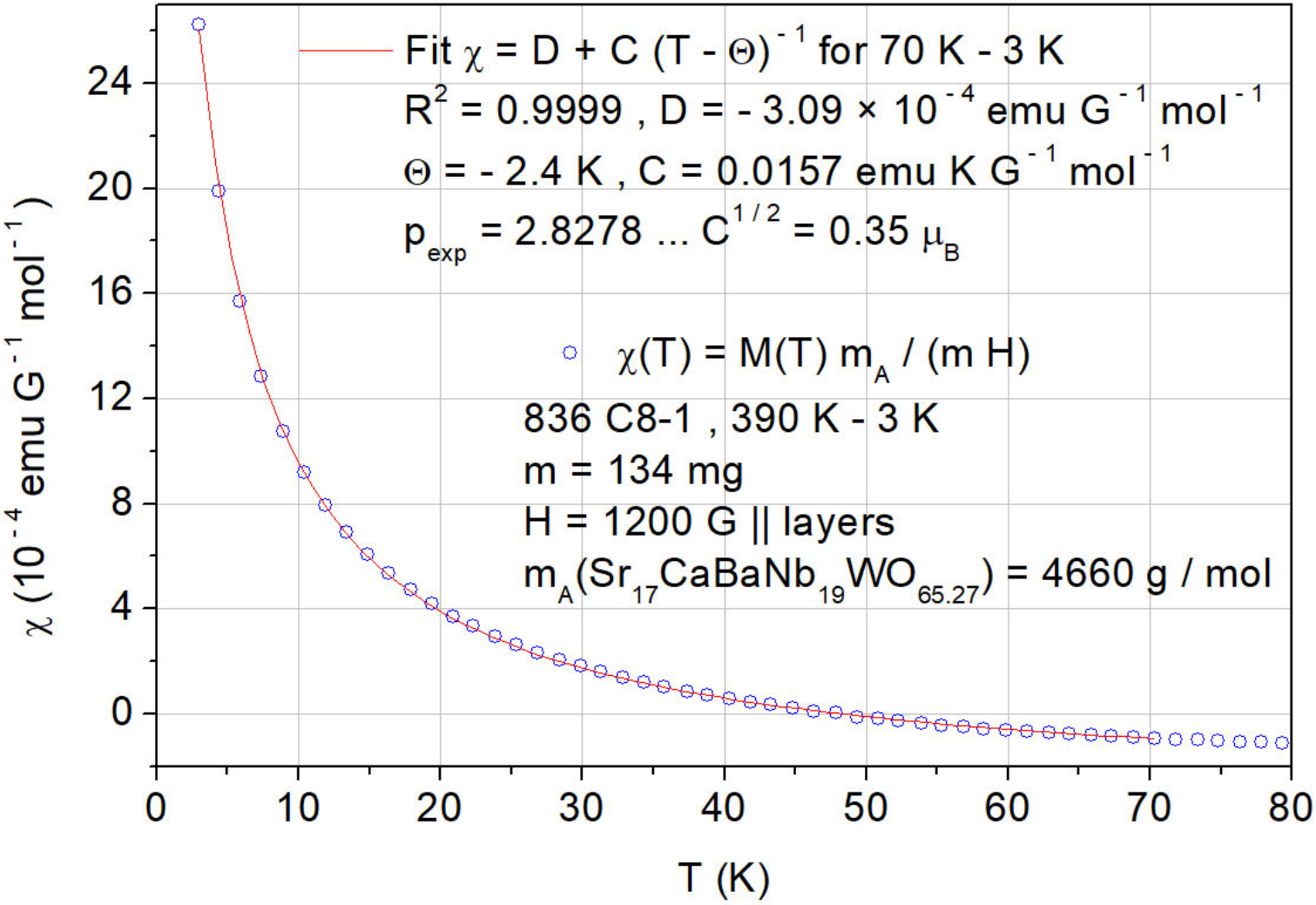

Ref. for the calculation of p_{exp}: Progress in Solid State Chemistry 36 (2008) 253

6 Conducting and metallic Carpy-Galy phases $A_nB_nO_{3n+2} = ABO_x$

6.9.5 A Schückel-Müller-Buschbaum type phase: Synthesis and properties of $Sr_{17}CaBaNb_{19}WO_{64}$ ...

Melt-grown synthesis of $(Sr,Ca,Ba)_{19}Nb_{19}WO_{69.5-y}$ under 95 % Ar + 5 % H_2

Run / sample No. 838 (this part 6.9.5) and 826 (part 6.9.6)

In the previous part 6.9.4 , 6.9.3 , and 6.9.2 the run / sample No. 836 , 828 , and 812 is presented, respectively. It describes the melt-grown synthesis of materials $(Sr,Ca,Ba)_{19}Nb_{19}WO_{69.5-y}$ which were prepared by reducing the fully oxidized composition $(Sr,Ca,Ba)_{19}Nb_{19}WO_{69.5}$ under flowing 97.2 % Ar + 2.8 % H_2

This part 6.9.5 and the following part 6.9.6 present the results of attempts to achieve a higher degree of reduction by using a flowing argon-hydrogen atmosphere with a higher hydrogen content, namely 5 % H_2 instead of 2.8 % H_2 . In this way it was possible to synthesize materials with an oxygen content of $x = 69.5 - y = 64$

Powder with composition $Sr_{17}CaBaNb_{19}WO_{69.5}$ Run No. 838

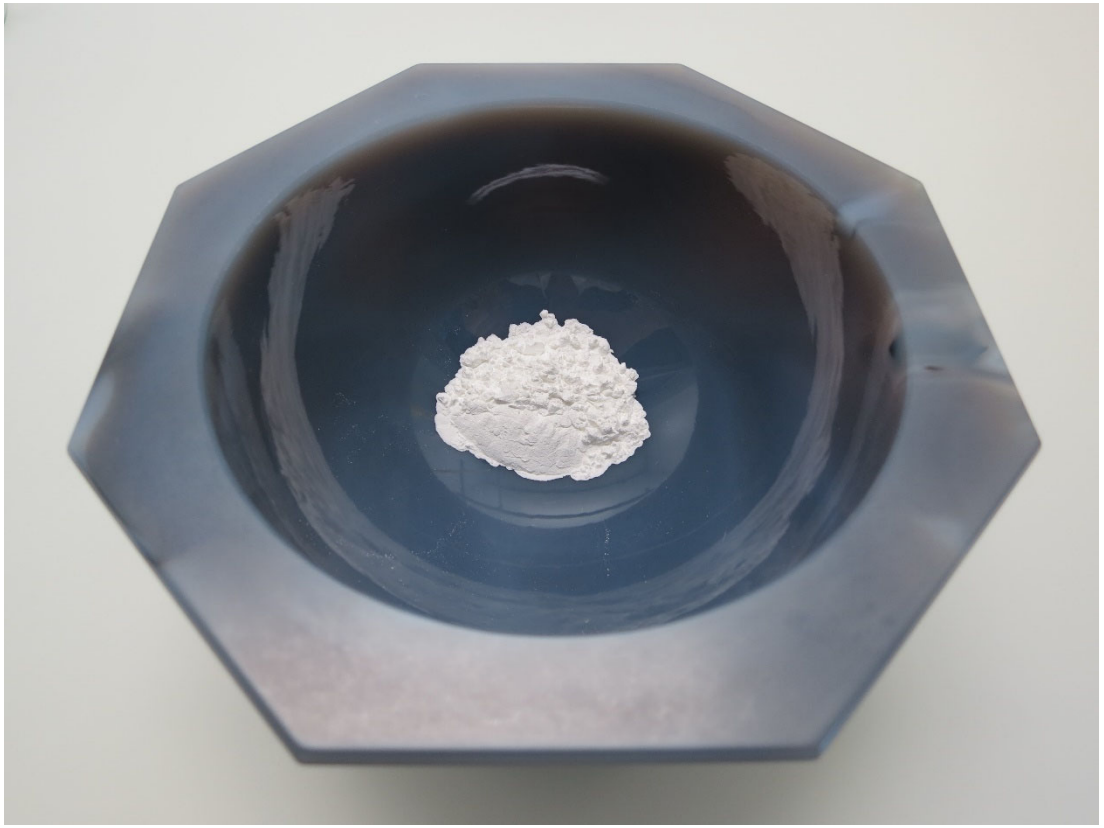

Powder with fully oxidized composition $Sr_{17}CaBaNb_{19}WO_{69.5}$ in an agate mortar. This powder was prepared by heating the mingled starting materials for 4 h at 1190 °C under air. Subsequently the somewhat sintered material was grinded into powder and mingled again. A part of this powder was pressed into two rectangular rods

As-pressed rods with composition $Sr_{17}CaBaNb_{19}WO_{69.5}$

Run No. 838

As-pressed rods with fully oxidized composition $Sr_{17}CaBaNb_{19}WO_{69.5}$, i.e. all Nb and W ions are in their highest valence or oxidation state Nb^{5+} and W^{6+}, respectively

As-pressed rods in an alumina box. Ready for sintering under air. The as-pressed rods are located on a lower punch which is made of alumina. The length of the long rod is 9 cm

Sintered rods with composition $Sr_{17}CaBaNb_{19}WO_{69.5}$ Run No. 838

The as-pressed rods were 4 h sintered at 1225 °C under air.
The sintering did result in a shrinkage of their length, namely
$\Delta L \approx$ - 4 mm for the long rod and $\Delta L \approx$ - 2 mm for the short rod

Sintered rods with composition $Sr_{17}CaBaNb_{19}WO_{69.5}$ Run No. 838

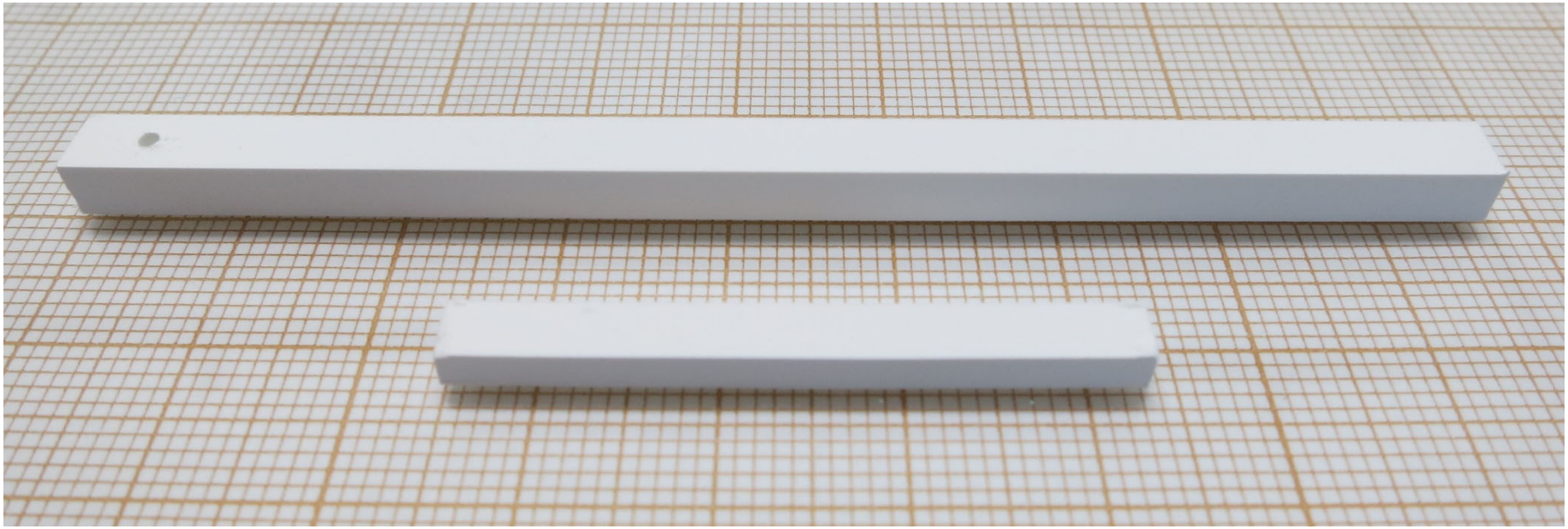

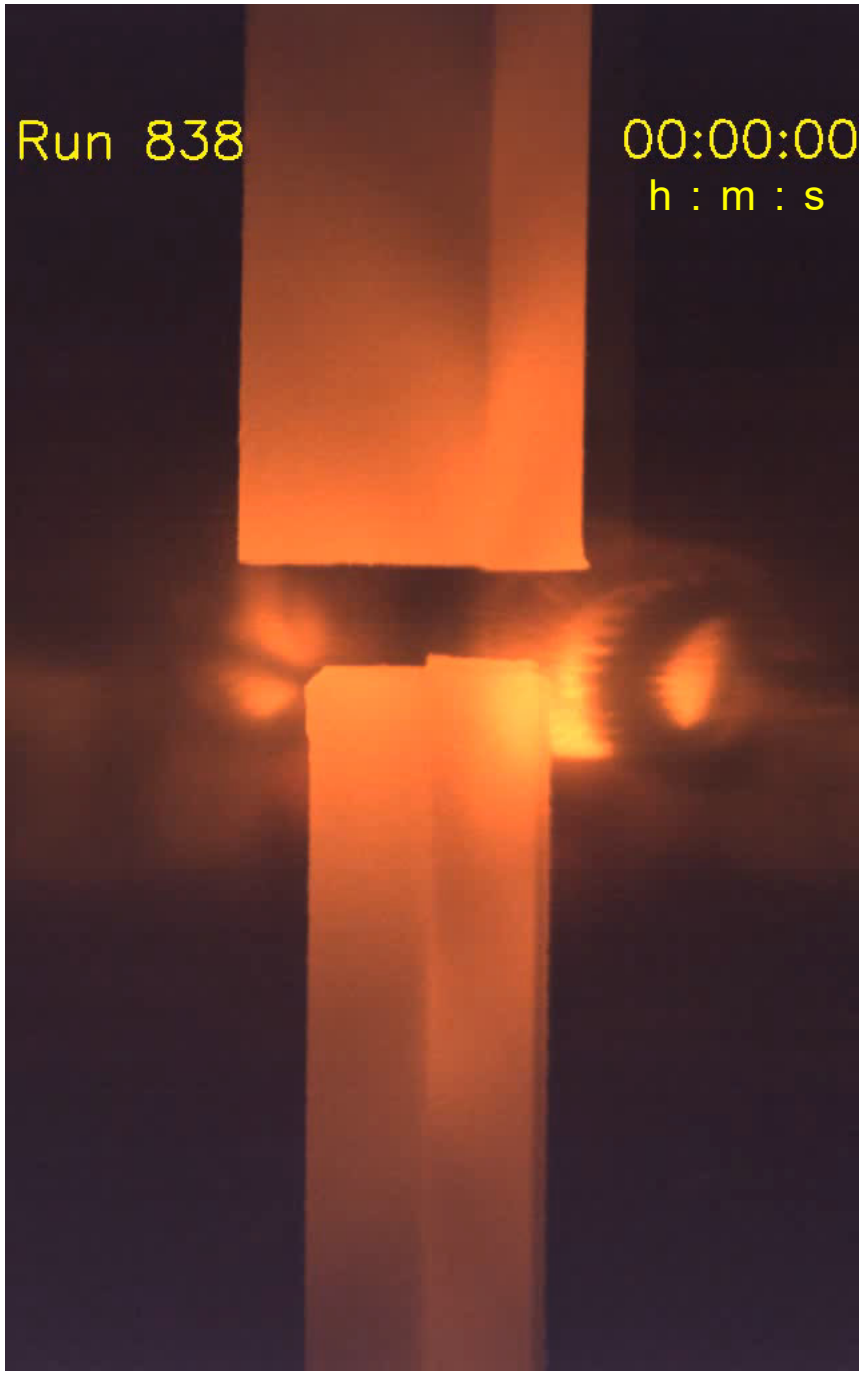

Melt-grown synthesis of $Sr_{17}CaBaNb_{19}WO_{69.5 - y}$

Starting materials for the mirror furnace run: Polycrystalline sintered rods with fully oxidized composition $Sr_{17}CaBaNb_{19}WO_{69.5}$

Fast mode video from the overall melt-grown synthesis of $Sr_{17}CaBaNb_{19}WO_{69.5 - y}$ under 95 % Ar + 5 % H_2 in the Cyberstar mirror furnace. The video is only running in the ppsx type version of this publication, see page 2

Gas flow rate: 400 sccm (24 L / h)
Gas type setting at the mass flow controller: Ar

Lamp power to maintain the molten zone: 2 × (396 - 405) W

Speed of the lower shaft and seed rod (crystal growth speed): 14 mm / h

Melt-grown synthesis of $Sr_{17}CaBaNb_{19}WO_{69.5 - y}$

Starting materials for the mirror furnace run: Polycrystalline sintered rods with fully oxidized composition $Sr_{17}CaBaNb_{19}WO_{69.5}$

Real time video of a short section from the melt-grown synthesis of $Sr_{17}CaBaNb_{19}WO_{69.5 - y}$ under 95 % Ar + 5 % H_2 in the Cyberstar mirror furnace. The video is only running in the ppsx type version of this publication, see page 2

Gas flow rate: 400 sccm (24 L / h)
Gas type setting at the mass flow controller: Ar

Lamp power to maintain the molten zone: 2 × (396 - 405) W

Speed of the lower shaft and seed rod (crystal growth speed): 14 mm / h

As-grown crystalline $Sr_{17}CaBaNb_{19}WO_{69.5-y}$ and polycrystalline rods

Run / Sample No. 838

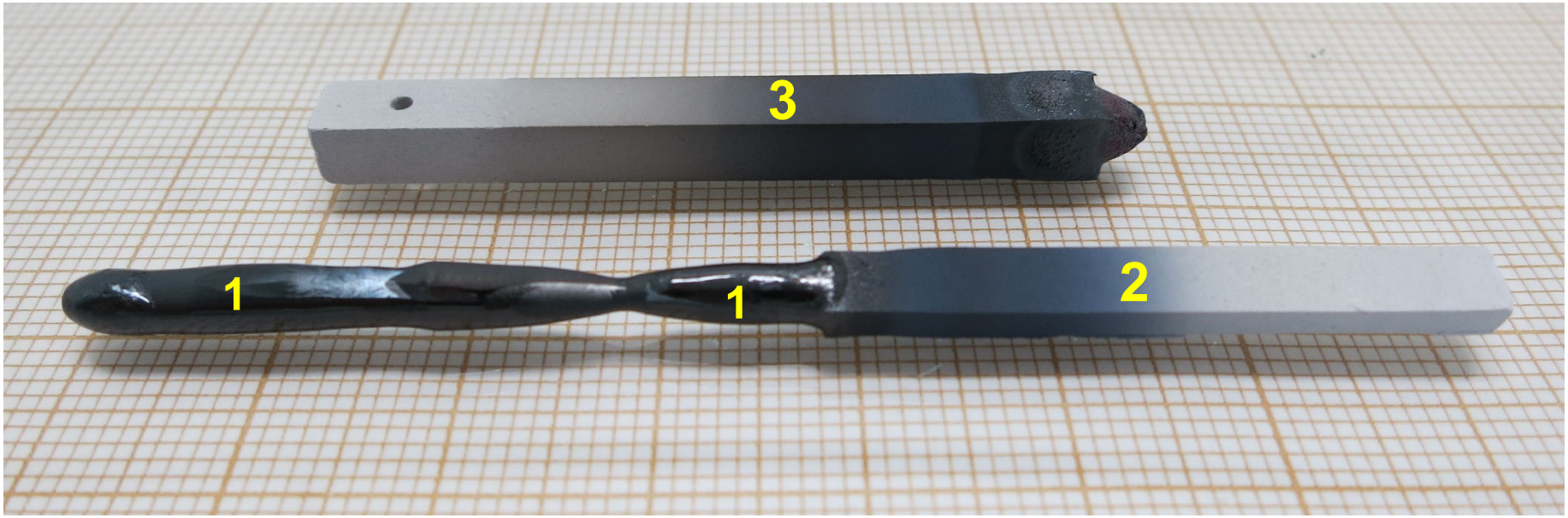

38 mm long as-grown crystalline material (1) plus polycrystalline seed rod (2) and remaining part of the polycrystalline feed rod (3)

Prepared at the ETH Zurich in 2019

As-grown crystalline material $Sr_{17}CaBaNb_{19}WO_{69.5 - y}$

Sample No. 838

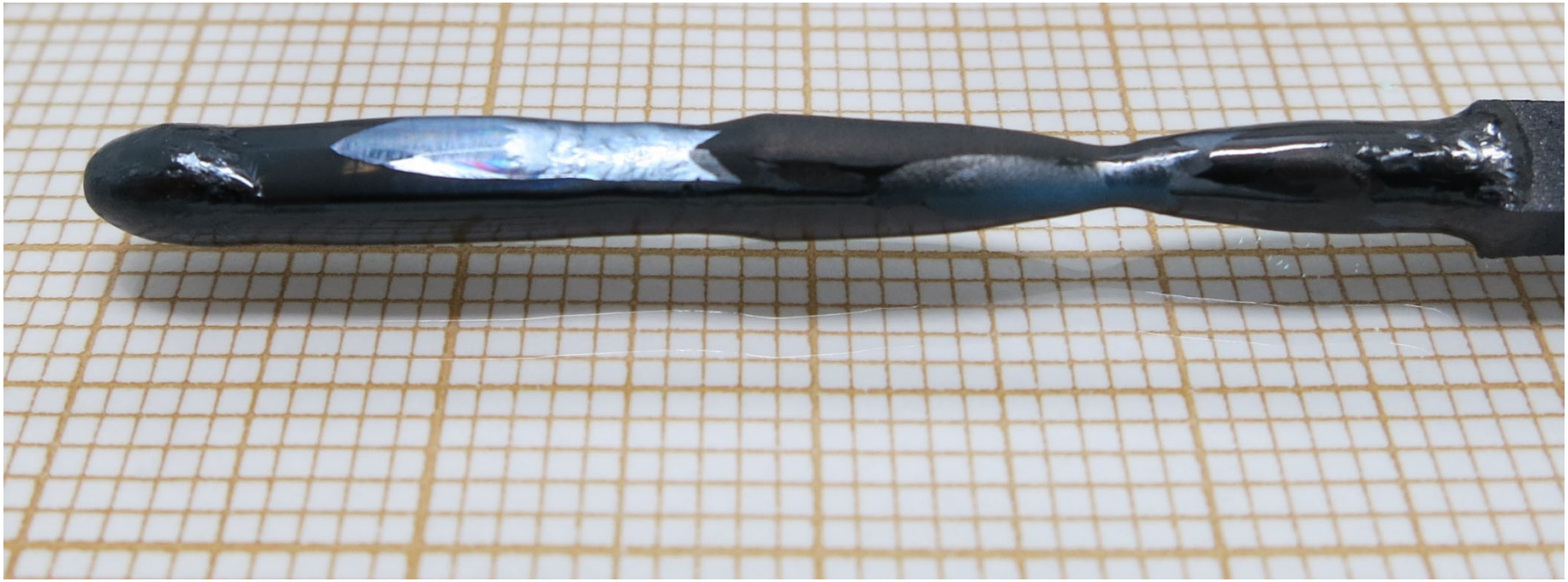

38 mm long as-grown crystalline material

As-grown crystalline material $Sr_{17}CaBaNb_{19}WO_{69.5 - y}$

Sample No. 838

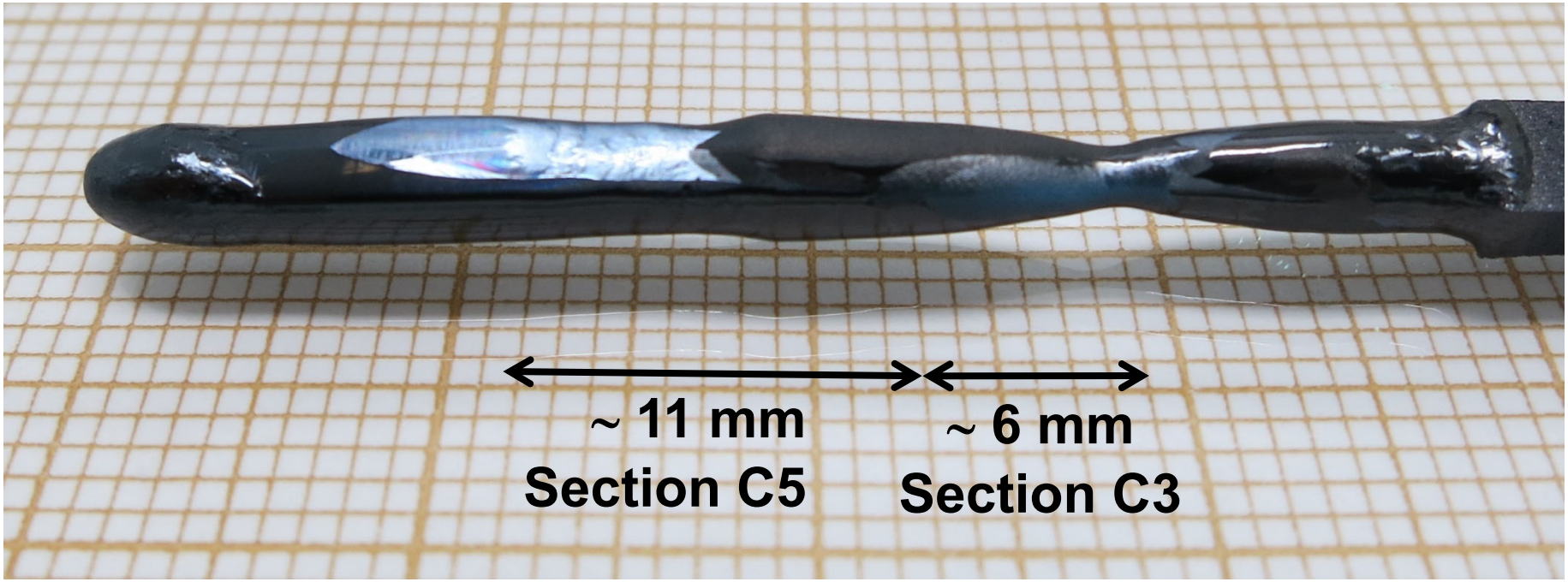

38 mm long as-grown crystalline material

As-grown crystalline material $Sr_{17}CaBaNb_{19}WO_{69.5 - y}$

Sample No. 838

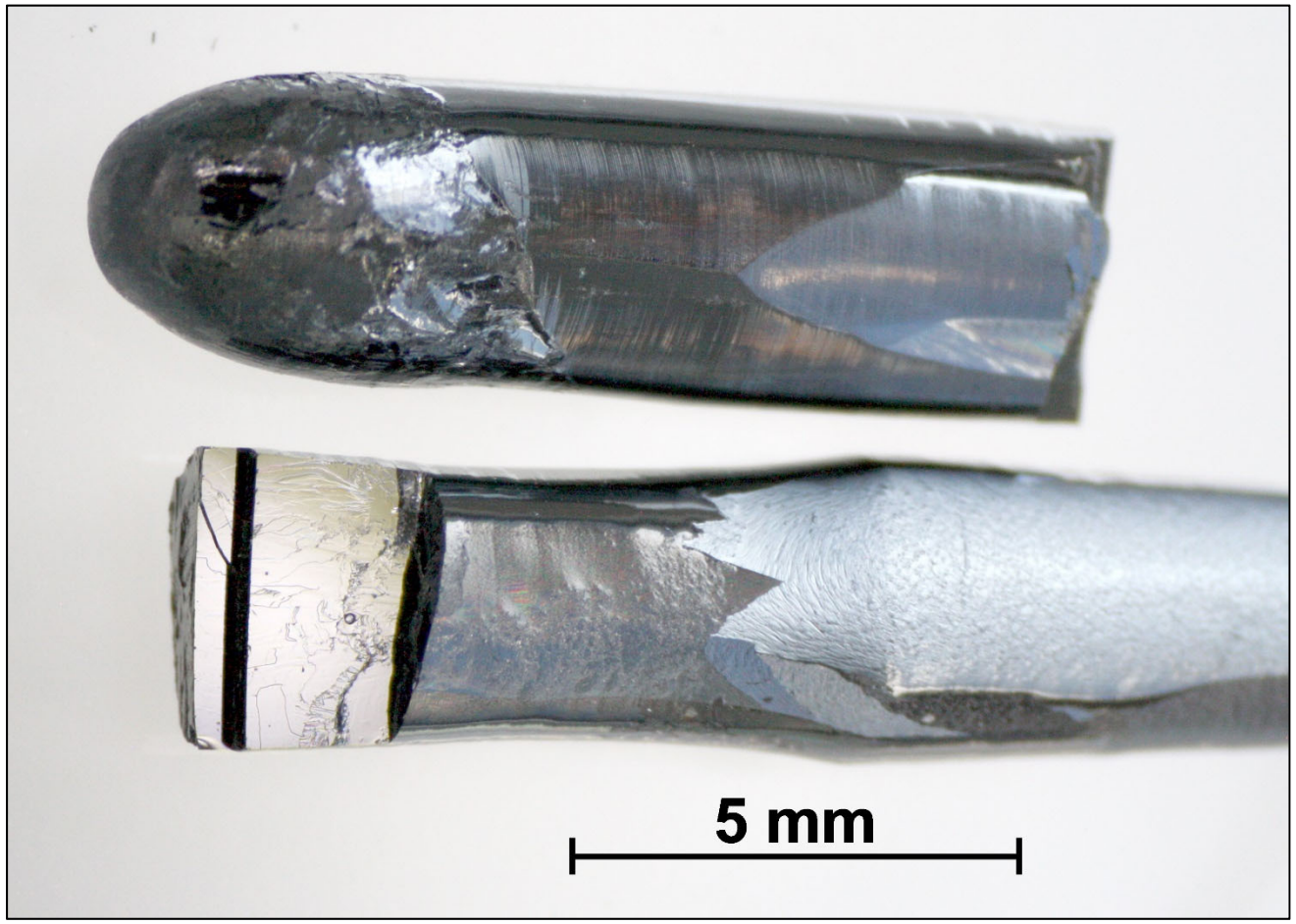

Crystalline pieces from the as-grown material

As-grown crystalline material $Sr_{17}CaBaNb_{19}WO_{69.5 - y}$

Sample No. 838

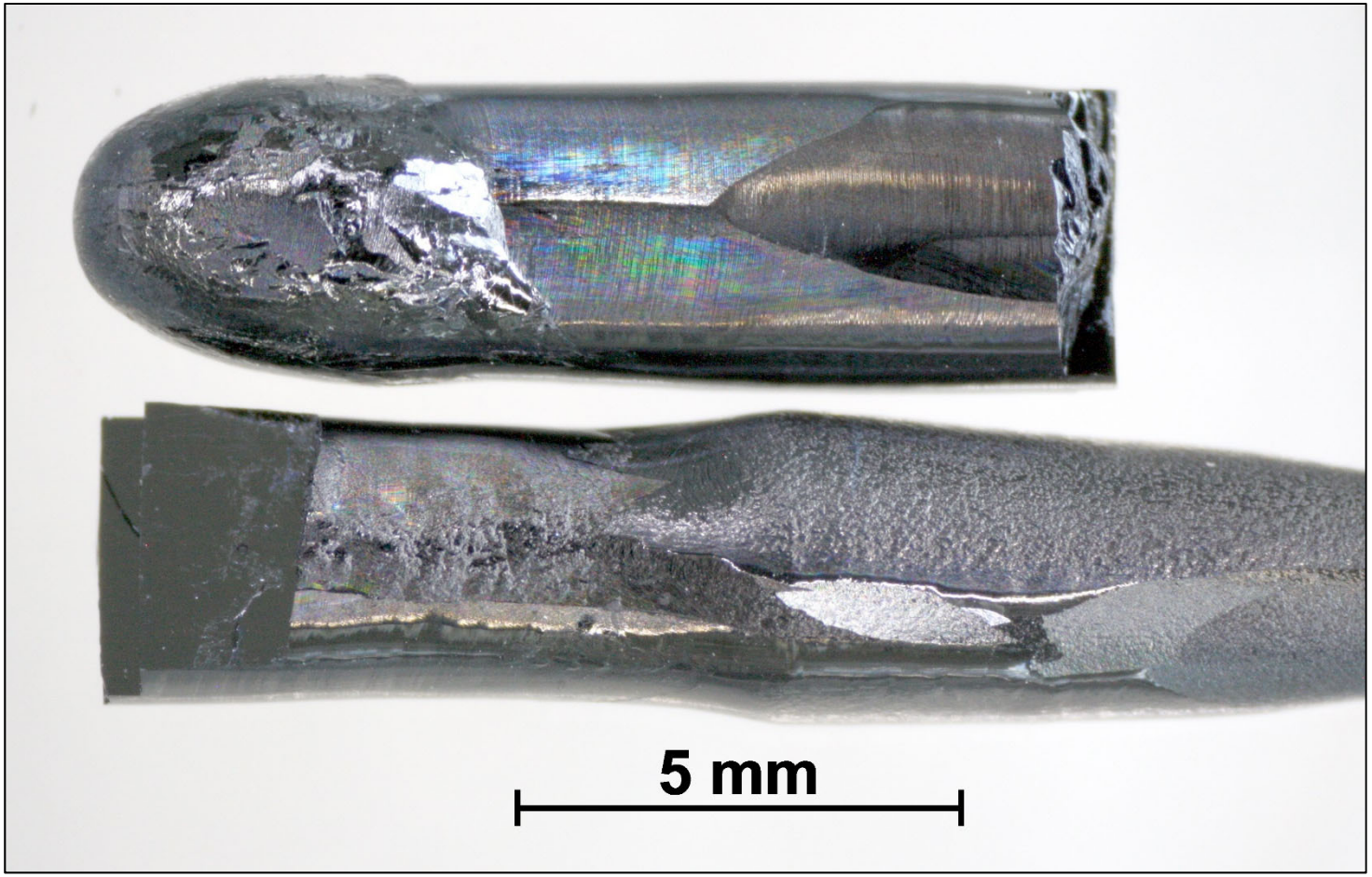

Another picture from the same pieces

As-grown crystalline material $Sr_{17}CaBaNb_{19}WO_{69.5 - y}$

Sample No. 838

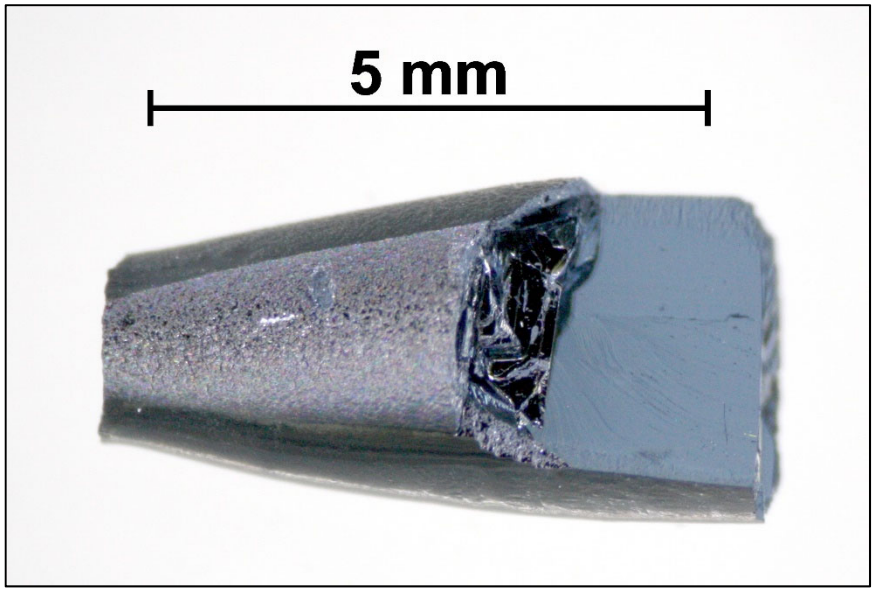

From section C3

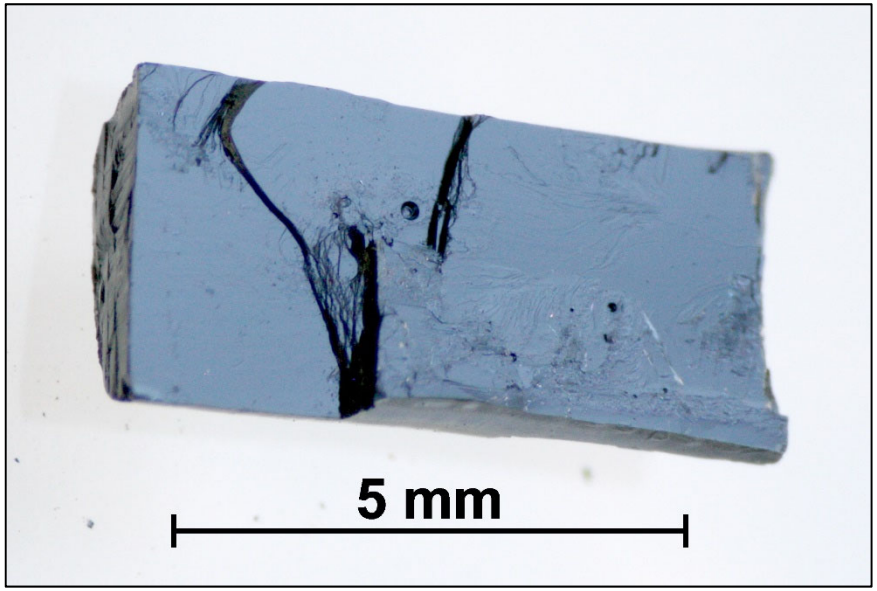

From section C5

Crystalline pieces of the as-grown material

838 C5 $Sr_{17}CaBaNb_{19}WO_x$ Thermogravimetry

Thermogravimetric oxidation in flowing synth. air up to the fully oxidized composition with $x = x_F = 69.5$ for the determination of the oxygen content $x = 69.5 - y$ by using a thermogravimetric analyzer NETZSCH TG 209 F1 Libra

Pulverized crystalline material from section C5 of the as-grown sample → $x = 64.06$

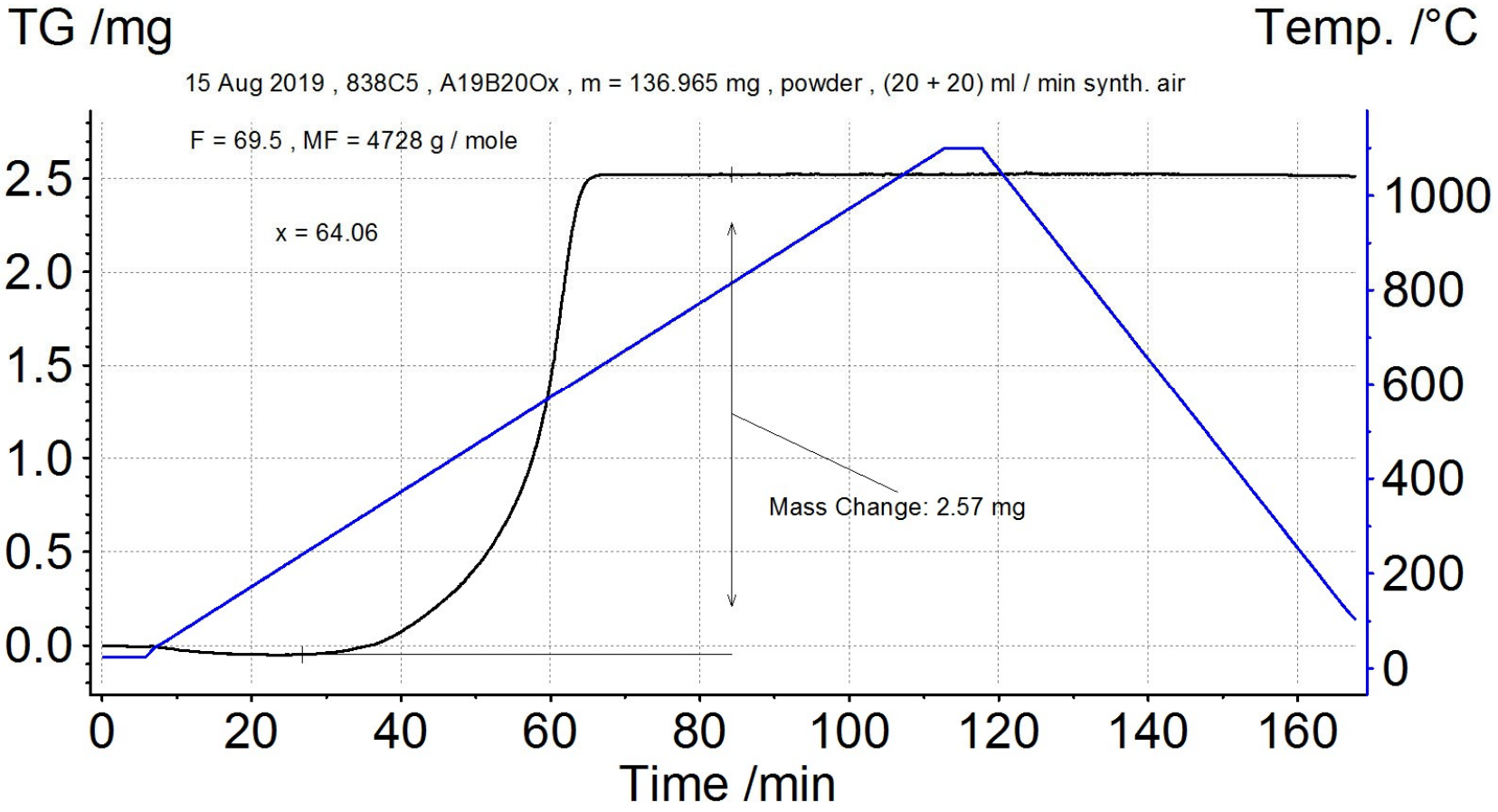

$Sr_{17}CaBaNb_{19}WO_{64.06}$ Valences of the Nb and W ions

Valence or oxidation states of the
Nb and W ions in $Sr_{17}CaBaNb_{19}WO_{64.06}$

The most likely scenario is W^{4+} / $5d^{2}$

↓

Charge neutrality and Sr^{2+}, Ca^{2+}, Ba^{2+}, and O^{2-} → $Nb^{4.53+}$ / $4d^{0.47}$

↓

2 (5d) + 19 × 0.47 (4d) = 10.9 d-electrons
per formula and assumed size of the unit cell

838 C5 $Sr_{17}CaBaNb_{19}WO_{64}$ Powder x-ray diffraction

Powder x-ray diffraction pattern of pulverized crystalline material from section C8

Square root - linear plot • Background subtracted

All observed peaks fit to an orthorhombic *n* = 5 type structure

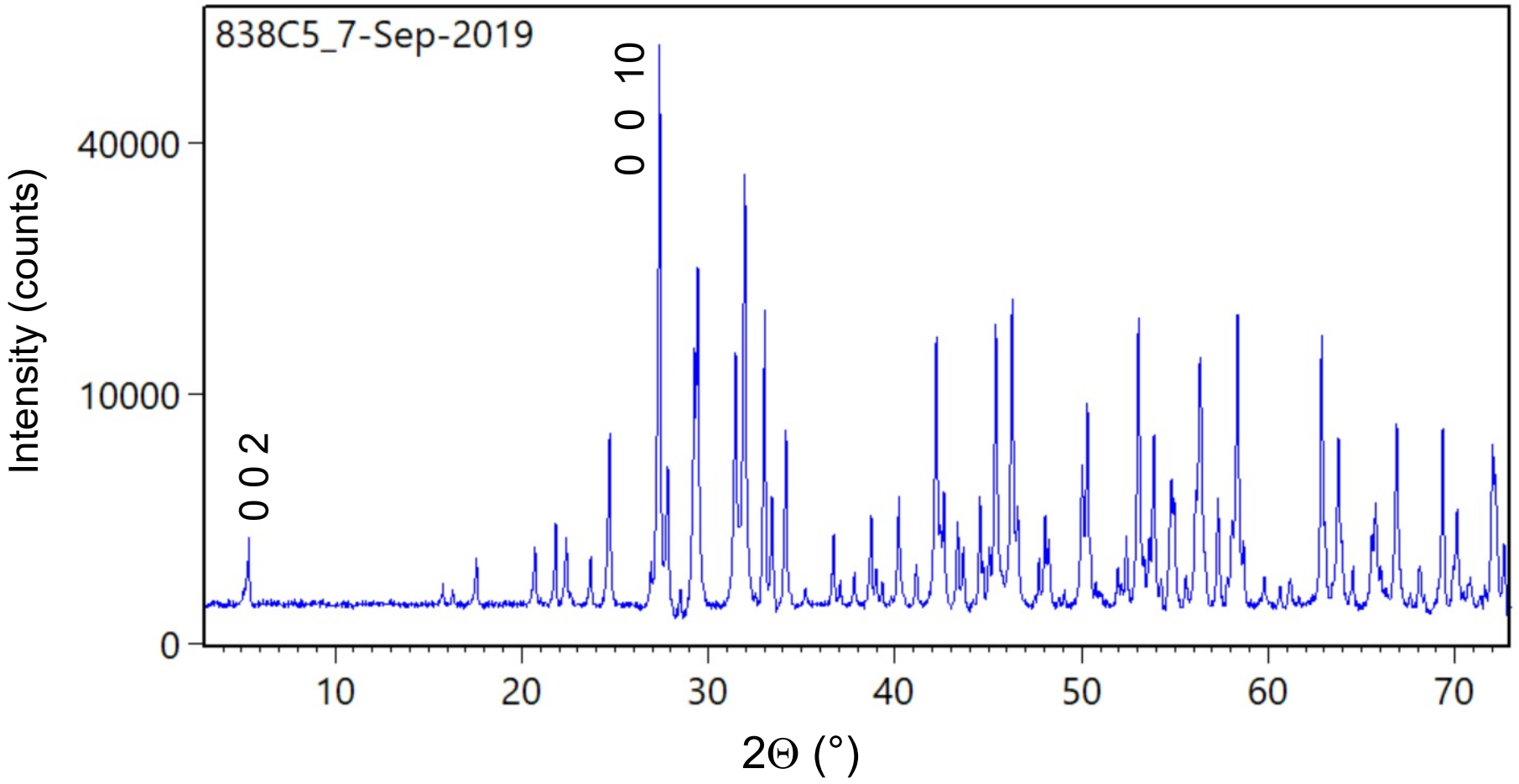

838 C5 $Sr_{17}CaBaNb_{19}WO_{64}$ Powder x-ray diffraction

	Observed peak position (°2θ)	d-spacing (Å)	Relative intensity (%)	h k l from lattice parameter refinement
Lowest angle peak Its position indicates the structure type of $A_nB_nO_{3n+2}$, namely n = 5 in this case	5.38	16.41	3	0 0 2
Highest intensity peak	27.39	3.25	100	0 0 10

838 C5 $Sr_{17}CaBaNb_{19}WO_{64}$ Powder x-ray diffraction

Results of lattice parameter refinement with $(h\ k\ l)_{max}$ = (10 10 20)

Number of observed peaks	103
Number of indexed peaks	103
Number of unindexed peaks	0
Crystal structure type	n = 5 of $A_nB_nO_{3n+2}$
Crystal system	Orthorhombic
Bravais lattice	P
a (Å)	7.98
b (Å)	5.68
c (Å)	32.50
V (Å^3)	1473
$\lvert 2\theta_{obs} - 2\theta_{calc} \rvert$ for all observed and calculated peaks	$\leq 0.059°$
Figure of merit of the refinement or fit	14.2
Chi square of the refinement or fit	3.5×10^{-6}

838 C5 $Sr_{17}CaBaNb_{19}WO_{64}$ Magnetic measurements

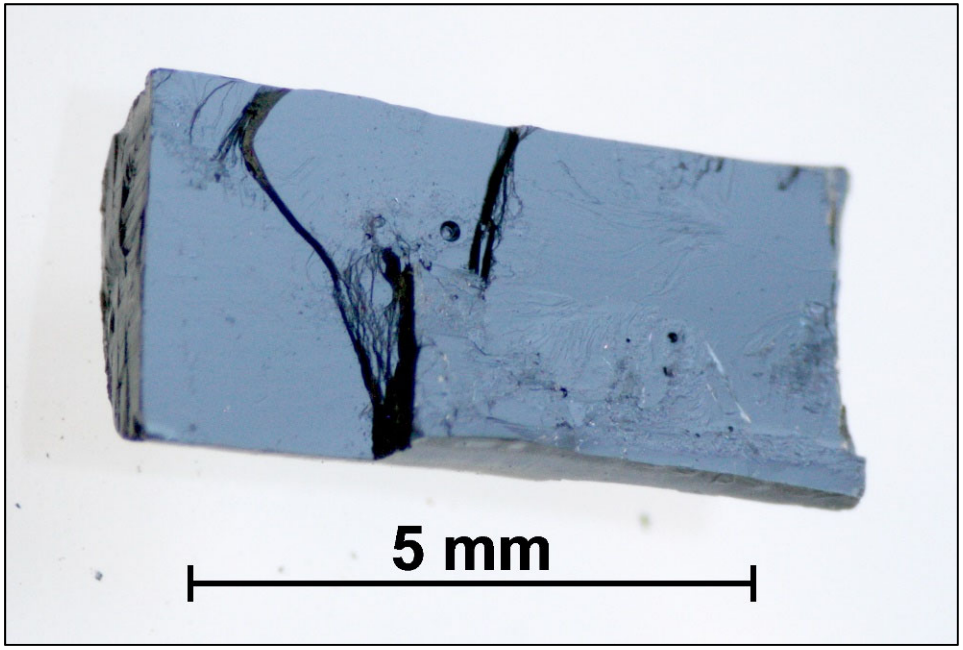

Crystalline piece C5-1 with m = 118 mg
from section C5 of the as-grown material

This piece was used to study its magnetic
properties by a SQUID magnetometer

838 C5 $Sr_{17}CaBaNb_{19}WO_{64}$ Magnetic susceptibility $\chi(T)$

DC magnetic moment M(T) measured by a Quantum Design SQUID magnetometer MPMS3

10.9 d-electrons from Nb^{4+} / $4d^1$ and W^{4+} / $5d^2$

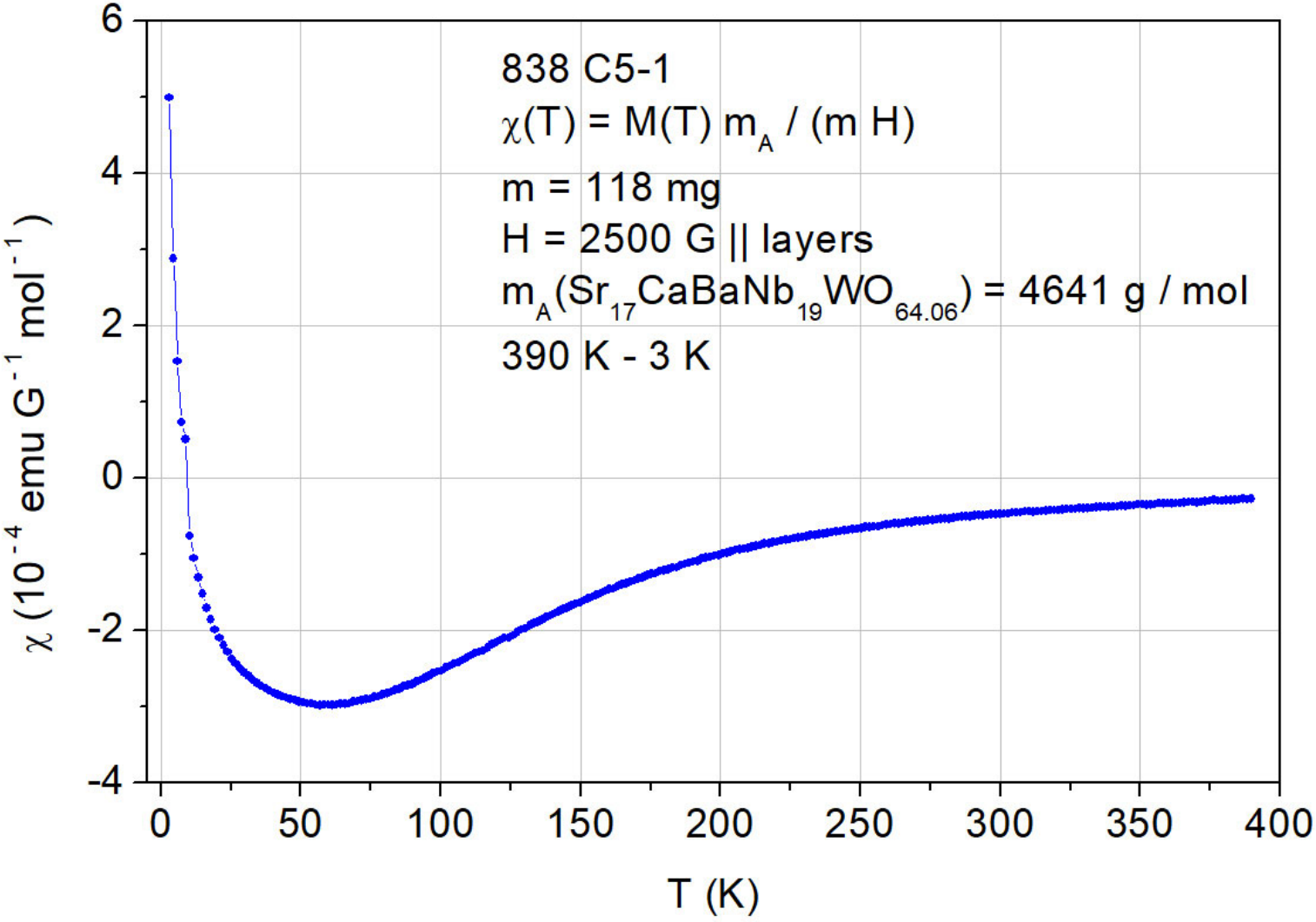

838 C5 $Sr_{17}CaBaNb_{19}WO_{64}$ Magnetic susceptibility $\chi(T)$

DC magnetic moment M(T) measured by a Quantum Design SQUID magnetometer MPMS3

10.9 d-electrons from Nb^{4+} / $4d^1$ and W^{4+} / $5d^2$

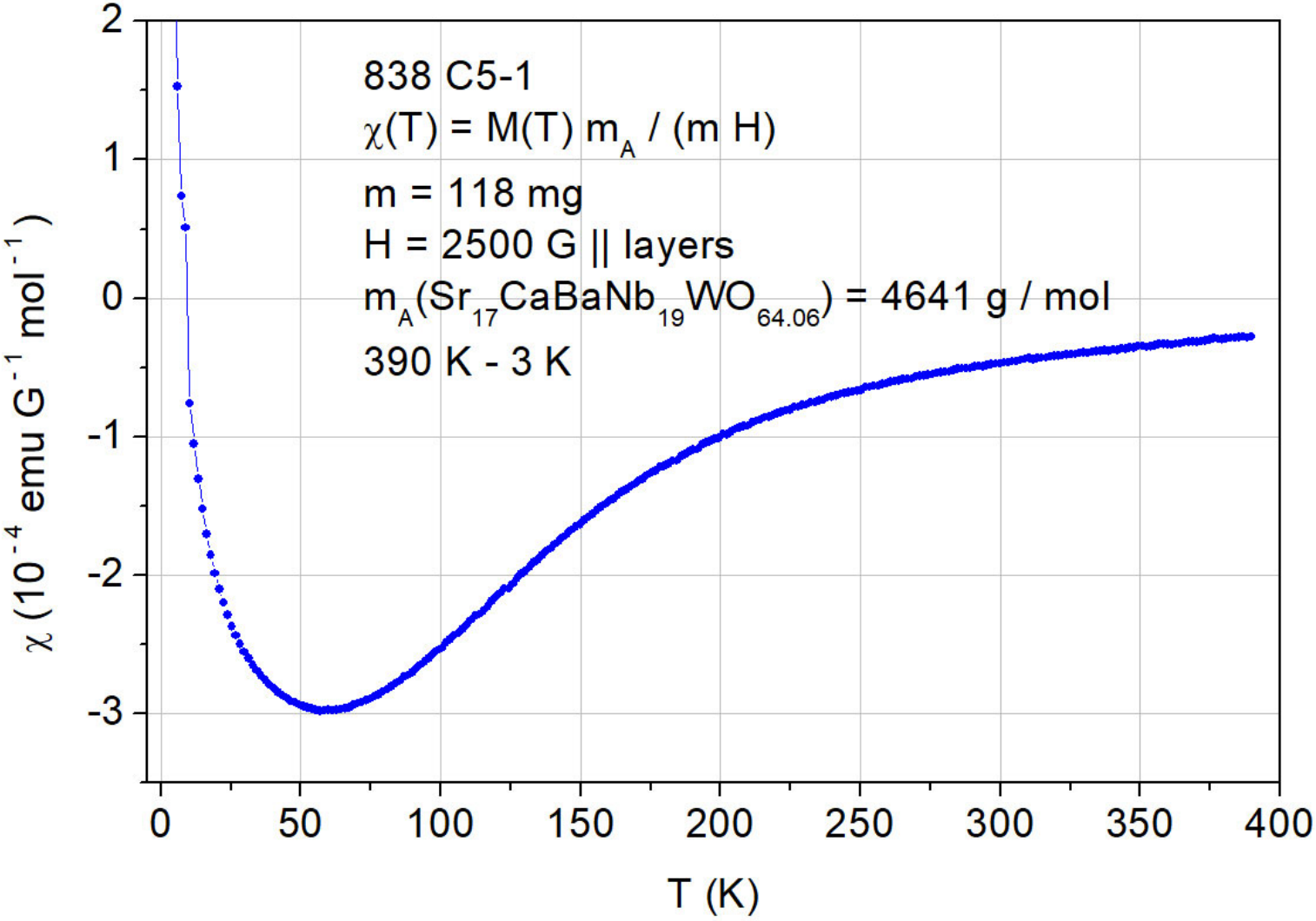

The behavior of $\chi(T)$ in the range from 390 K to 65 K is similar to that of $A_nB_nO_{3n+2}$ type quasi-1D metals. Thus this n = 5 type material is potentially also a quasi-1D metal

838 C5 $Sr_{17}CaBaNb_{19}WO_{64}$ Magnetic susceptibility $\chi(T)$

DC magnetic moment M(T) measured by a Quantum Design SQUID magnetometer MPMS3

10.9 d-electrons from Nb^{4+} / $4d^1$ and W^{4+} / $5d^2$

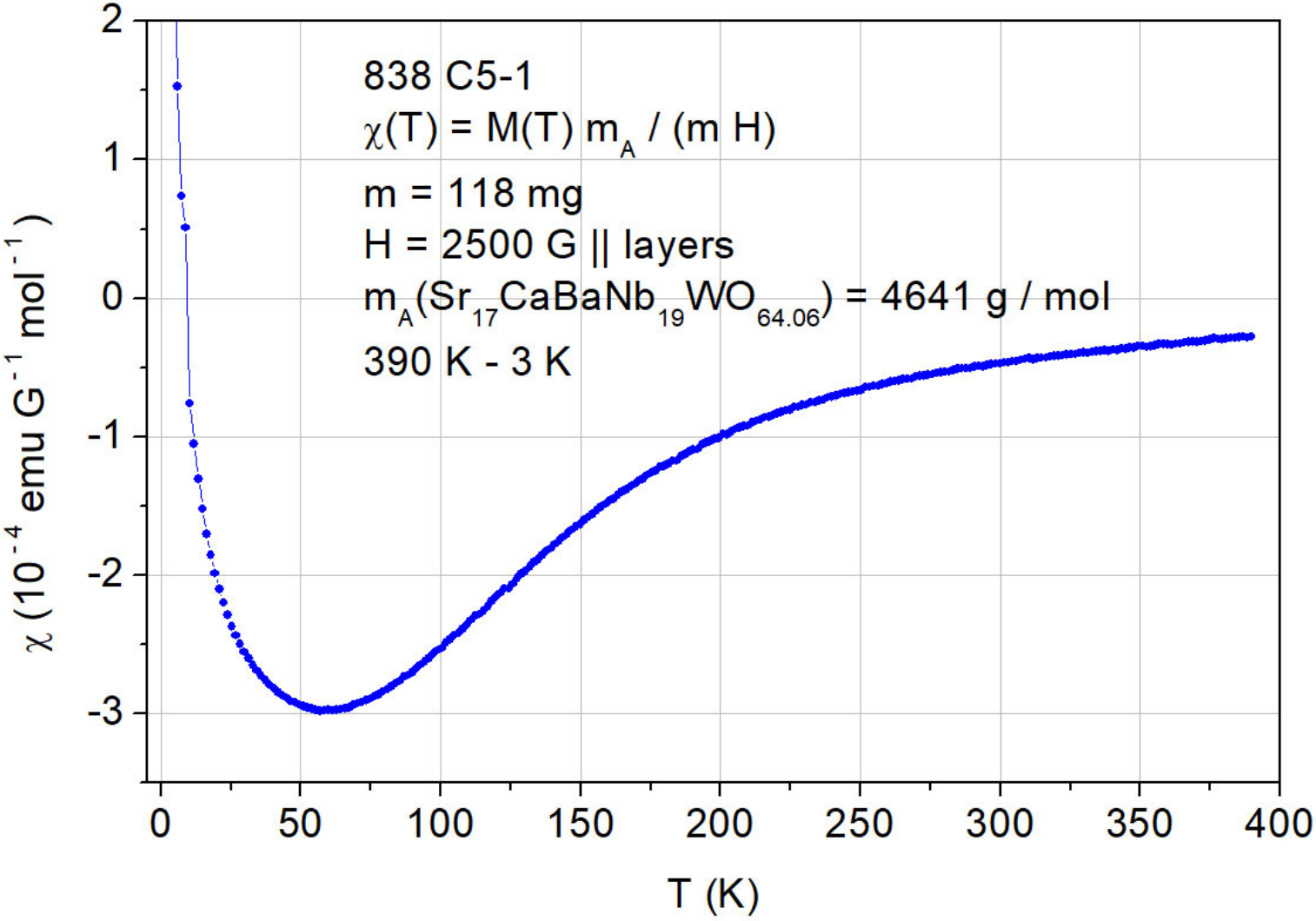

Increase of $\chi(T)$ below 55 K due to paramagnetic impurities or defect states or 5d electrons which become localized ?

838 C5 $Sr_{17}CaBaNb_{19}WO_{64}$ Magnetic susceptibility $\chi(T)$

DC magnetic moment M(T) measured by a Quantum Design SQUID magnetometer MPMS3

10.9 d-electrons from Nb^{4+} / $4d^1$ and W^{4+} / $5d^2$

D = diamagnetic contribution from closed electron shells of Sr^{2+}, Ca^{2+}, Ba^{2+}, Nb^{5+}, W^{6+}, and O^{2-}

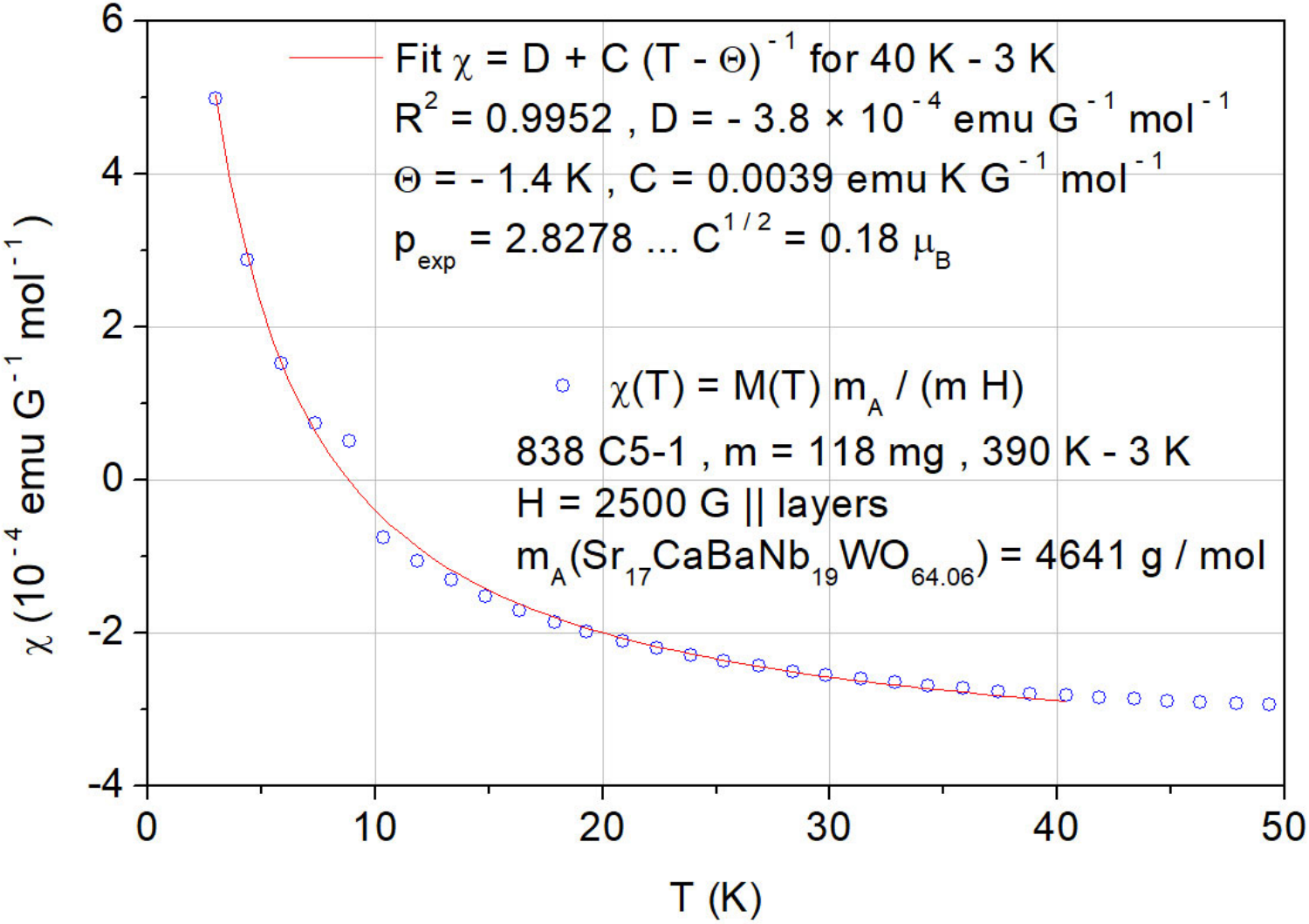

Ref. for the calculation of p_{exp}: Progress in Solid State Chemistry 36 (2008) 253

6 Conducting and metallic Carpy-Galy phases $A_nB_nO_{3n+2} = ABO_x$

6.9.6 A Schückel-Müller-Buschbaum type phase: Synthesis and properties of $Sr_{17}Ca_2Nb_{19}WO_{64}$ ...

As-pressed rods with composition $Sr_{17}Ca_2Nb_{19}WO_{69.5}$

Run No. 826

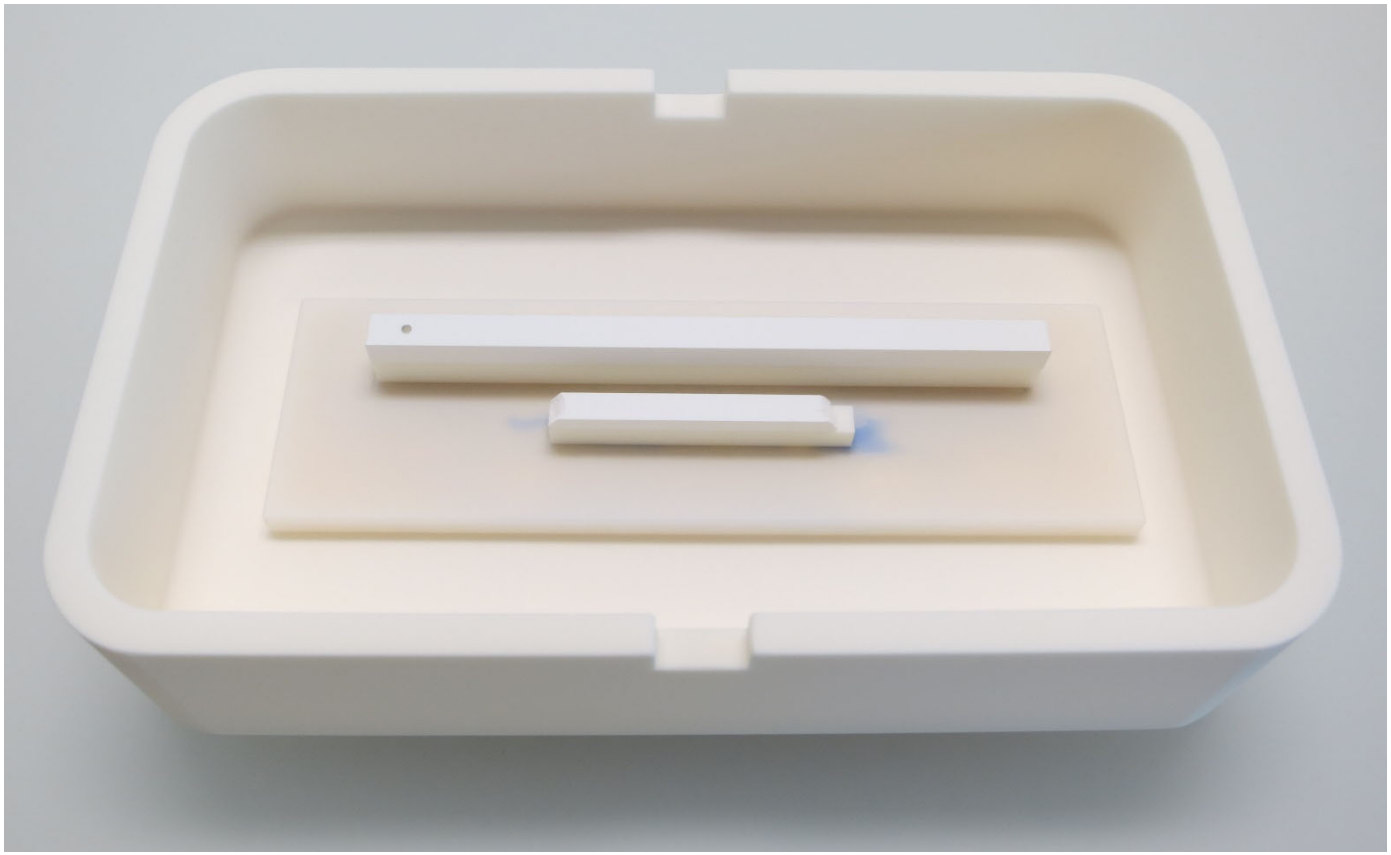

As-pressed rods in an alumina box. Ready for sintering under air. The as-pressed rods are located on a lower punch which is made of yttria-stabilized zirconia. The length of the long rod is 9 cm

As-pressed rods with fully oxidized composition $Sr_{17}Ca_2Nb_{19}WO_{69.5}$, i.e. all Nb and W ions are in their highest valence or oxidation state Nb^{5+} and W^{6+}, respectively.

At the both ends of the short rod somewhat material is missing. That damage did happen accidentally during the preparation of the rod. However, its overall length is still appropriate for the mirror furnace run

Sintered rods with composition $Sr_{17}Ca_2Nb_{19}WO_{69.5}$ Run No. 826

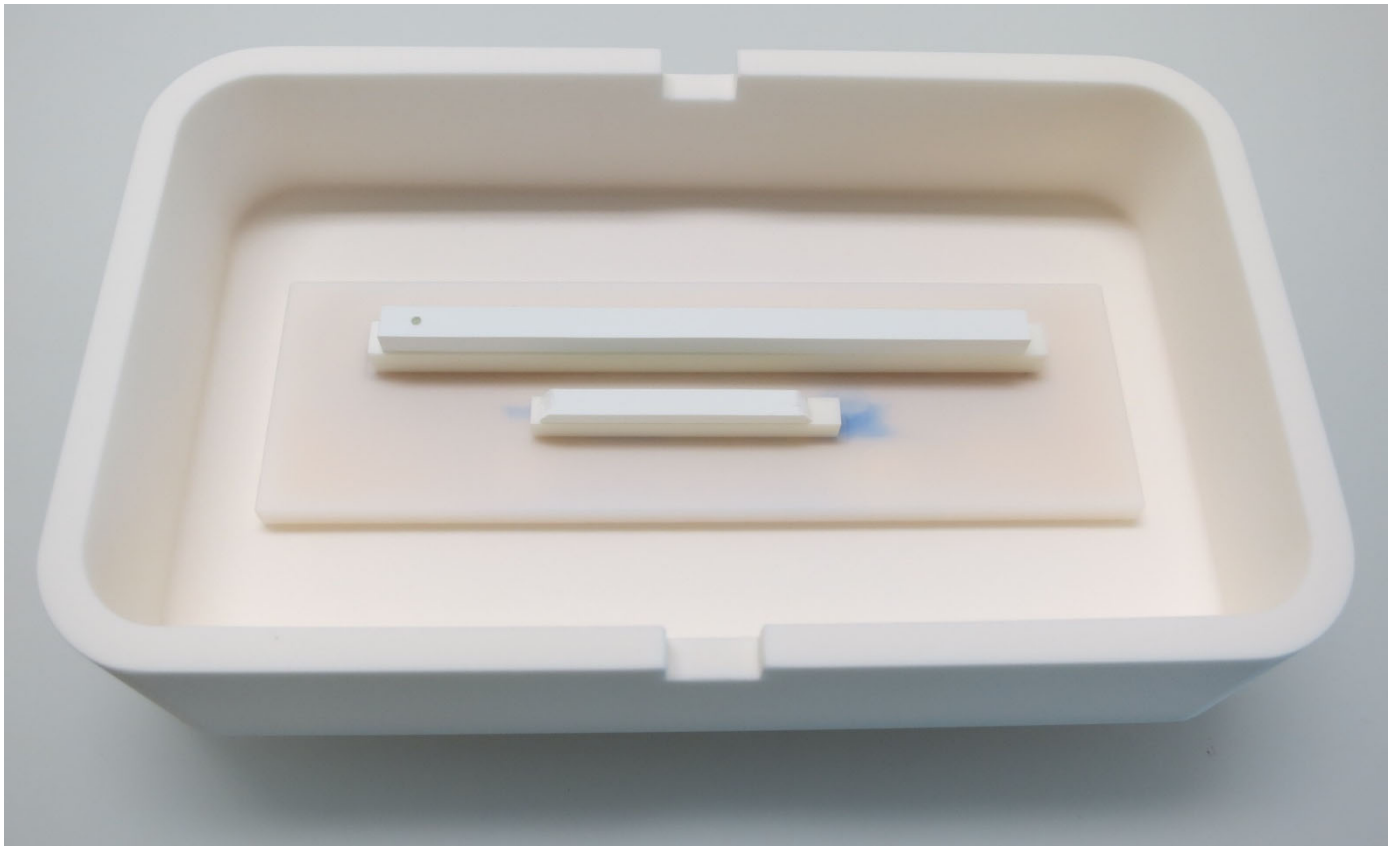

The as-pressed rods were 4 h sintered at 1260 °C under air.
The sintering did result in a shrinkage of their length

A somewhat lower sintering temperature would have been better because the sintered rods were attached on their lower punch. Fortunately it was possible to remove the rods from their lower punch without damaging the rods.
Later related experiments revealed that lower punches made of alumina are more suitable

Sintered rods with composition $Sr_{17}Ca_2Nb_{19}WO_{69.5}$ Run No. 826

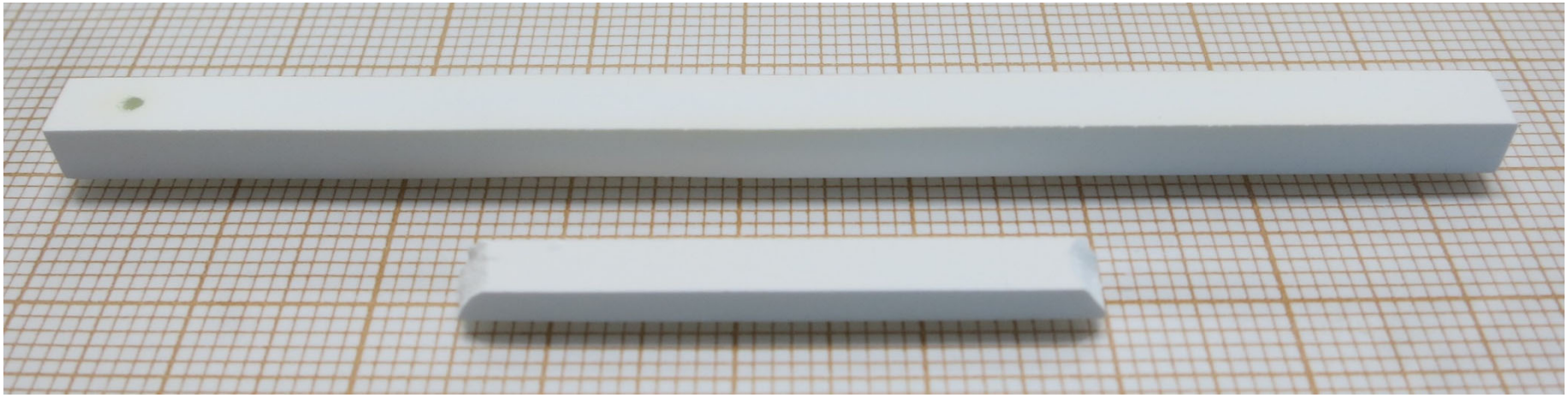

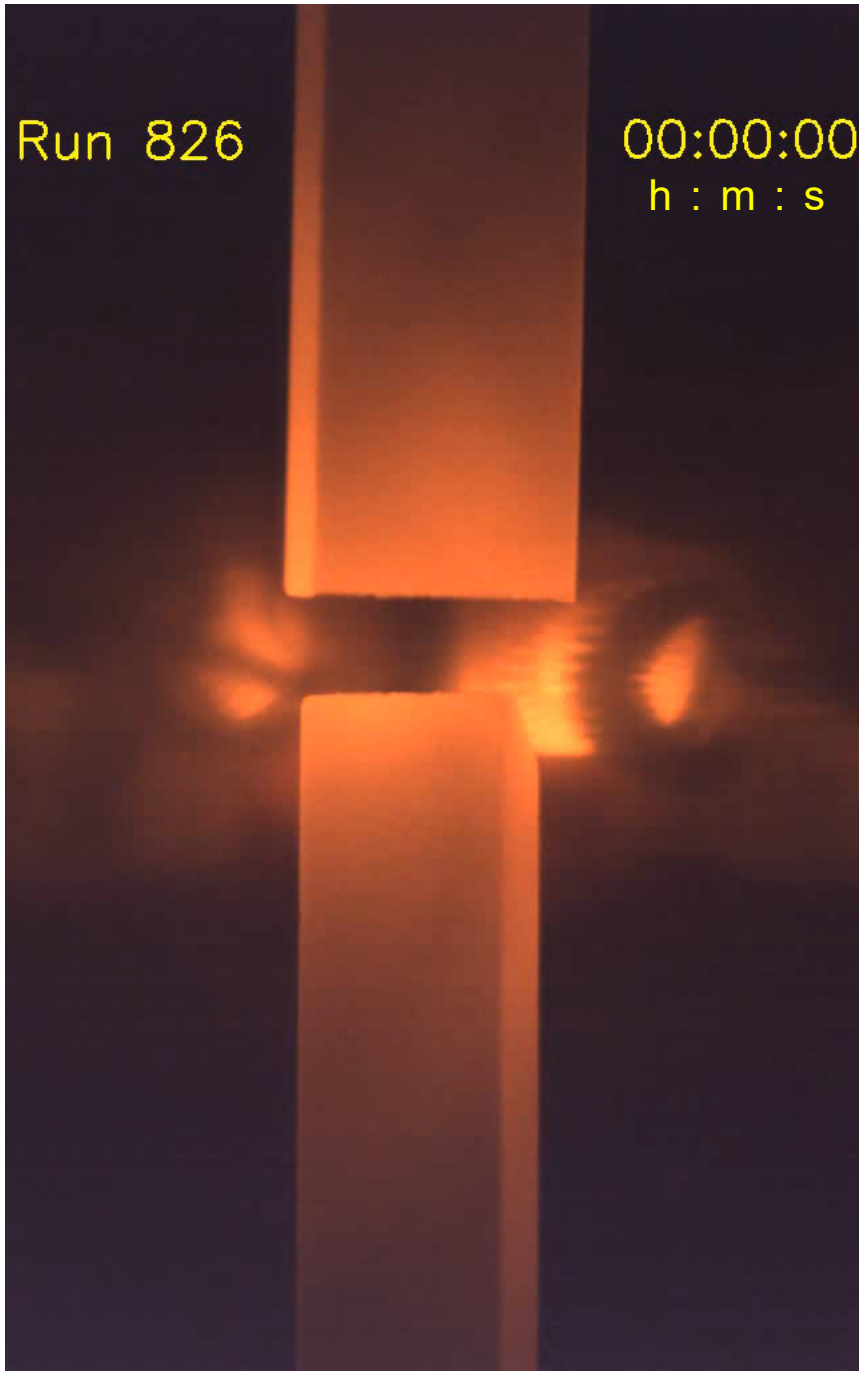

Melt-grown synthesis of $Sr_{17}Ca_2Nb_{19}WO_{69.5-y}$

Starting materials for the mirror furnace run: Polycrystalline sintered rods with fully oxidized composition $Sr_{17}Ca_2Nb_{19}WO_{69.5}$

Fast mode video from the overall melt-grown synthesis of $Sr_{17}Ca_2Nb_{19}WO_{69.5-y}$ under 95 % Ar + 5 % H_2 in the Cyberstar mirror furnace. The video is only running in the ppsx type version of this publication, see page 2

Gas flow rate: 400 sccm (24 L / h)
Gas type setting at the mass flow controller: Ar

Lamp power to maintain the molten zone: 2 × (385 - 404) W

Speed of the lower shaft and seed rod (crystal growth speed): 14 mm / h

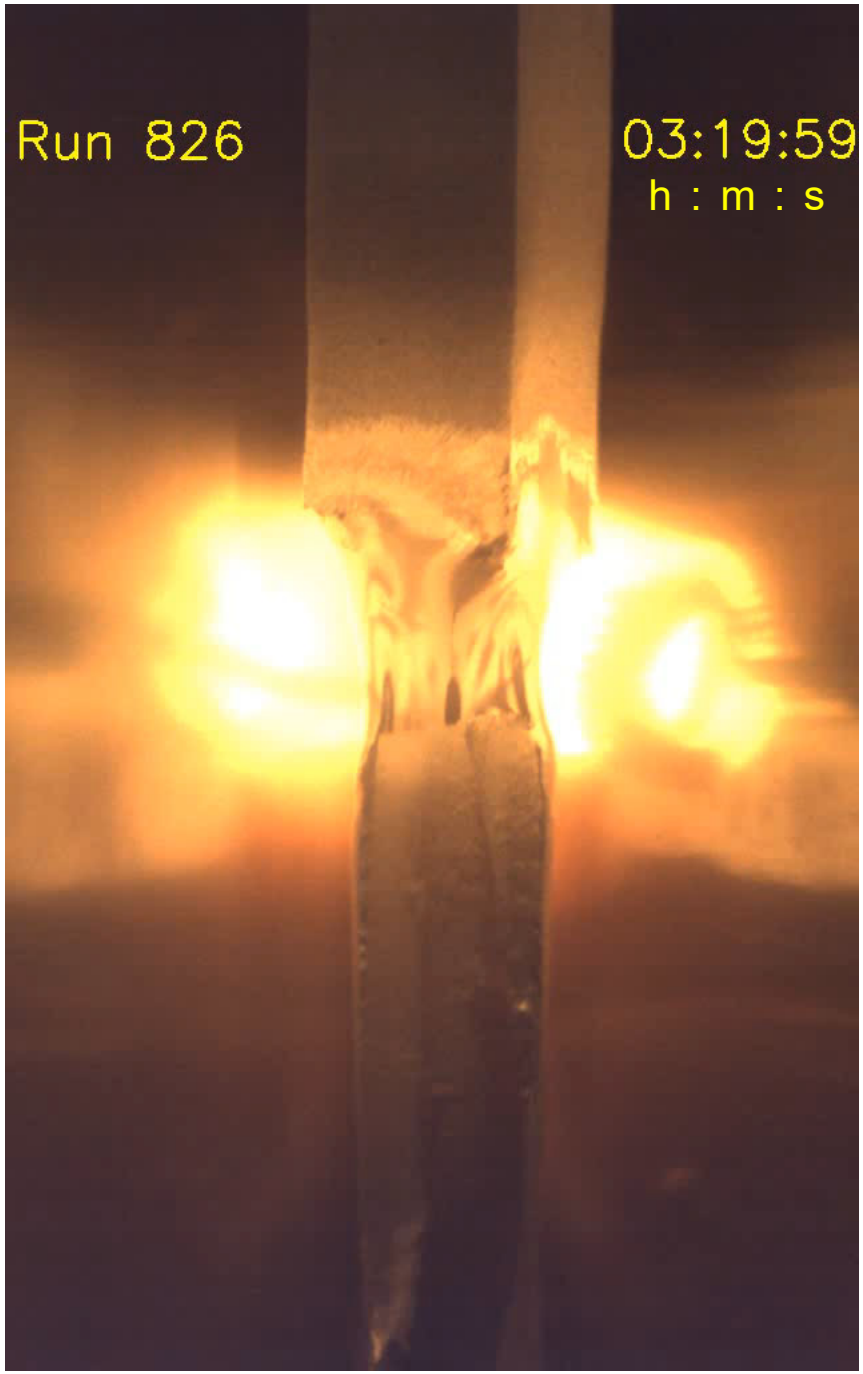

Melt-grown synthesis of $Sr_{17}Ca_2Nb_{19}WO_{69.5-y}$

Starting materials for the mirror furnace run: Polycrystalline sintered rods with fully oxidized composition $Sr_{17}Ca_2Nb_{19}WO_{69.5}$

Real time video of a short section from the melt-grown synthesis of $Sr_{17}Ca_2Nb_{19}WO_{69.5-y}$ under 95 % Ar + 5 % H_2 in the Cyberstar mirror furnace. The video is only running in the ppsx type version of this publication, see page 2

Gas flow rate: 400 sccm (24 L / h)
Gas type setting at the mass flow controller: Ar

Lamp power to maintain the molten zone: 2 × (385 - 404) W

Speed of the lower shaft and seed rod (crystal growth speed): 14 mm / h

As-grown crystalline $Sr_{17}Ca_2Nb_{19}WO_{69.5-y}$ and polycrystalline rods

Run / Sample No. 826

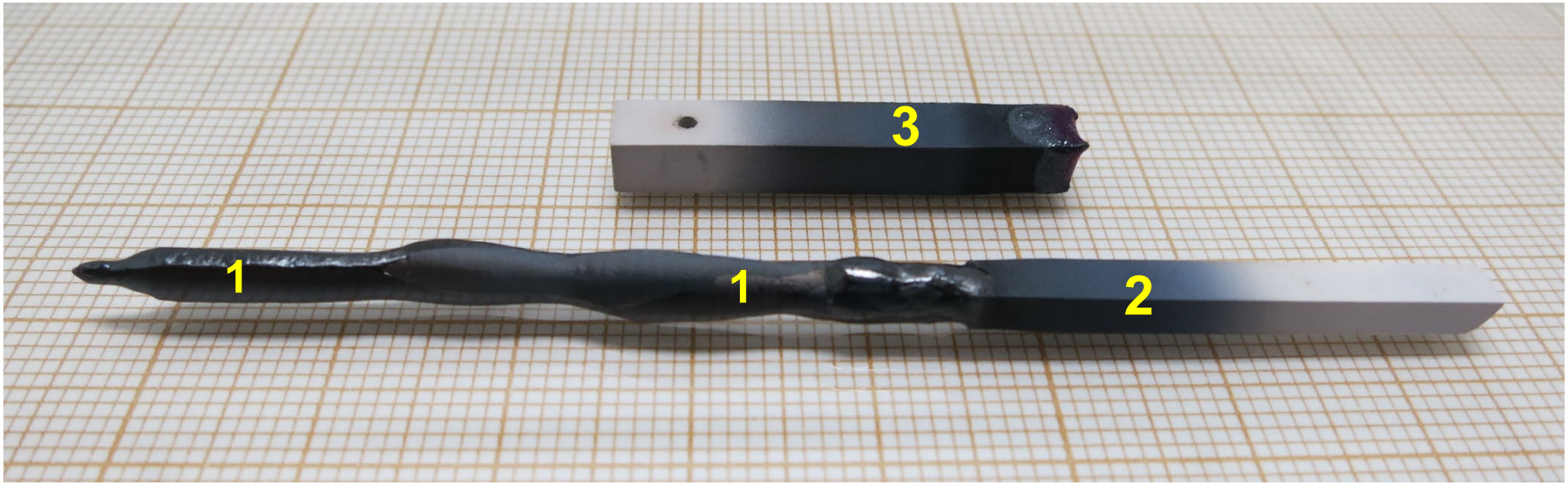

5 cm long as-grown crystalline material (1) plus polycrystalline seed rod (2) and remaining part of the polycrystalline feed rod (3)

Prepared at the ETH Zurich in 2019

As-grown crystalline material $Sr_{17}Ca_2Nb_{19}WO_{69.5 - y}$

Sample No. 826

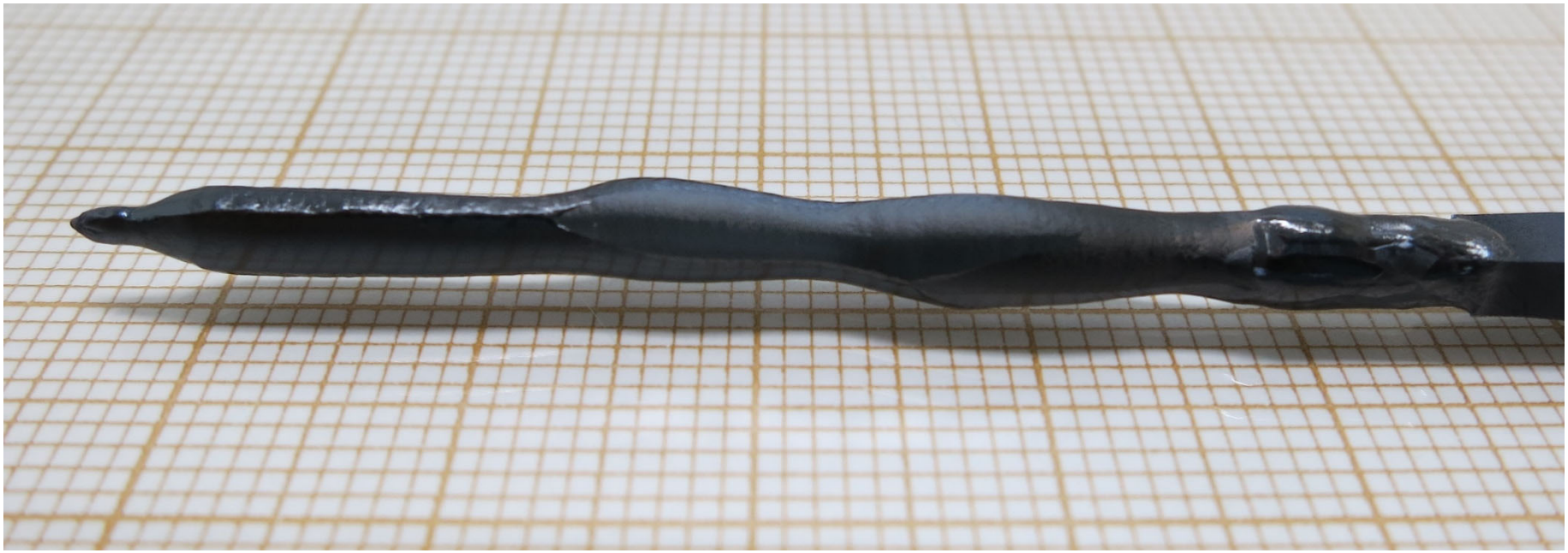

5 cm long as-grown crystalline material

As-grown crystalline material $Sr_{17}Ca_2Nb_{19}WO_{69.5 - y}$

Sample No. 826

Another view from the 5 cm long as-grown crystalline material

As-grown crystalline material $Sr_{17}Ca_2Nb_{19}WO_{69.5-y}$

Sample No. 826

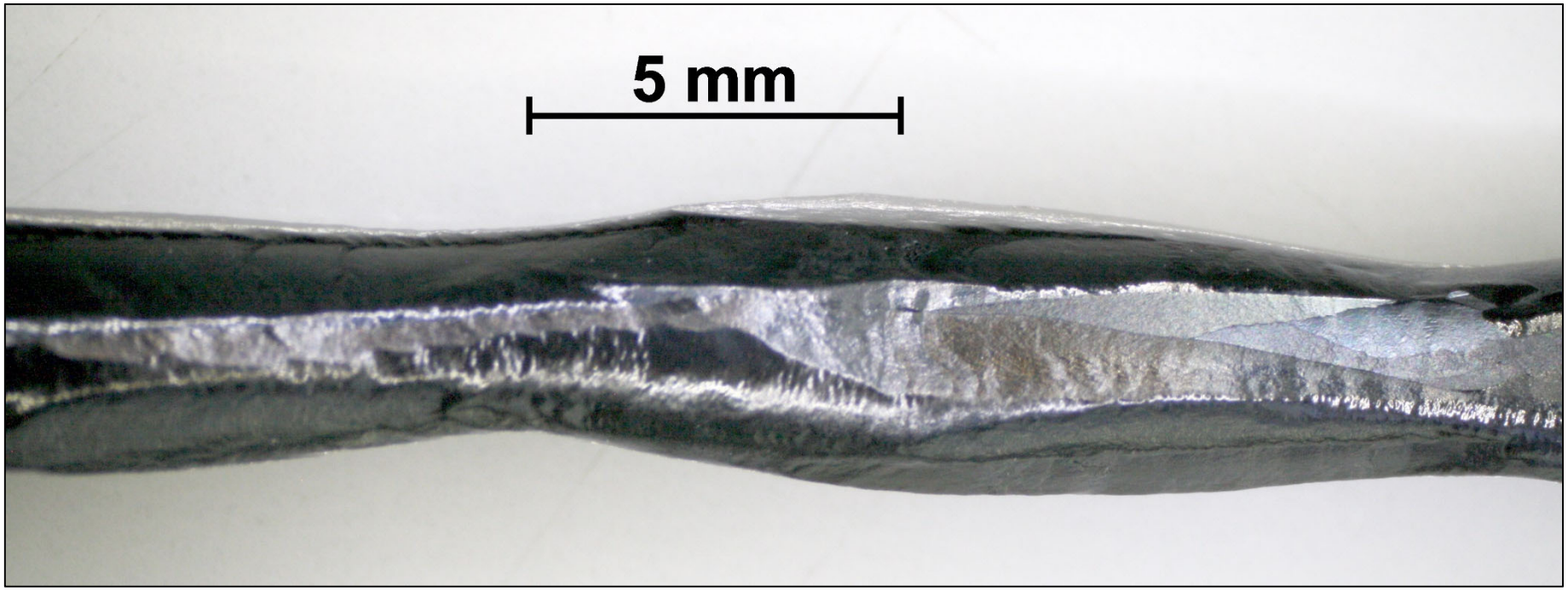

A section from the 5 cm long as-grown crystalline material

As-grown crystalline material $Sr_{17}Ca_2Nb_{19}WO_{69.5-y}$

Sample No. 826

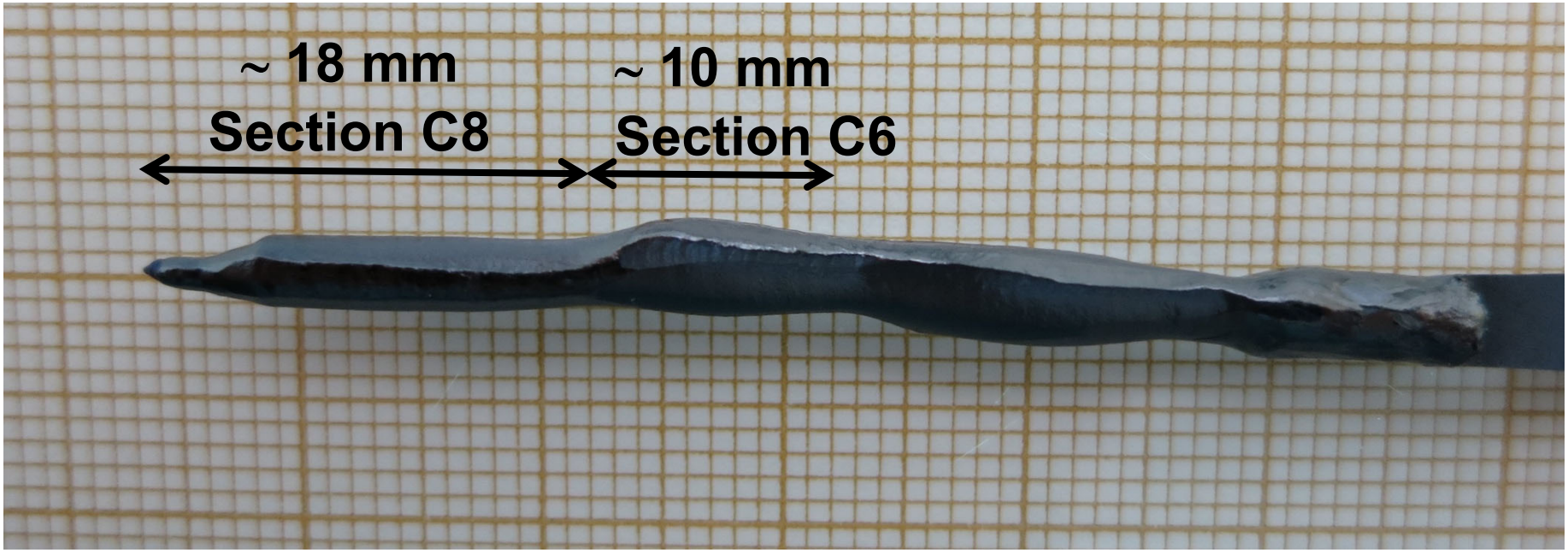

5 cm long as-grown crystalline material

As-grown crystalline material $Sr_{17}Ca_2Nb_{19}WO_{69.5-y}$

Sample No. 826

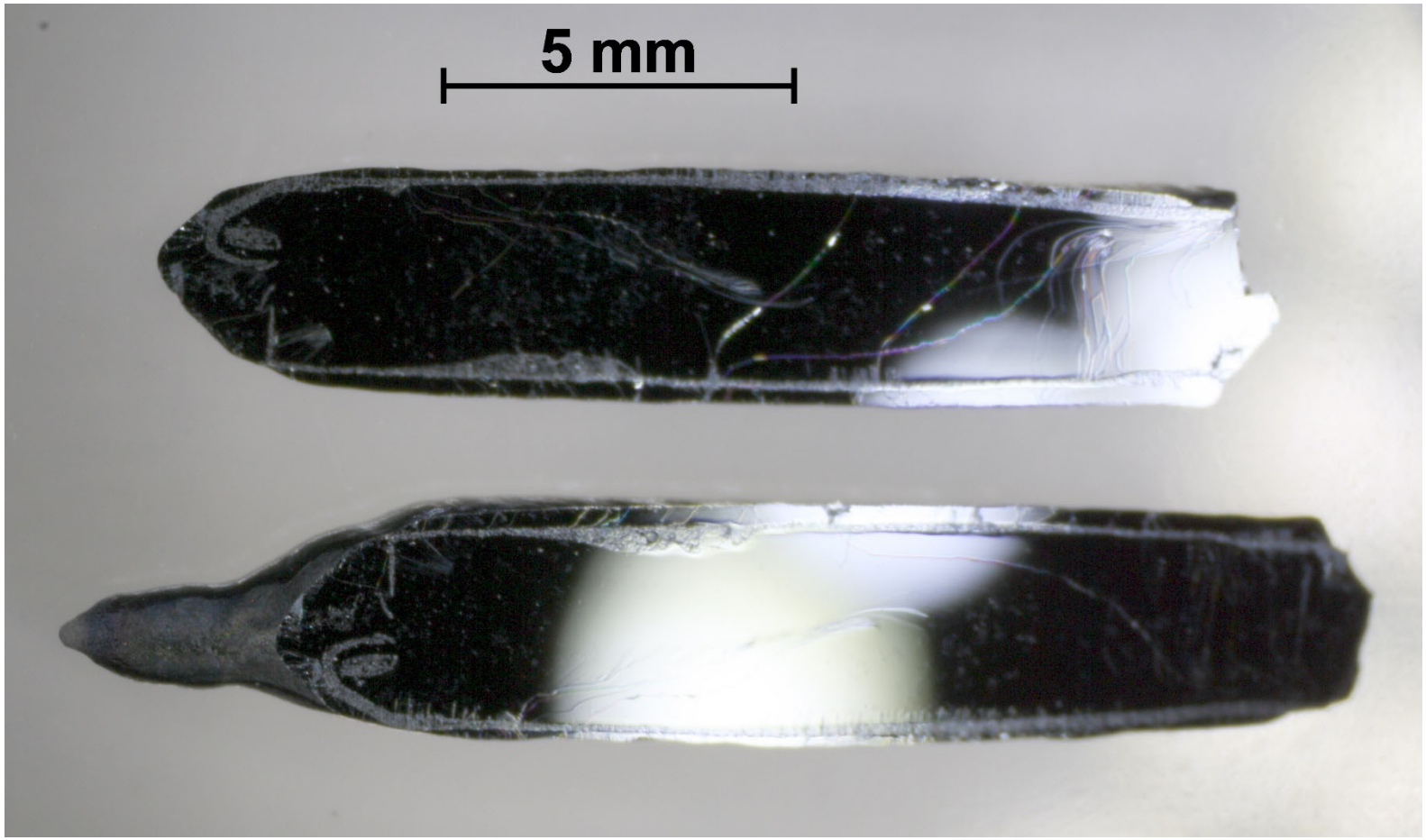

Crystalline pieces from section C8 of the as-grown material

As-grown crystalline material $Sr_{17}Ca_2Nb_{19}WO_{69.5-y}$

Sample No. 826

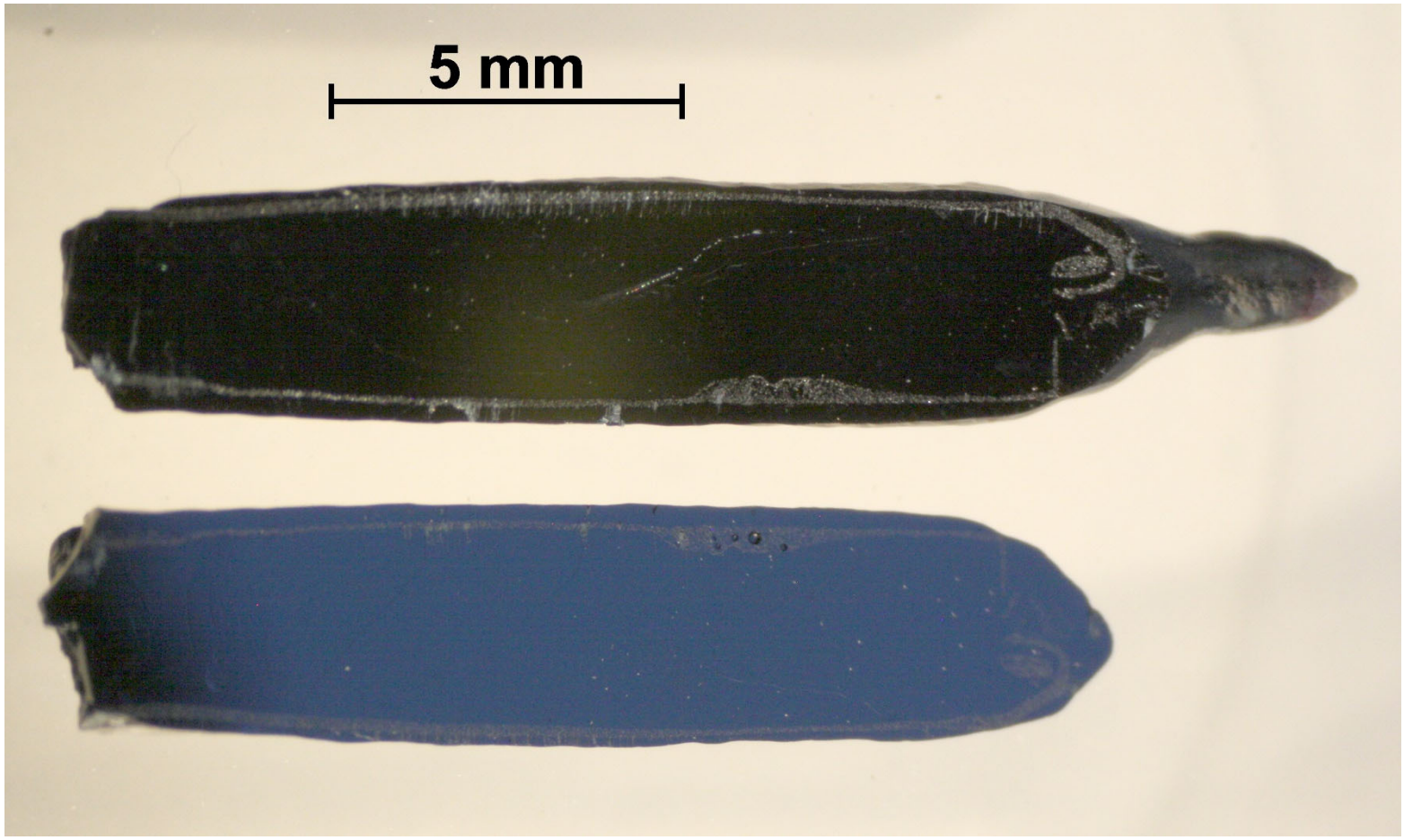

Another picture from the same crystalline pieces
from section C8 of the as-grown material

As-grown crystalline material $Sr_{17}Ca_2Nb_{19}WO_{69.5-y}$

Sample No. 826

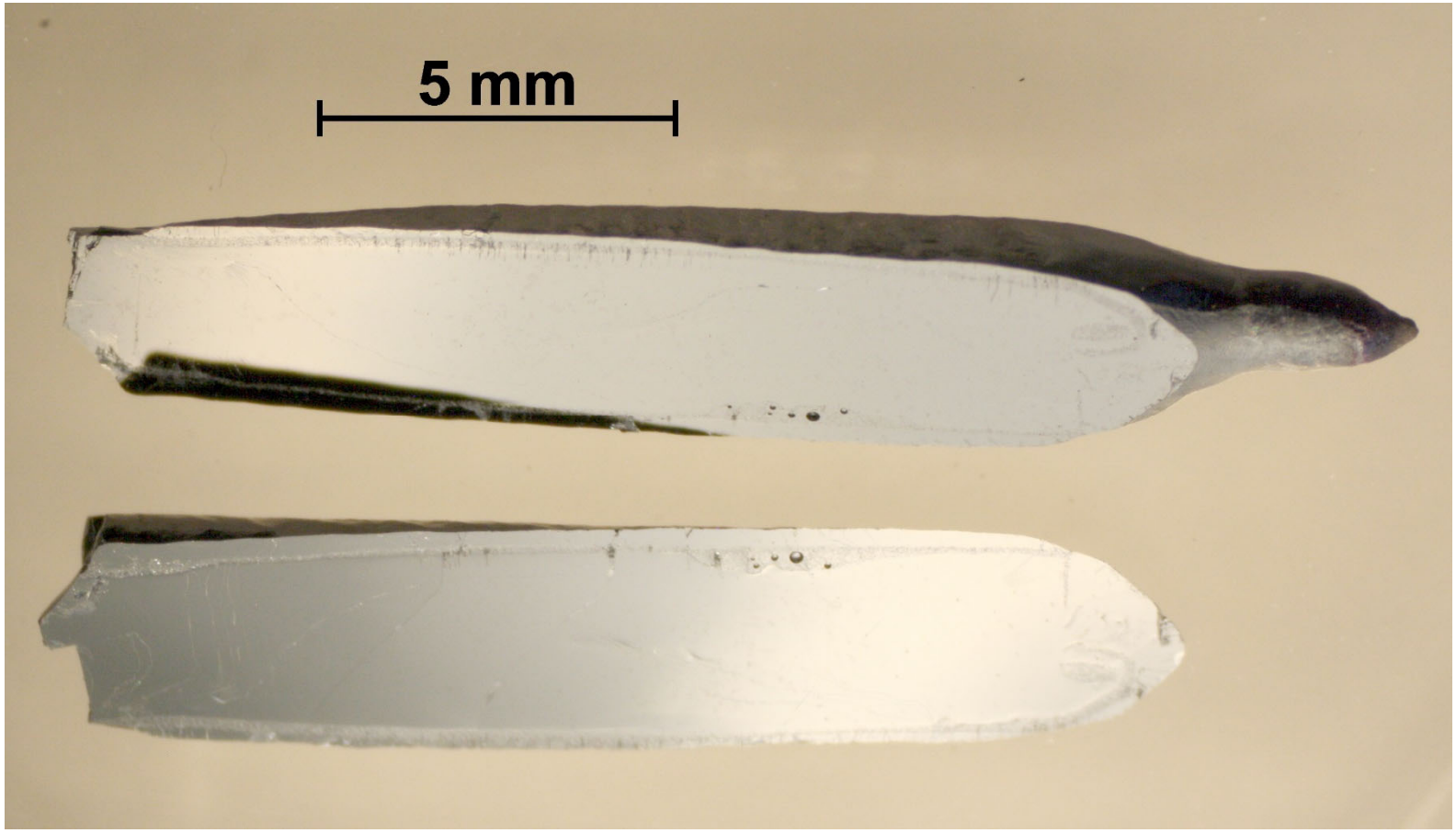

Further picture from the same crystalline pieces
from section C8 of the as-grown material

As-grown crystalline material $Sr_{17}Ca_2Nb_{19}WO_{69.5-y}$

Sample No. 826

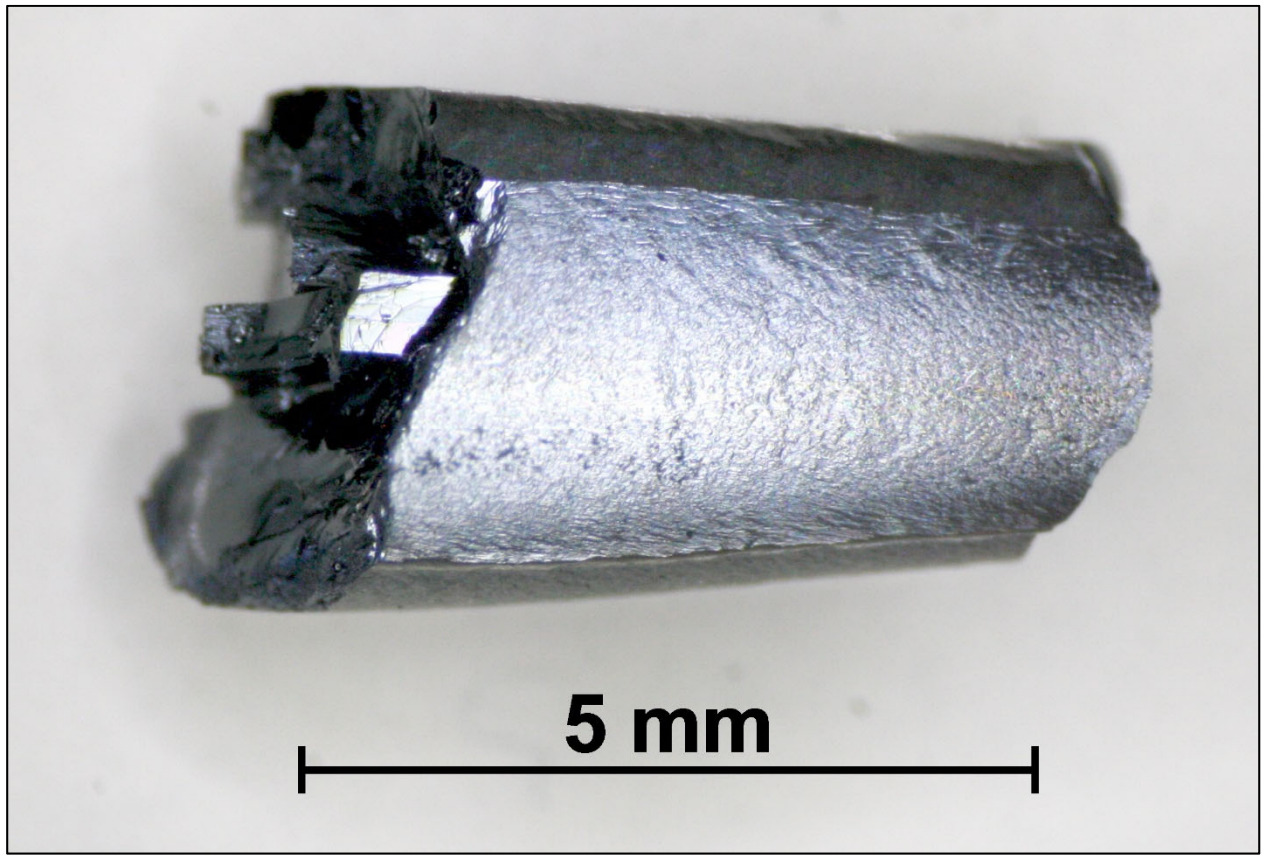

Crystalline piece from section C6 of the as-grown material

826 C6 $Sr_{17}Ca_2Nb_{19}WO_x$ Thermogravimetry

Thermogravimetric oxidation in flowing synth. air up to the fully oxidized composition with $x = x_F = 69.5$ for the determination of the oxygen content $x = 69.5 - y$ by using a thermogravimetric analyzer NETZSCH TG 209 F1 Libra

Pulverized crystalline material from section C6 of the as-grown sample $\rightarrow$ $x = 63.97$

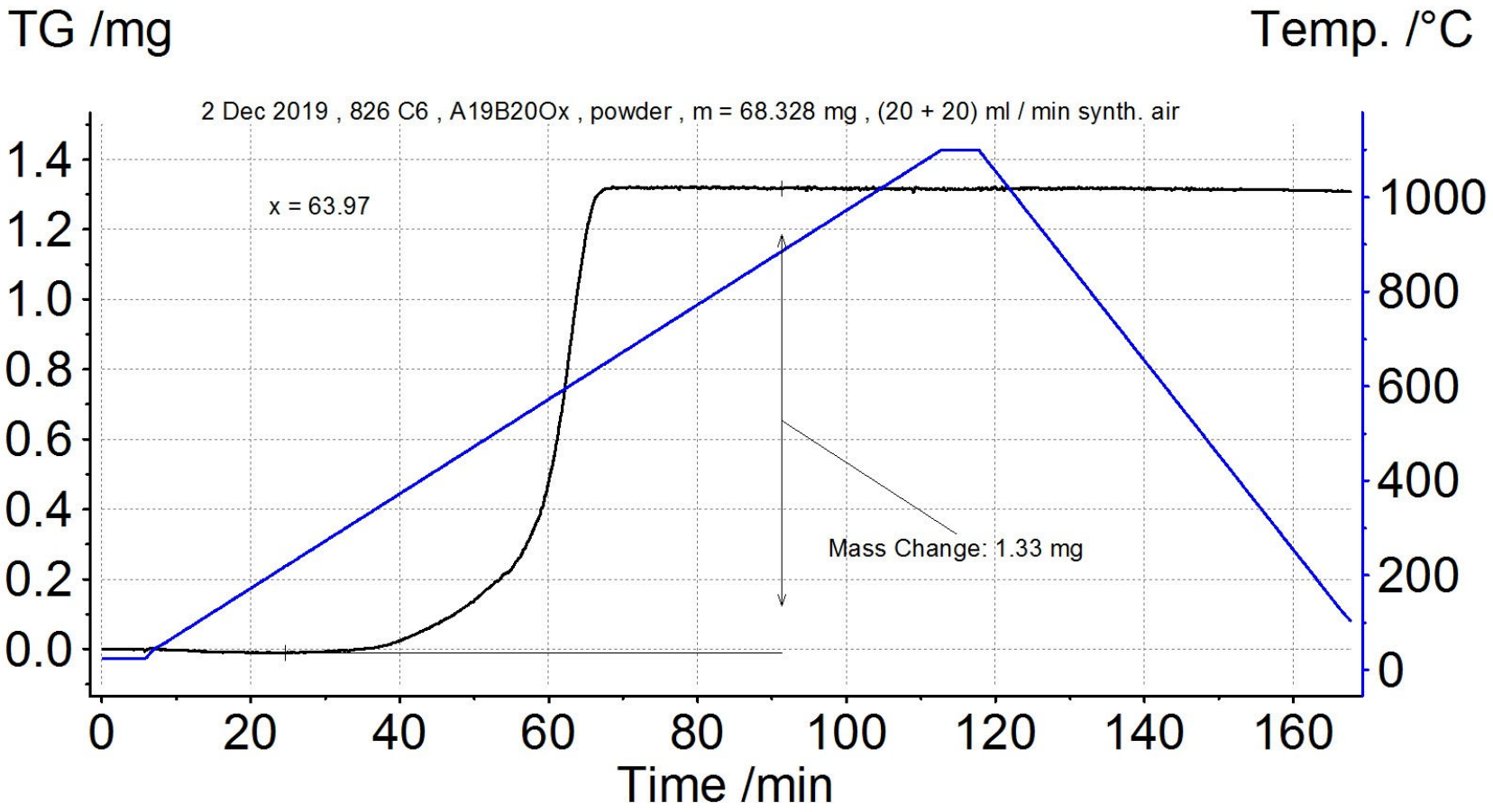

$Sr_{17}Ca_2Nb_{19}WO_{63.97}$ Valences of the Nb and W ions

Valence or oxidation states of the
Nb and W ions in $Sr_{17}Ca_2Nb_{19}WO_{63.97}$

The most likely scenario is W^{4+} / $5d^2$

↓

Charge neutrality and Sr^{2+}, Ca^{2+}, and O^{2-} → $Nb^{4.52+}$ / $4d^{0.48}$

↓

2 (5d) + 19 × 0.48 (4d) = 11.1 d-electrons
per formula and assumed size of the unit cell

826 C6 $Sr_{17}Ca_2Nb_{19}WO_{64}$ Powder x-ray diffraction

Powder x-ray diffraction pattern of pulverized crystalline material from section C6

Square root - linear plot • Background subtracted

All observed peaks fit to an orthorhombic *n* = 5 type structure

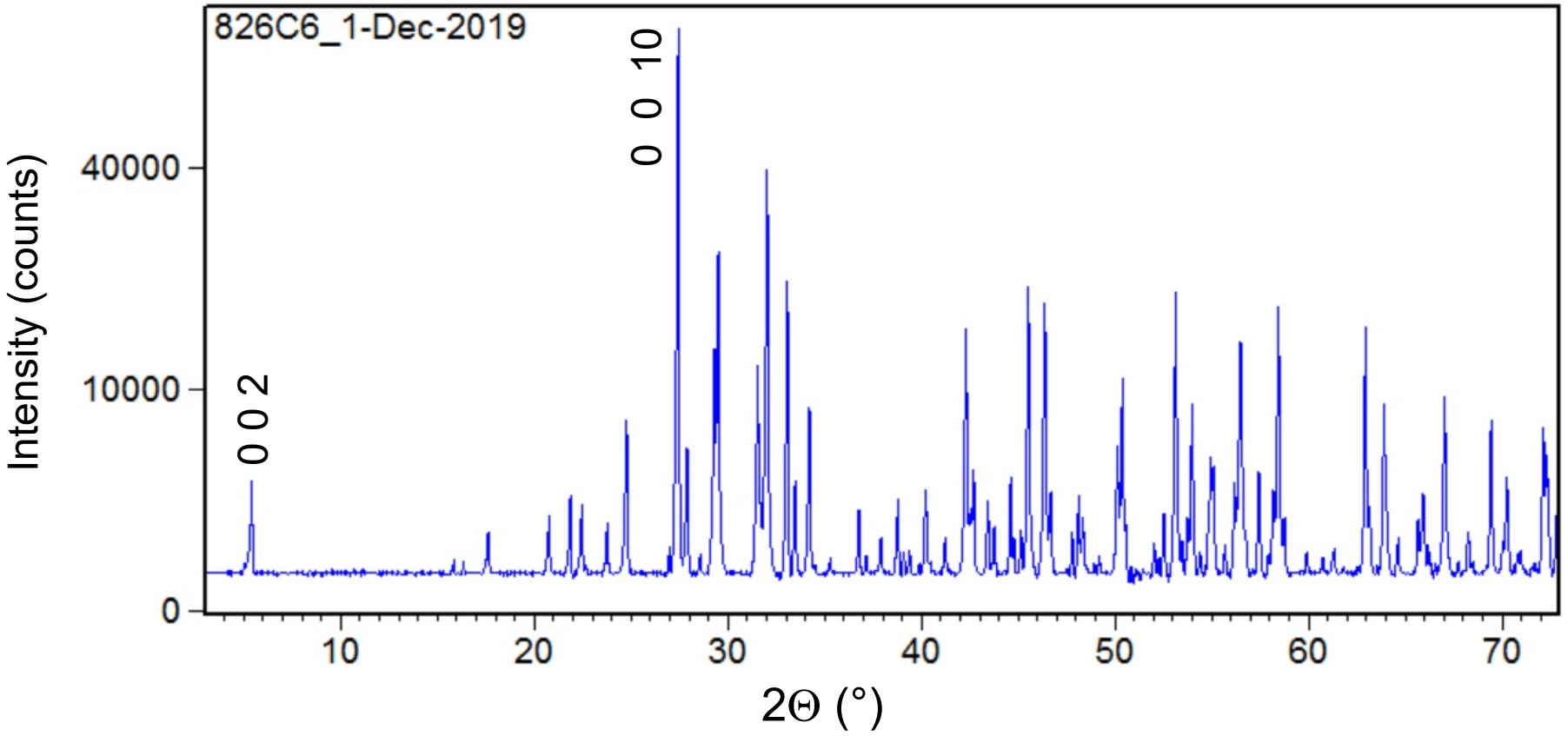

Available is an Excel file with the powder-x-ray diffraction data.
It is provided via the link which is specified on page 2

826 C6 $Sr_{17}Ca_2Nb_{19}WO_{64}$ Powder x-ray diffraction

	Observed peak position (°2θ)	d-spacing (Å)	Relative intensity (%)	h k l from lattice parameter refinement
Lowest angle peak Its position indicates the structure type of $A_nB_nO_{3n+2}$, namely n = 5 in this case	5.41	16.31	5	0 0 2
Highest intensity peak	27.44	3.25	100	0 0 10

Available is an Excel file with the powder-x-ray diffraction data.
It is provided via the link which is specified on page 2

826 C6 $Sr_{17}Ca_2Nb_{19}WO_{64}$ Powder x-ray diffraction

Results of lattice parameter refinement with $(h\ k\ l)_{max} = (10\ \ 10\ \ 20)$

Number of observed peaks	97
Number of indexed peaks	97
Number of unindexed peaks	0
Crystal structure type	$n = 5$ of $A_nB_nO_{3n+2}$
Crystal system	Orthorhombic
Bravais lattice	P
a (Å)	7.96
b (Å)	5.67
c (Å)	32.46
V (Å^3)	1465
$\lvert 2\theta_{obs} - 2\theta_{calc} \rvert$ for all observed and calculated peaks	$\leq 0.071°$
Figure of merit of the refinement or fit	16.8
Chi square of the refinement or fit	4.4×10^{-6}

Available is an Excel file with the powder-x-ray diffraction data.
It is provided via the link which is specified on page 2

826 C6 $Sr_{17}Ca_2Nb_{19}WO_{64}$ Magnetic measurements

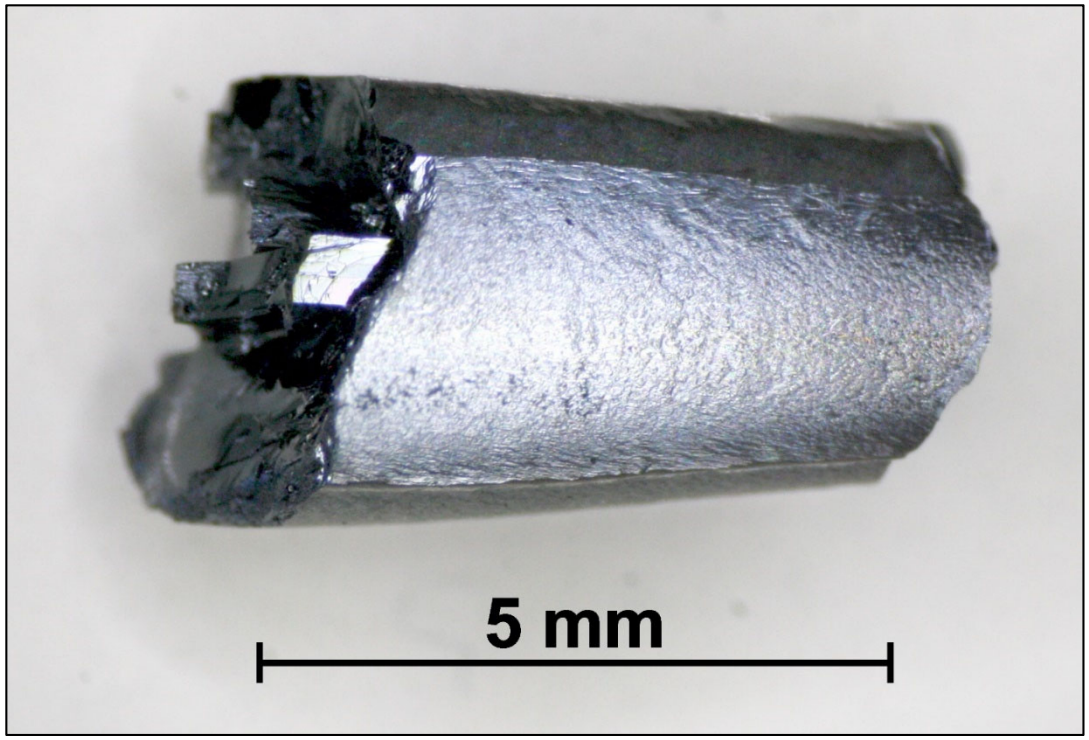

Crystalline piece C6-1 with m = 221 mg
from section C6 of the as-grown material

This piece was used to study its magnetic
properties by a SQUID magnetometer

826 C6 $Sr_{17}Ca_2Nb_{19}WO_{64}$ Magnetic susceptibility $\chi(T)$

DC magnetic moment M(T) measured by a Quantum Design SQUID magnetometer MPMS3

11.1 d-electrons from Nb^{4+} / $4d^1$ and W^{4+} / $5d^2$

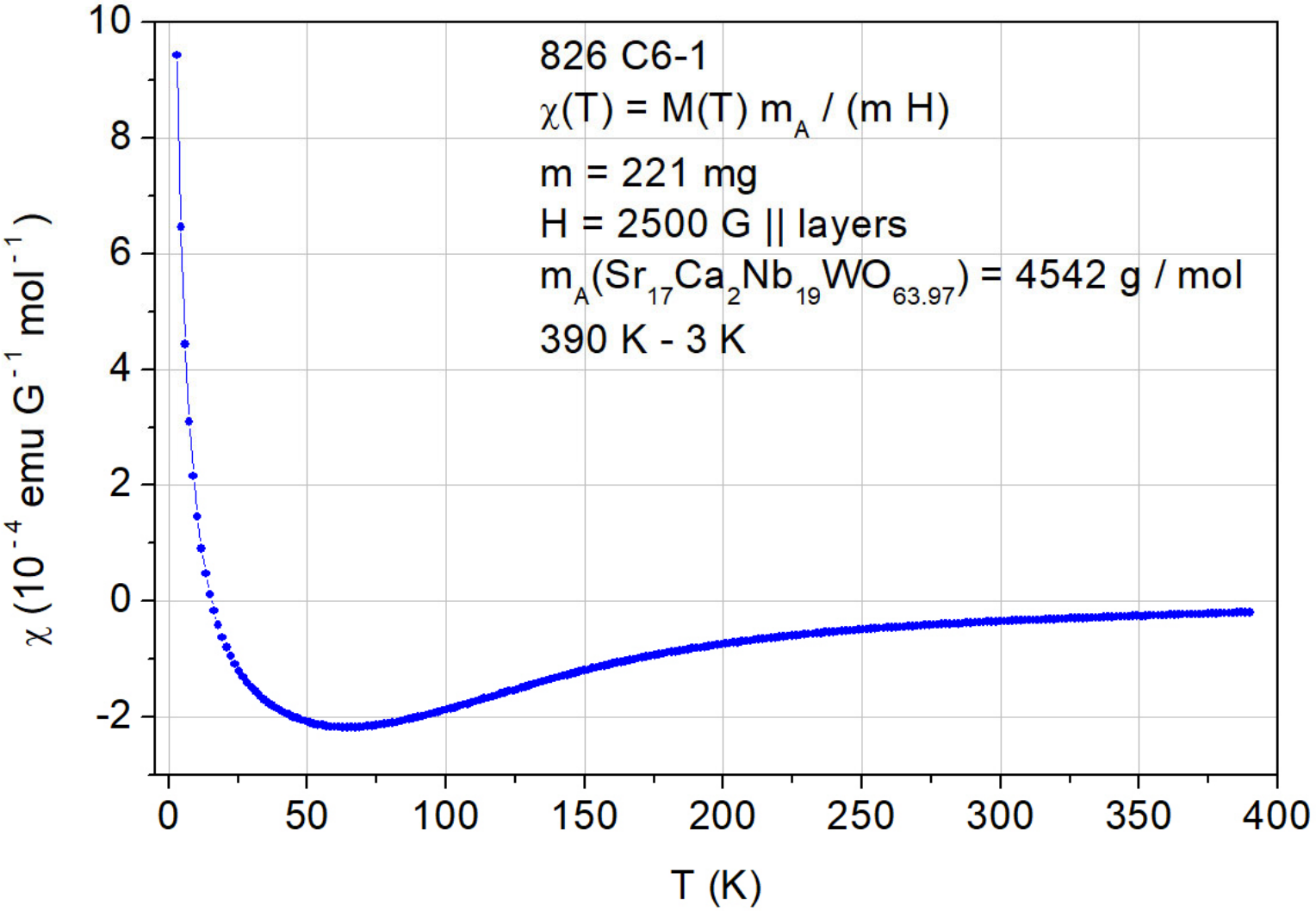

826 C6 $Sr_{17}Ca_2Nb_{19}WO_{64}$ Magnetic susceptibility $\chi(T)$

DC magnetic moment M(T) measured by a Quantum Design SQUID magnetometer MPMS3

11.1 d-electrons from Nb^{4+} / $4d^1$ and W^{4+} / $5d^2$

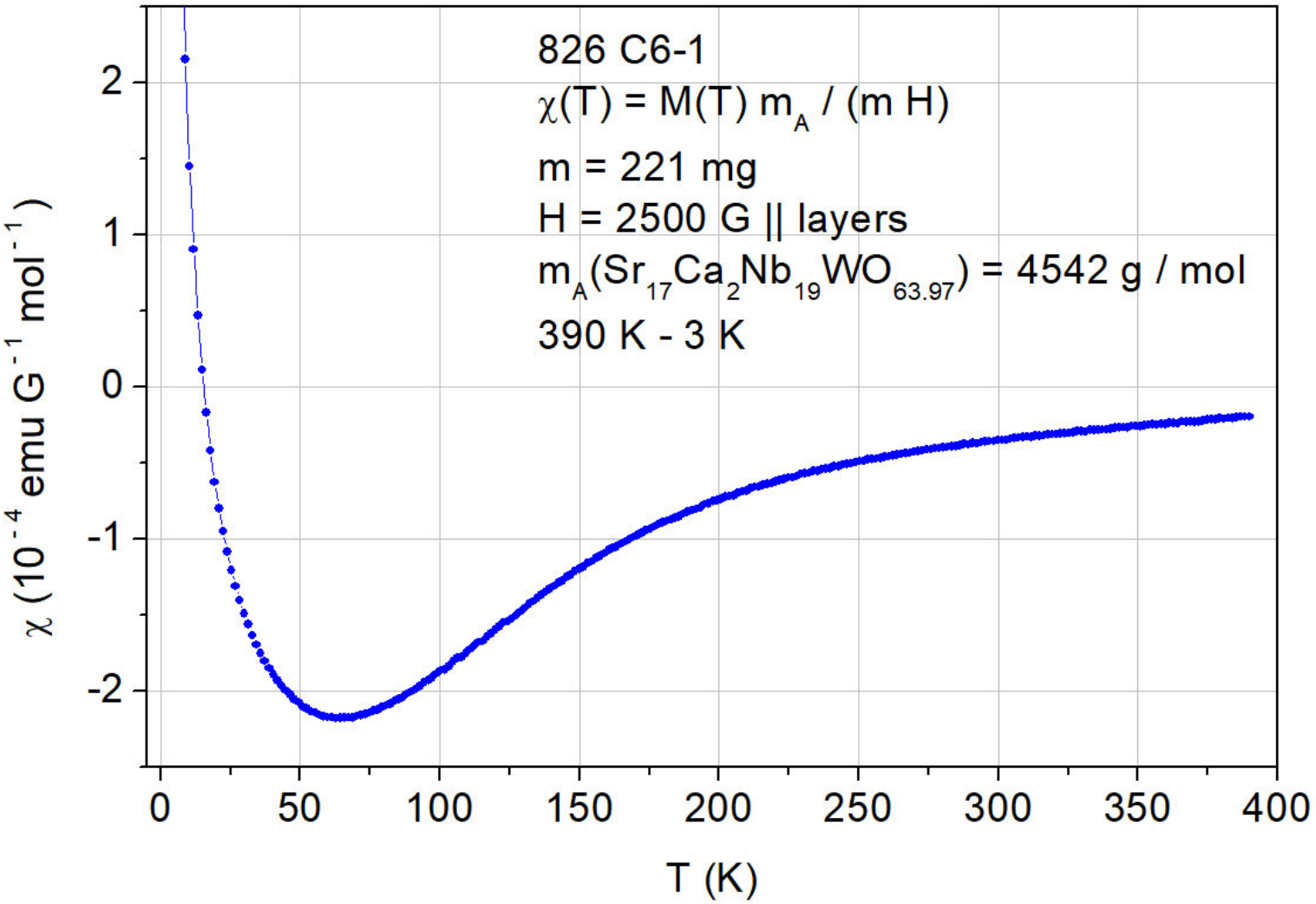

The behavior of $\chi(T)$ in the range from 390 K to 70 K is similar to that of $A_nB_nO_{3n+2}$ type quasi-1D metals. Thus this n = 5 type material is potentially also a quasi-1D metal

826 C6 $Sr_{17}Ca_2Nb_{19}WO_{64}$ Magnetic susceptibility $\chi(T)$

DC magnetic moment M(T) measured by a Quantum Design SQUID magnetometer MPMS3

11.1 d-electrons from Nb^{4+} / $4d^1$ and W^{4+} / $5d^2$

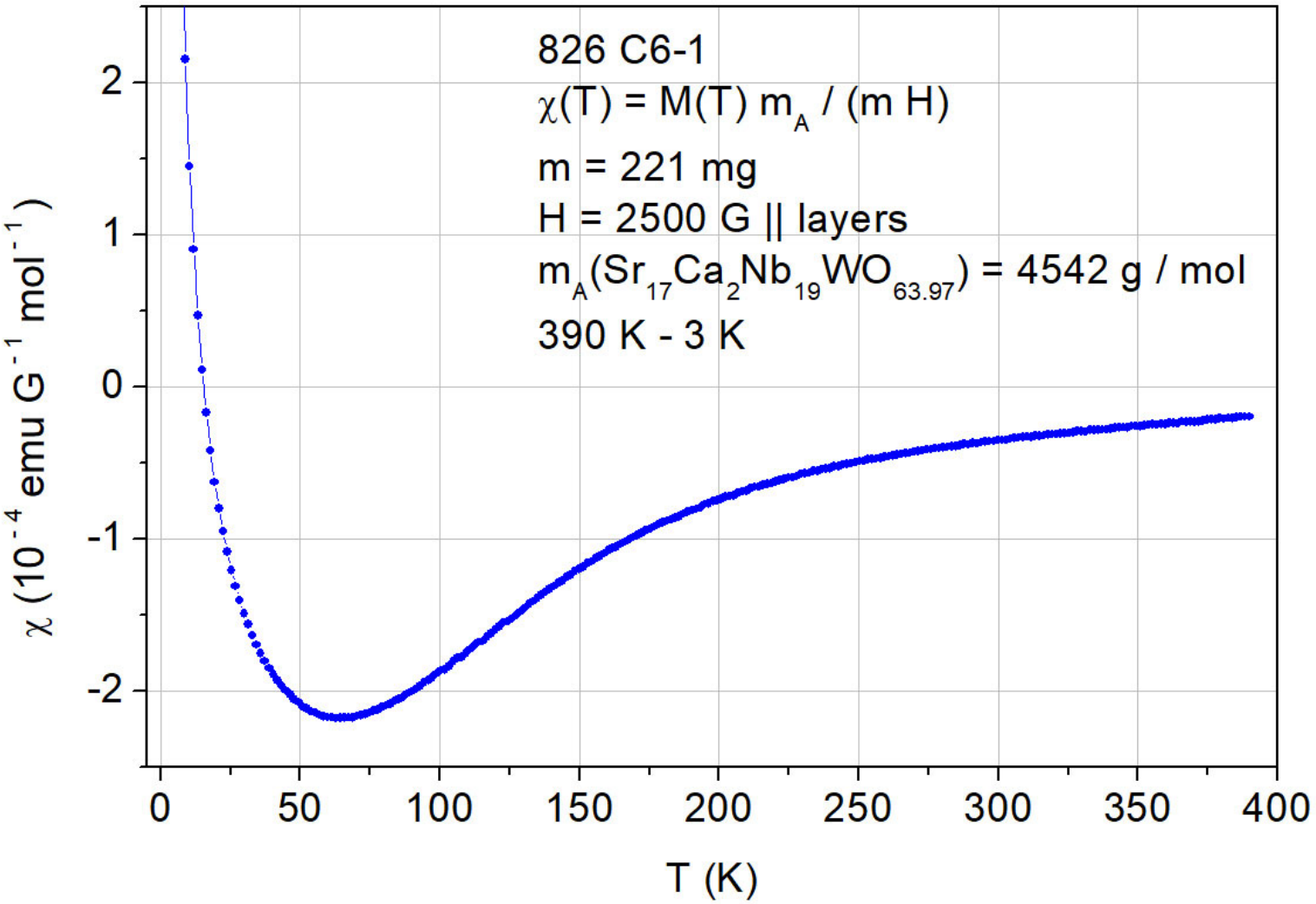

Increase of $\chi(T)$ below 60 K due to paramagnetic impurities or defect states or 5d electrons which become localized ?

826 C6 $Sr_{17}Ca_2Nb_{19}WO_{64}$ Magnetic susceptibility $\chi(T)$

DC magnetic moment M(T) measured by a Quantum Design SQUID magnetometer MPMS3

11.1 d-electrons from Nb^{4+} / $4d^1$ and W^{4+} / $5d^2$

D = diamagnetic contribution from closed electron shells of Sr^{2+}, Ca^{2+}, Nb^{5+}, W^{6+}, and O^{2-}

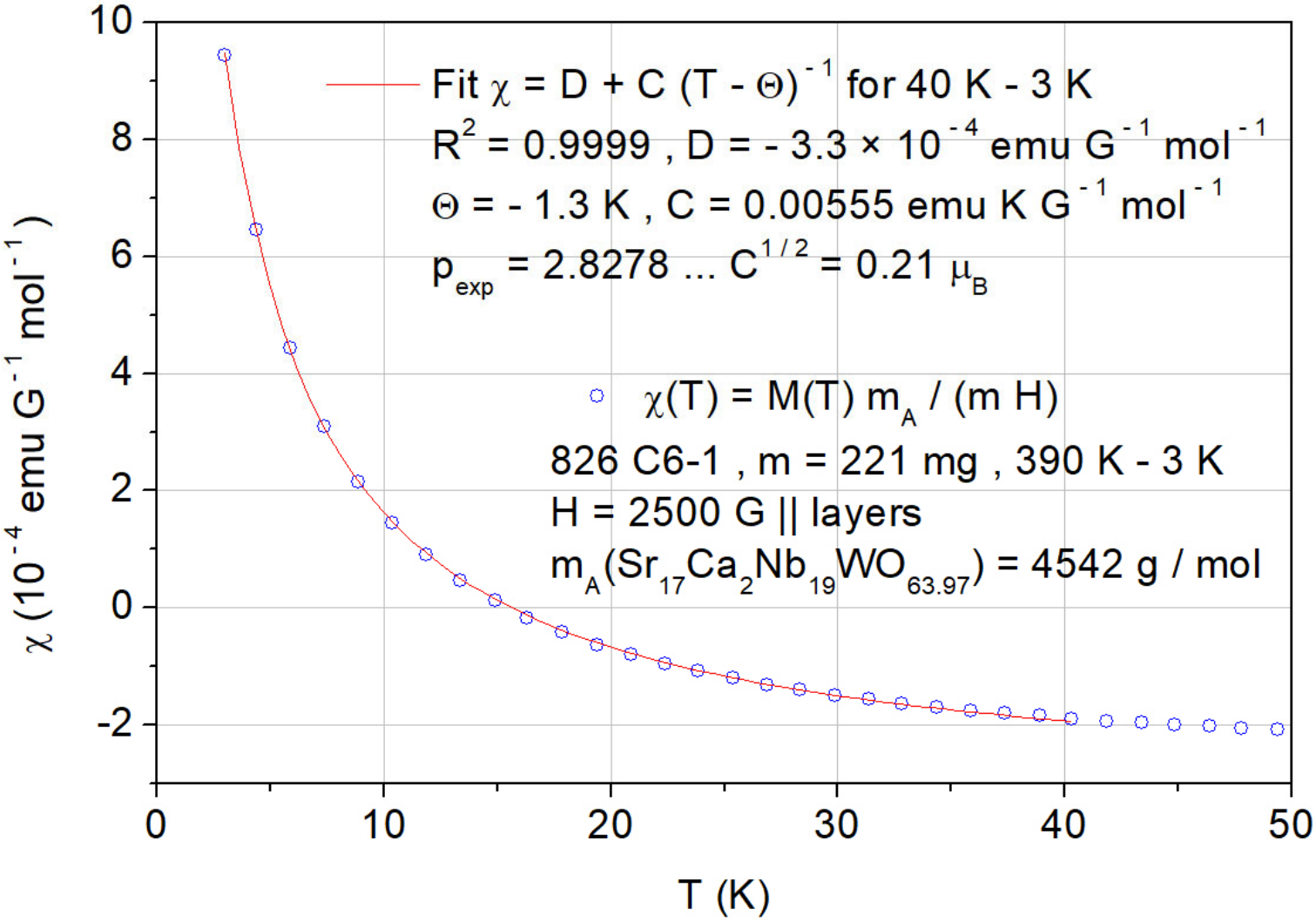

Ref. for the calculation of p_{exp}: Progress in Solid State Chemistry 36 (2008) 253

6.9.7 Magnetic susceptibility curves $\chi(T)$ of five compounds of the type $(Sr,Ca,Ba)_{19}Nb_{19}WO_x$ ($64 \leq x \leq 66$) in one graphics ...

Magnetic susceptibility χ(T) of melt-grown Sr- and O-deficient *n* = 5 type $(Sr,Ca,Ba)_{19}Nb_{19}WO_x$ ($64 \leq x \leq 66$)

χ(T) of the materials which are presented in the previous parts 6.9.2 - 6.9.6

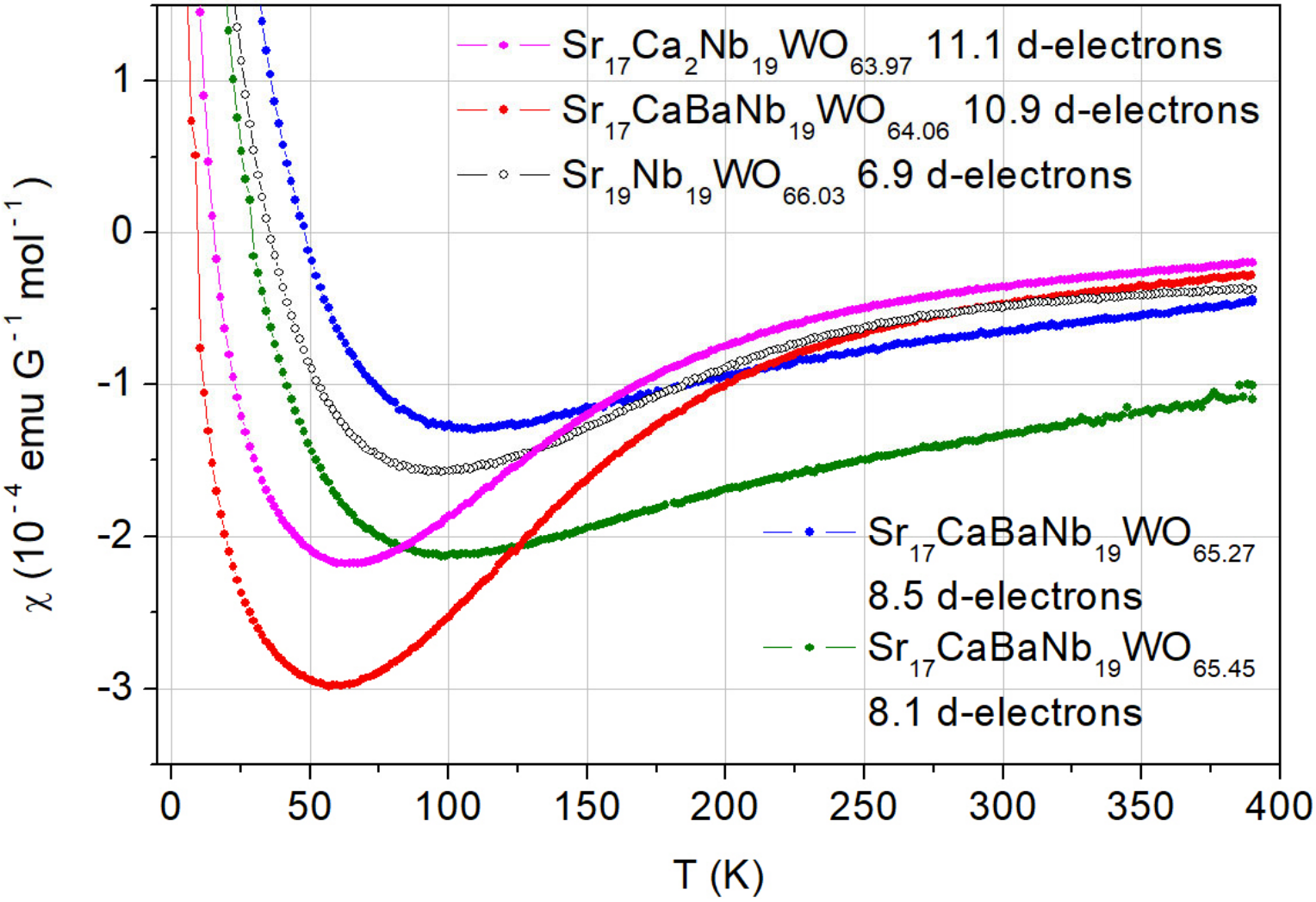

The specified number of d-electrons per formula and assumed size of the unit cell are from Nb^{4+} / $4d^1$ and W^{4+} / $5d^2$

Magnetic susceptibility χ(T) of melt-grown Sr- and O-deficient $n = 5$ type $(Sr,Ca,Ba)_{19}Nb_{19}WO_x$ ($64 \leq x \leq 66$)

The Sr-deficient Schückel-Müller-Buschbaum type phases $Sr_{17}Ca_2Nb_{19}WO_{64}$ and $Sr_{17}CaBaNb_{19}WO_{64}$ differ from the other compounds

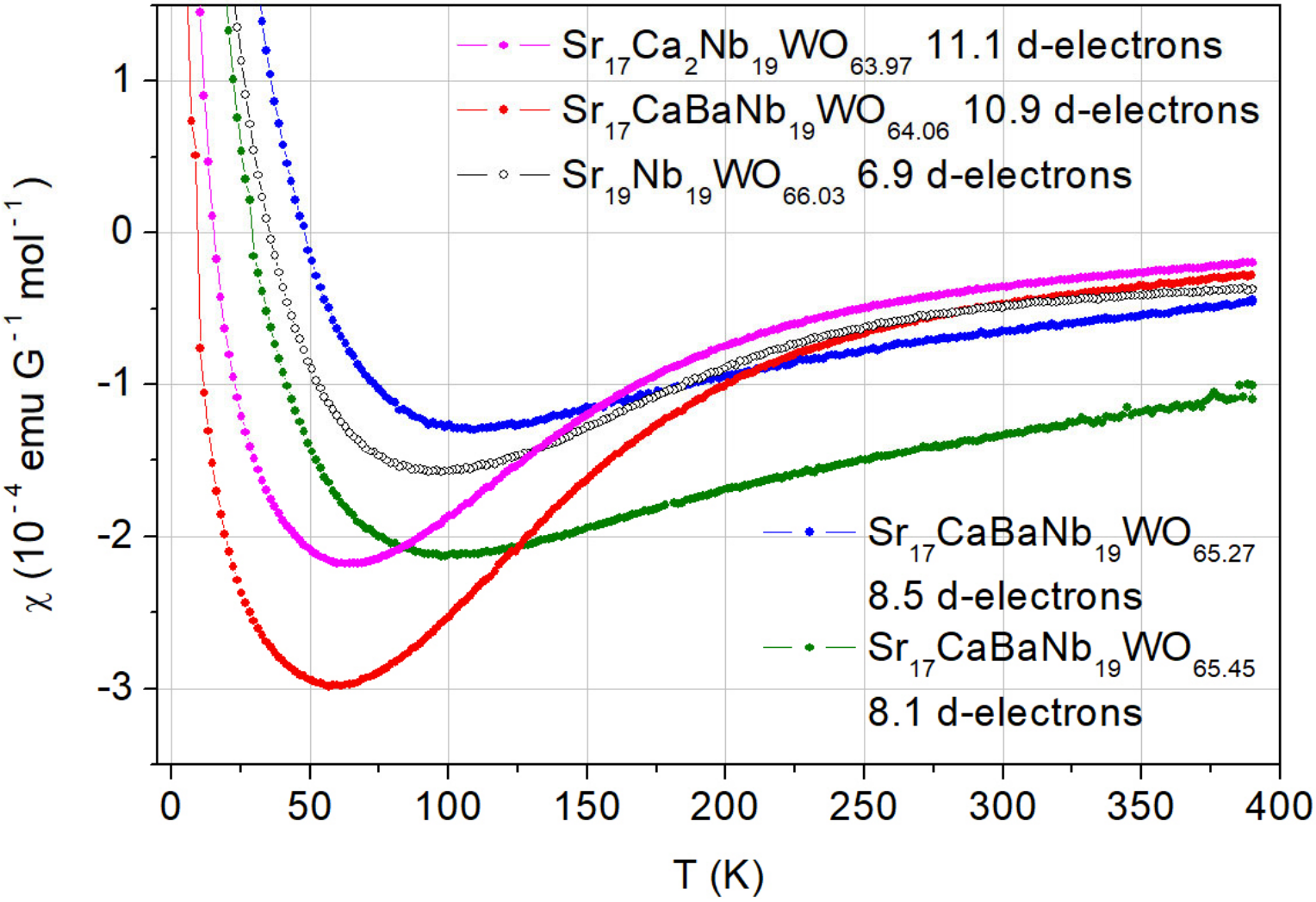

The specified number of d-electrons per formula and assumed size of the unit cell are from Nb^{4+} / $4d^1$ and W^{4+} / $5d^2$

6.9.8 The Sr-deficient Schückel-Müller-Buschbaum type phases $Sr_{17}Ca_2Nb_{19}WO_{64}$ and $Sr_{17}CaBaNb_{19}WO_{64}$: Comments and open questions ...

Let's first recall from part 6.7 the crystal structure of the *n* = 5 type Schückel-Müller-Buschbaum phase $SrNbO_{3.2} = Sr_5Nb_5O_{16} = Sr_{20}Nb_{20}O_{64}$ and the *n* = 5 type quasi-1D metal $SrNbO_{3.4} = Sr_5Nb_5O_{17} = Sr_{20}Nb_{20}O_{68}$ ...

The crystal structure of the *n* = 5 types $Sr_{20}Nb_{20}O_{64}$ and $Sr_{20}Nb_{20}O_{68}$

= NbO_6 octahedra (O located at the corners, Nb hidden in the center)

= NbO_4 (O located at the corners, Nb in the center)

= Sr

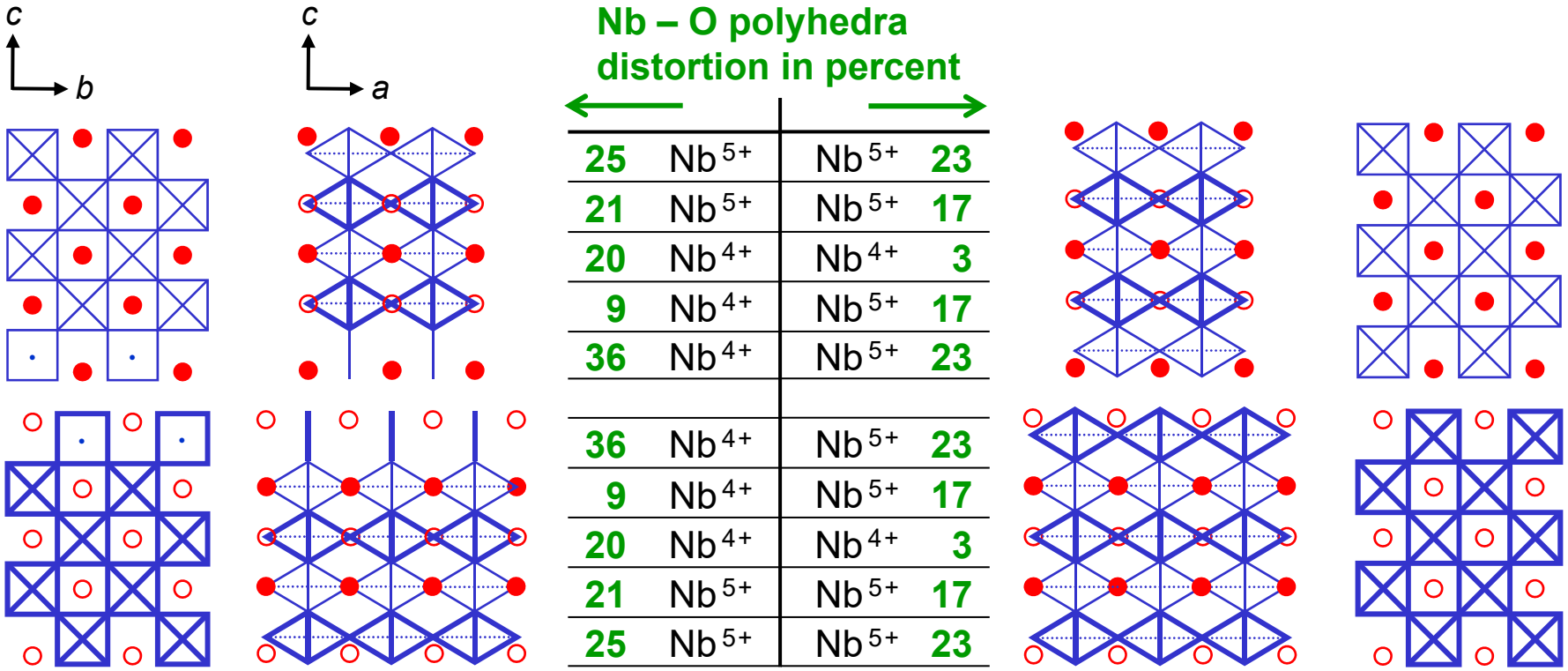

Nb – O polyhedra distortion in percent

25	Nb^{5+}	Nb^{5+}	23
21	Nb^{5+}	Nb^{5+}	17
20	Nb^{4+}	Nb^{4+}	3
9	Nb^{4+}	Nb^{5+}	17
36	Nb^{4+}	Nb^{5+}	23
36	Nb^{4+}	Nb^{5+}	23
9	Nb^{4+}	Nb^{5+}	17
20	Nb^{4+}	Nb^{4+}	3
21	Nb^{5+}	Nb^{5+}	17
25	Nb^{5+}	Nb^{5+}	23

$SrNbO_{3.2} = Sr_5Nb_5O_{16} = Sr_{20}Nb_{20}O_{64}$

Non-centrosymmetric !

Physical properties = ?

K. Schückel and Hk. Müller-Buschbaum
Z. Anorg. Allg. Chem. 528 (1985) 91

Nb^{5+} / $4d^0$

Nb^{4+} / $4d^1$

F. Lichtenberg et al., Prog. Solid State Chem. 36 (2008) 253

$SrNbO_{3.4} = Sr_5Nb_5O_{17} = Sr_{20}Nb_{20}O_{68}$

Centrosymmetric

Quasi-1D metal

S. C. Abrahams et al.
Acta Cryst. B 54 (1998) 399

The crystal structure of the n = 5 types $Sr_{20}Nb_{20}O_{64}$ and $Sr_{20}Nb_{20}O_{68}$

= NbO_6 octahedra (O located at the corners, Nb hidden in the center)

= NbO_4 (O located at the corners, Nb in the center)

(Fully ordered) oxygen vacancies are located at opposite boundaries of the layers or slabs

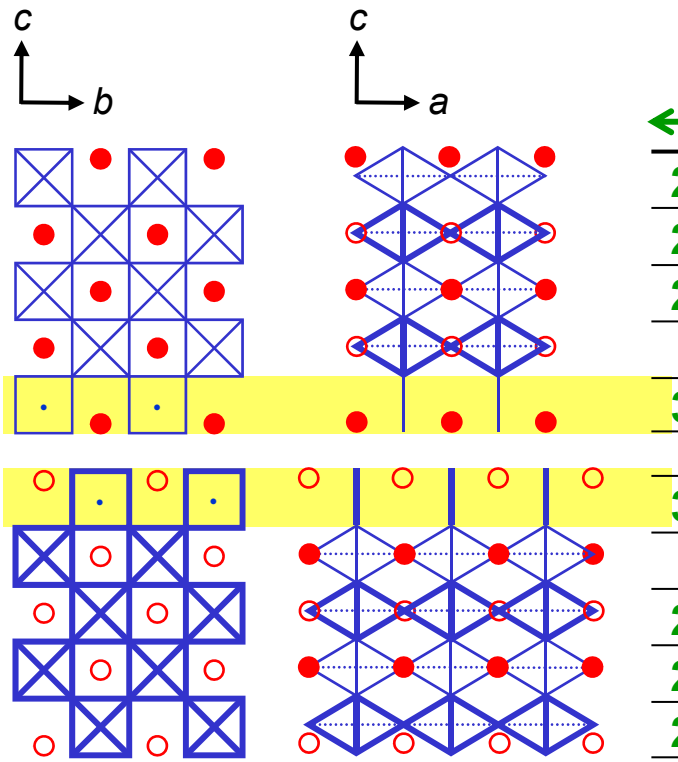

Nb – O polyhedra distortion in percent

25	Nb^{5+}	Nb^{5+}	23
21	Nb^{5+}	Nb^{5+}	17
20	Nb^{4+}	Nb^{4+}	3
9	Nb^{4+}	Nb^{5+}	17
36	Nb^{4+}	Nb^{5+}	23
36	Nb^{4+}	Nb^{5+}	23
9	Nb^{4+}	Nb^{5+}	17
20	Nb^{4+}	Nb^{4+}	3
21	Nb^{5+}	Nb^{5+}	17
25	Nb^{5+}	Nb^{5+}	23

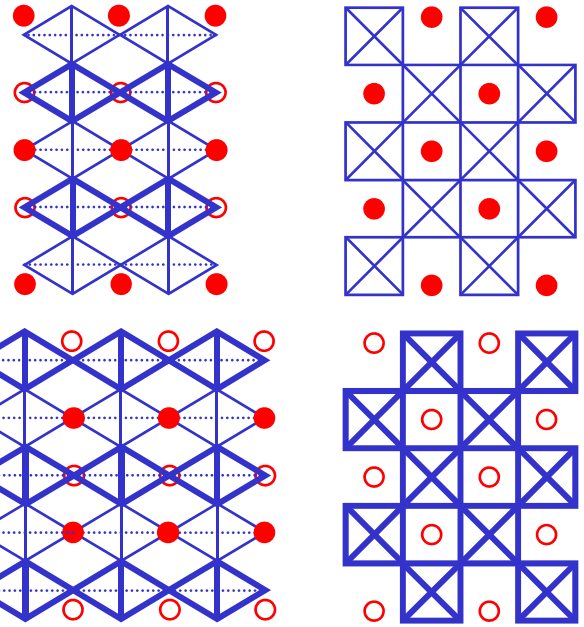

$SrNbO_{3.2} = Sr_5Nb_5O_{16} = Sr_{20}Nb_{20}O_{64}$

Non-centrosymmetric !

Physical properties = ?

K. Schückel and Hk. Müller-Buschbaum
Z. Anorg. Allg. Chem. 528 (1985) 91

Nb^{5+} / $4d^0$

Nb^{4+} / $4d^1$

F. Lichtenberg et al., Prog. Solid State Chem. 36 (2008) 253

$SrNbO_{3.4} = Sr_5Nb_5O_{17} = Sr_{20}Nb_{20}O_{68}$

Centrosymmetric

Quasi-1D metal

S. C. Abrahams et al.
Acta Cryst. B 54 (1998) 399

The crystal structure of the *n* = 5 type $Sr_{20}Nb_{20}O_{64}$

= NbO_6 octahedra (O located at the corners, Nb hidden in the center)

= NbO_4 (O located at the corners, Nb in the center)

(Fully ordered) oxygen vacancies are located at opposite boundaries of the layers or slabs

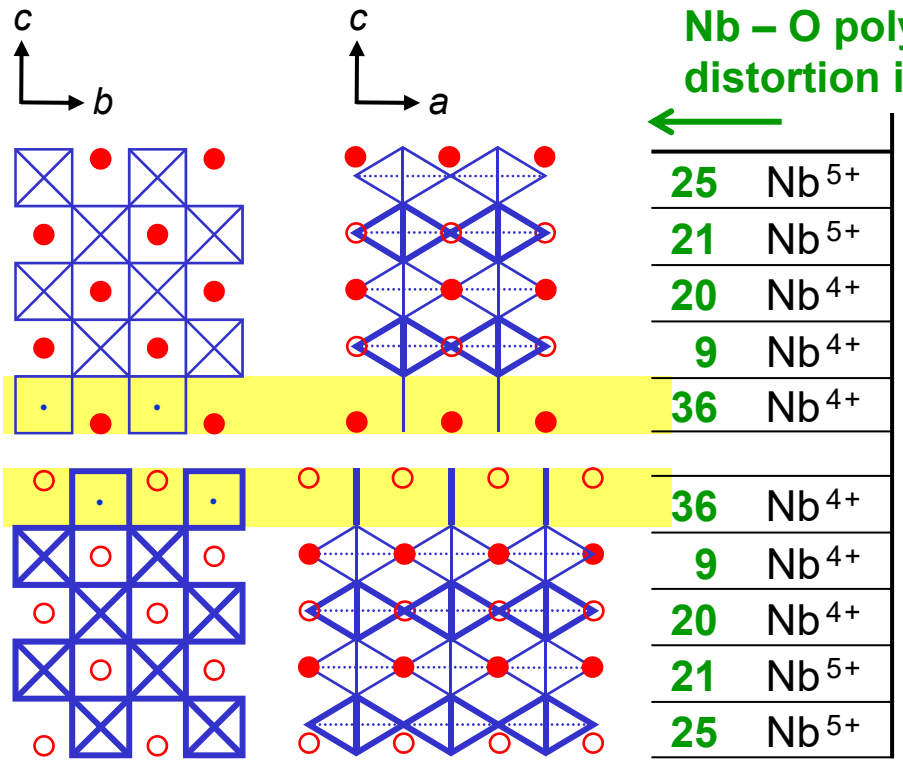

Nb – O polyhedra distortion in percent

25	Nb^{5+}
21	Nb^{5+}
20	Nb^{4+}
9	Nb^{4+}
36	Nb^{4+}
36	Nb^{4+}
9	Nb^{4+}
20	Nb^{4+}
21	Nb^{5+}
25	Nb^{5+}

In case of the Sr-deficient Schückel-Müller-Buschbaum type phases $Sr_{17}Ca_2Nb_{19}WO_{64}$ and $Sr_{17}CaBaNb_{19}WO_{64}$ the non-occupied Sr sites are probably also located at the boundary of the layers or slabs because there the bonding forces are probably smaller than in the other regions

$SrNbO_{3.2} = Sr_5Nb_5O_{16} = Sr_{20}Nb_{20}O_{64}$

Non-centrosymmetric !

Physical properties = ?

Nb^{5+} / $4d^0$

Nb^{4+} / $4d^1$

K. Schückel and Hk. Müller-Buschbaum
Z. Anorg. Allg. Chem. 528 (1985) 91

F. Lichtenberg et al., Prog. Solid State Chem. 36 (2008) 253

The crystal structure of the *n* = 5 types $Sr_{20}Nb_{20}O_{64}$ and $Sr_{20}Nb_{20}O_{68}$

= NbO_6 octahedra (O located at the corners, Nb hidden in the center)

= NbO_4 (O located at the corners, Nb in the center)

Along *c*-axis symmetric distribution of Nb^{5+} and Nb^{4+} and distortions

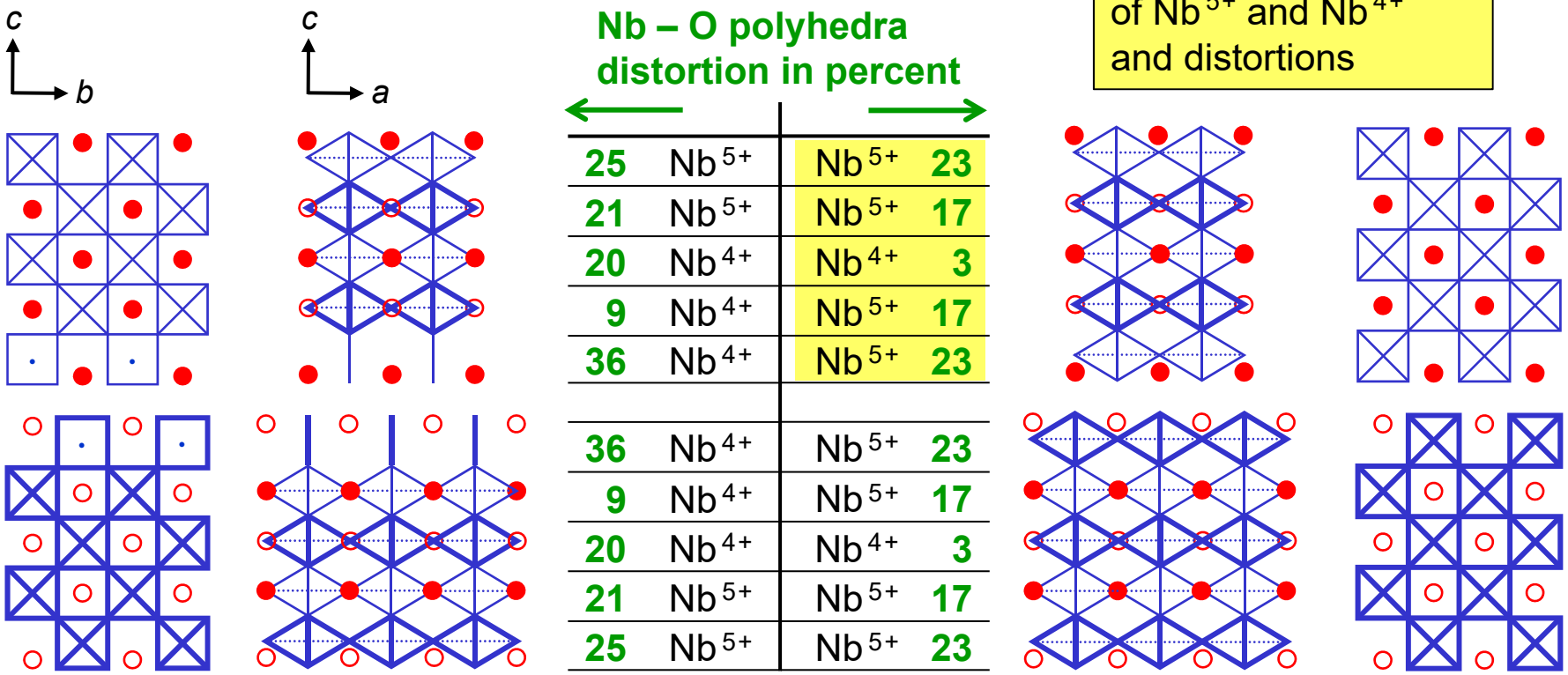

Nb – O polyhedra distortion in percent

25	Nb^{5+}	Nb^{5+}	23
21	Nb^{5+}	Nb^{5+}	17
20	Nb^{4+}	Nb^{4+}	3
9	Nb^{4+}	Nb^{5+}	17
36	Nb^{4+}	Nb^{5+}	23
36	Nb^{4+}	Nb^{5+}	23
9	Nb^{4+}	Nb^{5+}	17
20	Nb^{4+}	Nb^{4+}	3
21	Nb^{5+}	Nb^{5+}	17
25	Nb^{5+}	Nb^{5+}	23

$SrNbO_{3.2} = Sr_5Nb_5O_{16} = Sr_{20}Nb_{20}O_{64}$

Non-centrosymmetric !

Physical properties = ?

K. Schückel and Hk. Müller-Buschbaum
Z. Anorg. Allg. Chem. 528 (1985) 91

Nb^{5+} / $4d^0$

Nb^{4+} / $4d^1$

F. Lichtenberg et al., Prog. Solid State Chem. 36 (2008) 253

$SrNbO_{3.4} = Sr_5Nb_5O_{17} = Sr_{20}Nb_{20}O_{68}$

Centrosymmetric

Quasi-1D metal

S. C. Abrahams et al.
Acta Cryst. B 54 (1998) 399

The crystal structure of the *n* = 5 types $Sr_{20}Nb_{20}O_{64}$ and $Sr_{20}Nb_{20}O_{68}$

= NbO_6 octahedra (O located at the corners, Nb hidden in the center)

= NbO_4 (O located at the corners, Nb in the center)

Along *c*-axis asymmetric distribution of Nb^{5+} and Nb^{4+} and distortions

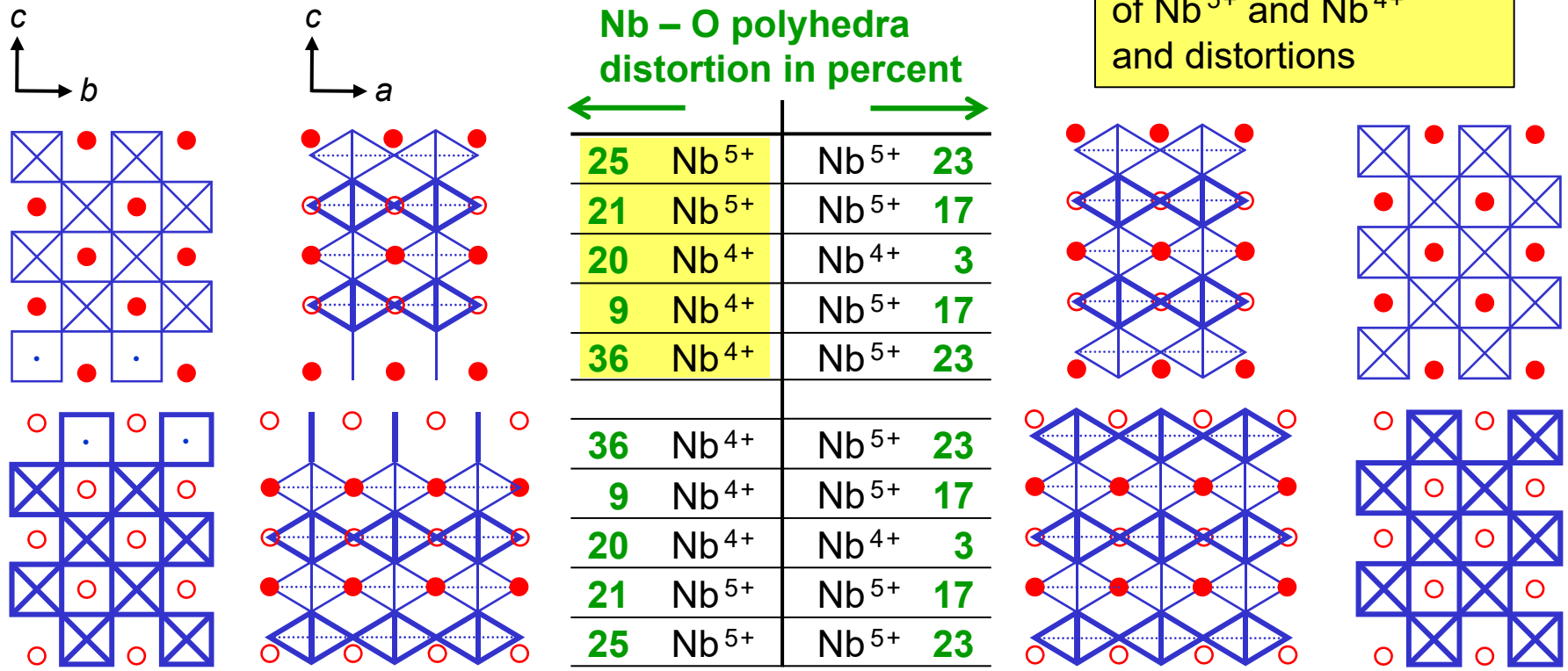

Nb – O polyhedra distortion in percent

25	Nb^{5+}	Nb^{5+}	23
21	Nb^{5+}	Nb^{5+}	17
20	Nb^{4+}	Nb^{4+}	3
9	Nb^{4+}	Nb^{5+}	17
36	Nb^{4+}	Nb^{5+}	23
36	Nb^{4+}	Nb^{5+}	23
9	Nb^{4+}	Nb^{5+}	17
20	Nb^{4+}	Nb^{4+}	3
21	Nb^{5+}	Nb^{5+}	17
25	Nb^{5+}	Nb^{5+}	23

$SrNbO_{3.2} = Sr_5Nb_5O_{16} = Sr_{20}Nb_{20}O_{64}$

Non-centrosymmetric !

Physical properties = ?

K. Schückel and Hk. Müller-Buschbaum
Z. Anorg. Allg. Chem. 528 (1985) 91

Nb^{5+} / $4d^0$

Nb^{4+} / $4d^1$

F. Lichtenberg et al., Prog. Solid State Chem. 36 (2008) 253

$SrNbO_{3.4} = Sr_5Nb_5O_{17} = Sr_{20}Nb_{20}O_{68}$

Centrosymmetric

Quasi-1D metal

S. C. Abrahams et al.
Acta Cryst. B 54 (1998) 399

The crystal structure of the *n* = 5 types $Sr_{20}Nb_{20}O_{64}$ and $Sr_{20}Nb_{20}O_{68}$

= NbO_6 octahedra (O located at the corners, Nb hidden in the center)

= NbO_4 (O located at the corners, Nb in the center)

Largest contribution to electronic DOS / metallic behavior from these regions, see part 6.2

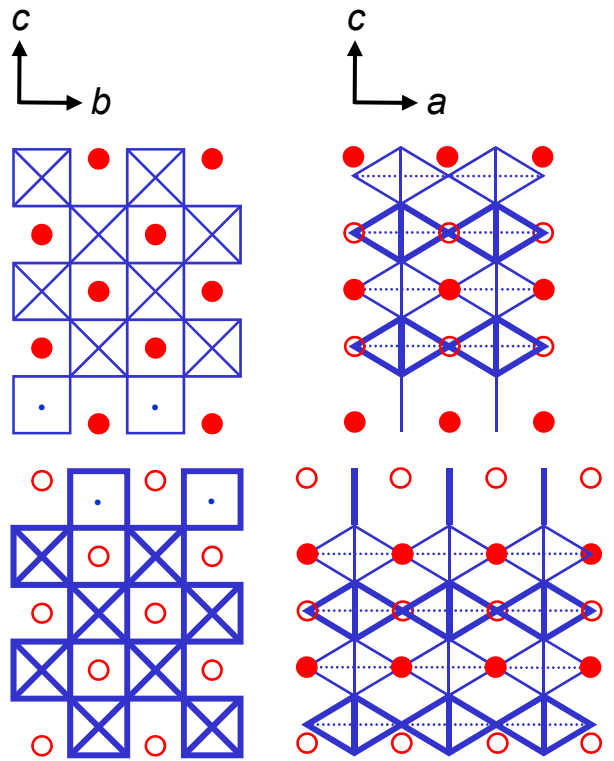

Nb – O polyhedra distortion in percent

25	Nb^{5+}	Nb^{5+}	23
21	Nb^{5+}	Nb^{5+}	17
20	Nb^{4+}	Nb^{4+}	3
9	Nb^{4+}	Nb^{5+}	17
36	Nb^{4+}	Nb^{5+}	23
36	Nb^{4+}	Nb^{5+}	23
9	Nb^{4+}	Nb^{5+}	17
20	Nb^{4+}	Nb^{4+}	3
21	Nb^{5+}	Nb^{5+}	17
25	Nb^{5+}	Nb^{5+}	23

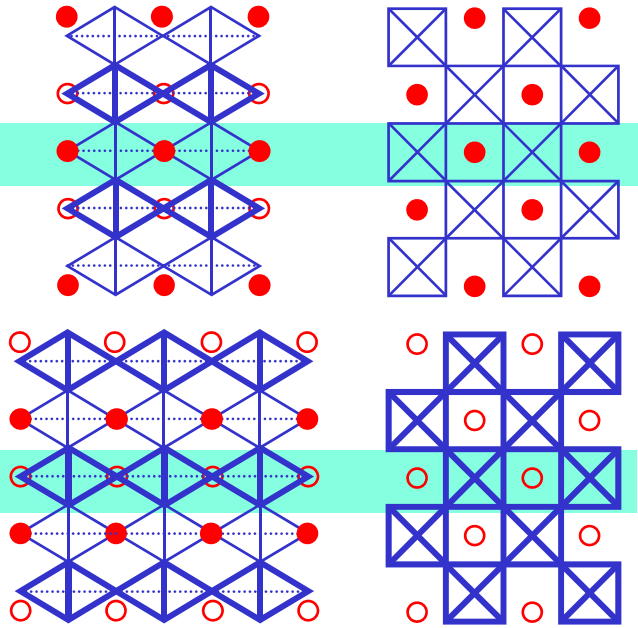

$SrNbO_{3.2} = Sr_5Nb_5O_{16} = Sr_{20}Nb_{20}O_{64}$

Non-centrosymmetric !

Physical properties = ?

K. Schückel and Hk. Müller-Buschbaum
Z. Anorg. Allg. Chem. 528 (1985) 91

Nb^{5+} / $4d^0$

Nb^{4+} / $4d^1$

F. Lichtenberg et al., Prog. Solid State Chem. 36 (2008) 253

$SrNbO_{3.4} = Sr_5Nb_5O_{17} = Sr_{20}Nb_{20}O_{68}$

Centrosymmetric

Quasi-1D metal

S. C. Abrahams et al.
Acta Cryst. B 54 (1998) 399

The crystal structure of the *n* = 5 types $Sr_{20}Nb_{20}O_{64}$ and $Sr_{20}Nb_{20}O_{68}$

= NbO_6 octahedra (O located at the corners, Nb hidden in the center)

= NbO_4 (O located at the corners, Nb in the center)

Largest contribution to electronic DOS / potential metallic behavior from these regions ?

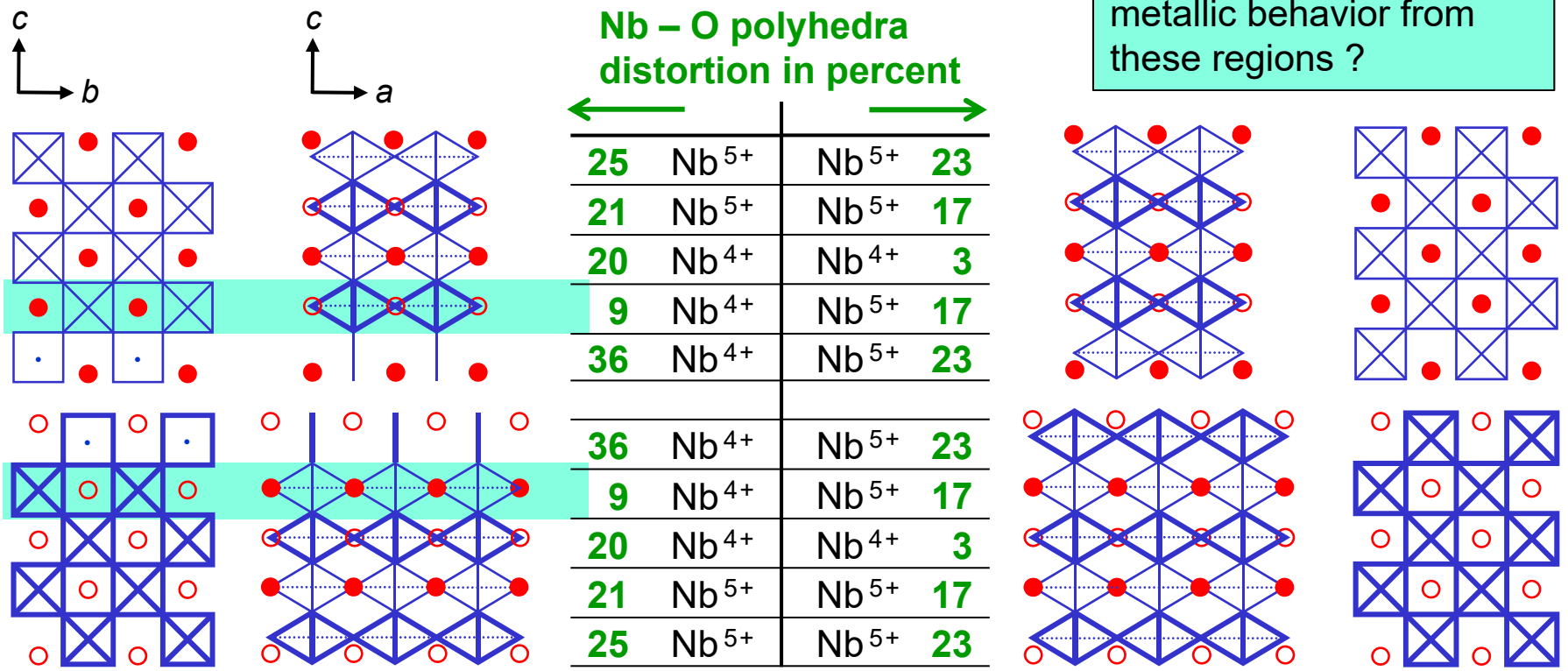

Nb – O polyhedra distortion in percent

25	Nb^{5+}	Nb^{5+}	23
21	Nb^{5+}	Nb^{5+}	17
20	Nb^{4+}	Nb^{4+}	3
9	Nb^{4+}	Nb^{5+}	17
36	Nb^{4+}	Nb^{5+}	23
36	Nb^{4+}	Nb^{5+}	23
9	Nb^{4+}	Nb^{5+}	17
20	Nb^{4+}	Nb^{4+}	3
21	Nb^{5+}	Nb^{5+}	17
25	Nb^{5+}	Nb^{5+}	23

$SrNbO_{3.2} = Sr_5Nb_5O_{16} = Sr_{20}Nb_{20}O_{64}$

Non-centrosymmetric !

Physical properties = ?

K. Schückel and Hk. Müller-Buschbaum
Z. Anorg. Allg. Chem. 528 (1985) 91

Nb^{5+} / $4d^0$

Nb^{4+} / $4d^1$

F. Lichtenberg et al., Prog. Solid State Chem. 36 (2008) 253

$SrNbO_{3.4} = Sr_5Nb_5O_{17} = Sr_{20}Nb_{20}O_{68}$

Centrosymmetric

Quasi-1D metal

S. C. Abrahams et al.
Acta Cryst. B 54 (1998) 399

The crystal structure of the n = 5 types $Sr_{20}Nb_{20}O_{64}$ and $Sr_{20}Nb_{20}O_{68}$

= NbO_6 octahedra (O located at the corners, Nb hidden in the center)

= NbO_4 (O located at the corners, Nb in the center)

Region with a metal-insulator-like interface, see part 6.3

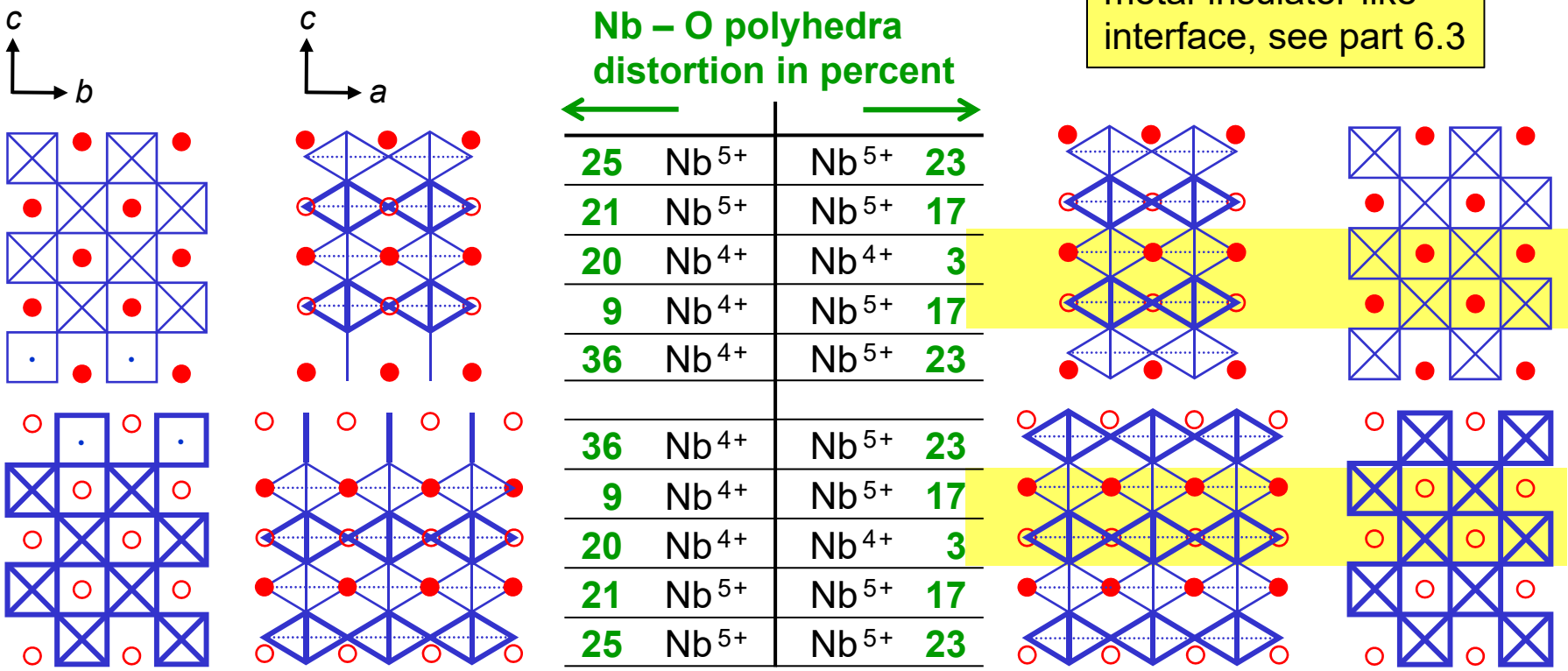

$SrNbO_{3.2} = Sr_5Nb_5O_{16} = Sr_{20}Nb_{20}O_{64}$

Non-centrosymmetric !

Physical properties = ?

Nb^{5+} / $4d^0$

Nb^{4+} / $4d^1$

$SrNbO_{3.4} = Sr_5Nb_5O_{17} = Sr_{20}Nb_{20}O_{68}$

Centrosymmetric

Quasi-1D metal

K. Schückel and Hk. Müller-Buschbaum
Z. Anorg. Allg. Chem. 528 (1985) 91

F. Lichtenberg et al., Prog. Solid State Chem. 36 (2008) 253

S. C. Abrahams et al.
Acta Cryst. B 54 (1998) 399

The crystal structure of the *n* = 5 types $Sr_{20}Nb_{20}O_{64}$ and $Sr_{20}Nb_{20}O_{68}$

= NbO_6 octahedra (O located at the corners, Nb hidden in the center)

= NbO_4 (O located at the corners, Nb in the center)

Region with a metal-insulator-like interface ?

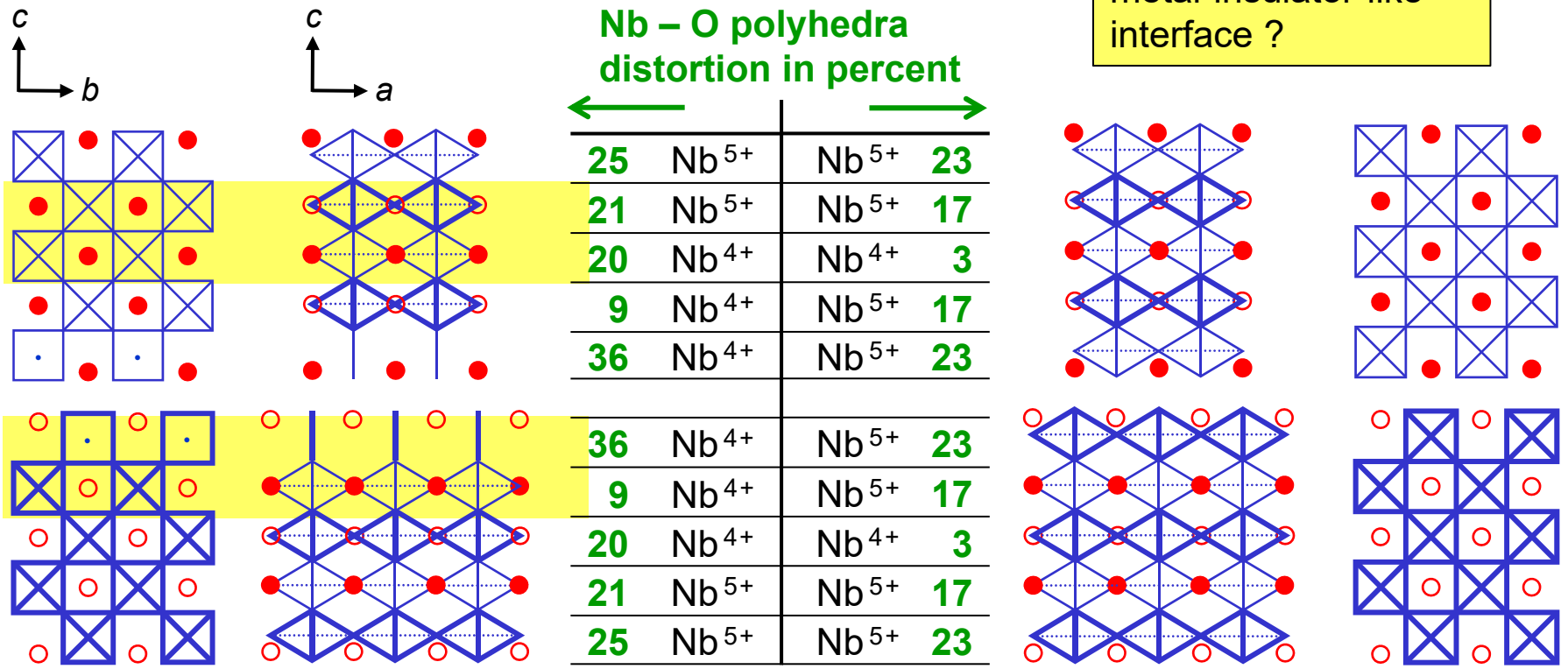

Nb – O polyhedra distortion in percent

25	Nb^{5+}	Nb^{5+}	23
21	Nb^{5+}	Nb^{5+}	17
20	Nb^{4+}	Nb^{4+}	3
9	Nb^{4+}	Nb^{5+}	17
36	Nb^{4+}	Nb^{5+}	23
36	Nb^{4+}	Nb^{5+}	23
9	Nb^{4+}	Nb^{5+}	17
20	Nb^{4+}	Nb^{4+}	3
21	Nb^{5+}	Nb^{5+}	17
25	Nb^{5+}	Nb^{5+}	23

$SrNbO_{3.2} = Sr_5Nb_5O_{16} = Sr_{20}Nb_{20}O_{64}$

Non-centrosymmetric !

Physical properties = ?

K. Schückel and Hk. Müller-Buschbaum
Z. Anorg. Allg. Chem. 528 (1985) 91

Nb^{5+} / $4d^0$

Nb^{4+} / $4d^1$

F. Lichtenberg et al., Prog. Solid State Chem. 36 (2008) 253

$SrNbO_{3.4} = Sr_5Nb_5O_{17} = Sr_{20}Nb_{20}O_{68}$

Centrosymmetric

Quasi-1D metal

S. C. Abrahams et al.
Acta Cryst. B 54 (1998) 399

The reported and a hypothetical structure of the *n* = 5 type $Sr_{20}Nb_{20}O_{68}$

= NbO_6 octahedra (O located at the corners, Nb hidden in the center)

= NbO_4 (O located at the corners, Nb in the center) ● ○ = Sr

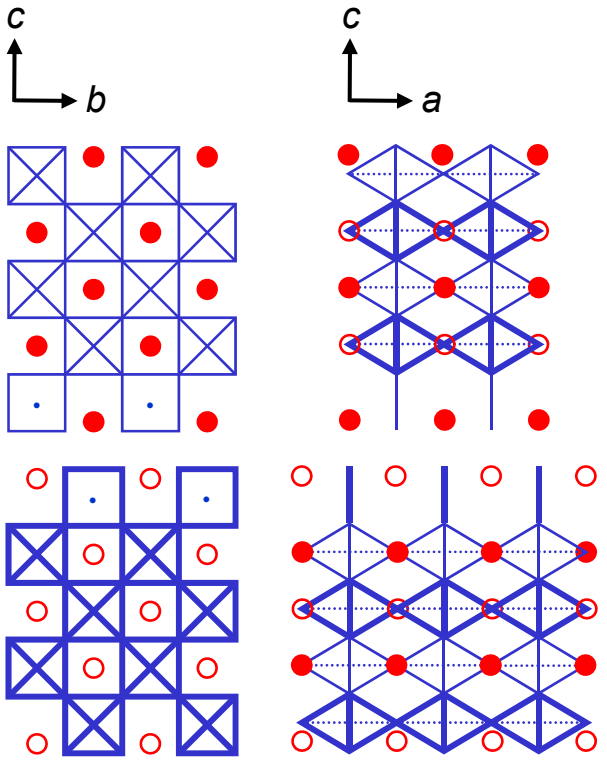

Reported by K. Schückel and Hk. Müller-Buschbaum

Nb – O polyhedra distortion in percent

25	Nb^{5+}	Nb^{5+}
21	Nb^{5+}	Nb^{4+}
20	Nb^{4+}	Nb^{4+}
9	Nb^{4+}	Nb^{4+}
36	Nb^{4+}	Nb^{5+}
36	Nb^{4+}	Nb^{5+}
9	Nb^{4+}	Nb^{4+}
20	Nb^{4+}	Nb^{4+}
21	Nb^{5+}	Nb^{4+}
25	Nb^{5+}	Nb^{5+}

Nb^{5+} / $4d^0$

Nb^{4+} / $4d^1$

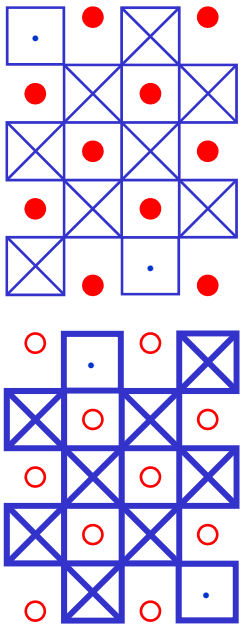

A hypothetical variant with a symmetric distribution of Nb^{4+} and Nb^{5+} in one slab or layer along the *c*-axis

Energetically unfavorable ?

NbO_4 polyhedra with Nb^{5+} ?

Z. Anorg. Allg. Chem. 528 (1985) 91 and
Prog. Solid State Chem. 36 (2008) 253

The Sr-deficient Schückel-Müller-Buschbaum type phases $Sr_{17}Ca_2Nb_{19}WO_{64}$ and $Sr_{17}CaBaNb_{19}WO_{64}$

Comments and open questions

- Do they have the same but Sr-deficient crystal structure as that of $Sr_5Nb_5O_{16} = Sr_{20}Nb_{20}O_{64}$ reported by K. Schückel and Hk. Müller-Buschbaum, i.e. do they have
  - a non-centrosymmetric space group ?
  - within a single layer or slab along the *c*-axis an asymmetric distribution of the Nb^{4+} and Nb^{5+} ions ?
  - within a single layer or slab along the *c*-axis an asymmetric distribution of the Nb – O polyhedra distortions ?
  - with reference to the stoichiometric *n* = 5 type $Sr_{20}Nb_{20}O_{68}$ fully ordered oxygen vacancies which are located at opposite boundaries of the layers or slabs ?

- Can the assumed doubled *a*-axis be confirmed by single crystal x-ray diffraction ?

The Sr-deficient Schückel-Müller-Buschbaum type phases $Sr_{17}Ca_2Nb_{19}WO_{64}$ and $Sr_{17}CaBaNb_{19}WO_{64}$

Comments and open questions

- Do the W ions occupy only specific *B* or Nb sites within the unit cell or are they randomly distributed ?

- Can the assumed valence state of tungsten, namely W^{4+} / $5d^2$, experimentally be verified ?

- Are these materials quasi-1D metals like the related stoichiometric *n* = 5 type quasi-1D metal $Sr_5Nb_5O_{17} = Sr_{20}Nb_{20}O_{68}$? If yes: Do the 5d electrons from the W ions contribute to the metallic behavior like the 4d electrons from Nb^{4+} ?

- The composition of the layered perovskite-related Sr- and O-deficient *n* = 5 type $(Sr,Ca,Ba)_{19}Nb_{19}WO_{64} = (Sr,Ca,Ba)_{0.95}Nb_{0.95}W_{0.05}O_{3.2} = A_{0.95}BO_{3.2}$ is close to that of the non-layered perovskite $A_{20}B_{20}O_{60} = ABO_3$. For comparison it should be mentioned that in the system $LaTiO_x$ the homogeneity range of the non-layered perovskite structure extends from *x* = 3 to *x* = 3.2 , see part 6.1

The Sr-deficient Schückel-Müller-Buschbaum type phases $Sr_{17}Ca_2Nb_{19}WO_{64}$ and $Sr_{17}CaBaNb_{19}WO_{64}$

Comments and open questions

- Are there related but insulating $n = 5$ type compounds $A_{19}B_{20}O_{64}$ or $A_{20}B_{20}O_{64}$ which are non-centrosymmetric, magnetoelectric, ferroelectric, and / or mulitiferroic ?

- Many of these comments and open questions can also be applied to the related melt-grown compounds which have a higher oxygen content, namely
  - $Sr_{17}CaBaNb_{19}WO_{65.3}$ which is presented in part 6.9.4
  - $Sr_{17}CaBaNb_{19}WO_{65.5}$ which is presented in part 6.9.3
  - $Sr_{19}Nb_{19}WO_{66}$ which is presented in part 6.9.2

- If the oxygen content of such type of materials is about 66.7 or smaller, then in principle an $n = 6$ type phase could arise but there are no indications for that. An example of an $n = 6$ type compound is the ferrorelectric insulator $Sr_6Nb_4Ti_2O_{20} = Sr_{20}Nb_{13.33}Ti_{6.67}O_{66.67}$ (Nb^{5+} / $4d^0$ and Ti^{4+} / $3d^0$)

The Sr-deficient Schückel-Müller-Buschbaum type phases $Sr_{17}Ca_2Nb_{19}WO_{64}$ and $Sr_{17}CaBaNb_{19}WO_{64}$

Comments and open questions

- When considering a series of such type of materials with a higher oxygen content that approaches stepwise from higher values towards 64:
  Is there a specific oxygen content x_c or a two-phase oxygen content range which separates the two single phases
  - centrosymmetric / non-centrosymmetric ?
  - symmetric / asymmetric distribution of the Nb^{4+} and Nb^{5+} ions ?
  - symmetric / asymmetric distribution of the Nb – O polyhedra distortions ?

6.9.9 A nonlinear behavior of the magnetic moment M(H) of the crossover region from a polycrystalline to a crystalline material suggests the existence of ferromagnetism in the system Sr - Ca - Ba - Nb - W - O or in one of its subsystem ...

As-grown crystalline $Sr_{17}CaBaNb_{19}WO_{69.5-y}$ and polycrystalline rods
Run / Sample No. 828 • See part 6.9.3

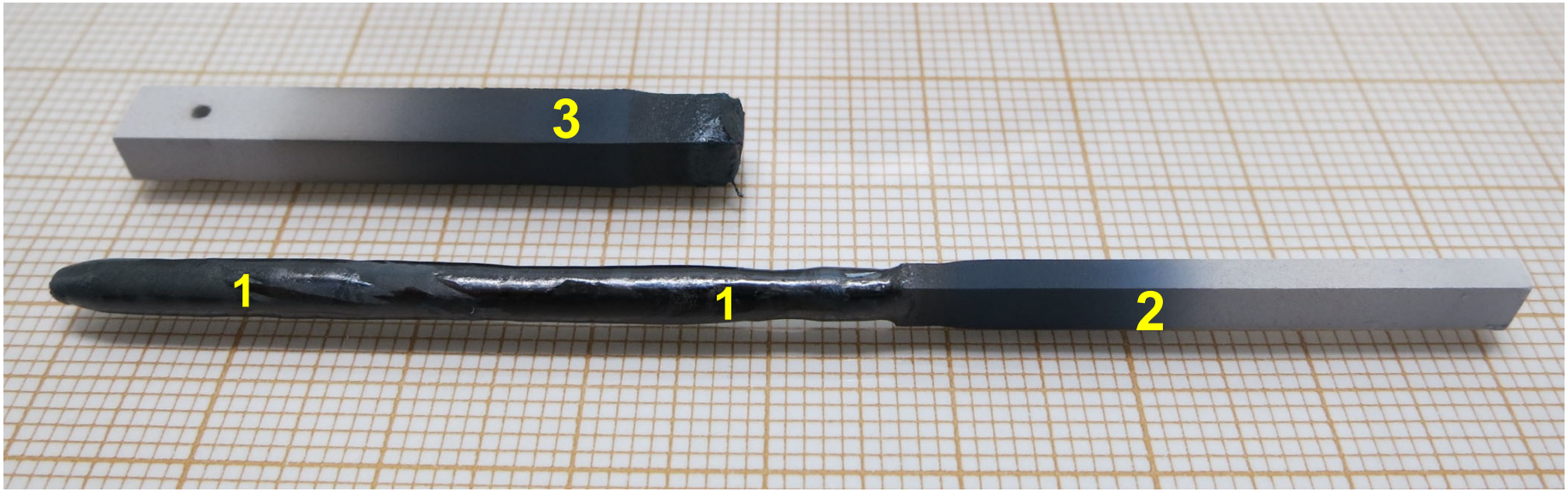

47 mm long as-grown crystalline material (1) plus polycrystalline seed rod (2) and remaining part of the polycrystalline feed rod (3)

As-grown crystalline $Sr_{17}CaBaNb_{19}WO_{69.5-y}$ and polycrystalline rods

Run / Sample No. 828

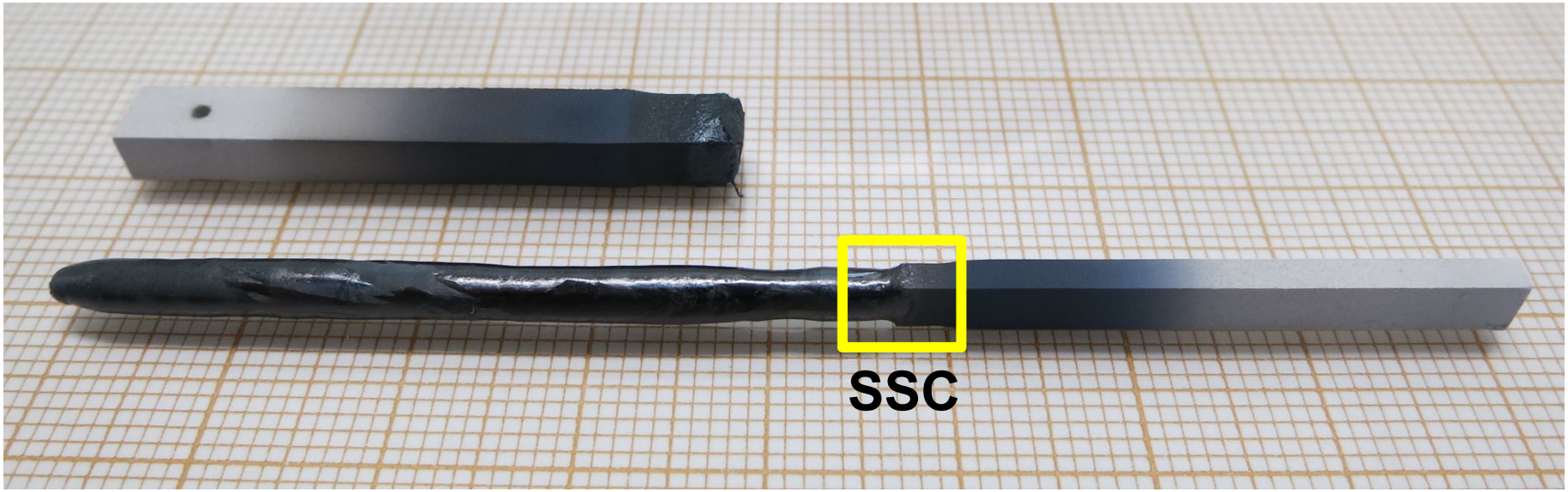

SSC: A piece which comprises reduced polycrystalline material from the Sintered Seed rod and melt-grown Crystalline material, i.e. such a piece comprises the crossover region from sintered polycrystalline to crystalline. It is very likely that the reduced and fully oxidized polycrystalline material is multiphase

Crossover region crystalline / polycrystalline of $Sr_{17}CaBaNb_{19}WO_{69.5 - y}$

Sample No. 828

Crossover region crystalline / polycrystalline of $Sr_{17}CaBaNb_{19}WO_{69.5 - y}$

Sample No. 828

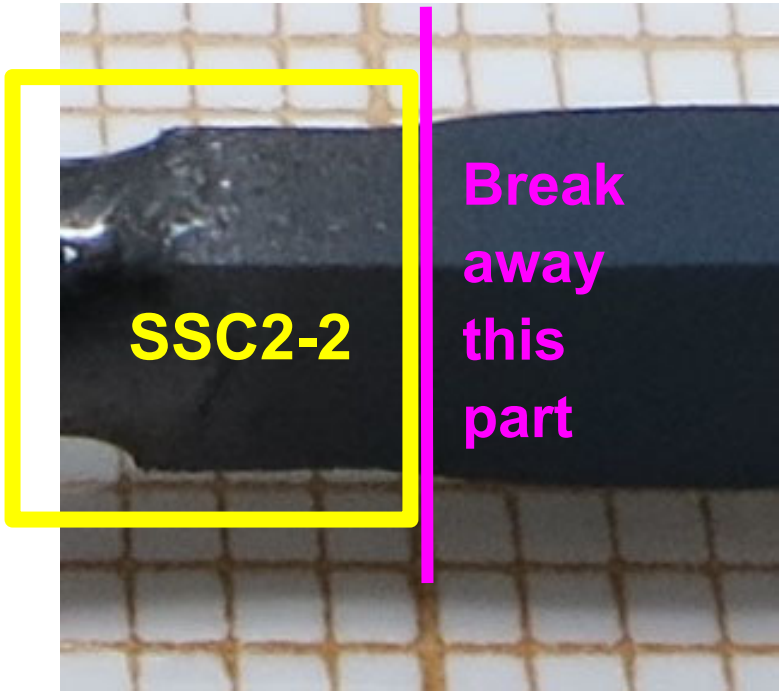

Crossover region crystalline / polycrystalline of $Sr_{17}CaBaNb_{19}WO_{69.5-y}$

Sample No. 828 • Magnetic measurements

Orientation of the magnetic field H with respect to specimen SSC2-2

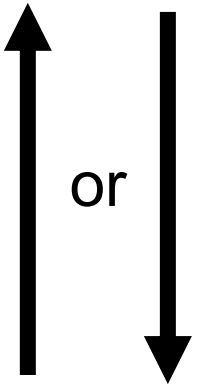

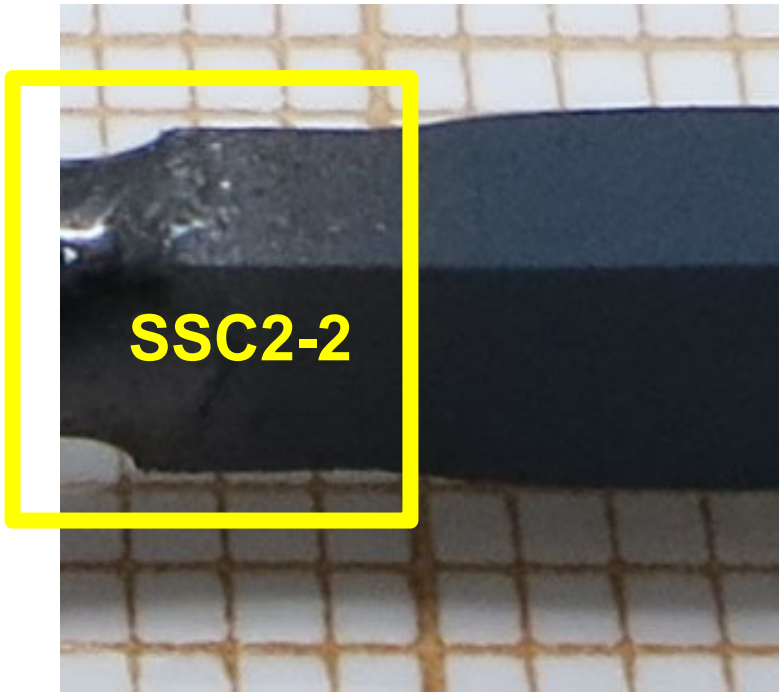

Crossover region crystalline / polycrystalline of $Sr_{17}CaBaNb_{19}WO_{69.5-y}$

Sample No. 828 • Magnetic moment M(H)

DC magnetic moment M(H) measured by a Quantum Design SQUID magnetometer MPMS3

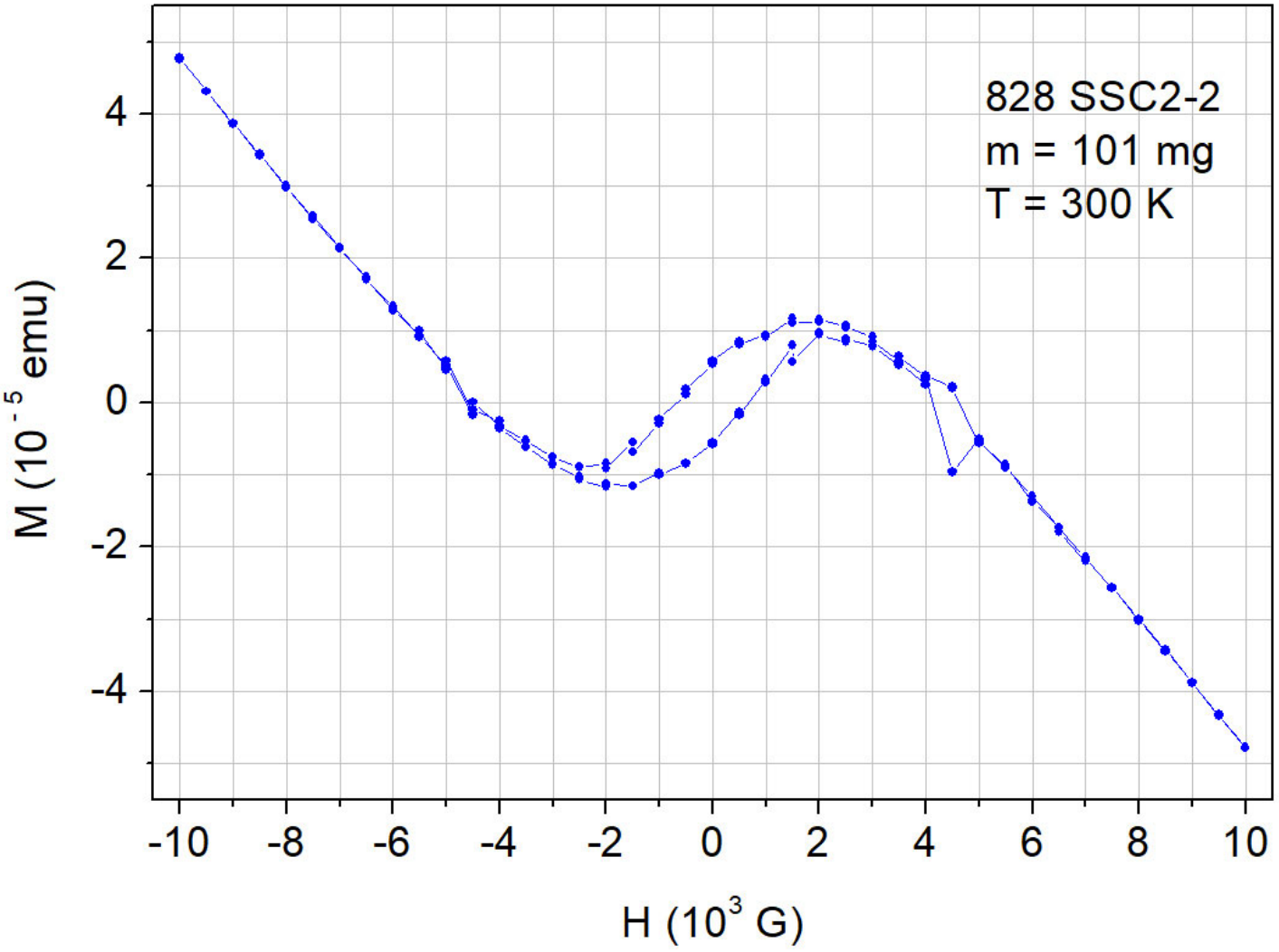

Magnetic field H:
$0 \rightarrow 10000\ G \rightarrow 0$
$\rightarrow -10000\ G \rightarrow 0$

$|\Delta H| = 500\ G$

Field changing rate 20 G / s

20 s waiting time before starting a DC measurement when the set field was reached

Crossover region crystalline / polycrystalline of $Sr_{17}CaBaNb_{19}WO_{69.5-y}$

Sample No. 828 • Magnetic moment M(H)

DC magnetic moment M(H) measured by a Quantum Design SQUID magnetometer MPMS3

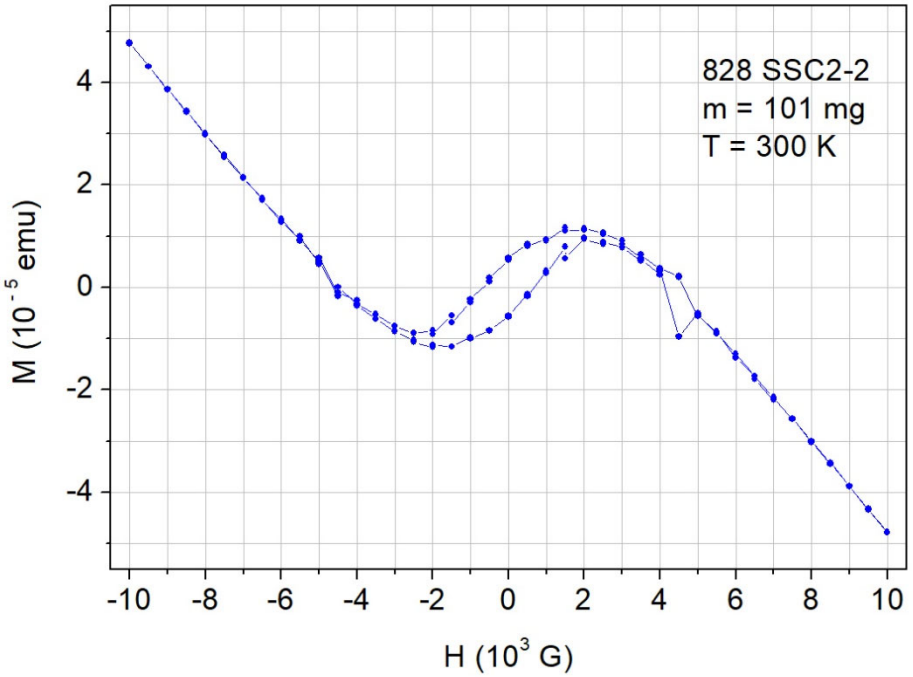

Instead of an usual linear M(H) behavior this particular curve is observed. It suggests the presence of a small amount of a ferromagnetic phase whose magnetic moment saturates with increasing field so that with further increasing field the linear contribution from a diamagnetic material appears.

Is it possible that the specimen was accidentally contaminated with a small amount of a ferromagnetic material during its preparation for the magnetic measurements ? This cannot be completely ruled out. However, this appears unlikely because all specimens which were used for magnetic measurements were broken off from the crystalline material and / or seed rod and then mechanically fixed within a straw without using any metallic or magnetic tools / things / materials ...

Crossover region crystalline / polycrystalline of $Sr_{17}CaBaNb_{19}WO_{69.5-y}$

Sample No. 828 • Magnetic moment M(H)

DC magnetic moment M(H) measured by a Quantum Design SQUID magnetometer MPMS3

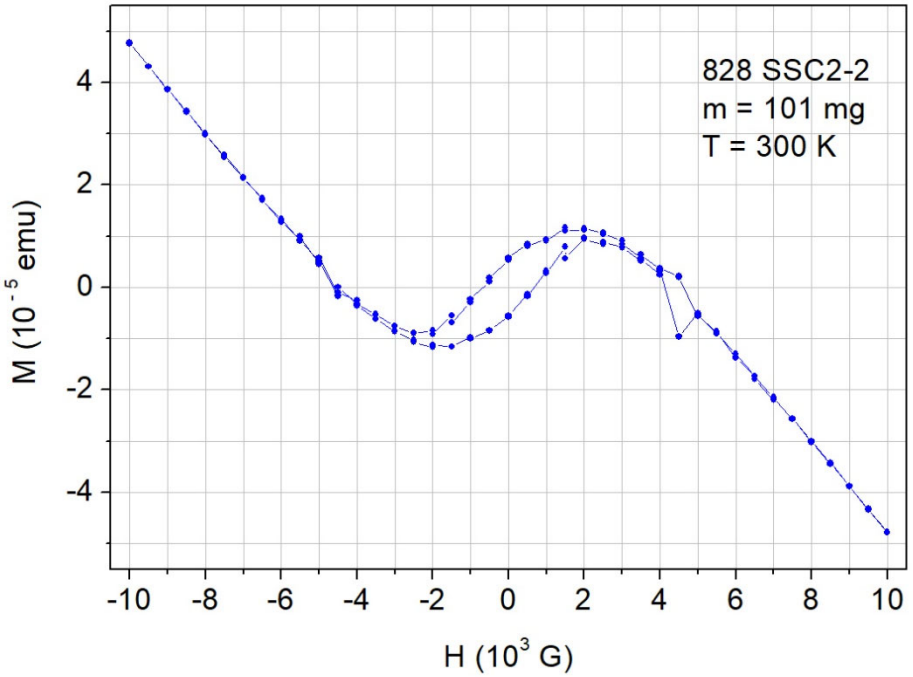

Therefore this particular M(H) curve suggests the existence of a ferromagnetic compound or ferromagnetic interface phenomenon in the system Sr - Ca - Ba - Nb - W - O or in one of its subsystem

Also other samples were investigated. Some of them display a similar M(H) behavior but most of them show an usual linear M(H) curve. Examples are presented on the following pages ...

As-grown crystalline $Sr_{18}CaBaNb_{19}WO_{70.5-y}$ and polycrystalline rods
Run / Sample No. 840 • See part 6.10

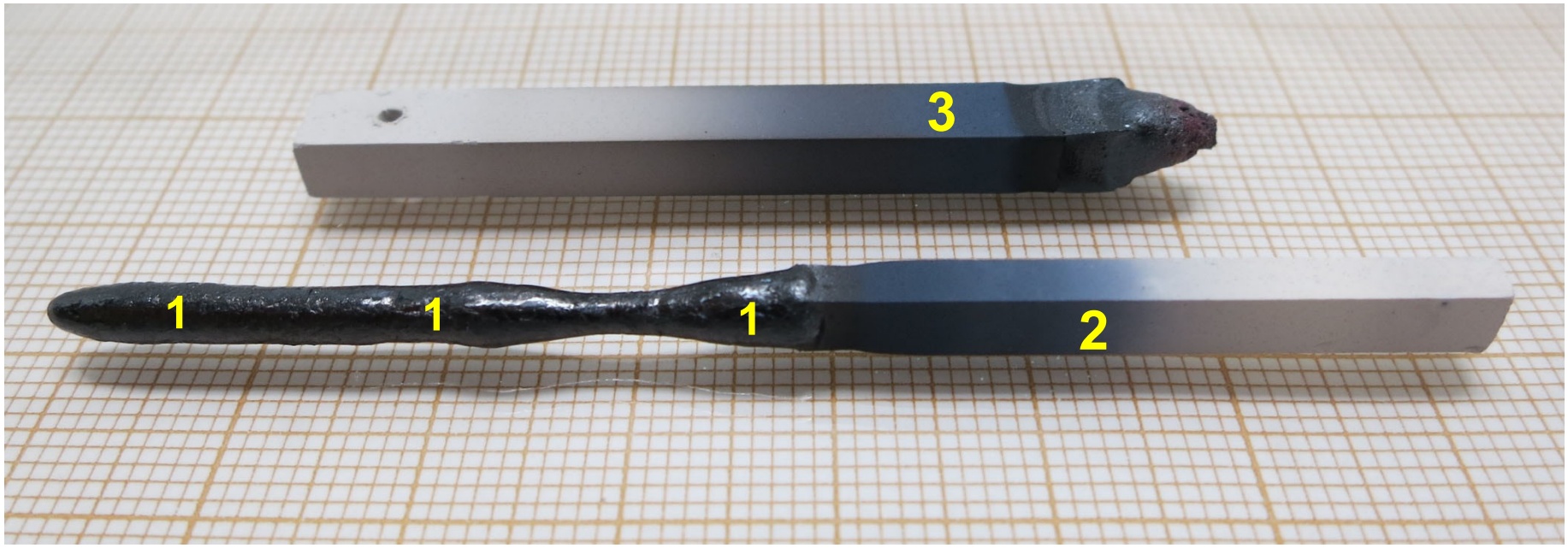

39 mm long as-grown crystalline material (1) plus polycrystalline seed rod (2) and remaining part of the polycrystalline feed rod (3)

The crystalline material is not single phase, see part 6.10

As-grown crystalline $Sr_{17}CaBaNb_{19}WO_{69.5-y}$ and polycrystalline rods

Run / Sample No. 840

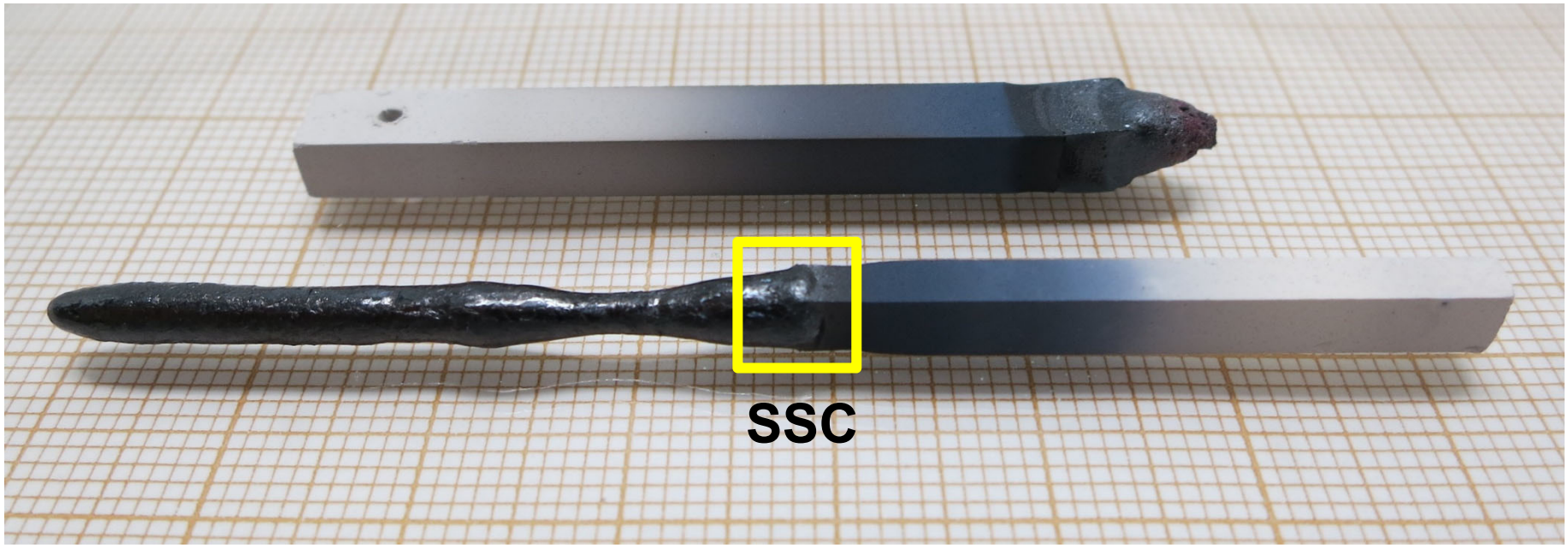

SSC: A piece which comprises reduced polycrystalline material from the Sintered Seed rod and melt-grown Crystalline material, i.e. such a piece comprises the crossover region from sintered polycrystalline to crystalline. It is very likely that the reduced and fully oxidized polycrystalline material is multiphase

Crossover region crystalline / polycrystalline of $Sr_{18}CaBaNb_{19}WO_{70.5-y}$

Sample No. 840 • Magnetic moment M(H)

DC magnetic moment M(H) measured by a Quantum Design SQUID magnetometer MPMS3

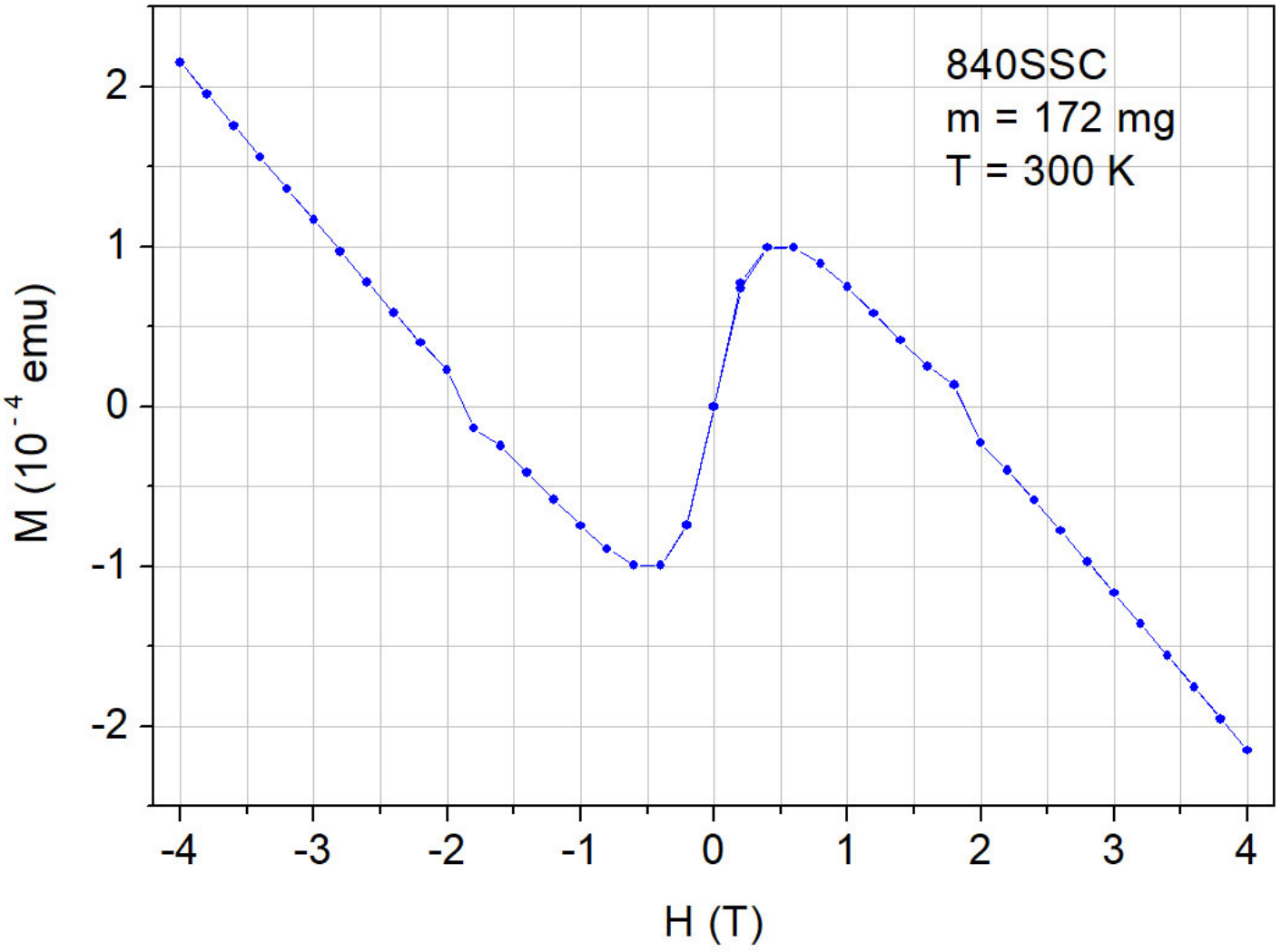

Magnetic field H:
$0 \rightarrow 4\ T \rightarrow 0$
$\rightarrow -4\ T \rightarrow 0$

$|\Delta H| = 0.2\ T$

20 s waiting time before starting a DC measurement when the set field was reached

Crossover region crystalline / polycrystalline of $Sr_{18}CaBaNb_{19}WO_{70.5-y}$

Sample No. 840 • Magnetic moment M(H)

DC magnetic moment M(H) measured by a Quantum Design SQUID magnetometer MPMS3

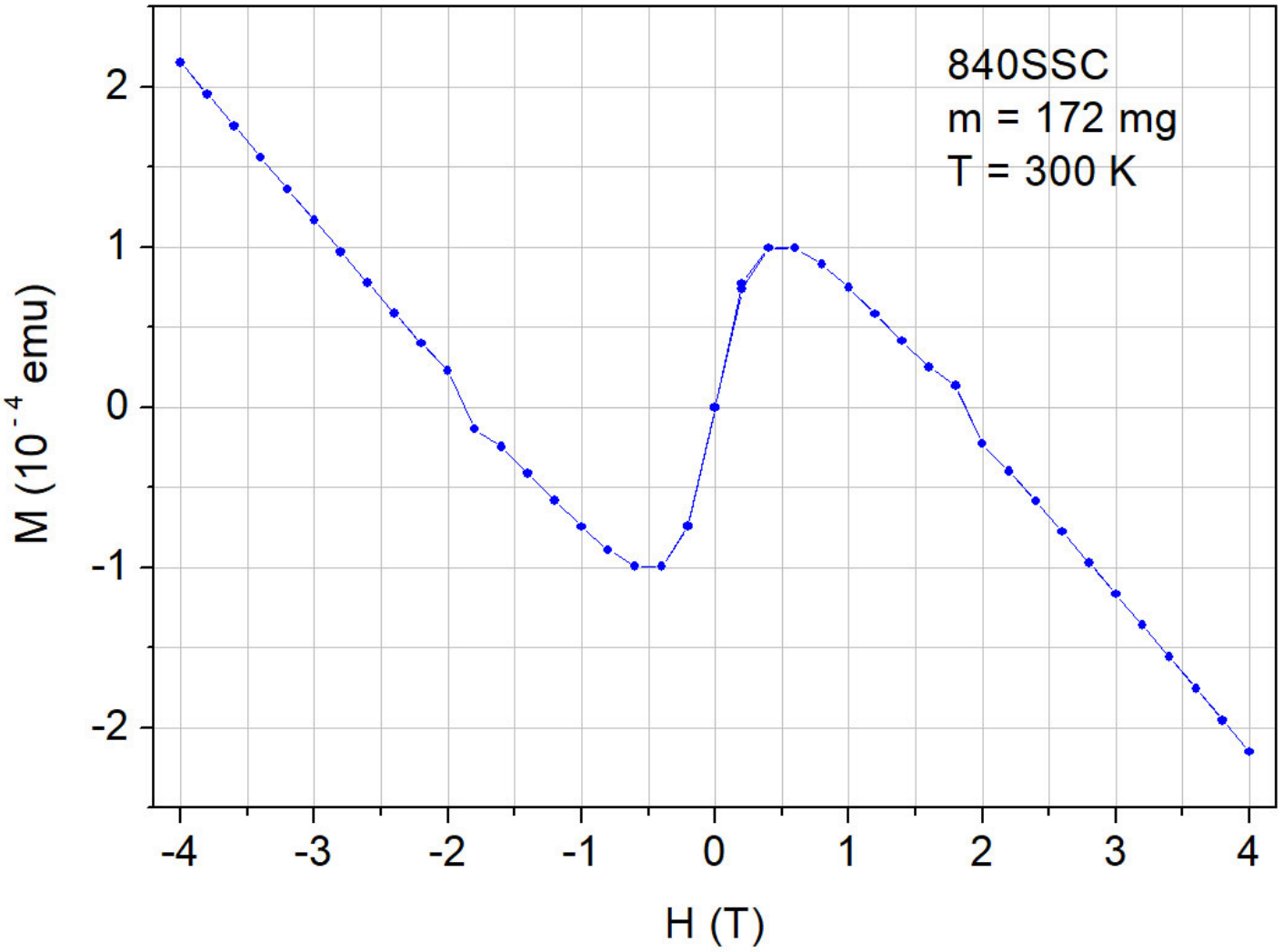

This M(H) curve is similar to that of specimen 828 SSC2-2 , however it does not show a hysteresis

For comparison also M(H) of a melt-grown crystalline piece was measured ...

Pieces of melt-grown $Sr_{18}CaBaNb_{19}WO_{67.4}$
Sample 840 • See part 6.10

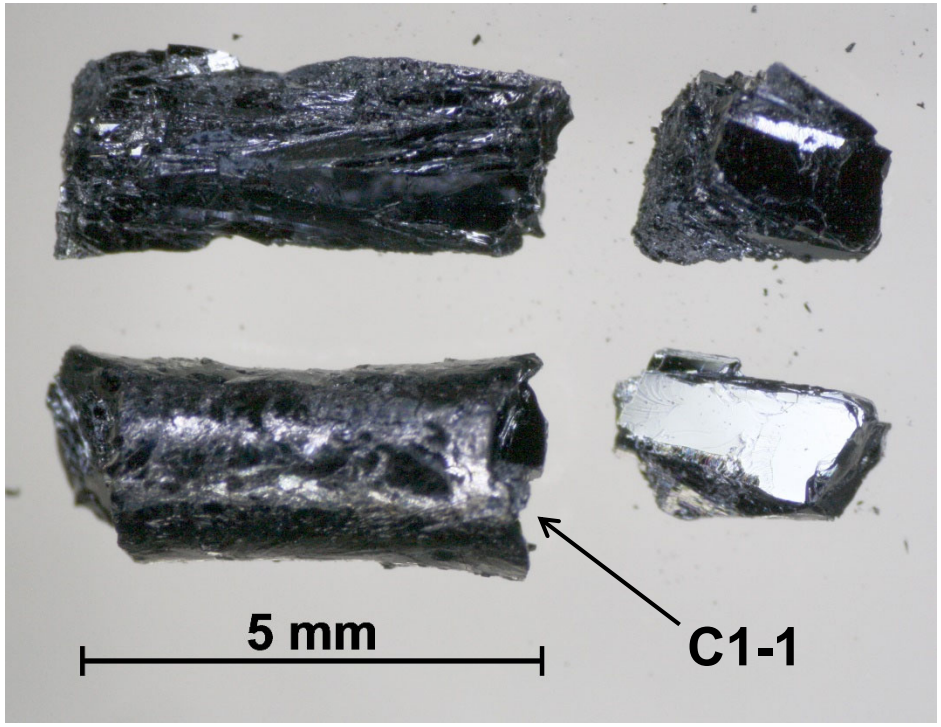

Crystalline pieces from section C1 of the as-grown material which is not single phase, see part 6.10

The piece C1-1 with m = 91 mg was used to measure M(H) ...

Melt-grown $Sr_{18}CaBaNb_{19}WO_{67.4}$

Sample No. 840 • Magnetic moment M(H)

DC magnetic moment M(H) measured by a Quantum Design SQUID magnetometer MPMS3

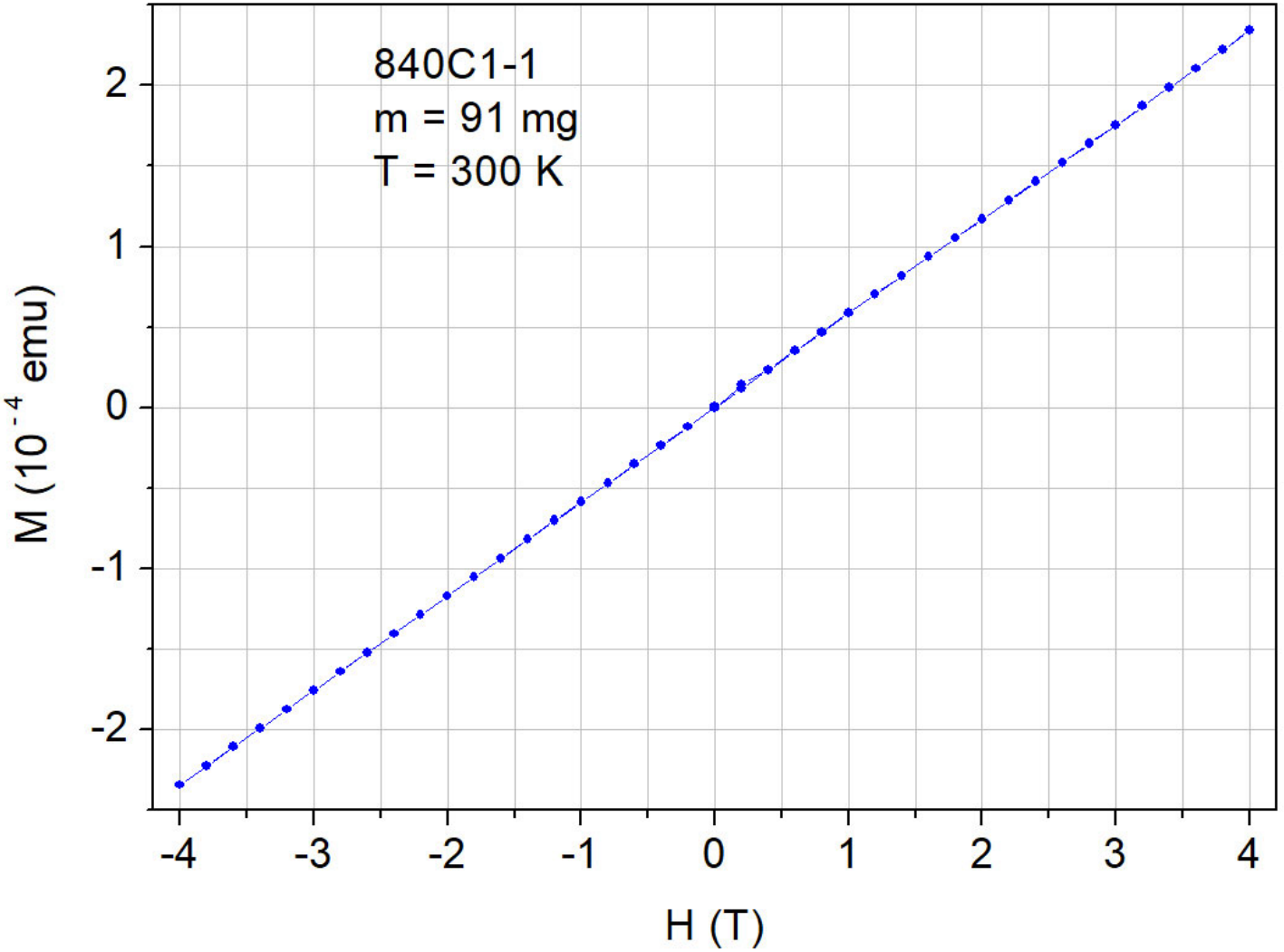

Magnetic field H:
$0 \rightarrow 4\ T \rightarrow 0$
$\rightarrow -4\ T \rightarrow 0$

In contrast to specimen 840 SSC this crystalline piece 840 C1-1 displays an usual linear behavior

As-grown crystalline $Sr_{17}CaBaNb_{19}WO_{69.5-y}$ and polycrystalline rods
Run / Sample No. 836 • See part 6.9.4

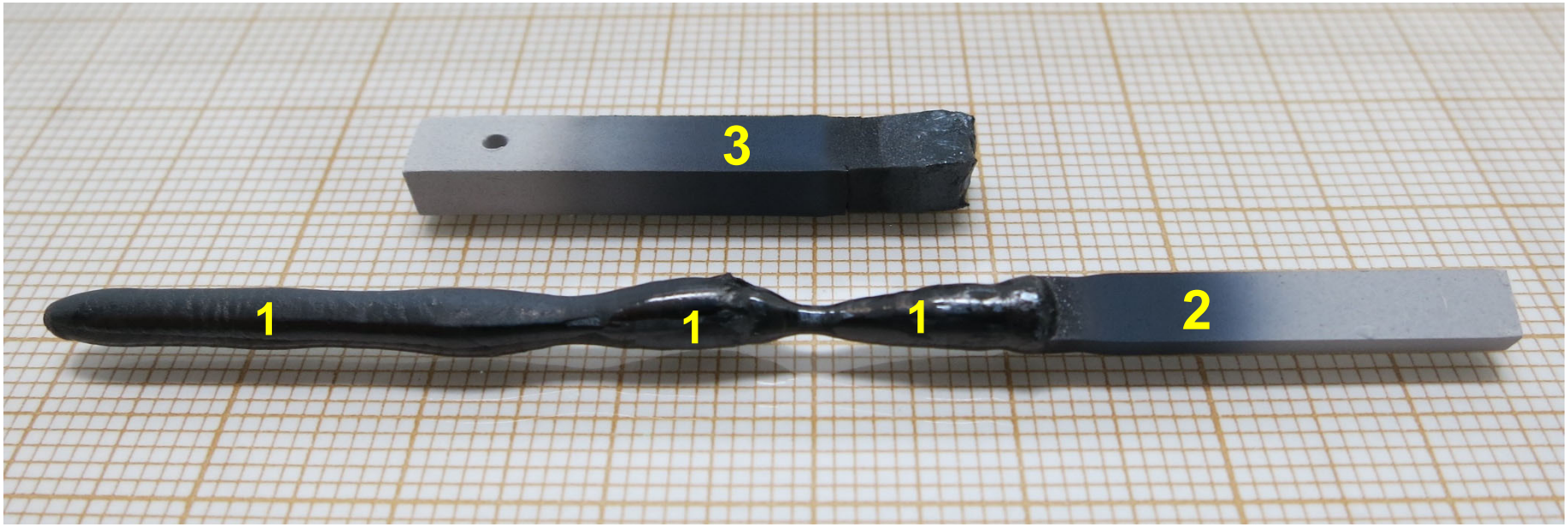

5 cm long as-grown crystalline material (1) plus polycrystalline seed rod (2) and remaining part of the polycrystalline feed rod (3)

As-grown crystalline $Sr_{17}CaBaNb_{19}WO_{69.5-y}$ and polycrystalline rods

Run / Sample No. 836

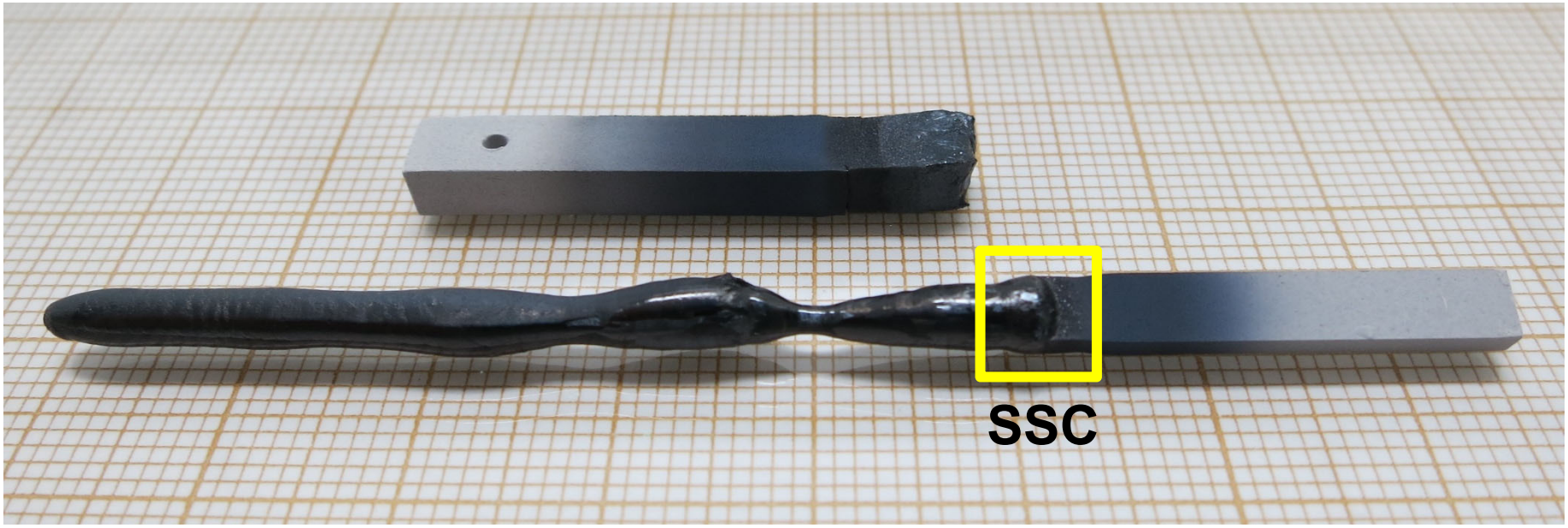

SSC: A piece which comprises reduced polycrystalline material from the Sintered Seed rod and melt-grown Crystalline material, i.e. such a piece comprises the crossover region from sintered polycrystalline to crystalline. It is very likely that the reduced and fully oxidized polycrystalline material is multiphase

Crossover region crystalline / polycrystalline of $Sr_{17}CaBaNb_{19}WO_{69.5-y}$

Sample No. 836 • Magnetic moment M(H)

DC magnetic moment M(H) measured by a Quantum Design SQUID magnetometer MPMS3

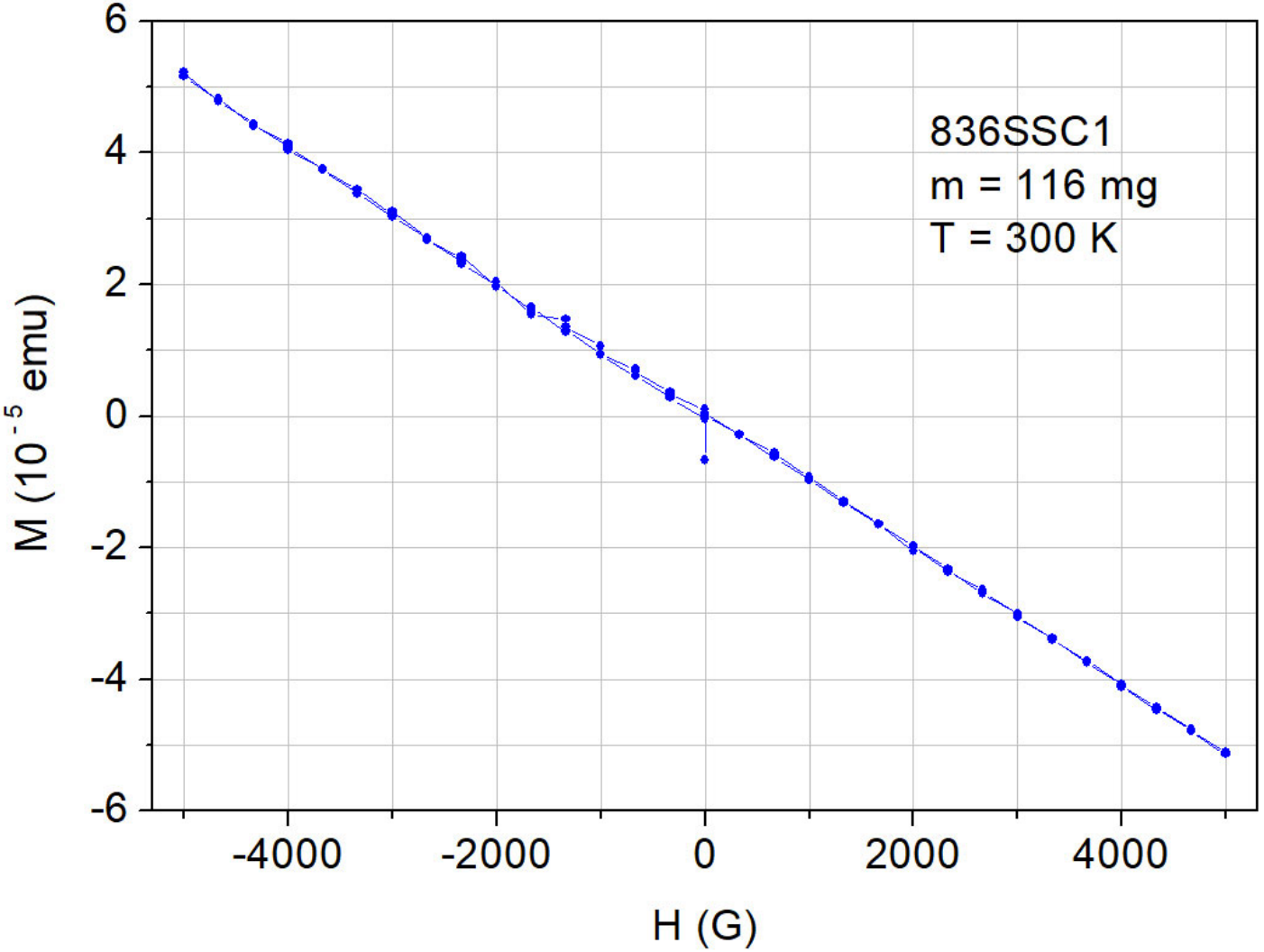

Magnetic field H:
0 → 5000 G → 0
→ - 5000 G → 0

This specimen 836 SSC1 displays an usual linear behavior

Also M(H) of a polycrystalline piece was measured ...

As-grown crystalline $Sr_{17}CaBaNb_{19}WO_{69.5-y}$ and polycrystalline rods
Run / Sample No. 836 • See part 6.9.4

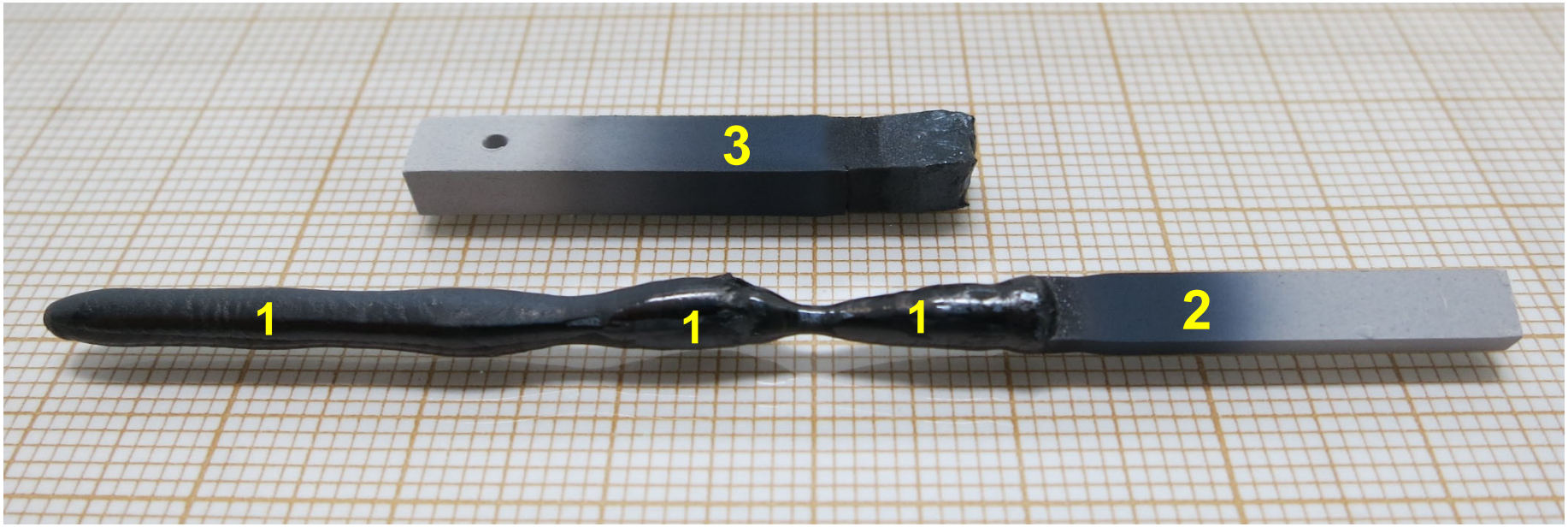

5 cm long as-grown crystalline material (1) plus polycrystalline seed rod (2) and remaining part of the polycrystalline feed rod (3)

As-grown crystalline $Sr_{17}CaBaNb_{19}WO_{69.5-y}$ and polycrystalline rods

Run / Sample No. 836

SS: A piece from the reduced and fully oxidized polycrystalline Sintered Seed rod. It is very likely that the reduced and fully oxidized polycrystalline material is multiphase

A piece of polycrystalline $Sr_{17}CaBaNb_{19}WO_{69.5-y}$

Sample No. 836 • Magnetic moment M(H)

DC magnetic moment M(H) measured by a Quantum Design SQUID magnetometer MPMS3

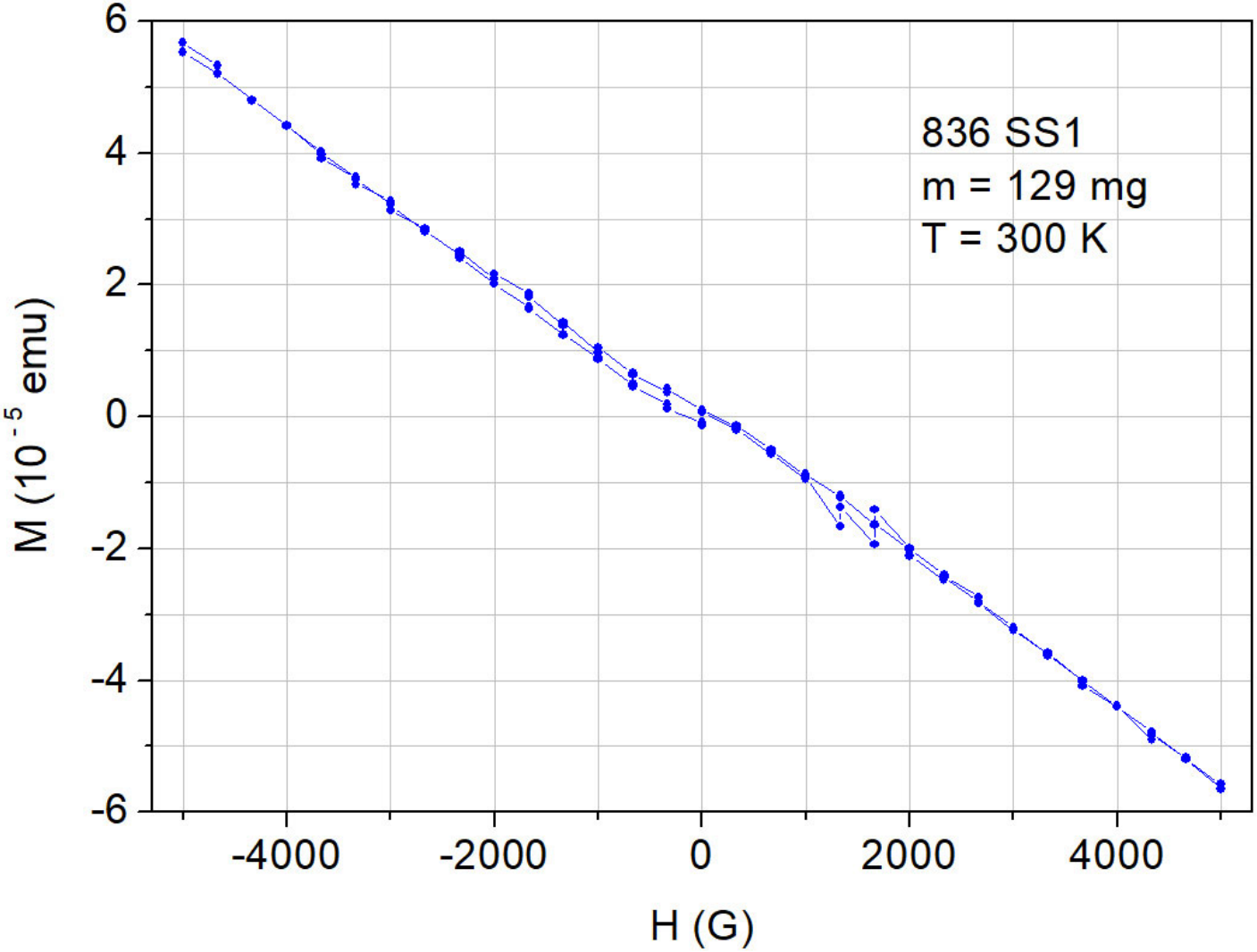

Magnetic field H:
$0 \rightarrow 5000\ G \rightarrow 0$
$\rightarrow -5000\ G \rightarrow 0$

$|\Delta H| = 333\ G$

Field changing rate 10 G / s

20 s waiting time before starting a DC measurement when the set field was reached

This specimen 836 SS1 displays nearly an usual linear behavior

As-grown crystalline $Sr_{19}Nb_{19}WO_{69.5-y}$ and polycrystalline rods
Run / Sample No. 812 • See part 6.9.2

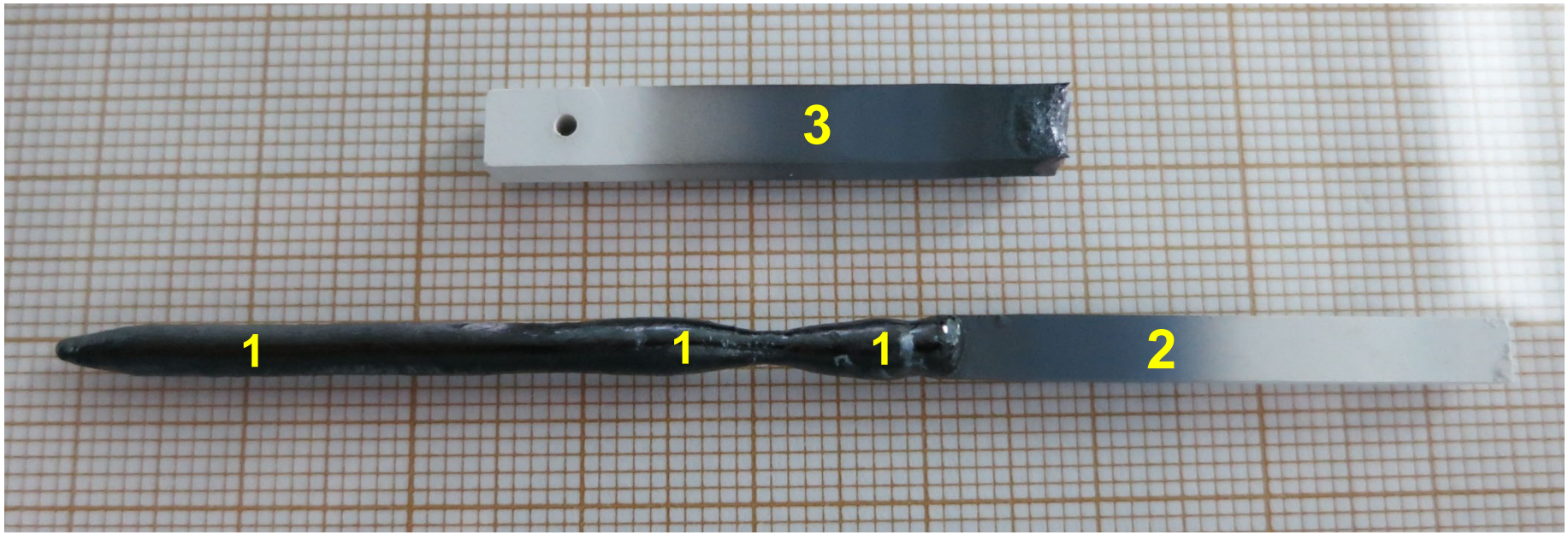

5 cm long as-grown crystalline material (1) plus polycrystalline seed rod (2) and remaining part of the polycrystalline feed rod (3)

As-grown crystalline $Sr_{19}Nb_{19}WO_{69.5-y}$ and polycrystalline rods

Run / Sample No. 812

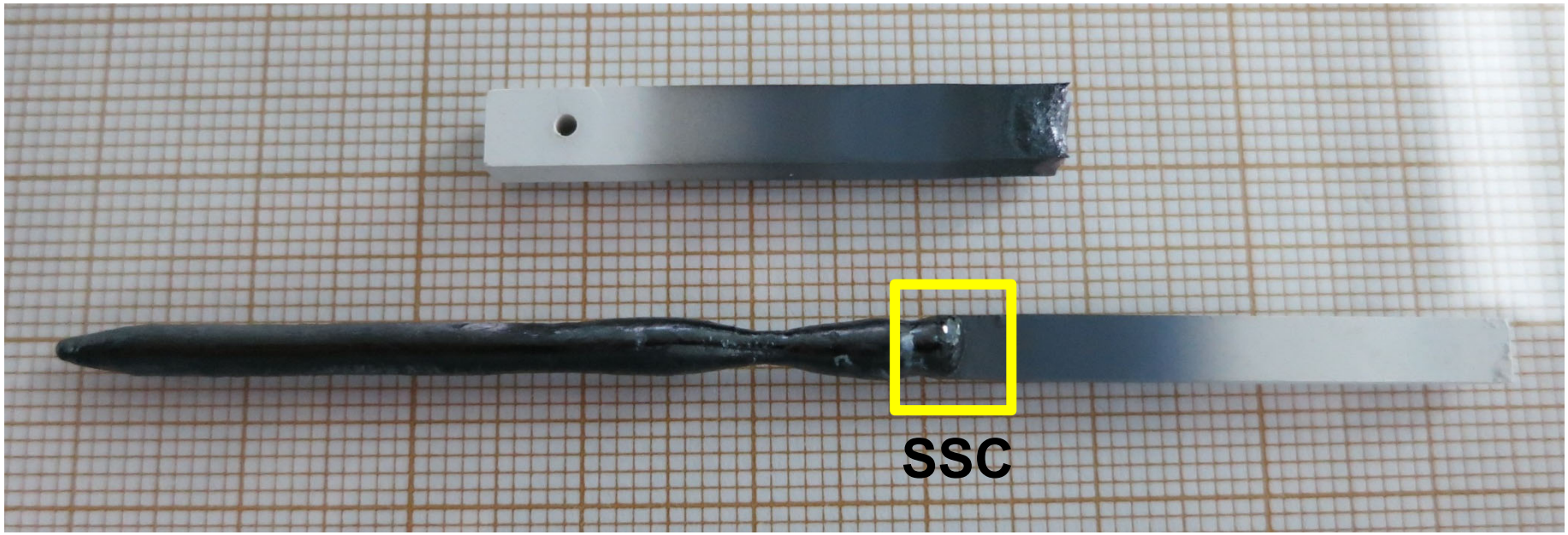

SSC: A piece which comprises reduced polycrystalline material from the Sintered Seed rod and melt-grown Crystalline material, i.e. such a piece comprises the crossover region from sintered polycrystalline to crystalline. It is very likely that the reduced and fully oxidized polycrystalline material is multiphase

Crossover region crystalline / polycrystalline of $Sr_{19}Nb_{19}WO_{69.5-y}$

Sample No. 812 • Magnetic moment M(H)

DC magnetic moment M(H) measured by a Quantum Design SQUID magnetometer MPMS3

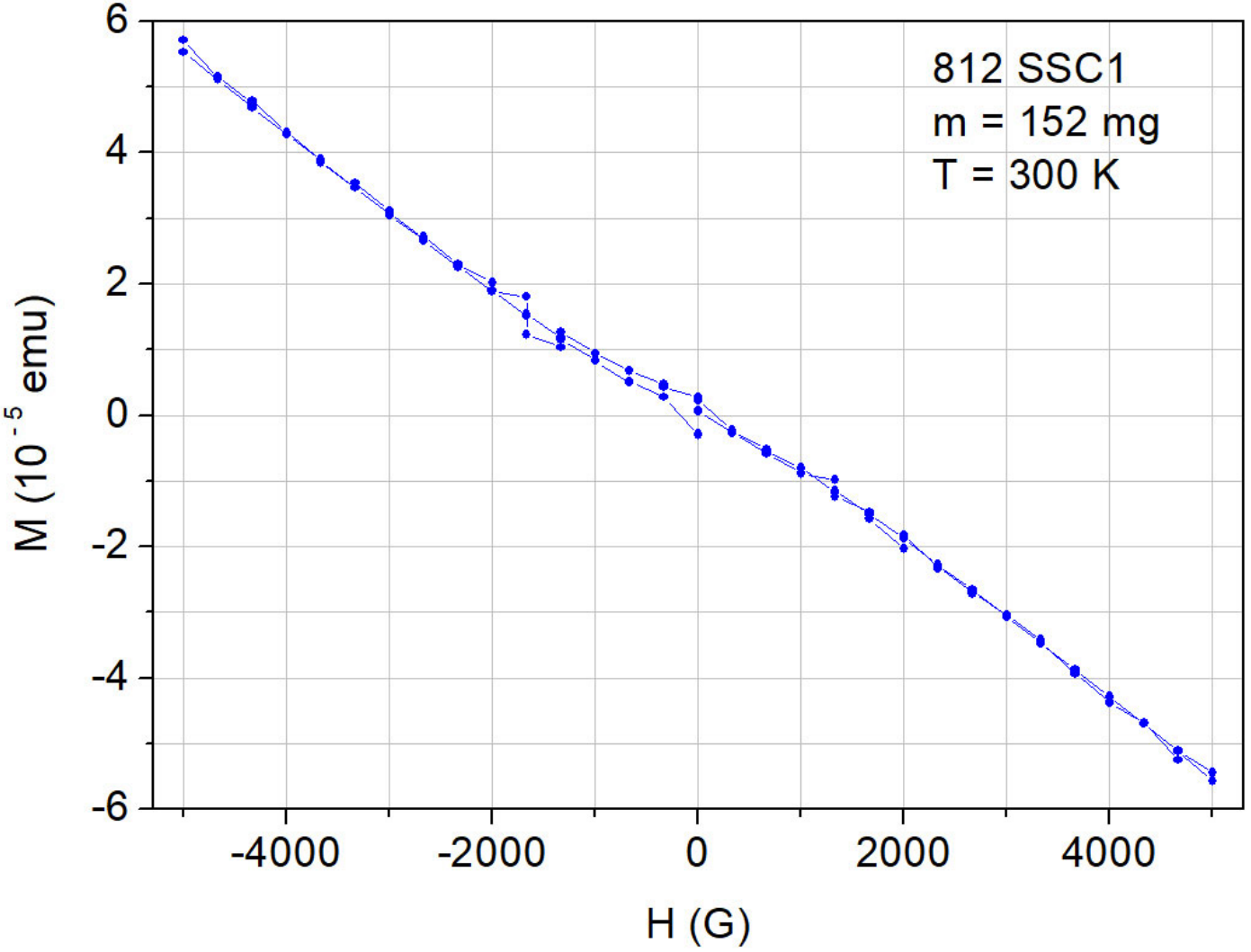

Magnetic field H:
$0 \rightarrow 5000\ G \rightarrow 0$
$\rightarrow -5000\ G \rightarrow 0$

$|\Delta H| = 333\ G$

Field changing rate 10 G / s

20 s waiting time before starting a DC measurement when the set field was reached

This specimen 812 SSC1 displays nearly an usual linear behavior

6.10 Examples of synthesis experiments and processed compositions which did not result in a single phase melt-grown

n = 5 type material: $Sr_{19}Nb_{18}W_2O_{70-y}$, $Sr_{18}CaBaNb_{19}WO_{70.5-y}$, $Ca_{19}BaNb_{19}WO_{68}$, $Sr_{20}Nb_{19}O_{67.5-y}$, $Ca_{20}Nb_{19}O_{65}$, and $Eu_{20}Ti_{20}O_{67}$ ...

Run / Sample No. 819:

$Sr_{19}Nb_{18}W_2O_{70-y}$ ...

Sintered rods with composition $Sr_{19}Nb_{18}W_2O_{70}$ Run No. 819

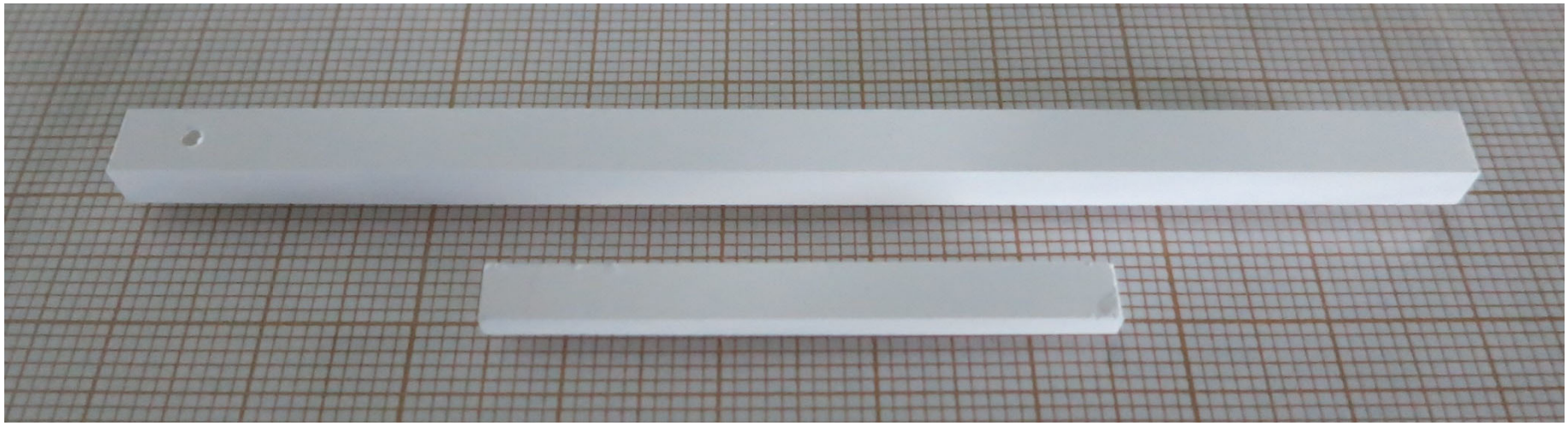

Polycrystalline sintered rods with fully oxidized composition $Sr_{19}Nb_{18}W_2O_{70}$, i.e. all Nb and W ions are in their highest valence or oxidation state Nb^{5+} and W^{6+}, respectively

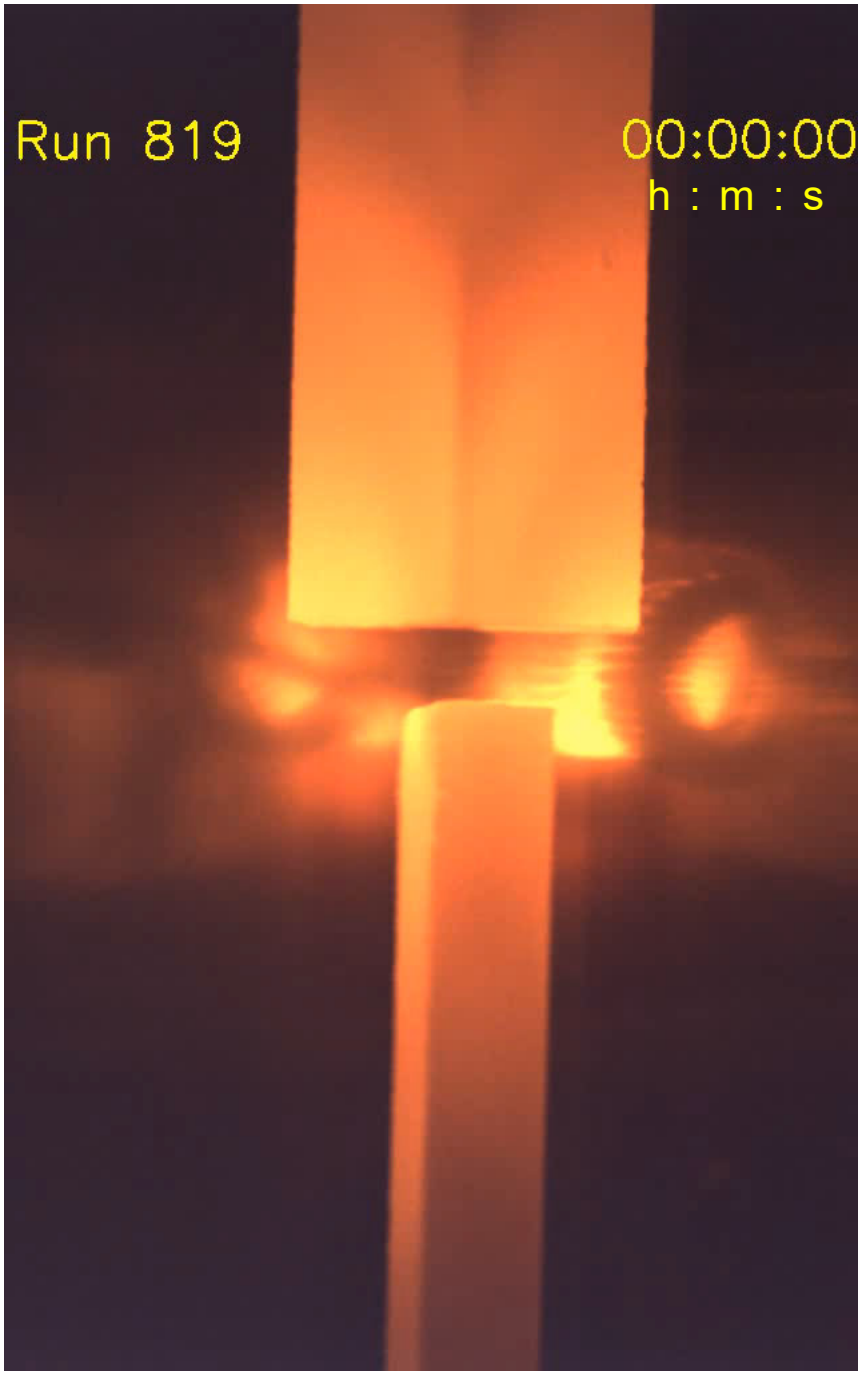

Melt-grown synthesis of $Sr_{19}Nb_{18}W_2O_{70-y}$

Starting materials for the mirror furnace run: Polycrystalline sintered rods with fully oxidized composition $Sr_{19}Nb_{18}W_2O_{70}$

Fast mode video from the overall melt-grown synthesis of $Sr_{19}Nb_{18}W_2O_{70-y}$ under 97.2 % Ar + 2.8 % H_2 in the Cyberstar mirror furnace. The video is only running in the ppsx type version of this publication, see page 2

Gas flow rate: 400 sccm (24 L / h)
Gas type setting at the mass flow controller: Ar

Lamp power to maintain the molten zone: 2 × (380 - 435) W

Speed of the lower shaft and seed rod (crystal growth speed): 14 mm / h

The video shows a stepwise development of a viscous zone above the molten zone. This and the needed increase of the lamp power indicates the presence of an incongruent melting and solidification

As-grown crystalline $Sr_{19}Nb_{18}W_2O_{70-y}$ and polycrystalline rods

Run / Sample No. 819

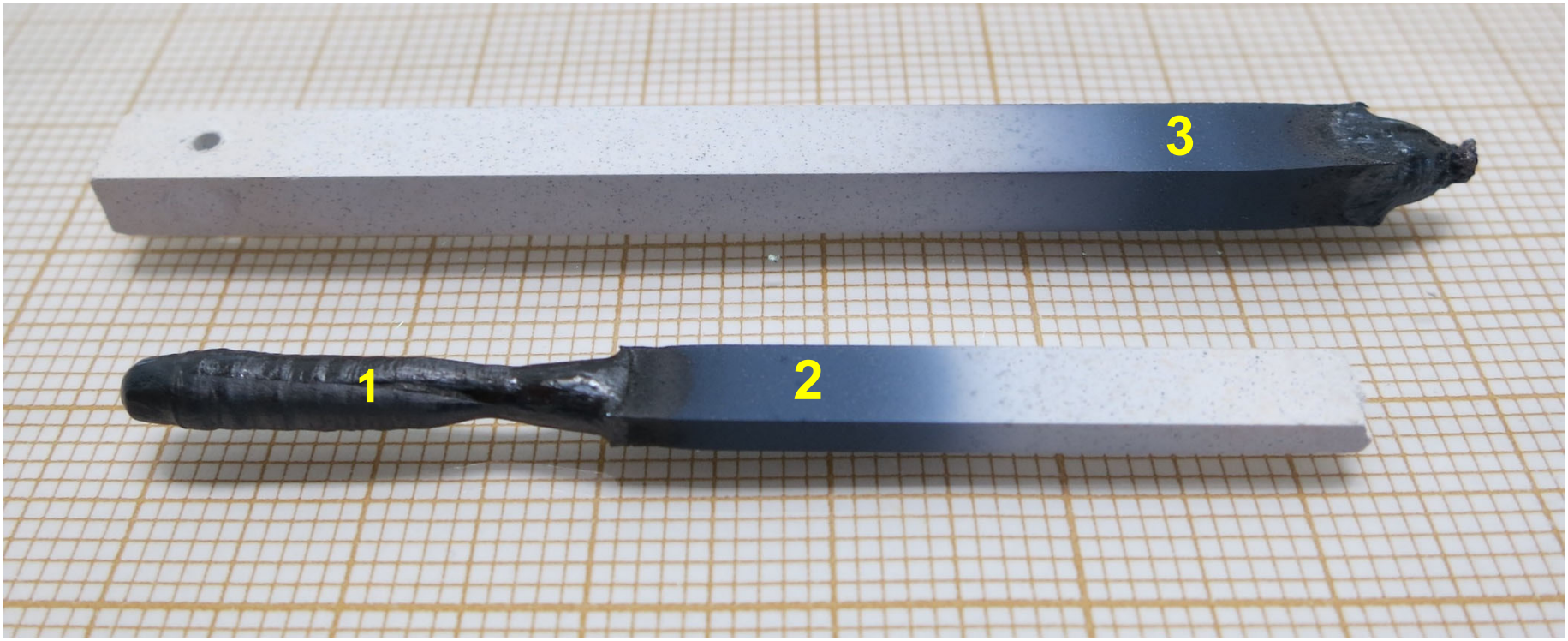

2 cm long as-grown crystalline material (1) plus polycrystalline seed rod (2) and remaining part of the polycrystalline feed rod (3)

Prepared at the ETH Zurich in 2018

As-grown crystalline material $Sr_{19}Nb_{18}W_2O_{70-y}$

Sample No. 819

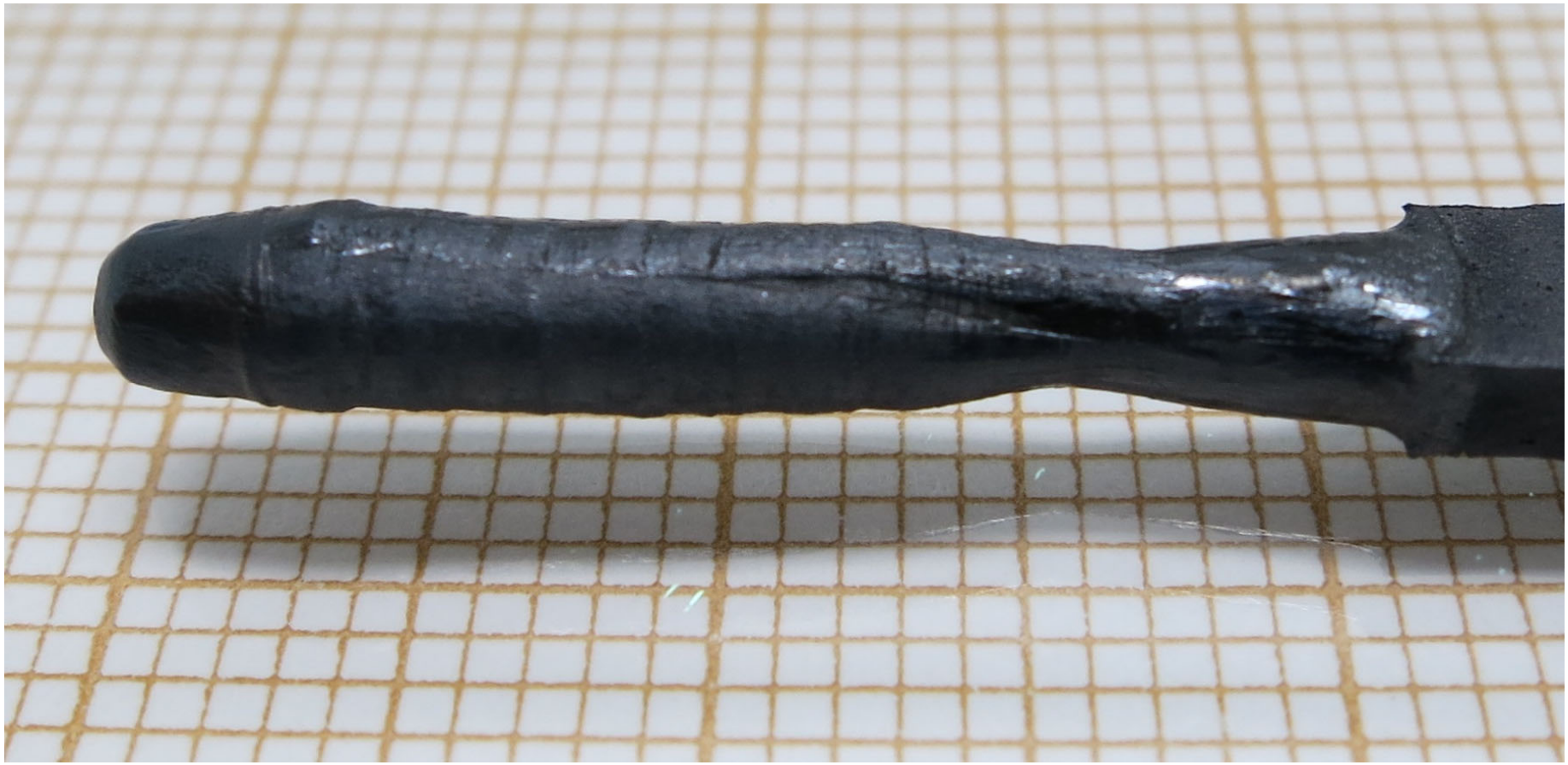

2 cm long as-grown crystalline material

As-grown crystalline material $Sr_{19}Nb_{18}W_2O_{70-y}$

Sample No. 819

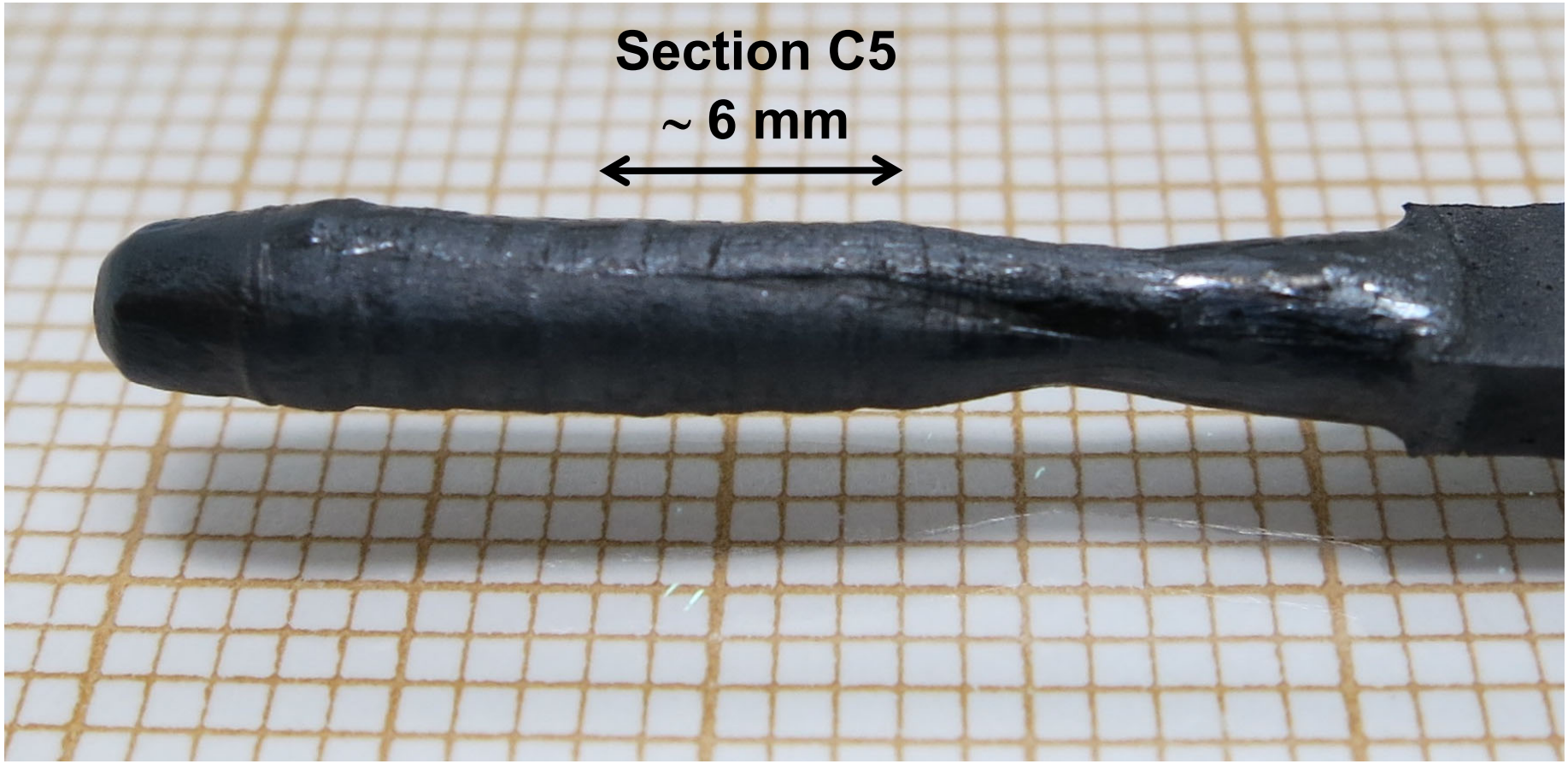

2 cm long as-grown crystalline material

As-grown crystalline material $Sr_{19}Nb_{18}W_2O_{70-y}$

Sample No. 819

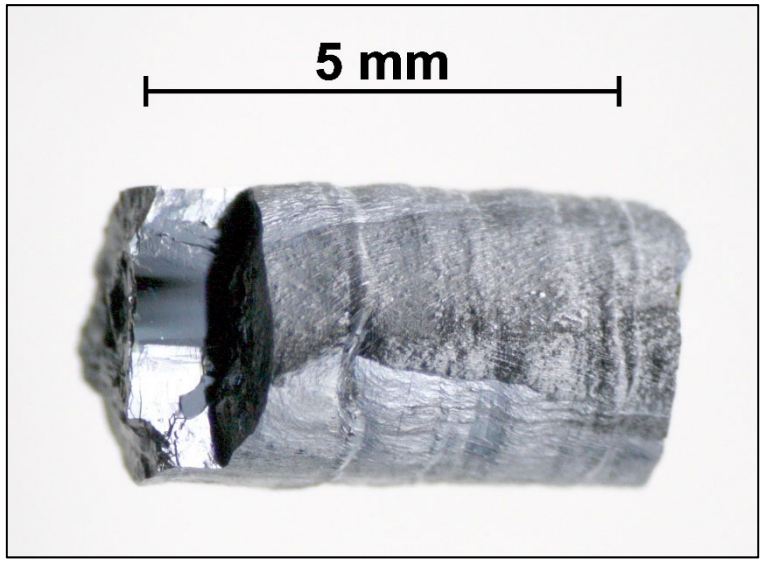

Crystalline piece from section C5 of the as-grown material

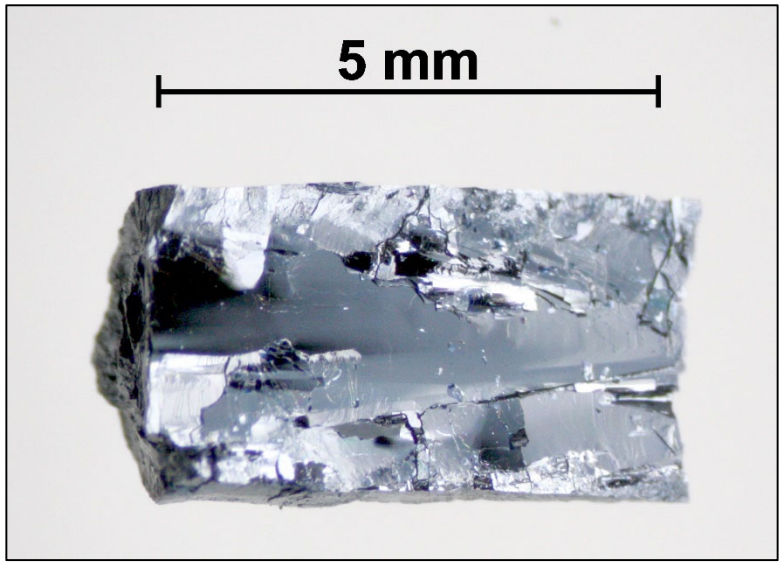

Part of the crystalline piece which is shown in the picture on the left

A thermogravimetric oxidation of pulverized material from section C5 resulted in an oxygen content $x = 70 - y = 68.36$, i.e. $\Delta y = -1.64$

For comparison: The melt-grown synthesis of $Sr_{19}Nb_{19}WO_{69.5-y}$ likewise under 97.2 % Ar + 2.8 % H_2 resulted in $x = 69.5 - y = 66.03$, i.e. $\Delta y = -3.47$, see run / sample No. 812 which is presented in part 6.9.2

As-grown crystalline material $Sr_{19}Nb_{18}W_2O_{70-y}$

Sample No. 819

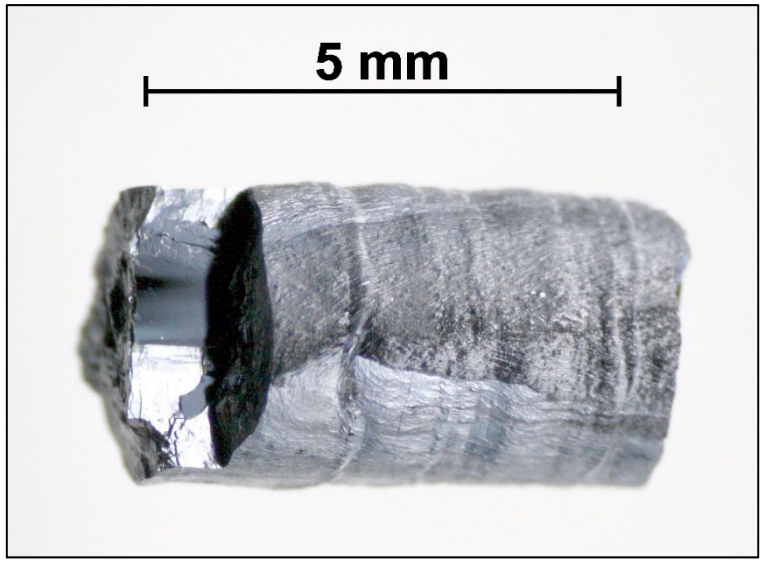

Crystalline piece from section C5 of the as-grown material

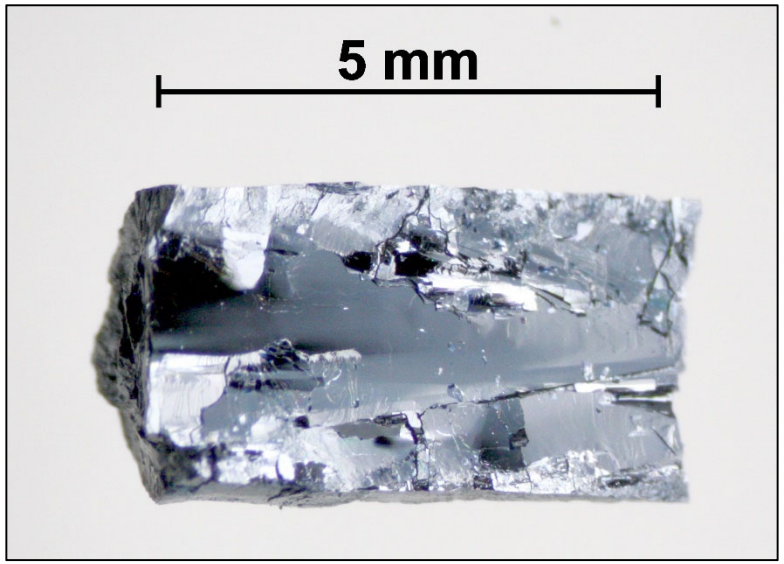

Part of the crystalline piece which is shown in the picture on the left

Powder x-ray diffraction of pulverized material from section C5 indicates a multiphase material which consists of an n = 4.5 type phase, an n = 5 type phase, and hexagonal $Sr_{11}Nb_9O_{33}$ which is reported in Progress in Solid State Chemistry 36 (2008) 253

Run / Sample No. 840:

$Sr_{18}CaBaNb_{19}WO_{70.5 - y}$ ...

Sintered rods with composition $Sr_{18}CaBaNb_{19}WO_{70.5}$ Run No. 840

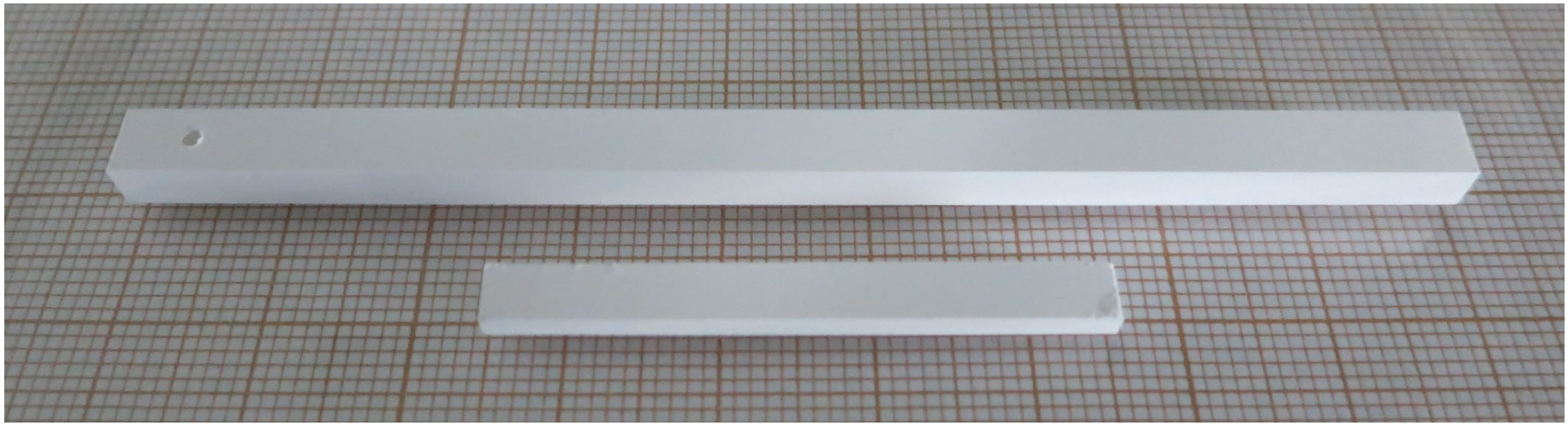

Polycrystalline sintered rods with fully oxidized composition $Sr_{18}CaBaNb_{19}WO_{70.5}$, i.e. all Nb and W ions are in their highest valence or oxidation state Nb^{5+} and W^{6+}, respectively

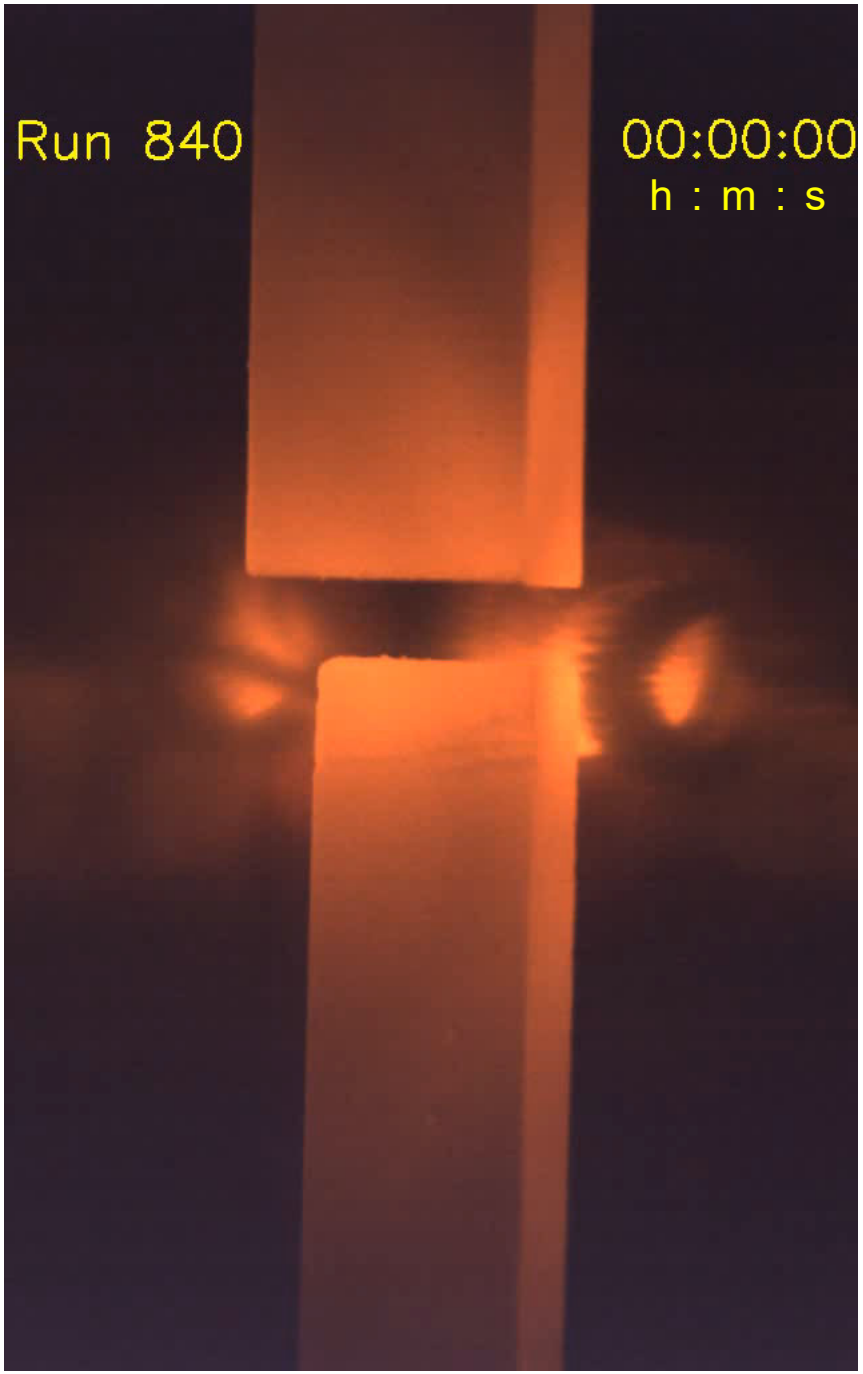

Melt-grown synthesis of $Sr_{18}CaBaNb_{19}WO_{70.5 - y}$

Starting materials for the mirror furnace run: Polycrystalline sintered rods with fully oxidized composition $Sr_{18}CaBaNb_{19}WO_{70.5}$

Fast mode video from the overall melt-grown synthesis of $Sr_{18}CaBaNb_{19}WO_{70.5 - y}$ under 95% Ar + 5 % H_2 in the Cyberstar mirror furnace. The video is only running in the ppsx type version of this publication, see page 2

Gas flow rate: 400 sccm (24 L / h)
Gas type setting at the mass flow controller: Ar

Lamp power to maintain the molten zone: 2 × (398 - 468) W

Speed of the lower shaft and seed rod (crystal growth speed): 14 mm / h

The video shows after some time a stepwise development of a viscous zone above the molten zone. This and the needed increase of the lamp power indicates the presence of an incongruent melting and solidification

As-grown crystalline $Sr_{18}CaBaNb_{19}WO_{70.5-y}$ and polycrystalline rods

Run / Sample No. 840

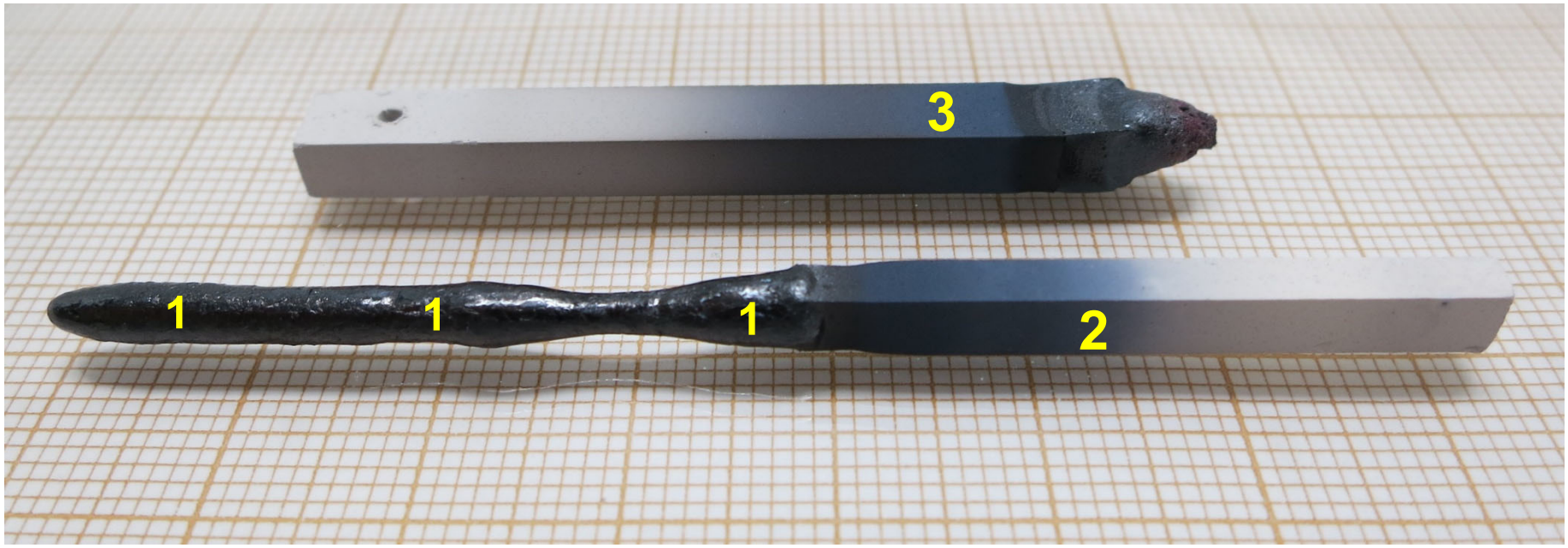

39 mm long as-grown crystalline material (1) plus polycrystalline seed rod (2) and remaining part of the polycrystalline feed rod (3)

Prepared at the ETH Zurich in 2019

As-grown crystalline material $Sr_{18}CaBaNb_{19}WO_{70.5 - y}$

Sample No. 840

39 mm long as-grown crystalline material

As-grown crystalline material $Sr_{18}CaBaNb_{19}WO_{70.5 - y}$

Sample No. 840

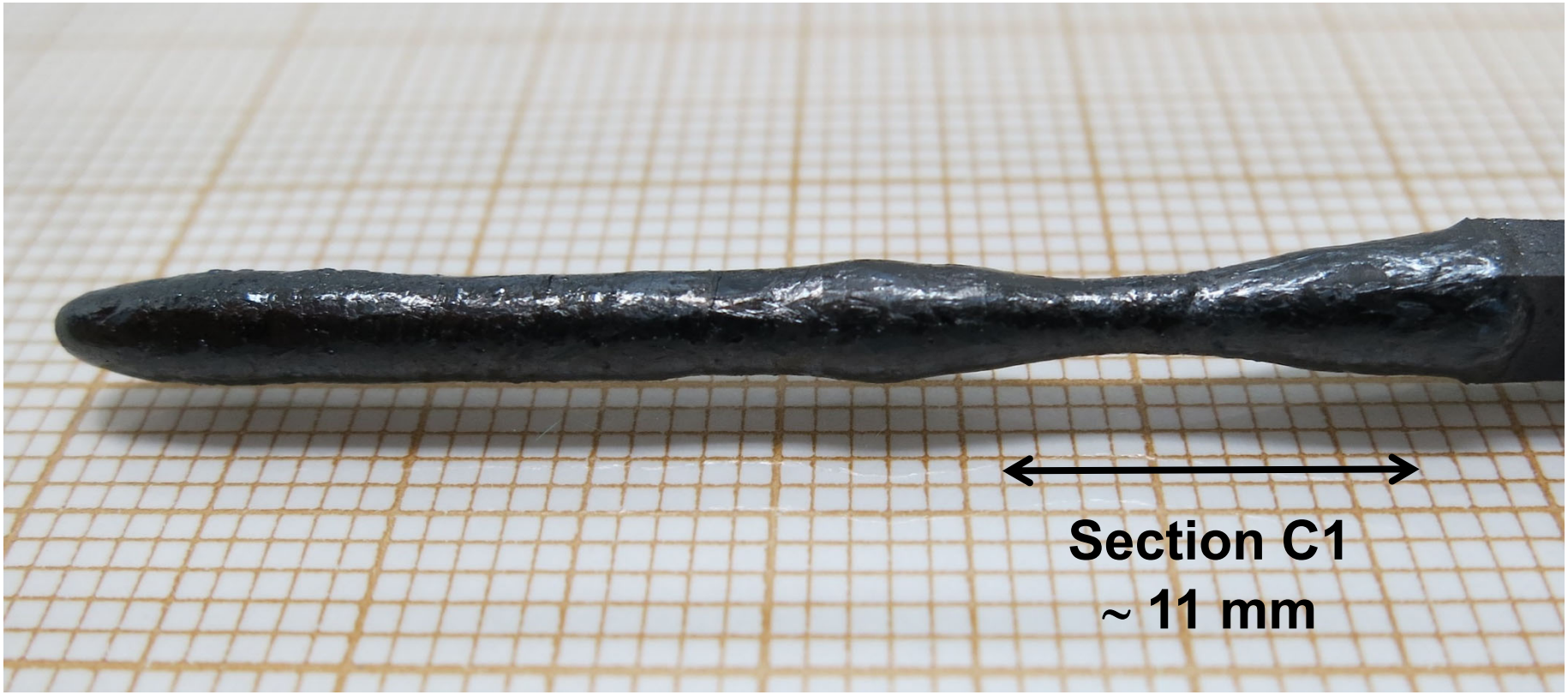

39 mm long as-grown crystalline material

As-grown crystalline material $Sr_{18}CaBaNb_{19}WO_{70.5 - y}$

Sample No. 840

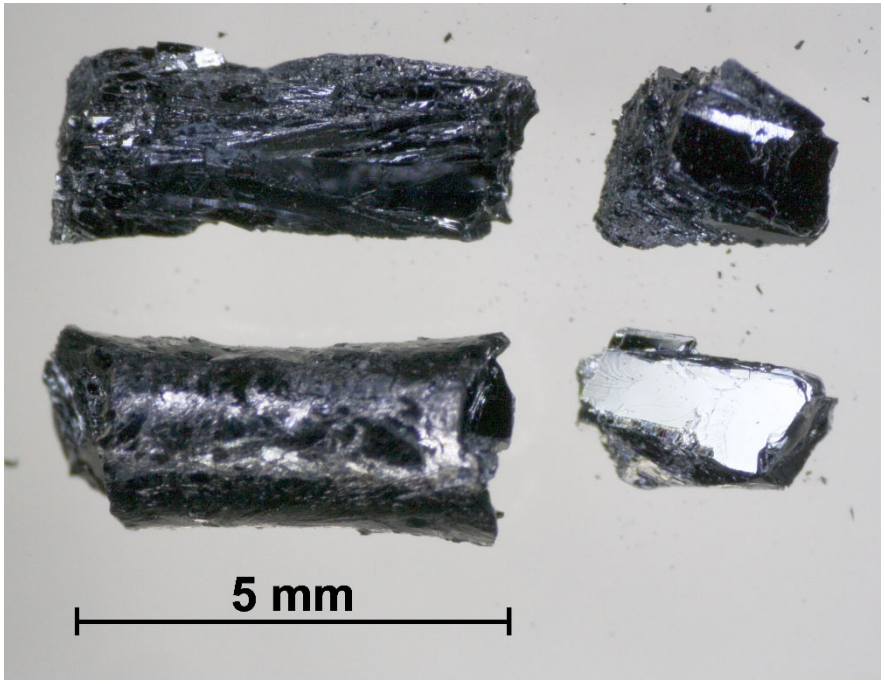

Crystalline pieces from section C1 of the as-grown material

A thermogravimetric oxidation of pulverized material from section C1 resulted in an oxygen content $x = 70.5 - y = 67.42$, i.e. $\Delta y = - 3.08$

For comparison: The melt-grown synthesis of $Sr_{17}CaBaNb_{19}WO_{69.5 - y}$ likewise under 95 % Ar + 5 % H_2 resulted in $x = 69.5 - y = 64.06$, i.e. $\Delta y = - 5.44$, see run / sample No. 838 which is presented in part 6.9.5

As-grown crystalline material $Sr_{18}CaBaNb_{19}WO_{70.5 - y}$

Sample No. 840

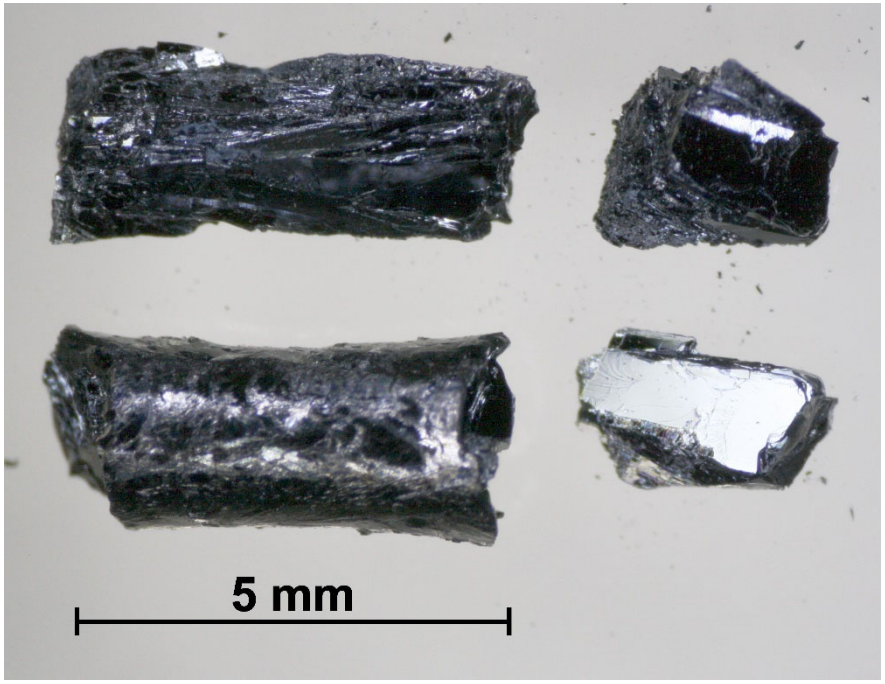

Crystalline pieces from section C1 of the as-grown material

Powder x-ray diffraction of pulverized material from section C1 indicates the presence of an *n* = 5 type phase and 1 unindexed peak at 2Θ = 29.84° with I_{rel} = 16 %. This suggests the presence of hexagonal $Sr_{11}Nb_9O_{33}$ and / or hexagonal $Sr_6Nb_5O_{18}$ which are reported in Progress in Solid State Chemistry 36 (2008) 253. Their highest intensity peak positions are 2Θ = 29.82° and 2Θ = 29.96°

Run / Sample No. 834:

$Ca_{19}BaNb_{19}WO_{68}$ ...

Preparation of rods with composition $Ca_{19}BaNb_{19}WO_{68}$ Run No. 834

Approach: $19\ CaCO_3 + BaCO_3 + 9.5\ (1 - y)\ Nb_2O_5 + 19\ y\ NbO_{2.01} + WO_3$

$= Ca_{19}BaNb_{19}WO_{67.9} + 20\ CO_2 \uparrow$

The starting material $NbO_{2.01}$ is niobium dioxide NbO_2 (Nb^{4+}) with a thermogravimetrically determined or verified oxygen content of 2.01

Equation for oxygen: $20 + 9.5 \times 5\ (1 - y) + 19 \times 2.01\ y + 3 = 67.9$

$\Rightarrow$ $y = 260 / 931 = 0.2793$

$9.5\ (1 - y) = 10749 / 1862 = 6.8469$

$19\ y = 4940 / 931 = 5.3061$

Preparation of rods with composition $Ca_{19}BaNb_{19}WO_{68}$ Run No. 834

Appropriate amounts of the starting materials

19 $CaCO_3$ + $BaCO_3$ + 6.8469 Nb_2O_5 + WO_3

were calculated, weighed, mingled, and pre-reacted for 4 h at 1210 °C under air which results in the CO_2-free composition

19 CaO + BaO + 6.8469 Nb_2O_5 + WO_3 (color white)

Subsequently the somewhat sintered material was grinded into powder and a calculated and weighed amount of

5.3061 $NbO_{2.01}$ (black powder)

was added. The picture shows the white and black powder in an agate mortar

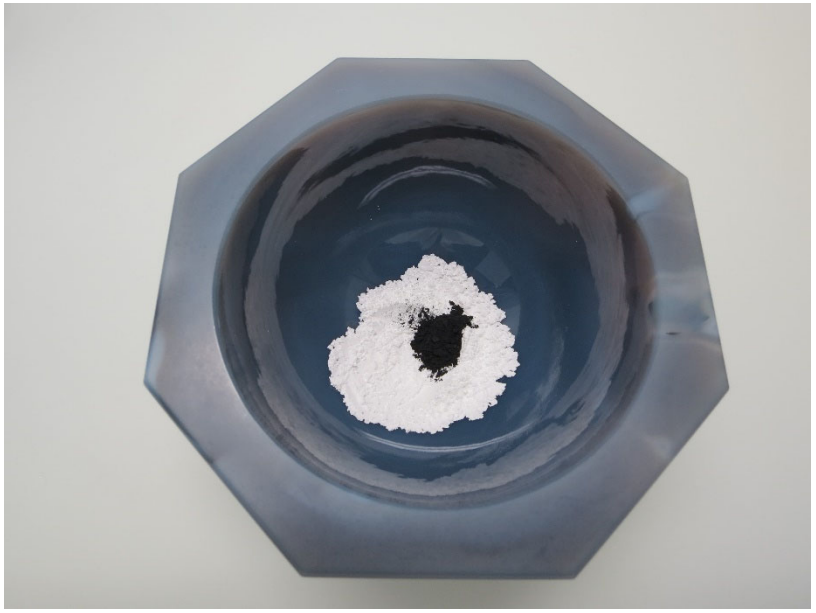

Preparation of rods with composition $Ca_{19}BaNb_{19}WO_{68}$ Run No. 834

The powders were mingled which results in a powder with composition

$$19\ CaO + BaO + 6.8469\ Nb_2O_5 + WO_3 + 5.3061\ NbO_{2.01} = Ca_{19}BaNb_{19}WO_{67.9}$$

The picture shows this powder in an agate mortar

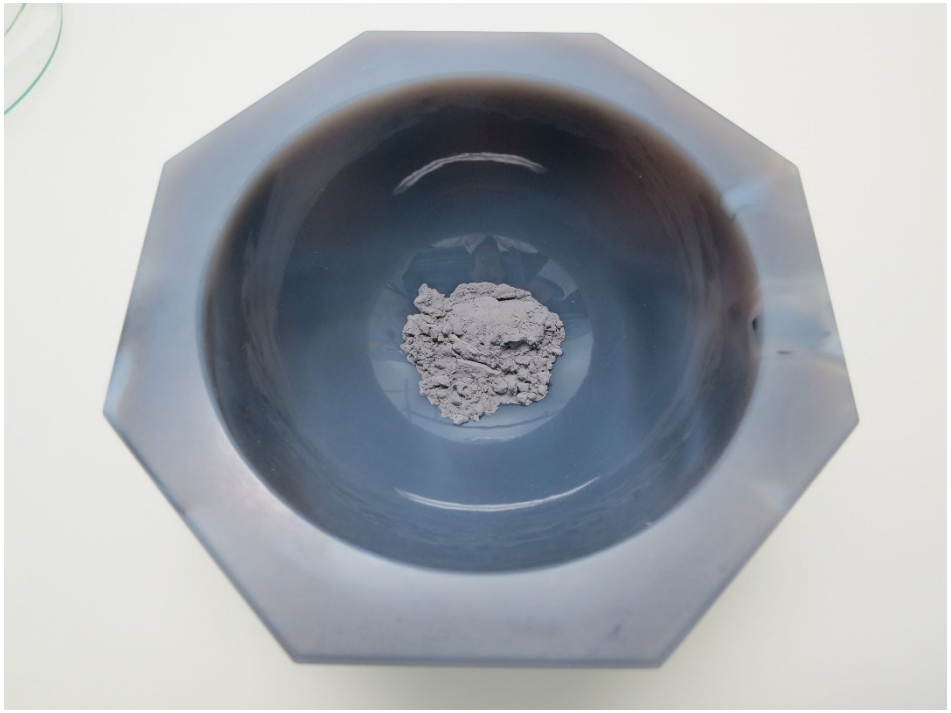

A small part of this powder was used to verify its composition by thermo-gravimetric oxidation which resulted in an oxygen content of 67.90

A part of this powder was pressed into two rectangular rods ...

Preparation of rods with composition $Ca_{19}BaNb_{19}WO_{68}$ Run No. 834

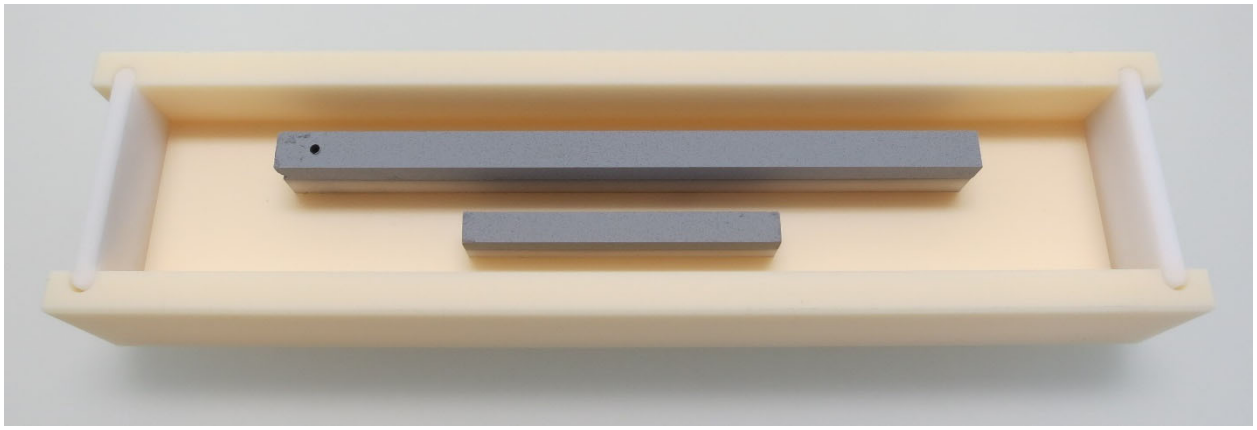

As-pressed rods with composition $Ca_{19}BaNb_{19}WO_{67.9}$ on their lower punch made of alumina in an alumina box. The length of the long rod is 9 cm

The alumina box is covered with a niobium sheet which acts as oxygen getter when the rods are sintered under flowing argon in the GERO tube furnace ...

Preparation of rods with composition $Ca_{19}BaNb_{19}WO_{68}$ Run No. 834

Log-linear plot of recorded data of a tube furnace run on 26 and 27 March 2019 with rods No. 834 on lower punches in an alumina box which is covered with a Nb sheet. Before starting the run: 2 × evacuated (2.3×10^{-3} / 1.4×10^{-3} mbar at the gas outlet after 6 / 6 min) and flushed with Ar. Gas (Ar) flow rate 24 L / h. Heating and cooling rate 250 °C / h (set values). Dwell time 2 h at 1300 °C . The O_2 content of Ar at the gas outlet becomes zero at elevated temperatures because the Nb sheet getters O_2 . Ar purity 6.0

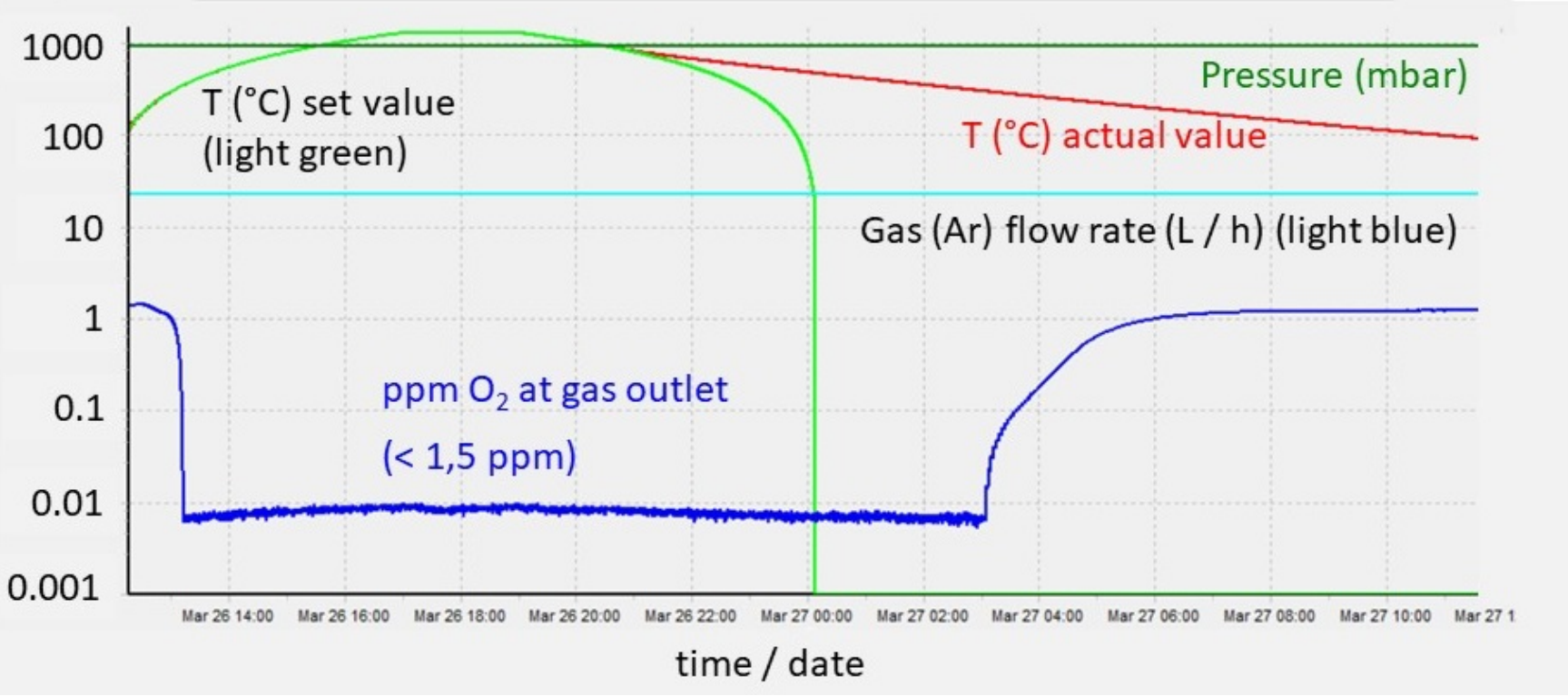

Preparation of rods with composition $Ca_{19}BaNb_{19}WO_{68}$ Run No. 834

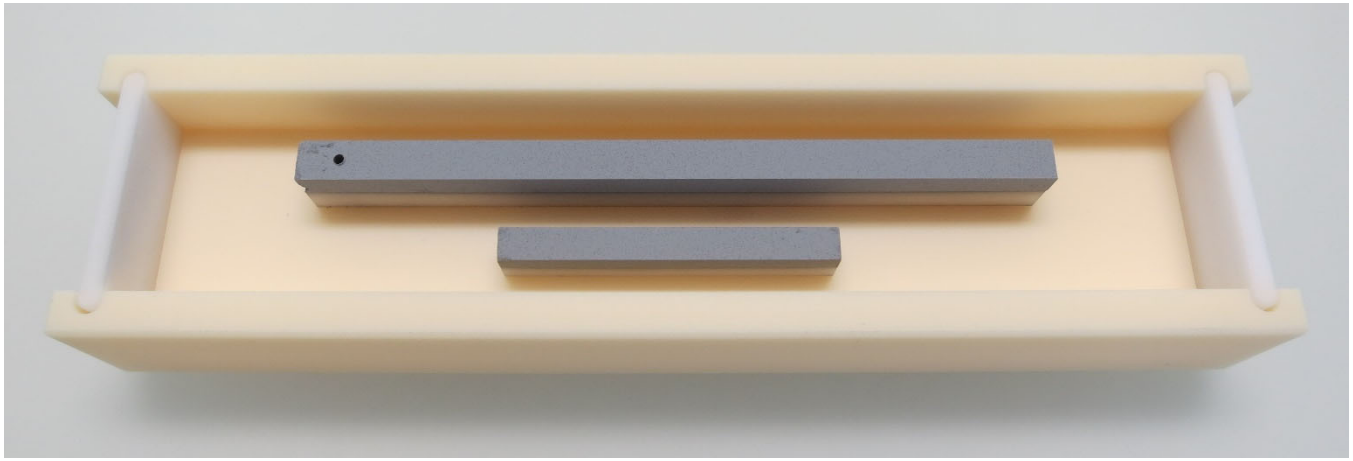

As-pressed rods with composition $Ca_{19}BaNb_{19}WO_{67.9}$

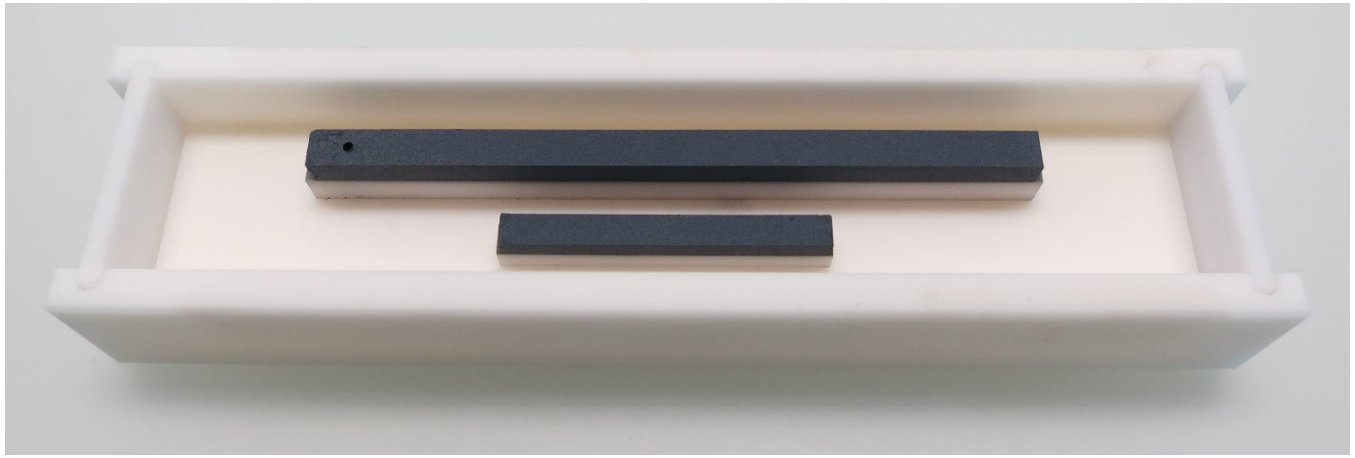

Rods after sintering for 2 h at 1300 °C under flowing argon in the GERO tube furnace

Preparation of rods with composition $Ca_{19}BaNb_{19}WO_{68}$ Run No. 834

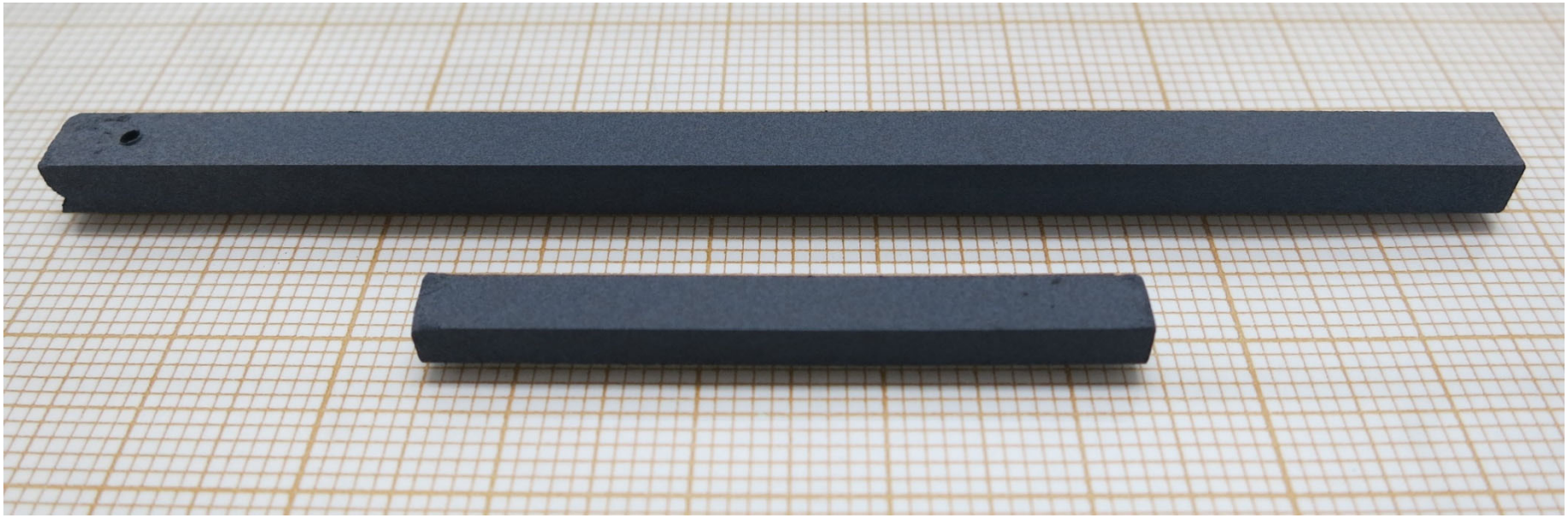

Polycrystalline sintered rods with composition $Ca_{19}BaNb_{19}WO_{68}$

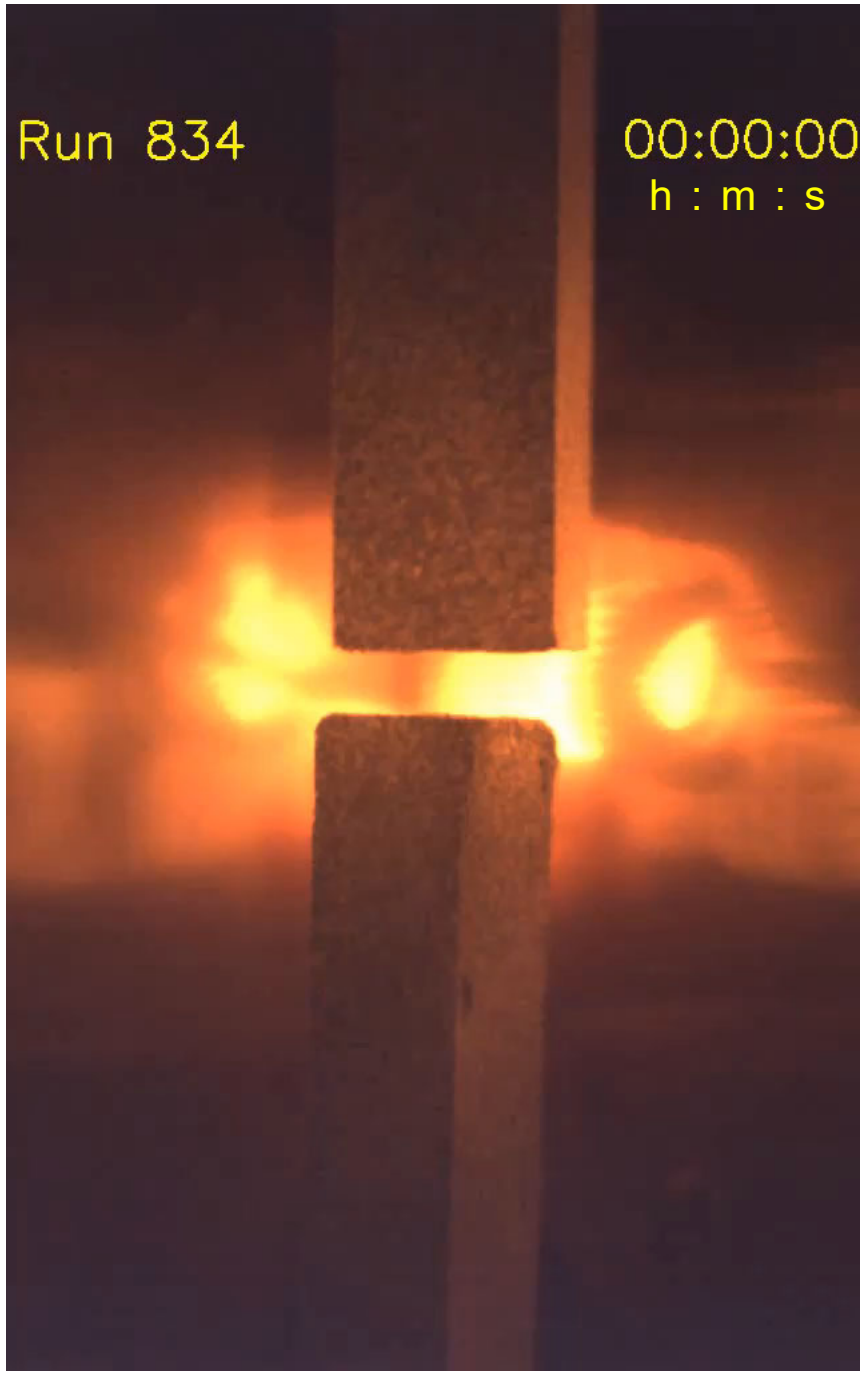

An attempt to prepare melt-grown $n = 5$ type $Ca_{19}BaNb_{19}WO_{68}$

Starting materials for the mirror furnace run: Polycrystalline sintered rods with composition $Ca_{19}BaNb_{19}WO_{68}$

Fast mode video from the overall mirror furnace run under Ar in the Cyberstar mirror furnace. The video is only running in the ppsx type version of this publication, see page 2

Gas flow rate: 400 sccm (24 L / h)

Lamp power to maintain the molten zone: 2 × (336 - 349) W

Speed of the lower shaft and seed rod (crystal growth speed): 14 mm / h

The video shows after some time a stepwise development of a viscous zone above the molten zone. That indicates the presence of an incongruent melting and solidification. Actually, as revealed later by powder XRD, from the beginning no $n = 5$ (oxygen content $x \sim 68$) but an $n \sim 4$ type material ($x = 70$) crystallizes from the melt

Result of an attempt to prepare melt-grown $n = 5$ type $Ca_{19}BaNb_{19}WO_{68}$

Run / Sample No. 834

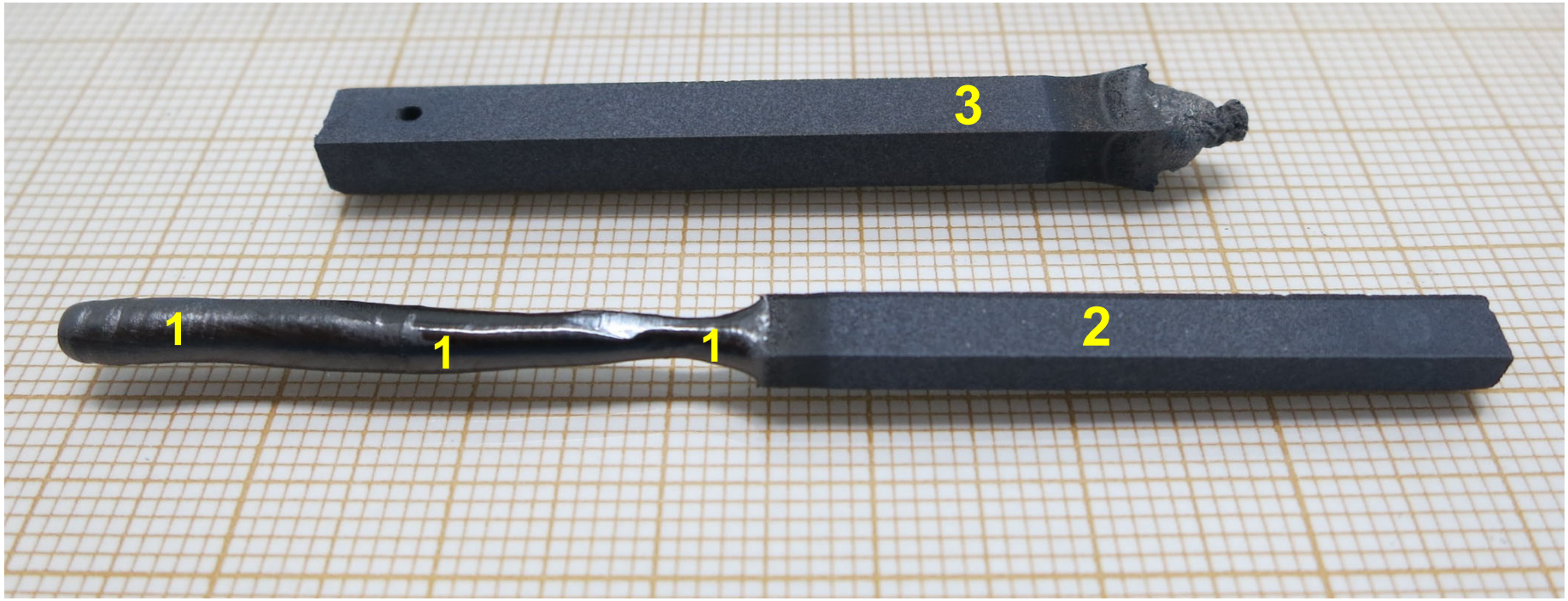

34 mm long as-grown crystalline material (1) plus polycrystalline seed rod (2) and remaining part of the polycrystalline feed rod (3)

Prepared at the ETH Zurich in 2019

Result of an attempt to prepare melt-grown *n* = 5 type $Ca_{19}BaNb_{19}WO_{68}$

Sample No. 834

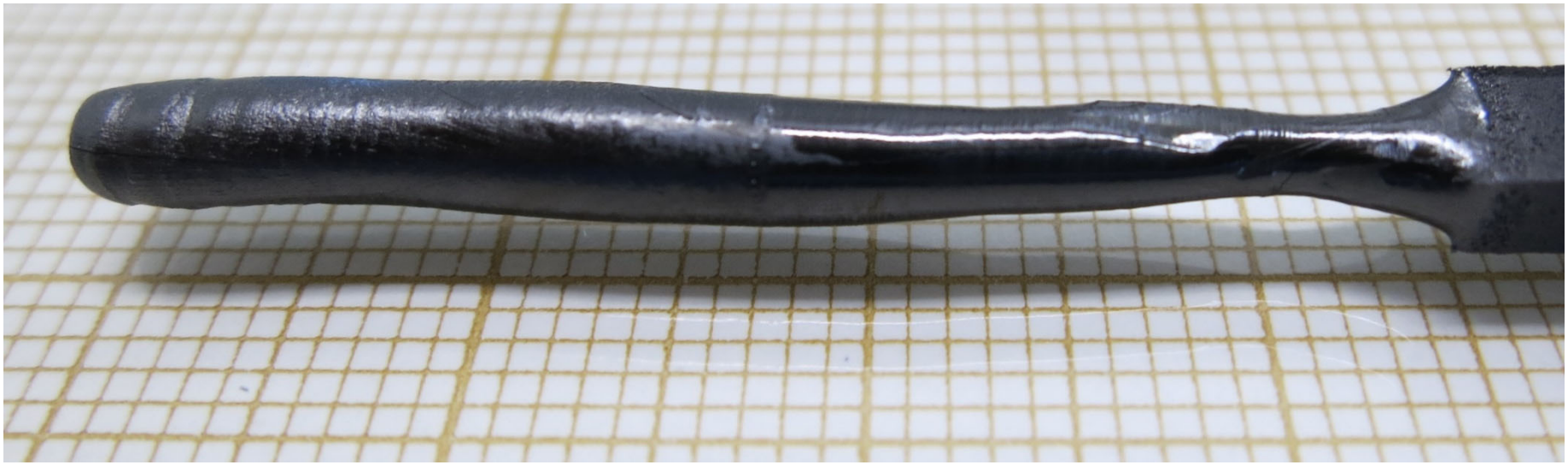

34 mm long as-grown crystalline material

Result of an attempt to prepare melt-grown $n = 5$ type $Ca_{19}BaNb_{19}WO_{68}$

Sample No. 834

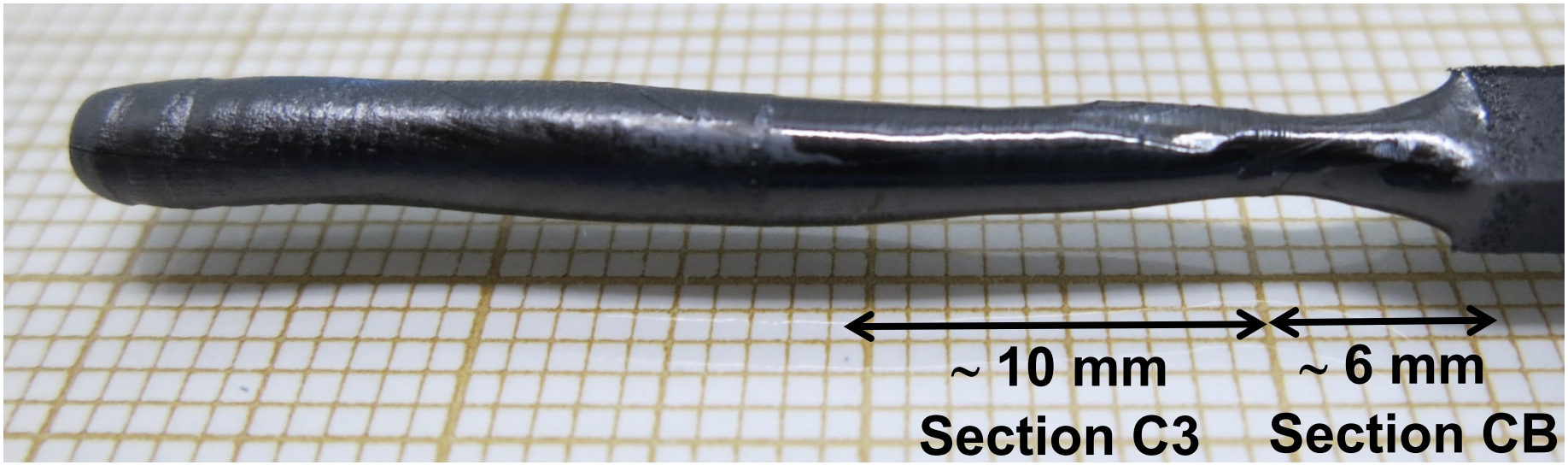

34 mm long as-grown crystalline material

Result of an attempt to prepare melt-grown *n* = 5 type $Ca_{19}BaNb_{19}WO_{68}$

Sample No. 834

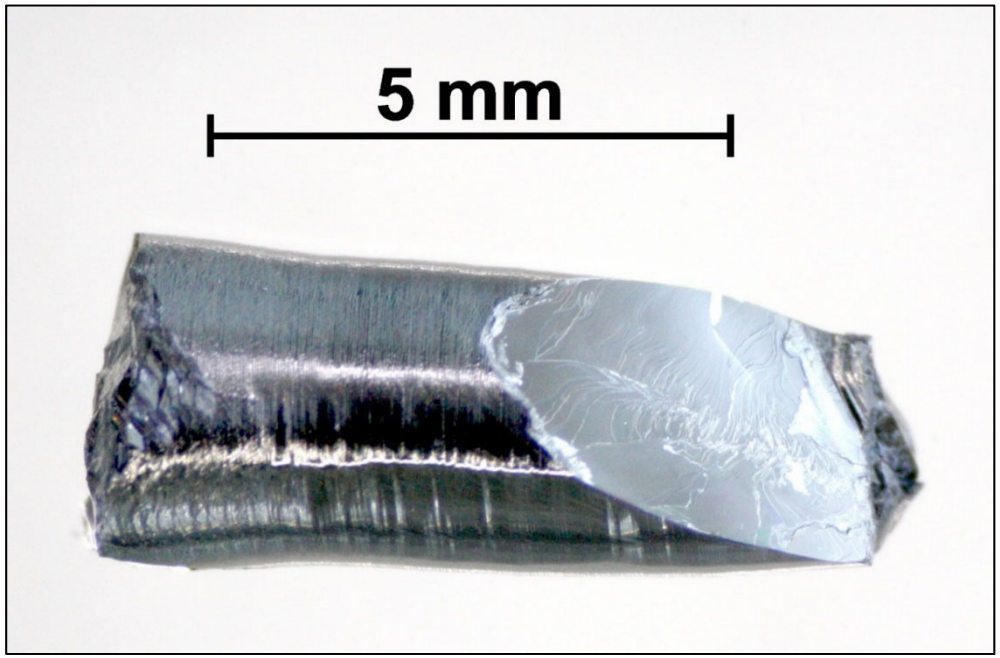

Crystaliine piece from section C3 of the as-grown material

Result of an attempt to prepare melt-grown $n = 5$ type $Ca_{19}BaNb_{19}WO_{68}$

Sample No. 834

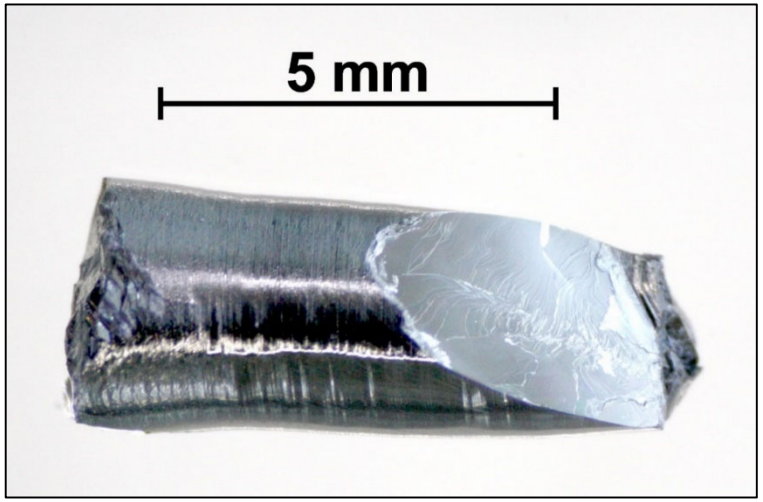

Crystalline piece from section C3 of the as-grown material

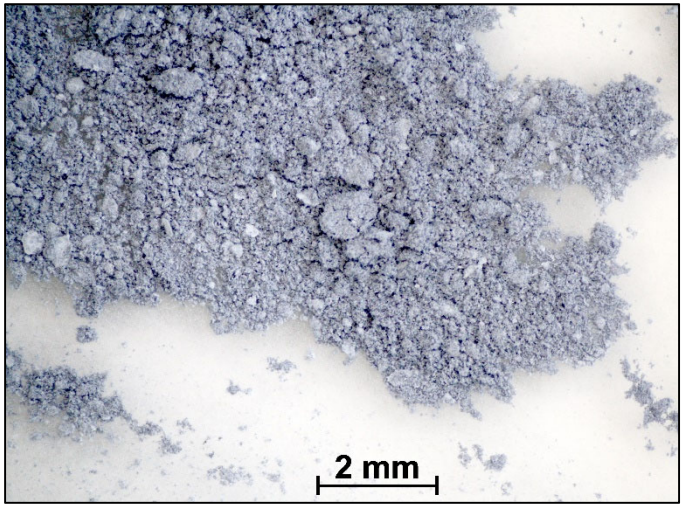

Pulverized crystalline material from section C3 and CB

Powder x-ray diffraction of pulverized material from section C3 and CB of the as-grown sample indicates the presence of an $n = 4$ type phase plus another minor phase(s) but no presence of an $n = 5$ type phase. An $n = 4$ type phase has a higher oxygen content x than an $n = 5$ type, namely $x \sim 70$ instead of $x \sim 68$. The color of pulverized crystalline material is not black but gray which indicates that its oxygen content and composition is nearby that of the fully oxidized and non-conducting composition $Ca_{19}BaNb_{19}WO_{70.5}$

Another examples

in short form ...

Another examples of processed compositions which did not result in a single phase melt-grown *n* = 5 type material

Run / Sample No.	Composition of the melt-grown material	Desired phase or structure type	Actual phase(s) from powder XRD	Synthesis procedure
797	$Sr_{20}Nb_{19}O_{66.1}$	Conducting Nb- and O-deficient *n* = 5 with Nb^{5+} / Nb^{4+}	*n* = 5 plus hexagonal $Sr_6Nb_5O_{18}$	Reducing the fully oxidized composition $Sr_{20}Nb_{19}O_{67.5}$ under 97.2 % Ar + 2.8 % H_2 with a gas flow rate 24 L / h and a growth speed 14 mm / h
800	$Ca_{20}Nb_{19}O_{65.2}$		*n* = 5 plus another phase(s)	Processing the composition $Ca_{20}Nb_{19}O_{65}$ under Ar with a growth speed 14 mm / h

Samples prepared at the ETH Zurich in 2017

Another example of a processed composition which did not result in a single phase melt-grown *n* = 5 type material

Run / Sample No.	Composition of the melt-grown material	Desired phase or structure type	Actual phase(s) from powder XRD	Synthesis procedure
724	$Eu_{20}Ti_{20}O_{67}$	Conducting *n* = 5 with Ti^{4+} / Ti^{3+} and Eu^{3+} or Eu^{3+} / Eu^{2+}	Cubic pyrochlore $Eu_2Ti_2O_7$ with Eu^{3+} / Ti^{4+} plus perovskite $EuTiO_3$ with Eu^{2+} / Ti^{4+}	As-pressed rods with composition $Eu_{20}Ti_{20}O_{66.6}$ were sintered for 1 h at 1325 °C under 750 sccm Ar + 0.14 sccm (90 % Ar + 10 % O_2) without Nb sheet , ~ 20 ppm O_2 in Ar at gas outlet. Composition of sintered rods was $Eu_{20}Ti_{20}O_{66.8}$. Sintered rods were processed in the Cyberstar mirror furnace under 1000 sccm Ar + 0.15 sccm (90 % Ar + 10 % O_2) , ~ (16 - 1 - 9) ppm O_2 in Ar at gas outlet. Growth speed 14 mm / h

Sample prepared at the ETH Zurich in 2014

6 Conducting and metallic Carpy-Galy phases $A_nB_nO_{3n+2} = ABO_x$

6.11 Magnetic properties of lanthanide ions Ln^{3+} in titanates of the type $Ln_nTi_nO_{3n+2} = LnTiO_x$ ...

Magnetic properties of some lanthanide ions

Ion	Ce^{4+} La^{3+}	Ce^{3+}	Pr^{3+}	Nd^{3+}	Sm^{3+}	Sm^{2+} Eu^{3+}	Eu^{2+} Gd^{3+}	Yb^{3+}
Electronic configuration	$4f^0$	$4f^1$	$4f^2$	$4f^3$	$4f^5$	$4f^6$	$4f^7$	$4f^{13}$
Multiplet ground state $^{2S+1}L_J$	$^1S_0$	$^2F_{5/2}$	$^3H_4$	$^4I_{9/2}$	$^6H_{5/2}$	$^7F_0$	$^8S_{7/2}$	$^2F_{7/2}$
g	–	6/7	4/5	8/11	2/7	–	2	8/7
q_{th} [μ_B]	0	2.54	3.58	3.62	0.84	0	7.94	4.54
Δ [K]		3150	3100	2750	1450	500	– [2]	14800
χ_V [10^{-6} emu G^{-1} mol^{-1}]		45	97	174	739	6000	–	8
ξ [10^{-6} K^{-1}] in $\chi_V/\chi_C = \xi T$		56	61	106	8276	∞ [1]	–	3

Table 64. Magnetic properties of some rare earth ions after Ref. [89,104]. Recall that L = S, P, D, F, G, H, I stands for L = 0, 1, 2, 3, 4, 5, 6, respectively. g is the free-ion Lande factor after Eq. (19). q_{th} is the theoretical free-ion value of the effective magnetic moment in units of the Bohr magneton μ_B after Eq. (18). Δ is the energy difference between the first excited state $^{2S+1}L_{J+1}$ and the ground state $^{2S+1}L_J$ of the multiplet. χ_V is the molar Van Vleck paramagnetic susceptibility after Eq. (14). The parameter $\xi = 2S(L+1)/[g^2 J(J+1)^2 \Delta]$, when multiplied with the temperature T, represents the ratio of the temperature-independent Van Vleck susceptibility χ_V to the Curie susceptibility $\chi_C = C/T$. [1]Here $\xi = \infty$ indicates symbolically the exclusive presence of the Van Vleck paramagnetism because the Curie susceptibility is absent owing to $J = 0$. [2]Due to $L = 0$ there is no spin-orbit interaction and therefore Δ does not exist because the different levels of a multiplet arise from the spin-orbit coupling.

Progress in Solid State Chemistry 36 (2008) 253 and references therein

Magnetic susceptibility of (free) samarium and europium ions

Sm^{3+} ($4f^5$) $\rightarrow$ Langevin paramagnetism (Curie or Curie-Weiss behavior)
plus significant contribution of Van Vleck paramagnetism

Sm^{2+} and Eu^{3+} (both $4f^6$) $\rightarrow$ Only Van Vleck (total angular momentum $J = 0$)

Eu^{2+} ($4f^7$) $\rightarrow$ Only Langevin (orbital angular momentum $L = 0$)

Langevin paramagnetism results from states with different m_J

Van Vleck paramagnetism results from states J and $J + 1$

Magnetic susceptibility $\chi(T)$ of conducting $n = 5$ type Carpy-Galy phases $Ln_nTi_nO_{3n+2} = LnTiO_x$ and the cubic pyrochlore $EuTiO_{3.5}$

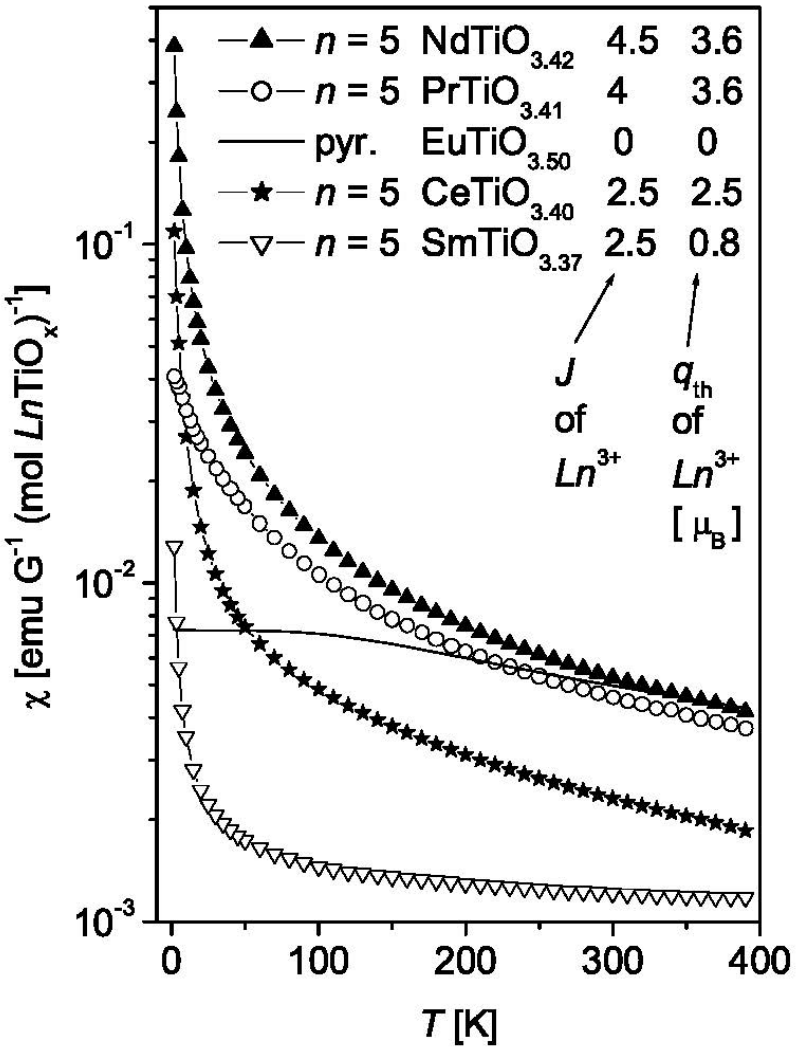

The conducting materials (quasi-1D metals ?) comprise a mixed valence Ti^{4+} ($3d^0$) / Ti^{3+} ($3d^1$) and χ is dominated by the Ln^{3+} ions

$EuTiO_{3.5}$ is a Ti^{4+} ($3d^0$) insulator

Fig. 56. Log-linear plot of the molar magnetic susceptibility $\chi(T)$ in fields of $H \leq 500$ G of some titanates $LnTiO_x$: The $n = 5$ electrical conductors $CeTiO_{3.40}$ ($3d^{0.20}$), $PrTiO_{3.41}$ ($3d^{0.18}$), $NdTiO_{3.42}$ ($3d^{0.16}$), $SmTiO_{3.37}$ ($3d^{0.26}$), and the insulator $EuTiO_{3.50}$ ($3d^0$) with pyrochlore structure. The susceptibility results predominantly from the paramagnetic moments of the rare earth ions Ln^{3+}. Therefore this plot represents a comparison of the magnitude and the temperature dependence of $\chi(T)$ resulting from Ce^{3+}, Pr^{3+}, Nd^{3+}, Sm^{3+} and Eu^{3+}. J is the quantum number of the total angular momentum of Ln^{3+} and q_{th} the associated theoretical free-ion value of the effective magnetic moment, see Table 64. The susceptibility of the Ce^{3+}, Pr^{3+} and Nd^{3+} titanates displays a Curie-Weiss behavior, see Fig. 52, 59 and Table 65, 67 and 69. The susceptibility of $SmTiO_{3.37}$ is markedly influenced by the Van Vleck type paramagnetism, see Table 64 and also Fig. 51 and 52. The paramagnetic susceptibility of $EuTiO_{3.50}$ results exclusively from the Van Vleck type paramagnetism, see Table 64 and also Fig. 54.

Progress in Solid State Chemistry 36 (2008) 253

Enhancement of magnetic interactions by vacancies ?

Curie-Weiss behavior of magnetic susceptibility: $\chi = C / (T - \Theta)$

Curie-Weiss temperature Θ indicates strength of magnetic exchange interaction between localized paramagnetic moments of Ln^{3+} ions in $Ln_nTi_nO_{3n+2} = LnTiO_x$

Nearly stoichiometric $LnTiO_x$ and significantly non-stoichiometric $Ln_{1-y}TiO_{x-w}$

Structure type	Compound	Average Ti valence	V [Å^3]	Θ (K)
n = 4.33	$CeTiO_{3.47}$	$Ti^{3.94+} / 3d^{0.06}$	3499	– 43
	$Ce_{0.95}TiO_{3.39}$	$Ti^{3.93+} / 3d^{0.07}$	3497	– 98
n = 5	$NdTiO_{3.42}$	$Ti^{3.84+} / 3d^{0.16}$	1330	– 28
	$NdTiO_{3.31}$	$Ti^{3.62+} / 3d^{0.38}$	1318	– 30
	$Nd_{0.95}TiO_{3.34}$	$Ti^{3.83+} / 3d^{0.17}$	1332	– 60

Progress in Solid State Chemistry 36 (2008) 253

Ln-deficiency results approximately in a doubling of Θ:

- Is this of general relevance in magnetism ?
- Enhancement of T_c in magnetically ordered systems by non-stoichiometry ?
- Is this also valid for deficiencies at the *B* site of $A_nB_nO_{3n+2} = ABO_x$?

7 Stability ranges of Carpy-Galy phases $A_nB_nO_{3n+2} = ABO_x$ and polymorphism in the systems $LnTiO_{3.5}$, $(Pr,Ca)(Ti,Nb)O_{3.5}$, $SmTiO_x$, $Ln_6Ti_4Fe_2O_{20}$, and $NaWO_{3.5}$ ...

The system $LnTiO_{3.5} = Ln_2Ti_2O_7$

Increasing *Ln* atomic number and decreasing ionic radius of Ln^{3+} →

***Ln* in $LnTiO_{3.5}$**	**La**	**Ce**	**Pr**	**Nd**	**Pm**	**Sm**	**Eu**	**Gd**
Structure type after normal pressure synthesis	*n* = 4 non-centrosymmetric ferroelectric					Cubic pyrochlore		
Structure type after high pressure synthesis or another special approach						*n* = 4 , non-centrosymmetric (potentially) ferroelectric 7 - 8 kbar at 1400 - 1900 °C or by annealing $SmTiO_3$ powder at 800 °C in air	80 kbar at 1750 °C	Strain-stabilized thin films

Progress in Solid State Chemistry 36 (2008) 253 and references therein

Journal of Materials Chemistry 22 (2012) 24894 and 22 (2012) 9806, see the two pages after the following page

Melt-grown $n = 4$ type $La_{0.1}Sm_{0.9}TiO_{3.5} = La_{0.2}Sm_{1.8}Ti_2O_7$ (Sm^{3+}, Ti^{4+})

Pieces from as-grown material

Sample No. 385

Grown under air

Yellow transparent (ferroelectric) insulator

Composition nearby the stability limit of the $n = 4$ type structure because $SmTiO_{3.5} = Sm_2Ti_2O_7$ crystallizes in the cubic pyrochlore structure

Progress in Solid State Chemistry 36 (2008) 253

Material prepared at the University of Augsburg - Photo taken at the ETH Zurich

Stability limits of *n* = 4 type $LnTiO_{3.5}$ = $Ln_2Ti_2O_7$ thin films grown on (110)-oriented $SrTiO_3$

Stability limit of the layered-perovskite structure in $Ln_2Ti_2O_7$ (Ln = lanthanide) thin films grown on (110)-oriented $SrTiO_3$ substrates by the sol-gel route

Zhenmian Shao, Sébastien Saitzek, Pascal Roussel, and Rachel Desfeux

Journal of Materials Chemistry 22 (2012) 24894 - 24901

https://doi.org/10.1039/C2JM34729F

Abstract: The stability limit between the layered-perovskite and pyrochlore structures was investigated for $Ln_2Ti_2O_7$ (Ln = lanthanide) thin films grown on (110)-oriented $SrTiO_3$ substrate by the sol–gel route. In bulk, for standard conditions of pressure and temperature, these oxides adopt the layered-perovskite structure for Ln = La to Nd while they crystallize in the pyrochlore one for Sm to Lu. When grown in thin films on (110)-oriented $SrTiO_3$ substrates, the frontier separating these two structures is shifted. High-resolution X-ray diffraction measurements evidence the stabilization of a metastable (00*l*) oriented layered-perovskite structure for $Sm_2Ti_2O_7$, $Eu_2Ti_2O_7$, and $Gd_2Ti_2O_7$. Such stabilization is explained by a combination of both the strains induced by the substrate in the film and the good lattice match between the substrate and the metastable layered-perovskite oxide. The stabilization of layered-perovskite structures in thin films opens interesting perspectives in terms of development of new ferroelectric/piezoelectric devices, keeping in mind that the isostructural $La_2Ti_2O_7$ and $Nd_2Ti_2O_7$ possess a very high Curie temperature ($T_c \approx 1500$ °C). Finally, the role played by the lanthanide precursor (nitrate or chloride) in the stabilization of the layered-perovskite structure is highlighted and prediction for stabilization of other new layered-perovskite compounds in the $Ln_2B_2O_7$ (B = Zr, Mn) system for thin films deposited on the (110)-oriented $SrTiO_3$ substrate is reported.

Evidence of ferroelectricity in a metastable $n = 4$ type $SmTiO_{3.5} = Sm_2Ti_2O_7$ thin film

Evidence of ferroelectricity in metastable $Sm_2Ti_2O_7$ thin film

ZhenMian Shao, Sebastien Saitzek, Anthony Ferri, Mohamed Rguiti, Loïc Dupont, Pascal Roussel, and Rachel Desfeux

Journal of Materials Chemistry 22 (2012) 9806 - 9812

https://doi.org/10.1039/C2JM16261J

Abstract

The synthesis by the sol-gel route of metastable $Sm_2Ti_2O_7$ thin film is reported. While for standard conditions of pressure and temperature, the $Sm_2Ti_2O_7$ compound crystallizes in a cubic pyrochlore structure, in the form of a thin film (grown on (110)-oriented $SrTiO_3$ substrate), a monoclinic layered perovskite structure is stabilized by strain effects induced by the substrate. Under these conditions, (00l)-oriented $Sm_2Ti_2O_7$ oxide is isostructural to ferroelectric $Ln_2Ti_2O_7$ (with Ln = La, Ce, Pr and Nd) phases, which is already well known. Studies by Selected Area Electron Diffraction (SAED) reveal the existence of a systematically twinned structure and the presence of a fault in the stacking of the perovskite layers. Piezoresponse Force Microscopy (PFM) measurements confirm undoubtedly the ferroelectricity in this metastable phase.

The system $Pr_{1-y}Ca_yTi_{1-y}Nb_yO_{3.50}$ (Pr^{3+}, Ti^{4+}, and Nb^{5+})

Powder x-ray diffraction pattern of melt-grown $Pr_{1-y}Ca_yTi_{1-y}Nb_yO_{3.50}$

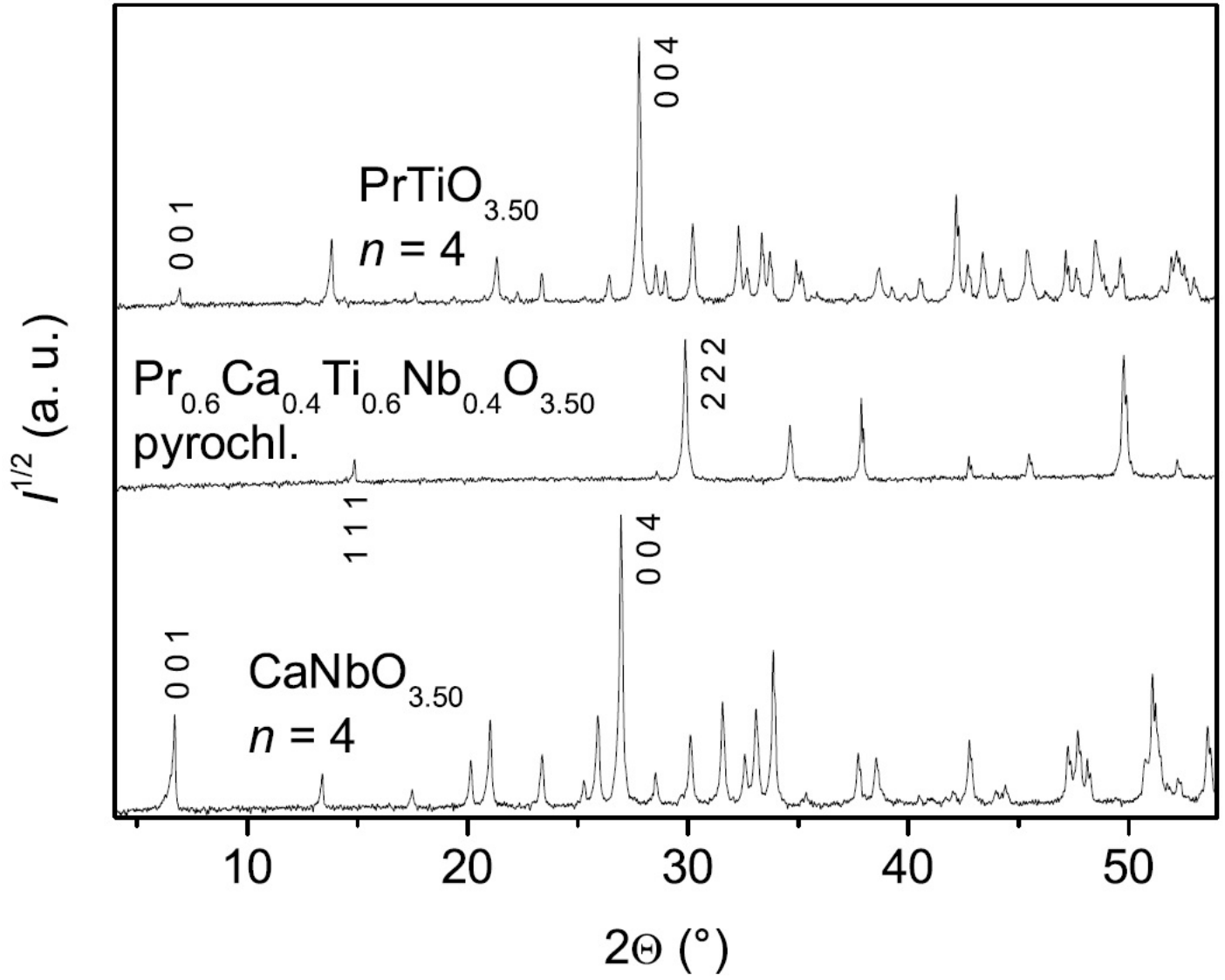

$PrTiO_{3.50}$ and $CaNbO_{3.50}$ are $n = 4$ type ferrolectric insulators

Nevertheless, some intermediate compositions crystallize in the cubic pyrochlore structure, e.g. that with $y = 0.4$

Progress in Solid State Chemistry 36 (2008) 253

The system $SmTiO_x$

x in $SmTiO_x$	x = 3.50	x = 3.44	x = 3.37
Structure type after normal pressure synthesis	Cubic pyrochlore	Two phases: n = 5 and cubic pyrochlore	n = 5
Structure type after high pressure synthesis or another special approach	n = 4 non-centrosymmetric ferroelectric 7 - 8 kbar at 1400 - 1900 °C Annealing $SmTiO_3$ powder at 800 °C in air Strain-stabilized thin films		

Progress in Solid State Chemistry 36 (2008) 253 and references therein
Journal of Materials Chemistry 22 (2012) 24894 and 22 (2012) 9806

The system $SmTiO_x$

Crystalline pieces from the melt-grown material

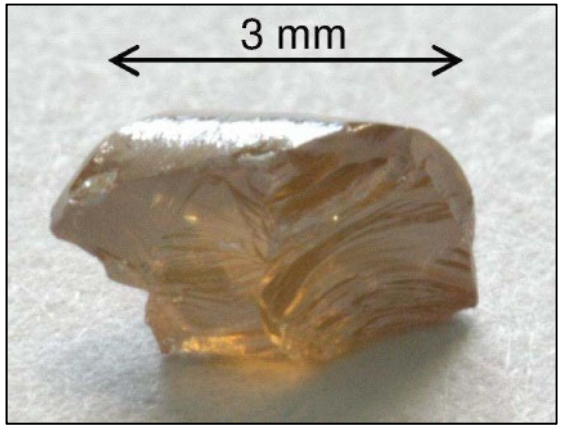

$SmTiO_{3.50} = Sm_2Ti_2O_7$

Sm^{3+} / $4f^5$ and Ti^{4+} / $3d^0$

Sample No. 252

Grown with 15 mm / h in air

Structure type pyrochlore

Yellow transparent insulator

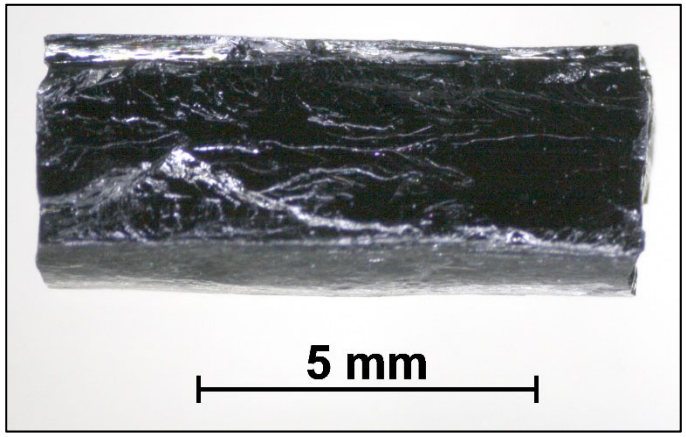

$SmTiO_{3.37}$

Sm^{3+} / $4f^5$ and $Ti^{3.74+}$ / $3d^{0.26}$

Sample No. 299

Grown with 15 mm / h in argon

Structure type $n = 5$

Black electrical conductor (quasi-1D metal ?)

Samples prepared at the University of Augsburg - Picture of $SmTiO_{3.37}$ taken at the ETH Zurich

Progress in Solid State Chemistry 36 (2008) 253

Melt-grown n = 5 type $SmTiO_{3.37}$

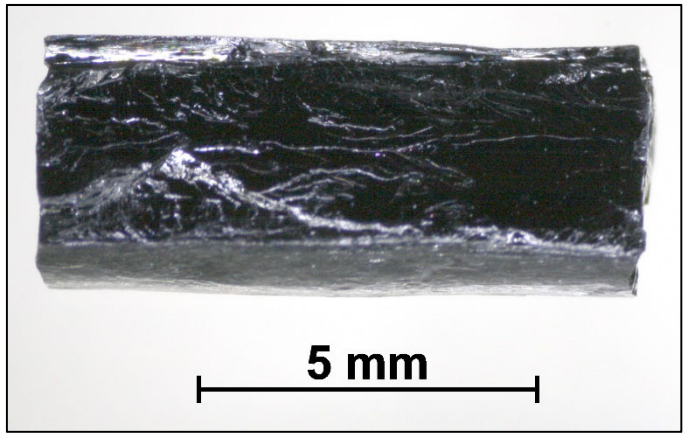

$SmTiO_{3.37}$ Sample No. 299

Sm^{3+} / $4f^{5}$ and $Ti^{3.74+}$ / $3d^{0.26}$

Grown with 15 mm / h in argon

Black electrical conductor (quasi-1D metal ?)

Sample prepared at the University of Augsburg

Picture taken at the ETH Zurich

Progress in Solid State Chemistry 36 (2008) 253

Sample preparation: A thermogravimetrically confirmed composition (powder)

$$0.5\ Sm_2O_3 + 0.897\ TiO_2 + 0.103\ TiO_{1.03} = SmTiO_{3.40}$$

was pressed in form of two rectangular rods and sintered for 4 h at 1375 °C under argon. Thermogravimetry of a small piece from the sintered rods revealed an oxygen content of x = 3.37, i.e. the rods released somewhat oxygen, namely Δx = - 0.03. Melt-grown $SmTiO_{3.37}$ was prepared by processing the sintered rods by floating zone melting under argon in a GERO mirror furnace. The oxygen content x = 3.37 of the melt-grown crystalline material was thermogravimetrically determined.

Titanium monoxide with thermogravimetrically determined oxygen content 1.03

Melt-grown $Ln_6Ti_4Fe_2O_{20}$ (see part 5.3.1 and 5.3.2)

Increasing *Ln* atomic number and decreasing ionic radius of Ln^{3+} →

Ln **in** $Ln_6Ti_4Fe_2O_{20}$	**La**	**Ce**	**Pr**	**Nd**	**Pm**	**Sm**	$Sm_{0.9}Eu_{0.1}$	**Eu**
Structure type	$n = 6$	Attempts to prepare an $n = 6$ type material were not successful	$n = 6$			$n = 6$		Multiphase material: Pyrochlore $Eu_2Ti_2O_7$ and perovskite $EuTiO_3$ and ?

Orthorhombic $NaWO_{3.5} = Na_2W_2O_7$ and $A_nB_nO_{3n+2} = ABO_x$

$NaWO_{3.5} = Na_2W_2O_7$ W^{6+} ($5d^0$) insulator	
Structure type after normal pressure synthesis	Orthorhombic Centrosymmetric WO_6 octahedral and WO_4 tetrahedra $[W_2O_7]^{2-}$ chains along *a*-axis K. Okada, H. Morikawa, F. Marumo, and S. Iwai, Acta Crystallographica Section B 31 (1975) 1200
Structure type after high pressure synthesis	Orthorhombic $n = 4$ Non-centrosymmetric Potentially ferroelectric Single crystals were grown by cooling normal pressure synthesized $Na_2W_2O_7$ slowly from 1200 °C under 20 – 30 kbar K.-J. Range and H. Haase, Acta Crystallographica Section C 46 (1990) 317

8 Carpy-Galy phases

$A_nB_nO_{3n+2} = ABO_x$ allow a special kind of micro or nano patterning by an electron beam

8 Carpy-Galy phases $A_nB_nO_{3n+2} = ABO_x$ allow a special kind of micro or nano patterning by an electron beam

8.1 A basic observation which was published in 1993 ...

Creation of $n = \infty$ perovskite type $Sr_{0.8}La_{0.2}NbO_{3+\delta}$ regions in $n = 4$ type $Sr_{0.8}La_{0.2}NbO_{3.5}$ by an electron beam in a TEM

In 1992 / 1993 Tim Williams discovered that the $n = 4$ type $Sr_{0.8}La_{0.2}NbO_{3.5}$ can be reduced to the $n = \infty$ perovskite type $(Sr,La)NbO_{3+\delta}$ by an electron beam in a transmission electron microscope (TEM)

Highly distorted perovskite regions appear after lenghty irradiation

HRTEM image made by Tim Williams

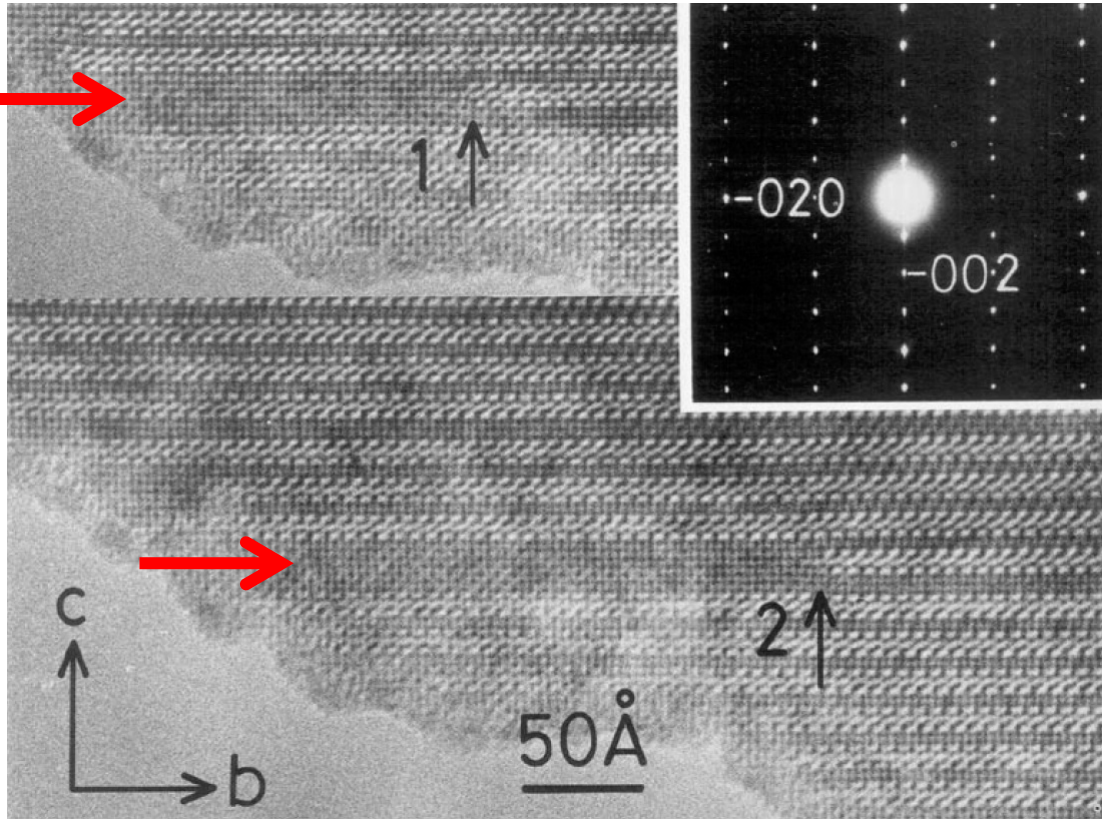

T. Williams, F. Lichtenberg, D. Widmer, J. G. Bednorz, and A. Reller, Journal of Solid State Chemistry 103 (1993) 375

This observation triggered the following research ...

8 Carpy-Galy phases

$A_nB_nO_{3n+2} = ABO_x$ allow a special kind of micro or nano patterning by an electron beam

8.2 Conducting $n = \infty$ type $SrNbO_3$ micropillars or nanopillars in an $n = 4$ type ferroelectric $SrNbO_{3.5}$ matrix or in an $n = 5$ type $SrNbO_{3.4}$ matrix ...

$n = \infty$ perovskite type $SrNbO_3$ nanopillars in a $n = 5$ type $SrNbO_{3.4}$ matrix

A crystalline piece of melt-grown $n = 5$ type $SrNbO_{3.4}$ - prepared at the IBM Zurich Research Laboratory by an IBM mirror furnace - was thinned and locally reduced and transformed to $n = \infty$ type perovskite $SrNbO_3$ by an electron beam in a scanning transmission electron microscope (STEM)

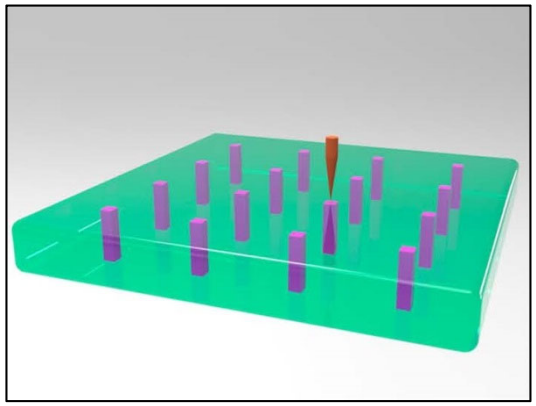

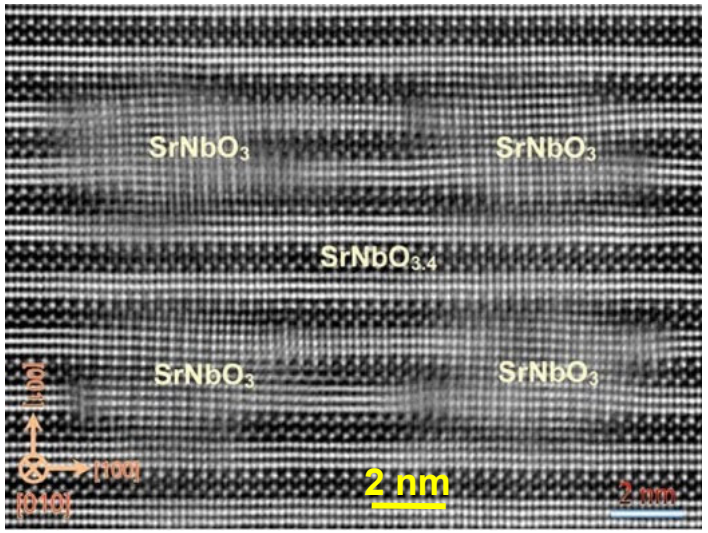

HAADF STEM image of patterned $SrNbO_3$ nanopillars in a $SrNbO_{3.4}$ matrix

If one could find a system in which the matrix is para- or diamagnetic and the transformed phase is ferromagnetic, then such a nanodevice can perhaps be applied as storage media for perpendicular magnetic recording

C. Chen, Z. Wang, F. Lichtenberg, Y. Ikuhara, J. G. Bednorz, Nano Letters 15 (2015) 6469

Conducting $SrNbO_3$ nano/micropillars in a ferroelectric $SrNbO_{3.5}$ matrix

Conducting $SrNbO_3$ ($n = \infty$) nano/micro-pillars were introduced into a ferroelectric $SrNbO_{3.5}$ ($n = 4$) thin film via a phase transformation or reduction from $SrNbO_{3.5}$ to $SrNbO_3$ triggered by a focused electron beam

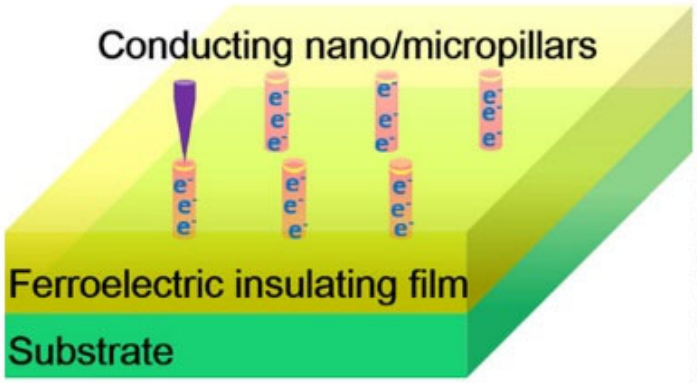

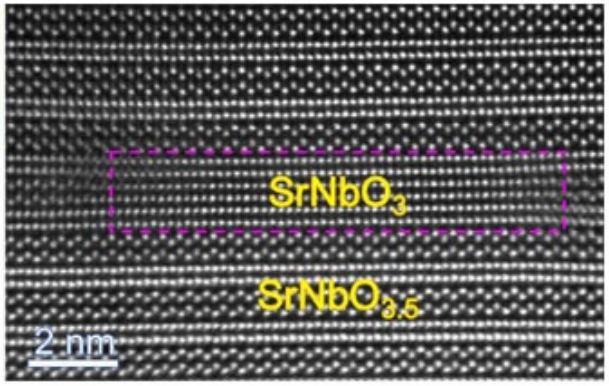

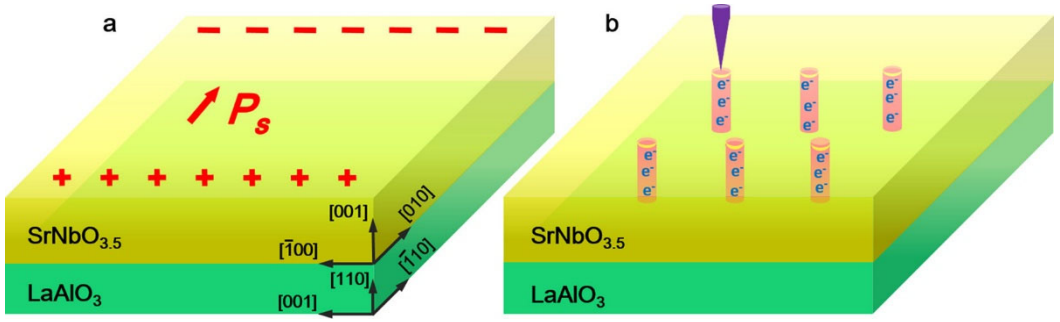

Reference including images:

Ferroelectric Oxide Thin Film with an Out-of-Plane Electrical Conductivity

Tingting Yao, Yixiao Jiang, Chunlin Chen, Xuexi Yan, Ang Tao, Lixin YangLixin Yang, Cuihong Li, Kenyu Sugo, Hiromichi Ohta, Hengqiang Ye, Yuichi Ikuhara, and Xiuliang Ma

Nano Letters 20 (2020) 1047 - 1053

https://doi.org/10.1021/acs.nanolett.9b04210

Conducting $SrNbO_3$ nano/micropillars in a ferroelectric $SrNbO_{3.5}$ matrix

Conducting $SrNbO_3$ ($n = \infty$) nano/micro-pillars were introduced into a ferroelectric $SrNbO_{3.5}$ ($n = 4$) thin film via a phase transformation or reduction from $SrNbO_{3.5}$ to $SrNbO_3$ triggered by a focused electron beam

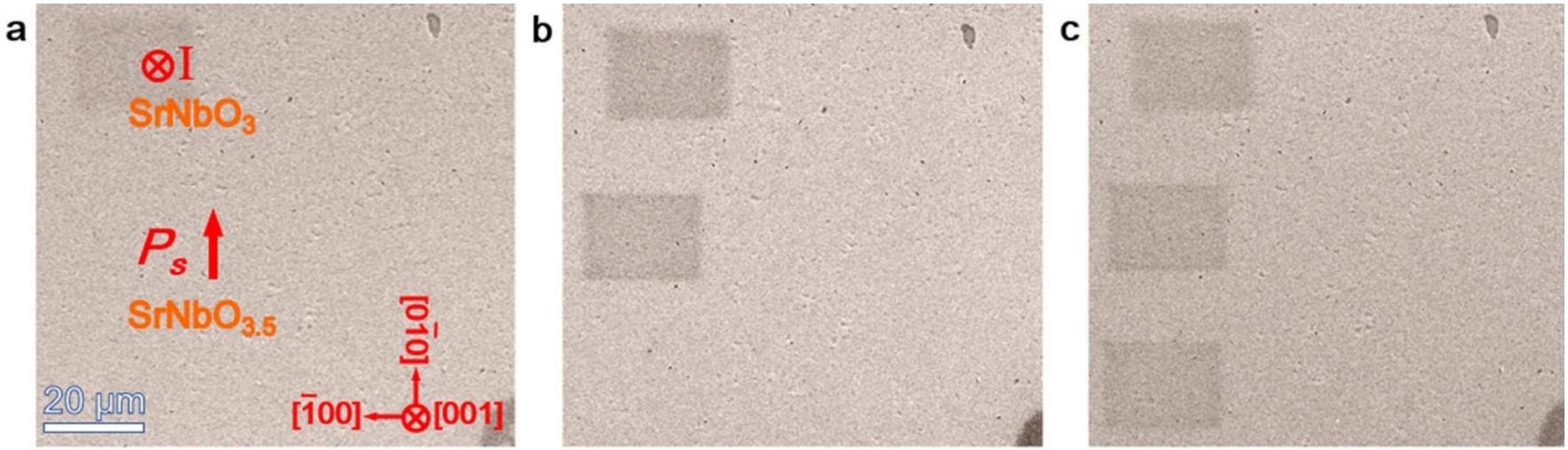

Reference including images:

Ferroelectric Oxide Thin Film with an Out-of-Plane Electrical Conductivity

Tingting Yao, Yixiao Jiang, Chunlin Chen, Xuexi Yan, Ang Tao, Lixin YangLixin Yang, Cuihong Li, Kenyu Sugo, Hiromichi Ohta, Hengqiang Ye, Yuichi Ikuhara, and Xiuliang Ma

Nano Letters 20 (2020) 1047 - 1053

https://doi.org/10.1021/acs.nanolett.9b04210

8 Carpy-Galy phases $A_nB_nO_{3n+2} = ABO_x$ allow a special kind of micro or nano patterning by an electron beam

8.3 A potential novel magnetoelectric or multiferroic system: Weak ferromagnetic $LaTiO_3$ micropillars in a ferroelectric matrix $LaTiO_{3.5}$ ...

A potential novel magnetoelectric or multiferroic system: Weak ferromagnetic $LaTiO_3$ micropillars in ferroelectric $LaTiO_{3.5}$

The $n = \infty$ perovskite type $LaTiO_3$ is known as a weak ferromagnet / canted antiferromagnet with $T_N \approx 150$ K. The $n = 4$ type $LaTiO_{3.5}$ is known as a high-T_c ferroelectric with $T_c = 1770$ K.

If it is possible to create weak ferromagnetic $LaTiO_3$ micropillars in a ferroelectric $LaTiO_{3.5}$ matrix, then this raises the question if the electric and magnetic properties / quantities are coupled. If yes, then this represents a novel magnetoelectric system and potentially also a novel multiferroic system.

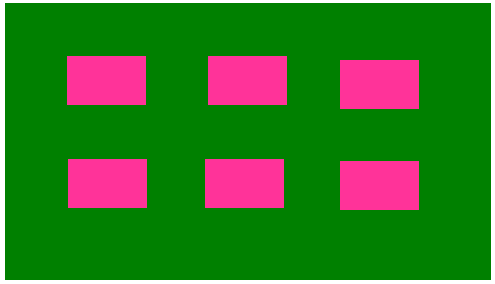

Sketch of a hypothetical system:
Weak ferromagnetic $LaTiO_3$ micropillars
in a ferroelectric $LaTiO_{3.5}$ matrix

8 Carpy-Galy phases $A_nB_nO_{3n+2} = ABO_x$ allow a special kind of micro or nano patterning by an electron beam

8.4 Another suggested system: $NaWO_x$ ($3 \leq x < 3.5$) micropillars in a $NaWO_{3.5}$ matrix ...

$NaWO_x$ ($3 \leq x < 3.5$) micropillars in a $NaWO_{3.5}$ matrix ?

As shown on the page after next the insulating $NaWO_{3.5} = Na_2W_2O_7$ (W^{6+} / $5d^0$) displays two structural modifications which are both orthorhombic. When synthesized under high pressure it adopts the $n = 4$ type structure which is potentially ferroelectric. Maybe it is also possible to stabilize the $n = 4$ type structure in a $NaWO_{3.5}$ thin film by strain by an appropriate substrate.

Stoichiometric $n = \infty$ pervoskite type $NaWO_3$ (W^{5+} / $5d^1$) was synthesized under high pressure and displays a metallic resistivity behavior.

Yuya Ikeuchi et al., Inorganic Chemistry 58 (2019) 6790

Perhaps $NaWO_3$ micropillars or $NaWO_x$ ($3 < x < 3.5$) micropillars can be created in a $NaWO_{3.5}$ matrix.

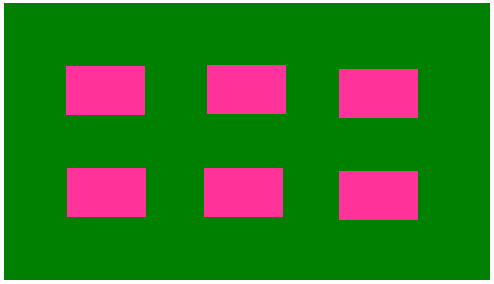

Sketch of a hypothetical system:
$NaWO_3$ or $NaWO_x$ ($3 < x < 3.5$) micropillars
in a $NaWO_{3.5}$ matrix

Among others, such a system appears interesting with respect to the reported evidence for high-T_c superconductivity in the system Na – W – O which is presented in the following part 9 ...

9 Indications for high-T_c superconductivity in the system Na – W – O and a hypothetical involvement of Carpy-Galy phases $A_nB_nO_{3n+2} = ABO_x$ ...

Indications for high-T_c superconductivity in the system Na – W – O

WO_3 (W^{6+} / $5d^0$)

- Antiferroelectric insulator with $T_c \approx 1000$ K
- Distorted ReO_3 type crystal structure which can be considered as distorted perovskite ABO_3 with absent A

Sodium tungsten bronze Na_xWO_3 (W^{6+} / $5d^0$ and W^{5+} / $5d^1$) with $0 < x < 1$

- Na-deficient perovskite structure and metallic conductor
- Superconducting with $T_c < 2$ K for $0.16 \leq x \leq 0.4$, T_c increases with decreasing x

B. W. Brown and E. Banks, Journal of the American Chemical Society 76 (1954) 963 • Ch. J. Raub et al., Physical Review Letters 13 (1964) 746 • N. N. Garif'yanov et al., Czechoslovak Journal of Physics 46 Supplement S2 (1996) 855 • A. Garcia-Ruiz and Bokhimi, Physica C 204 (1992) 79

Superconducting islands with $T_c \approx 90$ K on the surface of Na-doped WO_3

S. Reich et al., The European Physical Journal B 9 (1999) 1 • A. Shengelaya et al., The European Physical Journal B 12 (1999) 13 • S. Reich et al., Journal of Superconductivity 13 (2000) 855

- Strong experimental evidence for high-T_c superconductivity without Cu
- In spite of many efforts the superconducting phase could not be identified

Speculation: High-T_c superconducting phase Na_xWO_y could be of the type $A_nB_nO_{3n+2}$

Progress in Solid State Chemistry 36 (2008) 253

$NaWO_x$ ($3.5 \geq x \geq 3$) and $A_nB_nO_{3n+2} = ABO_x$

x in $NaWO_x$	$x = 3.5$ W^{6+} ($5d^0$) insulator	$3.5 > x > 3$ Conducting	$x = 3$ W^{5+} ($5d^1$) metal
Structure type after normal pressure synthesis	Orthorhombic Centrosymmetric WO_6 octahedra and WO_4 tetrahedra $[W_2O_7]^{2-}$ chains along *a*-axis K. Okada, H. Morikawa, F. Marumo, and S. Iwai, Acta Cryst. B 31 (1975) 1200	W^{6+} ($5d^0$) / W^{5+} ($5d^1$) ? Hypothetical $4 \leq n \leq 6$ Supercon-ducting ? Progress in Solid State Chemistry 36 (2008) 253	
Structure type after high pressure synthesis	Orthorhombic $n = 4$ Non-centrosymmetric Potentially ferroelectric Single crystals were grown by cooling normal pressure synthesized $Na_2W_2O_7$ slowly from 1200 °C under 20 – 30 kbar K.-J. Range and H. Haase, Acta Cryst. C 46 (1990) 317		Cubic perovskite Yuya Ikeuchi et al., Inorganic Chemistry 58 (2019) 6790

No indications for superconductivity in a polycrystalline sintered *n* = 5 type composition $NaWO_{3.4}$

Synthesis approach:

$0.5\ Na_2CO_3 + 0.8921\ WO_3 + 0.1079\ WO_{1.98} \rightarrow NaWO_{3.39} + 0.5\ CO2 \uparrow$

$WO_{1.98}$ = Tungsten dioxide with thermogravimetrically determined oxygen content 1.98

Pre-reacted for 6 h at 600 °C under air. After mingling the pre-reacted material with $WO_{1.98}$ the obtained powder was pressed into a reactangular shape and heated and sintered for 6 h at 700 °C under argon in the GERO tube furnace.

A polycrystalline sintered *n* = 5 type composition $NaWO_{3.4}$

Sample No. 704 • Prepared at the ETH Zurich in 2012

Material is probably multiphase

Powder x-ray diffraction was not performed

The magnetic moment M(T) and susceptibility $\chi(T)$ of a piece from this material was measured by a SQUID magnetometer in the temperature range $2\ K \leq T \leq 330\ K$. $\chi(T)$ is weakly diamagnetic and nearly temperature-independent and no indication for superconductivity was detected.

Acknowledgement: F. L. thanks Bertram Batlogg (ETH Zurich) who performed the magnetic measurement with his Qantum Design SQUID Magnetometer MPMS XL

No indications for superconductivity in a polycrystalline sintered *n* = 6 type composition $NaWO_{3.33}$

Synthesis approach analogous to what is described on the previous page but with another appropriate ratio WO_3 / $WO_{1.98}$

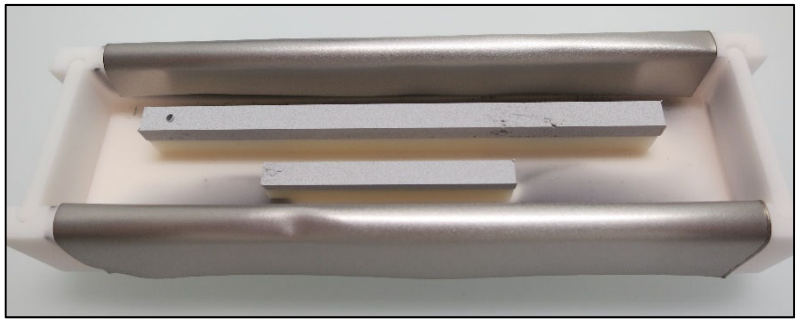

Two as-pressed rods with composition $NaWO_{3.33}$

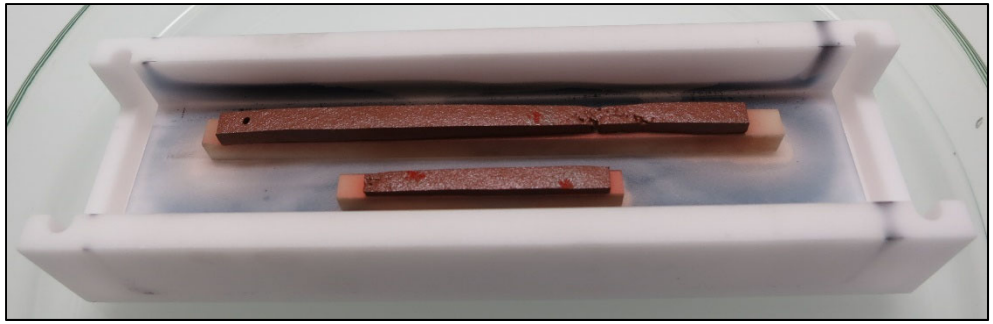

Rods with composition $NaWO_{3.33}$ after they were heated and sintered under argon

Run / Sample No. 711 • Prepared at the ETH Zurich in 2013

Material is probably multiphase • Powder x-ray diffraction was not performed

Processing the sintered rods by floating zone melting did not work because of a difficult melting behavior and strong bending of the seed rod in the mirror furnace

The magnetic moment M(T) of a piece from the sintered rods was measured by a SQUID magnetometer in the temperature range 2 K ≤ T ≤ 300 K and no indication for superconductivity was detected. **Acknowledgement:** F. L. thanks Marisa Medarde (PSI) and Mickael Morin (PSI) for performing a magnetic measurement with a Quantum Design SQUID magnetometer MPMS XL and Nicholas Bingham (PSI) for performing a magnetic measurement with a Quantum Design SQUID magnetometer MPMS3

10 Pictures and properties of some melt-grown perovskite-related layered oxides which are not Carpy-Galy phases such as Sr_2RuO_4 , $SrLaFeO_4$, $BaCa_{0.6}La_{0.4}Nb_2O_7$, $Sr_5Nb_4O_{15}$, and $Sr_6Nb_5O_{18}$ ...

2D sketch of perovskite-related layered oxides of the type

$A_{j+1}B_jO_{3j+1}$, $A'A_{k-1}B_kO_{3k+1}$, $A_nB_nO_{3n+2}$, and hexagonal $A_mB_{m-1}O_{3m}$

B = Al, Ti, V, Cr, Mn, Fe, Cu, Ru ... Comprises j = 1 type $(La,Ba)_2CuO_4$ in which J. G. Bednorz and K. A. Müller discovered in 1986 superconductivity up to 30 K

B = Ti, Nb, Ta

- Layers are constituted by corner-shared BO_6 octahedra and extend along *ab*-plane
- Layer thickness along *c*-axis: $j = k = n = m - 1$ BO_6 octahedra
- $j = k = n = m = \infty \rightarrow$ Perovskite structure ABO_3

Progress in Solid State Chemistry 36 (2008) 253

= BO_6 octahedra (O located at corners, *B* hidden in center)

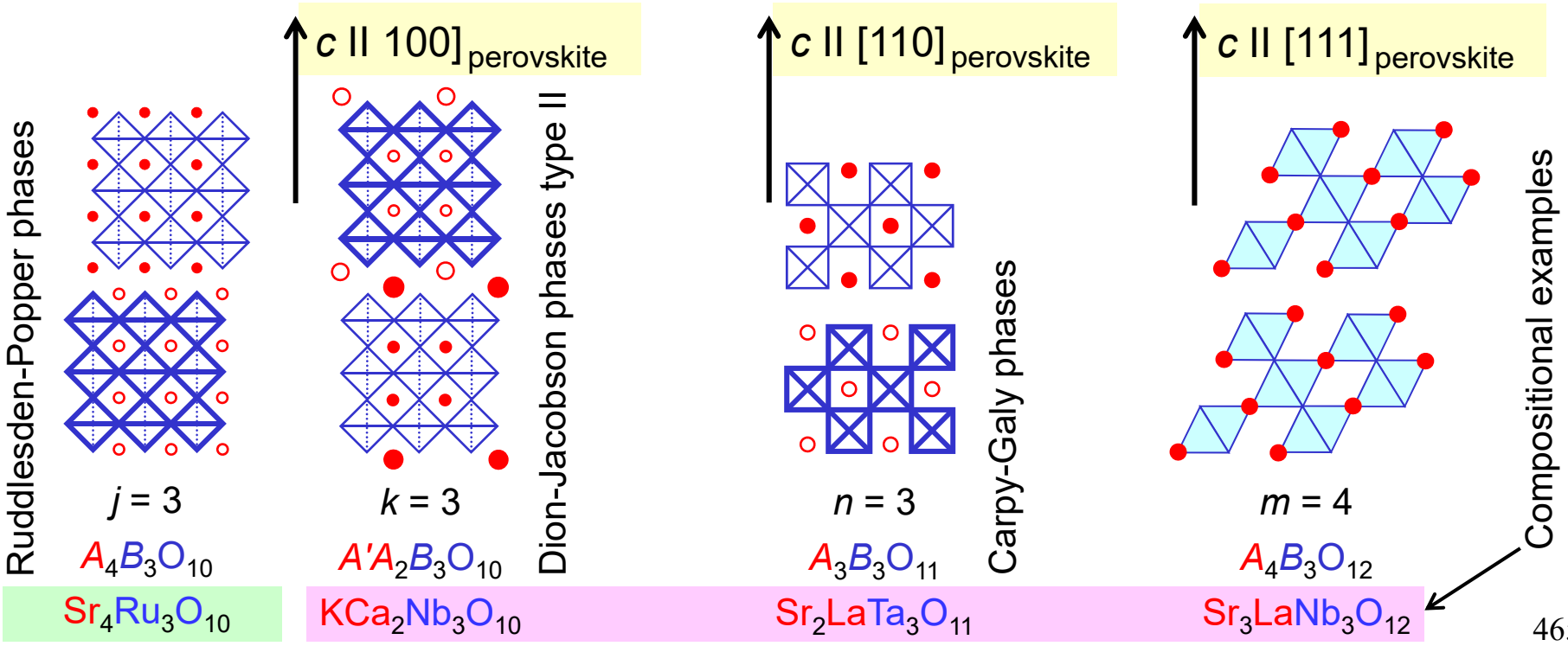

2D sketch of perovskite-related layered oxides of the type

$A_{j+1}B_jO_{3j+1}$, $A'A_{k-1}B_kO_{3k+1}$, $A_nB_nO_{3n+2}$, and hexagonal $A_mB_{m-1}O_{3m}$

Presented on the following pages are pictures and properties of some melt-grown materials of these three homologous series

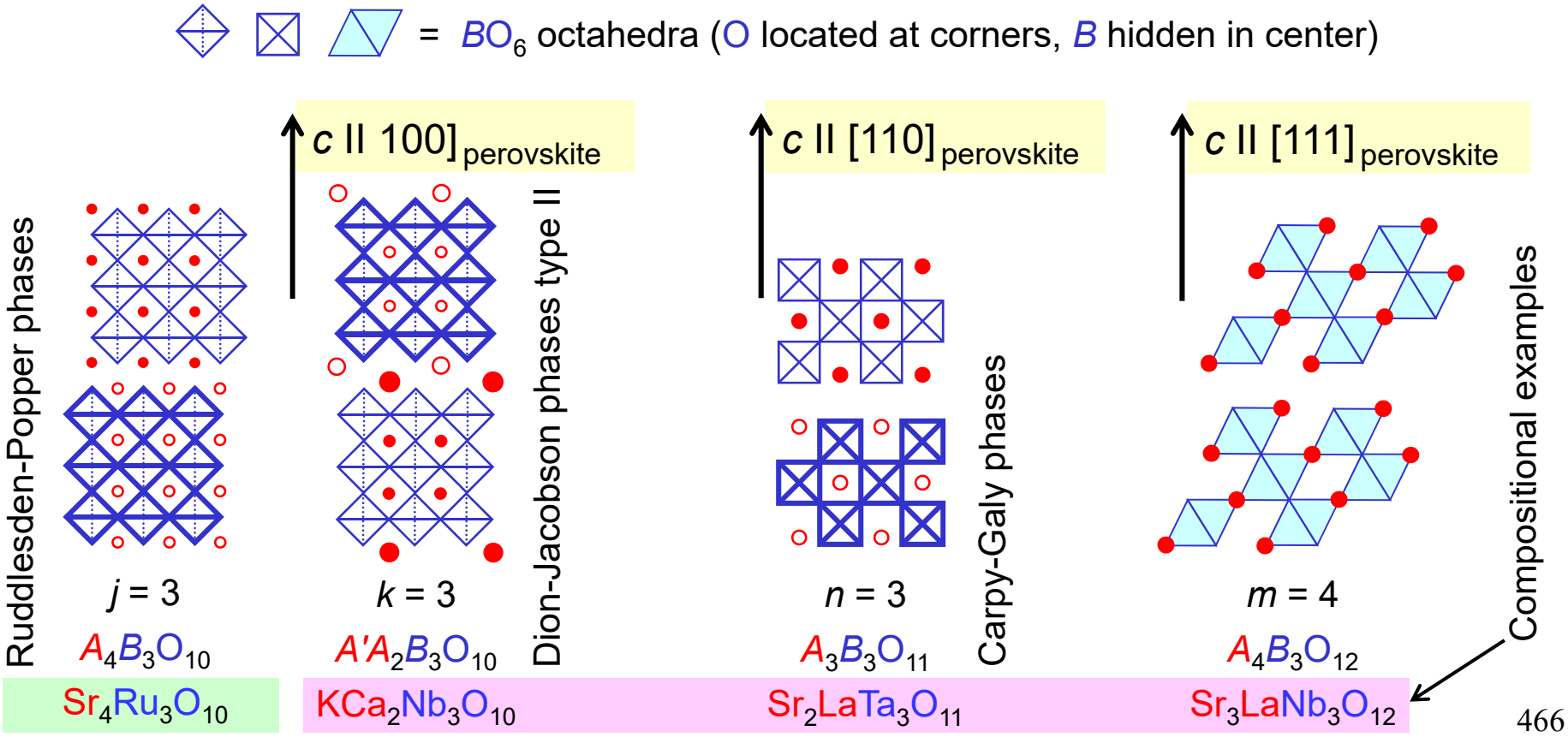

Example of a melt-grown oxide prepared by an IBM mirror furnace

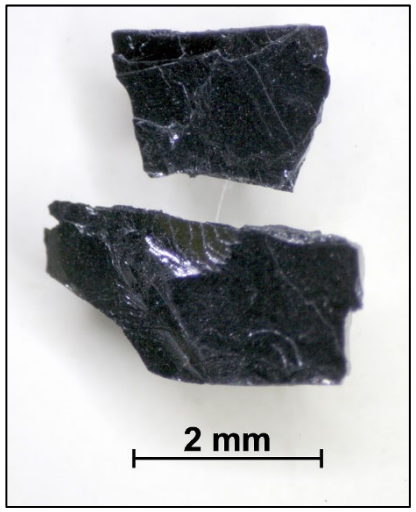

Sr_2RuO_4 Sample No. Z 111

Structure type $j = 1$
of $A_{j+1}B_jO_{3j+1}$

Grown under synth. air

Samples prepared at the
IBM Zurich Research Laboratory

Photos taken at the ETH Zurich

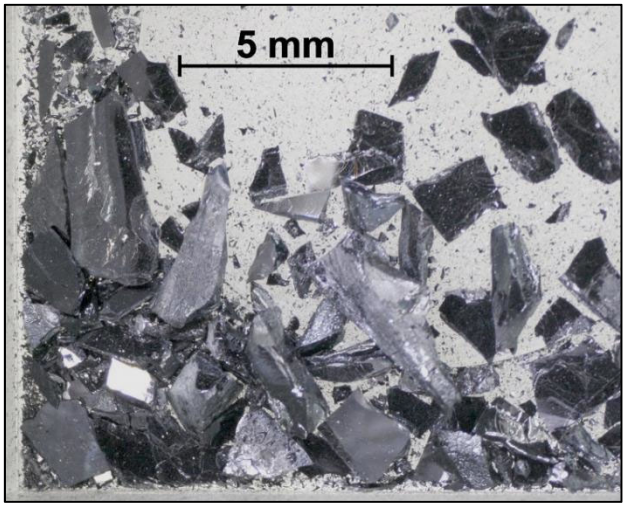

The original intention was to try to synthesize the $j = 2$ type $Sr_3Ru_2O_7$ via the melt. However, $Sr_3Ru_2O_7$ did never appear and always Sr_2RuO_4 did arise, nearly independent of the ratio Sr / Ru. The experiments were difficult because of a strong evaporation of RuO_x . Nevertheless, nice crystalline pieces of Sr_2RuO_4 could be obtained from the inner part of the melt-grown material. Resistivity measurements on Sr_2RuO_4 crystals revealed a metallic behavior along the layers. In crystalline form Sr_2RuO_4 was the first metallic substrate for the epitaxial growth of thin films of high-T_c superconductors like $YBa_2Cu_3O_{7-\delta}$

Tim Williams, Frank Lichtenberg, Armin Reller, and Georg Bednorz, Materials Research Bulletin 26 (1991) 763
F. Lichtenberg, A. Catana, J. Mannhart, and D. G. Schlom, Applied Physics Letters 60 (1992) 1138
L. Walz and F. Lichtenberg, Acta Crystallographica Section C 49 (1993) 1268

Example of a melt-grown oxide prepared by an IBM mirror furnace

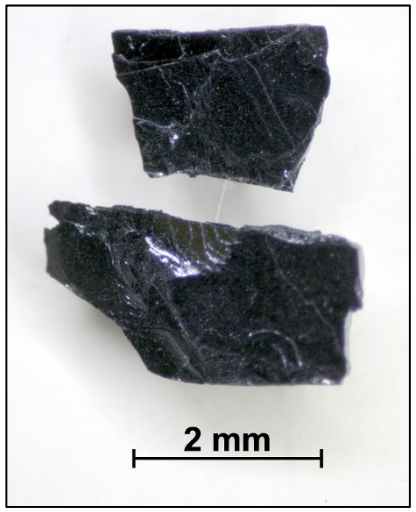

Sr_2RuO_4 Sample No. Z 111

Structure type $j = 1$
of $A_{j+1}B_jO_{3j+1}$

Grown under synth. air

Samples prepared at the
IBM Zurich Research Laboratory

Photos taken at the ETH Zurich

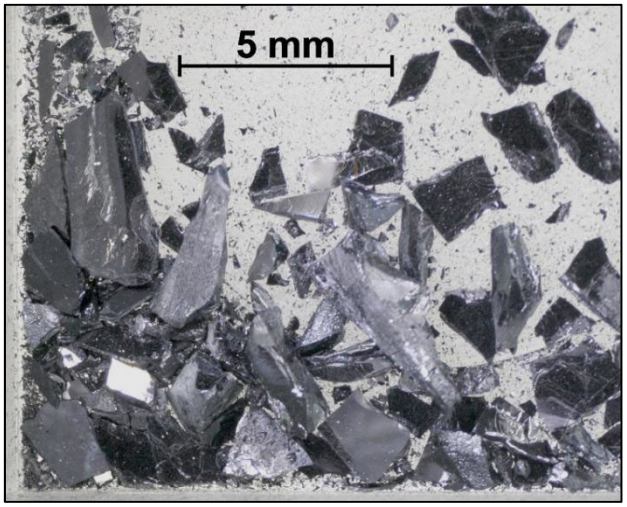

Later it was discovered that the Sr_2RuO_4 crystals itself are superconducting at low temperatures with $T_c \approx 1$ K. Despite of its low T_c the Sr_2RuO_4 gained considerable attention because of its unconventional superconducting properties. Sr_2RuO_4 is isostructural to $(La,Ba)_2CuO_4$ in which J. G. Bednorz and K. A. Müller discovered in 1986 superconductivity up to 30 K. For updates and references until May 2019 see the program of the conference "Strontium Ruthenate - 25 years of a puzzling superconductor" which took place in May 2019 at the ETH Zurich:

https://sro214.ethz.ch and https://sro214.ethz.ch/files/sro214_full.pdf

Y. Maeno, H. Hashimoto, K. Yoshida, S. Nishizaki, T. Fujita, J. G. Bednorz, and F. Lichtenberg, Nature 372 (1994) 532 • F. Lichtenberg, Progress in Solid State Chemistry 30 (2002) 103 • Andrew Peter Mackenzie and Yoshiteru Maeno, Reviews of Modern Physics 75 (2003) 657 • Y. Maeno, S. Kittaka, T. Nomura, S. Yonezawa, and K. Ishida, Journal of the Physical Soceity of Japan 81 (2012) 011009 • Ying Liu and Zhi-Qiang Mao, Physica C 514 (2015) 339

Examples of melt-grown oxides prepared by a GERO mirror furnace

Layered perovskite-related $A_{j+1}B_jO_{3j+1}$

Crystalline pieces from as-grown brown-black antiferromagnetic insulators with Fe^{3+} / $3d^5$ which were grown with 15 mm / h under synthetic air

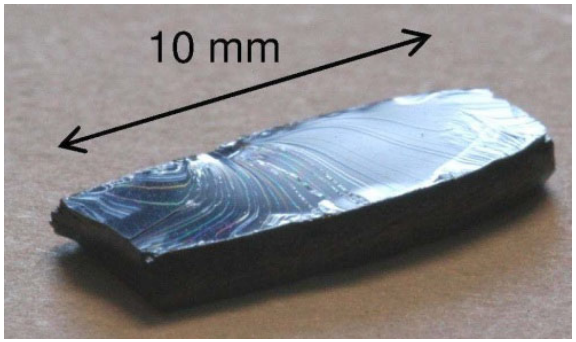

$LaSrFeO_4$

Sample No. 475

Structure type $j = 1$

Ruddlesden-Popper phase

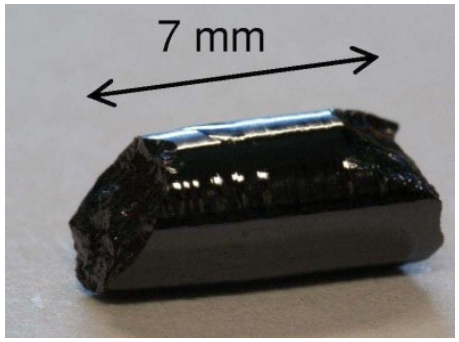

$LaFeO_3$

Sample No. 530

$j = \infty$ type perovskite ABO_3

Samples prepared at the University of Augsburg - Progress in Solid State Chemistry 36 (2008) 253

Example of a melt-grown oxide prepared by a GERO mirror furnace

Layered perovskite-related Dion-Jacobson phase $A'A_{k-1}B_kO_{3k+1}$ without alkali metal

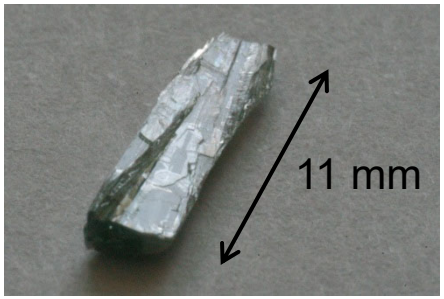

Crystalline piece from the as-grown material

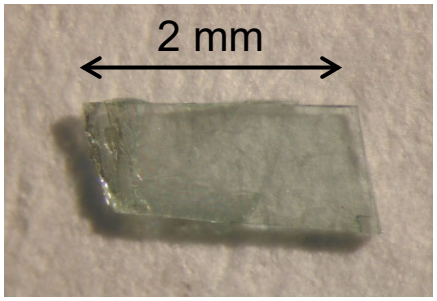

Plate-like crystal cleaved from the as-grown material

$BaLa_2Ti_3O_{10}$

Ti^{4+} / $3d^0$

Sample No. 149

Grown under synthetic air

Structure type k = 3

Light green transparent insulator

Samples prepared at the University of Augsburg - Progress in Solid State Chemistry 36 (2008) 253

Examples of melt-grown oxides prepared by a GERO mirror furnace

Layered perovskite-related Dion-Jacobson phases $A'A_{k-1}B_kO_{3k+1}$ without alkali metal

Crystalline pieces of as-grown materials which are black-blue metallic conductors

$BaCa_{0.6}La_{0.4}Nb_2O_7$

$Nb^{4.8+}$ / $4d^{0.2}$

Sample No. 134

Grown in argon

Structure type k = 2

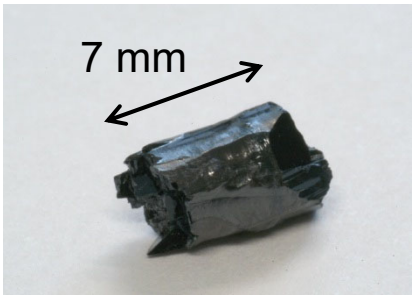

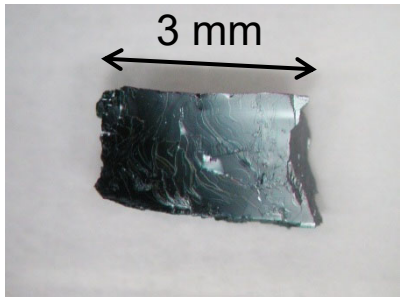

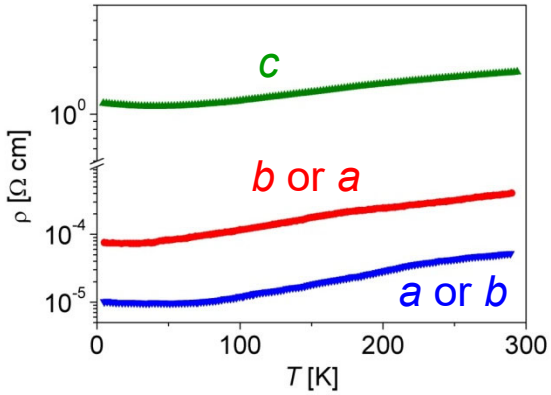

$BaCa_2Nb_3O_{10.07}$

$Nb^{4.71+}$ / $4d^{0.29}$

Sample No. 150

Grown in argon

Structure type k = 3

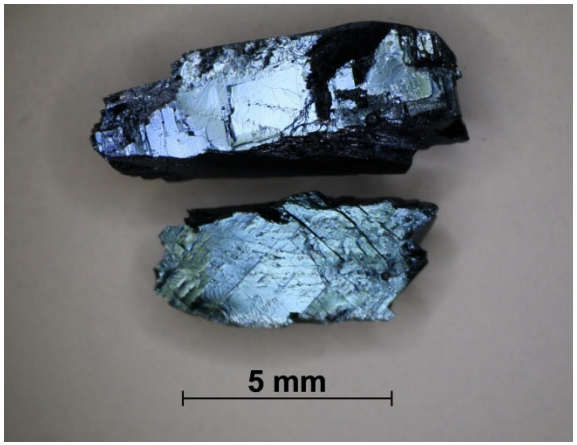

Resistivity ρ(T) along

a- , *b*- and *c*-axis

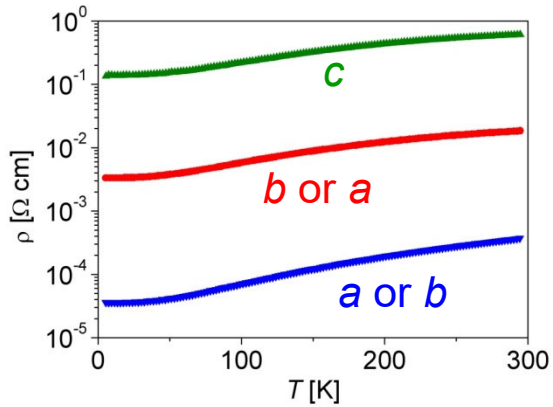

Progress in Solid State Chemistry 36 (2008) 253

Samples prepared at the University of Augsburg - Photo of $BaCa_2Nb_3O_{10.07}$ taken at the ETH Zurich

Example of a Laue image of melt-grown crystalline platelets

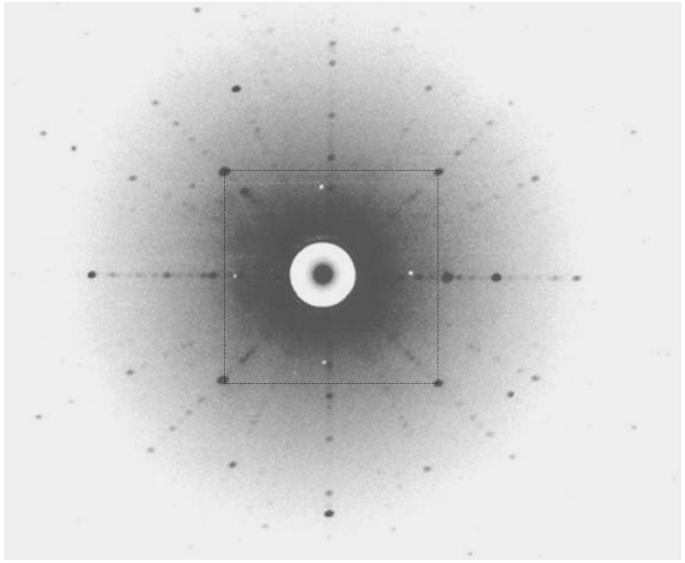

Orthorhombic $BaCa_{0.6}La_{0.4}Nb_2O_7$

Structure type $k = 2$ of perovskite-related layered $A'A_{k-1}B_kO_{3k+1}$

Dark / bright - inverted image

$a = 4.00$ Å , $b = 7.80$ Å , $c = 19.96$ Å

a and b cannot be distinguished because $a \approx b / 2$

Progress in Solid State Chemistry 36 (2008) 253

Example of a melt-grown oxide prepared by a GERO mirror furnace

Niobates of hexagonal layered perovskite-related $A_mB_{m-1}O_{3m}$

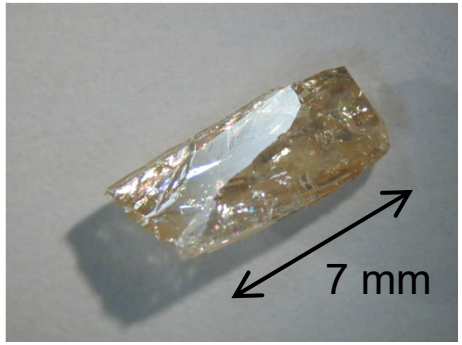

Crystalline piece
from the
as-grown material

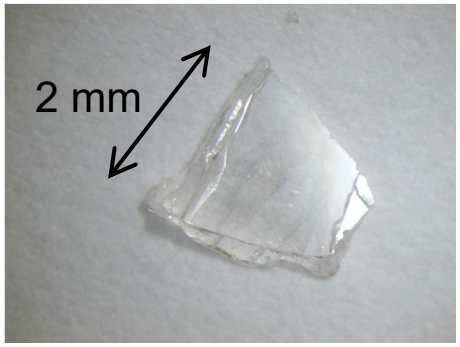

Plate-like crystal
cleaved from the
as-grown material

$Sr_5Nb_4O_{15}$

Nb^{5+} / $4d^0$

Sample No. 431

Grown with 15 mm / h
under synthetic air

Structure type m = 5

Yellow transparent insulator

Samples prepared at the University of Augsburg - Progress in Solid State Chemistry 36 (2008) 253

Example of melt-grown oxides prepared by a GERO mirror furnace

Niobates of layered hexagonal perovskite-related $A_mB_{m-1}O_{3m}$

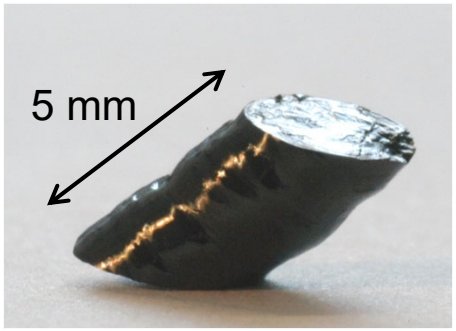

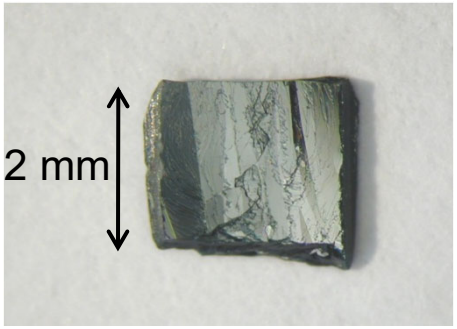

Crystalline pieces from the as-grown material

$Sr_6Nb_5O_{18.07}$ $Nb^{4.83+}$ / $4d^{0.17}$

Sample No. 433

Grown with 8 mm / h in argon

Structure type m = 6

Blue-black quasi-2D metal and temperature-driven metal-to-semiconductor transition at 160 K

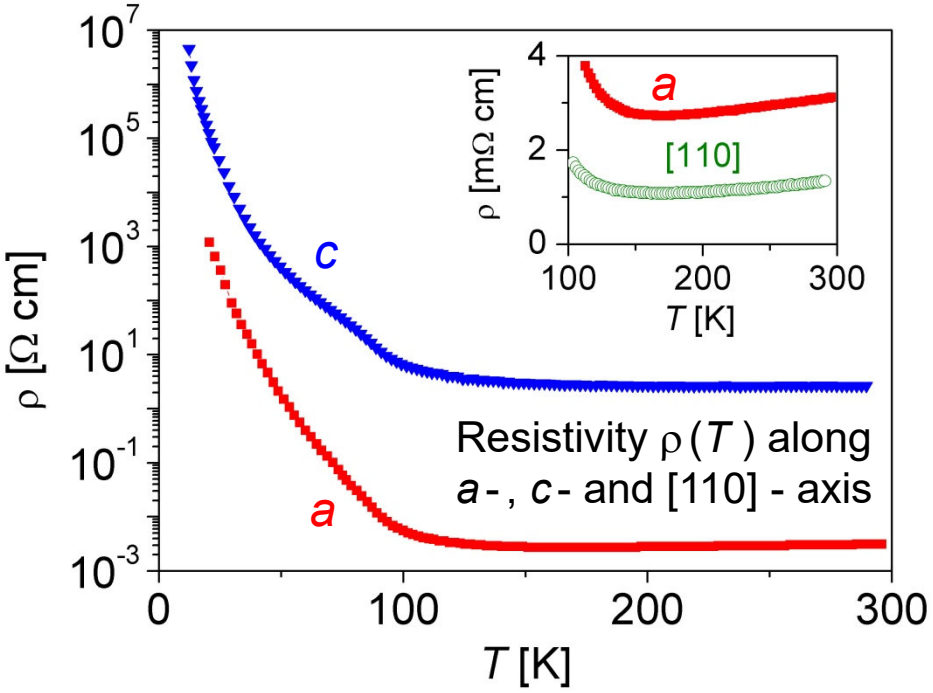

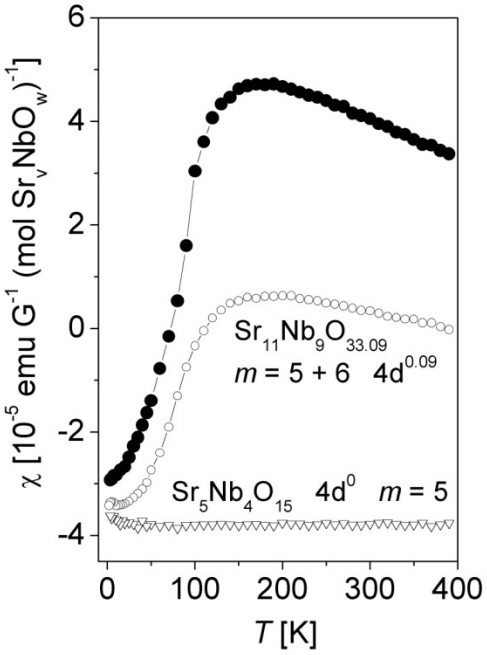

Magnetic susceptibility $\chi(T)$ without Curie contribution from paramagnetic impurities

Samples prepared at the University of Augsburg - Progress in Solid State Chemistry 36 (2008) 253

Example of a Laue image of melt-grown crystalline platelets

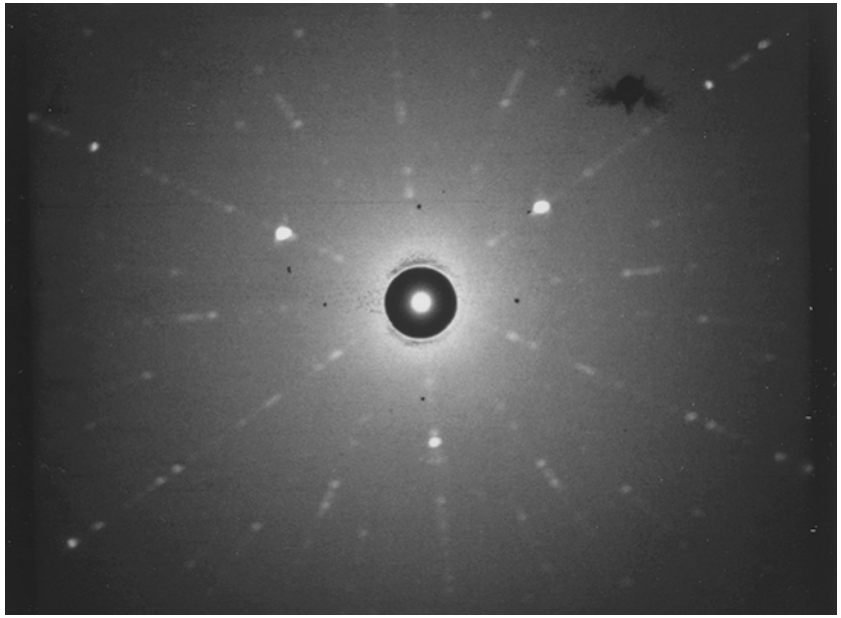

Hexagonal $Sr_{11}Nb_9O_{33.1}$

Structure type m = 5 + 6 of perovskite-related layered $A_mB_{m-1}O_{3m}$

a = 5.66 Å , c = 75.67 Å

Progress in Solid State Chemistry 36 (2008) 253

Example of a melt-grown oxide prepared by a GERO mirror furnace

Niobates of hexagonal layered perovskite-related $A_mB_{m-1}O_{3m}$

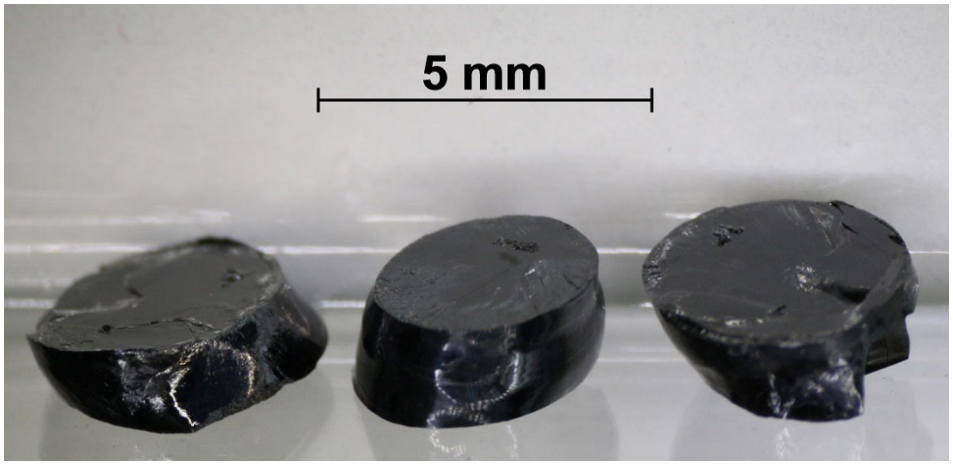

Crystalline pieces from the as-grown material

$Sr_{4.6}La_{0.4}Nb_4O_{15.06}$ $Nb^{4.93+}$ / $4d^{0.07}$

Sample No. 433

Grown with (15 - 6) mm / h by reducing the fully oxidized Nb^{5+} composition $Sr_{4.6}La_{0.4}Nb_4O_{15.20}$ under 98 % Ar + 2 % H_2

Structure type m = 5

Blue-black electrical conductor

Observation at melt-grown layered oxides:

Usually the layers grow parallel or 45 degrees declined to the axial direction of the as-grown material. Concerning own experiments this compound is one of very few examples where the layers did grow perpendicular to the axial direction of the as-grown material

Progress in Solid State Chemistry 36 (2008) 253

Samples prepared at the University of Augsburg - Photo taken at the ETH Zurich
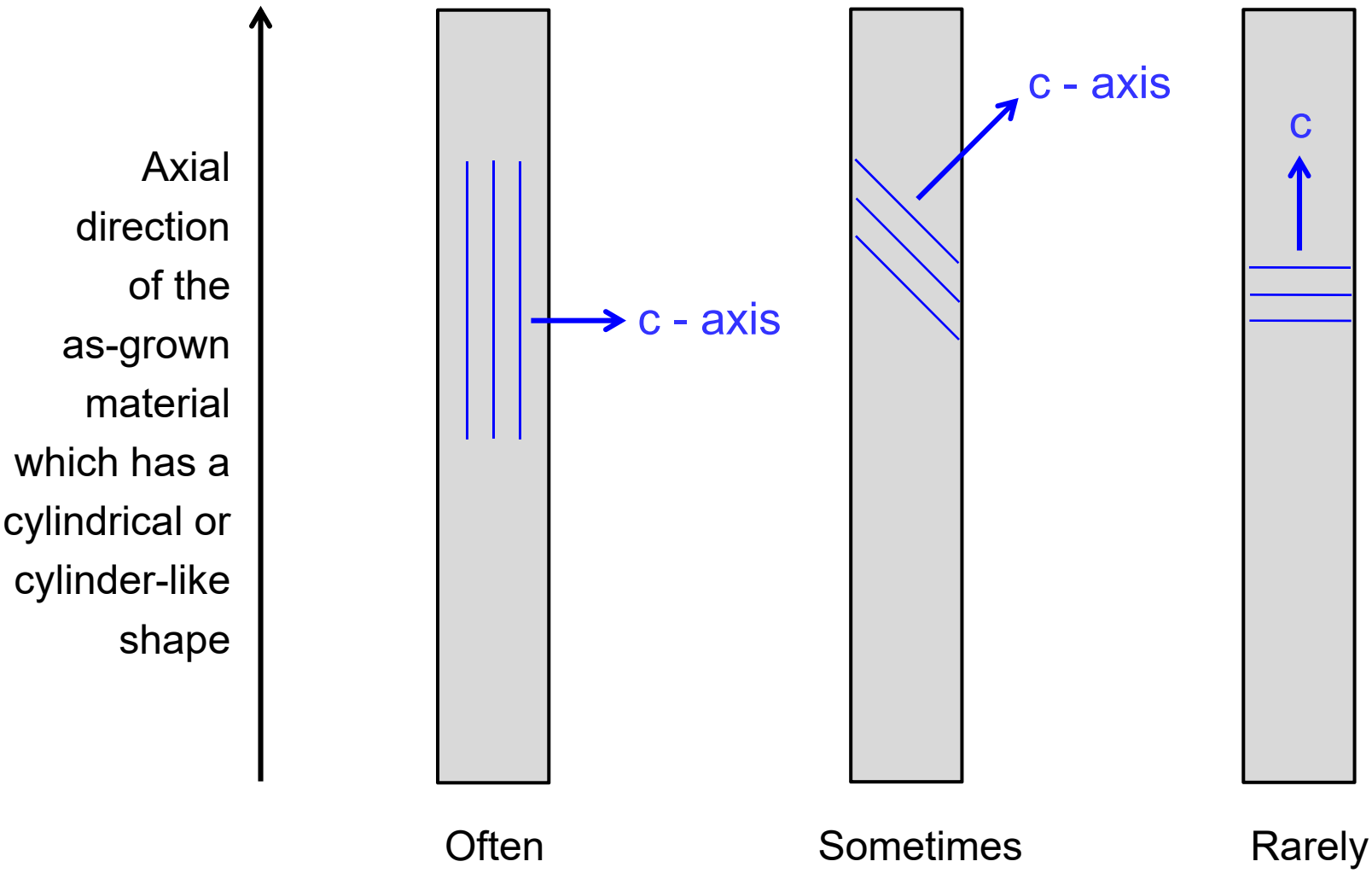
Observed orientation of the layers in melt-grown layered oxides